The Development of Computational Tools for Theoretical Predictions in Particle Physics at the Large Hadron Collider

Thomas Henri Cridge

Christ's College

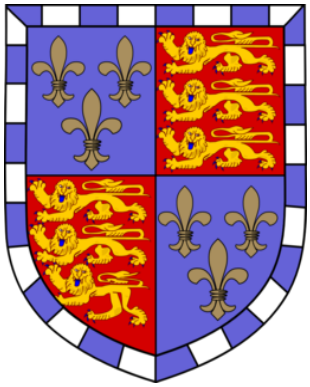

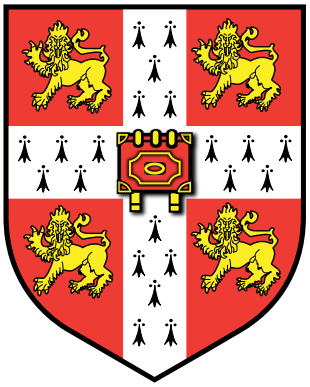

This dissertation is submitted for the degree of Doctor of Philosophy.

Department of Applied Mathematics and Theoretical Physics

University of Cambridge

Supervisor: Professor Benjamin Allanach

September 2018

UNIVERSITY OF CAMBRIDGE

The Development of Computational Tools for Theoretical Predictions in Particle Physics at the Large Hadron Collider

Thomas Henri Cridge

The Large Hadron Collider (LHC) experiments are an excellent tool for the improvement of our knowledge of the Standard Model and the examination of Beyond Standard Model theories. Nonetheless, to maximise the learning-potential of the LHC, clear and precise theoretical predictions are needed, for both the Standard Model and its extensions, to allow critical comparison of these models with data. In particular, given the complexity of the collision environment at the LHC, and the expansive nature of many parameter spaces of Beyond Standard Model theories, computational programs to perform theoretical calculations are increasingly required.

The work presented in this thesis fits this role, it is focused on two computational programs developed with the aim of producing such theoretical predictions for LHC phenomenology in two key areas. These are the precision Standard Model predictions of transverse momentum spectra for a wide class of processes at the LHC, and Beyond Standard Model predictions for the decay widths of as-yet undiscovered particles in the context of supersymmetry.

Chapter 1 presents a brief chronology and review of the Standard Model. Following this, the work reported in this thesis is split into two parts, focused on the two main projects undertaken. Chapters 2, 3 and 4 describe the development of the `SoftSusy` decay calculator program to determine the partial widths and branching ratios of supersymmetric and Higgs particles in the Minimal Supersymmetric Standard Model and the Next-to-Minimal Supersymmetric Standard Model. The theoretical and phenomenological background, methodology, assumptions, and the vast array of decay modes calculated by the program are described. This is followed by details of the extensive validation of the decay calculator program and a selection of results. Chapter 5 begins the second part of the thesis, providing theoretical background for Chapters 6 and 7, which discuss the newly-developed `reSolve` program, designed to undertake the theoretically-demanding calculations associated with transverse momentum resummation for a wide range of LHC processes. Details of the methods, assumptions, validation and results for channels so far included are all provided, these show excellent agreement with previous theoretical results and experimental data. Both projects are then summarised in Chapter 8. Further information is provided in the appendices; Appendix A presents explicitly all formulae incorporated into the `SoftSusy` decay calculator program; whilst Appendix B provides further details on the theoretical underpinning of the transverse momentum resummation calculations performed by the `reSolve` program.

Abstract

The Large Hadron Collider (LHC) experiments are an excellent tool for the improvement of our knowledge of the Standard Model and the examination of Beyond Standard Model theories. Nonetheless, to maximise the learning-potential of the LHC, clear and precise theoretical predictions are needed, for both the Standard Model and its extensions, to allow critical comparison of these models with data. In particular, given the complexity of the collision environment at the LHC, and the expansive nature of many parameter spaces of Beyond Standard Model theories, computational programs to perform theoretical calculations are increasingly required.

The work presented in this thesis fits this role, it is focused on two computational programs developed with the aim of producing such theoretical predictions for LHC phenomenology in two key areas. These are the precision Standard Model predictions of transverse momentum spectra for a wide class of processes at the LHC, and Beyond Standard Model predictions for the decay widths of as-yet undiscovered particles in the context of supersymmetry.

Chapter 1 presents a brief chronology and review of the Standard Model. Following this, the work reported in this thesis is split into two parts, focused on the two main projects undertaken. Chapters 2, 3 and 4 describe the development of the `SoftSusy` decay calculator program to determine the partial widths and branching ratios of supersymmetric and Higgs particles in the Minimal Supersymmetric Standard Model and the Next-to-Minimal Supersymmetric Standard Model. The theoretical and phenomenological background, methodology, assumptions, and the vast array of decay modes calculated by the program are described. This is followed by details of the extensive validation of the decay calculator program and a selection of results. Chapter 5 begins the second part of the thesis, providing theoretical background for Chapters 6 and 7, which discuss the newly-developed `reSolve` program, designed to undertake the theoretically-demanding calculations associated with transverse momentum resummation for a wide range of LHC processes. Details of the methods, assumptions, validation and results for channels so far included are all provided, these show excellent agreement with previous theoretical results and experimental data. Both projects are then summarised in Chapter 8. Further information is provided in the appendices; Appendix A presents explicitly all formulae incorporated into the `SoftSusy` decay calculator program; whilst Appendix B provides further details on the theoretical underpinning of the transverse momentum resummation calculations performed by the `reSolve` program.

Declaration

This dissertation is the result of my own work and includes nothing which is the outcome of work done in collaboration except as declared in the Preface and specified in the text.

It is not substantially the same as any that I have submitted, or, is being concurrently submitted for a degree or diploma or other qualification at the University of Cambridge or any other University or similar institution except as declared in the Preface and specified in the text. I further state that no substantial part of my dissertation has already been submitted, or, is being concurrently submitted for any such degree, diploma or other qualification at the University of Cambridge or any other University or similar institution except as declared in the Preface and specified in the text. As described in detail in the Preface the work described is available in my published papers [1] and [2].

It does not exceed the prescribed word limit for the relevant Degree Committee - for the mathematics department there is no prescribed word limit.

Preface

This thesis contains the majority of the work undertaken during my PhD in Theoretical Particle Physics and is the result of my work unless otherwise specified here or in the text. The first chapter offers an introduction to the general area of research, and consequently is necessarily review material, although of course in my words and with my own explanation.

Chapters 2, 3 and 4 are the result of my first PhD project on the `SoftSusy` program, which was performed in collaboration with my supervisor, Professor Benjamin Allanach. Chapter 2 provides a specific introduction into the theoretical and experimental context in this area and so is further review material, collated and written by myself using the references contained therein. Chapters 3 and 4 detail the exact research I performed in this area. In this project the vast majority of the work was my own, the initial idea was that of my supervisor and the decay calculator program is designed to be part of the `SoftSusy` package which is also my supervisor's creation. Nonetheless the development of the decay calculator as part of this program, which I focus my comments on in this thesis, was overwhelmingly my own. I was responsible for re-deriving and verifying all the decay formulae included (with the exception of the three body modes which are adapted from `sPHENO` [3, 4]) and the subsequent coding, validation of the decay modes and the results. The only exceptions to this are the chargino to neutralino pion modes mentioned briefly in Chapters 3.4.1 and 3.4.5 and presented in Chapter 4.11, these were added by my supervisor; in addition he wrote the numerical integrator used in my code to evaluate the 3-body decay numerical integrals. He also undertook some occasional overall restructuring of the whole `SoftSusy` package. All formulae used in the program are given in Appendix A, which appears also in our published paper on this work [1], which acts as a manual and validation of the `SoftSusy` decay calculator. Several of the sections in these chapters have been adapted and extended from our work presented there.

Chapters 5, 6 and 7 present the results of my work in collaboration with Dr Francesco Coradeschi at the Department of Applied Mathematics and Theoretical Physics (DAMTP) on developing the new `reSolve` transverse momentum resummation program. Chapter 5 is again review material on this area and is therefore my understanding of the context of this research, with many references used in its writing. Chapters 6 and 7 demonstrate the culmination of our work in this area - the `reSolve` program. Chapter 6 begins explaining the theoretical formalism, this formalism was developed by many others and references are given in the text, we simply apply and

adapt the formalism in our research. This work was very much a collaborative effort, with Dr Coradeschi offering the initial theoretical expertise in this area, the initial idea and the overall framework for the structure of the program. I was responsible for the explicit programming, testing, validation and results of the program. In particular, the code is largely my own based on the theoretical formalism and using private programs in this area such as `2gRes` [5, 6] and `DYRes` [7, 8] as inspiration and as useful comparisons. Francesco developed the histogrammer and parallelisation of the program, as well as the built-in Monte Carlo integrator (`k_vegas`), and offered much effort in the general development and debugging of the initial program version. As I was responsible for the validation and results, the figures presented in Chapter 7 are all completely my own as are the comparisons and comments associated. The work presented represents the first main version of many of the `reSolve` program, again this has been collated in our paper [2], which contains a shorter version of much of the information presented here and serves as the manual for the program. Appendix B provides further details on many aspects of the resummation formalism and its application in `reSolve`, the resummation coefficients in Appendix B.1 were gathered by Francesco from several references as described. Appendices B.2 and B.3 give details on Mellin space and Monte Carlo integration and are my explanation of how and why this is done in the `reSolve` program.

Both the `SoftSusy` and `reSolve` programs are provided on memory sticks in addition to this thesis for the examiners; for other readers they are also available online on Github, where the most up-to-date versions will always be found, at the links https://github.com/BAllanach/softsusy and https://github.com/fkhorad/reSolve. The two programs are also available with their published papers [1] [2], whilst `SoftSusy` can additionally be found on its web page "http://softsusy.hepforge.org/". Each of these projects displayed in the following thesis are first stages in what we hope to be a long continuous path of development, extension and augmentation for both programs - we hope they will prove of great use to the particle physics community. This thesis therefore serves as a meticulous and detailed summary of my PhD efforts over the past four years and so I hope that the reader will find this thesis as informative and as rewarding as it was to work in this area.

Acknowledgements

This PhD thesis has been the culmination of many years of effort, not just by myself and not just over the last four years. There are many people I would like to thank for their support and encouragement during my life and without which it would not have been possible to reach this stage.

First of all, of course, I would like to thank my parents, I will be forever grateful for their continuous support and effort. Both through my childhood, encouraging me to delve deeper into my interest in mathematics and physics and pushing teachers and schools to foster its development, and beyond. This required an unbelievable amount of work and I believe it has ultimately paid dividends through this work. In the same breath I must also mention my brothers, we shared a great childhood and they have always been around to support and encourage me wherever required, including into adulthood where we are now pursuing our separate interests but are always available to support one other. It is no exaggeration to say that without my parents and my brothers I doubt my life would have taken the wonderful track it has, which I will follow into my post-doctoral physics research. Similarly I would like to extend my thanks to the rest of my family, who are always there for me.

From a physics and mathematics perspective I wish to express my gratitude for many teachers during my school years, without their efforts this PhD would not have been possible. At university I am grateful to my supervisors and tutors and Christ's College, where I have completed the vast majority of my formal physics education in undertaking my Bachelor's, Master's and PhD degrees. Christ's has been somewhere I have had the pleasure to call home for the past 8 years and I am thankful for all those I have shared my time at Christ's with. There are several members of staff at Cambridge I would like to personally thank; including Dr Winter and Dr Batley at Christ's, Professor Parker and Professor Gripaios at the Cavendish Laboratory, and Professor Allanach and Dr Coradeschi at the Department of Applied Mathematics and Theoretical Physics (DAMTP). In particular Professor Allanach, as my PhD supervisor, has offered innumerable hours of help and advice throughout my PhD, including being my collaborator for my first PhD paper, `SoftSusy`. Dr Coradeschi meanwhile has been my collaborator for the second project, `reSolve`, offering his theoretical expertise in this area to enable us to complete the project. I consequently have learnt a great deal of physics from them both and they have therefore been key to my PhD research, which I present in this thesis. There are also many others with whom I have discussed physics and my research, in particular the members of the Cambridge Supersymmetry Working

Group, to whom I therefore owe a debt of gratitude.

Finally, as well as my friends at Christ's College and elsewhere during my time in Cambridge, I wish also to express special thanks to my officemates Sebastian Cespedes, Felipe Contatto and Kai Roehrig; these have been a key part of my PhD experience and I have thoroughly enjoyed discussing physics and much more besides with them. Similarly, Matthew Lim and Benjamin Brunt at the physics department were colleagues and friends with whom I shared many enjoyable times at the Cavendish and elsewhere.

I should also thank STFC for funding me through the majority of my PhD, this has enabled me to focus on physics and therefore contributed significantly to this work, with DAMTP and the Cambridge Philosophical Society providing further funding. In addition I spent an enjoyable five months at the Kavli Institute for Theoretical Physics at UCSB in California as a Graduate Fellow during the final year of my PhD and I am grateful too for their support.

As for the necessities, this thesis was typeset using LaTeX, whilst the Feynman diagrams were produced using the web interface https://feynman.aivazis.com/ and the Tikz-Feynman [9] package.

Contents

Chapter 1

Introduction

Particle physics as a field has grown tremendously over the past century since its genesis as an experimentally testable and verifiable area of research, beginning with J.J. Thomson's discovery of the electron in Cambridge in 1897. Since then our understanding of the fundamental constituents of matter and the laws that govern them has progressed with undeniable fervour fuelled by human curiosity. It has been marked by many achievements; through Rutherford's probing of the atom, the development of quantum mechanics and quantum field theory, starting from the 1920s with the efforts of Dirac to quantise the electromagnetic field and leading to the postulation of antimatter. This was followed theoretically by the formulation of QED, renormalisation and other techniques in the 1950s by Schwinger, Feynman, Tomanaga and others; whilst experimentally the 1950s and 60s were marked by the somewhat confusing days of the "particle zoo" as new mesons and baryons were discovered at times on an almost weekly basis. This situation was clarified theoretically with the development of the quark model by Gell-Mann and others and the subsequent development of QCD through the 1970s by David Gross and Frank Wilczek. Meanwhile, electroweak theory was also being developed by Glashow, Salam and Weinberg, to be verified experimentally later in the 1980s by the UA1 and UA2 collaborations at CERN. The discovery of the top particle in 1995 at Fermilab [10, 11] and the key discovery of the Higgs boson at the Large Hadron Collider (LHC) in 2012 [12, 13] have since completed the contemporary picture of particle physics, described by a Standard Model based on $SU(3) \times SU(2) \times U(1)$ gauge symmetry and with fermions as fundamental matter particles and gauge bosons as force mediators. This involved the efforts of thousands of physicists - be they experimental or theoretical - including many making crucial contributions that have been skipped in this brief chronology.

1.1 Standard Model

This "Standard Model" of particle physics is itself ever-adapting, absorbing new concepts and changing to reflect new developments and knowledge, for example the addition of neutrino masses. It is described here in its current form, which is only slightly altered from its initial formulations. The Standard Model encompasses three fundamental interactions, and is governed by the fundamental gauge group $SU(3)_c \times SU(2)_L \times U(1)_Y$, with each gauge group having couplings g_s, g and g' respectively. This theory contains all of the fundamental matter particles currently known in addition to 4 types of gauge boson to mediate particle interactions, and 1

scalar. There are therefore 17 fundamental fields in the Standard Model - 12 matter particles split into 6 quarks and 6 leptons; 4 gauge bosons; which are the gluons, photon, W and Z bosons; and 1 scalar, the Higgs boson. These themselves are grouped into structures and bound by symmetries constraining their properties. The 12 matter particles split into quarks, which interact under the $SU(3)$ gauge group, and leptons, which do not, and for each of which there are 6 fermionic particles. These fermions are divided into 3 generations, demonstrating the same overall properties but having increasing masses: up and down, charm and strange, top and bottom; and electron and electron neutrino, muon and muon neutrino and tau and tau neutrino respectively for the quarks and leptons, with the precise reasons behind these generation copies unknown. These matter particles and the gauge bosons governing their interactions live in specific representations of the gauge groups which specify their behaviour and properties via their quantum numbers.

The quarks are triplets of the $SU(3)_c$ gauge group in the fundamental representation, they interact under the strong interaction of QCD via the gluons which are the 8 generators of $SU(3)_c$ and are correspondingly in the adjoint representation. The leptons, and indeed all other particles, meanwhile are singlets of $SU(3)_c$ and so feel no interactions under this gauge group. The $SU(2)_L$ gauge group is chiral, acting on the left-hand chiral components of $SU(2)_L$ doublets of the fermions, with each doublet containing one generation; $(u_L \quad d_L)^T$, $(c_L \quad s_L)^T$, $(t_L \quad b_L)^T$, $(\nu_{eL} \quad e_L)^T$, $(\nu_{\mu_L} \quad \mu_L)^T$, $(\nu_{\tau L} \quad \tau_L)^T$, whilst the right-hand components of these fields are singlets under $SU(2)_L$ due to its chiral nature u_R, d_R, c_R, s_R, t_R, b_R, e_R, μ_R, τ_R[1]. The $SU(3)_c$ and $SU(2)_L$ groups commute so the QCD interactions do not change flavour, whilst the $SU(2)_L$ interactions do not change colour. Just as for the QCD interactions, the gauge bosons of $SU(2)_L$ are in the adjoint and so there are 3 generator gauge bosons of the $SU(2)_L$ group, denoted W_1^μ, W_2^μ, W_3^μ. As for the final $U(1)_Y$ group, it also treats left-hand and right-hand fields differently. All of the Standard Model fields carry hypercharge (Y), defined by $Y = Q - T_L^3$, where Q is the electromagnetic charge and I_W^3 is the third component of weak isospin (eigenvalue of the third $SU(2)_L$ generator), this $U(1)_Y$ group comes with the gauge boson B. All the matter particles also are accompanied by antiparticle partners of the same mass but opposite charges. The field content of the Standard Model, and the fields' quantum numbers under the three fundamental Standard Model gauge groups, are given in Table 1.1.

1.1.1 Standard Model Lagrangian

The interactions of the various matter and force particles are described by the Standard Model Lagrangian, which can be broken up in several different ways; here it is broken into gauge, fermion, Higgs and Yukawa pieces:

$$\mathcal{L}_{\text{SM}} = \mathcal{L}_{\text{gauge}} + \mathcal{L}_{\text{f}} + \mathcal{L}_{\phi} + \mathcal{L}_{\text{Yukawa}}. \tag{1.1}$$

[1]It should be noted that there may also be right-handed neutrinos $\nu_{e\,R}$, $\nu_{\mu\,R}$, $\nu_{\tau\,R}$ in extensions to the Standard Model, for example to generate neutrino masses.

Field name	Symbol	Representation
Left-handed quarks	q_L	(3, 2, $\frac{1}{6}$)
Left-handed leptons	l_L	(1, 2, -$\frac{1}{2}$)
Right-handed up quark	u_R	(3, 1, $\frac{2}{3}$)
Right-handed down quark	d_R	(3, 1, -$\frac{1}{3}$)
Right-handed electron	e_R	(1, 1, -1)
Gluons	G	(8, 1, 0)
Weak Isospin Gauge Bosons	W_i	(1, 3, 0)
Weak Hypercharge Gauge Boson	B	(1, 1, 0)
Higgs	H	(1, 2, $\frac{1}{2}$)

Table 1.1: The Standard Model field content and their quantum numbers under the Standard Model gauge group $SU(3)_c \times SU(2)_L \times U(1)_Y$, the quark and lepton left and right-handed parts are repeated for each of the three generations.

First, consider the gauge part:

$$\mathcal{L}_{\text{gauge}} = -\frac{1}{4}G^i_{\mu\nu}G^{\mu\nu i} - \frac{1}{4}W^l_{\mu\nu}W^{\mu\nu l} - \frac{1}{4}B_{\mu\nu}B^{\mu\nu}, \tag{1.2}$$

this contains the kinetic and self-interaction terms of the $SU(3)_c$, $SU(2)_L$ and $U(1)_Y$ gauge bosons. Here $i, j, k = 1, \ldots, 8$ and $l, m, n = 1, \ldots, 3$; the $U(1)_Y$ gauge boson B_μ has no self-interactions and so no structure constants f_{ijk} appear, in contrast the $SU(2)_L$ and $SU(3)_c$ groups are non-Abelian and so have non-zero commutators of their gauge generators which are described by their structure constants ϵ_{lmn} and f_{ijk} respectively[2]:

$$G^i_{\mu\nu} = \partial_\mu G^i_\nu - \partial_\nu G^i_\mu - g_s f_{ijk} G^j_\mu G^k_\nu, \tag{1.3}$$

$$W^l_{\mu\nu} = \partial_\mu W^l_\nu - \partial_\nu W^l_\mu - g\epsilon_{lmn} W^m_\mu W^n_\nu, \tag{1.4}$$

$$B_{\mu\nu} = \partial_\mu B_\nu - \partial_\nu B_\mu, \tag{1.5}$$

where for example the structure constants of QCD are given in terms of the Gell-Mann matrices, which are the generators of $SU(3)_c$, by:

$$[\frac{\lambda_a}{2}, \frac{\lambda_b}{2}] = i f_{abc} \frac{\lambda_c}{2} \tag{1.6}$$

The fermionic part of the Standard Model Lagrangian, $\mathcal{L}_f$ consists of covariant derivatives of the fields, encompassing kinetic terms and the fermion interactions with the gauge bosons of $SU(3)_c$, $SU(2)_L$ and $U(1)_Y$:

$$\mathcal{L}_f = \sum_{n=1}^{3} (\bar{q}_{nL} i \not{D} q_{nL} + \bar{l}_{nL} i \not{D} l_{nL} + \bar{u}_{nR} i \not{D} u_{nR} + \bar{d}_{nR} i \not{D} d_{nR} + \bar{e}_{nR} i \not{D} e_{nR}), \tag{1.7}$$

here $n = 1, 2, 3$ is the generation index, whilst colour indices have been suppressed. Each of

[2]The possibility of θ_{QCD} terms and similar have been neglected here.

the covariant derivatives contains appropriate interactions for that particle type, based on the particle quantum numbers as listed in Table 1.1; the term for the left-handed quark fields is:

$$\bar{q}_{nL} i \not{D} q_{nL} = i \sum_{\alpha,\beta=1}^{3} (\bar{u}^{\alpha}_{nL} \quad \bar{d}^{\alpha}_{nL}) \gamma^{\mu} \Big[D_{\mu} \delta_{\alpha\beta} + \frac{i g_s}{2} \vec{\lambda}_{\alpha\beta} . \vec{G}_{\mu} I_2 \Big] (u^{\beta}_{nL} \quad d^{\beta}_{nL})^T. \tag{1.8}$$

The α, β are colour indices, $\vec{\lambda}_{\alpha\beta}$ is a vector of the 8 Gell-Mann matrices[3] (the generators of $SU(3)_c$) and $\vec{G}_{\mu}$ a corresponding vector of the 8 gluon gauge fields. Of course, the $SU(3)_c$ part only acts for the quark q_{nL}, u_{nR}, d_{nR} fields. The covariant derivative here is that for the $SU(2)_L \times U(1)_Y$ gauge bosons:

$$D_{\mu} X_{nh} = \Big(\partial_{\mu} + \frac{ig}{2} \delta_{hL} \vec{\sigma} . \vec{W}_{\mu} + i g' Y_X B_{\mu} \Big) X_{nh}. \tag{1.9}$$

X is one of the fields, n is again a generation index, $h = L, R$ is the handedness so δ_{hL} turns off the $SU(2)_L$ interaction for the right-handed fields, $\vec{\sigma}$ is a vector of the Pauli matrices (which are the generators of $SU(2)_L$), $\sigma_1 = \begin{pmatrix} 0 & 1 \\ 1 & 0 \end{pmatrix}$, $\sigma_2 = \begin{pmatrix} 0 & -i \\ i & 0 \end{pmatrix}$ and $\sigma_3 = \begin{pmatrix} 1 & 0 \\ 0 & -1 \end{pmatrix}$, $\vec{W}_{\mu} = (W^1_{\mu}, W^2_{\mu}, W^3_{\mu})$ and Y_X is the hypercharge of the given field.

The Higgs part of the Standard Model Lagrangian is

$$\mathcal{L}_{\phi} = (D^{\mu}\phi)^{\dagger} D_{\mu} \phi - V(\phi). \tag{1.10}$$

This contains the covariant derivatives of the Higgs:

$$D_{\mu} \phi = \Big(\partial_{\mu} + \frac{ig}{2} \vec{\sigma} . \vec{W}_{\mu} + \frac{ig'}{2} B_{\mu} \Big) \phi, \tag{1.11}$$

ϕ is an $SU(2)_L$ doublet $\phi^T = (\phi^+ \quad \phi^0)$. The covariant derivatives themselves involve the kinetic terms and the $SU(2)_L \times U(1)_Y$ interactions of gauge bosons with the Higgs, as they must to break these in electroweak symmetry breaking (EWSB) and give the gauge bosons masses. This EWSB occurs as a result of the Higgs potential $V(\phi) = -\mu^2 \phi^{\dagger}\phi + \lambda(\phi^{\dagger}\phi)^2$ acquiring a vacuum expectation value (VEV) different from 0, due to its "Mexican-Hat" shape, which occurs for $\mu^2 > 0$. For such a potential the minimum occurs at:

$$\sqrt{\phi^{\dagger}\phi} = \sqrt{\frac{\mu^2}{2\lambda}} \equiv \frac{v}{\sqrt{2}}, \tag{1.12}$$

here v is the non-zero VEV of the Higgs potential. The Higgs field in the potential minimum at its VEV may then replace the Higgs field in the covariant derivative terms of the Higgs Lagrangian; indeed by taking the unitary gauge we remove the Goldstone modes which are "eaten" and allow the explicit development of the $W^{\pm}$ and Z gauge boson masses to be observed. In this gauge

[3] Rather than the Gell-Mann matrices λ_a, in QCD the t_a matrices are often used, here the factor of $\frac{1}{2}$ is absorbed into the matrices so $t_a = \frac{\lambda_a}{2}$.

make the replacement $\phi \to \frac{1}{\sqrt{2}}(0 \quad v+h)^T$ so that h represents excitations about the VEV (i.e. the physical Higgs boson) and expand the covariant derivative squared term:

$$\begin{aligned} D_\mu\phi &= \left(\partial_\mu + \frac{ig}{2}\begin{pmatrix} gW_3^\mu & \sqrt{2}W_\mu^+ \\ \sqrt{2}W_\mu^- & -W_3^\mu \end{pmatrix} + \frac{ig'}{2}B_\mu\right) I_2 \begin{pmatrix} 0 \\ v+h \end{pmatrix} \\ &= \begin{pmatrix} 0 + \frac{i}{2\sqrt{2}}\sqrt{2}W_\mu^+(v+h)g \\ \partial_\mu(v+h) + \frac{i}{2\sqrt{2}}(-gW_\mu^3 + g'B_\mu)(v+h) \end{pmatrix}. \end{aligned} \tag{1.13}$$

Here we have identified the charged W bosons as linear combinations of the W_μ^1 and W_μ^2, $W_\mu^\pm = \frac{1}{\sqrt{2}}(W_\mu^1 \mp iW_\mu^2)$. The overall covariant derivative term, which is hiding the gauge boson masses and gauge boson - Higgs interactions, may therefore be expanded as:

$$\begin{aligned} (D^\mu\phi)^\dagger D_\mu\phi =& \partial^\mu(v+h)^\dagger\partial_\mu(v+h) - \frac{i}{2\sqrt{2}}\Big[(v+h)^\dagger(-gW_3^\mu + g'B^\mu)\partial_\mu(v+h) \\ &- \partial^\mu(v+h)^\dagger(-gW_\mu^3 + g'B_\mu)\times(v+h)\Big] + \frac{1}{8}\Big(2W^{\mu+}W_\mu^- g^2 \\ &+ (-gW_3^\mu + g'B^\mu)(-gW_\mu^3 + g'B_\mu)\Big)(v+h)^\dagger(v+h). \end{aligned} \tag{1.14}$$

Analysing this expression reveals that we now have gauge boson mass and interaction terms for the $W_\mu^\pm$, but also more subtly for linear combinations of the remaining W_3^μ and B^μ gauge bosons. Specifically, we obtain mass and interaction terms for new gauge bosons which are rotations of the W_3^μ and B^μ gauge bosons through some angle, called the weak mixing angle (or "Weinberg" angle) - these are the physical Z boson and photon we observe in nature:

$$\begin{pmatrix} W_\mu^3 & B_\mu \end{pmatrix} = \begin{pmatrix} \cos\theta_W & \sin\theta_W \\ -\sin\theta_W & \cos\theta_W \end{pmatrix} \begin{pmatrix} Z_\mu & A_\mu \end{pmatrix}. \tag{1.15}$$

With this we can rearrange the $(D^\mu\phi)^\dagger D_\mu\phi$ term to look for mass terms $m_W^2 W^{\mu+}W_\mu^-$ and $\frac{1}{2}m_Z^2 Z^\mu Z_\mu$ for the W and Z bosons respectively[4], as well as their interaction terms. However, first it can be noted that the only linear combination of the W_3^μ and B^μ which appears is $-gW_3^\mu + g'B^\mu = -g(\cos\theta_W Z^\mu + \sin\theta_W A^\mu) + g'(-\sin\theta_W Z^\mu + \cos\theta_W A^\mu) = -Z^\mu\sqrt{g^2+g'^2} + 0A^\mu$. This arises as the Weinberg mixing angle is related to the gauge couplings for the $SU(2)_L$ and $U(1)_Y$ groups, these are set by identifying the charges under QED with the relevant Lagrangian terms. The result is no mass term for the photon, and correspondingly no Higgs-photon couplings, at tree-level. We have therefore managed to break $SU(2)_L \times U(1)_Y \to U(1)_{\text{em}}$ and give the W and Z bosons mass whilst leaving the photon massless:

$$(D^\mu\phi)^\dagger D_\mu\phi = \partial^\mu h^\dagger\partial_\mu h + \Big(\frac{gv}{2}\Big)^2\left[1 + \frac{2h}{v} + \frac{h^2}{v^2}\right]W^{\mu+}W_{\mu-} + \frac{1}{2}(g^2+g'^2)\frac{v^2}{2}\left[1 + \frac{2h}{v} + \frac{h^2}{v^2}\right]Z^\mu Z_\mu + 0A^\mu A_\mu. \tag{1.16}$$

The mass terms are $m_W = \frac{gv}{2}$, $m_Z = \frac{v}{2}\sqrt{g^2+g'^2} = \frac{m_W}{\cos\theta_W}$ and $m_A = 0$, giving a prediction for the ratio of the W and Z masses on the basis of the chosen representations of the fields and

[4]The different normalisations arise as the $W^\pm$ is a complex field whilst the Z is a real field.

the fact that charges must match observation upon EWSB, this prediction is experimentally verified. There are also 3- and 4-point vertices of the Higgs with gauge bosons here, but again (as it is massless) no direct Higgs-photon coupling.

We can verify that in this process we have conserved the number of degrees of freedom as a complex Higgs doublet with 4 degrees of freedom has become a real scalar and masses for the W^+, W^- and Z. Furthermore we can view this process of electroweak symmetry breaking in the context of Goldstone's theorem, which states that for each spontaneously broken generator a Goldstone boson is generated. In our case we break three generators in breaking $SU(2)_L \times U(1)_Y$ down to $U(1)_{\text{em}}$. These three massless Goldstone modes are then eaten by the previously-massless gauge bosons $W^\pm$ and Z; the Goldstone modes become the longitudinal degrees of freedom of the gauge bosons which thereby acquire a mass. The Higgs boson then corresponds to the remaining unbroken generator.

The same replacement of the Higgs doublet via its VEV must be made in the Higgs potential in order to extract the Higgs mass and 3- and 4-point self-interaction terms

$$V(\phi) = -\mu^2\phi^\dagger\phi + \lambda(\phi^\dagger\phi)^2 = -\frac{\mu^2}{2}(v+h)^2 + \frac{\lambda}{4}(v+h)^4 = -\frac{1}{4}v^2\lambda + \lambda v^2 h^2 + \lambda v h^3 + \frac{\lambda}{4}h^4, \tag{1.17}$$

this reveals that $m_h^2 = 2\lambda v^2$. Given that the Higgs VEV v is known through our knowledge of the gauge couplings by equating the expressions for the W and Z boson masses in electroweak symmetry breaking with experimental measurements, this means that once the mass of the Higgs boson (125 GeV [12, 13]) is measured the self-coupling is theoretically known, although is yet to be measured experimentally.

Finally, whilst the Higgs mechanism has given mass to the gauge bosons, there are still no fermion masses at this stage in the discussion as a result of electroweak gauge symmetry. The masses are instead generated in the spontaneous breaking of electroweak symmetry via Higgs - fermion couplings, these couplings are the "Yukawa" couplings which are matrices linking left-handed and right-handed fermion fields as follows[5,6]:

$$\mathcal{L}_{\text{Yukawa}} = -\sum_{n=1}^{3}[-y^u\bar{q}_{nL}H^c u_R - y^d\bar{q}_{nL}Hd_R - y^e\bar{l}_{nL}He_R + \text{h.c.}], \tag{1.18}$$

here $H^c = i\sigma_2 H^*$ so it has hypercharge $-\frac{1}{2}$ as required to conserve hypercharge in the up quark Yukawa term. These interaction terms generate fermion masses in EWSB as the Higgs field is replaced by its VEV, and they generate Higgs-fermion couplings proportional to these Yukawas and so also to the fermion masses:

$$m_f = \frac{y_f v}{\sqrt{2}}. \tag{1.19}$$

[5] The Yukawa matrices therefore have generation indices so that the first term in the Yukawa Lagrangian is $-(y^u)_{ij}\bar{q}_{nLi}H^c u_{Rj}$.

[6] "h.c." indicates here the hermitian conjugate of the terms included must also be added.

1.1.2 Perturbation Theory

Following this introduction detailing the Standard Model Lagrangian, we can now use the interactions between the particles it encompasses to build up Feynman diagrams for processes of interest. These Feynman diagrams are then converted into matrix elements for each process which are in turn squared, summed over final states and averaged over initial states, before being integrated over the relevant 4-momenta state space ("phase space") to obtain expressions for cross-sections, decays and transition rates. However, as well as "tree-level diagrams" at leading order, incorporating the minimum number of intermediates and vertices possible, we can build up an infinite series of diagrams "beyond Leading order" (beyond LO) for each process by adding loops or vertices with additional particles. These processes are suppressed by the necessary additional couplings at the vertices, therefore we are able to build up a perturbative series in the relevant coupling to describe the overall total transition rate, this is given in Figure 1.1.

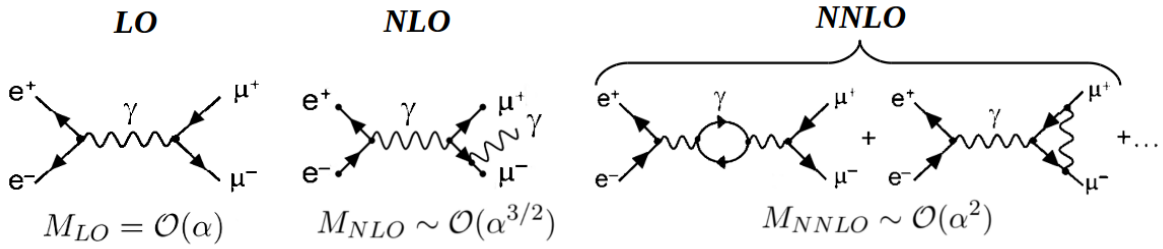

Figure 1.1: The Leading Order (LO), Next-to-Leading order (NLO) and Next-to-Next-to-Leading order (NNLO) QED contributions to the matrix element for electron positron annihilation into a muon and antimuon. In the NLO case the emission of the photon can occur off any initial of final state leg; while in the NNLO case there are further diagrams which have not been included here. Each additional contribution in the series has a higher power of the gauge coupling.

Any loops added have momenta which, unlike in the tree-level processes, are undetermined and so add additional integrals to be performed in the phase space.

In fact, the couplings themselves are attached to sub-diagrams representing their vertices and so they can also be loop-corrected, they therefore build up energy dependence as they "run" to different values as the energy scale is changed, this is described further in Chapter 1.1.4.

1.1.3 Divergences

Thus far our picture of the Standard Model has been a little naive; whilst we have established a Lagrangian giving the required masses and couplings of the observed particles and introduced perturbation theory, we have not given it foundations in quantum field theory. In fact the picture we have given is, on closer inspection, plagued by divergences at both low (infrared - IR) and high (ultraviolet - UV) energies. If one attempts to determine the Feynman rules along with amplitudes for various processes, several features immediately become apparent, aspects which greatly troubled our predecessors in particle physics. First of all, it quickly becomes clear that

loop contributions to amplitudes offer corrections to the "bare" masses and coupling constants found in the Standard Model Lagrangian and that the associated loop integrals are divergent. At first sight this causes the theory to lose all predictivity as any calculations are swamped by infinite contributions. These UV divergences appear due to arbitrarily high allowed loop momentum and are generically of the form:

$$\int d^4k \frac{k^2}{k^4} \sim \int kdk \to \infty, \text{ as k} \to \infty. \tag{1.20}$$

An example of such a divergence is given in the next section in the context of the photon propagator and the running electromagnetic coupling, whilst a quadratic UV divergence is derived for contributions to the Higgs mass in Chapter 1.2. However, this is not all - more subtle divergences also appear at low energies, typically due to propagators of massless particles. These are a key part of our work in Chapters 5-7. Such IR divergences, in contrast, arise at low momenta $k \to 0$ from integrals generically of the form below, with logarithmic divergences being produced:

$$\int \frac{d^4k}{k^4} \sim \int \frac{dk}{k} \to \infty, \text{ as k} \to 0. \tag{1.21}$$

1.1.4 Renormalisation

In order to remove the UV divergences appearing from loop corrections, we may "renormalise" the bare parameters in the theory, which have infinite corrections, to physical finite parameters by cancelling infinite contributions against one another. As an example consider Figure 1.2(a), for any photon propagator one can add loop corrections of this form (known as vacuum polarisation diagrams). The issue arises as the loop momentum is not fixed by the external momenta - rather any loop momentum on one side of the loop can be balanced by one on the other side, therefore the loop contributions contain integrals over an infinite range of loop momenta. Such problems were a great source of consideration for theoretical particle physicists through the 1930s and 1940s until the work of Kramers, Bethe, Schwinger, Feynman, Tomonaga and Dyson.

Schematically, considering for example these photon propagator corrections in the case of electron scattering in Figure 1.2(b) and (c), in order to determine the full amplitude an infinite tower of insertions of loop corrections of the form of the photon vacuum polarisation must be summed. Each of the loops included on the photon propagator provides a divergent loop integral correction of the form

$$-1(-ie_0)^2 \int_0^\Lambda \frac{d^4k}{(2\pi)^4} \gamma^\mu \frac{i}{(\not{k}+\not{q})-m} \gamma^\nu \frac{i}{\not{k}-m} \equiv i\Pi_2^{\mu\nu}(q). \tag{1.22}$$

Here e_0 is the bare, unrenormalised electron charge, as appearing in the Standard Model Lagrangian, k is the four-momentum scale of the loop and q is the 4-momentum transfer of the photon mediating the scattering, whilst Λ is some UV cut-off. The bare photon progagator can

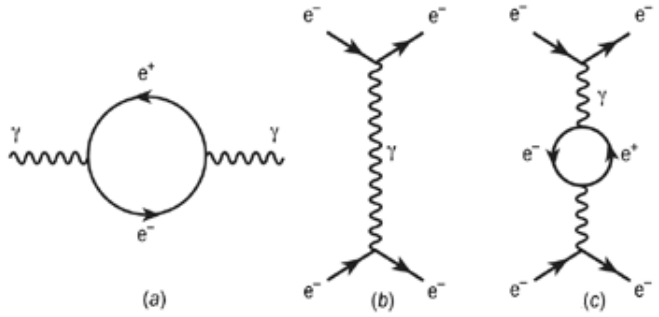

Figure 1.2: (a) Vacuum polarisation contribution to the photon propagator, it offers an infinite correction to any diagrams containing photons, ostensibly creating a problem for the predictivity of QED. (b) The tree-level diagram for electron-electron scattering in QED. (c) The vacuum polarisation 1-loop correction to electron-electron scattering. The vacuum polarisation can be inserted an arbitrary number of times, creating an infinite sum of corrections to the amplitude, each of which diverges.

be denoted $P_0 = \frac{e_0^2}{q^2}$, the effective photon propagator accounting for all possible vacuum polarisation insertions may then be written as a geometric series which can be summed to infinity. Skipping over details of the tensor structure and contractions for brevity and simplicity here, it can be shown each insertion adds a factor of $e_0^2\Pi(q^2)$ where $\Pi(q^2)$ is related to $\Pi_2^{\mu\nu}(q)$, but with the tensor structure accounted for. As a result the series is:

$$P_0 + P_0 e_0^2 \Pi(q^2) + P_0 e_0^2 \Pi(q^2) e_0^2 \Pi(q^2) + \cdots = P_0[1 + \sum_{j=1}^{\infty} (e_0^2 \Pi(q^2))^j] = \frac{e_0^2}{q^2} \frac{1}{1 - e_0^2 \Pi(q^2)} \equiv \frac{e^2(q^2)}{q^2}. \tag{1.23}$$

Therefore the effect of the loop contributions is to modify the Standard Model Lagrangian bare charge e_0 into a momentum-scale dependent charge $e(q^2)$. We can rewrite the bare charge in terms of this effective charge and the one-loop self-energy (or vacuum polarisation) $\Pi(q^2)$ in order to extract how this new momentum-dependent effective charge varies with energy scale.

$$e^2(q^2) = \frac{e^2(\mu^2)}{1 - e^2(\mu^2)[\Pi(q^2) - \Pi(\mu^2)]}. \tag{1.24}$$

Given that experimentally we can measure $e(q^2)$ and see that it is finite, this means that the renormalisation cancels two separately divergent quantities $\Pi(q^2)$ and $\Pi(\mu^2)$ against each other to leave a finite quantity. This difference can be calculated in quantum field theory and results in a logarithmic running of the fine structure constant with momentum, more details on these calculations can be found in [14]. The minus sign in the denominator meaning the QED interaction becomes stronger at higher energies (shorter distances) - for example whilst $\alpha(q^2 \approx 0) = 1/137$, at the LHC the relevant interaction strength is $\alpha(q^2 = m_Z^2) = 1/127$.

$$\alpha(q^2) = \frac{\alpha(\mu^2)}{1 - \alpha(\mu^2) \frac{1}{3\pi} \ln\left(\frac{q^2}{\mu^2}\right)}. \tag{1.25}$$

If we expand this to form a perturbative series in α we see each term contains a logarithm of the ratio of scales to the power of the order of that term in α:

$$\alpha(q^2) = \alpha(\mu^2)\left[1 + \frac{\alpha(\mu^2)}{3\pi}\ln\left(\frac{q^2}{\mu^2}\right) + \left(\frac{\alpha(\mu^2)}{3\pi}\ln\left(\frac{q^2}{\mu^2}\right)\right)^2 + \dots\right]. \tag{1.26}$$

Therefore the renormalisation group running of the fine structure constant $\alpha(q^2)$ absorbs an infinite series of logarithms of the ratio of scales, it thereby "resums" potentially large logarithmic terms $\frac{\alpha(\mu^2)}{3\pi}\ln\left(\frac{q^2}{\mu^2}\right)$, which will be large when $\alpha^{-1} \sim \frac{1}{3\pi}\ln\left(\frac{q^2}{\mu^2}\right)$.

There is an alternative manner by which to derive the running of the coupling $\alpha(q^2)$ however; rather than considering loop corrections to the Feynman diagram for the relevant vertex, we may instead consider that we expect any observable to be formally independent of the scale it is evaluated at when calculated to all orders, this must be true as the scales are purely arbitrary choices made in our calculations. For an arbitrary observable $\mathcal{A}$ at each order of its evaluation it will depend on α and the ratio of scales considered Q^2/μ^2, we then expect the sum of all orders to be independent of the scale and so

$$\mu^2\frac{d}{d\mu^2}\mathcal{A}\Big(\alpha, \frac{Q^2}{\mu^2}\Big) = \left[\mu^2\frac{\partial}{\partial\mu^2} + \mu^2\frac{\partial\alpha}{\partial\mu^2}\frac{\partial}{\partial\alpha}\right]\mathcal{A} = 0. \tag{1.27}$$

We may introduce the logarithm of the ratio of scales and a β function, incorporating the dependence of the gauge coupling on the energy scale:

$$t \equiv \ln\Big(\frac{Q^2}{\mu^2}\Big), \qquad \beta(\alpha) \equiv \mu^2\frac{\partial\alpha}{\partial\mu^2} \equiv \frac{\partial\alpha}{\partial\ln\mu^2}. \tag{1.28}$$

So we have

$$\left[-\frac{\partial}{\partial t} + \beta(\alpha)\frac{\partial}{\partial\alpha}\right]\mathcal{A} = 0, \tag{1.29}$$

solving this differential equation for any observable $\mathcal{A}\Big(\alpha, \frac{Q^2}{\mu^2}\Big)$ requires:

$$t = \int_{\alpha(\mu^2)}^{\alpha(Q^2)}\frac{dx}{\beta(x)}. \tag{1.30}$$

We may then differentiate equation 1.30 with respect to t to obtain

$$\beta(\alpha(Q^2)) = \frac{\partial\alpha(Q^2)}{\partial t}. \tag{1.31}$$

The β function may then be expanded as a function of α (corresponding to 1-loop, 2-loop, etc considerations in our previous method) as

$$\beta(\alpha) = -\alpha\sum_{n=0}^{\infty}\beta_n\Big(\frac{\alpha}{4\pi}\Big)^{n+1}. \tag{1.32}$$

Taking the first order correction only we have from equation 1.31 that:

$$Q^2\frac{\partial\alpha(Q^2)}{\partial Q^2} = -\alpha^2\Big(\frac{\beta_0}{4\pi}\Big), \tag{1.33}$$

integrating both sides we obtain an expression for the running of $\alpha(Q^2)$ at 1-loop order:

$$\alpha(Q^2) = \frac{\alpha(\mu^2)}{1 + \frac{\beta_0}{4\pi}\alpha(\mu^2)t} = \frac{\alpha(\mu^2)}{1 + \frac{\beta_0}{4\pi}\alpha(\mu^2)\ln\left(\frac{Q^2}{\mu^2}\right)}. \tag{1.34}$$

This is of the same form as obtained considering the 1-loop corrections directly in equation 1.25, all that remains is the determination of $\beta_0 = -\frac{4}{3}$, which may be calculated from Feynman diagrammatic calculations as before.

The dependences of the gauge couplings on energy are therefore encoded in their respective β functions, which may be calculated up to a given order accuracy. Similar calculations can be performed for the electron propagator, with self-energy diagrams via loops of photons now causing the electron mass to run with energy scale. Meanwhile in QCD, although the situation is complicated by the fact it is a non-Abelian theory (i.e. its structure constants are non-zero) and consequently there are additional loop corrections from gluon self-interactions on top of those from fermion loops, analogous calculations (via either method) follow through for the running of the coupling α_s. As a result of the additional loop corrections, in QCD the difference of the self-energy contributions is altered relative to QED, resulting in a plus sign in the denominator of the running expression. This sign flip has remarkable consequences for its phenomenology; it causes α_s to run to smaller values at higher energies ("asymptotic freedom"), or equally to run to large values at large distances (low energies), indicating confinement of quarks and gluons. For example, $\alpha_s(\Lambda_{QCD} \approx 250\,\text{MeV}) \sim 1$, $\alpha_s(1\,\text{GeV}) \approx 0.5$ and $\alpha_s(m_Z) \approx 0.1184$.

This renormalisation procedure, removing infinities in physical observed quantities, has some ambiguities - there are also renormalisation schemes, different methods for exactly how to remove the infinities in renormalisation of the masses and couplings, which result in differences in the values of the couplings and masses even when renormalised at the same order. The differences in such schemes largely come down to different choices of factors to absorb in the renormalisation in the so-called "counter-terms" to cancel the divergences, and to different choices of UV regulation (i.e. using a cut-off as above or an alternative method to deal with the UV divergent integrals). The most common examples are the "Minimal Subtraction" MS and "Modified Minimal Subtraction" $\overline{MS}$ schemes, whilst supersymmetry (SUSY) uses the "Dimensional Reduction" DR and $\overline{DR}$ schemes, this will be mentioned briefly in Chapter 2 but more information on renormalisation schemes may be found in [14]. The conversions between masses and coupling parameters evaluated in different schemes can be determined at given loop order. Meanwhile, the subtraction of the divergence at a given scale μ in the first method introduces an arbitrary scale into the calculation - termed the "renormalisation scale". As seen in the second method, we require that observables are formally independent of this scale when evaluated to all orders; however, any quantity in reality is evaluated as a perturbative expansion, truncated at given order, and therefore scale dependence remains in theoretical quantities. As a result of these scheme differences and scale dependences theoretical predictions to the same order often produce different numerical values. Such differences of parameters evaluated in different schemes

and with different scales simply correspond to higher-order effects, nonetheless they can have significant consequences for theoretical predictions at a given order. Many texts cover this in far more detail, for example refer to the books [14, 15] for more information.

As well as divergences in the UV (high-energy scale) for the Standard Model, divergences may also arise in the IR (low-energy scale) as a result of poles in the propagators, these divergences can too be absorbed into running of parameters, and indeed IR divergences in initial states can be absorbed into PDFs at some factorisation scale in an analogous manner. This will be described in more detail in Chapter 5 for our work in QCD.

1.1.5 QCD

Finally, whilst we have introduced Quantum Chromodynamics as an $SU(3)$ gauge theory with gauge quantum number "colour" as part of the Standard Model Lagrangian, we focused much of our attention on the electroweak sector and the Higgs, as this is of relevance to our work in Chapters 2-4. QCD however is a theory of rich complexity and is a key component of our research in Chapters 5-7, we therefore wish to highlight a few salient features here.

QCD is a sector of the Standard Model of particular intricacy and of rich and varied phenomenology, and, given the premier contemporary collider is a hadron-hadron collider, it is an area of great relevance to ongoing particle physics theory, phenomenology and experiments. First of all, in QCD the gauge coupling α_s offers distinct behaviour to the electroweak gauge couplings, α_s is larger than α at collider energies so QCD processes necessitate many more orders of corrections be calculated in our perturbative series for theoretical predictions. Furthermore, the value of the α_s coupling increases at lower energies causing non-perturbative effects at low energies such as hadronisation, whilst thankfully reducing at collider energies ("asymptotic freedom") and thereby allowing perturbative calculations to be performed for theoretical predictions at colliders in a similar way to in QED. These large α_s values at low energies lead to confinement and the "colour confinement hypothesis" that all long-lived particles are colour singlets, with quarks and gluons both coloured and permanently dressed in QCD radiation causing hadronisation at long distances. As a result, at hadron colliders we must separate the long distance non-perturbative behaviour from the short distance hard scattering, this leads to "QCD factorisation theorems" (see Chapter 5.5), the parton model of QCD and its QCD improvements allowing parton splittings. In order to describe the fact that we collide composite objects we incorporate such intricate non-perturbative effects into parton distribution functions (PDFs) which give the probability of obtaining a given particle (aka "parton") of given momentum fraction from the overall composite hadron being collided. The large value of α_s at low scales also ensures the probability of additional emissions becomes very large as the energy is reduced, ensuring "soft" (i.e. low energy) emissions can dominate processes and phenomenology and causing divergences which must be treated (such as absorbing them into PDFs) and subsequently the resummation that is the subject of our research in this area. This leads to splitting and fragmentation behaviour of partons, which we will not touch upon in great detail, but is further complicated

by the non-Abelian nature of QCD allowing gluon-gluon interactions. This whistle-stop tour of QCD is simply to give a flavour of some of the effects and its importance, much greater detail is given later, focusing on areas of specific interest for our applications (Chapters 5-7). For a full exposition there are a great many textbooks ranging from pedagogical introductions [16] to more detailed descriptions [17, 18] and many in between [19].

1.2 Problems with the Standard Model

This completes a brief review of the mathematical formulation of the Standard Model, summarising only its features salient to our work in this thesis. It is a theory which contains 30 elementary particles (counting antiparticles as well as particles) and 26 parameters - 9 fermion masses, 3 quark mixing angles, 1 (Charge Parity (CP)-violating) phase, 3 gauge couplings, 1 further angle (QCD vacuum angle), 1 Higgs mass and one Higgs vacuum expectation value, 3 neutrino masses[7] and 4 neutrino mixing matrix (PMNS matrix) parameters. Its development and experimental verification have been the subjects of extensive efforts throughout the past century and it has proved remarkably successful, both in extending our theoretical knowledge of fundamental particle physics and in describing experimental results at colliders and elsewhere, often up to unprecedented accuracy via loop calculations. Nonetheless, despite its obvious success, the Standard Model is known to be incomplete, having several theoretical and experimental problems and absences. A brief summary of several of the key issues is presented here; again targeted on those most relevant to our work, nonetheless more comprehensive reviews can be found in [20–22].

1. **Technical Hierarchy Problem** - As demonstrated in the discussion of renormalisation and running of parameters within the Standard Model, loop corrections can offer interesting problems for the Standard Model as a quantum field theory. In an exactly analogous manner to the computations of loop corrections to fermion masses and gauge couplings in the context of running, loop corrections to the Higgs mass must also be considered in order to determine their effect upon its mass. The Higgs boson couples to all particles with mass, therefore there are corrections from scalar loops, fermion loops and vector boson loops as demonstrated in Figure 1.3.

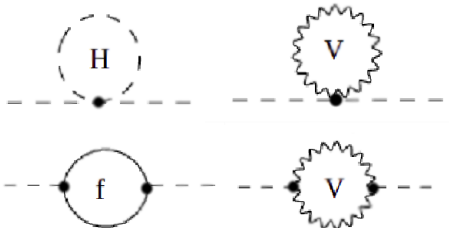

Figure 1.3: 1-loop corrections to the Higgs mass arising in the Standard Model; starting from the top left and proceeding anticlockwise there are corrections from scalars (i.e. the Higgs itself) due to the Higgs self-interaction, fermions due to the Higgs Yukawa couplings, and Vector bosons due to the 3- and 4-point interactions resulting from Electroweak Symmetry Breaking (EWSB).

[7] In fact, as only the mass squared differences of the 3 neutrinos are known, the lightest may be massless, reducing the number of parameters by 1.

The Higgs however couples to particles in proportion to their masses, therefore the dominant correction to the Higgs mass comes from a top-antitop fermion loop. Using the Standard Model Feynman rules this 1-loop Higgs mass correction can be written down and evaluated, here the correction is ultimately determined at zero Higgs momentum ($q = 0$) for simplicity, we introduce a UV cut-off to demonstrate that the divergence naturally pushes the Higgs mass to the largest scale in the theory:

$$\begin{aligned}(\delta^{(t)}_{m_h})^2 =& -\frac{|y_t|^2}{2}\int^{\Lambda}\frac{d^4k}{(2\pi)^4}Tr\Big[\frac{\not{k}+\not{q}+m_t}{(k+q)^2-m_t^2}\frac{\not{k}+m_t}{k^2-m_t^2}\Big] \\ &\sim -2|y_t|^2\int^{\Lambda}\frac{d^4k}{(2\pi)^4}\Big[\frac{1}{(k^2-m_t^2)}+\frac{2m_t^2}{(k^2-m_t^2)^2}\Big] \\ &\sim -2|y_t|^2\int^{\Lambda}\frac{2\pi^2k^3dk}{(2\pi)^4}\frac{1}{(k^2-m_t^2)} \sim -2|y_t|^2\int^{\Lambda}\frac{kdk}{8\pi^2} \sim -\frac{|y_t|^2}{8\pi^2}\Lambda^2. \end{aligned} \tag{1.35}$$

Therefore the Higgs boson mass-squared receives corrections at 1-loop which are quadratic in the UV cut-off of the Standard Model and this indicates that the Higgs mass has a very sensitive dependence upon higher scale physics. This implies that either new physics should be seen very soon at energy scales being probed at colliders and elsewhere, or there must be some delicate cancellation present at the higher-than-expected new physics scale whereby new physics particle loop corrections to the Higgs mass are fine-tuned to be very close to one another and hence delicately cancel to provide a Higgs boson at the lower scale of electroweak physics. There are in fact two related but subtly different questions here - first, is the Higgs boson mass stable with respect to loop corrections? As we have just seen it is not in the Standard Model, this is called the "Technical" Hierarchy Problem. Second of all, why do these different scales arise in the first place, i.e. why is the scale of the Higgs boson (and hence electroweak physics) significantly lower than the scale of new physics even if the Higgs boson mass satisfies this Technical Hierarchy Problem (is "technically natural")? This is the Hierarchy or Naturalness Problem. There are many potential new physics solutions to these hierarchy and naturalness issues, however often to avoid constraints (such as smallness of observed flavour-changing-neutral currents, small CP violation (CPV), precision electroweak tests or collider search bounds) the new physics in these models is pushed to higher energies, thereby reintroducing a "little" hierarchy problem between this scale and the electroweak (EW) scale.

2. **Dark Matter** - Evidence from a variety of astrophysical distance scales clearly indicates the presence of some non-Standard Model mass component in the universe which has so far only been detected interacting gravitationally. This evidence comes from a variety of sources; from rotational velocity curves of stars around galaxies through cluster dynamics (the Bullet Cluster being a classic example) to large-scale structure formation. There are many reviews on this subject [23, 24] so the details are skipped here. Nonetheless the conclusion is that there is an additional fundamental component of the universe not accounted for by the Standard Model. There are many potential suggestions for what this

component could be; from new Weakly Interacting Massive Particles (WIMPS) at around the electroweak and collider scale, to axions which are a very light pseudoscalar particle behaving as a collectively oscillating field (as a result of the low mass), to primordial black holes. One of many reviews on the subject is given in [25]. Many new physics models include various dark matter candidate particles, for example the Lightest (stable) Susy Particles (LSPs) of supersymmetry, see Chapter 2. The common features of these dark matter candidates are that they are either too light/heavy, too weakly interacting, or both, to have so far been detected at experiments; nevertheless this is an active area of research with many current and proposed experiments aiming to target different candidates and regions of parameter space in the search for the nature of dark matter.

3. **Matter-Antimatter Asymmetry** - It is observed astrophysically that the universe has a discrepancy between the number of baryons (n_B) and the number of antibaryons ($n_{\bar{B}}$): $\xi_B = \frac{n_B - n_{\bar{B}}}{n_\gamma} = 10^{-9}$, with n_γ the number of photons. However, given it is assumed that the Big Bang produced equal numbers of baryons and antibaryons and that these were in equilibrium with photons, the question of how such an asymmetry could have emerged arises. As the universe expanded in its early history we expect $\gamma + \gamma \Leftrightarrow B + \bar{B}$ backward and forward processes to be in equilibrium as the photon temperature is initially high. As the temperature drops the forward process becomes disfavoured and so only the reverse annihilation reaction of baryon-antibaryon annihilation to photons remains, depleting the number of baryons and antibaryons in favour of photons. This continues until the baryon and antibaryon density becomes such that the reverse reaction freezes out as it eventually becomes slower than the expansion rate of the universe, as set by the Hubble scale. Therefore it is expected that the number of photons be much greater than the number of baryons and antibaryons, but also naively that the baryon and antibaryon densities in the universe are equal. In order to create a matter-antimatter asymmetry 3 "Sakharov" conditions [26] must be satisfied. In the Standard Model there is allowance for the number of baryons to exceed the number of antibaryons and so create a small asymmetry as a result of CP violation, arising via the complex phase of the Cabbibo-Kobayashi-Maskawa (CKM) matrix which relates the mass and gauge eigenstates of quarks. In addition to this measured CP violation in the quark sector, there may also be CPV in the lepton sector, nonetheless the scale of the CPV in the Standard Model is $\xi_B^{\mathrm{SM}} = 10^{-18}$, much lower than observed in the universe. As a result, new sources of CPV are required beyond the Standard Model in order to explain the observed asymmetry.

4. **Neutrino Masses** - The observation of neutrino oscillations at a variety of experiments around the world [27–32] (a review is presented in [33]) means that the 3 neutrino mass eigenstates must have different masses, i.e. $\Delta m^2_{12} \neq 0$ and $\Delta m^2_{13} \neq 0$. Masses for at least 2 of the 3 neutrinos must therefore be incorporated into the Standard Model. As seen previously in this chapter, Dirac particle mass terms can be generated in EWSB of the form $m_f^{(D)}(\bar{f}_L \phi f_R + \bar{f}_R \phi f_L)$, where $m_f^{(D)} = \frac{y_f v}{\sqrt{2}}$, requiring the addition of right-handed

neutrinos to obtain a neutrino mass. However this would not explain the smallness of the neutrino masses without accepting a correspondingly small Yukawa coupling for the neutrinos. Given the right-handed neutrinos are gauge singlets however, arbitrary additional terms involving them may be added to $\mathcal{L}_{SM}$ whilst respecting the overall gauge symmetries. Consequently, "Majorana" mass terms of the form $-\frac{1}{2}M\bar{\nu}_R^c\nu_R$ may be added[8]. Such Majorana terms can be understood to be allowed as a result of the fact the right-handed neutrinos are singlets and so may act as their own antiparticles, such terms therefore violate lepton number. Consequently the overall Lagrangian for the neutrino masses would contain Dirac and Majorana mass contributions, and the diagonalisation of the mass matrix can then generate a "see-saw" mechanism [36–40] (a review is available in [41]) pushing the left-handed neutrinos to small masses and the right-handed neutrinos to large masses, explaining the suppressed masses of the former and the lack of experimental observation of the latter.

5. **Many other issues** - In addition to these issues, there are a number of other problems and absences of the Standard Model which are listed here for brevity and in no particular order. There is no Standard Model explanation for the manner in which fermions are replicated into 3 near-identical copies differing only by mass, the complicated flavour structure of the Standard Model and the highly hierarchical nature of the CKM matrix are unexplained as they are input parameters in the Standard Model, and no reason behind the apparent quantisation of the electromagnetic charges is offered. Why there are 3 gauge groups and the combined $SU(2)_L \times U(1)_Y$ is chiral are also not answered, furthermore there is no inclusion of gravity or dark energy (on top of the exclusion of a viable dark matter candidate). Similarly, the strong CP problem of why the θ_{QCD} parameter in the Lagrangian term $\theta_{QCD}\frac{\alpha_s}{8\pi}F_{\mu\nu}\tilde{F}^{\mu\nu}$ is observed to be smaller than 10^{-11} (this results in no measurable electric dipole moment for the neutron) is unexplained. Subsets of such issues may be explained by a variety of Beyond Standard Model theories, many of which are not relevant for the discussion of the work undertaken in this thesis and are therefore not detailed. Grand Unified Theories may offer solutions for charge quantisation and for the existence of 3 generations and 3 gauge groups, the strong CP problem can be accounted for via the introduction of the axion through the Peccei-Quinn mechanism [42] perhaps also offering a dark matter candidate, flavour structure may be explained by a variety of new physics theories, and the list goes on. Several reviews of some of the issues of the Standard Model and their possible solution in Beyond Standard Model theories are available, for example in [20–22].

The Standard Model therefore suffers from many issues. Nonetheless it also has great scope for improvement and adaptation, hopefully explaining many of these matters whilst retaining the successes of our predecessors in developing such an accurate description of physics up to collider scales. This has therefore led to a wide and blossoming field of Beyond Standard Model

[8] More information is available in [34] and [35].

physics, with many theories, adaptations and hypotheses built to resolve various subsets of these issues.

In general, the aims of these Beyond Standard Model theories are to offer some minimal extension or additional framework within which to set the Standard Model in order to provide all its innumerable successes on top of further resolutions of some of these issues and intricacies left unresolved. There are correspondingly two approaches, the first are UV complete models offering a "top-down" approach with the well-tested Standard Model physics at collider scales and lower arising naturally out of these models as a lower energy scale manifestation of some more fundamental picture. The second are those offering minimal theoretical or phenomenological extensions ("bottom-up" models) to explicitly maintain the Standard Model as a fundamental basis for particle physics but with slight modifications to rectify some of its issues and absences. The wide range of Beyond Standard Model theories will not be reviewed here, the only one of specific relevance to the work discussed will be supersymmetry (one of the most popular of these theories), a UV complete model that serves as an extension of the Standard Model at low scales and which we shall therefore describe in Chapter 2. Further information and more detailed discussions of the Standard Model, its issues and Beyond Standard Model theories may be found in the books [14, 16, 34].

1.3 Contemporary Particle Physics

All of this makes the current epoch of particle physics a very exciting one; from a theoretical point of view there is a very successful model with clear problems to be explained and resolved, meanwhile experimentally there is also the Large Hadron Collider at CERN, the world's largest machine and the biggest scientific experiment ever assembled, specifically aimed at targeting these issues. This combination of the Standard Model and its issues along with the LHC as a microscope to hone in on its properties has already revealed significant results. The first run of the LHC reinforced our belief in the Standard Model via the discovery of one of its key missing pieces - the Higgs boson [12] [13], the fundamental scalar providing mass to the gauge bosons and fermions. With this discovery, LHC run 2 has been able to focus its efforts on both the precise testing of our knowledge of the Standard Model, and on direct and indirect searches for the new particles postulated in Beyond Standard Model (BSM) theories. With this run near completion there are now numerous constraints on many of these BSM theories and their parameter spaces (for example recent results include [43–46]). Such constraints in the context of supersymmetry are described in Chapter 2. As of yet, there have been no unarguable hints for any such new physics, and despite concerted efforts and the multitude of LHC data available many possibilities remain. Nonetheless, with significant constraints on the parameter spaces of some of the most minimal BSM theories (such as the Minimal Supersymmetric Standard Model, MSSM), whilst such direct searches for new physics continue unabated, there is a growing appetite for complementary searches looking for indirect signs of new physics. Foremost amongst these are precision physics measurements, aiming to look for tiny deviations from Standard

Model expectations as signs for Beyond Standard Model physics. These also have the benefit of acting as tests of the Standard Model, further improving our theoretical understanding of it as a description of nature. For any of these approaches, whether direct and indirect searches for new physics at colliders or precision physics measurements of the Standard Model alone, in this era of vast swathes of data and the unclean environment provided by a hadron-hadron collider at high energies, determining theoretical predictions for all searches and all interaction setups becomes increasingly difficult. This difficulty will only increase as we move to higher luminosities at run 3 of the LHC and the subsequent High-Luminosity LHC (HL-LHC) machine. Moreover, this is further complicated by the extensive parameter spaces of many Beyond Standard Model theories, particularly those offering UV completions (such as supersymmetry). The needs either to scan such parameter spaces or to evaluate very difficult integrals and simulate events via Monte Carlo integration methods (whether in the Standard Model or beyond) therefore often preclude by-hand analytic calculations, or at least make them inefficient and intractable. As a result, computational tools are not only increasingly desired for producing theoretical predictions, but are in fact required. Only with such computational tools for theoretical predictions is the particle physics community able to maximise the potential of the LHC (and other experiments) for the extension of our knowledge of fundamental particle physics. Such tools allow precise experimental searches to be carried out via comparisons of theory predictions with LHC data, whilst also offering the ability to extend theoretical understanding; as a consequence there has been a growing focus on the development of computational tools for LHC phenomenology. It is this area in which our research has been undertaken, and our efforts in this area are detailed in the remaining chapters of this thesis.

1.4 Thesis Outline

In this work we will describe the development of two new computational tools designed to produce theoretical predictions for phenomenology at the LHC, both in the Standard Model and beyond. These are: `SoftSusy decay calculator` [1], which is a new tool built onto an existing widely used program and predicts the branching ratios of supersymmetric and Higgs particles; and `reSolve` [2], a completely new program for computing differential spectra for a wide class of processes at the LHC, focusing upon transverse momentum resummation. The work will be described in two halves, ordered chronologically, with the first half describing the research, development and results of the decay calculator program for `SoftSusy`, and the second half detailing the production, validation and results of the `reSolve` transverse momentum (q_T) resummation program. Chapter 2 therefore begins our discussions with an overview of the theory of supersymmetry from a phenomenological perspective, aiming to put our endeavours in this area into context. This is followed by Chapter 3, which provides specific details of the decay calculator program; its assumptions, methodology and implementation, as well as a summary of the decay modes included. Chapter 4 builds on this, providing particulars on how to use the `SoftSusy decay calculator` program, before giving a comprehensive examination of the validation and results of the program. Subsequently it also outlines limitations of the work and areas of priority for future developments. Chapter 5 begins the second half of this work, describing the background for our research efforts in transverse momentum resummation by detailing the need for differential spectra and resummation at the LHC, this will provide theoretical background with a phenomenological focus. An overview of the `reSolve` program, its methodology, the implementation of its theoretical formalism and its structure, along with the channels so far incorporated, is provided next in Chapter 6. The specifics of how to use the `reSolve` program are then given in Chapter 7, along with an extensive description and analysis of the careful validation of the program and results produced. Thereafter, the current limitations of this work and consequent topics for future developments in this program and in this area are discussed. Finally, the research in both projects is summarised in Chapter 8. The Appendices provide further details on several points, with the complete set of supersymmetric and Higgs particle decay formulae given in Appendix A, along with information on the contributions included and assumptions made. Further information on the theoretical ideas behind the `reSolve` program are given in Appendix B, including a list of the resummation coefficients involved in the formalism.

Chapter 2

Supersymmetry and the LHC

2.1 Supersymmetry Theoretical Background

Supersymmetry is one of the most popular Beyond Standard Model theories available to explain many of the issues of the Standard Model and does so by extending it to a more fundamental theory, it thereby retains all of the numerous successes of the Standard Model as a theory of nature. However, supersymmetry was not originally developed or proposed as a remedy to issues of the Standard Model; rather these solutions were only understood later, following its development. This therefore makes the successes of supersymmetry as a Beyond Standard Model theory all the more remarkable. In order to appreciate the phenomenology of supersymmetry, and consequently the motivations for our work in this area of supersymmetric particle decays, we first take a brief sojourn into the theoretical background of supersymmetry.

2.1.1 Superspace, Superfields, Supermultiplets

Symmetry is a key element of the quantum field theory of the Standard Model, whether via the gauge symmetries controlling the interactions, the discrete C, P, T symmetries, or other symmetries (whether deliberate or accidental) such as baryon and lepton number conservation. These symmetries therefore are the key element determining the theory and phenomenology of the Standard Model, and the same applies for its extensions. An example of such an additional symmetry which may be applied is supersymmetry. We shall focus on its general properties in this introduction, avoiding many of the precise mathematical details as they are unnecessary here, highlighting only aspects relevant to this research. A more detailed review is [47].

At its most basic level, supersymmetry transforms bosons into fermions and vice versa, consequently it must have fermionic generators;

$$Q|fermion\rangle \propto |boson\rangle, \qquad Q|boson\rangle \propto |fermion\rangle. \tag{2.1}$$

The supersymmetry generators therefore produce superpartners of each of the known particles, which differ by $\frac{1}{2}$ in spin. Particles and their superpartners are linked, living together in the same irreducible representations of the supersymmetry algebra - termed "supermultiplets". A variety of properties of these supermultiplets may be straightforwardly derived.

- Particles and their superpartners are in the same supermultiplet and must have the same mass, assuming the supersymmetry is unbroken.
- The number of fermionic and bosonic degrees of freedom must be equal; this is somewhat intuitive given the link the supersymmetry generators form between bosons and fermions.
- Particles and their superpartners must have the same gauge quantum numbers as the supersymmetry generators Q, $Q^\dagger$ commute with the generators of the Standard Model gauge transformations.

There are two obvious classes of supermultiplets[1]: containing either a spin-$\frac{1}{2}$ fermion (in Weyl 2-component spinor form so the number of fermionic degrees of freedom, $n_F = 2$) and 2 spin-0 real scalars ("sfermions") (so the number of bosonic degrees of freedom, $n_B = 2 \times 1 = 2$) - these are "chiral supermultiplets"; or containing a spin-1 massless gauge boson (so $n_B = 2$) and a spin-$\frac{1}{2}$ fermionic partner ("gaugino") (again in Weyl 2-component form so that $n_F = 2$) - these are "vector supermultiplets", also referred to as "gauge supermultiplets". In order to apply supersymmetry to the Standard Model, one must group the existing particles and their superpartners into appropriate chiral and vector supermultiplets, this is detailed in Chapter 2.2 in introducing the Minimal Supersymmetric Standard Model.

A key overall result of supersymmetry is that as the particles and their superpartners are contained within the same superfields (i.e. in the same supermultiplets) then the requirements of invariance of the supersymmetric Lagrangian under the supersymmetry transformation fixes the coupling of the superpartners by relating them to those of their partner particles. Couplings between superpartners can therefore be regarded simply as "supersymmetrisations" of those in the Standard Model. As a result supersymmetry guarantees set relationships between fermionic/bosonic and superpartner bosonic/fermionic particles (respectively), this is key to the resolution of the technical hierarchy problem in supersymmetry, as described further in Chapter 2.3.

These supermultiplets of separate bosonic and fermionic fields may be combined into single objects, $\Phi(X)$, known as superfields [48,49]. These superfields are a function of superspace coordinates, x^μ, θ^α and $\theta^\dagger_{\dot{\alpha}}$. The motivation for the development of a new mathematical framework of superspace and superfields lies in the ease of deriving various properties of supersymmetric field theories in this language, as opposed to using the standard quantum field theory language of the Standard Model. We will not go into details on the topics of superspace and superfields here as a precise understanding is not necessary for the research presented in this thesis.

The formal and rigorous mathematical background of supersymmetry is an area of great interest, and further information on this can be found in many texts, including [50,51]. Nonetheless, we end our outline here and now focus on specific aspects relevant to the work undertaken. The general information provided thus far is more than sufficient to detail the work carried out in Chapters 3 and 4.

[1]There are actually other combinations of particles and superpartners possible in supermultiplets, however these may be reduced to combinations of chiral and gauge supermultiplets.

2.1.2 Supersymmetry Breaking

A key result of our introduction to supersymmetry in the previous section was that the masses of particles and their superpartners must be the same as they live in the same supermultiplets. However, this provides significant problems for supersymmetry as a Beyond Standard Model explanation of nature as this implies any superpartner particles would have been observed long ago (given their couplings are also linked to their partner particles and so are of the same scale). Therefore it is obvious that supersymmetry must be broken in nature, i.e. that the vacuum state is not invariant under action by the supersymmetry generators, $Q|0\rangle \neq 0$ and $Q^\dagger|0\rangle \neq 0$. This will occur if the scalar potential $V(\phi)$ has a non-zero global minimum, or at least a non-zero metastable minimum whose instability with respect to the global minimum gives a lifetime greater than the age of the universe.

There are two ways to break a symmetry, either directly - for example in the way that the fermion masses explicitly break the $[U(3)]^5$ flavour symmetry of the Standard model, or spontaneously - where the Lagrangian of the theory satisfies the symmetry but develops a vacuum value which does not, in the way the Higgs mechanism breaks the electroweak symmetry (see Chapter 1.1.1). We restrict our attention to the case of supersymmetry breaking relevant to the MSSM and NMSSM; in this case neither a direct nor a spontaneous breaking in the same sector can occur as these would both preserve the "Supertrace" (STr) over particle masses:

$$STr(m^2) = \sum_i (-1)^{2i+1}(2i+1)m_i^2 = 0, \tag{2.2}$$

where i is the spin of each particle. As supersymmetry commutes with the gauge group generators, this supertrace can be applied to each supermultiplet, or indeed each particle and its partners (as these have the same charge). Generically therefore one expects to have superpartners either equal (or a fixed ratio) in mass to their partner Standard Model particles, or spaced around the Standard Model particle masses with some lighter and some heavier, depending upon the particle spin. Applying this to the W boson and down quark and their partners we then find that there would be a "wino" of mass $\sqrt{\frac{3}{2}}m_W^2$, whilst the $\tilde{d}_L$ ("sdownL") and $\tilde{d}_R$ ("sdownR") would be spaced equally around the down quark mass:

$$-3m_W^2 + 2m_{\tilde{W}}^2 = 0, \tag{2.3}$$

$$2m_d^2 - \tilde{d}_L^2 - \tilde{d}_R^2 = 0. \tag{2.4}$$

Such similar mass superpartners have not been observed, therefore clearly it must be the case that supersymmetry is spontaneously broken in the MSSM/NMSSM in a hidden sector so as to avoid the supertrace constraint and this breaking is assumed to be radiative, or at least indirect. The topic of supersymmetry breaking and the associated supertrace sum rules is one with many subtleties; our discussion here is general and rather schematic, thereby broad-brushing many specifics which affect the arguments here (more details are available in [47, 52, 53]).

As a result of these difficulties in breaking supersymmetry directly, a two-sector system has become the archetype model, whereby the supersymmetry breaking occurs spontaneously in some hidden sector and is communicated into the visible MSSM sector via some messenger fields. This setup evades the supertrace relations linking the particle and superpartner masses. Typically, the hidden sector is assumed charged under some additional gauge group $G_{\not{\text{SUSY}}}$, the MSSM and hidden sector are then singlets under the Hidden sector gauge group and the Standard Model gauge group respectively. Only the mediating fields are charged under the combined $G_{\not{\text{SUSY}}} \times (SU(3)_c \times SU(2)_L \times U(1)_Y)$ group, as illustrated in Figure 2.1.

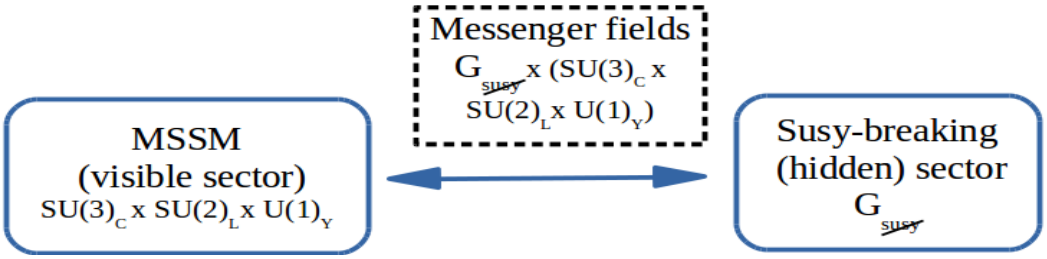

Figure 2.1: Archetypal two-sector model for spontaneous supersymmetry breaking, with a hidden sector of some additional gauge group where the supersymmetry breaking occurs which is linked to the visible sector via some mediating fields charged under both the Standard Model gauge group and the additional gauge group.

There are many options for the breaking in the hidden sector and how it is communicated into the visible sector. We list the three most popular supersymmetry-breaking mediation mechanisms relevant to LHC phenomenology here:

- **Gravity-mediated Supersymmetry-Breaking** - New physics arising near the Planck scale (such as gravity) communicates the breaking in the hidden sector into the visible sector via tree-level interactions causing mass splittings of particles and their superpartners of order

$$\Delta m \sim \frac{M^2_{\not{\text{SUSY}}}}{M_{\text{Pl}}}, \tag{2.5}$$

where M_{Pl} is the Planck mass. For desired mass splittings of 1 TeV, this requires the supersymmetry breaking scale to be $M_{\not{\text{SUSY}}} \sim 10^{11}$ GeV.

In gravity mediated supersymmetry breaking [54–57], the minimal model is called "mSUGRA" (minimal supergravity). In this model the scalar masses, fermion masses and the trilinear couplings (of fermions, sfermions and Higgses) are each assumed unified at the Grand-Unification (GUT) scale; consequently there are only 5 additional parameters relative to the Standard Model: m_0, $m_{\frac{1}{2}}$, A_0, $\tan\beta$ and $\text{sign}(\mu)$; where m_0 is the unified scalar mass, $m_{\frac{1}{2}}$ is the unified fermion mass, A_0 is the unified trilinear coupling, $\tan\beta$ is the ratio of the vacuum expectation values of the two Higgs doublets and μ is the dimensionful parameter setting the scale of the Higgs and Higgsino masses. This setup is arguably the most well-studied form of supersymmetry breaking, theoretically and experimentally, with LHC searches often focusing upon the "Constrained Minimal Supersymmetric Standard Model" (CMSSM), which features the MSSM with the parameters arising from mSUGRA at the GUT scale.

- **Gauge-Mediated Supersymmetry Breaking (GMSB)** - In this mechanism, gauge loops (perhaps of the ordinary electroweak or QCD interactions) transmit the supersymmetry breaking from the hidden sector into the MSSM [58, 59]. Consequently we expect the mass splitting of particles and superpartners to be of order

$$\Delta m \sim \frac{M_{\not{\text{SUSY}}}}{16\pi^2}, \tag{2.6}$$

where here the $16\pi^2$ is the usual factor arising from loop integration. For mass splittings of order 1 TeV we therefore require $M_{\not{\text{SUSY}}} \sim 10^5\,\text{GeV}$, which is much lower than the corresponding supersymmetry breaking scale in mSUGRA. The reason for this essentially is that one expects the mass scale of the superpartner masses is now only suppressed by the messenger fields mass scale, rather than by M_{Pl}.

The minimal model is called mGMSB and has 6 additional parameters relative to the Standard Model; $M_{\not{\text{SUSY}}}$ (the supersymmetry breaking scale), M_m (the mass scale associated with the messenger fields), n_5 (the number of messenger field multiplets), $\tan\beta$, sign(μ) and C_{grav} (which parametrises the decay rate to gravitinos and hence their mass). GMSB models can have unique phenomenology depending upon the gravitino mass (see later Chapter 2.1.3 for details).

- **Anomaly-Mediated Supersymmetry Breaking (AMSB)** - In the supergravity setups which may cause gravity-mediated supersymmetry breaking, there are also always 1-loop contributions arising when supersymmetry is broken, giving contributions to mass splittings via supergravity VEVs [60, 61]. These contributions are loop-suppressed, and so are usually sub-dominant to the gravity-mediated tree-level mediation. However, if the tree-level contributions are prevented or suppressed themselves (for example exponential suppression may arise in extra-dimensional models due to separation of branes) then the anomaly-mediated loop contributions may become important.

The minimal model is called mAMSB and has 4 additional parameters relative to the Standard Model; m_0 (universal scalar mass), $m_{\frac{3}{2}}$ (gravitino mass), $\tan\beta$ and sign(μ). The key phenomenological feature of AMSB models is that the gaugino masses are given by

$$M_i \propto \frac{b_i g_i^2}{16\pi^2} m_{\frac{3}{2}}, \tag{2.7}$$

again the $16\pi^2$ occurs due to the mediation being 1-loop. The important point is that the gaugino masses are in proportion to their gauge couplings squared multiplied by their gauge group factors b_i (which are given later in equation 2.37). As a result the lightest supersymmetric particle (LSP) (if it is a neutralino) will be dominated by the superpartners of the charged W bosons, the wino (not the superpartner of the B gauge field, the bino as is usually assumed). Moreover, the lightest chargino and lightest neutralino will correspondingly be near degenerate in mass (as both are dominantly wino in this scenario), such small mass splittings lead to phase-space suppressed decays, greatly affecting the phenomenology of these models in this case.

Regardless of their precise form, all supersymmetry breaking mechanisms relate the supersymmetric masses, couplings and other parameters to one another at some higher supersymmetry-breaking or GUT scale, thereby reducing the number of free parameters in the theory. The parameters at this high scale may then be run down to the collider and electroweak scale via the MSSM renormalisation group equations to obtain the full mass spectra, mixings and couplings which are potentially observable at colliders. In any case, none of the known supersymmetry breaking mechanisms are perfect or completely prescriptive, and the scale of the supersymmetry breaking is unknown. For this reason, our ignorance of its exact details is often parametrised phenomenologically by the explicit addition, by hand, of supersymmetry breaking terms[2] to the Lagrangian of the supersymmetric theory being considered;

$$\mathcal{L} = \mathcal{L}_{\text{SUSY}} + \mathcal{L}^{\text{soft}}_{\not{\text{SUSY}}}. \tag{2.8}$$

Nonetheless, one must be careful to only add terms which, whilst they break the supersymmetry and accordingly result in mass splittings between the supersymmetric and Standard Model particles, do not reintroduce quadratic divergences. Only these retain a natural explanation of the hierarchy of the electroweak and higher (e.g. GUT) scales[3], in particular the supersymmetric relationships linking the couplings of bosons and fermions must hold. Such terms are termed "soft" supersymmetry breaking terms [62]. In the case of softly-broken supersymmetry, whilst there are mass splittings between supersymmetric and Standard Model particles, the quadratic divergences in scalar masses are still cancelled to all orders in perturbation theory, leaving only logarithmic divergences which do not destabilise the hierarchy.

The terms which may be added to softly break the supersymmetry are scalar masses (m^2), gaugino masses (M), and trilinear couplings (a^{ijk}); clearly these are supersymmetry breaking as they give masses to only the scalars and gauginos, not their respective Standard Model partners[4]. The Lagrangian for the MSSM, along with the soft breaking terms, is given in Chapter 2.2.

Unfortunately however, the addition of these explicit parametrisations of potential soft supersymmetry breaking terms which may be induced introduces to our phenomenological theory all possible such parameters with no relationships amongst them. As a result, the parameter space to search for these supersymmetric models is expanded drastically with ≈ 120 new parameters. It is the supersymmetry breaking mechanism which links these together, often enforcing relations between them at the high scale, reducing these to the $4-6$ parameters of mSUGRA, mGMSB and mAMSB. Consequently, dropping any assumptions about the breaking and parametrising all possibilities leaves a vast parameter space to search. Nonetheless, there are phenomenological

[2] As this addition is explicit and only made to parametrise possible supersymmetry breaking terms which may arise as a result of some unexplained indirect mechanism, it avoids the supertrace considerations.

[3] The cancellation of quadratically divergent contributions to the Higgs mass is shown explicitly in Chapter 2.3.

[4] In the case where there are no gauge singlet chiral superfields then additional non-holomorphic (i.e. functions of superfield conjugates as well as of the superfields themselves) scalar trilinear couplings c_{ijk} may also be added, for example in the MSSM. However, these terms tend to be negligibly small. In theories, such as the NMSSM, where there is a gauge singlet chiral superfield they reintroduce quadratic divergences. These terms are consequently colloquially referred to as "maybe soft". There are also tadpole terms $t^i\phi_i$ which are possible for gauge singlet scalars ϕ_i, there are none of these in the MSSM.

guides: the extended parameter space is not arbitrary - many parts of it introduce unacceptable amounts of CP violation, flavour violation and similar phenomenologically undesirable effects. Therefore constraints are often placed to generate the "phenomenological" MSSM (pMSSM), a 19 parameter sub-space, which is described further in Chapter 2.5.

2.1.3 Gravitino and Goldstino

In the Standard Model, gravity is glaringly absent, posing an issue for considering it as a complete description of nature; however, as alluded to in the discussions of gravity-mediated supersymmetry breaking and AMSB, gravity may be incorporated into supersymmetry producing "supergravity" theories. These supergravity theories often arise from GUT-scale models; usually involving string theory and a fundamental, enlarged gauge group out of which our Standard Model gauge group appears. In light of these theoretical motivations, it is therefore interesting to consider the consequences of including gravity in our supersymmetric models. In order to do so, the particle spectrum of our supergravity models must include a spin-2 graviton and its supersymmetric partner the spin-$\frac{3}{2}$ gravitino (both are massless) and supersymmetry must also be promoted to a local symmetry. When supersymmetry is spontaneously broken, a Goldstone mode appears (as usual for a spontaneously broken symmetry), however as supersymmetry has fermionic generators it is a Goldstone fermion, the massless spin-$\frac{1}{2}$ "Goldstino". However, in direct analogy with the Higgs mechanism, a "super-Higgs" mechanism now occurs [63] whereby, during spontaneous supersymmetry breaking, the massless gravitino (the equivalent of the Higgs mechanism's massless gauge boson) "eats" the massless Goldstino (equivalent of the scalar Higgs doublet components). The Goldstino therefore becomes the longitudinal (i.e. spin-$\frac{1}{2}$) components of the now massive gravitino.

The result of this mechanism is that the gravitino, rather than interacting purely with gravitational strength, now has longitudinal components which interact more strongly via the Goldstino components [64]. It may therefore produce signatures of relevance to LHC phenomenology and so must be included in the particle spectrum. The mass of the gravitino induced determines the phenomenological relevance of the signals. The gravitino has no Standard Model gauge interactions and so will only be observed through missing energy/transverse momentum. In general, the mass of the gravitino is of order

$$m_{\tilde{G}} := m_{\frac{3}{2}} \sim \frac{M^2_{\cancel{\text{SUSY}}}}{M_{\text{Pl}}}. \tag{2.9}$$

However, the precise mass scale to which this corresponds varies significantly as a result of the differences in the supersymmetry breaking scales in different supersymmetry breaking mediations. For the case of gravity mediated supersymmetry breaking models, the mass splitting of particles and their superpartners is also of order $\Delta m \sim \frac{M^2_{\cancel{\text{SUSY}}}}{M_{\text{Pl}}}$, therefore the gravitino mass is of order $m_{\tilde{G}} \sim 1\,\text{TeV}$ and so the gravitino will be of limited relevance to phenomenology. In gauge mediated supersymmetry breaking models on the other hand, the mass splitting is set

via a 1-loop effect, not via Planck scale physics, therefore the supersymmetry breaking scale is much lower and $m_{\tilde{G}} \sim \frac{M_{\cancel{SUSY}}^2}{M_{\mathrm{Pl}}} \sim 10\,\mathrm{eV}$. As a result, the gravitino will be the LSP and so R-parity conserving GMSB models will have cascades of decays ending in the gravitino; this produces phenomenologically interesting signatures described in further detail in Chapters 2.5 and 4. For a description of R-parity we refer the reader to Chapter 2.2.4.

2.2 Minimal Supersymmetric Standard Model

2.2.1 Particle Content

In the Minimal Supersymmetric Standard Model (MSSM), we wish to extend the Standard Model by the minimal additional particle/field content in order to make it consistent with supersymmetry. This therefore requires the grouping of the Standard Model particles into as few supermultiplets as possible. The requirement that each supermultiplet may only contain particles with the same gauge quantum numbers however severely restricts this. Looking back at the field content of the Standard Model in Table 1.1, this illustrates that none of the Standard Model particles can be grouped to form the supermultiplets of each other. In other words, the fermions cannot be the gaugino partners of gauge bosons, and the Higgs cannot be the scalar partners of the fermions (and vice versa). Therefore for each Standard Model particle we must introduce an additional supersymmetric superpartner (or more strictly superpartners in order to equate the bosonic and fermionic degrees of freedom - for example there are two scalar sfermions for each fermion). The fermions are chiral, and therefore must exist in chiral superfields with their sfermion superpartners. Chiral superfields may only be left-handed and so any right-handed particles are included via their charge conjugates, which are left-handed. The gauge bosons meanwhile are promoted to exist in vector supermultiplets with their gaugino superpartners. All told, there are 5 chiral superfields for the fermions of each generation - Q_i, U_i^c, D_i^c, L_i, E_i^c (i is a generation index) - and 3 vector superfields B, W, G.

In addition, given the Higgs boson is spin 0 it must be assigned to a chiral supermultiplet. However, this is insufficient - in fact two Higgs chiral superfields must be present and correspondingly there are two Higgs doublets in the MSSM[5]. The reasons for this are twofold:

- Fermion Masses - Firstly, the Higgs doublets must give mass to the fermions, which occurs via the superpotential in the MSSM. The terms desired to give mass to the fermions are therefore $y_u Q H U^c$, $y_d Q H^c D^c$ and $y_e L H^c E^c$ for the up quarks, down quarks and leptons respectively. However, the superpotential must be a holomorphic function of the chiral superfields - holomorphic meaning depending only on the chiral superfields and not on their conjugates - and so terms including H^c are forbidden. Two Higgs doublets are therefore required, the first Higgs doublet is called H_u, having the standard Higgs quantum numbers and giving mass to the up type quarks, the second Higgs doublet H_d is introduced with opposite hypercharge to give mass to the down type quarks and the leptons.

[5]The MSSM is therefore an example of a "Two Higgs Doublet Model" (2HDM). These come in several types, the MSSM is type II as the up quarks couple to a different Higgs doublet to the down quarks and leptons.

- Gauge Anomalies - The second reason is for the cancellation of gauge anomalies associated with the electroweak $SU(2)_L \times U(1)_Y$ gauge symmetry. In general, chiral fermions may generate gauge anomalies, which break gauge symmetries at loop-level. The triangle diagrams shown in Figure 2.2 illustrate the gauge anomalies relevant for this discussion.

  The diagrams in Figures 2.2a and 2.2b are $(U(1)_Y)^3$ and $U(1)_Y(SU(2)_L)^2$ anomalies. In the case of the Standard Model, the particle quantum numbers are such that they both cancel, as demonstrated in equations (2.10) and (2.11). For the $(U(1)_Y)^3$ anomaly the contributions will generate a logarithmic divergence proportional to the trace over the Y^3 values of the chiral fermions in the loop, with left-handed (LH) and right-handed (RH) fermions contributing with opposite sign due to the trace over the Dirac structure. Here the factors of 3 are for colour and factors of 2 are for the fact $SU(2)_L$ doublets contain 2 particles of the same hypercharge.

(a) $(U(1)_Y)^3$ (b) $U(1)_Y(SU(2)_L)^2$

Figure 2.2: Electroweak gauge anomalies at 1-loop in the Standard Model (and in the MSSM). All chiral fermions can contribute to the $(U(1)_Y)^3$ anomaly in (a), whilst only $SU(2)_L$ doublets may contribute to the $U(1)_Y(SU(2)_L)^2$ anomaly in (b). The amplitudes are proportional to the traces over the Y^3 or Y of the chiral fermions contributing, with LH and RH chiral fermions contributing with opposite sign. There are also diagrams with crossed outgoing particles, these have identical expressions for the anomalies.

$$\begin{aligned} Tr(Y^3) &= \sum_{f_L} Y_{f_L}^3 - \sum_{f_R} Y_{f_R}^3 \\ &= \Big[\underbrace{3 \times 2 \times (\frac{1}{6})^3}_{\text{LH quarks}} + \underbrace{2 \times (-\frac{1}{2})^3}_{\text{LH leptons}}\Big] - \Big[\underbrace{3 \times (\frac{2}{3})^3}_{\text{RH up quarks}} + \underbrace{3 \times (-\frac{1}{3})^3}_{\text{RH down quarks}} + \underbrace{(-1)^3}_{\text{RH electrons}}\Big] = 0. \end{aligned} \tag{2.10}$$

Meanwhile for the $Y(I_W^{(3)})^2$ case (remember $I_W^{(3)}$ is the third component of weak isospin) only the $SU(2)_L$ doublets contribute, again the factor of 3 is as the quarks are coloured:

$$\begin{aligned} Tr(Y(I_W^{(3)})^2) &= \sum_{f_L} Y_{f_L}(I_W^{(3)})^2) \\ &= \underbrace{3 \times \frac{1}{6} \times \Big[(\frac{1}{2})^2 + (-\frac{1}{2})^2\Big]}_{\text{LH quarks}} + \underbrace{-\frac{1}{2} \times \Big[(\frac{1}{2})^2 + (-\frac{1}{2})^2\Big]}_{\text{LH leptons}} = 0. \end{aligned} \tag{2.11}$$

The addition of Higgsinos in the MSSM, as chiral fermions, may ruin this anomaly cancellation. If there was a single H_u Higgs doublet then its Higgsino, which has hypercharge of $\frac{1}{2}$, would contribute an additional $(\frac{1}{2})^3$ to the $Tr(Y^3)$, and an additional $\frac{1}{2} \times (\frac{1}{2})^2$ to the $Tr(Y(I_W^{(3)})^2)$, rendering both non-zero and introducing a 1-loop breaking of the elec-

troweak gauge symmetry. These problems are avoided with two Higgs doublets of opposite hypercharge, as the H_d doublet then provides equal but opposite contributions to those of the H_u doublet to both anomalies, returning the overall trace to 0.

With two Higgs doublets, electroweak symmetry breaking (EWSB) is slightly altered in the MSSM. In the Standard Model, there was one complex Higgs doublet corresponding to four degrees of freedom, two of which were charged degrees of freedom and two of which were neutral. In EWSB, the two charged degrees of freedom give mass to the $W^{\pm}$ and one neutral degree of freedom (the neutral CP odd degree of freedom as it turns out) gives mass to the Z boson, leaving one CP even neutral Higgs boson. In the MSSM, there are two complex Higgs doublets (each with a charged Higgsino and a neutral Higgsino superpartner), this is therefore eight degrees of freedom - now four charged and four neutral degrees of freedom. In EWSB, as in the Standard Model, two charged degrees of freedom form the longitudinal degrees of freedom of the $W^{\pm}$, giving these mass, meanwhile one CP odd neutral degree of freedom gives the Z boson mass. This therefore leaves two CP even neutral Higgs degrees of freedom, forming two CP even neutral Higgs bosons, one CP odd neutral Higgs boson, and two charged Higgs bosons.

Following all these considerations, the particle and superfield content of the MSSM is given in Tables 2.1 and 2.2. To summarise there are 12 squarks (one superpartner for each of the left- and right-handed quarks of the Standard Model), 9 sleptons (one superpartner for each of the left- and right-handed charged leptons and one superpartner for each of the left-handed neutrinos, assuming no right-handed neutrinos), the gluino, bino, winos (charged and neutral), and 5 Higgs fields and 4 Higgsinos (two neutral, two charged). After mixing, as described in Chapter 2.2.3, these form the 32 additional particles listed in Table 2.1; the R-parity is also listed, this is explained in Chapter 2.2.4.

Particle Type	Spin	R_p	Label
gluino	$\frac{1}{2}$	-1	$\tilde{g}$
squark	0	-1	$\tilde{u}_L$ $\tilde{u}_R$ $\tilde{d}_L$ $\tilde{d}_R$ $\tilde{c}_L$ $\tilde{c}_R$ $\tilde{s}_L$ $\tilde{s}_R$ $\tilde{t}_1$ $\tilde{t}_2$ $\tilde{b}_1$ $\tilde{b}_2$
slepton	0	-1	$\tilde{e}_L$ $\tilde{e}_R$ $\tilde{\nu}_e$ $\tilde{\mu}_L$ $\tilde{\mu}_R$ $\tilde{\nu}_\mu$ $\tilde{\tau}_1$ $\tilde{\tau}_2$ $\tilde{\nu}_\tau$
chargino	$\frac{1}{2}$	-1	$\tilde{W}_1^{\pm}$ $\tilde{W}_2^{\pm}$
neutralino	$\frac{1}{2}$	-1	$\tilde{Z}_1^0$ $\tilde{Z}_2^0$ $\tilde{Z}_3^0$ $\tilde{Z}_4^0$
Higgs bosons	0	+1	h^0 H^0 H^+ H^- A^0

Table 2.1: The 32 additional particles of the Minimal Supersymmetric Standard Model (MSSM) after mixing of particles with the same quantum numbers in electroweak symmetry breaking, only intra-generational mixing and only in the third generation is allowed for the sfermions here. Whilst the sfermions have L and R subscripts they have no handedness, the subscript denotes the quark-handedness to which their couplings are linked via supersymmetry. The lightest CP even neutral Higgs h is listed, although this is expected to be Standard Model-like and so it not technically an additional particle.

Type	Name	Symbol	Particle content		Representation $(SU(3)_C, SU(2)_L, U(1)_Y)$
			Spin-0	Spin-$\frac{1}{2}$	
chiral supermultiplets	LH Quark supermultiplet	Q_i	$\begin{pmatrix}\tilde{u}_L & \tilde{d}_L\end{pmatrix}$	$\begin{pmatrix}u_L & d_L\end{pmatrix}$	$(3, 2, \frac{1}{6})$
	RH Up quark supermultiplet	$(U_i)^c$	$\tilde{u}_R^*$	$u_R^\dagger$	$(\bar{3}, 1, -\frac{2}{3})$
	RH Down quark supermultiplet	$(D_i)^c$	$\tilde{d}_R^*$	$d_R^\dagger$	$(\bar{3}, 1, \frac{1}{3})$
	LH Lepton supermultiplet	L_i	$\begin{pmatrix}\tilde{\nu}_L & \tilde{e}_L\end{pmatrix}$	$\begin{pmatrix}\nu_L & e_L\end{pmatrix}$	$(1, 2, -\frac{1}{2})$
	RH electron supermultiplet	$(E_i)^c$	$\tilde{e}_R^*$	$e_R^\dagger$	$(1, 1, 1)$
	Higgs-up supermultiplet	H_u	$\begin{pmatrix}H_u^+ & H_u^0\end{pmatrix}$	$\begin{pmatrix}\tilde{H}_u^+ & \tilde{H}_u^0\end{pmatrix}$	$(1, 2, \frac{1}{2})$
	Higgs-down supermultiplet	H_d	$\begin{pmatrix}H_d^0 & H_d^-\end{pmatrix}$	$\begin{pmatrix}\tilde{H}_d^0 & \tilde{H}_d^-\end{pmatrix}$	$(1, 2, -\frac{1}{2})$
			Spin-$\frac{1}{2}$	Spin-1	
vector supermultiplets	Gluino supermultiplet	G	$\tilde{g}$	g	$(8, 1, 0)$
	Wino supermultiplet	W	$\tilde{W}^\pm\ \tilde{W}^0$	$W^\pm\ W^0$	$(1, 3, 0)$
	Bino supermultiplet	B	$\tilde{B}^0$	B^0	$(1, 1, 0)$

Table 2.2: The chiral and vector supermultiplets of the MSSM, their symbols, particle content and gauge group representations are all given. These supermultiplets contain all the 17 particles of the Standard Model and the 32 MSSM additional particles. "LH" and "RH" indicate left/right-handed. Note that as chiral supermultiplets may only be left-handed, any right-handed supermultiplets are written as conjugates to produce left-handed chiral supermultiplets, this flips the representations so the 3 of $SU(3)_C$ becomes $\bar{3}$ and the hypercharge assignments are also flipped. For the quark and lepton supermultiplets only those of the first generation are given, the index i is a generation index running from 1 to 3.

2.2.2 MSSM Lagrangian

Now the particle and supermultiplet content of the MSSM has been outlined, let us provide the MSSM Lagrangian. It has two main parts, the supersymmetry-conserving part, and the soft supersymmetry-breaking part which purely parametrises all the supersymmetry breaking which may arise as a result of an unknown supersymmetry breaking mechanism. Beginning with the supersymmetry-conserving part, there are three parts to this: the superpotential, the Kähler potential and the gauge kinetic function. For a renormalisable supersymmetric theory, the only component that needs to be provided once the particle content and gauge quantum numbers are given is the superpotential, as the Kähler potential and gauge kinetic function are fixed by renormalisability requirements.

- Superpotential, W - The superpotential is a holomorphic function of the chiral superfields of mass dimension 3 and, for the MSSM (assuming R-parity conservation - see Chapter 2.2.4) is given by

$$W_{\text{MSSM}} = (y_u)_{ij} H_u Q_i U_j^c + (y_d)_{ij} H_d Q_i D_j^c + (y_e)_{ij} H_d L_i E_j^c + \mu H_u H_d. \tag{2.12}$$

  This contains, as the first three terms, the usual Yukawa interaction terms for the fermions and sfermions, which also give mass to these particles just as in the Standard Model. The last term is the Higgsino mass term which sets the masses of the Higgs bosons and Higgsinos. The gauge indices have been suppressed with only the generation indices $i, j = 1, 2, 3$ explicitly included. The first term for example may be written in full as $(y_u)_{ij}(H_u)_\alpha(Q_i)_{\beta a}(U_j)^c_a\epsilon^{\alpha\beta}$ with $a = 1, 2, 3$ the colour index and the α, β as $SU(2)_L$ indices contracted in a gauge invariant manner via the epsilon tensor.
- Kähler Potential, K - The Kähler potential is a real function of the chiral and antichiral superfields (i.e. left and right-handed) of mass dimension 2 and incorporates the vector superfields in order to ensure supergauge invariance. It is fixed by the particle content, quantum numbers and renormalisability requirements to be

$$K = \Phi_i^\dagger \exp(2V)\Phi_i. \tag{2.13}$$

  Here the Φ are each of the chiral superfields of the MSSM, whilst $V = g_s\frac{\lambda^a}{2}G^a + \frac{g}{2}\sigma^i W^i + g'YB$ is a vector superfield of all the gauge interactions in the MSSM, with the λ^a the Gell-Mann matrices and the σ_i the Pauli matrices. This form of Kähler potential ensures it is invariant under the generalised gauge transformations of the chiral and vector superfields. The Kähler potential provides the kinetic terms for the matter and Higgs fields[6].
- Gauge Kinetic Function, f - This is the prefactor function for the kinetic term of the field-strength superfields, which are functions of the vector superfields, and so provides the kinetic terms for the gauge bosons and gauginos. In general, it is a holomorphic function of the chiral superfields and has mass dimension 0, for renormalisable theories it is just proportional to a $\delta_{\alpha\beta}$ function. This ensures the kinetic terms are products of field strength superfields for the same gauge interactions, the constant of proportionality depends on normalisation, it is usually $\frac{1}{g_a^2}$, where g_a (for $a = 1, 2, 3$) is the coupling for each of the gauge groups.

These three pieces specify everything needed to construct the overall supersymmetry conserving part of the MSSM Lagrangian; we will not repeat this process here. A detailed overview of how to construct supersymmetric Lagrangians in general, with the MSSM as an example, is available in [65].

[6]The reader may be concerned that the vector superfield V is exponentiated and appears dimensionful, this issue is avoided as it is expanded in superspace and Grassmanian variables have inverse dimensions which ensure the overall expanded exponential is dimensionless.

The soft supersymmetry-breaking part of the Lagrangian must also be stated. The soft supersymmetry-breaking Lagrangian in the R-parity conserving case[7] (which is all that is considered later in the `SoftSusy` decay calculator in Chapters 3 and 4) consists of gaugino mass terms, scalar mass terms for the sfermions and Higgs bosons, and trilinear couplings of the scalars. Such terms are clearly supersymmetry breaking as they provide additional masses to the superpartners but not their Standard Model partner particles:

$$\begin{aligned}\mathcal{L}_{\cancel{\text{SUSY}}} =& \frac{1}{2}M_1\tilde{B}\tilde{B} + \frac{1}{2}M_2\tilde{W}\tilde{W} + \frac{1}{2}M_3\tilde{g}\tilde{g} + m_2^2|H_u|^2 + m_1^2|H_d|^2 + (m_3^2 H_u H_d + h.c.) \\ &+ \tilde{Q}^*_{Li}(m^2_{\tilde{Q}})_{ij}\tilde{Q}_{Lj} + \tilde{L}^*_{Li}(m^2_{\tilde{L}})_{ij}\tilde{L}_{Lj} + \tilde{u}_{Ri}(m^2_{\tilde{U}})_{ij}\tilde{u}^*_{Rj} + \tilde{d}_{Ri}(m^2_{\tilde{D}})_{ij}\tilde{d}^*_{Rj} + \tilde{e}_{Ri}(m^2_{\tilde{E}})_{ij}\tilde{e}^*_{Rj} \\ &+ (A_U)_{ij}\tilde{Q}_{Li}H_u\tilde{u}^*_{Rj} + (A_D)_{ij}\tilde{Q}_{Li}H_d\tilde{d}^*_{Rj} + (A_E)_{ij}\tilde{L}_{Li}H_d\tilde{e}^*_{Rj}.\end{aligned} \tag{2.14}$$

Supersymmetry breaking mechanisms link these soft parameters together at the supersymmetry-breaking scale. For example in the CMSSM at the GUT scale there are unified scalar masses, unified fermion masses, and unified trilinear couplings; therefore $M_1 = M_2 = M_3 \equiv M_{\frac{1}{2}}$, $m_1^2 = m_2^2 = m^2_{\tilde{Q}} = m^2_{\tilde{L}} = m^2_{\tilde{U}} = m^2_{\tilde{D}} = m^2_{\tilde{E}} \equiv m_0^2$, $A_U = A_0 Y_U$, $A_D = A_0 Y_D$ and $A_E = A_0 Y_E$.

2.2.3 Mixing

In Standard Model electroweak symmetry breaking, the B and W_3 fields mix according to the weak mixing angle θ_W to produce the observable Z boson and photon. The quarks also have a misalignment between mass and gauge eigenstates, as parametrised by the CKM matrix, leading the mass eigenstates to be mixtures of the gauge eigenstates; a similar structure is also encoded in the lepton sector via the PMNS matrix. In all these cases we have particles of the same quantum numbers mixing. In particular, for mixing in electroweak symmetry breaking, particles of the same charge and colour representation may mix (even if they have different weak isospin or hypercharge) as only the $SU(3)_c \times U(1)_{em}$ group remains unbroken. These mixing effects in electroweak symmetry breaking will be phenomenologically important for our additional Higgs and supersymmetric particles of supersymmetry.

There are four sets of gauge eigenstates in the MSSM which may therefore mix to form the potentially observable supersymmetric mass eigenstates.

2.2.3.1 Higgs Bosons

In the Higgs sector of the MSSM, there are three neutral Higgs bosons and 2 charged Higgs bosons; the neutral and charged Higgs bosons may not mix as this breaks the unbroken $U(1)_{\text{em}}$ symmetry left after EWSB. Therefore the mixing is confined to the neutral Higgs sector[8]. In

[7] The concept of R-parity will be introduced later in Chapter 2.2.4.

[8] For the interests of brevity, here we do not detail the mixing that occurs in the charged Higgs sector between the charged Goldstone and the charged Higgs gauge eigenstate to give the physical charged Higgs, or the mixing

addition, since we assume CP invariance in the Higgs sector, the two CP even neutral Higgs bosons may not mix with the one CP odd neutral Higgs, leaving a 2×2 mixing matrix in the CP even neutral Higgs sector:

$$\mathcal{L} \supset \frac{1}{2} \begin{pmatrix} \mathcal{R}(H_u^0) & \mathcal{R}(H_d^0) \end{pmatrix} \mathcal{M}_{\mathcal{R}(H^0)} \begin{pmatrix} \mathcal{R}(H_u^0) \\ \mathcal{R}(H_d^0) \end{pmatrix}. \tag{2.15}$$

Here $\mathcal{R}(H_{u/d}^0)$ indicates the real part of the complex Higgs field. The elements of the matrix $\mathcal{M}_{\mathcal{R}(H^0)}$ for the gauge eigenstates of the neutral CP even Higgs bosons are set via partial derivatives of the scalar potential with respect to the neutral CP even Higgs fields, with these then set to their VEVs. The elements therefore are dependent upon m_A, $\tan\beta$ and m_Z:

$$\mathcal{M}_{\mathcal{R}(H^0)} = \begin{pmatrix} m_A^2 \cos^2\beta + m_Z^2 \sin^2\beta & -(m_A^2 + m_Z^2)\sin\beta\cos\beta \\ -(m_A^2 + m_Z^2)\sin\beta\cos\beta & m_A^2 \sin^2\beta + m_Z^2 \cos^2\beta \end{pmatrix}. \tag{2.16}$$

As this mass matrix is real and symmetric, it may be diagonalised via an orthogonal transformation to find its mass eigenstates and their eigenvalues (masses). We may parametrise this orthogonal transformation as a rotation matrix with mixing angle α:

$$\begin{pmatrix} h^0 \\ H^0 \end{pmatrix} = \begin{pmatrix} \cos\alpha & \sin\alpha \\ -\sin\alpha & \cos\alpha \end{pmatrix} \begin{pmatrix} \mathcal{R}(H_u^0) \\ \mathcal{R}(H_d^0) \end{pmatrix}. \tag{2.17}$$

Given that the determinant of the mass matrix is positive ($\det\mathcal{M}_{\mathcal{R}(H^0)} = m_A^2 m_Z^2 \cos^2 2\beta \geq 0$) and the diagonal elements (which are the principal minors of the matrix) are all positive, the matrix is positive semi-definite and so the mass eigenstates are guaranteed to have positive masses. From the trace and determinant, it can be straightforwardly derived that:

$$m_{h,H} = \frac{1}{2}(m_Z^2 + m_A^2)\left[1 \mp \sqrt{1 - \frac{4m_A^2 m_Z^2 \cos^2 2\beta}{(m_A^2 + m_Z^2)^2}}\right], \tag{2.18}$$

where h is defined as the lighter of the two CP even neutral Higgs mass eigenstates. Meanwhile the mixing angle can be determined as:

$$\tan\alpha = \frac{(m_A^2 - m_Z^2)\cos 2\beta + \sqrt{(m_A^2 + m_Z^2)^2 - 4m_A^2 m_Z^2 \cos^2 2\beta}}{(m_A^2 + m_Z^2)\sin 2\beta}. \tag{2.19}$$

It should be noted at this stage that, whereas in the Standard Model the Higgs boson mass was a free non-predicted parameter $m_h = 2\lambda v^2$, in the MSSM the Higgs boson mass is predicted theoretically in terms of the Z mass (and hence the gauge couplings), the CP odd neutral Higgs mass (itself constrained in terms of the ratio of the Higgs VEVs, the mass parameter μ and others) and the ratio of the two Higgs doublet VEVs $\tan\beta$. In particular upper bounds on the

of the neutral Goldstone and the CP odd neutral Higgs to form the physical CP odd neutral Higgs. These mixings introduce factors of $\cos\beta$ and $\sin\beta$ into the interactions of these particles, where $\tan\beta$ is the ratio of the vacuum expectation values of the two Higgs doublets.

lightest Higgs mass can be obtained. The expectation value for a general vector admixture of the two eigenvectors of the mass matrix must lie between the two eigenvalues of the mass matrix, consequently we may evaluate an upper bound:

$$\begin{aligned} m_h^2 &\leq \begin{pmatrix} \cos\theta & \sin\theta \end{pmatrix} \begin{pmatrix} m_A^2 \cos^2\beta + m_Z^2 \sin^2\beta & -(m_A^2 + m_Z^2)\sin\beta\cos\beta \\ -(m_A^2 + m_Z^2)\sin\beta\cos\beta & m_A^2 \sin^2\beta + m_Z^2\cos^2\beta \end{pmatrix} \begin{pmatrix} \cos\theta \\ \sin\theta \end{pmatrix} \\ &\leq \cos^2\theta(m_A^2\cos^2\beta + m_Z^2\sin^2\beta) - \cos\theta\sin\theta(m_A^2 + m_Z^2)\sin 2\beta + \sin^2\theta(m_A^2\sin^2\beta + m_Z^2\cos^2\beta). \end{aligned} \tag{2.20}$$

The upper bound is generally saturated for large values of m_A and large $\tan\beta$ - in the decoupling limit of $m_A \gg m_Z$ the lightest MSSM Higgs boson is then Standard Model-like.

Now we may select the value of θ to extract bounds as the limits are true for any θ, in particular selecting $\theta = \frac{\pi}{2} - \beta$ obtains

$$m_h^2 \leq m_Z^2(\sin^4\beta + \cos^4\beta - 2\sin^2\beta\cos^2\beta) = m_Z^2(\cos^2\beta - \sin^2\beta)^2 = m_Z^2\cos^2 2\beta, \tag{2.21}$$

this implies that at tree-level $m_h \leq m_Z$ (occurs if $\beta \approx 0, \frac{\pi}{2}$ where the latter is the decoupling limit as there $\tan\beta$ is large). Given the measured value of $m_h = 125\,\text{GeV}$, this may seem as though it causes issues for the MSSM. Fortunately however, radiative corrections raise this upper bound. Details can be found in Chapter 2.3.4.

2.2.3.2 Sfermions

Sfermions are also of the same colour representations and electric charge as each other, therefore they may also mix in electroweak symmetry breaking. In this discussion, we limit the mixing to intra-generation sfermion mixing as we assume no additional flavour violation relative to the Standard Model (a standard pMSSM assumption), which means the trilinear coupling matrices and Yukawa matrices are proportional ($A_f \propto Y_f$), i.e. they are diagonal in the same basis. In general there are 5 contributions to sfermion masses; three which give the $\tilde{f}_L$ and $\tilde{f}_R$ separate mass contributions, and two which cause mixing in EWSB [65]. Both intra-generation mixing terms are proportional to m_f as they arise during EWSB and so are proportional to the VEV of the relevant up/down-Higgs doublet. For this reason it is often assumed that mixing in the first two generations of sfermions is negligible; this assumption will be made in Chapter 3. Taking this assumption, along with the alignment of the trilinear and Yukawa matrices, essentially results in approximating these 3×3 matrices via their $(3,3)$ element, which is overwhelmingly dominant due to the hierarchy of the Yukawa couplings. As a result, let us consider the stop sfermions from here as an example. The mass matrix in the Lagrangian for the stops, incorporating all 5 contributions, is therefore given by:

$$\mathcal{L}_{\tilde{t}_i} \ni \begin{pmatrix} \tilde{t}_L^\dagger & \tilde{t}_R^\dagger \end{pmatrix} \begin{pmatrix} m_{\tilde{t}_L}^2 + m_t^2 + m_Z^2\cos 2\beta(\frac{1}{2} - \frac{2}{3}\sin^2\theta_W) & m_t(\mu\cot\beta - A_t) \\ m_t(\mu\cot\beta - A_t) & m_{\tilde{t}_R}^2 + m_t^2 + m_Z^2\cos 2\beta(\frac{2}{3}\sin^2\theta_W) \end{pmatrix} \begin{pmatrix} \tilde{t}_L \\ \tilde{t}_R \end{pmatrix}. \tag{2.22}$$

Once more this is real symmetric, and so it may be diagonalised by a rotation matrix linking the gauge and mass eigenstates.

$$\begin{pmatrix} \tilde{t}_1 \\ \tilde{t}_2 \end{pmatrix} = \begin{pmatrix} \cos\theta_t & \sin\theta_t \\ -\sin\theta_t & \cos\theta_t \end{pmatrix} \begin{pmatrix} \tilde{t}_L \\ \tilde{t}_R \end{pmatrix}. \tag{2.23}$$

Again, one may determine the masses of the lightest ($\tilde{t}_1$) and heaviest stops ($\tilde{t}_2$) via the eigenvalues and the mixing angle θ_t may be determined; we do not provide these here. This same exposition applies for the other third generation sfermions and their mixings; the sbottoms and the staus. There is no mixing of the third generation ν_τ as this only exists in its left-handed form.

2.2.3.3 Neutralinos

The MSSM contains four spin-$\frac{1}{2}$ neutralino states, in the form of the bino ($\tilde{B}$), neutral wino ($\tilde{W}_3$), and two Higgsinos ($\tilde{H}_u$, $\tilde{H}_d$); these all share the same electric charge of 0, the same spin and the same colour representation (singlets) and so will mix in electroweak symmetry breaking to give 4 neutral spin-$\frac{1}{2}$ states, the lightest of which may be a good dark matter candidate (see Chapter 2.3). The Lagrangian and neutralino mass matrix for these particles has contributions from the last term of the superpotential in equation 2.12 (unsurprisingly as this is the Higgsino mass term), a contribution from EWSB, and one from the soft supersymmetry breaking gaugino mass terms of equation 2.14; the physical neutralino mass eigenstates are often denoted $\tilde{\chi}_i^{(0)}$, however here they will be denoted $\tilde{Z}_i$ for ease of reading.

$$\mathcal{L}_{\tilde{Z}_i} \ni -\frac{1}{2}\begin{pmatrix} -i\tilde{B} & -i\tilde{W}_3 & \tilde{H}_u & \tilde{H}_d \end{pmatrix} \mathcal{M}_{\tilde{Z}_i} \begin{pmatrix} -i\tilde{B} & -i\tilde{W}_3 & \tilde{H}_u & \tilde{H}_d \end{pmatrix}^T, \tag{2.24}$$

where

$$\mathcal{M}_{\tilde{Z}_i} = \begin{pmatrix} M_1 & 0 & -M_Z\cos\beta\sin\theta_W & M_Z\sin\beta\sin\theta_W \\ 0 & M_2 & M_Z\cos\beta\cos\theta_W & -M_Z\sin\beta\cos\theta_W \\ -M_Z\cos\beta\sin\theta_W & M_Z\cos\beta\cos\theta_W & 0 & -\mu \\ M_Z\sin\beta\sin\theta_W & -M_Z\sin\beta\cos\theta_W & -\mu & 0 \end{pmatrix}. \tag{2.25}$$

As before, the neutralino mass matrix is real and symmetric and so is diagonalised by an orthogonal transformation[9]:

$$\begin{pmatrix} \tilde{Z}_1 \\ \tilde{Z}_2 \\ \tilde{Z}_3 \\ \tilde{Z}_4 \end{pmatrix} = \begin{pmatrix} v_1^{(1)} & v_1^{(2)} & v_1^{(3)} & v_1^{(4)} \\ v_2^{(1)} & v_2^{(2)} & v_2^{(3)} & v_2^{(4)} \\ v_3^{(1)} & v_3^{(2)} & v_3^{(3)} & v_3^{(4)} \\ v_4^{(1)} & v_4^{(2)} & v_4^{(3)} & v_4^{(4)} \end{pmatrix} \begin{pmatrix} -i\tilde{B} \\ -i\tilde{W}_3 \\ \tilde{H}_u \\ \tilde{H}_d \end{pmatrix}, \tag{2.26}$$

here the $\tilde{Z}_i$ are mass ordered (by absolute values of their masses), with $\tilde{Z}_1$ the lightest neutralino.

[9]Our orthogonal transformation matrix N (where $N_{(i,j)} = v_i^{(j)}$) here is the transpose of the O matrix of [66], and is also transformed (transposed and with rows swapped) relative to that of [65] as a result of a different ordering of the gauge eigenstates.

Now in this case, the fact there are 0s on the diagonal indicates that the mass matrix is not positive definite, and so generically we must expect the possibility of neutralino mass eigenstates with negative masses. In general, in our discussions in this thesis in Chapters 3 and 4 we will therefore have the possibility of negative neutralino masses. However, given that we have ordered the neutralinos via their absolute values of their masses, it is often customary to define their masses to be positive (although we shall not). In this case the sign of the mass is changed via a field redefinition, absorbing a factor of $i\gamma_5$ into the relevant row of the neutralino mixing matrix. Performing this field redefinition can be shown to simultaneously change the sign of the mass term in the Lagrangian, whilst leaving the kinetic term unchanged; it does however affect neutralino couplings as additional γ_5 matrices and factors of i appear which can have significant effects in interferences. The effects of negative masses are accounted for in the `SoftSusy` code and in Appendix A via factors of the form $(-1)^{\theta_i}$ which are ± 1 depending on the sign of the mass of the neutralino being considered.

2.2.3.4 Charginos

In the MSSM, there are also two charginos of each charge ($\pm$), arising from the charged winos and the charged Higgsinos of the gauge eigenbasis. The mass matrix present in the MSSM Lagrangian is given by

$$\mathcal{L}_{\tilde{W}_i} \ni -\frac{1}{2}\begin{pmatrix} -i\tilde{W}^+ & \tilde{H}_u^+ & -i\tilde{W}^- & \tilde{H}_d^- \end{pmatrix} \mathcal{M}_{\tilde{W}_i} \begin{pmatrix} -i\tilde{W}^+ & \tilde{H}_u^+ & -i\tilde{W}^- & \tilde{H}_d^- \end{pmatrix}^T. \tag{2.27}$$

However, given the charge symmetry here, the mass matrix $\mathcal{M}_{\tilde{W}_i}$ reduces to 2×2 block form:

$$\mathcal{M}_{\tilde{W}_i} = \begin{pmatrix} 0 & N^T \\ N & 0 \end{pmatrix}, \quad \text{where} \quad N = \begin{pmatrix} M_2 & gv_u \\ gv_d & \mu \end{pmatrix} = \begin{pmatrix} M_2 & \sqrt{2}m_W \sin\beta \\ \sqrt{2}m_W \cos\beta & \mu \end{pmatrix}. \tag{2.28}$$

Accordingly, we may reduce the whole Lagrangian mass expression to 2×2 form:

$$\mathcal{L}_{\tilde{W}_i} \ni -\frac{1}{2}\begin{pmatrix} -i\tilde{W}^- \\ \tilde{H}_d^- \end{pmatrix} N \begin{pmatrix} -i\tilde{W}^+ & \tilde{H}_u^+ \end{pmatrix} + h.c.. \tag{2.29}$$

Unlike all our previous diagonalisations, this chargino mass matrix is not symmetric. As the γ_5 matrix acts in similar block diagonal form we can therefore relate the asymmetry of the mass matrix to γ_5 (i.e. handedness) dependence. The generalisation of the usual diagonalisation of a real symmetric matrix via an orthogonal transformation to a non symmetric matrix is to perform a singular value decomposition. We act on the mass matrix $\mathcal{M}_{\tilde{W}_i}$ with different matrices U and V on its left- and right-hand side such that $U^\dagger D V = \mathcal{M}_{\tilde{W}_i}$, for unitary matrices U and V and a diagonal matrix of singular values D. As a result of the 2×2 block structure, we can consequently consider diagonalising the 2×2 blocks separately by different rotations, essentially rotating the left-hand and right-hand chiral components differently.

$$\begin{pmatrix}\tilde{W}_1^+\\ \tilde{W}_2^+\end{pmatrix} = V\begin{pmatrix}-i\tilde{W}^+\\ \tilde{H}_u^+\end{pmatrix}, \qquad \begin{pmatrix}\tilde{W}_1^-\\ \tilde{W}_2^-\end{pmatrix} = U\begin{pmatrix}-i\tilde{W}^-\\ \tilde{H}_d^-\end{pmatrix}. \tag{2.30}$$

We can therefore exploit the separate LH and RH rotations to remove any chirality dependence:

$$U^* N V^{-1} = D = \begin{pmatrix} m_{\tilde{W}_1} & 0\\ 0 & m_{\tilde{W}_2}\end{pmatrix}, \tag{2.31}$$

where the eigenvalues $m_{\tilde{W}_{1/2}}$ are necessarily real but may be negative (in which case we may perform the field redefinitions exactly as described in the context of neutralinos). U and V may be parametrised in terms of rotation angles in the usual manner:

$$U = \begin{pmatrix}\cos\theta_L & -\sin\theta_L\\ \sin\theta_L & \cos\theta_L\end{pmatrix}, \qquad V = \begin{pmatrix}\cos\theta_R & -\sin\theta_R\\ \sin\theta_R & \cos\theta_R\end{pmatrix}. \tag{2.32}$$

U is the unitary matrix which diagonalises $N^T N$ and V is similarly the unitary matrix which diagonalises NN^T (both $N^T N$ and NN^T are clearly symmetric and so permit diagonalisation via an orthogonal transformation). The NN^T and $N^T N$ matrices have eigenvalues $m^2_{\tilde{W}_1}$ and $m^2_{\tilde{W}_2}$, which again explains why the mass values themselves may be negative. As usual, the masses of the physical charginos ($\tilde{W}_1$, $\tilde{W}_2$, mass ordered from lowest to highest) may be determined and are

$$m^2_{\tilde{W}_{1,2}} = \frac{1}{2}\Big[|M_2|^2 + |\mu|^2 + 2m_W^2 \mp \sqrt{(|M_2|^2 + |\mu|^2 + 2m_W^2)^2 - 4|\mu M_2 - m_W^2 \sin 2\beta|^2}\,\Big]. \tag{2.33}$$

2.2.3.5 Further Mixing

In addition to this mixing of gauge eigenstates of the same colour, spin and charge in EWSB, in general there can be large amounts of additional mixing in the MSSM and its extensions as caused by particles running in loops. In particular, this is a concern where supersymmetric particles act in loops between Standard Model particles as this can cause effects already ruled out experimentally. Amongst the large general MSSM parameter space (as parametrised via the 120 possible supersymmetry breaking parameters), there are large sections where supersymmetric particles would cause large quark mixing, additional flavour violation and flavour-changing neutral currents (FCNCs) which have been ruled out by Standard Model measurements. We therefore expect that the precise but unknown supersymmetry breaking mechanism imposes constraints on these parameters to structure the parameter space such that these phenomenologically undesirable regions are ruled out. Some assumptions of this form can be made on the MSSM parameter space to reduce it, resulting in the phenomenological MSSM (pMSSM).

2.2.4 R-parity

In the Standard Model, baryon number (B) and lepton number (L) arise as accidental symmetries purely as a result of the gauge invariance, particle content and renormalisability requirements. In the MSSM however, this is no longer the case. The additional particle content, specifically the scalars carrying baryon and lepton number (the superpartners of the fermions), allow additional B and L violating terms to be written down in the superpotential. The superpotential given in equation 2.12 neglected these terms on the basis of minimality and phenomenology. In particular, phenomenologically, B and L number violation combined are excluded by processes such as proton decay, which currently has a measured lifetime of longer than 10^{34} years [67]. If the B and L number violating terms are not included then supersymmetry non-renormalisation theorems ensure they are not regenerated radiatively. Therefore provided such terms can be satisfactorily ruled out theoretically, we can explain such experimental measurements. In the MSSM the potential B and L number violating terms arising from the superpotential are

$$W_{RPV} = \lambda_{ijk} L_i L_j E^c_k + \lambda'_{ijk} L_i Q_j D^c_k + \lambda''_{ijk} U^c_i D^c_j D^c_k + \kappa_i L_i H_u. \tag{2.34}$$

In order to ban such terms, rather than just neglect them on the basis of minimality, a symmetry must be invoked - the most common of these symmetries is a Z_2 symmetry termed "R-parity"[10]. R-parity is a multiplicative conserved quantum number given by:

$$R_p = (-1)^{3(B-L)+2S}, \tag{2.35}$$

where S is the spin of the particle. Given all Standard Model particles and their superpartners have the same B and L number but differ in spin by $\frac{1}{2}$, Standard Model particles (including all Higgses) and their supersymmetric superpartner particles consequently have opposite sign R-parity. Conventionally, the Standard Model particles are given $R_p = 1$ and the supersymmetric superpartners have $R_p = -1$. A subtle point is how R-parity, a symmetry which explicitly distinguishes Standard Model particles and their supersymmetric partners, does not break supersymmetry. The resolution of this is that in reality it is an effective symmetry, which can be considered as arising from more fundamental symmetries such as "matter parity", which do not break supersymmetry, in addition to the conservation of angular momentum. Further details on this area may be found in [47, 65]. The precise method of generating this phenomenologically needed R-parity discrete symmetry is itself a subject of much interest, however we will not delve into it for this work. R-parity conservation is assumed in the standard meaning of the MSSM, and will be assumed in our work on supersymmetric decays in Chapters 3 and 4.

[10] There are actually many additional symmetries which can ban various subsets of the R-parity violating terms, for example see reference [47] for a summary.

2.2.4.1 R-parity conservation

The imposition of this R-parity symmetry, to produce the R-parity conserving ("RPC") MSSM, has tremendous consequences for phenomenology:

- All interactions in RPC models must involve an even number of supersymmetric particles in order to conserve R-parity: in particular it is this requirement that allows one to gain intuition of the allowed supersymmetric interactions in Chapter 2.2.5 by "supersymmetrising" Standard Model interactions via the exchange of an even number of Standard Model particles with their superpartners.
- In experiments Standard Model particles are necessarily collided; consequently conservation of R-parity ensures that supersymmetric particles must be pair produced, this has significant impacts on the kinematics and signatures.
- Any supersymmetric particle must decay to an odd number of supersymmetric particles, in addition to any number of Standard Model particles. Given decay kinematics favours fewer particles being produced (see Chapter 3.1) most supersymmetric particles undergo decays of the form $\text{SUSY} \to \text{SUSY} + \text{SM}$.
- The lightest supersymmetric particle (LSP) of the model, having no further supersymmetric particles to decay to, is stable and so may provide a good dark matter candidate, particularly if it is the lightest neutralino $\tilde{Z}_1$.
- These LSPs remain after cascades of supersymmetric particle decays and, if they are neutral (as they must be to provide a dark matter candidate), leave the experiments as missing energy and momentum.

For these reasons, most research in this area focuses on R-parity conserving models, as they offer the possibility of resolving the issues of dark matter in addition to the standard motivations for supersymmetry. Our `SoftSusy` decay calculator also assumes RPC for these reasons, nonetheless the spectrum generator part of the `SoftSusy` program [66] includes the possibility of allowing R-parity violation (RPV); therefore we discuss it briefly here.

2.2.4.2 R-parity violation

In spite of this focus in the field on R-parity conservation, it is possible to allow R-parity violating couplings or various subsets thereof, though they are constrained to be very small by experiments. In particular, with RPV one generically expects proton decay as demonstrated in Figure 2.3. However, proton decay requires both B number violation (via the first vertex corresponding to the third term in W_{RPV} in equation 2.34) and L number violation (via the second vertex corresponding to the second vertex in W_{RPV}) separately. Therefore preventing just one of B number violation and L number violation will prevent proton decay. Given there are strong bounds on B number violation via non-observation of processes such as neutron-antineutron mixing, it is often supposed that only L number is violated. In that case such small lepton number violation may also generate Majorana fermion masses and mixings for the neutrinos (for example see references [68–70]), whilst still preventing proton decay. In

general there are various UV models possible to generate a symmetry which prevents undesirable phenomenological consequences in this way whilst providing explanations for neutrino masses or other observations; a particular popular one is to note that whilst both B and L number are expected to be broken by non-perturbative effects in the Standard Model, B-L is not and is present in many GUT models. Therefore many models consider a gauged $U(1)_{B-L}$ symmetry broken by a scalar VEV [71], the remaining conserved unbroken subgroup can then correspond to R-parity conservation

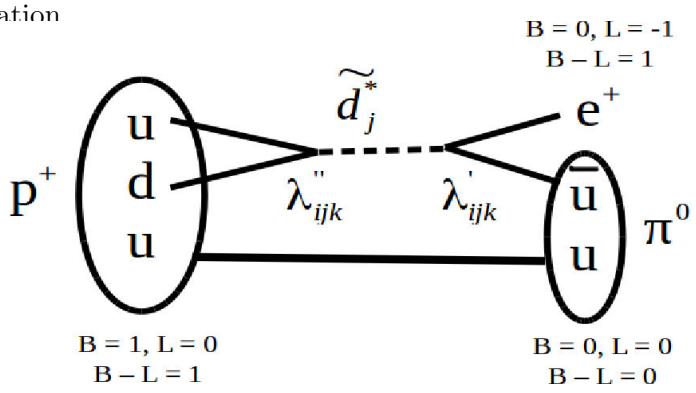

Figure 2.3: Proton decay allowed in the case of R-parity violation, the λ''_{ijk} is a baryon number violating coupling and the λ'_{ijk} is a lepton number violating coupling corresponding to the appropriate terms in the superpotential in equation 2.34. The B, L and B-L numbers are shown for each particle.

R-parity violation, even in very small amounts, may have significant phenomenological consequences (which will be outside the scope of our work in Chapters 3 and 4); the LSP may now decay offering a new array of signatures at the LHC.

2.2.5 Interactions

The particle interactions in the MSSM, and in supersymmetric models in general, are derived in a similar manner to the mass terms described in the Chapter 2.2.3; gathering all terms in the Lagrangian which may contribute to a given coupling and diagonalising and rotating states as required to obtain the couplings of the physical mass eigenstates. In general this process of deriving the various MSSM interactions is therefore very involved, nonetheless there are several guiding principles which may aid the intuition. Deriving the relevant interactions is vital to the calculation of the supersymmetric and Higgs decay branching ratios in our work in `SoftSusy` in Chapters 3 and 4.

First of all, as is the case in the Standard Model, all interactions must preserve all the quantum numbers of the MSSM, as any Lagrangian terms must be overall singlets of the $SU(3)_c \times SU(2)_L \times U(1)_Y$ gauge group. In addition, as we impose R-parity conservation in our work, we also expect baryon number and lepton number conservation. R-parity conservation also lends a second useful guide; as R-parity assigns a quantum number of $+1$ to Standard Model particles (and all Higgs bosons) and -1 to MSSM superpartners, all interactions must have an even number of supersymmetric particles. In particular, adding to this the fact that supersymmetry links particle and superpartner couplings, one may expect supersymmetric specific interactions to simply be "supersymmetrisations" of Standard Model interactions, where we take an even

number of the Standard Model particles present in a Standard Model allowed interaction and replace them by their superpartners. This will still be allowed by conservation of quantum numbers as particles and their superpartners are in the same overall gauge group representations, whilst transforming an even number of particles ensures R-parity conservation.

However, in reality, the only certain way to obtain the interactions of the MSSM is to perform the full derivations (this is demonstrated in many texts, including [65]), which were nonetheless performed in our work in this area. As an example of the need to rigorously perform such calculations rather than rely on guiding principles, an interaction vertex which one might naively expect to appear in the MSSM at tree-level is the H^+W^-Z vertex as it satisfies conservation of all quantum numbers and R-parity conservation. In reality however it is absent at tree-level (occurring only at 1-loop); the physical reason behind this is a cancellation resulting from the fact that the same angle β which is the ratio of the VEVs of the neutral Higgs fields also sets the mixing of the charged Higgs components of the doublets, thereby guaranteeing cancellation and the absence of this vertex at tree-level.

2.2.6 Renormalisation in the MSSM

In a manner exactly analogous to the Standard Model, supersymmetric (SUSY) models such as the MSSM and its extensions also have particle masses, couplings, mixings and gauge couplings which depend on the energy scale. However with additional particle content relative to the Standard Model this running of parameter values is altered, whilst the fundamental values of parameters matched onto the Standard Model or MSSM may also vary.

In generating the spectra of the MSSM, as performed by the `SoftSusy` spectrum generator, before the decay calculator aspect of the program our work has focused upon, one must take boundary conditions for physical masses and parameters at the electroweak scale (usually taken as M_Z); for example the top pole mass, the gauge coupling α in the $\overline{MS}$ scheme and the bottom mass in the $\overline{MS}$ scheme are usual boundary conditions. These boundary conditions then apply to the renormalisation group equation running between M_Z and $M_{\rm SUSY}$ or $M_{\rm GUT}$. These physical parameters are experimentally measured and so include corrections to all orders, in theoretical predictions these must then be matched onto Feynman diagrams up to the required order to extract the fundamental parameters of the theory. Given the MSSM has additional particles and interactions relative to the Standard Model, this means the fundamental theoretical parameters extracted are different. For example, the strong coupling constant α_s may be determined via gluon to quark-antiquark vertices. In the MSSM however there are 1-loop corrections from gluinos to this vertex (see Figure 3.3) in addition to the 1-loop Standard Model corrections, and so after subtracting off the various corrections at the specified loop level, the value extracted in the MSSM will be different from that of the Standard Model. Moreover, there can be different schemes for the mass extraction and different approximations made even within one theory in determining the fundamental parameters, and different numbers of loops included. These parameters are then used in the decay calculator expressions and so differences in numerical values here are a significant source of differences in the decay calculations.

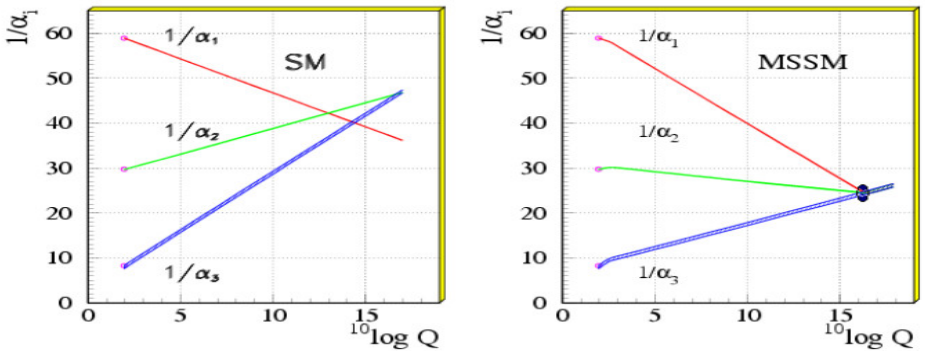

Figure 2.4: Running of the gauge couplings to higher scales in the Standard Model and the MSSM. This demonstrates how gauge coupling unification occurs in the MSSM but not in the SM, with the unification of the three gauge couplings occurring at around $M_{\text{GUT}} \approx 2 \times 10^{16}\,\text{GeV}$. Figure from [72].

Meanwhile, with addition particles, the running of the gauge couplings, as parametrised via the β functions, are also altered in the MSSM relative to the Standard Model. These additional particles typically appear around the TeV scale and so bend the running of the coupling constants beyond this point. The 1-loop expressions for the $\beta(g_i)$ functions in the Standard Model and MSSM are

$$\beta(g_i) = Q\frac{\partial g_i(Q)}{\partial Q} = \frac{\partial g_i(Q)}{\partial \log Q} = \frac{g_i^3}{16\pi^2}b_i, \tag{2.36}$$

where b_i differs for each gauge group and depends on the particle content[11]:

$$b_i = \begin{cases} 4.1, -\frac{19}{6}, -7 & \text{for SM for i=1,2,3;} \\ 6.6, 1, -3 & \text{for MSSM for i = 1,2,3.} \end{cases} \tag{2.37}$$

As a result, running the values of the gauge couplings to higher scales causes differences between the Standard Model and the MSSM. In the Standard Model the gauge couplings never unify, see Figure 2.4. In contrast, in the MSSM, with the altered values of the b_i coefficients (and in particular with the b_2 for the $SU(2)_L$ group changing sign and so running to larger values) Figure 2.4 shows all three gauge couplings unify approximately at a single scale (certainly within the errors that would be caused by corrections at the unification scale). This would indicate unification of the three fundamental forces relevant at particle scales, suggesting some GUT scale complete model arises at around $M_{\text{GUT}} \approx 2 \times 10^{16}\,\text{GeV}$. This is therefore regarded as a further motivation for supersymmetry and the MSSM. Investigations into the running of gauge couplings with different particle content or particle masses can be performed within `SoftSusy` [66].

As an aside, one may ask why the running of the gauge couplings with the log of the scale Q is linear in Figure 2.4, this is straightforward to demonstrate. Given $\alpha_i = g_i/4\pi^2$ then

$$\frac{\partial \alpha_i^{-1}}{\partial \log Q} = -\frac{8\pi}{g_i^3}\frac{\partial g_i}{\partial \log Q} = -\frac{8\pi}{g_i^3}\frac{g_i^3}{16\pi^2}b_i = -\frac{b_i}{2\pi}. \tag{2.38}$$

Therefore the gradient of α_i^{-1} is constant in units of $\log Q$ as observed.

[11] To be precise it should be noted that here the g_i are slightly different to the conventional Standard Model definitions as now $g_1 = \sqrt{5/3}g'$.

2.3 Motivations for Supersymmetry

There are consequently a great many motivations for supersymmetry from a theoretical and phenomenological perspective; this has contributed to its enduring popularity as a Beyond Standard Model theory, even in the face of a lack of discovery at the LHC. We summarise the motivations here, in the context of the MSSM.

2.3.1 Technical Hierarchy Problem and Naturalness

As demonstrated previously in Chapter 1.2, the Standard Model faces a problem of stability of the Higgs mass with respect to loop corrections, which raises questions of the origin of the difference of scales between electroweak and GUT/Planck scale physics and the stability of this scale difference. In Chapter 1.2, we explicitly evaluated the quadratic divergences to the Higgs boson mass m_h caused by the dominant top loop corrections in equation 1.35. If one were to repeat the calculation for the contribution of scalars to the Higgs boson mass, with the the Feynman diagram as shown in top left of Figure 1.3, then the mass correction due to a scalar 1-loop correction is

$$(\delta_{m_h})^2 = \lambda_S \int^{\Lambda} \frac{d^4k}{(2\pi)^4} \frac{1}{k^2 - m_s^2} \sim \lambda_S \int^{\Lambda} \frac{k^3 2\pi^2 dk}{(2\pi)^4} \frac{1}{k^2} \sim \frac{\lambda_S}{8\pi^2} \int^{\Lambda} k dk \sim \frac{\lambda_S \Lambda^2}{16\pi^2}. \tag{2.39}$$

The key differences relative to the fermionic corrections are - there is no minus sign as we have a loop of scalars, there is only one factor of the coupling as the Feynman diagrams involves a single 4-point vertex (c.f. two 3-point vertices for the fermionic case), and there is a factor of two difference arising from the coupling normalisation and lack of taking a trace in the scalar case. Crucially, the sign difference means that, if we can relate the scalar and fermionic couplings such that $\lambda_s = 2\lambda_f^2$ (where λ_f was the top Yukawa coupling y_t in equation 1.35), then the quadratically divergent contributions to m_h will cancel between scalar and fermion contributions, leaving only logarithmic divergences and resolving any issues of naturalness and stability. This is what happens in supersymmetry, each fermion is accompanied by two scalars - the $\tilde{f}_L$ and $\tilde{f}_R$ - in order to have the same number of fermionic and bosonic degrees of freedom in each supermultiplet, giving the necessary factor of two. Meanwhile, supersymmetry relates the fermions and their superpartners, linking their couplings and ensuring the cancellation.

2.3.2 Gauge Coupling Unification

As described in the previous section, Chapter 2.2.6, the gauge couplings unify when run to high scales in the MSSM, suggesting the presence of a GUT-scale UV complete model. This is theoretically satisfying, lending credence to work on grand unified theories (GUTs) and offers an indication of the scales at which new physics must be important in a way that does not arise from the Standard Model.

2.3.3 Dark Matter

One of the key obvious absences from the Standard Model, is its complete lack of any viable candidates for dark matter, as outlined in Chapter 1.2. However, the MSSM and its extensions naturally provide a good dark matter candidate in the case of R-parity conservation. In particular, the lightest supersymmetric particle is then stable, and so if it is neutral and colourless it is then a possible source for the dark matter observed astrophysically. Moreover the supersymmetric particles are generically expected to be WIMP-like ("Weakly Interacting Massive Particle"), given that they occur at masses just a few times the weak scale and with couplings linked to those of the Standard Model by supersymmetry. The requirement of neutral, colourless particles leaves 3 main types of supersymmetric particle which may be the LSP and dark matter - neutralinos $\tilde{Z}$, sneutrinos $\tilde{\nu}$ and gravitinos $\tilde{G}$. $\tilde{\nu}$ dark matter is largely ruled out experimentally [73], whilst LSP gravitino dark matter is possible in gauge-mediated supersymmetry breaking models. In this case constraints are generically weaker due to the very weak couplings of the gravitino, but may be set via long-lived NLSP decays to the LSP gravitino and Standard Model particles. In particular high energy photons produced in this manner would have cosmological effects, whilst gravitino masses in the certain mass ranges may result in displaced vertices at the LHC (see Chapter 4.2.4 for these modes in the `SoftSusy` decay calculator). In any case, collider experiments have focused on the possibility of neutralino dark matter, as this offers the most significant possibility of observation at such experiments. The exact nature of the lightest neutralino, i.e. its precise linear combination of bino, wino and Higgsino, along with its mass and the mass spectrum of the supersymmetric model, will alter its experimental and cosmological properties, and in particular whether or not it has the correct relic abundance in the universe. In the CMSSM, the LSP is usually a bino (as explained later below equation 2.52), this tends to be over-produced and so needs coannihilation with fermions and possibly significant Higgsino fraction to give the right relic abundance. There are many reviews available considering supersymmetric dark matter in great detail, including [74]. In generality, the calculation of the neutralino relic abundances for different supersymmetric parameter space points, and consequent restriction of the parameter space to that with viable dark matter candidates, is very complex. Fortunately however, public codes have been developed to perform this task, including `DarkSUSY` [75–77] and `micrOMEGAs` [78, 79], the latter of which can interface with the `SoftSusy` program.

2.3.4 Higgs mass prediction

In Chapter 1.1.1 we saw that the Higgs mass is not theoretically predicted by the Standard Model, but rather it may only be experimentally measured and input into the theory. In contrast, in the MSSM the Higgs mass is predicted as a function of other parameters of the theory and, as we demonstrated in Chapter 2.2.3.1, bounds may be placed on its mass. Specifically, in equation 2.21 it was shown that a tree-level upper bound of m_Z may be placed on m_h. Given then that the Higgs mass has been measured at the LHC to be $m_h = 125\,\text{GeV}$ [12, 13, 80], this

naively causes problems for the MSSM. In reality however there are also loop corrections to this bound, and given the Higgs couples to Standard Model particles and their superpartners in proportion to the mass of the Standard Model particles, the dominant contributions will be from tops and stops. The calculation of all the radiative corrections to the Higgs mass, including smaller contributions from gauge bosons and from bottoms and taus and their superpartners (which may be important in regions of larger $\tan\beta$), is very involved (excellent reviews of the techniques involved and the results are available in [81, 82]). In general however there are 3 requirements for large radiative corrections to the lightest Higgs boson mass:

- Large stop masses ($m_{\tilde{t}_i}$) increase the loop corrections to the Higgs mass caused by stop loops; these are usually the dominant contributions due to the large top Yukawa coupling. Under various simplifying assumptions ($m_{\tilde{t}_1} = m_{\tilde{t}_2} = m_{\tilde{t}}$ and no stop mixing ($X_t = 0$)) the stop loop contributions can be written as:

$$(\Delta m_h)^2 = \frac{3G_F}{\sqrt{2}\pi^2} m_t^4 \ln \frac{m_{\tilde{t}}^2}{m_t^2}. \tag{2.40}$$

  Whilst this contribution is only logarithmic in the stop mass squared, $m_{\tilde{t}}^2$, it is quartic in the large top mass and so may offer corrections of tens of GeV for stops of masses $m_{\tilde{t}} \sim \mathcal{O}(1\,\text{TeV})$.
- Large stop mixing, parametrised via the mixing parameter $X_t = A_t - \mu \cot\beta$, which is a measure of the amount of mixing between the two stop eigenstates $\tilde{t}_1$ and $\tilde{t}_2$. It may be shown that large mixing $X_t \sim m_{\tilde{t}}$, may increase the stop loop corrections to the lightest Higgs mass by $10 - 15\,\text{GeV}$ in these "maximal mixing" scenarios. The calculations to demonstrate this are somewhat complex and will not be included here, nonetheless the calculations can be performed and demonstrated using the `SoftSusy` spectrum generator [66]. The stop mixing corrections may be written as follows (more details are available in [83]):

$$(\Delta m_h)^2 = \frac{3G_F}{\sqrt{2}\pi^2} m_t^4 \left[\frac{X_t^2}{m_{\tilde{t}}^2} - \frac{X_t^4}{12 m_{\tilde{t}}^4} \right]. \tag{2.41}$$

- Large values of $\tan\beta$ increase the Yukawa couplings of the down type fermions such as the bottoms and taus. This allows the b, τ and their superpartners $\tilde{b}_i$ and $\tilde{\tau}_i$ to also make significant radiative contributions to m_h. Large m_A values are also required to maximise the tree-level Higgs mass. With these conditions the bottom and tau fermion and sfermion contributions may contribute an additional few GeV to the Higgs mass.

In addition to these one-loop effects, there are also 2-loop corrections, scheme dependences and various other effects. In general however, these radiative corrections allow the lightest Higgs mass of the MSSM to reach up to $m_h \sim 135\,\text{GeV}$, thereby providing an explanation of the LHC measured Higgs mass of $125\,\text{GeV}$. This may therefore be seen as a motivation for the MSSM; it should be noted however that reaching the value of the observed Higgs mass is not possible over much of the MSSM parameter space, and so it may be argued that this is

a little unsatisfactory, requiring some tuning. This is in fact one of the motivations for the Next-to-Minimal Supersymmetric Standard Model (NMSSM), described in Chapter 2.4, with the idea being that additional particle content allows m_h to be raised further, contributing an extra positive term to m_h across the parameter space and thereby allowing the observed Higgs mass to be achieved more naturally across the majority of the supersymmetric parameter space. More information on the Higgs mass in the MSSM may be found in the review [84].

2.3.5 Grand Unified Theories, Supergravity and String Theory

Supersymmetry is also a necessary part of many of the most compelling "top-down" models of the fundamental physics of the universe, including many Grand Unified Theories (GUTs). Local supersymmetry allows the formation of supergravity theories, incorporating general relativity into our description of particle physics. Meanwhile string theory, via superstring theories, often requires supersymmetry (or at least simplifies greatly in its presence). These may therefore be seen as theoretical indications of supersymmetry being an important part of the physics of the universe, particularly at high scales; however they offer no reason to suggest supersymmetry should be present at our current collider scales. These models are not relevant to our work in this thesis and so we go into no further details here.

2.4 Next-to-Minimal Supersymmetric Standard Model

Whilst the MSSM may be the most "minimal" of the phenomenologically testable supersymmetric models, it is by no means the sole possibility, indeed a plethora of extensions to the MSSM exist, all offering solutions to additional problems not resolved in the MSSM alone. Popular extensions include the Lepton-Number Violating MSSM ($\not{L}$MSSM) [70, 85–87], the $U(1)$ extended MSSM (UMSSM) [88, 89], Two Higgs Doublet Models (2HDMs) [90, 91] and many others; the only one of direct relevance to this work, and indeed one of the most popular for phenomenology, is the Next-to-Minimal Supersymmetric Standard Model (NMSSM).

The basic idea behind the NMSSM is to add a gauge singlet chiral superfield, S, to the MSSM. A chiral superfield contains an additional fermion - the "singlino" - and two additional scalars. This additional particle content has a significant effect upon the phenomenology; just as in the MSSM (see Chapter 2.2.3), gauge eigenstates with the same quantum numbers mix in electroweak symmetry breaking to form mass eigenstates. Now the additional singlino mixes with the two Higgsinos, the bino and neutral wino of the MSSM to form 5 neutralinos; the NMSSM therefore has an extended neutralino sector. Meanwhile, assuming CP conservation in the Higgs sector (which need not necessarily hold), the additional scalars form one CP even scalar and one CP odd scalar which each mix with the two CP even neutral scalars and the one CP odd neutral scalar of the MSSM respectively, forming an extended Higgs sector of 3 CP even neutral Higgs scalars and 2 CP odd neutral Higgs scalars.

More specifically, we define the NMSSM as the MSSM but with the superpotential now containing additional terms relative to the MSSM superpotential of equation 2.12:

$$W_{\text{NMSSM}} = W_{\text{MSSM}} + \lambda S H_u H_d + \xi_F S + \frac{1}{2}\mu' S^2 + \frac{\kappa}{3} S^3. \tag{2.42}$$

As the superpotential must have dimension 3, this makes the constants λ, κ dimensionless, whilst μ' has dimensions of mass and ξ_F has dimensions of [mass]^2. As the chiral superfield added is a gauge singlet, the singlino and two additional scalars may only interact with non Higgs/Higgsino particles via mixing.

The soft supersymmetry breaking contribution to the Lagrangian also contains extra pieces relative to the MSSM (see equation 2.14) as indicated in equation 2.43:

$$\mathcal{L}^{(\text{NMSSM})}_{\not{\text{SUSY}}} = \mathcal{L}^{(\text{MSSM})}_{\not{\text{SUSY}}} + m_S^2 |S|^2 + \left(\lambda A_\lambda H_u H_d S + \frac{1}{3}\kappa A_\kappa S^3 + \frac{1}{2} m_{S'}^2 S^2 + \xi_S S + h.c.\right). \tag{2.43}$$

The NMSSM consequently introduces several extra parameters: these are the dimensionless Yukawa couplings λ and κ, where λ sets the coupling of the gauge singlet superfield particles to the Higgs chiral superfields; it therefore sets the scalar and neutralino mixing as well as the Higgs and Higgsino mass, whilst κ also contributes to these mixings and mass parameters in both the extended neutralino and extended Higgs sectors. s is the vacuum expectation value of the S singlet scalar, which attains a VEV in EWSB in the same manner as occurs for the two Higgs

doublets; ξ_F and ξ_S are supersymmetry conserving and supersymmetry breaking tadpole terms respectively; μ' is a supersymmetric mass term for the new singlet (analogous to the μ parameter for the two Higgs doublets in the MSSM); m_S is a soft supersymmetry breaking mass for the new singlet; whilst A_λ and A_κ are soft supersymmetry breaking trilinear couplings associated with the new singlet and its interactions with the other two Higgs doublets. As a result of the additional parameters, many extra contributions are made to the corresponding parameters of the MSSM, and so several effective parameters are often defined for ease: $m_3^2 = B\mu$, $m_S^{'2} = B'\mu'$, $\mu_{\text{eff}} = \mu + \lambda s$, $B_{\text{eff}} = A_\lambda + \kappa s$ and $\hat{m}_3^2 = m_3^2 + \lambda(\mu' s + \xi_F)$. The details of this are unimportant for our work, however we have outlined them as these parameters appear in several of the expressions given in this section and later in Chapter 4 as well as in Appendix A.6. As in the MSSM, the parameters may be constrained and linked via considerations of the nature of the minimum of the scalar potential, requiring a minimum which is phenomenologically admissible. This is somewhat more complicated to deal with in the NMSSM as there may be several local minima. We do not go into details here, however they may be found in the excellent review on the NMSSM [92].

The first added term in the superpotential in equation 2.42 enables the singlino to mix with the usual 4 neutralinos of the MSSM forming the extended neutralino sector, so that the Lagrangian term in equation 2.24 becomes:

$$\mathcal{L}_{\tilde{Z}_i} \ni -\frac{1}{2}\left(-i\tilde{B} \quad -i\tilde{W}_3 \quad \tilde{H}_u \quad \tilde{H}_d \quad \tilde{S}\right)\mathcal{M}_{\tilde{Z}_i}\left(-i\tilde{B} \quad -i\tilde{W}_3 \quad \tilde{H}_u \quad \tilde{H}_d \quad \tilde{S}\right)^T, \tag{2.44}$$

where the neutralino mixing matrix previously given by equation 2.25, is now as follows[12]:

$$\mathcal{M}_{\tilde{Z}_i} = \begin{pmatrix} M_1 & 0 & -\frac{g'v_d}{\sqrt{2}} & \frac{g'v_u}{\sqrt{2}} & 0 \\ 0 & M_2 & \frac{gv_d}{\sqrt{2}} & -\frac{gv_u}{\sqrt{2}} & 0 \\ -\frac{g'v_d}{\sqrt{2}} & \frac{gv_d}{\sqrt{2}} & 0 & -\mu_{\text{eff}} & -\lambda v_u \\ \frac{g'v_u}{\sqrt{2}} & -\frac{gv_u}{\sqrt{2}} & -\mu_{\text{eff}} & 0 & -\lambda v_d \\ 0 & 0 & 0 & 0 & 2\kappa s + \mu'. \end{pmatrix} \tag{2.45}$$

Diagonalising this mass matrix then gives each of the 5 physical mass eigenstate neutralinos a singlino component. This may significantly affect the phenomenology of the supersymmetric model, in particular if the LSP is singlino-like then the NLSPs may have long lifetimes, potentially producing displaced vertex signatures in colliders such as the LHC.

As for the Higgs sector of the NMSSM, the same first term of the superpotential also generates mixing of the singlet scalars with the scalars of the MSSM. Therefore we obtain a 3×3 mass matrix in the CP even sector and a 2×2 mass matrix in the CP odd sector (splitting the complex scalar singlet into real and imaginary parts and assuming CP conservation in the extended Higgs

[12]The terms have been rewritten from functions of the variables m_Z, β and θ_W into functions of the variables g, g', v_u, v_d using $\tan\beta = \frac{v_u}{v_d}$, $\tan\theta_W = \frac{g'}{g}$, $m_W = \frac{g}{\sqrt{2}}\sqrt{v_u^2 + v_d^2}$ and $m_Z \cos\theta_W = m_W$, for example $m_Z \cos\beta \sin\theta_W = m_W \frac{g'}{g}\cos\beta = m_W \frac{g'}{g}\frac{v_d}{\sqrt{v_u^2+v_d^2}} = \frac{g'v_d}{\sqrt{2}}$.

sector). The CP even neutral Higgs mixing matrix is now given in equation 2.46 and again must be diagonalised to obtain the masses and mixing matrix between the different eigenbases, where $\mathcal{R}(S)$ has been added as the third component of vectors in this space:

$$\mathcal{M}_{\mathcal{R}(H^0)} = \begin{pmatrix} g^2 v_d^2 + (\mu_{\text{eff}} B_{\text{eff}} + \hat{m}_3^2)\tan\beta & (2\lambda^2 - g^2) v_u v_d - \mu_{\text{eff}} B_{\text{eff}} - \hat{m}_3^2 & \lambda(2\mu_{\text{eff}} v_d - (B_{\text{eff}} + \kappa s + \mu') v_u) \\ (2\lambda^2 - g^2) v_u v_d - \mu_{\text{eff}} B_{\text{eff}} - \hat{m}_3^2 & g^2 v_u^2 + (\mu_{\text{eff}} B_{\text{eff}} + \hat{m}_3^2)/\tan\beta & \lambda(2\mu_{\text{eff}} v_u - (B_{\text{eff}} + \kappa s + \mu') v_d) \\ \lambda(2\mu_{\text{eff}} v_d - (B_{\text{eff}} + \kappa s + \mu') v_u) & \lambda(2\mu_{\text{eff}} v_u - (B_{\text{eff}} + \kappa s + \mu') v_d) & \lambda(A_\lambda + \mu')\frac{v_u v_d}{s} + \kappa s(A_\kappa + 4\kappa s + 3\mu') - (\xi_S + \xi_F \mu')/s \end{pmatrix}. \quad (2.46)$$

Meanwhile, in the NMSSM there are therefore two physical CP odd neutral Higgs bosons (in addition to the usual Goldstone which essentially gives mass to the Z boson), the mass matrix for the two CP odd neutral Higgs bosons of the NMSSM is given in equation 2.47 and must be diagonalised to obtain the masses and mixing matrix. Here the ordering of the gauge eigenstates is $\begin{pmatrix} \mathcal{I}(H_d^0) & \mathcal{I}(H_u^0) & \mathcal{I}(S) \end{pmatrix}^T$.

$$\mathcal{M}_{\mathcal{I}(H^0)} = \begin{pmatrix} (\mu_{\text{eff}} B_{\text{eff}} + \hat{m}_3^2)\tan\beta & \mu_{\text{eff}} B_{\text{eff}} + \hat{m}_3^2 & \lambda v_u (A_\lambda - 2\kappa s - \mu') \\ \mu_{\text{eff}} B_{\text{eff}} + \hat{m}_3^2 & (\mu_{\text{eff}} B_{\text{eff}} + \hat{m}_3^2)/\tan\beta & \lambda v_d (A_\lambda - 2\kappa s - \mu') \\ \lambda v_u (A_\lambda - 2\kappa s - \mu') & \lambda v_d (A_\lambda - 2\kappa s - \mu') & \lambda(B_{\text{eff}} + 3\kappa s + \mu')\frac{v_u v_d}{s} - 3\kappa A_\kappa s - 2m_S'^2 - \kappa\mu' s - \xi_F(4\kappa + \frac{\mu'}{s}) - \frac{\xi_S}{s} \end{pmatrix}. \quad (2.47)$$

The effect of the extended Higgs sector is to significantly alter the phenomenology of the expected Higgs bosons, now there may be a lighter CP odd or CP even Higgs than the Standard Model-like Higgs at 125 GeV. This can significantly affect the decay signatures of the NMSSM as now there may be large invisible widths of the Standard Model-like Higgs to lighter scalar degrees of freedom.

2.4.1 Motivations for the NMSSM

Given all the additional complications of the extra contributions and extended neutralino and Higgs sectors of the NMSSM, the question naturally arises of what the motivations are for disrupting the minimality of the MSSM via the addition of the gauge singlet chiral superfield. In fact, there are two general motivations, both associated with naturalness and fine tuning, with the first more theoretical and the second more phenomenological:

- μ problem of the MSSM - In the MSSM superpotential of equation 2.12, the term $\mu H_u H_d$ introduces an additional dimensionful parameter into the theory as μ has mass dimension 1. This μ parameter therefore sets the mass scale of the Higgses and Higgsinos and consequently must be of order the electroweak scale in order to ensure the H_u and H_d scalars get VEVs after electroweak symmetry breaking of the correct order of magnitude. However, setting μ by hand to this value with no additional explanation is rather unsatisfactory when the origin of the scale of μ is nominally completely independent of the electroweak

scale and would therefore naturally be expected to be of order the cut-off scale M_{GUT} or M_{Pl}. In fact, this is a big problem for the MSSM as it essentially reintroduces naturalness issues involving the hierarchies of scales, the resolution of which in the context of the electroweak scale and the Higgs mass value and stability was a key motivation for supersymmetry.

The NMSSM resolves this issue by allowing the dynamical generation of the μ parameter. In an exactly analogous manner to the generation of fermion masses in the Standard Model (or MSSM) via Yukawa couplings and VEVs of the Higgs doublet(s), we may generate the μ parameter at the EW/SUSY scale when the singlet S gets a VEV s in electroweak symmetry breaking. In order to do this, we must replace the superpotential μ term with a coupling of the singlet to the two Higgs doublets:

$$\mu H_u H_d \xrightarrow{replace} \lambda S H_u H_d \xrightarrow{EWSB} \lambda \langle S \rangle H_u H_d = \lambda s H_u H_d \Rightarrow \mu_{\text{eff}} = \lambda s. \tag{2.48}$$

As the VEV s occurs in EWSB it is naturally at the electroweak scale, avoiding any issues of naturalness. This therefore removes the need to add an additional scale to the theory. The NMSSM therefore resolves the μ problem of the MSSM.

- Higgs mass m_h - In the MSSM in Chapter 2.3.4 we saw that the MSSM provides an explanation of the size of the Higgs mass, in a way the Standard Model is unable to, however it was also apparent that only a small particularly fine-tuned part of the overall supersymmetric parameter space for the MSSM, i.e. one with heavy stops and large stop mixing, was able to reach $m_h = 125\,\text{GeV}$. So once again, in the MSSM we still have the question of why it should be that only a very specific and restricted part of the parameter space seems to have arisen in nature. In the NMSSM however, with the addition of the singlet scalars, we have additional contributions to the Higgs mass m_h. In order to extract the Higgs masses we must diagonalise the mass matrix for the CP even neutral Higgs bosons. In order to obtain an upper bound on the Higgs mass we may rotate the upper 2×2 sub-matrix by an angle β and find:

$$m_h^2 \leq m_Z^2 \Big(\cos^2 2\beta + \frac{\lambda^2}{g^2} \sin^2 2\beta \Big). \tag{2.49}$$

Therefore in the NMSSM there is an additional positive contribution to the upper bound on the Higgs mass set by λ. This raises the obtainable Higgs mass at tree-level such that the upper bound is larger than m_Z, adding on the radiative corrections as in the MSSM then allows $m_h = 125\,\text{GeV}$ to be reached over much of the parameter space of the NMSSM, avoiding any questions of selection of specific regions of parameter space[13].

[13]The overall upper bound, including radiative corrections, on m_h is now $\sim 150\,\text{GeV}$ due to this additional positive tree-level contribution to its mass.

2.4.2 Z_3 invariant NMSSM

There is a clear problem with the NMSSM as we have thus far presented it as a resolution of the μ problem; whilst it is true that we may now dynamically generate a contribution to the μ_{eff} parameter dynamically via the VEV of S, we still must explain why a contribution of the form of the μ term in the MSSM is not present. In addition, we have also added in further dimensionful parameters in μ', ξ_F to the superpotential and corresponding soft supersymmetry breaking dimensionful mass parameters m_3^2, $m_S'^2$ and ξ_S exist in $\mathcal{L}_{\not{\text{SUSY}}}$, all of which must be around the electroweak and SUSY scales with no prior justification, again removing naturalness as a motivation for the NMSSM. Thankfully, one may ban such terms by instead considering the "scale-invariant" NMSSM: by requiring the addition of no new scales to the theory we set $\mu = \mu' = \xi_F = m_3^2 = m_S'^2 = \xi_S = 0$, recovering naturalness. However, we must ban such terms for a good reason - examining the superpotential of the NMSSM given in equation 2.42, it is clear that the dimensionless terms exhibit a Z_3 symmetry which is not present in the dimensionful terms. In other words, as the superpotential is cubic, any transformation of the form $\Phi \to \Phi e^{2\pi i/3}$ on all of the chiral superfields will exclude any terms with dimensionful parameters, leaving only the scale invariant superpotential as this has an accidental Z_3 symmetry.

We can therefore distinguish the general NMSSM, which we have discussed so far, from the Z_3-invariant NMSSM (often referred to as the NMSSM in the literature). The Z_3-invariant NMSSM is naturally scale-invariant, therefore resolving the μ problem of the MSSM whilst retaining naturalness as a motivation. The superpotential for the Z_3-invariant NMSSM is:

$$W_{\text{NMSSM}}^{Z_3} = W_{\text{MSSM}}\Big|_{\mu=0} + \lambda S H_u H_d + \frac{\kappa}{3} S^3. \tag{2.50}$$

However, adding a discrete Z_3 symmetry to the theory also poses problems. After EWSB this Z_3 is spontaneously broken as the scalar fields get VEVs and so the universe would contain regions of space with equivalent (i.e. same vacuum energy) values but different phases of the VEVs v_u, v_d, s, with the VEVs in different regions related by Z_3 transformations. These "bubbles" of different vacua would be separated by domain walls interpolating between the different phase but equivalent solutions and which would contain significant fractions of the energy density of the universe and have observable impacts on the Cosmic Microwave Background. There has been much work on avoiding such issues. Generally it is assumed that the Z_3 is an accidental symmetry and so there is an explicit Z_3 breaking term at late times to break the degeneracy of energy between the different vacuum bubbles and so cause the domain walls to evaporate. This still maintains the ability to effectively ban the scale invariant terms of the superpotential as the Z_3 violation is small. Alternatively, embedding the discrete Z_3 symmetry in a continuous symmetry, for example $U(1)'$ added symmetries in extensions of NMSSM models, can avoid domain walls. More information on these topics is available in references [92, 93].

`SoftSusy` works for both the Z_3-conserving and Z_3-violating NMSSM in both the spectrum generation (i.e. particle mass calculation) and decay calculation aspects of the program. This is detailed further in Chapter 4.

2.5 Supersymmetric Phenomenology

Supersymmetry, as demonstrated diligently throughout this chapter, is therefore a very well theoretically motivated extension to the Standard Model, and consequently has been a very popular model amongst theorists, phenomenologists and experimentalists alike. Nonetheless, the acid test for any theory is its discovery in nature; the LHC experiments at CERN offer an ideal environment to search for low-energy supersymmetry and so there has been a conscientious, meticulous effort since its inception to determine the possible signatures of supersymmetric particles at the LHC. Pedagogical reviews of supersymmetric phenomenology are available in [94,95] and we detail some of the key features of supersymmetry phenomenology in the remaining sections of this chapter.

2.5.1 Searching for Supersymmetry at the LHC

Supersymmetry adds many new particles and interactions to the Standard Model and consequently supersymmetric models offer a rich and varied phenomenology with many different classes of signatures at the LHC. We focus on R-parity conserving signatures, which are the subject of both our work and the majority of the research efforts in this area. As a result, supersymmetric particles are necessarily pair produced. First of all, the supersymmetric particles produced can have direct signatures at the LHC, with charged particles such as squarks, charged sleptons, charginos and charged Higgses all leaving charged tracks, whilst coloured particles such as gluinos or squarks will produce jets of QCD particles. In general however, these direct signatures are not the optimal means by which to search for supersymmetric particles as they sit on top of very large backgrounds of charged particles and QCD objects of the Standard Model produced naturally and copiously in a hadron-hadron collider. Consequently, indirect searches for supersymmetric particles afford the greatest potential for their discovery.

Regardless of the type of supersymmetric particle produced, under the assumption of R-parity conservation, each supersymmetric particle must decay into an odd number of supersymmetric particles (in addition to Standard Model particles). Given decays producing fewer particles are kinematically favoured (see Chapter 3.1), this results in each supersymmetric particle produced decaying into a supersymmetric particle and a Standard Model particle in a "2-body" decay. This process continues in a cascade of decays until the LSP (lightest supersymmetric particle) is produced, which must be stable by R-parity. Each of these cascades of decays is typically very prompt in the absence of both unnaturally small couplings and any kinematic suppression such as small mass differences, all occurring within the body of the LHC detectors. As a result, a signature for a broad array of supersymmetric models at the LHC is missing energy and momentum corresponding to a neutral (and hence undetectable) LSP particle carrying energy and momentum out of the detector. Given hadron-hadron colliders have no control over the longitudinal momentum of a given event (as it is set via the parton distribution functions determining the momentum fractions of the colliding partons), the signature is re-

ferred to as missing transverse energy/momentum ("MET"). Whilst Standard Model processes involving neutrinos will also produce MET, this is typically much less than would be expected from supersymmetric cascades of decays. The MET produced in the supersymmetric cascades will also typically come with multi-jet and/or multi-lepton signatures arising as Standard Model by-products from the cascade of decays to the LSP, see Figure 2.5 for an example.

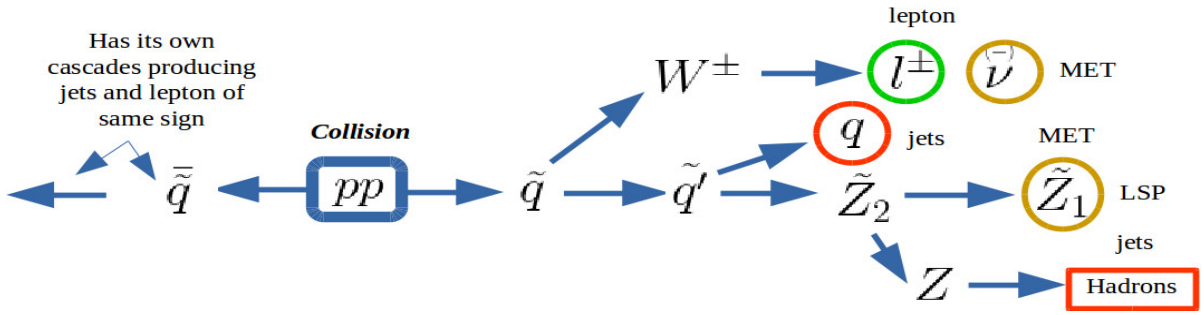

Figure 2.5: Supersymmetric particles pair-produced in proton-proton collisions at the LHC each cascade down to the LSP (usually the lightest neutralino $\tilde{Z}_1$) producing missing transverse energy and momentum (MET) along with other signatures. In the cascade given here each supersymmetric decay chain produces a lepton and jets and therefore the overall signature for the pair production is MET + jets + same sign dileptons (same sign dileptons have a small Standard Model background).

The specifics of which particles are produced, which decay modes are dominant, which are suppressed and the like are very much dependent on the model parameters, the mass spectrum and the admixtures of gauginos and Higgsinos in the electroweakinos. Indeed the `SoftSusy` decay calculator is specifically designed to perform the decay calculations for any supersymmetric parameter point of the MSSM or NMSSM in order to guide experimental searches for superparticles as to which decay modes are most promising or most constraining. Nonetheless, general points can be made - in particular there are a range of signals which occur for broad ranges of (N)MSSM parameters; whilst given the importance of the supersymmetric cascade decays to the LSP for supersymmetric searches, generic comments can be made which depend largely only on the nature of the LSP, which can have a notable impact on the phenomenology.

The LHC is generically able to place stronger bounds on the strong production of supersymmetric particles ($\tilde{g}$, $\tilde{q}$) than on electroweakinos ($\tilde{W}_j^{\pm}$, $\tilde{Z}_i^0$). This occurs as coloured supersymmetric particles are easier to search for, producing more jets and usually more MET than the lighter electroweakinos due to their heavier masses, whilst also tending to be more copiously produced at a hadron-hadron collider. For this reason, searches for neutralinos and charginos frequently have to use lepton signatures to suppress backgrounds, but even so produce less stringent bounds.

The LSP is a key aspect of supersymmetric phenomenology and so its composition (i.e. its amounts of each of the gauginos and Higgsinos) as well as that of the other light electroweakinos has important effects on the nature of the decays which occur and accordingly on the Standard Model products produced, which determines the lepton signatures, jet activity and other features. The gauge eigenstates of the electroweakinos are related by supersymmetry to their su-

perpartner electroweak gauge bosons and the Higgs bosons; as these all interact differently with different particles, so do the electroweakinos. Consequently the fraction of each electroweakino gauge eigenstate in the mass eigenstates for the lighter neutralinos and charginos affects their interactions and decays. These considerations may allow more precise searches for given model points or more information to be gleaned for given signatures. This situation is complicated further in the NMSSM, where the neutralinos may also have singlino components, as these couple to non-Higgs boson particles only via mixing, neutralinos with large singlino components will interact very weakly, allowing long-lived NLSPs in the case where the LSP is dominantly singlino. These NLSPs may then produce displaced vertex signatures. In general the admixtures of singlino will also reduce the rates of decays and reduce branching ratios, making searches more difficult.

Given the large extent of the supersymmetric parameter space, even within the MSSM, assumptions are often made simplifying the setup and phenomenology of the associated models. In particular, insight into the nature of the LSP in different models is welcome given its key importance to the phenomenology. One such common assumption is "gaugino mass unification", given in supersymmetry the gauge couplings unify at a high scale it is often also assumed the gaugino masses unify, for example in the Constrained MSSM (CMSSM) a common gaugino mass of $M_1(\text{GUT}) = M_2(\text{GUT}) = M_3(\text{GUT}) = m_{\frac{1}{2}}$ is taken. This assumption has important consequences as the ratios of the gaugino masses to their gauge couplings, $\frac{M_i}{g_i^2}$ are fixed as the scales are changed as a result of the form of the 1-loop β functions. The proof is straightforward and is summarised here. In Chapter 2.2.6 in equation 2.36 we gave the MSSM 1-loop β functions (for the gauge couplings) in terms of the scale Q, if we were to derive the β function for the gaugino masses at 1-loop we would obtain

$$\beta(M_i) = \frac{\partial M_i(Q)}{\partial \log Q} = \frac{1}{8\pi^2} g_i^2 M_i b_i. \tag{2.51}$$

Then combining the β functions for the gauge couplings and their matching gauginos we then observe the β functions for the ratios $\frac{M_i}{g_i^2}$ are 0:

$$\beta\Big(\frac{M_i}{g_i^2}\Big) = \frac{\frac{\partial M_i}{\partial \log Q} g_i^2 - M_i \frac{\partial g_i^2}{\partial \log Q}}{g_i^4} = \frac{\Big(\frac{1}{8\pi^2} g_i^2 M_i b_i\Big) g_i^2 - M_i 2 g_i \Big(\frac{g_i^3}{16\pi^2} b_i\Big)}{g_i^4} = 0. \tag{2.52}$$

The result of this is that, under the assumption of gaugino mass unification, given the gauge couplings also unify at M_{GUT}, the ratios $\frac{M_1}{g_1^2} = \frac{M_2}{g_2^2} = \frac{M_3}{g_3^2}$ are fixed at all scales. Consequently the ratio $M_1 : M_2 : M_3$ is approximately $1 : 2 : 7$ at all scales and therefore the gluino will be the heaviest gaugino and the lightest neutralino (LSP) will be dominantly bino. This allows us to make largely model independent comments about gluinos producing more boosted events (and hence more MET) than electroweakinos, whilst having a dominantly bino LSP also affects the signatures of the supersymmetric cascades of decays. Having a dominantly bino LSP can however cause problems astrophysically as it interacts weakly and so freezes out with relic

abundance larger than that expected for dark matter - it must therefore be further depleted by some resonance in its interactions or via coannihilation. More detail about the dark matter phenomenology of different supersymmetric LSPs can be found in [96]. However, given the lack of discovery of gluinos, and the consequent stringent bounds placed on the gluino mass, the lightest possible gluino mass is ever-increasing, under the assumption of gaugino mass unification this pushes up the values of the bino and wino masses too; contrastingly however, the Higgsinos can never be too heavy as, to avoid unacceptably large fine-tuning, they must always be of order the electroweak scale. Therefore it is becoming increasingly favoured to have Higgsino-like LSPs [97], whose phenomenology is significantly different - for example Higgsinos tend to be under-produced as a result of large annihilation cross-sections, whilst as the masses of the gauginos all increase the lighter electroweakinos become more and more dominantly Higgsino and accordingly have smaller mass splittings. This ensures 3-body and phase-space suppressed decays become more likely, perhaps offering displaced vertex signatures.

There are, nonetheless, specific setups in which other LSP types are dominant. One classic example is that in Anomaly-mediated supersymmetry breaking models the gaugino masses are found in approximate proportion to their β functions (i.e. the b_i coefficients of equations 2.36 and 2.37), ergo the lightest electroweakinos are predominantly wino and nearly degenerate. As a result, decays of the lightest chargino $\tilde{W}_1^{\pm}$ to the lightest neutralino $\tilde{Z}_1^0$ may be 3-body phase-space suppressed decays, or even produce pions. These decays therefore require special treatment and offer interesting signatures such as kinks and disappearing tracks. This setup is consequently included in the `SoftSusy` decay calculator and more information is given later in Chapter 4.2.5. There is also the possibility of gravitino LSPs in supergravity models. As described in Chapter 2.1.3, in GMSB models the gravitino is often the LSP, therefore NLSP decays to the gravitino LSP and a Standard Model particle (photon, Z, Higgs, gluon or fermion depending on the NLSP particle) become important, the weaker interactions present for a gravitino enable the possibility of displaced vertex signatures. This configuration is also available in the `SoftSusy` decay calculator and so is described further in Chapter 4.2.4.

Of course, this discussion of the importance of the LSP for supersymmetric phenomenology is nominally redundant in the case of R-parity violating (RPV) models. However with small RPV some of this may still hold as the LSP may be stable on the scales of the size of the LHC detectors; alternatively RPV decays of the LSP to Standard Model particles may allow unusual displaced vertex and other signatures. Nonetheless, RPV models are not included in our decay research and so we make no further mention of these.

In addition to these searches for specific decay signatures or specific final state LSPs, the indirect effects of supersymmetric particles as intermediates or in loops can also be sought in otherwise purely Standard Model processes. One means of searching for supersymmetric intermediates in a general manner is to perform searches for resonances looking for the effects of new species of intermediate particles affecting the differential distributions of known Standard Model processes. In these searches, sharp peaks are searched for in the invariant mass spectra of Standard Model particles, with the idea being that if these are produced via intermediate

unknown particles one would expect a Breit-Wigner type resonance (see equation 3.3 in Chapter 3.1) in the production cross-section as the intermediate particle decays into the observed Standard Model particles. This type of search was crucial in the discovery of the Higgs boson in the diphoton invariant mass spectrum [12, 13].

As the main discovery of the LHC era, the discovery of the Higgs boson itself offers the opportunity to search for an extended Higgs sector, whilst the Standard Model loop decays of the Higgs boson to two photons, two gluons or a Z boson and a photon may be measured to test for additional contributions from supersymmetric particles. For example, whilst in the Standard Model the $h \to \gamma\gamma$ 1-loop decay only has dominant contributions for fermions (of which top is dominant due to its Yukawa coupling) and gauge bosons running in the loop, in the MSSM and NMSSM there are also contributions from charginos, charged Higgses and sfermions; similar considerations hold for the $h \to Z\gamma$ decay, the Feynman diagrams are given in Figure 2.6. The contributions and expressions for the partial widths of these modes are listed in the expressions A.150 to A.204 in Appendix A.3.6. So far, no evidence for additional contributions to these Standard Model loop processes has been observed, with the $h\gamma\gamma$ coupling agreeing with the Standard Model within errors [98], whilst the $hZ\gamma$ coupling is yet to be observed with only an upper bound of 6.6 times the Standard Model prediction currently set [99]. Both modes are targets for more precise measurements in the remainder of run II of the LHC and in future runs.

In fact, the situation is more complicated in examining the decays and couplings of the Standard Model Higgs, as it is expected that the lightest Higgs of the MSSM, or the NMSSM eigenstate corresponding to the 125 GeV observation (which in the NMSSM may not be the lightest Higgs), is in the decoupling limit where all the supersymmetric mass parameters and the CP odd Higgs mass m_A are all large compared to the electroweak scale. In this limit, the decays and couplings of the supersymmetric Higgs at 125 GeV tend to that of the Standard Model Higgs, making distinguishing the (N)MSSM from the Standard Model potentially difficult [100]. This decoupling with increasing mass of the supersymmetric particles also enables the MSSM to replicate the Standard Model results for electroweak precision tests, thereby foregoing potential discrepancies. As a result of such possible similarities between the supersymmetric Higgs at 125 GeV and the Standard Model Higgs, searches for higher mass resonances in the same outgoing states produced by the 125 GeV Higgs but at much larger masses are performed in order to search directly for the heavier Higgs bosons of the extended Higgs sector of the (N)MSSM. Nonetheless, as of yet there have only been exclusion limits set [101].

Further information on the contributions to Standard Model and MSSM Higgs loop decays, and on Higgs physics in general in the Standard Model and supersymmetric extensions, can be found in the excellent book [102] and in the relevant partial width formulae in Appendices A.3.6, A.6.1 and A.6.2 of this thesis, as well as in the figures in Chapter 4.2.2.

All of these varieties of signals of supersymmetry are being searched for at the LHC, there are therefore two main overall goals of the LHC at run II and beyond from the point of view of

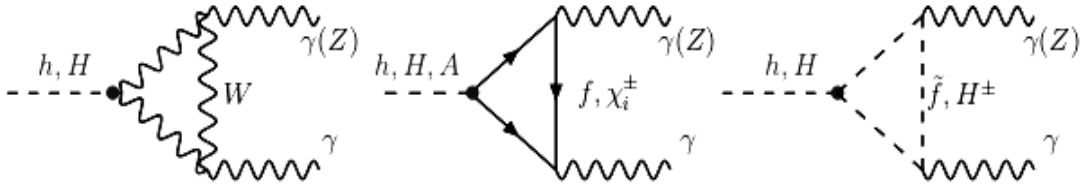

Figure 2.6: The dominant contributions to the $h \to \gamma\gamma$ and $h \to Z\gamma$ decays, these are W loops and fermion loops in the Standard Model. There are additional loop particles in the MSSM, however in practice sfermion, charged Higgs and chargino ($\chi_i^\pm$ in this notation means $\tilde{W}_i^\pm$) loops all have negligible effects as LHC bounds restrict their masses to large values. There are also crossed versions of these diagrams for the diphoton mode.

supersymmetry searches[14].

- Further inclusive and exclusive searches at yet higher energies looking for new BSM particles, via their decays to Standard Model and other supersymmetric particles. Included in this is the possibility of finding dark matter candidates.
- Study the discovered SM-like Higgs boson with greater precision, looking at its decays for deviations from the Standard Model. Loop decays are particularly important here as they can tell us about contributions of heavy particles yet to be discovered. Also search for the possibility of an extended Higgs sector via resonances in Higgs decay products or Higgs decay widths.

All of this requires knowledge of the decays predicted in supersymmetric models, in particular in the MSSM and extensions such as the NMSSM, in order to compare the LHC data with theoretical predictions and allow efficient search strategies to be carried out. This is the motivation behind the computational tools developed to produce decay tables for supersymmetric and Higgs particles, such as the `SoftSusy` program decay calculator that we have focused our research on, which is described in Chapters 3 and 4.

2.5.2 Experimental constraints

The foremost challenge to supersymmetry is that whilst it is very well motivated theoretically, there has been no direct evidence for it experimentally; rather there is only indirect evidence when experimental measurements are cast in a theoretical light (naturalness, gauge unification, dark matter and the like). If supersymmetry is to be discovered it would therefore represent a tremendous theoretical insight into the nature of our physical world. However, as of yet, despite significant efforts there have been no verifiable signs of supersymmetric particles or their effects. This lack of observation is used to put bounds on sparticle masses; which are summarised in their current form in Table 2.3.

[14]Outside of specific supersymmetry research, there is also the ambition of measuring Standard Model processes to greater precision in order to extend our knowledge of the Standard Model, whilst also enabling possible deviations from the Standard Model to be discovered which may offer hints of the form of new physics present. This aim is a motivation for our work in the second half of this thesis in Chapters 5, 6 and 7 on transverse momentum spectra and resummation.

Particle		Exclusion at 95% CL (i.e. lower bound on mass)	Reference
gluino	$\tilde{g}$	1.85 TeV	[103]
lightest stop	$\tilde{t}_1$	1 TeV	[104]
lightest sbottom	$\tilde{b}_1$	860 GeV	[105]
squarks of first two generations	$\tilde{q}$	1.55 TeV	[106]
lightest neutralino (LSP)	$\tilde{Z}_1^0$	650 GeV	[107]
lightest chargino/second lightest neutralino	$\tilde{W}_1^{\pm}/\tilde{Z}_2^0$	1.1 TeV	[107]
Heavier CP odd neutral Higgs	A	440 GeV	[108]
sleptons	$\tilde{l}$	500 GeV	[107]

Table 2.3: Bounds on the various supersymmetric and Higgs particles of the MSSM by the ATLAS experiment. These bounds are at 95% confidence level (approximately 2σ) and each rely on a series of assumptions and so are only a guide to the approximate order of the mass range searched, in particular they rely on the masses of other supersymmetric particles. There are many different searches and exclusion limits set for each particle depending upon the model assumptions made and channels searched. Moreover an extensive search was not performed to produce the table, the limits are those available at [109].

These bounds present potential problems given the motivation for supersymmetry to resolve problems of naturalness. There are nonetheless possible explanations for the non-discovery of sub-TeV mass sparticles including RPV (which causes reduced missing energy by allowing the LSP to decay) and degenerate/compressed spectra (which reduces the transverse momentum in final states due to small mass splittings between initial and final state particles), as well as a variety of other supersymmetry (SUSY) models. In addition it may simply be that supersymmetry is present at slightly higher scales, out of the reach of the LHC in its current form.

In reality, these stated limits are in any case at best a guide: they depend on the model, assumptions and the masses of the other supersymmetric particles. They should consequently be viewed as the highest mass possible to exclude thus far rather than the lowest mass at which the specific supersymmetric particles may exist. Given the vastness of even the MSSM parameter space, rigorously excluding all possible models is very difficult and possibly even out of reach of the LHC. Rather, the experimental data are typically viewed in the light of a set of assumptions in order to simplify the setup, but which restrict the exclusions to specific models. For example, the experimental data are often viewed in the context of simplified models where the MSSM parameter space is reduced to a two dimensional plane, whilst branching ratios are often assumed to be 100% and direct decays to the LSP are usually assumed. All of these assumptions are invalid for many different regions of supersymmetric parameter space, the masses of the other supersymmetric particles not included in the two-dimensional reduction may be such that the specific decay mode searched for may be suppressed, whilst there may alternatively be many different relevant decay modes for the particle considered which would reduce its branching ratio for the mode assumed. Furthermore, as we have seen, supersymmetric decays do not come in isolation and instead take many steps to decay to the LSP in cascades of decays. These factors all significantly affect the phenomenology and signatures and likely reduce the exclusion reach

in the case of realistic models. Indeed, it is for these reasons and more that programs such as `SoftSusy` are desired in order to allow the examination of experimental data in the context of the full supersymmetric model theoretical predictions without such assumptions built in.

The LHC experiments do however also place model-dependent constraints for some of the more popular, reduced parameter space supersymmetric models. In particular, much of the early Run I work of the LHC focused on the Constrained Minimal Supersymmetric Standard Model (CMSSM), which features unified scalar masses, unified fermion masses, and unified trilinear couplings at the GUT scale and so reduces the parameter space to just 5 variables M_0, $M_{\frac{1}{2}}$, A_0, $\tan\beta$ and $\text{sign}(\mu)$. Consequently this model has now been largely ruled out around electroweak scales (see [110, 111]), although again there are various assumptions and caveats folded into these exclusion limits. At Run II there has correspondingly been a large focus on the "Phenomenological MSSM" (pMSSM), an enlarged model relative to the CMSSM and which has 19 free parameters. It is a bottom-up model based on taking the entire MSSM parameter space and making only assumptions based on reasonable expectations and required consistency with observed data elsewhere; it therefore assumes there are no new sources of CP violation relative to the Standard Model[15], no Flavour Changing Neutral Currents (FCNCs) added and assumes first and second generation universality. Given this parameter space is much much larger than the CMSSM, the exclusions placed on it are much less stringent and it is very experimentally challenging to rigorously exclude. For phenomenological studies of the pMSSM model exclusions from the LHC see [112]. There are further additional assumptions which can be made in order to simplify the parameter space further or explain to some degree the lack of CP or flavour violating effects. For example, "universality" (and reality) of soft parameters takes the scalar mass-squared matrices as proportional to the identity in the basis of the quark mass matrices (and takes the trilinear coupling matrices as proportional to the Yukawa matrices), whilst "alignment" takes them to be diagonal (or almost diagonal) in the basis of the quark mass matrices; both assumptions allow the scalar matrices to be diagonal in the required bases and thereby eliminate any FCNCs, whilst the matrices are also real eliminating any additional CPV. Alternatively, one may wish to be generic in the flavour structure and instead argue the masses of the first two generations of squarks are decoupled, being much higher than the electroweak scale (typically tens of TeV) so that loop effects causing FCNCs are suppressed. In this scenario one should endeavour to leave third generation squarks and gauginos around the TeV scale to continue to resolve issues of technical hierarchy, whilst Higgsinos must always be around the electroweak scale in order to set the Higgs mass of the correct order[16], though the hierarchy of supersymmetric masses may then be regarded as unnatural.

[15]The "SUSY CP Problem" is the question of why, given that most of the parameter space would introduce extra CP violation, there in fact appears to be little additional CP violation relative to the Standard Model. There is a similar "SUSY Flavour Problem" of why there are no large Flavour Changing Neutral Currents (FCNCs) arising from large off-diagonal elements in sfermion mixing matrices.

[16]If instead only gauginos and Higgsinos are left around the 1 TeV scale and third generation sfermions are also made heavy then one has a model of "Split Supersymmetry" [113].

Chapter 3

SoftSusy Overview

In this chapter and the next, we discuss our work on the `SoftSusy` program and the development of a decay calculator program which determines the branching ratios for supersymmetric and Higgs particles at the LHC. Further details are available in our paper associated with this work [1].

3.1 Particle Decays

As we have underlined in Chapter 2, decays are the key to experimental signatures of supersymmetry at the LHC, and form a crucial part of our work in this area. Therefore, ahead of the description of the research performed in the development of the decay calculator program for `SoftSusy` in the rest of the chapter and in Chapter 4, we provide a summary of particle decay theory in this context; more information is available in [16, 33, 114]. In our description in this section and the rest of the thesis, we classify decay modes according to both the number of daughter particles (with n-body meaning n decay products) and the order of the corrections included, i.e. tree-level, 1-loop or 2-loop.

Particles and their interactions are inherently quantum mechanical in their behaviour, therefore when considering particle interactions we may begin with Fermi's Golden Rule of quantum mechanics for the transition from one quantum mechanical state to another:

$$\Gamma_{fi} = 2\pi |T_{fi}|^2 \rho(E_i) = 2\pi \int |T_{fi}|^2 \delta(E_i - E) dn. \tag{3.1}$$

This describes the transition probability to go from one quantum mechanical state $|i\rangle$ to the state $|f\rangle$ in terms of the transition matrix element T_{fi} between the states and the $\rho(E_i)$ density of available states, encapsulating the physics of the transition and the number of possible equivalent transitions respectively. In this case, the integral ensures that all states are integrated over, whilst the delta function imposes energy conservation on the allowed states. The transition matrix element may be expanded, in the limit of weak interactions, as a perturbative expansion, essentially expanding the transitions order-by-order as is often done for expressions in quantum field theory.

We may then generalise this expression to the case of particle interactions in quantum field theory; in this case the transition matrix element and integral over states become the matrix element and integral over available phase space. In the case of a 2-body decay we now integrate

over the 3-momenta of the outgoing particles and ensure energy and momentum conservation with appropriate delta functions:

$$\begin{aligned}\Gamma(i \to f_1 f_2) &= \frac{(2\pi)^4}{2E_i} \int |M_{fi}|^2 \delta(E_i - E_{f1} - E_{f2}) \delta^3(\mathbf{p}_i - \mathbf{p}_{f1} - \mathbf{p}_{f2}) \frac{d^3\mathbf{p}_{f1}}{(2\pi)^3 2E_1} \frac{d^3\mathbf{p}_{f2}}{(2\pi)^3 2E_2} \\ &= \frac{(2\pi)^4}{2E_i} \int |M_{fi}|^2 \delta^4(p_i - p_{f1} - p_{f2}) \delta(p_{f1}^2 - m_{f1}^2) \delta(p_{f2}^2 - m_{f2}^2) d^4p_{f1} d^4p_{f2}.\end{aligned} \tag{3.2}$$

The matrix element M_{fi} contains the particle physics of how the interaction (here the decay) occurs, whilst the integration over the 3 or 4-momenta of the final states (i.e. over the phase space) sums up all the possible ways the interaction could occur, whilst ensuring 4-momentum conservation, thereby encoding the kinematics behind the calculation. In the second step here we rewrote the 3-momentum integrations in terms of integration over the entirety of a 2-dimensional 4-momentum phase space with additional delta functions ensuring the 4-momenta square to the mass squared of the particles considered. This simplifies the calculation as the matrix element and phase-space integration are both Lorentz invariant, and so may be evaluated separately in any frame and once only. All frame dependence occurs in the prefactor of the integral via the $1/E_i$ which provides the necessary factor expected - the decay rate is inversely proportional to the energy due to relativistic time dilation effects.

Such integrals of the matrix elements over phase space must be evaluated for each possible decay for each decaying (parent) particle. Each particle may however interact in a number of ways, therefore there are many possible decay modes for each parent particle, which all must be summed to give the total decay rate of the particle. This is termed the total "decay width" (Γ) of the particle, which is the inverse of the particle lifetime τ. The decay width is so-called as it is related to the form of resonances in the production of unstable particles, for example at colliders, with the energy spectrum for the production of an unstable particle of mass M and decay width Γ set by the Breit-Wigner form:

$$f(E) = \frac{k}{(E^2 - M^2) + M^2\Gamma^2}. \tag{3.3}$$

The total decay rate of a particle is consequently referred to as its "decay width" as Γ sets the full-width at half-maximum of the energy distribution of the decaying unstable particle. Each of the decay widths of the individual decay modes are then "partial widths" (PWs) (Γ_i), and so the probability of a specific decay mode occurring for a given parent particle is expressed as the "branching ratio" (BR) for that decay mode and is simply the ratio of the relevant partial width to the total width:

$$BR = \frac{\Gamma_i}{\Gamma}. \tag{3.4}$$

In the sample case of our 2-body decay $i \to f_1 f_2$ considered above, we may perform the

integrals present, first the 3-momentum conserving δ function removes the $d^3\mathbf{p}_2$ integral:

$$\Gamma(i \to f_1 f_2) = \frac{1}{8\pi^2 E_i} \int |M_{fi}|^2 \delta(E_i - E_{f1} - E_{f2}) \frac{d^3\mathbf{p}_{f1}}{4E_{f1}E_{f2}}. \tag{3.5}$$

Then as the integral is Lorentz invariant we choose to evaluate it in the centre of mass frame of the decaying particle so that $E_i = m_i$ and $E_{f2} = \sqrt{m_{f2}^2 + p_{f1}^2}$, and we convert to spherical polar coordinates, $d^3\mathbf{p}_{f1} = p_{f1}^2 dp_{f1} d\Omega$:

$$\Gamma(i \to f_1 f_2) = \frac{1}{8\pi^2 m_i} \int |M_{fi}|^2 \delta\Big(m_i - \sqrt{m_{f1}^2 + p_{f1}^2} - \sqrt{m_{f2}^2 + p_{f1}^2}\Big) \frac{p_{f1}^2 dp_{f1} d\Omega}{4\sqrt{m_{f1}^2 + p_{f1}^2}\sqrt{m_{f2}^2 + p_{f1}^2}}. \tag{3.6}$$

The integral may then be performed using the property of the delta function

$$\delta(f(x)) = \left|\frac{df}{dx}\right|_{x_0}^{-1} \delta(x - x_0), \tag{3.7}$$

which assumes there is only one root (zero) of the function $f(x)$ at x_0. If there are multiple roots these must be summed over. Applying this leads to the standard expression for the integral of a function of a variable with a delta function of the same variable:

$$\int g(x)\delta(f(x)) = g(x_0) \left|\frac{df}{dx}\right|_{x_0}^{-1}. \tag{3.8}$$

Consequently our expression in equation 3.6 may be considered as:

$$\Gamma(i \to f_1 f_2) = \frac{1}{8\pi^2 m_i} \int |M_{fi}|^2 \delta(f(p_{f1})) g(p_{f1}) dp_{f1} d\Omega = \frac{1}{8\pi^2 m_i} \int |M_{fi}|^2 \left|\frac{df}{dp_{f1}}\right|_{p^*}^{-1} g(p^*) d\Omega, \tag{3.9}$$

where $f(p_{f1}) = m_i - \sqrt{m_{f1}^2 + p_{f1}^2} - \sqrt{m_{f2}^2 + p_{f1}^2}$ and $g(p_{f1}) = \frac{p_{f1}^2}{4\sqrt{m_{f1}^2+p_{f1}^2}\sqrt{m_{f2}^2+p_{f1}^2}}$.

Therefore $\frac{df}{p_{f1}} = -\frac{p_{f1}}{\sqrt{m_{f1}^2+p_{f1}^2}} - \frac{p_{f1}}{\sqrt{m_{f2}^2+p_{f1}^2}}$, where x_0 is now p^* and is the value of the outgoing particle 3-momenta when the centre of mass momentum is 0, and so:

$$\Gamma(i \to f_1 f_2) = \frac{1}{8\pi^2 m_i} \int |M_{fi}|^2 \frac{p^*}{4(E_{f1} + E_{f2})} d\Omega = \frac{1}{8\pi^2 m_i} \int |M_{fi}|^2 \frac{p^*}{4m_i} d\Omega = \frac{p^*}{32\pi^2 m_i^2} \int |M_{fi}|^2 d\Omega, \tag{3.10}$$

which is the generic expression for the partial width for a 2-body decay of a parent particle i decaying to two daughter particles f_1 and f_2 in quantum field theory. Straightforward kinematics then reveals that:

$$p^* = \frac{1}{2m_i}\sqrt{[m_i^2 - (m_{f1} + m_{f2})^2][m_i^2 - (m_{f1} - m_{f2})^2]} = \frac{m_i}{2}\tilde{\lambda}^{\frac{1}{2}}(m_i, m_{f1}, m_{f2}). \tag{3.11}$$

The function $\tilde{\lambda}^{\frac{1}{2}}$ is a common kinematic function arising in decay formulae and is given by

$$\tilde{\lambda}^{\frac{1}{2}}(m_i, m_{f1}, m_{f2}) = \sqrt{\left[1 - \left(\frac{m_{f1} + m_{f2}}{m_i}\right)^2\right]\left[(1 - \left(\frac{m_{f1} - m_{f2}}{m_i}\right)^2\right]}. \tag{3.12}$$

Consequently we may rewrite the 2-body decay expression as:

$$\Gamma(i \to f_1 f_2) = \frac{1}{64\pi^2 m_i}\tilde{\lambda}^{\frac{1}{2}}(m_i, m_{f1}, m_{f2}) \int |M_{fi}|^2 d\Omega = \frac{1}{16\pi m_i}\tilde{\lambda}^{\frac{1}{2}}(m_i, m_{f1}, m_{f2})|M_{fi}|^2. \tag{3.13}$$

In the last stage we have assumed no solid angle dependence in the matrix element. In general, in order to complete the derivation for a given mode, one must evaluate the matrix element and integrate over any solid angle dependence. This involves evaluating a trace of Dirac spinors in the usual way for quantum field theory and then converting the dot products into momenta and angles before performing the integration.

In general however, particles may undergo not just 2-body decays, but n-body decays; each additional particle in the final state introduces an extra dimension to the phase space which must be integrated over, the corresponding 3-body decay formula may be straightforwardly written down:

$$\Gamma(i \to f_1 f_2 f_3) = \frac{(2\pi)^4}{2E_i} \int |M_{fi}|^2 \delta(E_i - E_{f1} - E_{f2} - E_{f3}) \delta^3(\mathbf{p}_i - \mathbf{p}_{f1} - \mathbf{p}_{f2} - \mathbf{p}_{f3}) \frac{d^3\mathbf{p}_{f1} d^3\mathbf{p}_{f2} d^3\mathbf{p}_{f3}}{(2\pi)^9 2E_{f1} 2E_{f2} 2E_{f3}}. \tag{3.14}$$

Such expressions are much more complicated to evaluate as they have an additional final state integral. Add to this the need to sum over different intermediates and consider interferences between such different contributions then it is understandable why such integrals are largely performed in the `SoftSusy` decay calculator via numerical integration. The exception to this are the Higgs decays to an on-shell vector boson and off-shell vector boson which goes on to decay into a fermion-antifermion pair; in that case the masses of the final state fermions may be neglected, simplifying the calculation and also giving the problem greater symmetry, which we exploit in determining the integrals.

In fact, the expressions may be generalised to an n-body decay[1] as:

$$\Gamma(i \to f_1 f_2 \dots f_n) = \frac{(2\pi)^4}{2E_i} \int |M_{fi}|^2 \delta^4(p_i - p_{f1} - p_{f2} - \dots - p_{fn}) \prod_{j=1}^{n} \frac{d^3\mathbf{p}_{fj}}{(2\pi)^3 2E_{fj}}. \tag{3.15}$$

Fortunately however, in determining the decays of particles at the LHC we do not have to consider all of the infinite set of many body decays available to each parent particle as every additional particle in the final state suppresses the partial width for that mode. This can be argued qualitatively by considering that every additional particle, whilst offering a new dimension to the phase space, spreads the same total incoming energy-momentum over one

[1] As an aside one can use this to deduce the number of independent variables, or Mandelstams, for a given process with n final state particles. Each additional final state particle has an additional 3-momentum integration whilst there is also overall 4-momentum conservation giving $3n - 4$.

additional particle. Energy-momentum conservation requires that the energies and momenta of the final state particles sum to that of the ingoing decaying parent, however in the phase space integration we integrate each particle over a factor $\frac{d^3\mathbf{p}}{2E(2\pi)^3}$ which essentially represents a fraction of the total energy-momentum in that final state particle. Therefore upon adding a particle to the final state, each such fraction is reduced and overall we therefore suppress the partial width, in fact Figure 4.9 in Chapter 4.2.3 demonstrates the dominance of 2-body modes over 3-body modes due to this suppression. Quantitatively this can be observed by comparing 1-body and 2-body phase space (as in [114]). The phase space for a "1-body decay", where a particle transforms into another particle (this cannot really be observed in quantum field theory as it would just be considered a mixing of particles which is accounted for to obtain the physical eigenstates) would be:

$$dPS_1 = (2\pi)^4 \frac{d^3\mathbf{p}_{f1}}{(2\pi)^3 2E_{f1}} \delta^4(p_i - p_{f1}) = (2\pi)\frac{d^3\mathbf{p}_{f1}}{2E_{f1}} \delta^4(p_i - p_{f1}), \tag{3.16}$$

but, using equation 3.7:

$$\int \delta(E_{f1}^2 - \mathbf{p}_{f1}^2 - m_{f1}^2) dE_{f1} = \int \delta(f(E_{f1})) dE_{f1} = \left|\frac{df}{dE_{f1}}\right|^{-1} = \frac{1}{2E_{f1}}. \tag{3.17}$$

Therefore we may write it instead as an integral over the full 4-dimensional phase space as:

$$dPS_1 = (2\pi) \int d^4 p_{f1} \delta^4(p_i - p_{f1}) \delta(p_{f1}^2 - m_{f1}^2) = (2\pi)\delta(s - m_{f1}^2), \tag{3.18}$$

and changing variables from s to $\sqrt{s}$ via equation 3.7 in the first step, and using $\delta(\alpha x) = \frac{\delta(x)}{|\alpha|}$ in the second we obtain

$$dPS_1 = (2\pi)\delta(\sqrt{s} - m_{f1}) \frac{1}{2\sqrt{s}} = \pi \frac{\delta\left(1 - \frac{m_{f1}}{\sqrt{s}}\right)}{s}. \tag{3.19}$$

The coefficient of this normalised δ function represents the volume of the phase space available for such "1-body" modes and is π, whilst s ensures the dimensions are correct.

Meanwhile for the 2-body case we can similarly extract this coefficient from the expression we derived previously in equation 3.13. The coefficient parametrising the size of the 2-body decay phase space is therefore $(1/16\pi)$ so the presence of the additional particle in the final state suppresses the decay width by $(1/(4\pi)^2)$. A similar suppression occurs for each additional particle in the final state; therefore our work on `SoftSusy` focuses on 2-body decay modes and also 3-body modes in regimes where there are no 2-body modes present.

The form of the kinematic functions produced by the phase space element integration also reveals information about the behaviour of partial widths in compressed spectra where the mass difference between the initial state and the final state $\delta_m = m_i - \sum_{j=1}^{N} m_{fj}$ is small. Take as an example the 2-body phase space element - in these compressed regions their behaviour is

dominated by kinematics, and for the 2-body decay case the kinematic function is $\tilde{\lambda}$ as given previously in equation 3.12. We can consider the behaviour of this function as $m_i \to (m_{f1}+m_{f2})$ to determine how the partial widths behave for compressed spectra. Figure 3.1 plots this function for $m_{f1}+m_{f2} = 300\,\text{GeV}$ in the region $m_{f1}+m_{f2}$ to $5(m_{f1}+m_{f2})$ for different mass differences between the two final state particles. The key feature is the sharp rise in the function in the compressed region near $m_i = m_{f1}+m_{f2}$, here changes of just a few percent in the masses of any of the initial and final state particles can cause the partial width to change considerably, particularly for extremely compressed decays. For example, for final state masses $m_{f1} = 250\,\text{GeV}$, $m_{f2} = 50\,\text{GeV}$ a change of 41% in the partial width arises in changing the initial state particle mass by less than 1% from $m_i = 300.25\,\text{GeV}$ to $m_i = 300.5\,\text{GeV}$. This is due to the change in the $\tilde{\lambda}$ function which behaves as $\tilde{\lambda} \sim \sqrt{\frac{\Delta m}{m_i}}$ as $\Delta m = m_i - m_{f1} - m_{f2} \to 0$ and so the expected factor increase in increasing Δm from 0.25 GeV to 0.5 GeV is $\sqrt{0.5/0.25} = 1.41$ as observed. As a result the accuracy of the mass spectrum predictions, as well as the approximations, schemes and order of the decay calculations, causes significant variations in the partial widths for very compressed spectra. In reality, compressed spectra typically produce 3-body decay modes, rather than 2-body modes as analysed here - nonetheless the conclusions and sensitivity to the mass predictions and decay assumptions are similar. The figure also confirms the expected behaviour that decay modes are forbidden kinematically (as they cannot conserve energy) if the final state particle masses sum to greater than the initial state particle masses, decay modes therefore "turn on" once the sum of the final state particle masses, the threshold, is reached: $m_i \geq m_{f1} + m_{f2} + \ldots m_{fn}$.

In addition to tree-level 2- and 3-body modes, we also consider loop decays and loop corrections where these are phenomenologically important modes or produce important corrections respectively. In general however, the addition of a loop to a process results in an additional integral to be performed over the loop momentum, as well as extra propagator and vertex terms; this additional integral therefore greatly increases the difficulty of evaluating the partial widths. Furthermore, there are often also many loop contributions to the 1-loop expression, meaning many different Feynman diagrams must be evaluated. In any case, all the loop decays and loop corrections in `SoftSusy` are performed explicitly and evaluated analytically. Propitiously for our applications in decay calculators, loop decays and loop contributions and corrections to amplitudes result in an extra factor of $\alpha_i = (g_i^2/4\pi)$ in the matrix element, and so 1-loop decays are typically suppressed relative to tree-level modes by at least factors of $(1/(4\pi)^2)$. As a result, for many of the modes included in `SoftSusy` only tree-level expressions for the partial widths are required. Exceptions occur when the tree-level mode is suppressed or not available and so the first such decay occurs at 1-loop, or when the corrections caused at 1-loop are particularly large - as in some QCD decays as $\alpha_s \sim \mathcal{O}(0.1)$ at collider energies. In particular, we include the 1-loop decays of the Higgs bosons to two photons, to two gluons or to a Z boson and a photon, which are not available at tree-level as the final state contains massless particles, but which are key experimental channels at the LHC. Moreover they are not as suppressed relative to tree-level modes as one might expect due to the Yukawa couplings of the top quark which enhance the

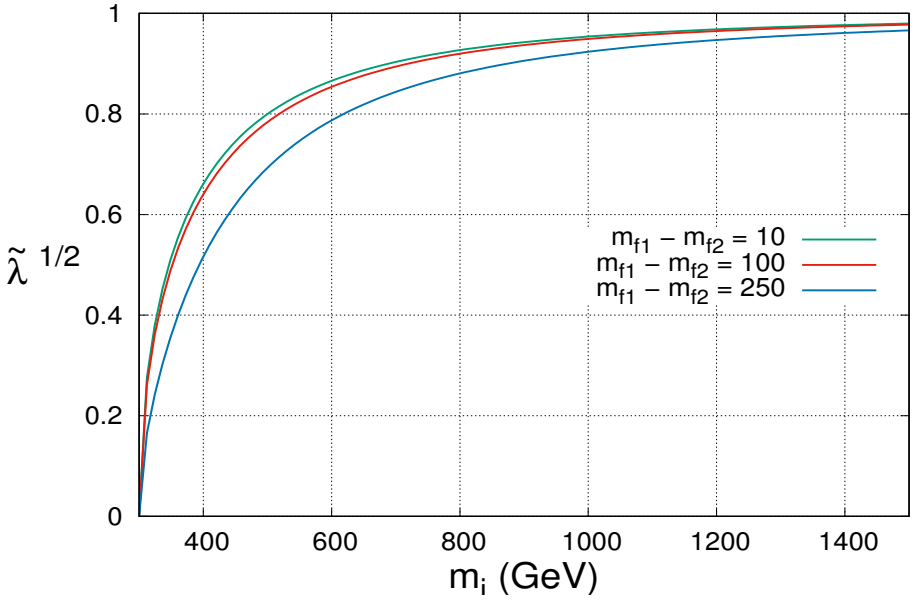

Figure 3.1: The kinematic function which dominates the behaviour of the partial width expressions as the initial and final state masses approach each other, demonstrating the sharp increase and significant dependence on the mass predictions near initial and final state mass degeneracy. This figure is made for the 2-body decay kinematic function $\tilde{\lambda}^{\frac{1}{2}}$ of equation 3.12, nonetheless the conclusions are general. Here the final state masses sum to 300 GeV and the figure demonstrates three different final state mass differences $m_{f1} - m_{f2}$, the kinematic function is plotted as the mass of the initial particle m_i is varied from degeneracy ($m_i = m_{f1} + m_{f2} = 300\,\text{GeV}$), where there is no available phase space, to $5(m_{f1} + m_{f2})$, where large amounts of phase space are available .

top 1-loop contribution by $(m_t/m_h)^2$. We also include beyond Leading Order QCD corrections to the Higgs boson decays to gluons (which is a 1-loop process so these are 2-loop corrections) and to the Higgs boson decays to quarks as it is well known that these have significant effects on the partial widths, reducing the partial widths to bottom and charm quarks by approximately 50% and 75% respectively, whilst increasing the partial width to gluons by around 50% [84,115]. These decay modes to quarks, particularly bottom quarks, are dominant modes for the Standard Model-like Higgs boson and so their accuracy affects all branching ratios significantly, whilst the Higgs to gluon gluon decay amplitude is the reverse of the key gluon gluon fusion production mechanism for the Higgs.

It should also be noted that the factor gained from an additional particle in the final state is approximately the same factor as is gained by adding a loop to an expression, so in regimes where we consider 3-body tree-level modes, 2-body 1-loop modes may be important also, depending on the relative couplings and the kinematics. We will endeavour to add 2-body 1-loop modes in these cases in future developments.

3.2 Decay Calculator Context

In order to produce theoretical predictions for the phenomenology of supersymmetric models at the LHC and elsewhere, several different types of computational tools are required. The analysis flow and different classes of programs needed at each stage of the calculation are summarised in Figure 3.2 and more details are available in [116].

The first stage is the determination of the supersymmetric mass spectrum, i.e. the calculation of the supersymmetric and Higgs particle masses for the model and parameter point considered - this is performed by "Supersymmetric Spectrum Generators", of which `SoftSusy` [66] has been a premier example. `SoftSusy` is able to calculate the particle masses and couplings in the following cases: the R-parity conserving MSSM, with three-loop renormalisation group equations (RGEs) and some leading two-loop threshold corrections to gauge and Yukawa unification [117] (both one order higher than comparable alternative programs); the R-parity violating MSSM [68] including neutrino masses and mixings [69]; or in the R-parity conserving NMSSM [118]. Both the MSSM and NMSSM have two-loop corrections to the squark and gluino pole masses [119] as the production of these strongly interacting supersymmetric particles offers key signatures for supersymmetry at the LHC. `SoftSusy` has therefore developed into a comprehensive, publicly available, key program in the determination of the properties of supersymmetric particles for searches at the LHC. Nonetheless, other programs exist which also determine the mass spectrum of supersymmetric particles in various approximations, and to various degrees of accuracy; for the MSSM there are the codes `FLEXIBLESUSY` [120, 121], `ISASUSY` [122], `SUSEFLAV` [123], `SUSPECT` [124] and `sPHENO` [3, 4], whilst Higgs masses can be calculated in supersymmetric models in `FeynHiggs` [125]. For the NMSSM the choices are more limited, with only one alternative stand-alone program to `SoftSusy` for the spectrum generation: this is the `NMSSMTools` [126–128] program. Nevertheless, the `SARAH` [129] `Mathematica` package (which produces vertices, mass matrices and RGEs for supersymmetric models) can be combined with `FLEXIBLESUSY` or `sPHENO` to calculate the spectrum. Meanwhile, `NMSSMCALC` [130] can be used for the computation of the Higgs masses and decays in the NMSSM.

Following the calculation of the supersymmetric and Higgs masses, as well as their couplings, the next stage is the determination of their decays. This is performed by "Supersymmetric Decay Calculators", and the development of such a program for `SoftSusy` was the primary focus behind our research in this area. The `SoftSusy` decay calculator program can compute the partial widths and branching ratios of supersymmetric and Higgs particles in the MSSM and NMSSM [1], including all tree-level 2-body decay modes as well as 3-body modes at tree-level for the Higgs particles, gluino, chargino and neutralinos, and the phenomenologically crucial 1-loop decay modes of the Higgs particles into two photons, two gluons or a photon and a Z boson. QCD corrections are also included for Higgs decays to quarks (1-loop corrections) and to gluons (2-loop corrections). The decay modes included, implementation, validation and results of the `SoftSusy` decay calculator program that we have written and developed as part of our research in this area are elucidated in much greater detail in the remainder of this chapter and the next. Again,

a variety of alternative programs are available, each able to compute to differing accuracies different subsets of the supersymmetric and Higgs decays for given supersymmetric models. Some programs have incorporated this task into their calculations, such as event generators (described in the next paragraph), however the majority of programs for supersymmetric decay calculation are dedicated tools: foremost amongst them being `SUSYHIT` [131] (itself a combination of two codes, `HDECAY` [132, 133] and `SDECAY` [134]); `FeynHiggs` [125], which determines only the Higgs boson decays; and `sPHENO` [3, 4], which contains a decay calculator for the MSSM along with its spectrum generator. The options for decay calculations in the NMSSM, exactly as for the spectrum generation, are much more limited, with the `NMSSMTools` [126–128] program once more the sole stand-alone option, whilst again `SARAH` [129, 135] can be combined with `sPHENO`. Meanwhile, in the area of Higgs decays of the NMSSM, as well as determining the masses, `NMSSMCALC` [130] can calculate the branching ratios. This includes CP violating effects, which may in general be present in the NMSSM, once more some dominant QCD loop corrections are incorporated.

The information about the mass spectrum and decay widths of the supersymmetric particles may then be passed to event generator programs to simulate the supersymmetric particle events produced at the LHC and elsewhere. "Matrix Element Generators" first simulate the collision of the 2 protons in the LHC beam, producing N particles, these particles are then allowed to shower into hadrons, and decay using the input of the supersymmetric decay calculators to govern the ratio of different decay modes undertaken. The production of such events is generated randomly via Monte Carlo integrations. Examples of such supersymmetric event generator programs include `PYTHIA` [136], `Herwig++` [137, 138] and `SHERPA` [139, 140], all of which carry out both the matrix element generation and the parton showering and hadronisation. This showering and hadronisation produces many Standard Model particles and QCD jets which may also be used as event signatures, depending upon if they can be discriminated from the general large QCD backgrounds which are also produced. There are also specific programs dedicated to matrix element generation, including `MadGraph` [141] (which also then matches the results onto parton showering algorithms), `PROSPINO` [142], and many others. The list here is not exhaustive and only representative of a large area of previous and ongoing research - more can be found in the literature, including in [116].

As well as these cross-section estimates and event production information, in order to confront experimental data with theoretical predictions detector simulations are also required; these impose various cuts, efficiencies and acceptances based on the precise morphology and design of the detector used experimentally. This stage is usually performed partially in the Monte Carlo event generators, but the details of the experimental setup are known only to the relevant collaboration and so further such collider simulations may have to be done "in-house" within the experimental collaborations themselves. Nonetheless, general conclusions can be drawn and searches can often be approximated outside of this by phenomenologists, perhaps using detector simulation tools such as `DELPHES` [143].

In addition to all of this, calculations of specific further observables may also be desired, in

order to address the relevant supersymmetric model or parameter space point with further constraints and evidence outside of the specific signatures simulated. One such class of constraints comes from dark matter and associated observables. As described in Chapter 2, supersymmetric models may provide an LSP as a viable dark matter candidate, several programs are therefore available to calculate the associated dark matter relic density and direct and indirect dark matter detection observables arising from the considered supersymmetric model parameter point(s). Examples of programs that can perform these calculations include `DarkSUSY` [75–77] and `micrOMEGAs` [78, 79].

Further observables not directly related to the collider signatures but which offer indirect collider constraints on supersymmetric models include the $b \to s\gamma$ branching ratio, which is sensitive to supersymmetric particles at 1-loop (such as charginos and charged Higgses). This decay itself is only present at 1-loop in the Standard Model (via W bosons) and so beyond Standard Model effects can be very significant. Constraints also arise from the anomalous magnetic moment of the muon $(g-2)_\mu$, to which there can also be a substantial non-zero supersymmetric contribution. A review of this area is available in [144], whilst there is currently a 3.4σ discrepancy.

Finally, electroweak observables are also key constraints on supersymmetric models: all spectrum generators, including `SoftSusy` use electroweak masses such as the Z boson mass or top mass and other masses as constraints at the electroweak scale, nonetheless they also determine the mass of the lightest Higgs boson m_h to varying levels of accuracy, with `SoftSusy` offering particularly high precision via 3-loop corrections to the Higgs mass by linking with the `Himalaya` program [145, 146]. As indicated previously in Chapter 2.3.4, the necessity to reproduce the Standard Model-like Higgs boson of mass 125 GeV places significant constraints on many parts of the supersymmetric parameter space.

There are also global fitting codes which aim at producing either a χ^2 or likelihood value or perhaps a posterior probability map over the supersymmetric parameter space given input collider, cosmological and precision constraints. These tools often rely on many of the programs already mentioned to carry out the supersymmetric calculations, before they themselves evaluate the fits. As with the rest of this field, there are several different options available in the literature including: `SuperBayeS` [147, 148], which uses `SoftSusy`, `DarkSUSY` and `FeynHiggs` input; `SFITTER` [149] and `FITINO` [150] are other options; whilst recently the `GAMBIT` tool has been released as a further Beyond Standard Model fitting code, again incorporating elements of several programs, including `SoftSusy`, `DarkSUSY` and `ISAJET`. We go into no further details on these programs as they are not of direct relevance to the work presented here.

As should be now obvious, there are a great number of computer programs available in this field, and this plethora of computer programs is useful, enabling all possible calculations for supersymmetric models to be made in a way that would be inconceivable to manage within any single program. Moreover, the different programs themselves also have different benefits, using different approximations and covering different models. Our research focuses in particular on

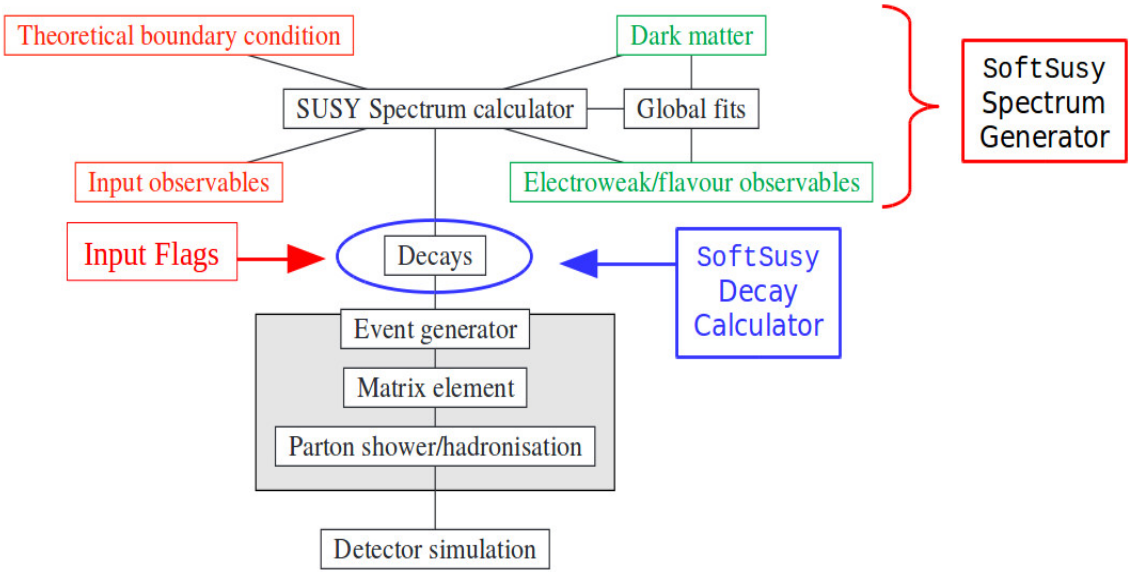

Figure 3.2: The analysis flowchart for producing theoretical predictions for the phenomenology of supersymmetric modes, detailing the types of programs required and which tasks may be performed by `SoftSusy`. This figure is adapted from [116].

the mass spectrum generation and decay partial widths calculation aspects of these analyses and so our comments will now be aimed at these programs. A summary of the capabilities of the mass spectrum generation and decay calculation programs relevant to our work is given in Table 3.1, which is a projection of the program abilities of each code onto the plane of relevance to our work and so is far from exhaustive; moreover it is based on reading the available program manuals and web pages and so is only schematic. For full details we encourage the user to refer themselves to the manuals of the appropriate programs, whose version numbers are listed.

It is clear that the programs available differ in many subtle aspects. In fact, even programs having apparently the same approximations and assumptions for a given calculation often will differ in their numerical answers due to the incorporated higher order corrections being different. For example decay widths can vary because of the use of different schemes, scales and orders of running masses and couplings in order to approximate higher order corrections not explicitly included in the formulae. The same effects are true in the sparticle spectrum [151] and in the Higgs masses calculated [152–154]. As a result, numerous comparisons have been performed between the different codes, such as [116, 155], whilst we explicitly demonstrate comparisons in the decay widths in our validation of the `SoftSusy` decay calculator code in Chapter 4, based on our own paper in [1]. As a result of these differences, and the complexity of the calculations, one key means by which to gauge the theoretical errors associated with the calculations is the comparison of the results of different spectrum generator and decay calculator programs. Meanwhile, different codes also serve the purpose of allowing cross-checking and error-finding to be performed more easily, ensuring the accuracy of the predictions.

The different programs also have to be compatible with one another, allowing each to interface with other codes to perform different parts of the calculations. This can lead to potential

issues with different versions of different codes not matching or potentially making inconsistent assumptions or approximations. To attempt to ameliorate this situation as much as possible, as well as make the lives of the users much easier should they have to use many different programs to complete their calculations, the SUSY Les Houches Accord (SLHA) [156] and SUSY Les Houches Accord 2 (SLHA2) [157] were produced. These are designed to allow the more straightforward interfacing of different programs via input and output ASCII text files listing the relevant masses, couplings and other model parameters in separate blocks. This has been largely successful, although some issues occasionally remain, still thereby favouring single programs determining as many steps of the calculations as possible. Before the advent of the `SoftSusy` decay calculator program, `SoftSusy` has been interfaced with various different programs, including `SUSYHIT` [131] to determine the branching ratios of supersymmetric and Higgs particles in the MSSM, `NMSSMTools` [126–128] to calculate the branching ratios of supersymmetric and Higgs particles in the NMSSM, and `micrOMEGAs` [78, 79] to determine dark matter observables. The `SoftSusy` decay calculator, which is the focus of our research in this area, now supersedes the former two, with all decay calculations able to be performed within `SoftSusy`.

The situation with many separate programs with separate assumptions and methodologies is, of course, far from ideal; it is preferable to have as many of the calculations as possible implemented in a single program or even in each of the single programs. This has clear benefits in usability as users only have to download and compile a single program; avoids interfacing programs which, even with the SLHA, can introduce bugs; and is cleaner from the point of view of programming. This would ensure that exactly the same approximations and assumptions are made throughout a calculation and the same parameter values used, thereby reducing possible sources of error. Moreover, there are also physics motivations, by performing many calculations in each program this means multiple programs carry out each calculation, enabling cross-checking between programs as well as permitting a greater understanding of the theoretical errors involved. This should lead to a better awareness of what can be inferred from experimental data about theoretical SUSY models. For these reasons the all-in-one `SoftSusy` spectrum generator and decay calculator package, now available as a result of our work, offers many benefits over the previous setup and enables theoretical predictions for searches for supersymmetric signatures to be made with greater certainty and ease. We hope that this addition of functionality to `SoftSusy` will facilitate collider studies of sparticle and supersymmetric Higgs searches, both through the study of differences between it and the other programs as an estimate of the size of theoretical uncertainty in the prediction and through a fast and unified computation.

	SoftSusy (4.1.4)	SusyHit (1.5)	sPHENO (4.0.3)	NMSSMTools (5.3.0)	FeynHiggs (2.14.1)	PYTHIA (8.2)	NMSSMCALC (2.00)
Spectrum Calculator	✓	✓ SUSPECT	✓	✓ NMSpec	✓(Higgses only)	✗	✓(Higgses only)
RGEs	3-loop	2-loop	3-loop	2-loop	- (different approach)	-	-
Highest Order Mass Corrections	3-loop (Higgs)	2-loop	2-loop (Higgs)	2-loop (Higgs)	2-loop (+ resummations and EFTs)	-	2-loop
NMSSM	✓	✗	(✗) Only with SARAH	✓	✗	-	✓
FV	✓	✓	✓	✗	✓	-	✗
RPV	✓	✗	✓	✗	✗	-	✗
ν masses mixings	✓	✗	✓	✗	✗	-	✗
Experimental constraints	✗ (Only EW)	✓	✓	✓	✓	-	✓ (some)
Decay Calculator	✓	✓ HDECAY, SDECAY	✓	✓	✓	✓	✓
SUSY decays	✓	✓ SDECAY	✓	✓	✗	✓	✗
Higgs decays	✓	✓ HDECAY	✓	✓	✓(high accuracy)	✓	✓
Loop corrections	✓ (Higgses only, $h \to q\bar{q}, gg$)	✓	✓ (Higgs only)	✓ (Mainly Higgs decays)	✓ (Higgs only)	✗	✓ ($h \to q\bar{q}, gg$)
Decays to Gravitinos	✓	✓	✓	✓	✗	✗	✗
3-body decays	✓ (not $\tilde{f}$ yet)	✓	✓	✓	(✓) ($h \to VV^*$ only)	(✓) some	(✓) ($h \to VV^*$ only)
NMSSM	✓	✗	(✗) Only with SARAH	✓	✗	✗	✓
RPV	✗	✗	✓	✗	✗	✗	✗
CPV	✗	✗	✗	✓	✗	✗	✓

Table 3.1: A comparison of the programs available for calculation of SUSY mass spectra and decay branching ratios, version numbers are given for each program. The presence and corresponding capabilities of a spectrum generator in the programs is given in rows 2-9. Rows 10-18 similarly reveal whether each program has a decay calculator and its capabilities. The features of the SoftSusy decay calculator which is the focus of our work, are given in the second column in rows 10-18. Only a subset of all public programs in this area can be included in a single table therefore a selection has been made of programs against which we have performed explicit comparisons and programs demonstrating the breadth of possibilities in this area. The programs included are SoftSusy [1,66,68,69,117–119,145,146], SUSYHIT [131–134], sPHENO [3,4,158], NMSSMTools [126–128, 159–162], FeynHiggs [125, 163–167], PYTHIA [136] and NMSSMCalc [130, 168–171]. Other relevant programs not included are given in the text and this table is not exhaustive.

3.2.1 Mass Spectrum Generator Approach

We now provide a detailed description of the overall workings of spectrum generator and decay calculator programs. We begin with the first stage of such calculations, the supersymmetric mass spectrum generation. Mass spectrum generators solve a system of linked differential equations with boundary conditions at each end. These are the renormalisation group equations of the supersymmetric model with boundary conditions at the low electroweak scale provided by physical measurements, such as the top mass, Z mass, fine structure constant at m_Z and others; and theoretical boundary conditions on the soft supersymmetry breaking parameters at the high GUT scale. In addition, there are requirements on the solution of successful radiative electroweak symmetry breaking. In order to solve this system, to determine the supersymmetric masses and couplings at the SUSY scale, spectrum generators must run particle masses, couplings and mixing parameters between two disparate scales. To complete this process in full generality and with complete rigour, one would have to integrate out each particle below its mass and match the theory above each particle mass to a reduced effective theory below each particle mass; however given the number of additional particles present in the MSSM (with even more in its extensions), this is intractable. Moreover, with the particles able to order themselves in mass in all possible ways, N additional particles would therefore result in $\sim N!$ effective theories to be run, each needing its own renormalisation group equations. Given this situation there are two approaches used in the literature, each relevant in a different regime.

The first approach, and the method adopted in `SoftSusy` as well as `SUSPECT` (and also in versions of `sPHENO` prior to version 4.0), is to match the Standard Model parameters used as inputs at the low scale immediately onto the full MSSM at m_Z [2]. This matching involves the conversion of the Standard Model parameters extracted from experiment into MSSM parameters. For example, considering α_s, this is determined via jet cross-sections with vertices such as $g \to q\bar{q}, gg$. The measurements for such cross-sections are then used to determine the vertex factors (proportional to α_s at the scale it is measured) including Standard Model loop corrections up to the desired order in perturbation theory. However, if the theory is taken to be the MSSM rather than the Standard Model, there are additional loop corrections which we must subtract off the calculated α_s value to obtain our boundary condition on $\alpha_s(m_t)$ for the MSSM. At 1-loop, such corrections come from gluino loops via processes such as that in Figure 3.3. These "finite term" corrections are proportional to $m_Z^2/(16\pi^2 m_{\rm SUSY}^2)$ and are included by matching straight onto the MSSM at the low scale[3]. However, by matching at an electroweak scale, logarithmic pieces in the β function are not resummed which arise in the RGEs between m_t and $m_{\rm SUSY}$ due to mass splittings between the various supersymmetric particles (i.e. as not all supersymmetric particles appear at $m_{\rm SUSY}$); these are proportional to $(1/16\pi^2)\log[(\Delta m)^2/m_Z^2]$ and alter the gradient of the running. In order to account for such missing pieces, `SoftSusy` and other programs that use this method add "threshold corrections" to a given order, these account

[2] Traditionally the low matching scale is m_Z, however as of `SoftSusy` version 4.1.1 the matching is done at m_t, this may have effects on the numerical values of the parameters obtained, such as m_h [83].

[3] In spectrum generators $m_{\rm SUSY} = \sqrt{m_{\tilde{t}_1} m_{\tilde{t}_2}}$ although this can be altered by the user.

for the difference in gradient over the m_Z to $m_{\rm SUSY}$ running with additional intercept corrections on top of the finite pieces[4]. This approach deals with the effects of sparticle thresholds by using the MSSM (or its extensions as appropriate) as an effective theory between m_Z and $m_{\rm SUSY}$. Even within this prescription, there are choices which represent different higher order terms - for the gluino correction of Figure 3.3 for example, the question of which gluino mass value should one use in the loop ensues. Using the pole mass or the $\overline{DR}$ running mass will lead to distinct α_s values essentially corresponding to 2-loop effects. In order to minimise such effects, higher orders must be included; in this respect `SoftSusy` is state of the art, containing 3-loop RGEs and many 2-loop threshold corrections to the third generation Yukawas and the strong gauge coupling α_s as these have particularly large effects on the Higgs mass [117].

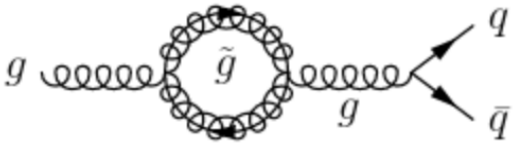

Figure 3.3: Supersymmetric correction to the vertex used to provide the value of $\alpha_s(m_t)$, the contribution of this diagram must be factored in to obtain our value of α_s at the low scale in the MSSM. There is also a similar contribution from squark loop corrections.

The alternative approach, as used by `ISAJET`, `NMSSMTools`, `sPHENO` (since version 4.0 released in March 2017) [158] and `FlexbileSUSY`, is to integrate out the sparticles from the RGEs at a higher scale ($m_{\rm SUSY}$) and then run in an effective theory between $m_{\rm SUSY}$ and m_Z. This naturally resums the logarithmic terms due to mass splittings in the RGEs, but misses finite terms due to loop corrections via sparticles in loops. Generically, these two approaches have different regimes of validity, with the `SoftSusy` approach missing terms of order $\mathcal{O}(\log[(\Delta m)^2/m_Z^2])$, whilst the `NMSSMTools` and `sPHENO` approach misses some terms of order $\mathcal{O}(m_Z^2/m_{\rm SUSY}^2)$. Therefore the former approach will be most accurate for lower values of the $m_{\rm SUSY}$ scale, whilst the latter is more accurate for higher values of $m_{\rm SUSY}$ where the mass splittings increase but the finite terms reduce in size. Where the exact boundary of the two approaches occurs is a model-dependent question, and one of increasing interest given the LHC constraints on low-scale supersymmetry. It has been addressed by the paper [83] in the context of the accuracy of the Standard Model-like Higgs mass, which offers a key constraint on supersymmetric models. The different approaches therefore offer another source of potential mass, mixing and coupling differences between spectrum generators; these parameters are then used as inputs to the decay calculators and so may cause significant differences in partial widths obtained, depending upon the nature of the mass spectrum and model considered. Nonetheless, as previously mentioned, any such differences between codes can be used as an estimator of associated theoretical errors for these difficult calculations and offer an order of magnitude estimate for the size of higher order effects.

Aside from these differences in approach at the low end of the renormalisation group running,

[4]Note we distinguish between these threshold corrections, and those obtained between $m_{\rm SUSY}$ and the high scale whose logarithms are resummed up to the order of the renormalisation group equations included: 3-loop with Next-to-Next-to-Leading-Logarithms.

the basic methodology of the fixed point iteration solution of the two boundary RGE problem to determine the supersymmetric and Higgs masses and couplings is the same and is illustrated in a simplified form in Figure 3.4. It is described here:

1. Match the low energy boundary conditions on fermion masses, gauge couplings and other electroweak parameters onto either the MSSM or the Standard Model, depending on which of the two approaches are used. Threshold corrections are included at this stage in `SoftSusy` to account for leading missing logarithmic pieces arising due to the sparticle mass splitting. Guesses are required for the parameters on which there are no boundary conditions, such as the supersymmetric masses, these are made approximately and are irrelevant, being overwritten the next time the iteration reaches the low scale.
2. If the latter approach is used match, onto the full MSSM at $m_{\rm SUSY}$; if the former is used, there is no need for this step as the spectrum generator already runs in the full MSSM.
3. The particle masses, couplings and other parameters are then run in the full MSSM up to the high scale (however it is defined) - often this is the GUT scale, defined as the point where the $SU(2)_L$ and $U(1)_Y$ coupling unify: $\alpha_1(M_{\rm GUT}) = \alpha_2(M_{\rm GUT})$.
4. At the high scale, the supersymmetric parameters are compared with the theoretical boundary conditions (such as unification of scalar masses, fermion masses and trilinear couplings in the case of minimal supergravity models); the parameters for which there are theoretical boundary conditions are replaced by the boundary condition values, leaving the remaining parameters unaltered.
5. The new set of parameters are all run down to the low scale in the full MSSM (perhaps via matching at $m_{\rm SUSY}$ and running in the Standard Model as an EFT below this if the second approach is used). These parameters at the low scale are compared with the low scale boundary conditions and replaced as appropriate, the whole new set of parameters is then run back to the high scale.
6. Steps 3-5 are then repeated in fixed point iteration until the parameters reach convergence within the level of the tolerance defined, by default this numerical precision is 10^{-4} but this may be changed in the input file[5]. Usually a self-consistent solution satisfying both low scale and high scale boundary conditions is found within 3-5 iterations. The number of iterations required is dependent on the model and the precise setup as well as the low and high energy scales set.
7. Finally, once the solution is found, the parameters are run to the supersymmetry scale $m_{\rm SUSY}$ and the supersymmetric and Higgs masses, mixings and couplings are output in the mass spectrum at this scale. This information is then used as an input to the decay calculator program.

There are potential issues which may arise from such an iterative approach, in particular can we be certain there is just one solution and if not does the fixed point iteration method necessarily produce the "best" solution, however that may be defined. For example, it may

[5]Specifically it is set in item 1 of the SOFTSUSY block, information on the `SoftSusy` input file is given in Chapter 4.1.1.

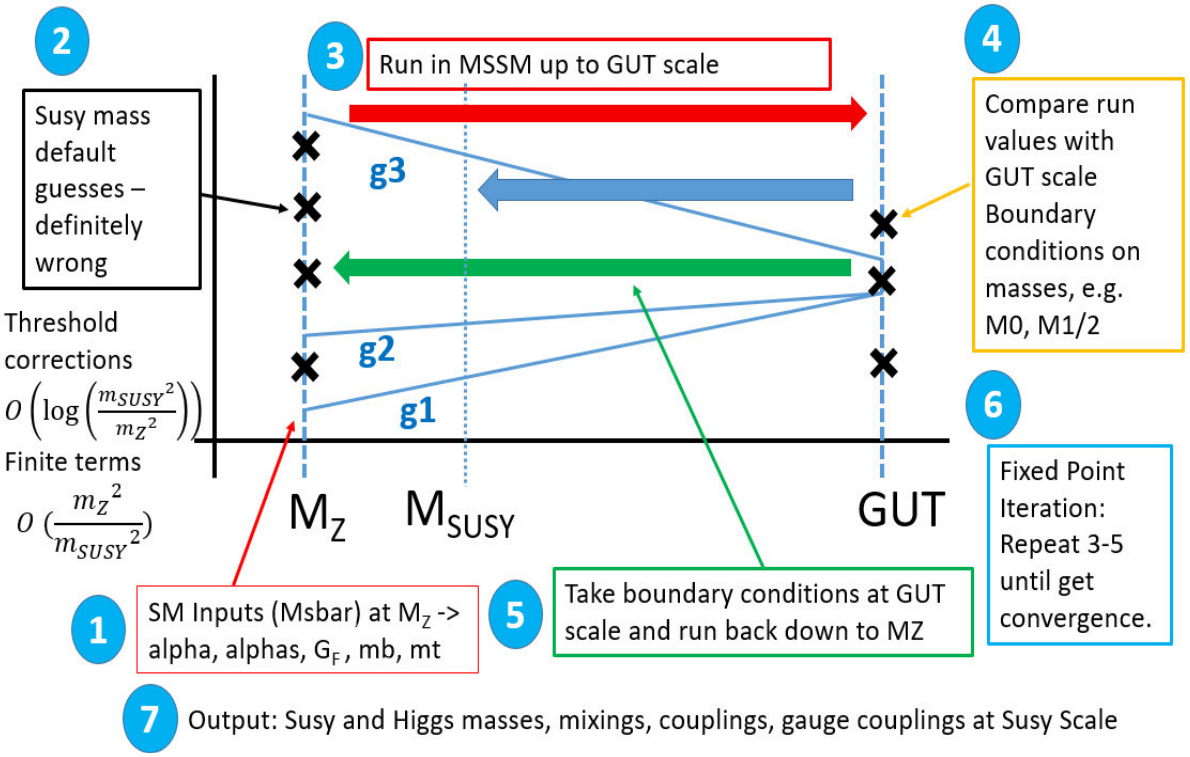

Figure 3.4: Schematic overview of how a spectrum generator program solves the two boundary differential equation problem posed to determine the masses of the supersymmetric and Higgs particles. It does so by repeatedly running between the low and high scales in fixed point iteration, taking the boundary conditions at each end as inputs each time, until the masses are determined and consistent within a given tolerance.

appear that it would be prone to finding local minima in the solution "fit", rather than the global minimum or even that the fixed point algorithm may be unstable in the region of some solutions. This has been studied in the literature, in particular in the context of `SoftSusy` itself an alternative "shooting" approach was investigated [172] and demonstrated that the fixed point iterative method may in some instances only provide one of several solutions, although cases where the phenomenology of these new solutions is markedly different are comparatively rare.

3.2.2 Decay Calculator Approach

The second stage of the calculation, and the one most relevant to our research, is the calculation of the partial widths of the available decay modes given the mass spectrum of sparticles and Higgs bosons and their associated mixings and couplings. This part of the program is computationally more straightforward, with the difficulty lying in the number of modes to calculate and in the physics associated with difficult decay modes, particularly beyond tree-level or with more than 2 final state particles where there are additional difficult integrals to perform and many contributions and interferences to consider.

As is the case in the vast majority of decay calculator programs, we have chosen in `SoftSusy` to set up the program to deal with specific models, these being any MSSM or NMSSM models

satisfying a small number of assumptions as described in Chapter 3.3.4. Therefore the decay calculation aspects are applicable for all three classes of MSSM supersymmetry breaking at the high scale (see Chapter 2.1.2), or more generally for the pMSSM, or indeed user specified high scale and breaking conditions in the spectrum generation, as well as for the NMSSM; provided the assumptions accompanying our decay calculator are satisfied in such approaches. The decay partial widths are hard-coded into the program, therefore extensions to further models would require further coding, for example if an extension to the RPV case was desired additional modes and coupling contributions would need to be added explicitly. This general model-specific approach is used by all decay calculators in their stand-alone forms (`SusyHit`, `sPHENO`, `NMSSMTools`, `ISAJET`, `NMSSMCalc`, `FeynHiggs`, `PYTHIA`, etc). An alternative is to produce decay calculators that can determine the branching ratios for any given model and model extensions. The `Mathematica` package `SARAH` is able to generate the vertices and mass matrices for any given supersymmetric model, the decay calculator `sPHENO` with `SARAH` can then analyse additional models and model extensions not directly coded into the decay calculator. Whilst this approach has advantages in enabling the analysis of a wider variety of models, we have chosen the former approach for its simplicity, usability and accuracy, with explicitly coding and analysing certain classes of models under strict decay calculator assumptions enabling more specific modes to be added and potentially offering greater insights into the phenomenology of these models.

The mechanics of any decay calculator program involves the computation of a vast number of different decay modes; first checking which modes are kinematically available, and then evaluating relevant couplings for the decay modes, before evaluating the partial widths of relevant modes, obtaining total widths and branching ratios, and finally outputting them in a series of decay tables for each parent particle. An overall schematic of the functioning of the `SoftSusy` decay calculator is provided in Figure 3.5; this is similar for all decay calculators, with differences arising as a result of different modes being evaluated and different approximations, choices and assumptions within equivalent decay modes. First the input mass, coupling and mixing parameters are read at the SUSY scale from the `SoftSusy` spectrum generator. Next the decay modes are calculated one by one for each parent supersymmetric or Higgs particle, with switches used to call MSSM or NMSSM decay formulae. 3-body modes and decays to gravitino LSPs may also be evaluated depending upon the flags used and by default will be evaluated where they are relevant to the phenomenology of the model, these can be turned off however (in the input file for 3-body decays or in the code for decays to LSP gravitino). Branching ratios are only output for modes with branching ratios above the branching ratio tolerance and 3-body modes are only called where 2-body modes of the same particles are not available. Even in this case, if there are other 2-body modes (to different final state particles), the 3-body modes calculated will typically not be output as the 2-body modes often dominate the branching ratios, forcing the 3-body mode branching ratios below the branching ratio output tolerance. Additional complications arise from QCD corrections, which may be applied to some Higgs modes (as described in Chapter 3.4). 1-loop modes also involve intricacies, with the masses and couplings often first run to the scale of the decaying parent particle mass so as to endeavour to reduce the size of any

corrections and hopefully produce a more accurate partial width. Many of these specific details of the assumptions, choices and decay modes are given in Chapter 3.3, whilst more information is also available in Appendix A and in our paper [1]. In Figure 3.5, dashed lines represent calls that are only made if the appropriate input flags and conditions are met.

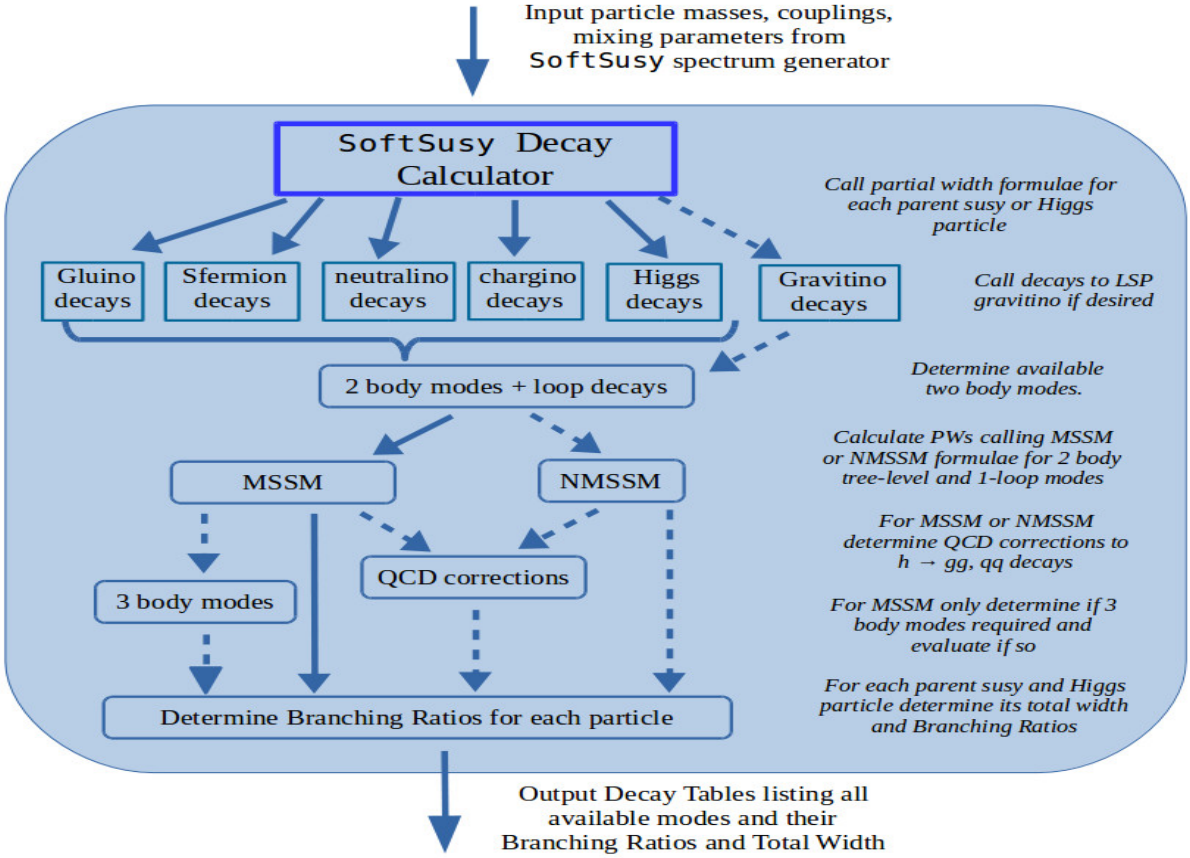

Figure 3.5: Schematic overview of the `SoftSusy` decay calculator, dashed lines represent calls that are only made if the appropriate input flags and conditions are met, only the MSSM is always called (even for the NMSSM as several decays are identical in the MSSM and NMSSM), the NMSSM specific modes (involving the extended Higgs and neutralino sectors) are only called for NMSSM models. By default QCD corrections are added to Higgs decays to quarks or gluons in the MSSM or NMSSM, by default 3-body modes are also calculated where required, although only in the MSSM, however both 3-body modes and QCD corrections may be turned off by the user. Decays to gravitino LSPs are evaluated by default but this may be turned off in the code.

Care has been taken to ensure consistency throughout the decay calculations with the `SoftSusy` spectrum generator, with the masses and couplings used evaluated and applied in the same schemes and under the same approximations in order to eliminate additional sources of errors which may arise from theoretical inconsistencies. In addition, the spectrum generation and decay calculation aspects of the `SoftSusy` program are largely independent; the spectrum generator is only called after the inputs are provided if parameters are run to the scale of the decaying parent particle mass in order to improve the accuracy of the partial widths calculated. Consequently, the decay calculator may be used as a stand-alone provided all necessary input parameters for the partial width functions are input.

3.3 Conventions, Methodology and Implementation

We now outline the conventions, choices, assumptions and methodology used in our work on the `SoftSusy` decay calculator, in our associated paper [1], and in the decay calculator program.

Throughout $\tilde{Z}_i$ and $\tilde{W}_j$ are used for neutralinos ($i = 1, 2, 3, 4$ in the MSSM or $i = 1, 2, 3, 4, 5$ in the NMSSM) and charginos ($j = 1, 2$), respectively. This is different to the commonly used $\tilde{\chi}_i^0$ and $\tilde{\chi}_j^+$ notation for ease of reading, particularly when they appear in subscripts. The notation for the mass-ordered CP even and CP odd neutral Higgs bosons is that $h_i \in \{h, H, H3\}$ for $i = 1, 2, 3$ are the CP even neutral Higgs bosons in order of increasing mass, whilst $A_i \in \{A, A2\}$ for $i = 1, 2$ are the CP odd neutral Higgs bosons again in order of increasing mass, remembering that $H3$ and $A2$ occur only in the NMSSM.

The partial width formulae for all of the decay modes included in the `SoftSusy` decay calculation[6] are listed in Appendix A; many of these were re-derived in the development of the program and have been written in one consistent set of conventions. The latest version of the whole `SoftSusy` program itself is also submitted with this thesis.

3.3.1 MSSM

While the conventions used in the decays code are largely those used in `SoftSusy` [66], there are differences in a few places in order to allow easier comparison with partial width (PW) formulae provided elsewhere. The few differences with respect to Ref. [66] are as listed below[7]:

- In our calculations, it is convenient to work in a basis where the third generation sfermions are mass ordered with $m_{\tilde{f}_1} < m_{\tilde{f}_2}$. In order to ensure this, the mixing angle θ_f is transformed accordingly ($\theta_f \to \theta_f + \pi/2$) in the case where the `SoftSusy` spectrum generator has $m_{\tilde{f}_1} > m_{\tilde{f}_2}$.
- The mixing angles for the charginos are transformed with respect to the `SoftSusy` spectrum generator in order to match conventions used elsewhere (e.g. [124]). Therefore $\theta_{L/R}$ as indicated below is given by $\theta_{L/R}^{decays} = -\theta_{L/R}^{spectrum} + \pi/2$.
- The neutralino mixing matrix employed here is $N = O^T$, where O is the neutralino mixing defined in Ref. [66].

3.3.2 NMSSM

The conventions used in the decay code are predominantly those described previously in the `SoftSusy` NMSSM manual [118], but there are differences in a few places. As well as those listed above, there are a few changes specific to the NMSSM, to allow straightforward comparison with `NMSSMTools` [126–128, 159]:

[6] The source code for the calculations is in the folder `src` in the files `decays.cpp`, `mainDecay.cpp`, `twoBodyDecays.cpp` and `threeBodyDecays.cpp`, which are in the `C++` programming language.

[7] In the decay code itself, the neutralino mixing matrix used (N in `SoftSusy notation`) is transposed.

- The Charge Parity (CP) even neutral Higgs mixing matrix, S, is altered relative to the matrix R provided by `SoftSusy` [118]. The matrix S used in the decay formulae is obtained via an orthogonal transformation exchanging eigenstates:

$$S = R \begin{pmatrix} 0 & 1 & 0 \\ 1 & 0 & 0 \\ 0 & 0 & 1 \end{pmatrix} = \begin{pmatrix} R(1,2) & R(1,1) & R(1,3) \\ R(2,2) & R(2,1) & R(2,3) \\ R(3,2) & R(3,1) & R(3,3) \end{pmatrix}, \tag{3.20}$$

  i.e. the first two columns are interchanged.

- The CP odd neutral Higgs mixing matrix is altered relative to the matrix provided by `SoftSusy` [118], the matrix P detailed in the decay formulae (different to the P in Ref. [118] which we write here as P^{prov}) is given below. The differences are that the first row of P^{prov} is dropped (as this refers to the Goldstone boson) and the first and second columns are interchanged. The mixing angles β and θ_A are as used elsewhere in `SoftSusy` [66, 118].

$$P = \begin{pmatrix} P^{\text{prov}}(2,2) & P^{\text{prov}}(2,1) & P^{\text{prov}}(2,3) \\ P^{\text{prov}}(3,2) & P^{\text{prov}}(3,1) & P^{\text{prov}}(3,3) \\ 0 & 0 & 0 \end{pmatrix} = \begin{pmatrix} \cos\beta\cos\theta_A & \sin\beta\cos\theta_A & \sin\theta_A \\ \cos\beta\sin\theta_A & \sin\beta\sin\theta_A & -\cos\theta_A \\ 0 & 0 & 0 \end{pmatrix}. \tag{3.21}$$

3.3.3 Mass Choices and Scales Used

As described previously, at any given order of calculation in the mass spectrum generation, there are assumptions, schemes and approximations that can result in numerically different values for quantities corresponding to the same physical parameter. Subsequently however, there are also potential differences originating from the choices and assumptions made in the decay calculations themselves as well as the corrections included. In this case, as for the spectrum generators, these choices correspond to different higher order effects and are theoretically equivalently valid choices at the order of approximation applied, nonetheless they of course lead to further differences in the numerical partial widths and branching ratios output. One particularly pervasive choice is that of the renormalisation scale at which to evaluate the parameters input into each partial width formula. For example, consider the decay of a gluino into a top and a stop. One must choose a renormalisation scale for the coupling, whilst the masses of the particles involved could be running masses evaluated at different scales or pole masses. Each choice affects the numerical value of the partial width, but all choices are equivalent at tree-level. In `SoftSusy` the following choices are made:

- In general, unless explicitly stated otherwise, the masses of the supersymmetric (SUSY) and Higgs particles and other parameters, such as mixing angles and gauge couplings, are evaluated at the scale $M_{\text{SUSY}} = x\sqrt{m_{\tilde{t}_1}(M_{\text{SUSY}})m_{\tilde{t}_2}(M_{\text{SUSY}})}$, where x by default is 1 but can be set by the user. Here, $m_{\tilde{t}_i}(M_{\text{SUSY}})$ is the running i^{th} stop mass evaluated at a modified dimensional reduction [173] ($\overline{DR}$) renormalisation scale M_{SUSY}.

- For Higgs loop decays the gauge coupling strengths α_s and α are evaluated at the mass of the decaying Higgs, with the hope of improving the accuracy obtained for these important modes.
- For Higgs loop decays to $\gamma\gamma$ or $Z\gamma$ the masses of the important quarks (i.e. m_t, m_b, m_c) are evaluated at the mass of the decaying Higgs in order to attempt to improve the accuracy of the partial width evaluated. Below M_Z, these are run in 3 loop QCD and 1 loop in QED, as they are in the case of the lightest CP even Higgs h's decays. In the calculation of decays of H, $H3$, A and $A2$ quark masses are run to m_H, m_{H3}, m_A, m_{A2} in the (N)MSSM as appropriate.
- Throughout the program, unless otherwise stated here, we use two different quark masses; "kinematic masses" for the kinematics (i.e. for masses of particles in the initial or final states) and "running masses" for the evaluation of couplings. This hopefully allows a large part of some higher order corrections to be incorporated into the quark legs via the mass running. The way in which these masses are evaluated is listed in Table 3.2.
- In addition to the above quark masses, there are extra masses `mcpole` and `mspole` defined in `decays.h` which are used only for the neutral Higgs boson decays to $q\bar{q}$ or gg and are set to avoid double counting in the QCD corrections [174].
- If the QCD corrections to these decays are turned off then the running masses for the quarks are used in order to attempt to hopefully incorporate some of the NLO corrections to the quark legs.

As detailed in Table 3.2, for the third generation sfermions the "kinematic" masses are pole masses obtained from the propagators whilst the "running (coupling)" masses are in the $\overline{DR}$ scheme. For the "kinematic" masses of the first two generation fermions, the $\overline{MS}$ mass at M_Z is used, whilst the "running" masses are extracted from the running Yukawa couplings. For the electron and muon, the running is small as there are only QED effects. The "kinematic" masses for the vector bosons are pole masses, whilst for the "running (coupling)" masses they are running $\overline{DR}$ masses evaluated at $M_{\rm SUSY}$. $\overline{MS}$ masses include only SM corrections within `SoftSusy`, with 3-loop QCD and 1-loop QED corrections; whilst Yukawa-extracted masses are in the $\overline{DR}$ scheme and include SM and SUSY corrections. Quark input masses can be reset by the user within the `SMINPUTS` block of the SLHA/SLHA2 input file and the kinematic and running masses used will then change accordingly.

The different choices of scales for the input parameters is one of the key sources of differences between different decay calculator programmes. It is worth noting that an experimental value of Fermi's constant, G_F, is also used; this is inconsistent with the tree-level expression $\frac{G_F}{\sqrt{2}} = \frac{g^2}{8m_W^2}$ as it is an empirical quantity and so incorporates higher order terms.

kinematic masses		running (coupling) masses	
`mtPole`	pole mass from propagator	`runmt`	$\overline{DR}$ mass at M_Z
`mbPole`	pole mass from propagator	`runmb`	$\overline{DR}$ mass at M_Z
`mtauPole`	pole mass from propagator	`runmtau`	$\overline{DR}$ mass at M_Z
`mc`	$\overline{MS}$ mass at M_Z	`runmc`	Yukawa-extracted mass at M_Z
`ms`	$\overline{MS}$ mass at M_Z	`runms`	Yukawa-extracted mass at M_Z
`mup`	$\overline{MS}$ mass at M_Z	`runmu`	Yukawa-extracted mass at M_Z
`mdo`	$\overline{MS}$ mass at M_Z	`runmd`	Yukawa-extracted mass at M_Z
`mel`	$\overline{MS}$ mass at M_Z	`runmel`	Yukawa-extracted mass at M_Z
`mmu`	$\overline{MS}$ mass at M_Z	`runmmu`	Yukawa-extracted mass at M_Z
`polemw`	pole mass from propagator	`runmw`	running W mass at $M_{\rm SUSY}$
`polemz`	pole mass from propagator	`runmz`	running Z mass at $M_{\rm SUSY}$

Table 3.2: The two different types of masses used for the fermions and gauge bosons. The `names` given are those used in the code. "kinematic" masses are used for the masses of initial and final state particles whilst "running (coupling)" masses are used in couplings in the partial width formulae. Note that within `SoftSusy`, the $\overline{MS}$ masses include only SM corrections whilst the Yukawa-extracted masses ($\overline{DR}$ masses) include SM and SUSY corrections.

3.3.4 Assumptions Made

The following assumptions are made in the decay calculator:

- R-parity conservation in the MSSM and in the NMSSM.
- No additional CP violation relative to the SM.
- No additional flavour violation relative to the SM.
- Sfermion mixing has only been accounted for in the third generation of sfermions as it is proportional to the Yukawa couplings, which are negligible for the first two generations.
- We assume CP conservation in Higgs sector of the MSSM and in the extended Higgs sector of the NMSSM.

3.3.5 Method

The `SoftSusy` decay calculator is a `C++` program, matching the language of the vast majority of the `SoftSusy` spectrum generator package. This language is chosen as not only do most contemporary high energy physics experiments and computer programs use `C++` (with many previous `fortran` programs, such as `PYTHIA`, recently migrating over to `C++`), but also the object orientation allows a modular program to develop which is optimal for the many different calculations and models that may wish to be evaluated.

As for the implementation of the decay partial width formulae themselves within the decay calculator program, we have chosen to evaluate as many of the modes as is practicable analytically in order to favour speed of execution; for 2-body tree-level decay modes, the ana-

lytical expressions for the partial widths are explicitly used in order to provide fast evaluation. Similarly, for the 2-body 1-loop decays the loop integrals were performed analytically and the resulting formulae used. For 3-body decay modes (all tree-level), the phase space integral has been analytically reduced to a one-dimensional integral, which is then performed using adaptive Gaussian numerical integration [175].

The tree-level 3-body decay modes were therefore where most complications arose. In general for an n-body tree-level decay there are n integrals to perform, one over the three-momenta of each of the final state particles, as explained in Chapter 3.1. One of these integrals is always trivial to perform using the momentum-conserving delta function. For the 2-body tree-level decay widths this leaves one remaining integral with the energy delta function, this can then be performed easily. For tree-level 3-body decay widths however, one has two remaining integrals to perform and in general they are non-trivial to determine analytically. In certain cases the symmetry of the integrands, along with certain assumptions, may allow them to be performed. For $h \to VV^* \to Vf(')\bar{f}$ modes (V represents a vector boson), the mass of the Higgs boson ensures that the outgoing fermions may not be top quarks. Therefore one can neglect the masses of the outgoing fermions and greatly simplify the calculation. Passarino-Veltman reduction [176] can then allow reduction of the integrals to a one-dimensional integral, which in this case may be determined explicitly analytically; the result is given in Appendix A.3.6 equations A.144 and A.145, as well as in the "Higgs Hunter's Guide" [102]. For a general 3-body decay mode the calculations are however considerably more involved. There are two approaches that can be taken once the first trivial integral using the momentum-conserving delta function is performed; at this stage the partial width can be written as a double differential decay rate in two Mandelstam variables as is the case in `SUSYHIT-1.4`, following the work performed in reference [177], these two dimensional integrals can then be performed numerically. Alternatively, often one of the two integrals (remaining after the first trivial integral is performed) may be evaluated analytically, leaving a single one-dimensional integral to be performed numerically. This is the approach used in the work in reference [65,178] and is the method adopted in `sPHENO` [3,4], from which the expressions we use for the 3-body decays originate. The Feynman diagrams involved, effects included and any assumptions made for each of the 3-body decays are given in detail in Appendix A.4 with the corresponding partial width formulae.

In the case of very compressed regions, the 3-body decays often involve very fine cancellations between quantities, and this may cause issues with numerical precision, giving essentially random positive and negative numbers rather than reflecting the overall size of the integral (which must be positive definite). There can be negative integrands due to numerical precision close to both ends of the integration region for any of the 3-body modes, however these end regions are usually very phase space suppressed relative to the rest of the phase space, therefore issues only arise when the phase space region available itself is only "ends", i.e. is very compressed. In order to attempt to deal with potential issues originating here, we have implemented a check for negative partial widths, which may arise due to the numerical precision in the fine cancellations. If such negative partial widths arise anywhere in the program a warning is output and this partial width

is set to 0. Setting such partial widths to 0 is acceptable as these decay modes are very suppressed and so only important when they are the only modes available. One circumstance where these very compressed modes are the only ones available occurs for a gluino nearly degenerate with the lightest neutralino which is the LSP. In this case the only modes available are very suppressed decays to the lightest neutralino and quark-antiquark pairs of the first generation. Consequently the size of the integral determined in the 3-body decays is important for the phenomenology of the model and so (since `SoftSusy` version 4.1.4) we circumvent the numerical precision issues associated with the fine cancellations by taking the compressed spectrum limit of the integrand in this case and explicitly performing the cancellation analytically, leaving the remainder of the integrand. This is then calculated by `SoftSusy` and integrated numerically as before to give the partial widths (and hence branching ratios) and lifetime of the gluino. More information on the limit taken and formulae used are given in Appendix A.4.1. There may be similar regions in the 3-body decays of neutralinos, charginos (or sfermions when these are added to the program), which would benefit from increased accuracy gained from taking such limits; for now this is left to future work and greater study. In general, the outputs of spectrum generator and decay calculator programs for such very compressed spectra are of questionable accuracy in any case and should be used with caution; when the spectrum is so compressed the decay modes are dominated by the exact amount of the limited phase space available and consequently small differences in the masses of the supersymmetric particles and the quarks can significantly alter the partial widths. This was explained in the context of 2-body modes in Chapter 3.1 and illustrated in Figure 3.1[8].

Finally, for the loop decays the situation is of course more complicated than at tree-level, each loop provides an additional loop integral to be performed. In the case of the 1-loop decays included in `SoftSusy`, the integrals were performed explicitly with the help of Passarino-Veltman reduction [176] and formulae are available in Appendices A.3.6 and A.6 for the MSSM and NMSSM respectively.

3.4 Decay Modes

The following section provides a list of all the decay modes included in the decay part of the `SoftSusy` package along with some explanations; they are split into MSSM SUSY tree-level 2-body decays, MSSM Next-to-Lightest Supersymmetric Particle (NLSP) decays to the gravitino LSP, MSSM Higgs tree-level 2-body decays, MSSM Higgs 1-loop 2-body decays, MSSM tree-level 3-body decays, NMSSM SUSY and Higgs tree-level 2-body decays, NMSSM 1-loop 2-body decays and decays for which QCD corrections have been included. A comprehensive list of the formulae for all of the decays included is given explicitly in Appendix A for ease of reference, this also contains more details of the contributions and assumptions for the more complicated 3-body and loop decay modes. To summarise, we include:

[8] We refer here to very or highly compressed regions, rather than just compressed regions, the effects we discuss and the limited accuracy onsets around mass splittings of a few hundred MeV.

- All MSSM 2-body decays at (at least) tree-level, both sparticle and Higgs boson decays.
- Next-to-Lightest SUSY Particle (NLSP) 2-body decays to gravitinos in the MSSM at tree level.
- The phenomenologically most relevant 3-body decays of gluinos, charginos and neutralinos.
- Higgs decays to $\gamma\gamma$ and $Z\gamma$ at leading order (i.e. one-loop) in the MSSM and NMSSM.
- QCD corrections to neutral Higgs decays to quarks (1-loop) and to gluons (2-loop) in the MSSM and NMSSM.
- All NMSSM 2-body decays at (at least) tree-level, including the extended neutralino and extended Higgs sectors.

Whilst the majority of the decay modes are therefore calculated at tree-level, some effects of higher order corrections are approximated via the use of running masses and couplings, as calculated using the `SoftSusy` spectrum generator [66] - the details of the mass choices were given in Section 3.3.3. In Appendix A.1 there are a series of tables indicating all the modes included, along with appendix references for their partial width formulae as used in `SoftSusy`.

The branching ratios for each mode are grouped into decay tables for each parent SUSY or Higgs particle and are printed to standard output in the SLHA/SLHA2 convention [156, 157] to allow it to be passed straightforwardly to other programs (such as `PYTHIA` [136], `Herwig7` [137], `MadGraph` [141], for instance).

3.4.1 MSSM SUSY Tree-Level 2-Body Decays

The detailed formulae for these modes are in Appendix A.3. We begin with the gluino decays. The gluino $\tilde{g}$, being only charged under $SU(3)_c$ and with R-parity conservation, can only decay via squarks and so it decays dominantly to these on-shell squarks and quarks if it is heavy enough. The 2-body modes included are:

$$\tilde{g} \to q\tilde{q}^*_{L/R}, \bar{q}\tilde{q}_{L/R}, t\tilde{t}^*_{1/2}, \bar{t}\tilde{t}_{1/2}, b\tilde{b}^*_{1/2}, \bar{b}\tilde{b}_{1/2}.$$

If $m_{\tilde{g}} < m_{\tilde{q}} + m_q$ for all quark-squark partners, then such 2-body modes are kinematically unavailable and the 3-body modes via off-shell squarks are undertaken, these are given in Chapter 3.4.5. The radiative decay $\tilde{g} \to g\tilde{Z}_i$ has not yet been included in `SoftSusy` but will be added in a future version as it may be competitive with the 3-body decays included for compressed regions.

The sfermion $\tilde{f}$ decays included are, for the first two generations where there is no sfermion mixing[9]:

$$\tilde{q}_{L/R} \to \tilde{g}q, \qquad \tilde{f}_L \to \tilde{W}_j f', \qquad \tilde{f}_{L/R} \to \tilde{Z}_i f.$$

[9] f' indicates a fermion in the same generation as the f fermion but with opposite third component of weak isospin, i.e. f and f' could be u and d or ν_e and e^-.

The decays of the squarks to gluinos and quarks will routinely dominate if available as they occur via the strong interaction. The decays of left-handed sfermions tend to prefer wino-like neutralinos and charginos to bino-like as the gauge coupling of $SU(2)_L$ is greater than that of $U(1)_Y$. Nonetheless, for third generation sfermions decays to Higgsino-like neutralinos and charginos are also important, having potentially significant branching ratios due to the larger Yukawa couplings of the third generation. The 2-body decays of third generation sfermions are listed below; these are more exotic due to their larger Yukawa couplings, this opens up decay modes involving charged Higgses and neutral Higgs bosons. In addition, the larger Yukawas cause significant intra-generational mixing (not present for the first two generations) which allows decays involving W and Z bosons to occur more readily:

$$\begin{aligned}
\tilde{b}_{1/2} &\to \tilde{g}b, \tilde{W}_j t, \tilde{Z}_i b, \tilde{t}_{1/2} W^-, \tilde{t}_{1/2} H^-, \\
\tilde{t}_{1/2} &\to \tilde{g}t, \tilde{W}_j b, \tilde{Z}_i t, \tilde{b}_{1/2} W^+, \tilde{b}_{1/2} H^+, \\
\tilde{b}_2 &\to \tilde{b}_1 Z, \tilde{b}_1 h/H/A, \\
\tilde{t}_2 &\to \tilde{t}_1 Z, \tilde{t}_1 h/H/A, \\
\tilde{\tau}_{1/2} &\to \tilde{W}_j \nu_\tau, \tilde{Z}_i \tau, \tilde{\nu}_\tau W^-, \tilde{\nu}_\tau H^-, \\
\tilde{\nu}_\tau &\to \tilde{W}_j \tau, \tilde{Z}_i \nu_\tau, \tilde{\tau}_{1/2} W^+, \tilde{\tau}_{1/2} H^+, \\
\tilde{\tau}_2 &\to \tilde{\tau}_1 Z, \tilde{\tau}_1 h/H/A.
\end{aligned}$$

For charginos, the 2-body decay modes included are (where δ_{j1} is Kronecker delta):

$$\begin{aligned}
&\tilde{W}_j \to \tilde{q}_L \bar{q'}, \tilde{q}_{1/2} \bar{q'}, \tilde{l}_L \bar{\nu}_l, \tilde{\nu}_{l_L} \bar{l}, \tilde{\tau}_{1/2} \bar{\nu}_\tau, \tilde{\nu}_{\tau_L} \bar{\tau}, \tilde{Z}_i W^+, \tilde{Z}_i H^\pm, \delta_{j1} \tilde{Z}_1 \pi^\pm, \\
&\tilde{W}_2 \to \tilde{W}_1 Z, \tilde{W}_1 h/H/A.
\end{aligned}$$

The question of which of these are dominant is again a complicated one, for which decay calculators such as `SoftSusy` are specifically designed. There are general comments which can be made, with the decays to sfermions important either for Higgsino-like charginos, which have large branching ratios to third generation sfermions via their Yukawa couplings, or for wino-like charginos, which have moderate couplings to left-handed sfermions via the weak interaction. As expected, decays involving Higgs bosons (charged or neutral) are relevant as one chargino is more Higgsino-like and one more wino-like, both of which couple significantly to the Higgs. Decays involving Z bosons are more relevant when a Higgsino-like chargino is involved, similarly decays involving W bosons are more germane for wino-like charginos. Most of these general comments also apply to the case of neutralino 2-body decays.

We have also included a case which may be phenomenologically relevant, offering interesting signatures with long-lived charginos. This occurs when the lightest chargino and lightest neutralino are quasi-mass degenerate (such is the case when the lightest neutralino is wino dominated, for instance, as occurs often in AMSB models, see Chapter 2.1.2). In these cases it may be more appropriate to discuss decays into explicit hadrons rather than quark states if the mass splitting is of order a few times Λ_{QCD}. This includes 2-body chargino decay modes to the lightest neutralino and a pion. There are also 3-body modes which produce 2 pions and the

lightest neutralino, these are included in the 3-body SUSY modes listed in Chapter 3.4.5.

For neutralinos the 2-body decay modes are ($k > i$ as the neutralinos are mass ordered):

$$\tilde{Z}_i \to \tilde{f}_{L/R}\bar{f}, \tilde{f}_{1/2}\bar{f}, \tilde{W}_j W^+, \tilde{W}_j H^+,$$
$$\tilde{Z}_k \to \tilde{Z}_i Z, \tilde{Z}_i h/H/A.$$

The same comments as for the chargino decays apply regarding the favoured modes in scenarios with different admixtures of Higgsino and wino in the neutralinos. In addition there are also bino-like neutralinos, which interact little with any of the decay modes[10].

The 1-loop decay $\tilde{Z}_j \to \tilde{Z}_i\gamma$, for $j > i$, is yet to be included in the program, however it will soon be added as it may be competitive with the 3-body modes included in compressed regions of phase space.

3.4.2 MSSM Decays to Gravitinos

The following NLSP $\to \tilde{G} +$ SM decays are included (where SM indicates a Standard Model particle), for cases when the gravitino $\tilde{G}$ is the LSP. The gravitino often arises as the LSP in GMSB models as outlined in Chapter 2.1.3 - in this case these NLSP decays to gravitino LSPs offer interesting signatures at colliders, with long-lived NLSPs producing displaced vertices or even leaving the detector. The lifetime of the NLSP is governed by the mass of the gravitino. The decay modes included in `SoftSusy` are:

$$\tilde{g} \to g\tilde{G}, \qquad \tilde{q}_i \to q\tilde{G}, \qquad \tilde{l} \to l\tilde{G}, \qquad \tilde{Z}_i \to \gamma\tilde{G}, \qquad \tilde{Z}_i \to Z\tilde{G}, \qquad \tilde{Z}_i \to \phi\tilde{G}.$$

In these expressions ϕ denotes one of the neutral Higgs bosons h, H or A. The formulae for the partial widths are in Appendix A.5.

3.4.3 MSSM Higgs Tree-Level 2-Body Decays

The tree-level 2-body decay modes included for the Higgs particles in the MSSM are as follows, the formulae for the partial widths are explicitly given in Appendix A.3.6. The CP odd neutral Higgs boson has significantly fewer available decay modes than the CP even neutral Higgs bosons due to the constraint of CP conservation, this prevents decays of the A to two alike scalars or two alike vector bosons. Consequently, note that whilst all handedness combinations are allowed for the CP even Higgs in the decays to sfermions, the alike handedness combinations LL, RR are not allowed for the CP odd Higgs bosons. Similarly, for the third generation where there is squark mixing the combinations 11, 22 are not allowed for the CP odd Higgs bosons. For the decays to charginos however, alike combinations 11, 22 are allowed (in addition to unalike combinations) for the CP odd neutral Higgs bosons (as well as for the CP even neutral Higgs bosons as always) as the charginos are fermions:

[10]This is why bino-like LSPs are overproduced as a dark matter candidate, they interact little and so freeze-out early, leaving larger relic densities.

$$
\begin{aligned}
h/H/A &\to \tilde{f}_{L/R}\tilde{f}^*_{L/R}, \tilde{f}_{1/2}\tilde{f}^*_{1/2}, \tilde{W}_{1/2}\tilde{W}_{1/2}, \tilde{Z}_i\tilde{Z}_l, l^+l^-, \\
H^+ &\to \tilde{Z}_i\tilde{W}_j, q\bar{q'}, \nu_l\bar{l}, \tilde{f}_{L/R}\tilde{f}^*_{L/R}, \tilde{t}_{1/2}\tilde{b}^*_{1/2}, \nu_\tau\tilde{\tau}^*_{1/2}, hW^+, \\
h/H &\to AA, AZ, \\
H &\to H^+H^-, hh, VV, \\
A &\to h/HZ.
\end{aligned}
$$

The decay of the heavier CP even neutral Higgs boson to two vector bosons is listed here as it is typically heavy enough to decay into two on-shell vector bosons. In contrast, for the lightest (Standard Model-like) Higgs boson this decay is kinematically forbidden and instead the 3-body mode to a vector boson and fermion-antifermion pair via an off-shell vector boson occurs; this is listed later in Chapter 3.4.5. No $A \to VV$ decay is available due to CP conservation. The decays of the heavier CP even neutral Higgs H into two CP even or two CP odd Higgs bosons are relevant when both M_H and $\tan\beta$ have intermediate values [84].

The neutral Higgs decays to quarks are not included in this list as QCD corrections have been incorporated for these, see Chapter 3.4.8. It can be argued that QCD corrections for the charged Higgs decays to quarks are also important (although less so as the $H^\pm$ is an MSSM-only particle unlike the lightest CP even neutral Higgs boson), so QCD corrections to these decays will be added in a future version; they are particularly relevant for decays to the bottom quark at large $\tan\beta$ [84]. Meanwhile, the scenario where $m_{H^\pm} < m_t + m_b$ but $H^\pm$ undergoes a 3-body decay via an off-shell top to $W^\pm b\bar{b}$ is yet to be included. For H^+, decays to CKM suppressed combinations of q and q' are nonetheless considered in the program, for example $H^+ \to u\bar{s}$. Note however that the decays $H^+ \to H/AW^+$ are not included as they are kinematically forbidden in the MSSM assuming tree-level mass formulae, these modes are however included in the NMSSM.

3.4.4 MSSM Higgs 1-loop 2-body decays

The key Higgs 1-loop decays are also included as these are very important channels for LHC Higgs discovery and measurement:

$$h/H/A \to \gamma\gamma, Z\gamma.$$

The explicit expressions for their partial widths and the loop contributions included are in Appendix A.3.6 equations A.150 to A.204. The Feynman diagrams for these modes were given earlier in Chapter 2.5.1 in Figure 2.6. For the CP even neutral Higgs bosons the Standard Model contributions are fermion loops (dominantly top and bottom loops due to their larger Yukawa couplings) and W bosons, whilst in the MSSM there are also contributions from sfermions, charginos and charged Higgs bosons. In `SoftSusy` for the diphoton mode we include fermion contributions for top, bottom, charm and tau; sfermion contributions from stops, sbottoms and staus (as 3$^{\text{rd}}$ generation sfermions have larger Yukawa couplings and also tend to be lighter and so offer less suppressed contributions); charged Higgs contributions; W contributions and chargino contributions. For the $Z\gamma$ mode we include fewer contributions as the mode is yet to be observed

and so we need only potentially dominant contributions: we include top, bottom, charm, strange, W and charged Higgs contributions only. However with the lack of observation of a charged Higgs boson around the electroweak scale at the LHC and elsewhere, the charged Higgs contribution to $\gamma\gamma$ (and $Z\gamma$) is likely to be small as it is suppressed by $m_W^4/m_{H^\pm}^4$. Likewise, the contributions of the sfermions and charginos are increasingly small as their masses are pushed higher by LHC exclusions, with their contributions suppressed by $m_W^2/m_{\tilde{W}_i}^2$ and $m_W^2/m_{\tilde{f}}^2$ respectively. This pushes the partial width of the lightest CP even Higgs towards the Standard Model value as the supersymmetric particles in the loop decouple, producing the observed $h \to \gamma\gamma$ branching ratio. Meanwhile, the CP odd neutral Higgs only has contributions from fermion and chargino loops because of CP conservation.

The charged Higgs boson also has 1-loop decays to a photon and a W boson, or to a Z boson and a W boson, via top-bottom triangle loops dominantly [179]; however these are not phenomenologically important and are suppressed relative to the tree-level modes. These modes are not included in `SoftSusy`.

The loop decays to two gluons $\phi \to gg$ incorporate QCD corrections and so are listed in Chapter 3.4.8.

3.4.5 MSSM Tree-Level 3-Body Decays

The phenomenologically most important 3-body decays in the MSSM are included. For the neutralino decays to another neutralino and a fermion-antifermion pair $i > j$ as the neutralinos are mass-ordered:

$$
\begin{aligned}
h &\to V f \bar{f}. \\
\tilde{g} &\to \tilde{Z}_i q \bar{q}, \tilde{W}_i q \bar{q}'. \\
\tilde{Z}_i &\to \tilde{Z}_j f \bar{f}, \tilde{W}_j f \bar{f}'. \\
\tilde{W}_j &\to \tilde{Z}_i f \bar{f}', \delta_{j1} \tilde{Z}_1 \pi^\pm \pi^0.
\end{aligned}
$$

These 3-body modes are all typically suppressed relative to available 2-body modes and so are relevant largely in regions where no 2-body modes are available, such as compressed spectra. The Higgs 3-body modes to a vector boson and a fermion-antifermion pair via an off-shell vector boson intermediate have a large branching ratio for the Standard Model-like Higgs at 125 GeV as, whilst it is suppressed due to being 3-body, vector bosons have a large coupling to the Higgs boson via their large masses. Furthermore, for the Standard Model-like Higgs, these 3-body decays only compete with 2-body decays to fermions, for which the largest coupling is the (relatively small) bottom Yukawa coupling.

As for the gluino, its 3-body mode is available when the squarks are all heavier than the gluino[11]. The gluino 3-body modes to the lightest neutralino ordinarily dominate due to the larger phase space available, in addition the lightest stops are usually the lightest squarks and so

[11] This may occur if $M_3(M_{\rm GUT})$ is set lower than that expected from gaugino mass unification. It can even occur in the CMSSM - a CMSSM point in which the gluino is lighter than the squarks is given later in Figure 4.8.

the off-shell intermediate suppresses these modes less than for other heavier squark intermediates. Moreover, if the lightest neutralino is Higgsino-like then its couplings to squarks and quarks are proportional to the Yukawa couplings and so this further favours the 3-body decays to stops and tops, and to sbottoms and bottoms for large $\tan\beta$.

The 3-body modes of the neutralinos and charginos are particularly complex, having contributions from sfermion, Higgs and gauge boson intermediates, and so their relative strength depends on all of these couplings, making general comments more difficult. The neutralinos may only decay in 2-body modes to produce lighter neutralinos and Z bosons or neutral Higgs bosons, or lighter charginos and W bosons or charged Higgs bosons, or sfermion-fermion pairs; consequently typically the 3-body modes are the only decays available if the mass splitting between a neutralino and the lighter neutralinos is less than m_Z and the mass splitting between a neutralino and the lighter charginos is less than m_W. As a result, none of the fermions produced in the case of the neutralino 3-body decays decays will be a top quark in the relevant regions of parameter space. Which of the fermions are produced more abundantly depends on the exact nature of the spectrum. For larger mass splittings (although still smaller than the electroweak gauge boson masses) it is often the case that decays producing bottom quarks (and also tau leptons) dominate for the neutralino to neutralino decays as the large Yukawa couplings pull the sbottoms (staus) to lower masses so these sbottom intermediates suppress the partial widths less. In addition, the large Yukawa couplings also enhance their couplings to the Higgsino parts of the neutralinos. These effects are particularly relevant for the case of large $\tan\beta$ values as here the Yukawa couplings to bottoms and taus are amplified. As the mass splitting is reduced the phase space plays an increasing role and the necessity of additional mass energy in the case of the bottom quark (tau lepton) reduces the partial width relative to the first two generations until eventually the mass splitting is small enough that the 3-body decays producing these bottom quarks (tau leptons) are also kinematically forbidden, leaving only 3-body modes to the first and second generation fermions. Meanwhile, for the 3-body decays involving charginos the bottom is not relevant as it has to be produced in association with a top quark, which is too heavy to be relevant in these compressed phase space regions. Nonetheless the tau is particularly relevant as it is still third generation and is produced in association with a massless tau neutrino. Further information on the 3-body modes of electroweakinos is given in [180]. Once the mass splitting becomes very small, and the initial and final state electroweakino particles become quasi-degenerate, only first generation modes may become available. Eventually however as $\Delta m \to 0$ the quarks produced will not behave independently and instead hadronise together; consequently they must be considered together as hadrons in the final state and appropriate form factors accounted for, producing 2- and 3-body pion modes. We have included these for the phenomenologically interesting case of a near degenerate lightest chargino and neutralino LSP, as arising in AMSB.

As of yet, there are no 3-body decays of sfermions included; this will be resolved in future versions. The explicit formulae used for our 3-body decays, for which `sPHENO` [3] provided a useful reference, are given in Appendix A.4.

3.4.6 NMSSM SUSY and Higgs Tree-Level 2-Body decays

In the NMSSM, decays not involving the extended Higgs or neutralino sectors are the same as in the MSSM. For the extended neutralino and Higgs sectors the allowed decays are largely as before with the exception that now the neutralino index i runs from 1 to 5, whilst there is an additional CP even neutral Higgs and an additional CP odd neutral Higgs. All of the Higgs states are of course mixtures of the original MSSM states and the new NMSSM states, therefore the most "NMSSM-type" state need not necessarily be the heaviest. The $\tilde{Z}_{1,2,3,4}$, h and H (which we now use to label the lightest two CP even neutral Higgs bosons) and A have the same available modes as listed before; therefore we now list the decay modes of the additional states. As a guide, the same decays which can occur for the heaviest of the two CP even Higgs bosons of the MSSM, the H, may now also occur for the $H3$; similarly we can extend the decays of the A to the $A2$, and of the $\tilde{Z}_{1,2,3,4}$ of the MSSM to the $\tilde{Z}_5$. Additional decay modes in the NMSSM are therefore:

$$\begin{aligned}
\tilde{Z}_5 &\to W\tilde{W}_{1/2}, Z\tilde{Z}_n, H^{\pm}\tilde{W}_{1/2}, \tilde{Z}_n h/H/H3/A/A2, \tilde{f}_{L/R}\bar{f}, \tilde{f}_{1/2}\bar{f},\\
H3 &\to \tilde{f}_{L/R}\tilde{f}^*_{L/R}, \tilde{f}_{1/2}\tilde{f}^*_{1/2}, \tilde{W}_{1/2}\tilde{W}_{1/2}, \tilde{Z}_i\tilde{Z}_l, l^+l^-, AA, AA2,\\
H3 &\to A2A2, ZA/A2, H^+H^-, hh, hH, HH, W^-H^+, VV,\\
A2 &\to \tilde{f}_L\tilde{f}^*_R, \tilde{f}_1\tilde{f}^*_2, \tilde{W}_{1/2}\tilde{W}_{1/2}, \tilde{Z}_i\tilde{Z}_l, l^+l^-, Zh/H/H3, Ah/H/H3, W^-H^+,
\end{aligned}$$

where $VV \in \{W^+W^-,\ ZZ\}$, $i, l = 1, 2, 3, 4, 5$ and $n = 1, 2, 3, 4$ since the $\tilde{Z}_5$ decays into lighter neutralinos. As before, for the $A2$ there are fewer decays than the $H3$ as many decays are ruled out by CP conservation. For the decays to two sfermions, any combination of handedness is permitted LL, LR, RL, RR for the CP even Higgs decays and, similarly, for the decays to mixed sfermions all combinations 11, 12, 21, 22 are allowed; whilst for the CP odd Higgs decays the produced sfermions must be different by CP conservation and so only LR and RL, and 12 and 21 are available. Decays to all combinations 11, 12, 21, 22 are allowed for the charginos for both CP even and CP odd Higgs bosons. For the decays to quarks only charm, strange, top and bottom quarks are considered as the partial widths are proportional to the squares of the Yukawa couplings. Decays of the $H3$ or $A2$ to $q\bar{q}$ or gg are listed in Chapter 3.4.8 as QCD corrections are included in these channels.

The additional decays available in the NMSSM relative to the MSSM are similar, with the complication that the neutralinos have a supplementary singlino component and the CP even and CP odd neutral Higgs bosons have an extra singlet component. These singlino/singlet components have no interactions with the non-Higgs/Higgsino components in the model and so reduce the strengths of the interactions of the neutralinos and neutral Higgs bosons relative to the MSSM. Given the extended Higgs sector, it is now possible to have light CP even or CP odd Higgs bosons which are lighter than the Standard Model-like Higgs boson and therefore may significantly alter the phenomenology relative to the MSSM. Either the h or the H (i.e. the lightest or second lightest CP even neutral Higgs bosons) may now be identified with the

discovered Standard Model-like Higgs at 125 GeV. A light CP odd Higgs boson would allow Higgs to invisible decays to have a significant width due to $h \to AA$ decays. This can therefore be constrained via measurements of the visible decays to deduce the invisible width as the extra invisible width would suppress the other branching ratios, such as $h \to \tau\tau, bb$[12]. Searches for Higgs to two Higgs modes may be possible via searches for the decay products of the two produced Higgs bosons, such as $bb\tau^+\tau^-$ signals, if they can be observed above backgrounds. When such Higgs to Higgs decay modes are kinematically forbidden, the Higgs sector searches for the NMSSM are similar to those in the MSSM but with reduced couplings at tree-level and possible additional contributions at loop-level. We include more decay modes involving charged Higgs - gauge boson - neutral Higgs couplings as the theoretical mass constraints at tree-level in the NMSSM are far less stringent than in the MSSM. The effective MSSM is recovered from the NMSSM in the limit that $\lambda, \kappa \to 0$, $s \sim 1/\kappa \to \infty$ whilst keeping κ/λ and μ fixed, the Higgs sector then decouples into the MSSM doublet and a separate purely NMSSM singlet. Nonetheless with the additional Higgs states, if these couplings are slightly non-zero, the phenomenology can still therefore be quite different to the MSSM. In the neutralino sector in the NMSSM decoupling limit, the singlino neutralino decouples from the MSSM neutralinos and the neutralino sector of the NMSSM cannot be distinguished from the MSSM unless the singlino is the LSP. In this case NLSP MSSM neutralinos may leave the detector or produce displaced vertices. See references [92, 181] for further details of NMSSM phenomenology.

The explicit partial width expressions used within the decay calculator in the NMSSM in `SoftSusy` are given in Appendix A.6, the expressions were generalised from the MSSM corresponding decays with appropriate changes. `NMSSMTools` [126, 128, 159] proved a useful reference point with which to compare our decay widths and check the relevant formulae.

3.4.7 NMSSM 1-loop 2-Body Decays

As in the MSSM, in the NMSSM the important 1-loop decays of Higgs bosons are included:

$$h/H/H3/A/A2 \to \gamma\gamma, Z\gamma.$$

These modes are essentially identical to the 1-loop Higgs decays of the MSSM with the appropriate coupling changes. For the decay mode to diphotons we include fermion contributions from top, bottom, charm and tau; sfermion contributions from charm sfermions, strange sfermions, stops, sbottoms, staus and smuons; W contributions, charged Higgs contributions and chargino contributions. As in the MSSM case we need not include any first generation fermions or sfermions as their contributions are proportional to their Yukawas. In general only the 3$^{\text{rd}}$ generation contributions are important, particularly as the 3$^{\text{rd}}$ generation sfermions can be lighter and so the loop is less suppressed by the propagators. For the $Z\gamma$ mode as before we include fewer modes as it is yet to be observed at the LHC; the contributions included are

[12] Measurements via the total width of the Higgs directly are difficult as it is very narrow and so far only bounded experimentally rather than measured.

from tops, bottoms, charms, charginos, W bosons and charged Higgses. Meanwhile, whichever of the two lightest CP even Higgs bosons we identify with the Standard Model-like Higgs at 125 GeV must have its couplings very close to those of the Standard Model due to experimental constraints on its decay modes. The partial width expressions for these modes, and the loop contributions included, are listed in Appendix A.6 equations A.851 to A.902.

Again the decay to two gluons is listed in the next section as it includes QCD corrections. The detailed formulae used within the code for the partial widths of these modes are provided in Appendix A.7.

3.4.8 QCD Corrected Decays

NLO QCD corrections have been incorporated for the decays in which such effects are most important in both the MSSM and NMSSM, these are the neutral Higgs decays to quarks and decays to gluons:

$$h/H/H3/A/A2 \to q\bar{q}, gg.$$

The expressions used are given in Appendix A.7 and are based on those provided in the calculations in [182, 183]. Note that the quarks which are considered for neutral Higgs decays are only charm, strange and bottom for the lightest CP even neutral Higgs h, whilst the top is also included for the heavier CP even neutral Higgs boson(s) and for the CP odd neutral Higgs boson(s) of the (N)MSSM. Decays to u and d are negligible as a result of their small Yukawa couplings. For the decay to two quarks, the QCD corrections just offer an additional correction factor to the whole partial width, the corrections are identical in the MSSM and NMSSM with the difference arising in the tree-level formulae only. For the decay to two gluons, the situation is more complicated as there are both standard QCD and SUSY-QCD corrections, with the standard QCD corrections applying to all contributions but the SUSY-QCD contributions applying only to the scalar squark contributions. The corrections are therefore not just a simple factor to be applied. The QCD corrections for both the $q\bar{q}$ and gg case also differ between the CP even and CP odd neutral Higgs bosons as might be expected. These QCD corrections can be turned off if the user desires but by default are on as they result in significant changes to the partial widths, as detailed earlier at the end of Chapter 3.1.

Unlike in the case of the $\gamma\gamma$ and $Z\gamma$ decays, the masses used in the QCD corrected formulae cannot be running masses evaluated at the scale of the decaying Higgs mass - rather pole masses must be used in order to avoid double counting of corrections [174, 184]. The gauge coupling α_s is however evaluated at m_ϕ in order to attempt to include further additional corrections of higher orders.

3.5 Advantages of the SoftSusy Decay Calculator

Before moving on to the details of the use of the decay calculator for `SoftSusy`, its validation and a selection of results in the next chapter; we first summarise here the motivations and associated advantages of the `SoftSusy` decay calculator for the field:

- All-in-one spectrum generation and decay calculation: The program works straight out-of-the-box, performing the spectrum generation and decay calculation aspects automatically for each input file, producing one output file containing both the spectrum and decay information. There is no need to run model files or other programs in advance, it is absolutely self-contained for these aspects. This makes the program easy to use and straightforward to understand, both key features for any program to be used by the experimental and phenomenological communities. Moreover, with `SoftSusy` already a very popular spectrum generator, the addition of the decay calculator reduces the need to interface and pass information between many programs. It is at such junctions that issues typically occur, even with the SLHA, whether they be computational issues or issues of inconsistencies.

- NMSSM included in spectrum generation and decay calculation: Even amongst the many programs in this area it is very rare to have a program include both the spectrum generation and decay calculation aspects for the NMSSM, this will be of increasing importance to the field as the spotlight shifts from the most constrained MSSM models to its extensions. The only other options available are `NMSSMTools`, which, whilst it can perform spectrum calculation, typically was previously interfaced with `SoftSusy` to allow it to evaluate the spectrum before `NMSSMTools` evaluated the decay widths; meanwhile `SARAH` and `sPHENO` can be used together to perform spectrum generation and decay calculation in the NMSSM; whilst `NMSSMCalc` can evaluate the spectrum and widths for the Higgs sector only of the NMSSM. Consequently the inclusion of a spectrum generator and decay calculator within the same program for sparticle and Higgs decays of the NMSSM, with the program working without the need for any others, represents a significant advantage.

- Theoretical consistency: Interfaces and passing information between various programs for different aspects of these calculations, as they are very complicated, offer potential issues even with the SLHA. The decay calculator program has been explicitly built as part of the `SoftSusy` package and set up carefully to ensure the same assumptions and approximations are made in the same places. This ensures no additional theoretical errors originate from theoretical inconsistencies in the approaches and approximations taken, circumventing errors which may arise if separate programs are linked together.

- Additional decay calculator program: As should now be clear, the process of predicting the spectrum and partial widths for supersymmetric and Higgs particles is far from straightforward. Therefore the development of an additional decay calculator program allows for a further program against which to compare the theoretical predictions for given masses

and modes, allowing a greater awareness of the size of the theoretical errors involved in these calculations by observing the numerical differences produced by different approaches, approximations and included corrections. In addition, with the spectrum generator and decay calculator in one consistent package, error propagation can be examined, looking at how errors from the spectrum generation are enhanced or altered as they pass through the decay calculation in order to produce the theoretical predictions for experimentally observable branching ratios.

Chapter 4

Use and Results of the SoftSusy Decay Calculator

In this chapter we discuss how to use the `SoftSusy` program with an emphasis on the decay calculator program included in the package as a result of our work. We begin by explaining the input file flags and options, the decay information produced and the output file. This includes sample input and output files in addition to those provided directly with the program package. We then move on to outline the validation steps performed in the development of the decay calculator program. Finally, we present a comprehensive, but still far from exhaustive, catalogue of results produced by the `SoftSusy` decay program in order to provide an indication of the wide range of decay modes incorporated and the broad scope of the program for phenomenological applications. The paper associated with the `SoftSusy` decay calculator [1] contains further details and serves as its manual; the `SoftSusy` decay calculator incorporated into the overall `SoftSusy` program is also provided with this thesis.

4.1 How to use SoftSusy Decays

The `SoftSusy` program package is publicly available online at "http://softsusy.hepforge.org/", as well as with our paper at [1] and on `GitHub`; the `SoftSusy` web page being where the most up-to-date version is guaranteed to be found, along with a summary of changes made in each new version or sub-version released. The program comes with several test files and executables, for our uses we will primarily be interested in the main program executable `./softpoint.x` which runs the mass spectrum generation and decay calculation for a supersymmetric parameter point. For this executable itself there are several test files for the different models included:

- `./softpoint.x leshouches < inOutFiles/lesHouchesInput`
  - Runs the mass spectrum and decay calculation for a CMSSM model point.
- `./softpoint.x leshouches < inOutFiles/nmssmSLHAZ3Input`
  - Runs the mass spectrum and decay calculation for an NMSSM model point with Z_3 conservation.
- `./softpoint.x leshouches < inOutFiles/nmssmSLHAnoZ3Input`
  - Runs the mass spectrum and decay calculation for an NMSSM model point with Z_3 violation.

- `./softpoint.x leshouches < inOutFiles/rpvHouchesInput`
  - Runs the mass spectrum generation, but not the decay calculation, for an MSSM model point with R-parity violation, decay calculation can only be done with RPC currently.
- `./softpoint.x leshouches < inOutFiles/slha2Input`
  - Runs the mass spectrum for the CMSSM10.1.1 benchmark input point [185] - the decay calculation can be added via a line in the SOFTSUSY BLOCK to set item 0 to 1.
- `./softpoint.x leshouches < inOutFiles/pmssmInput`
  - Runs the mass spectrum for a pMSSM input point including the decay calculations.

More information on flags and options are given in the next section, whilst a number of additional input files will be explored later in Chapter 4.2 as we present the validation and a selection of results from the decay calculator program.

4.1.1 Input

The input file in `SoftSusy` contains a number of options for the mass spectrum generation and decay calculation. We focus on those of particular relevance to the partial width calculation aspects, further information on other options in the input file are available in the `SoftSusy` manuals [1, 66, 68, 69, 117–119]. A sample input file for the `SoftSusy` program is given in Figure 4.1; it is the `lesHouchesInput` file provided with the program and the different inputs are highlighted by the arrows. The input file is in SLHA form and split into 4 sections. The first BLOCK MODSEL is where the appropriate model is chosen: in the example in the figure item 1 in this block is chosen as 1 to indicate mSUGRA as the supersymmetry breaking model (this is the only option for the NMSSM), 2 indicates GMSB, 3 indicates AMSB; the item 3 in this block if present is set to 0 (default) to select the MSSM or 1 to select the NMSSM; item 4 indicates R-parity conservation if set to 0 (default) whilst 1 indicates RPV[1]; item 6 chooses no flavour violation if set to 0 (default). The second BLOCK, labelled "SMINPUTS", is where the input boundary conditions at the low scale are set on parameters such as the $\overline{MS}$ fine structure constant $\alpha^{\overline{\rm MS}}(m_Z)$ and strong coupling constant $\alpha_s^{\overline{\rm MS}}(m_Z)$, the Fermi constant, the Z, top and τ pole masses and the $\overline{MS}$ bottom mass $m_b^{\overline{\rm MS}}(m_b)$, amongst other possible inputs. The BLOCK "MINPAR" similarly is where the high scale boundary conditions for the RGEs are set, in the case of mSUGRA as in the sample input file this requires setting the unified scalar mass m_0, unified fermion mass $m_{\frac{1}{2}}$, ratio of VEVs of the two Higgs doublets $\tan\beta$, the unified trilinear coupling A_0 and the sign of the μ parameter. Further descriptions of these input options are available in the SLHA and SLHA2 papers [156] and [157]. An additional optional BLOCK "EXTPAR" may be also introduced to provide further non-standard inputs for high scale boundary conditions, for example for the pMSSM. Here NMSSM parameters may additionally be specified but only subsets of parameters which can be independently set and which lead to correct Higgs minimisation may be set together. Finally, the BLOCK "SOFTSUSY" sets the `SoftSusy` specific input flags for the spectrum generation and decay calculation. Item 0 is set to 1 to inform the program to perform decay calculations, by default the decay calculation

[1] RPV can only be run for the spectrum generation, not the decay calculation.

is not called. Items 24, 25 and 26 provide further information for the decay calculator program: item 24 sets the value of the minimum branching ratio output in the decay tables, the default is 10^{-6}; item 25 switches the 3-body decays on or off with 1 (default) calculating them if they are required and 0 switching 3-body decay calculations off. This may be useful in order to save time in large scans as the 3-body decays are performed numerically and so take longer. Finally, item 26 allows the partial widths to also be output in the decay tables, this can be useful if comparing different programs. The default option (0) has the partial widths not output, whilst the option 1 outputs the partial widths beyond the comments column in order to not disturb the SLHA format and still allow the output to be passed directly to other programs further down the analysis chain. Beyond these options there are the spectrum generator specific options, which are outlined in greater detail in [66]; these set the numerical precision for the convergence of the spectrum, the number of loops, gravitino mass and other inputs.

It is also possible to use command line input to set up the mass spectrum generation and decay calculation with the main executable `./softpoint.x`, rather than supply a "leshouches" input file. For the spectrum generator part the default format of the options is `./softpoint.x <SUSY-breaking-model> [SUSY-breaking-model options] [general options]` with the specific details provided in the MSSM RPC and the NMSSM `SoftSusy` manuals [66] and [118] respectively. The options relevant for the decay calculator are that `--decays` switches on the decay calculation, `--minBR=<value>` sets the minimum branching ratio to be output, `--dontCalculateThreeBody` switches off the 3-body decays, whilst `-outputPartialWidths` ensures the partial widths are output in addition to the branching ratios. For example, the `lesHouchesInput` file of Figure 4.1 can be replicated using the command line via:

```
./softpoint.x sugra --m0=125 --m12=500 --a0=0 --sgnMu=1 --tanBeta=10 --decays --higgsUncertainties.
```

There are further flags and switches inside the source code for users requiring finer control of the decay calculator. There are flags at the start of the code named `flag<particle name>` - when these flags have value 1 the particle decays are calculated, therefore by default all such flags are set to 1. These flags allow the user to turn off irrelevant decays for their analyses; for example in producing the scanning plots, such as Figure 4.9 in Chapter 4.2.3, all decays apart from those of the relevant decaying particle were turned off by setting these flags for all other particles to 0, allowing the plots to be produced more straightforwardly. Similarly there is a Boolean variable `QCDcorr`, which by default is `true`, which may be used to turn off QCD corrections. In case the user should want to run the parameters used to different scales, for example in performing comparisons with other decay calculators, it should be noted that running in `SoftSusy` is implemented using `MssmSoftsusy` and `NmssmSoftsusy` objects (detailed in references [66] and [118] respectively) and the `runto` command. If one alters the running scales within `SoftSusy` one must remember to instruct `SoftSusy` to recalculate the $\overline{DR}$ parameters at this scale using `calcDRbarPars()`. Nonetheless, any changes made to the code are at the user's risk. Finally, given the dependence of many of the partial widths on the input parameters, and in particular on the quark masses used, users may wish to alter the quark masses m_q. This

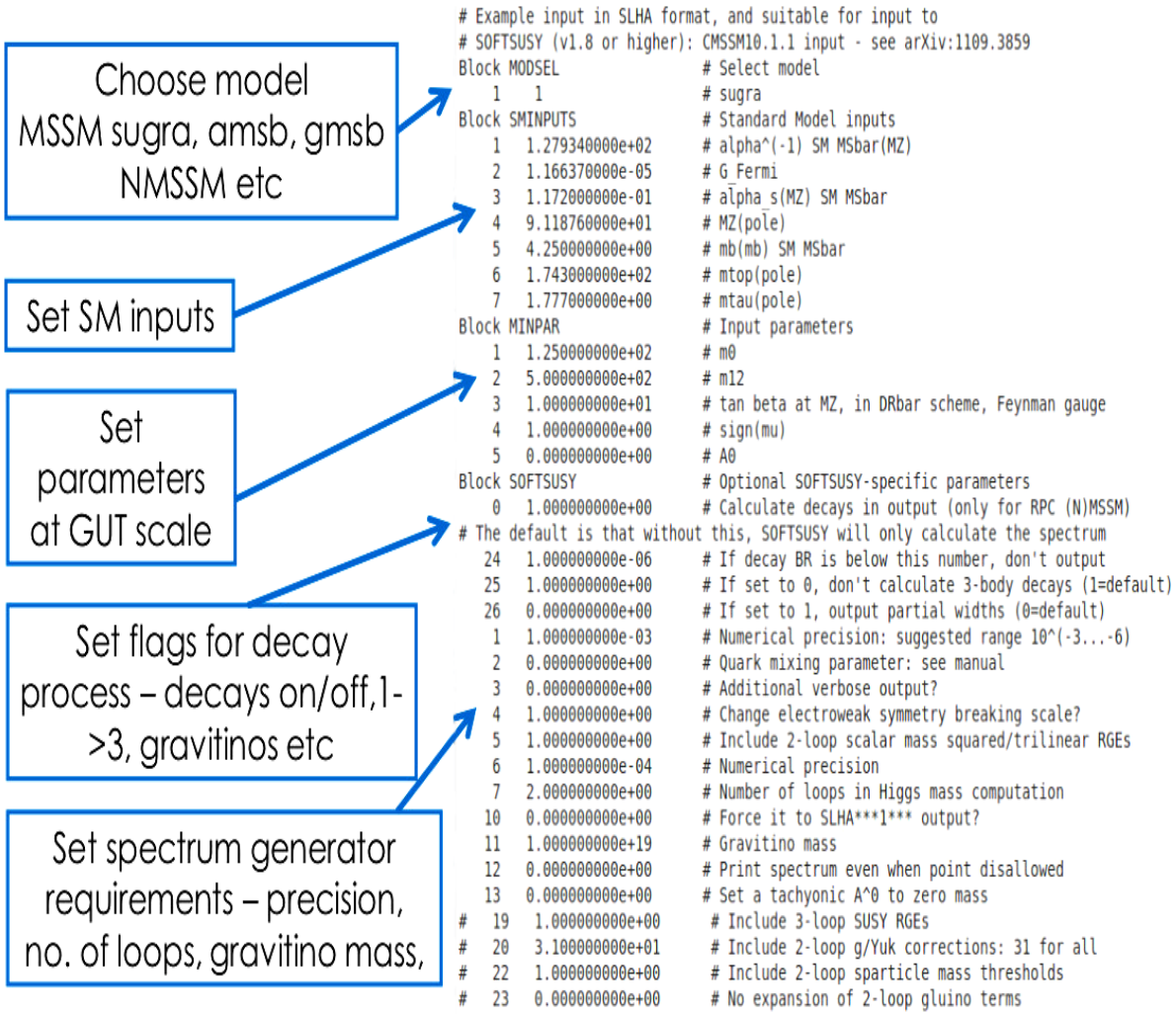


```
# Example input in SLHA format, and suitable for input to
# SOFTSUSY (v1.8 or higher): CMSSM10.1.1 input - see arXiv:1109.3859
Block MODSEL                # Select model
    1    1                  # sugra
Block SMINPUTS              # Standard Model inputs
    1   1.279340000e+02     # alpha^(-1) SM MSbar(MZ)
    2   1.166370000e-05     # G_Fermi
    3   1.172000000e-01     # alpha_s(MZ) SM MSbar
    4   9.118760000e+01     # MZ(pole)
    5   4.250000000e+00     # mb(mb) SM MSbar
    6   1.743000000e+02     # mtop(pole)
    7   1.777000000e+00     # mtau(pole)
Block MINPAR                # Input parameters
    1   1.250000000e+02     # m0
    2   5.000000000e+02     # m12
    3   1.000000000e+01     # tan beta at MZ, in DRbar scheme, Feynman gauge
    4   1.000000000e+00     # sign(mu)
    5   0.000000000e+00     # A0
Block SOFTSUSY              # Optional SOFTSUSY-specific parameters
    0   1.000000000e+00     # Calculate decays in output (only for RPC (N)MSSM)
# The default is that without this, SOFTSUSY will only calculate the spectrum
   24   1.000000000e-06     # If decay BR is below this number, don't output
   25   1.000000000e+00     # If set to 0, don't calculate 3-body decays (1=default)
   26   0.000000000e+00     # If set to 1, output partial widths (0=default)
    1   1.000000000e-03     # Numerical precision: suggested range 10^(-3...-6)
    2   0.000000000e+00     # Quark mixing parameter: see manual
    3   0.000000000e+00     # Additional verbose output?
    4   1.000000000e+00     # Change electroweak symmetry breaking scale?
    5   1.000000000e+00     # Include 2-loop scalar mass squared/trilinear RGEs
    6   1.000000000e-04     # Numerical precision
    7   2.000000000e+00     # Number of loops in Higgs mass computation
   10   0.000000000e+00     # Force it to SLHA***1*** output?
   11   1.000000000e+19     # Gravitino mass
   12   0.000000000e+00     # Print spectrum even when point disallowed
   13   0.000000000e+00     # Set a tachyonic A^0 to zero mass
#   19   1.000000000e+00      # Include 3-loop SUSY RGEs
#   20   3.100000000e+01      # Include 2-loop g/Yuk corrections: 31 for all
#   22   1.000000000e+00      # Include 2-loop sparticle mass thresholds
#   23   0.000000000e+00      # No expansion of 2-loop gluino terms
```

Figure 4.1: The input file `lesHouchesInput` included with the `SoftSusy` package. It is split into four sections for different input information and is SLHA-compliant. The first BLOCK MODSEL indicates the supersymmetric model and supersymmetry breaking to use, the section BLOCK SMINPUTS sets the Standard Model input values used as boundary conditions for the RGEs at the low scale. The third BLOCK MINPAR sets the high scale boundary conditions specific to the model of supersymmetry breaking, further information can be provided in an optional additional BLOCK "EXTPAR" (see [66, 156]). The final SOFTSUSY BLOCK contains the `SoftSusy` spectrum generator and decay calculator specific input, with items 0, 24, 25, 26 for the decay calculation.

may be done in the input file `BLOCK SMINPUTS`, the masses used within the decay calculator ("kinematic" and "running") will change accordingly.

4.1.2 Output

The output comes in the standard SLHA/SLHA2 format [156, 157]. In concordance with SLHA conventions the particle masses, total widths and partial widths (`PW`) are output in units of GeV.

Running the `./softpoint.x` executable with either an input file (such as that provided in Figure 4.1) or command line instructions produces a single output file in around 0.1-1s,

containing all the mass spectrum and decay branching ratios information for the supersymmetric and Higgs particles in the model. Furthermore, this information is all provided in SLHA/SLHA2 format [156, 157] and so may be passed straight into additional programs, for example `PYTHIA` if event generation is required. This makes the `SoftSusy` program straightforward to use. For the sample input file provided in Figure 4.1, the output file `lesHouchesOutput` provided with the `SoftSusy` package is generated, this is split into several parts with Figures 4.2 and 4.3 illustrating the parts containing the mass spectrum and one decay table[2]. The structure of the output file produced is as follows:

- Input information - At the top of the output file the input information provided to the `SoftSusy` program is listed so that output files can be identified with the input files.
- Mass spectrum - Next, the BLOCK MASS, lists the masses of all the supersymmetric and Higgs particles of the model, as seen in Figure 4.2.
- Couplings and Mixing Matrices - The couplings and mixing matrices calculated are output next.
- Decay information - For each possible parent supersymmetric and Higgs particle in the model a decay table is produced. This lists the total width of the particle followed by all available modes with branching ratio greater than `minBR` and their associated branching ratios. `NDA` indicates the number of daughter particles produced in the decay (2 or 3 in the current version of the `SoftSusy` decay calculator), the `PDGi` columns give the Particle Data Group (PDG) codes of the daughter particles produced in the decays (see Section 43 of Ref. [33] for a list of PDG codes) and the final column, following the `#` symbol, contains a human-readable comment listing the decay mode. Beyond this column the partial widths are output if Item 26 in the SOFTSUSY BLOCK is set to 1 or `--outputPartialWidths` is used as a command line option. The decay table for the gluino decays is shown in Figure 4.3 from the `lesHouchesOutput` file.
- Finally, as of recent versions of `SoftSusy`, the uncertainties in the predictions of the Higgs masses are output into a BLOCK DMASS at the bottom of the output file.

This output information may be more easily visualised using the program `pyslha` [186]; this allows the production of Figure 4.4 straight from the SLHA `SoftSusy` output file, here for the `lesHouchesOutput` file. It shows the mass spectrum produced as well as all the decays of branching ratio greater than `minBR`$= 10^{-5}$ shown with arrows, with bolder, thicker arrows indicating larger branching ratios.

4.1.3 Decay Information

The decay information produced by the `SoftSusy` decay calculator is stored in an object-oriented manner, with each possible parent supersymmetric and Higgs particle having a decay object of the `Particle` class containing all the relevant decay information determined. We display the class in Table 4.1, the user may wish to access this information if they seek to alter the code for their own purposes.

[2]The whole output file is available with the `SoftSusy` package but is too long to provide in full here.

```
Block MASS                  # Mass spectrum
# PDG code      mass        particle
        24     8.03604456e+01   # MW
        25     1.13377987e+02   # h0
        35     7.06258916e+02   # H0
        36     7.05981693e+02   # A0
        37     7.10783740e+02   # H+
   1000021     1.14489121e+03   # ~g
   1000022     2.04338616e+02   # ~neutralino(1)
   1000023     3.85279664e+02   # ~neutralino(2)
   1000024     3.85275816e+02   # ~chargino(1)
   1000025    -6.22425291e+02   # ~neutralino(3)
   1000035     6.36914220e+02   # ~neutralino(4)
   1000037     6.37189628e+02   # ~chargino(2)
   1000001     1.05321726e+03   # ~d_L
   1000002     1.05036934e+03   # ~u_L
   1000003     1.05321501e+03   # ~s_L
   1000004     1.05036709e+03   # ~c_L
   1000005     9.66192879e+02   # ~b_1
   1000006     8.06475613e+02   # ~t_1
   1000011     3.61526445e+02   # ~e_L
   1000012     3.52607618e+02   # ~nue_L
   1000013     3.61523108e+02   # ~mu_L
   1000014     3.52604199e+02   # ~numu_L
   1000015     2.22672378e+02   # ~stau_1
   1000016     3.51418985e+02   # ~nu_tau_L
   2000001     1.00857791e+03   # ~d_R
   2000002     1.01190679e+03   # ~u_R
   2000003     1.00857573e+03   # ~s_R
   2000004     1.01190423e+03   # ~c_R
   2000005     1.00538427e+03   # ~b_2
   2000006     1.01147162e+03   # ~t_2
   2000011     2.29807642e+02   # ~e_R
   2000013     2.29796987e+02   # ~mu_R
   2000015     3.62610867e+02   # ~stau_2
```

Figure 4.2: The second part of a `SoftSusy` output file, this contains the parameters determined by the spectrum generation, i.e. the masses of the supersymmetric and Higgs particles and their couplings and mixing matrices. This is from the file `lesHouchesOutput`.

```
#     PDG            Width
DECAY 1000021     1.41408172e+01   # Gluino decays
#     BR                NDA    PDG1         PDG2        Comments
      2.13758723e-02    2      1         -1000001   # ~g -> d ~d_L*
      2.13758723e-02    2     -1          1000001   # ~g -> db ~d_L
      4.53615031e-02    2      1         -2000001   # ~g -> d ~d_R*
      4.53615031e-02    2     -1          2000001   # ~g -> db ~d_R
      2.26657670e-02    2      2         -1000002   # ~g -> u ~u_L*
      2.26657670e-02    2     -2          1000002   # ~g -> ub ~u_L
      4.33066040e-02    2      2         -2000002   # ~g -> u ~u_R*
      4.33066040e-02    2     -2          2000002   # ~g -> ub ~u_R
      2.13768707e-02    2      3         -1000003   # ~g -> s ~s_L*
      2.13768707e-02    2     -3          1000003   # ~g -> sb ~s_L
      4.53628609e-02    2      3         -2000003   # ~g -> s ~s_R*
      4.53628609e-02    2     -3          2000003   # ~g -> sb ~s_R
      2.26663840e-02    2      4         -1000004   # ~g -> c ~c_L*
      2.26663840e-02    2     -4          1000004   # ~g -> cb ~c_L
      4.33077833e-02    2      4         -2000004   # ~g -> c ~c_R*
      4.33077833e-02    2     -4          2000004   # ~g -> cb ~c_R
      7.36731998e-02    2      5         -1000005   # ~g -> b ~b_1*
      7.36731998e-02    2     -5          1000005   # ~g -> bb ~b_1
      4.83144041e-02    2      5         -2000005   # ~g -> b ~b_2*
      4.83144041e-02    2     -5          2000005   # ~g -> bb ~b_2
      1.12588751e-01    2      6         -1000006   # ~g -> t ~t_1*
      1.12588751e-01    2     -6          1000006   # ~g -> tb ~t_1
```

Figure 4.3: The third part of a `SoftSusy` output file, this contains the parameters determined by the decay calculator, i.e. the total widths, available decay modes and branching ratios for each supersymmetric and Higgs particle in the model. Here we provide just the decay table for the gluino, this is followed by a similar table for each of the other parent particles in the model. This is from the file `lesHouchesOutput`.

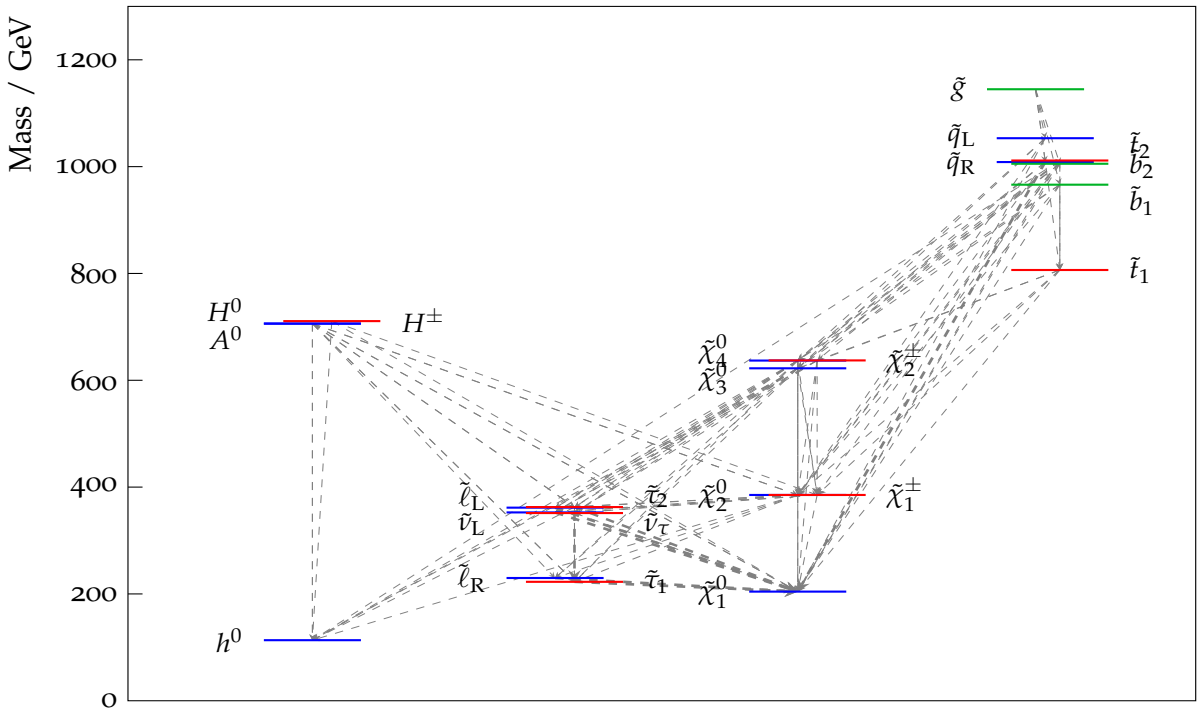

Figure 4.4: Visualisation of the output information contained in the `lesHouchesOutput` file and produced by `SoftSusy`, the mass spectrum is shown along with the decay branching ratios available (with branching ratio greater than 10^{-5}) to each particle, with bolder, thicker arrows indicating larger branching ratios. This figure has been produced by passing the SLHA output file lesHouchesOutput to the `slhaplot` executable of the `pyslha` interface program [186], the command line input required is `./slhaplot lesHouchesOutput --br=10e-5 --decaystyle=brwidth`.

data variable	description
`string name`	particle name
`double mass`	particle mass
`double PDG`	particle PDG code
`double No_of_Decays`	Total Number of possible decays of particle
`double No_1to2_Decays`	Total Number of possible 2-body decays of particle
`double No_1to3_Decays`	Total Number of possible 3-body decays of particle
`double No_grav_Decays`	Total Number of possible decays of particle to LSP gravitinos
`double No_NMSSM_Decays`	Total Number of possible decays of particle in the NMSSM
`double total_width`	Total Decay Width of the particle
`double two_width`	2-body decay partial width of the particle
`double three_width`	3-body decay partial width of the particle
`vector <vector<double>> Array_Decays`	A Nx6 array, where N = `No_of_Decays`. PDGs of the daughter particles are in columns 0 and 1 (and 4 for 3-body decays), the partial widths are in column 2, the number of daughters (NDA) in column 3 and the branching ratios in column 5.
`vector <string> Array_Comments`	A Nx1 array (vector), where N = `No_of_Decays`, listing each decay mode, e.g. $\tilde{g} \to \bar{u}\tilde{u}_L$.

Table 4.1: The information contained in the `Particle` object for each of the decaying particles. PDG codes are given in the reference [157]. Note that the numbers of decays contained in `double No_..._Decays` are the total number of such decays assuming non are kinematically forbidden. All these decays are checked by the program to see if they are allowed kinematically and calculated if so.

4.2 Validation and Results

We begin now comparisons of the results of the `SoftSusy` decay calculator against other publicly available decay programs, this also serves to illustrate a selection of the results which can be produced using the program. Specific and fairly extensive tests and comparisons were made for particular benchmark points against the programs `sPHENO`, `SUSYHIT` and `NMSSMTools`. Comparisons for some of these benchmark points are provided here for a selection of decaying SUSY and Higgs particles as illustrations; in addition scans over the mass of the decaying particle are given for the decays of the lightest SM-like Higgs and for the decays of a gluino $\tilde{g}$. The results given in this section represent only a small selection of the actual validation performed and only give a flavour of the results our program can produce. Nonetheless they allow both a qualitative check of the behaviour of the decays in the program and a quantitative comparison of the level of agreement with other programs. In particular the level of agreement with the same input parameters and with our set of input parameters is detailed in some specific cases.

4.2.1 Supersymmetric 2-body decays

All 2-body supersymmetric decay modes at tree-level are included in the `SoftSusy` program, therefore this is by far the biggest class of decay modes included. Nonetheless these modes are also amongst the simplest both from a physics point of view and computationally. To demonstrate this vast swathe of decay modes, we consider the decays of the lightest stop, $\tilde{t}_1$. The comparison of the results for this benchmark point between the new `SoftSusy` decay calculator and those of `SUSYHIT-1.4` is given in Table 4.2. The input values used for the various masses are: top pole mass `mtPole`= 174.3 GeV, bottom pole mass `mbPole`= 4.985 GeV, running top mass `runmt`= 145.555 GeV and running bottom mass `runmb`= 2.576 GeV. These differ from the default values used for these quantities in `SUSYHIT` and Table 4.2 illustrates the differences observed between `SoftSusy` and `SUSYHIT-1.4` branching ratios calculated as a result, as well as the differences when `SoftSusy` has the `SUSYHIT` mass inputs inserted by hand. This demonstrates that the level of agreement between the programs is around 10%, dropping down to 1% when the same input masses and coupling constants are used in both programs. These differences result from the different mass and scheme choices, as outlined in Chapter 3.3.3. The remaining disagreements in the neutralino decay modes occur as a result of differences in the neutralino mixing matrix due to differences in its calculation.

4.2.2 Higgs tree-level and 1-loop decays

The second key class of decay modes included in `SoftSusy` are those of the supersymmetric Higgs particles. These are of great importance due to the discovery of the Standard Model-like Higgs at the LHC. In Table 4.4, we perform similar comparisons between `SoftSusy` and `HDECAY-3.4` of `SUSYHIT-1.4` for Higgs decays. Here we have taken a SM-like Higgs, in the decoupling limit so all the SUSY decays are kinematically forbidden, given by a point in the

SoftSusy default inputs		SoftSusy SUSYHIT's inputs		SUSYHIT		mode
PW/GeV	BR	PW/GeV	BR	PW/GeV	BR	
1.833e+00	3.202e-01	1.708e+00	3.211e-01	1.708e+00	3.218e-01	$\tilde{t}_1 \to b\tilde{W}_1$
1.267e+00	2.218e-01	1.103e+00	2.073e-01	1.103e+00	2.078e-01	$\tilde{t}_1 \to b\tilde{W}_2$
1.304e+00	2.277e-01	1.299e+00	2.441e-01	1.299e+00	2.448e-01	$\tilde{t}_1 \to t\tilde{Z}_1$
7.181e-01	1.254e-01	6.848e-01	1.287e-01	6.729e-01	1.268e-01	$\tilde{t}_1 \to t\tilde{Z}_2$
6.009e-01	1.049e-01	5.250e-01	9.871e-02	5.249e-01	9.889e-02	$\tilde{t}_1 \to t\tilde{Z}_3$

Table 4.2: $\tilde{t}_1$ decays at the parameter point of the `lesHouchesInput` file provided with `SoftSusy`, which has a common scalar mass $m_0 = 125\,\text{GeV}$, a common gaugino mass $m_{1/2} = 500\,\text{GeV}$, ratio of Higgs vacuum expectation values $\tan\beta = 10$, sign of the superpotential μ parameter $\text{sign}(\mu) = +1$ and common soft SUSY breaking trilinear parameter $A_0 = 0$ in the constrained MSSM (CMSSM). This results in $m_{\tilde{t}_1} = 808.7\,\text{GeV}$, $m_{\tilde{W}_1} = 385.0\,\text{GeV}$, $m_{\tilde{W}_2} = 637.5\,\text{GeV}$, $m_{\tilde{Z}_1} = 204.0\,\text{GeV}$, $m_{\tilde{Z}_2} = 385.0\,\text{GeV}$, $m_{\tilde{Z}_3} = -622.7\,\text{GeV}$, $m_{\tilde{Z}_4} = 637.2\,\text{GeV}$. This table compares the partial widths and branching ratios as output by `SoftSusy` with our mass choices (and corresponding Yukawa couplings) and with the masses and Yukawa couplings in `SUSYHIT`, with the results of `SUSYHIT-1.4`. This illustrates the differences of order 10% that may arise depending upon mass ("kinematic" and "running") choices, the differences reduce to order 1% once the same masses are taken. `SoftSusy-4.0` was used for these results.

pMSSM parameter space which has Higgs mass 125 GeV - this point we call `pmssm1` and the SLHA [156] form of the input file is given verbatim in Table 4.3. The results of our decay calculator without QCD corrections included, with QCD corrections included, and with the same input quark and gauge boson masses and same input gauge couplings as `SUSYHIT`, again with QCD corrections, are compared with `HDECAY-3.4`. Note that the comparisons are done against the non-current version `HDECAY-3.4` as this is the version included in the `SUSYHIT-1.4` package. This allowed straightforward comparisons to be done between the new decay calculator and `SUSYHIT`'s version of `HDECAY` as one can input the spectrum as calculated by `SoftSusy` straight into `SUSYHIT`. This allowed the effects of the spectrum generator to be isolated as much as possible from the decay calculator which is being tested. Nonetheless, even with the same spectrum `SUSYHIT` first converts the mixing matrices and other inputs to its own conventions and assumptions, this accounts for the remaining numerical differences between the codes.

We include important QCD corrections for the neutral Higgs decays to quarks and to gluons. In Table 4.4, the comparison of the partial widths with QCD corrections switched on and switched off clearly demonstrates the significant difference these corrections make, as is widely known in the literature [84, 115, 183, 187]. Furthermore, it is clear that the main source of differences in partial widths between the decay calculator of `SoftSusy-4.0` and `HDECAY` is in the choice of masses used. Remaining differences tend to be small and are due largely to differences in other inputs, the exception being the decays to two vector bosons where order 10% differences are observed. This is due to `HDECAY` incorporating additional effects such as the width of the resonance and NLO corrections which are not included in `SoftSusy`. It should also be noted here that `HDECAY` performs a numerical integration whilst `SoftSusy` has an explicit expression with no integration required so the calculation methods are different. A comparison of the branching ratios output for this SM-like Higgs are given in Figure 4.5. In particular it should be noted that as `SoftSusy` predicts a larger partial width for the $h \to bb$ mode in this case due to a difference

```
Block MODSEL                # Select model
    1    0                  # non universal
    1    1                  # sugra input
Block SMINPUTS              # Standard Model inputs
    1   1.279340000e+02     # alpha^(-1) SM MSbar(MZ)
    2   1.166370000e-05     # G_Fermi
    3   1.172000000e-01     # alpha_s(MZ) SM MSbar
    4   9.118760000e+01     # MZ(pole)
    5   4.250000000e+00     # mb(mb) SM MSbar
    6   1.733000000e+02     # mtop(pole)
    7   1.777000000e+00     # mtau(pole)
Block MINPAR      # Input parameters
    1   1.000000000e+03     # m0
    2   3.000000000e+02     # m12
    3   3.000000000e+01     # tanb
Block SOFTSUSY              # Optional SOFTSUSY-specific parameters
    0   1.000000000e+00     # Calculate decays in output (only for RPC (N)MSSM)
    1   1.000000000e-03     # Numerical precision: suggested range 10^(-3...-6)
    2   0.000000000e+00     # Quark mixing parameter: see manual
    5   1.000000000e+00     # Include 2-loop scalar mass squared/trilinear RGEs
   24   1.000000000e-09     # If decay BR is below this number, don't output
   25   1.000000000e+00     # If set to 0, don't calculate 3-body decays (1=default)
   26   1.000000000e+00     # Output PWs
Block EXTPAR          # non-universal SUSY breaking parameters
      0   -1.000000000000000e+00         # Set MX=MSUSY
      3    1.000000000000000e+03         # M_3(MX)
     11   -7.700000000000000e+03         # At(MX)
     12    1.000000000000000e+03         # Ab(MX)
     13   -3.000000000000000e+03         # Atau(MX)
     23    3.000000000000000e+02         # mu(MX)
     26    3.000000000000000e+03         # mA(pole)
     33    3.000000000000000e+03         # mtauL(MX)
     36    3.000000000000000e+03         # mtauR(MX)
     43    3.500000000000000e+03         # mqL3(MX)
     46    3.800000000000000e+03         # mtR(MX)
```

Table 4.3: The pMSSM parameter space point used for the h decay comparisons in Table 4.4 and Figure 4.5, and for the $h \to \gamma\gamma$ loop contributions in Figure 4.7, this input file is in SLHA form [156].

in the default b mass used, then as this is a dominant decay mode this difference causes a larger total Higgs decay width in `SoftSusy` and so suppresses the branching ratios of the other modes slightly. For example, the partial widths for the $h \to cc$ mode are in exact agreement between `SoftSusy` and `HDECAY` in Table 4.4, however `SoftSusy` calculates a reduced branching ratio for this mode due to the larger predicted total width. Such effects are apparent in Figure 4.5 due to the logarithmic scale.

In order to provide a qualitative demonstration that the decay calculator is functioning correctly one may also scan the mass of the decaying particle and investigate how the partial widths and branching ratios change. Figure 4.6 shows how the branching ratios of a SM-like Higgs change as its mass is scanned from the Z^0 boson mass up to 200 GeV as calculated in (a) `SoftSusy` and in (b) a well-known plot produced by the LHC Higgs Cross Section Working Group [188] in 2011. This shows a good level of agreement, with small differences due to effects detailed previously in the quantitative comparison at $m_h = 125\,\text{GeV}$. The largest differences are in the cc, $\tau\tau$, gg, $\gamma\gamma$ channels and particularly at the low energy end near m_Z. There are several effects which cause this, in addition to those previously listed; firstly the amplitudes of the bb, cc channels are particularly sensitive to the value of α_s used. This dictates the size of the NLO QCD corrections, with larger α_s values enlarging the corrections and reducing the width; these effects

SoftSusy no QCD corrections		SoftSusy with QCD corrections		SoftSusy with SUSYHIT's masses and QCD corrections		HDECAY-3.4 with same QCD corrections		mode
PW	BR	PW	BR	PW	BR	PW	BR	
1.04e-04	3.30e-02	2.25e-04	4.03e-02	2.25e-04	4.31e-02	2.25e-04	4.24e-02	$h \to cc$
8.00e-07	2.55e-04	1.62e-06	2.91e-04	1.62e-06	3.11e-04	1.63e-06	3.06e-04	$h \to ss$
1.75e-03	5.56e-01	3.96e-03	7.10e-01	3.60e-03	6.90e-01	3.61e-03	6.80e-01	$h \to bb$
8.52e-07	2.71e-04	8.52e-07	1.53e-04	9.17e-07	1.76e-04	9.19e-07	1.73e-04	$h \to \mu\mu$
2.61e-04	8.30e-02	2.61e-04	4.67e-02	2.59e-04	4.97e-02	2.60e-04	4.90e-02	$h \to \tau\tau$
1.06e-05	3.36e-03	1.06e-05	1.89e-03	9.24e-06	1.77e-03	9.24e-06	1.74e-03	$h \to \gamma\gamma$
1.65e-04	5.27e-02	2.71e-04	4.86e-02	2.72e-04	5.22e-02	2.72e-04	5.13e-02	$h \to gg$
6.74e-06	2.15e-03	6.74e-06	1.21e-03	5.88e-06	1.13e-03	6.11e-06	1.15e-03	$h \to Z\gamma$
7.61e-04	2.42e-01	7.61e-04	1.36e-01	7.61e-04	1.46e-01	8.22e-04	1.55e-01	$h \to WW$
8.44e-05	2.69e-02	8.44e-05	1.51e-02	8.44e-05	1.62e-02	1.02e-04	1.92e-02	$h \to ZZ$
3.14e-03	1.00e+00	5.58e-03	1.00e+00	5.22e-03	1.00e+00	5.31e-03	1.00e+00	Total

Table 4.4: The h decay partial widths (in GeV) and branching ratios as output by SoftSusy first without QCD corrections, with QCD corrections, with QCD corrections and withSUSYHIT's quark and gauge boson masses and gauge couplings, and the results of HDECAY-3.4 from SUSYHIT-1.4. This illustrates the necessity of including QCD corrections for decays to quarks or gluons, as well as that masses are the primary source of differences between SoftSusy and HDECAY-3.4. The pMSSM point pmssm1 listed in Table 4.3 is used; it has $m_h = 125\,\text{GeV}$. The masses and gauge couplings from SUSYHIT inserted into the SoftSusy decay calculator in columns 5 and 6 are $\alpha_s = 0.11$ and $m_c = 1.40\,\text{GeV}$, $m_s = 0.19\,\text{GeV}$, $m_b = 4.77\,\text{GeV}$, $m_t = 173.30\,\text{GeV}$ for the $h \to q\bar{q}$ and $h \to gg$ decays; $m_\mu = 0.11\,\text{GeV}$, $m_\tau = 1.78\,\text{GeV}$ for $h \to l^+l^-$ decays; $\alpha(M_Z) = 7.29 \times 10^{-3}$ and $m_W = 80.35\,\text{GeV}$, $m_t = 188.72\,\text{GeV}$, $m_b = 3.47\,\text{GeV}$, $m_c = 0.74\,\text{GeV}$ and $m_\tau = 1.78\,\text{GeV}$ for $h \to \gamma\gamma$; $m_Z = 91.19\,\text{GeV}$, $m_t = 173.30\,\text{GeV}$, $m_b = 4.77\,\text{GeV}$, $\alpha = 7.29 \times 10^{-3}$ and $m_W = 80.36\,\text{GeV}$ for $h \to Z\gamma$ and for $h \to VV^*$. SoftSusy-4.0 was used.

are known to be particularly large for these Higgs to quark-antiquark channels. As a result, any subtle differences in the numerical values of α_s used, originating from different running schemes and methods for example, have a significant impact on the partial widths to these modes. Indeed, this effect is precisely the origin of the larger error regions seen in Figure 4.6b for this region for these modes, and whilst we have not evaluated such effects in SoftSusy we would expect similar size error regions for the SoftSusy predictions; this would bring the predictions into closer agreement. Specifically for this case our value of $\alpha_s(m_h)$ is lower than the corresponding value in HDECAY; this ensures our partial widths to the bb, cc channels are larger and correspondingly the branching ratios to other modes are reduced, as is seen in Figure 4.6. Additional effects are seen in the loop decays, particularly the gg, $\gamma\gamma$ modes; as always their partial widths depend upon the values of the quark and gauge boson masses running in the loop as well as the running values of the gauge couplings. Consequently, differences in the schemes of the running here alter the loop contributions. Furthermore, HDECAY also includes additional effects of electroweak NLO corrections which are not included in SoftSusy. It should also be noted that Figure 4.6b has been taken directly out of the relevant paper [188], and the input files used for HDECAY are not clear. We find that if we attempt to make the same plot again using HDECAY of SusyHit for our input file and with the same order corrections then the resulting plot is in better agreement still with our plot in Figure 4.6a, indicating some of the differences

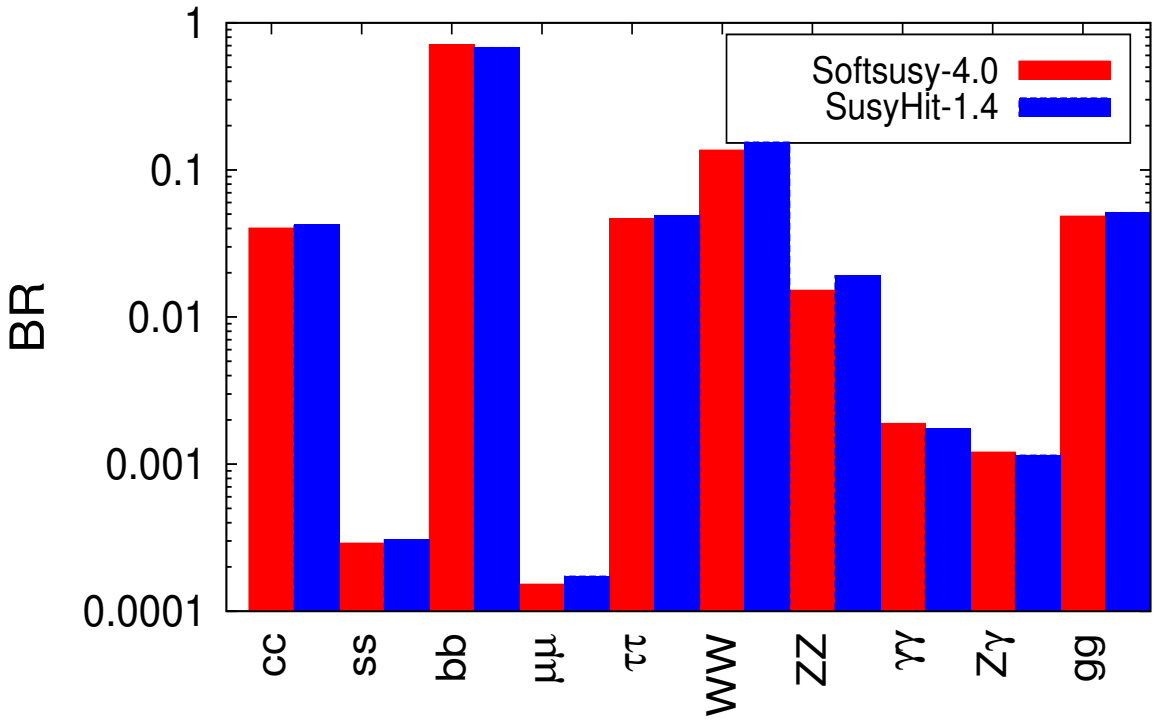

Figure 4.5: Branching ratios for a SM-like Higgs predicted by `SoftSusy` and by `HDECAY-3.4` in `SUSYHIT-1.4` for $m_h = 125\,\text{GeV}$. This is for the pMSSM point `pmssm1`, see Table 4.3. `SoftSusy-4.0` was used for these results.

arise as a result of different corrections included between the codes and different input setups. Nonetheless, the qualitative agreement is clear.

In conjunction with the results on the individual branching ratios of the Higgs particles, the sizes of different loop contributions to the Higgs 1-loop decays to $\gamma\gamma$, $Z\gamma$ and gg may also be extracted, offering potential insight into the effects of Standard Model and supersymmetric particles together on Standard Model loop decays. Should any deviation in the rate of one or more of the Standard Model Higgs loop decays be detected, or should a resonance be detected in a similar final state at higher energy, predictions of the size of different contributions will provide additional discriminating power to determine the possible supersymmetric models present. As a testimony to this, we present here in Figure 4.7 the loop contributions to the diphoton decay channel for the Standard Model-like Higgs and the heavier Higgs boson of the MSSM for the same pMSSM point, that given earlier in Table 4.3 (for which the heavier Higgs had mass $m_H = 3\,\text{TeV}$). In order to produce this figure the absolute values of the contributions have been taken in order to allow a logarithmic scale, this therefore hides some of the destructive interferences, for example between top and W boson for the lighter Higgs and between the two charginos for both the lighter and heavier Higgs. Figure 4.7(a) shows the contributions for the Standard Model-like Higgs, dominated by the top and W contributions as expected. There are contributions from the charginos but they largely cancel each other and experiments will not be sensitive to such contributions in the near future. Figure 4.7(b) shows the relative contributions of the different loops for the heavier Higgs of the pMSSM point. As expected, the contributions

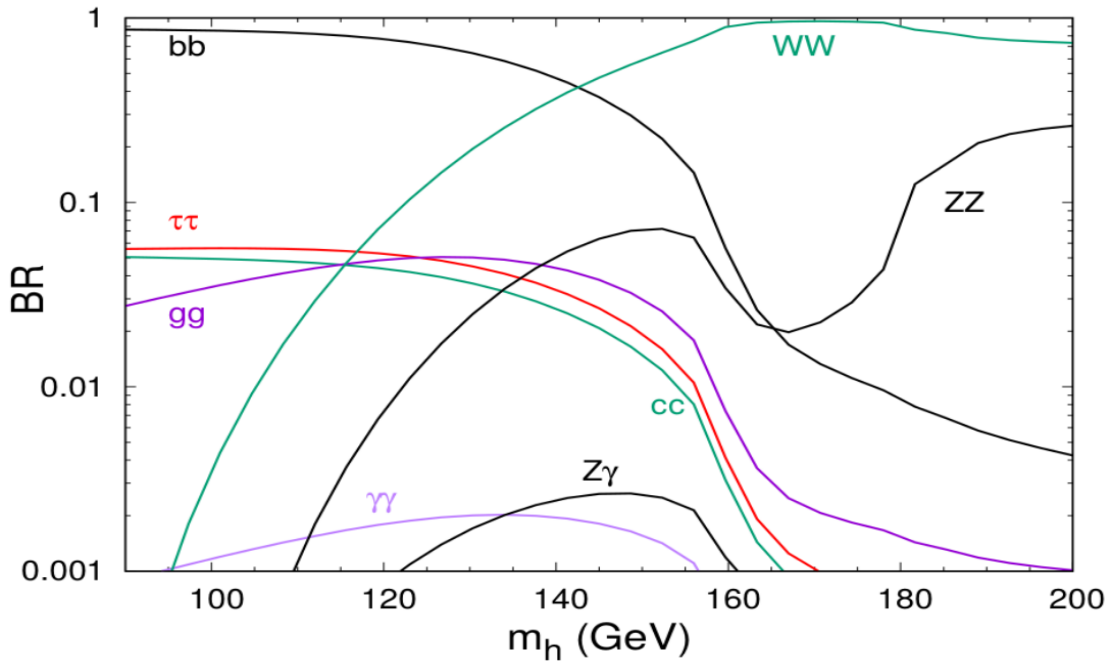

(a) `SoftSusy`

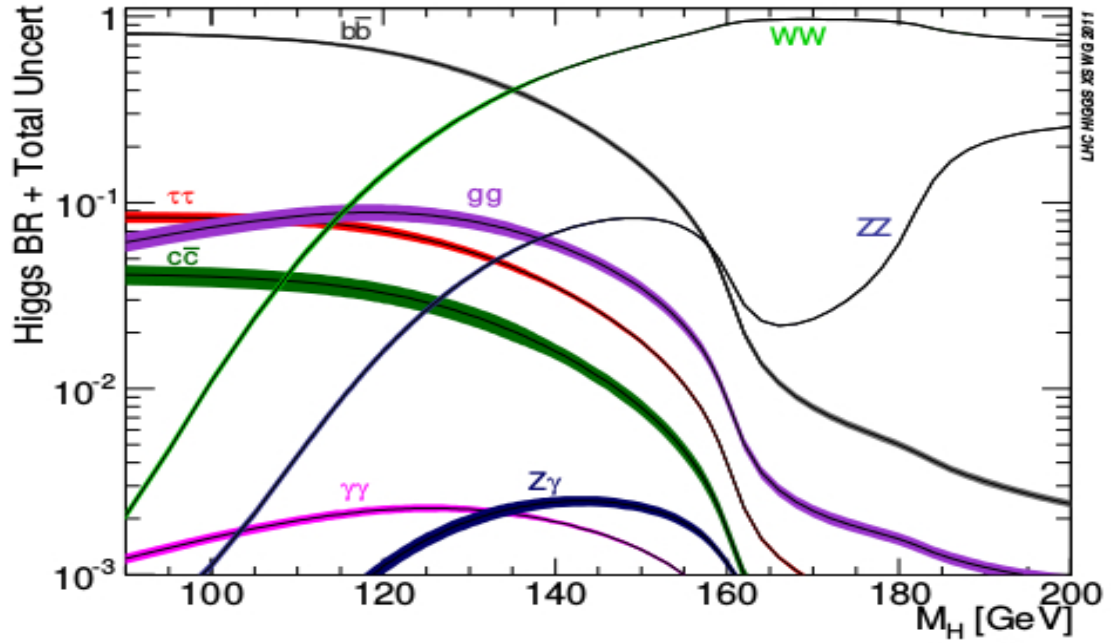

(b) LHC Higgs Cross-Section Working Group

Figure 4.6: Branching ratios for a SM(-like) Higgs as calculated in (a) by `SoftSusy-4.0` and in (b) by the LHC Higgs Cross-Section Working Group in [188]. This demonstrates a verification of the partial widths output by `SoftSusy`.

to the heavier Higgs loop decays are typically smaller as a result of the dependence of the loop contributions on the parameter $\tau_a = 4m_a^2/m_\phi^2$ (where $\phi = h, H$), which is much smaller for the heavier Higgs as a result of its larger mass. Note that the imaginary contributions to the loop decay appear when the loop particle has mass $2m_{\text{loop}} < m_\phi$ as in such cases the on-shell decay to two loop particles at tree-level is allowed; consequently there are more imaginary contributions for the heavier Higgs. Also note that the supersymmetric contributions to the heavier Higgs are relatively larger than for the Standard Model-like lighter Higgs, as it has enlarged couplings to supersymmetric particles whereas the Standard Model-like Higgs has reduced couplings to supersymmetric particles.

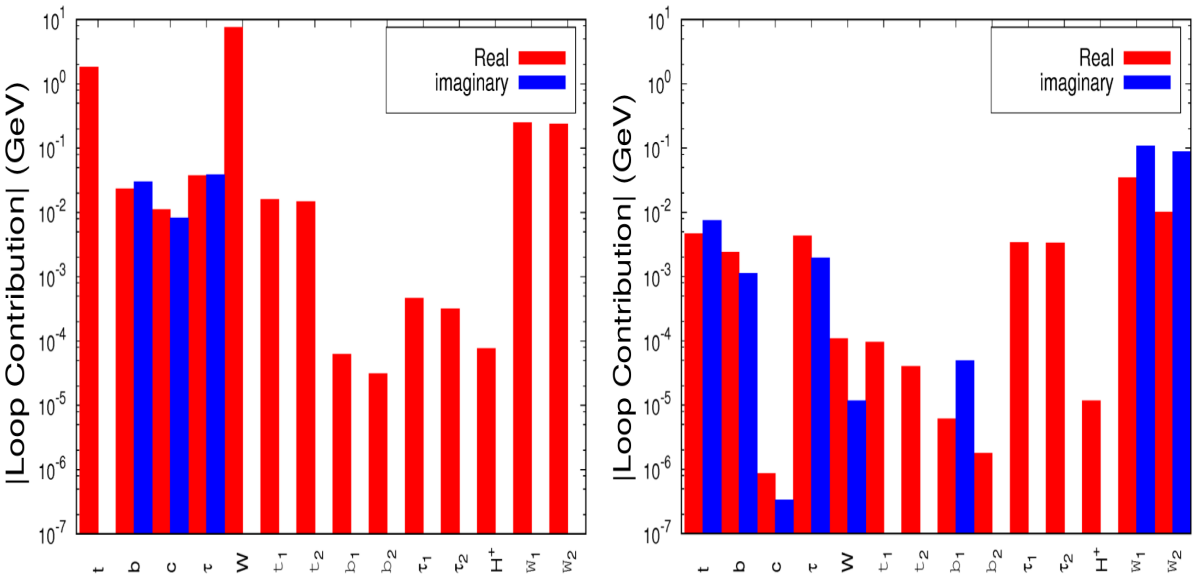

(a) $m_h = 125\,\text{GeV}$ (b) $m_H = 3\,\text{TeV}$

Figure 4.7: Absolute values of the matrix element contributions of different loop particles to the $h, H \to \gamma\gamma$ decay channels. Absolute values are taken so as to use a logarithmic scale and thereby allow all contributions to be viewed, nonetheless this does hide the sign of the contributions and so the presence of destructive interferences. Loop contributions shown against the y-axis scale here have dimensions of energy in GeV and are simply the size of the matrix element arising from that contribution. `SoftSusy-4.1.4` was used for these results.

4.2.3 Supersymmetric 3-body decays

So far we have demonstrated the validation of SUSY 2-body and Higgs MSSM decays, including the Higgs loop-decays, QCD corrections and Higgs 3-body decays. Similar validation and comparison was also performed for the MSSM 3-body decays and the NMSSM decays, as well as for special case decays to gravitinos and to pions, which we also examine later in this chapter.

First, let us consider the MSSM 3-body decays: an explicit comparison can be performed for the gluino 3-body decays with the spectrum given in Figure 4.8; the gluino 3-body decays to

neutralinos or charginos and quark-antiquark pairs are indicated, as are the appropriate Feynman diagrams for these modes. As the gluino only interacts via QCD, the only 2-body modes it has at tree-level are to squarks and quarks, however in this spectrum the gluino is lighter than all the squarks and so these modes are kinematically forbidden. At tree-level the dominant modes are therefore now the 3-body modes via an off-shell squark to neutralinos and a quark-antiquark pair or to charginos and a quark-antiquark pair, as illustrated. Radiative decays of the form $\tilde{g} \to g\tilde{Z}_i$ may also be important for such points but are yet to be included in `SoftSusy`. A comparison of the partial widths and branching ratios given by `SoftSusy-4.0`, `sPHENO-3.3.8` and `SUSYHIT-1.4` for this spectrum is presented in Table 4.5. This was performed taking the mass, coupling and other input decay parameters from `sPHENO` and inputting these directly by hand into the `SoftSusy` decay calculator in order to evaluate only differences due to the decay calculation, not any differences which might arise as a result of differing parameters from the spectrum generators. The agreement between the three programs is generally very good; in particular the agreement between `SoftSusy` and `sPHENO-3.3.8`, upon which the calculations of the 3-body decays is based, is usually between 1 and 5% with the larger differences often occurring where there are larger differences between `SUSYHIT-1.4` and `sPHENO-3.3.8`. The exceptions to this are the decays to third generation quark-antiquark pairs and the third and fourth heaviest neutralinos; i.e. $\tilde{g} \to t\bar{t}\tilde{Z}_3$, $\tilde{g} \to t\bar{t}\tilde{Z}_4$, $\tilde{g} \to b\bar{b}\tilde{Z}_3$ and $\tilde{g} \to b\bar{b}\tilde{Z}_4$. Here the differences observed are $10 - 20\%$ and they arise because of differences in the Yukawa couplings taken, for example for the b quark here the Yukawa coupling used in `SoftSusy` is determined by a running bottom mass of `runmb`$= 2.63\,\text{GeV}$, whereas `sPHENO` has a Yukawa coupling corresponding to a mass of `runmb`$= 2.37\,\text{GeV}$. In order to show this results in the differences observed, the running b mass in `SoftSusy` was temporarily set to that of `sPHENO` and the comparison for $\tilde{g} \to b\bar{b}\tilde{Z}_i$ is provided in Table 4.6. This demonstrates that the decays to $\tilde{Z}_1$ and $\tilde{Z}_2$ are not significantly altered by the new Yukawa coupling whereas the decays to $\tilde{Z}_3$ and $\tilde{Z}_4$ (i.e. those which showed differences with respect to `sPHENO`) now have significantly altered partial widths which are in much closer agreement with `sPHENO`, back down to the few percent level agreement seen in the other 3-body decays. This sensitivity to the b mass for the $\tilde{Z}_{3,4}$ indicates their increased proportions of Higgsino components.

A scan over the mass of the gluino to demonstrate the expected suppression of 3-body decays relative to 2-body decays was also performed, see Figure 4.9 where 3-body modes are shown as dashed lines and 2-body modes as solid lines. The result of this is that, phenomenologically, 3-body modes are only important when 2-body tree level modes are unavailable, as described in Chapter 3.1. This therefore verifies `SoftSusy` produces the expected behaviour for these decay modes. For this reason, `SoftSusy` only calculates 3-body modes when there are no similar 2-body modes available.

More details on the other 3-body modes included in the `SoftSusy` decay calculator, the contributions included, approximations made and the level of agreement seen between `SoftSusy` and other decay calculators for each mode are given in Appendix A.4. There, the relevant expressions used by our decay calculator to determine their partial widths are also provided.

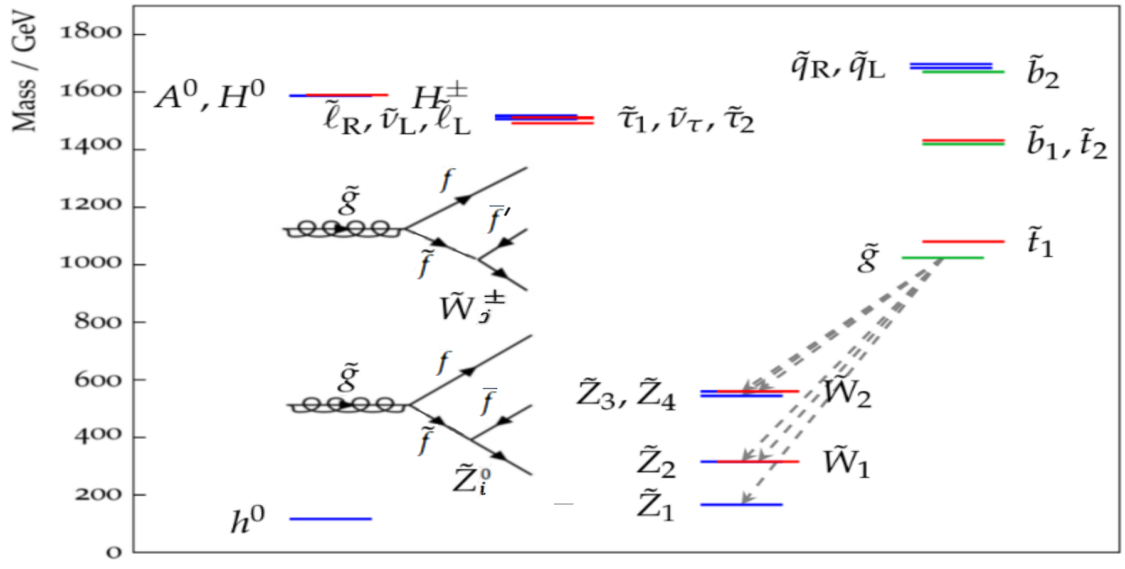

Figure 4.8: Spectrum used for quantitative comparison of gluino $\tilde{g}$ 3-body decays. Here the arrows indicate only the 3-body decay modes of the gluino: these are those investigated. This CMSSM spectrum has $m_0 = 1500\,\text{GeV}$, $m_{1/2} = 400\,\text{GeV}$, $\tan\beta = 10.37$, $\text{sign}(\mu) = +1$, $A_0 = -80\,\text{GeV}$ and was generated in `sPHENO`. The figure was produced using a modified version `slhaplot-3.0.4` from `pyslha` [186]. The Feynman diagrams for these 3-body modes are also given inset on the spectrum.

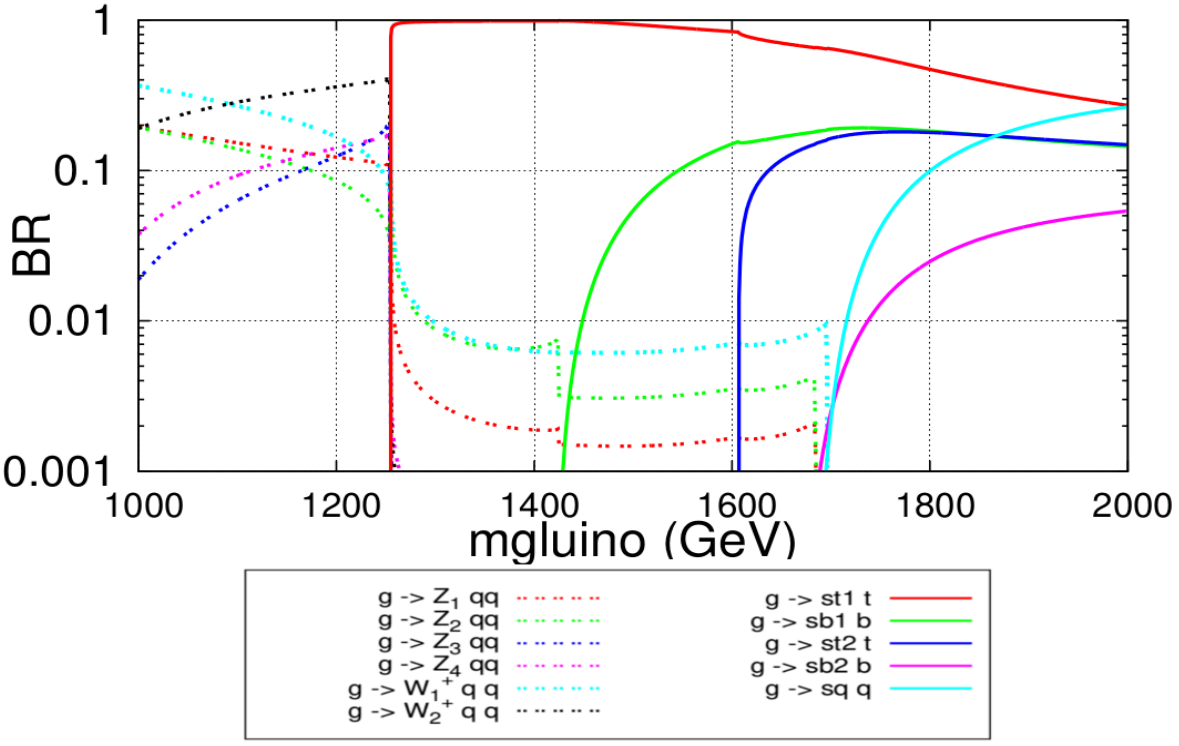

Figure 4.9: Branching ratios for the gluino $\tilde{g}$ of Figure 4.8 as its mass is scanned from 1 to 2 TeV. 3-body modes are shown in dashed lines and 2-body modes in solid lines. The suppression of 3-body modes relative to 2-body tree level modes is clearly evident in the drop in the 3-body branching ratios once the first 2-body mode $\tilde{g} \to \tilde{t}_1 t$ is available. Note that the "g" indicated in the plot are $\tilde{g}$ (i.e. gluinos), whilst "Z_i" are $\tilde{Z}_i$ (i.e. neutralinos) and "W_j" are $\tilde{W}_j$ (i.e. charginos). "st" indicates stops $\tilde{t}_i$, "sb" indicate sbottoms $\tilde{b}_i$, "sq" are $\tilde{q}$ squarks of the first two generations and "q" here are quarks of the first two generations in the case of the 2-body modes. For the 3-body modes however "q" indicates that they are instead summed over all three generations of quarks. `SoftSusy-4.0` was used for these results.

SoftSusy		sPHENO-3.38		SUSYHIT-1.4		mode
PW/GeV	BR	PW/GeV	BR	PW/GeV	BR	
2.90e-04	2.26e-02	2.89e-04	2.32e-02	2.89e-04	2.32e-02	$\tilde{g} \to \tilde{Z}_1 u\bar{u}$
3.21e-04	2.51e-02	3.19e-04	2.56e-02	3.19e-04	2.56e-02	$\tilde{g} \to \tilde{Z}_2 u\bar{u}$
1.35e-07	1.06e-05	1.35e-07	1.08e-05	1.35e-07	1.08e-05	$\tilde{g} \to \tilde{Z}_3 u\bar{u}$
5.52e-06	4.31e-04	5.49e-06	4.40e-04	5.49e-06	4.40e-04	$\tilde{g} \to \tilde{Z}_4 u\bar{u}$
9.06e-05	7.07e-03	9.02e-05	7.22e-03	9.02e-05	7.24e-03	$\tilde{g} \to \tilde{Z}_1 d\bar{d}$
3.07e-04	2.40e-02	3.06e-04	2.45e-02	3.06e-04	2.45e-02	$\tilde{g} \to \tilde{Z}_2 d\bar{d}$
1.75e-07	1.36e-05	1.74e-07	1.39e-05	1.74e-07	1.40e-05	$\tilde{g} \to \tilde{Z}_3 d\bar{d}$
6.67e-06	5.21e-04	6.64e-06	5.31e-04	6.64e-06	5.33e-04	$\tilde{g} \to \tilde{Z}_4 d\bar{d}$
2.90e-04	2.26e-02	2.89e-04	2.32e-02	2.89e-04	2.32e-02	$\tilde{g} \to \tilde{Z}_1 c\bar{c}$
3.21e-04	2.51e-02	3.19e-04	2.56e-02	3.19e-04	2.56e-02	$\tilde{g} \to \tilde{Z}_2 c\bar{c}$
1.35e-07	1.05e-05	1.41e-07	1.13e-05	1.35e-07	1.08e-05	$\tilde{g} \to \tilde{Z}_3 c\bar{c}$
5.52e-06	4.31e-04	5.50e-06	4.40e-04	5.49e-06	4.40e-04	$\tilde{g} \to \tilde{Z}_4 c\bar{c}$
9.06e-05	7.07e-03	9.02e-05	7.22e-03	9.02e-05	7.24e-03	$\tilde{g} \to \tilde{Z}_1 s\bar{s}$
3.07e-04	2.40e-02	3.06e-04	2.45e-02	3.06e-04	2.45e-02	$\tilde{g} \to \tilde{Z}_2 s\bar{s}$
1.75e-07	1.36e-05	1.77e-07	1.42e-05	1.74e-07	1.40e-05	$\tilde{g} \to \tilde{Z}_3 s\bar{s}$
6.67e-06	5.21e-04	6.64e-06	5.32e-04	6.64e-06	5.33e-04	$\tilde{g} \to \tilde{Z}_4 s\bar{s}$
1.47e-03	1.15e-01	1.47e-03	1.17e-01	1.44e-03	1.15e-01	$\tilde{g} \to \tilde{Z}_1 t\bar{t}$
2.56e-04	1.99e-02	2.46e-04	1.97e-02	2.67e-04	2.15e-02	$\tilde{g} \to \tilde{Z}_2 t\bar{t}$
3.48e-04	2.71e-02	3.10e-04	2.48e-02	3.34e-04	2.68e-02	$\tilde{g} \to \tilde{Z}_3 t\bar{t}$
6.13e-04	4.79e-02	5.66e-04	4.53e-02	5.21e-04	4.18e-02	$\tilde{g} \to \tilde{Z}_4 t\bar{t}$
1.27e-04	9.93e-03	1.25e-04	1.00e-02	1.25e-04	1.00e-02	$\tilde{g} \to \tilde{Z}_1 b\bar{b}$
7.80e-04	6.09e-02	7.74e-04	6.20e-02	7.74e-04	6.21e-02	$\tilde{g} \to \tilde{Z}_2 b\bar{b}$
2.20e-05	1.72e-03	1.77e-05	1.42e-03	1.78e-05	1.43e-03	$\tilde{g} \to \tilde{Z}_3 b\bar{b}$
3.48e-05	2.72e-03	3.24e-05	2.60e-03	3.23e-05	2.60e-03	$\tilde{g} \to \tilde{Z}_4 b\bar{b}$
6.28e-04	4.90e-02	6.24e-04	5.00e-02	6.24e-04	5.01e-02	$\tilde{g} \to \tilde{W}_1^- u\bar{d}$
6.28e-04	4.90e-02	6.24e-04	5.00e-02	6.24e-04	5.01e-02	$\tilde{g} \to \tilde{W}_1^+ d\bar{u}$
6.28e-04	4.90e-02	6.24e-04	5.00e-02	6.24e-04	5.01e-02	$\tilde{g} \to \tilde{W}_1^- c\bar{s}$
6.28e-04	4.90e-02	6.24e-04	5.00e-02	6.24e-04	5.01e-02	$\tilde{g} \to \tilde{W}_1^+ s\bar{c}$
1.20e-05	9.36e-04	1.19e-05	9.56e-04	1.19e-05	9.58e-04	$\tilde{g} \to \tilde{W}_2^- u\bar{d}$
1.20e-05	9.36e-04	1.19e-05	9.56e-04	1.19e-05	9.58e-04	$\tilde{g} \to \tilde{W}_2^+ d\bar{u}$
1.20e-05	9.36e-04	1.19e-05	9.56e-04	1.19e-05	9.58e-04	$\tilde{g} \to \tilde{W}_2^- c\bar{s}$
1.20e-05	9.36e-04	1.19e-05	9.56e-04	1.19e-05	9.58e-04	$\tilde{g} \to \tilde{W}_2^+ s\bar{c}$
9.29e-04	7.25e-02	9.21e-04	7.38e-02	9.21e-04	7.39e-02	$\tilde{g} \to \tilde{W}_1^- t\bar{b}$
9.29e-04	7.25e-02	9.21e-04	7.38e-02	9.21e-04	7.39e-02	$\tilde{g} \to \tilde{W}_1^+ b\bar{t}$
1.35e-03	1.05e-01	1.27e-03	1.01e-01	1.27e-03	1.02e-01	$\tilde{g} \to \tilde{W}_2^- t\bar{b}$
1.35e-03	1.05e-01	1.27e-03	1.01e-01	1.27e-03	1.02e-01	$\tilde{g} \to \tilde{W}_2^+ b\bar{t}$

Table 4.5: The $\tilde{g}$ decay partial widths and branching ratios in SoftSusy-4.0, sPHENO-3.3.8 and SUSYHIT-1.4 for the spectrum in Figure 4.8, for which the gluino only has 3-body decay modes available at tree-level.

SoftSusy with altered runmb		sPHENO-3.38		mode
PW/GeV	BR	PW/GeV	BR	
1.27e-04	9.93e-03	1.25e-04	1.00e-02	$\tilde{g} \to \tilde{Z}_1 b\bar{b}$
7.78e-04	6.10e-02	7.74e-04	6.20e-02	$\tilde{g} \to \tilde{Z}_2 b\bar{b}$
1.81e-05	1.42e-03	1.77e-05	1.42e-03	$\tilde{g} \to \tilde{Z}_3 b\bar{b}$
3.18e-05	2.50e-03	3.24e-05	2.60e-03	$\tilde{g} \to \tilde{Z}_4 b\bar{b}$

Table 4.6: The $\tilde{g}$ decay partial widths and branching ratios to $\tilde{Z}_i b\bar{b}$ as output by SoftSusy-4.0 with runmb taken so that the b Yukawa coupling in SoftSusy matches that in sPHENO. These decays showed significant differences between the two programs for $\tilde{Z}_3$ and $\tilde{Z}_4$, see Table 4.5. The agreement is now much improved, demonstrating that the differences result from a choice of the running b mass runmb.

4.2.4 Gravitino Decays

As outlined in Chapter 2.1.3, gravitinos inherit larger couplings via a super-Higgs mechanism, this can cause decays involving gravitinos to be relevant at colliders, particularly if the gravitino is the LSP as is often the case in GMSB models. In this case, the decays of NLSPs to the LSP gravitino can generate key signatures at the LHC, such as displaced vertex signatures. The decay formulae are given in detail in Appendix A.5, but the general form is given as an inset to Figure 4.10. The principal behaviour of these modes is that they are inversely proportional to the square gravitino mass, consequently the proper lifetimes $\tau_i \propto {m_{\tilde{G}}}^2$. Proper lifetimes are then converted into physical distances travelled in the detector by factoring in the velocity and time dilation effects, under the assumption the velocity is $v = 0.8c$ for the data in Figure 4.10. The figure is representative and only intended to illustrate the fundamental features of these decays - therefore the exact velocities are unimportant. A different assumption for the velocity will shift the curves parallel to the y-axis by a constant small amount (small as the y-axis is logarithmic). As the distances are all proportional to ${m_{\tilde{G}}}^2$, all the NLSP decays available have the same gradient on the logarithmic scale, with the prefactors determining the intercepts and hence separating the different decay modes. At ATLAS and CMS the typical distance scales relevant to displaced vertices are between 1mm and 1m, this corresponds to a given gravitino mass range which can be probed. Whilst Figure 4.10 shows an enlarged range of gravitino masses, cosmological and other observations place constraints on the gravitino masses allowed. These however tend to be model and assumption dependent and so are not summarised here - gravitino masses as light as eV and as heavy as 10 TeV [3] can be accommodated, depending on the model. As can be seen, this includes the range of gravitino masses over which displaced vertices would be expected to be produced via these NLSP to gravitino LSP decays.

[3] Although in that case the gravitino would not be the LSP.

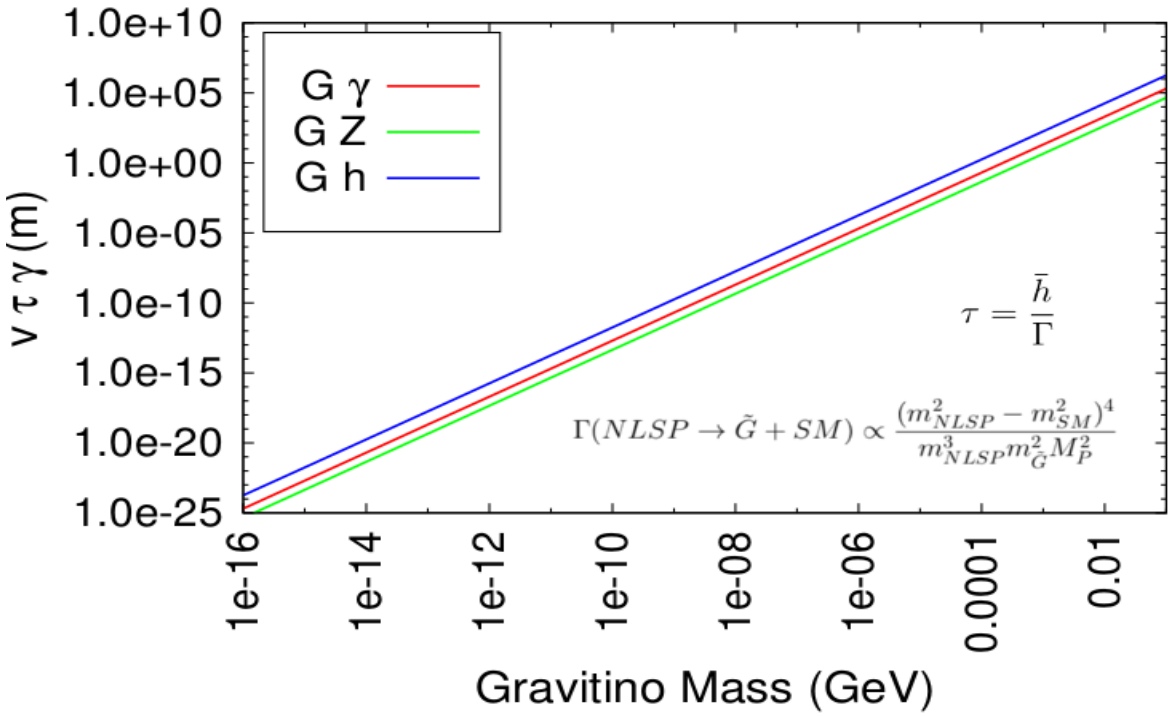

Figure 4.10: Next-to-Lightest Susy Particle (NLSP) decays to a gravitino LSP and Standard Model particle, such decays are relevant particularly for GMSB models, a randomly chosen example of which is provided here for which the NLSP is the lightest neutralino and the gravitino mass is scanned. The key feature is that the partial widths are proportional to $m_{\tilde{G}}{}^{-2}$ for all NLSPs, consequently the lifetimes are proportional to $m_{\tilde{G}}{}^2$ and so all decay modes have the same gradient in the log plot shown. The prefactors and mass differences alter the intercepts. `SoftSusy-4.0` was used for these results.

4.2.5 Chargino to Neutralino Pion Decays

A further special class of supersymmetric decay modes included are those of charginos decaying to quasi-degenerate neutralinos and pions. When chargino 2-body modes are unavailable[4], 3-body modes become important, specifically the 3-body decays to a neutralino and quark-antiquark pair such as $\tilde{W}_1 \to \tilde{Z}_1 u\bar{d}$. For standard mass splittings $\Delta m \equiv m_{\tilde{W}_j} - m_{\tilde{Z}_i}$, the quark-antiquark pair behave exactly as such, forming jets in the observed final state; however, as the mass splitting is reduced, eventually the quark and antiquark will hadronise together and so should be described together as pions. This includes various additional form factors which will alter their decay widths. We have included this particular case in the `SoftSusy` decay calculator program as such very compressed spectra modes lead to intriguing signatures at colliders. These include high transverse momentum chargino tracks decaying to pions and large missing transverse momentum (due to the neutralino LSP produced), and also kinks and disappearing tracks observed in one-pronged decays where a charged pion is detected produced from a chargino track but the neutralino produced is unseen. These signatures are a smoking gun for AMSB models, which typically produce a quasi-degenerate lightest chargino and lightest neutralino as the LSP is wino-like, with the more wino-like the LSP the smaller the mass splitting. In Figure 4.11,

[4]For example, typically chargino 2-body modes are not available for the lightest chargino when the mass splitting between it and the lightest neutralino is less than m_W.

we present the branching ratios and lifetime for a quasi-degenerate lightest chargino, scanning the mass splitting Δm between it and the lightest neutralino by scanning the $M_2(M_{\rm GUT})$ parameter as this in turn determines the size of the wino components in the lightest neutralino and chargino. The modes relevant at different mass splittings are given in Figure 4.11a, with the 3-body mode to electron and neutrino the only one available at mass splitting less than m_π. Once $\Delta m > m_\pi$, the pion modes dominate, with one and two pion modes included in `SoftSusy` as the two pion mode branching ratio increases with Δm as the phase space suppression reduces. Eventually, the standard 3-body modes to quarks and antiquarks again dominate and we switch to these once $\Delta m > \Lambda_H = 1.5\,\text{GeV}$. The exact point of the switch between the pion description and the quark description in `SoftSusy` was determined phenomenologically as the mass splitting at which the quark-antiquark modes and the corresponding pion modes each sum to the same branching ratio. Meanwhile, Figure 4.11b demonstrates the effect of the reduced phase space that occurs as Δm reduces on the lifetimes of the decaying lightest charginos; for small enough mass splittings these lifetimes become long enough to leave observable tracks at the LHC, with lifetimes of greater than around 10^{-11}s corresponding to the millimetre scales at which the LHC may resolve displaced and secondary vertices.

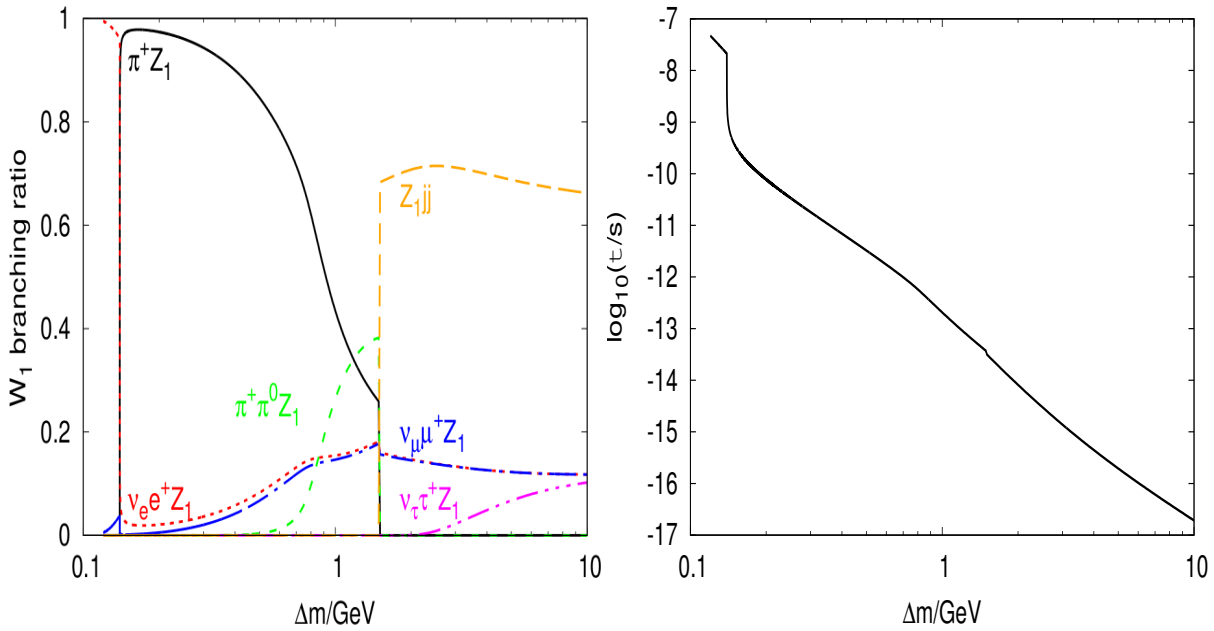

(a) Branching Ratios (b) Proper Lifetime

Figure 4.11: Decays of the lightest chargino near to degeneracy with the lightest neutralino for a deformed CMSSM point - the model begins with $m_0 = m_{\frac{1}{2}} = 500\,\text{GeV}$, $A_0 = 0$, $\tan\beta = 20$, $\text{sign}(mu) = +1$, but then gaugino non-universality is imposed by scanning $M_2(M_{\rm GUT})$ between 255 GeV and 280 GeV in order to zoom in on small $\Delta m = m_{\tilde{W}_1^+} - m_{\tilde{Z}_1^0}$. This scanning of the wino mass varies how wino-dominated the lightest chargino and lightest neutralino are, and correspondingly how similar their masses are. The dominant branching ratios are shown in (a), including the standard 3-body decays as well as the one and two pion modes and the switch-over point between the two descriptions at $\Delta m = \Lambda_H = 1.5\,\text{GeV}$, whilst (b) presents the lifetimes of the quasi-degenerate chargino. `SoftSusy-4.1.0` was used for these results.

4.2.6 NMSSM Decays

Similar detailed checks to those above were performed in the NMSSM and we provide some details here. In Table 4.7 we present a quantitative comparison of the decays of the second heaviest neutral CP even Higgs of the NMSSM, the H. The spectrum used, as generated by `SoftSusy`, is given in Figure 4.12 with decay modes of branching ratios (BRs) greater than 0.1 (also calculated automatically by `SoftSusy`) indicated by arrows, with thicker, bolder arrows representing larger BRs. For this parameter point, H is the CP even Higgs which has the largest singlet component, with $R(2,3) = 0.998$.

The comparison in Table 4.7 demonstrates that the level of agreement is usually better than 10% with the exception of a few of the decay modes. The decay modes which show larger differences are the decays to "down-type" fermions (i.e. fermions with third component of weak isospin $T_3 = -\frac{1}{2}$) and the 1-loop decay to two photons $H \to \gamma\gamma$. Note that the decays to two gluons here show good agreement with `NMSSMTools`: the scale of the decaying Higgs $m_H = 519.3\,\text{GeV}$ is relatively close to $M_{\text{SUSY}} = \sqrt{m_{\tilde{t}_1} m_{\tilde{t}_2}} = 675.5\,\text{GeV}$ so any differences in the running between the two programs have little effect. `SoftSusy` and `NMSSMTools` both run the gauge couplings to m_H, however there are potential differences in the running order and scheme.

For the case of the decays $H \to s\bar{s}$, $b\bar{b}$, $\mu^+\mu^-$ and $\tau^+\tau^-$, differences are seen between the default `SoftSusy` partial widths and those of `NMSSMTools`. Some of these differences can be explained by the use of different values for the masses from which Higgs couplings are extracted, particularly in the case of the decays to b, μ and τ pairs. `SoftSusy` uses $m_b(\text{pole}) = 4.97\,\text{GeV}$, $m_\mu(M_{\text{SUSY}}) = 0.103\,\text{GeV}$ and $m_\tau(M_{\text{SUSY}}) = 1.80\,\text{GeV}$; meanwhile `NMSSMTools` uses $m_b = 4.54\,\text{GeV}$, $m_\mu = 0.106\,\text{GeV}$ and $m_\tau = 1.78\,\text{GeV}$. However, most of the differences are due to the definition of the CP even mixing matrix S: the coupling of the singlet-like H to "down-type" fermions is given by $[S(2,2)/\cos(\beta)]^2$. `SoftSusy` obtains $S(2,2) = 2.71 \times 10^{-2}$, whilst `NMSSMTools` has $S(2,2) = 2.87 \times 10^{-2}$. Given that the partial widths are proportional to the square of the mixing matrix element, this results in an approximate 12% difference. The `SoftSusy` decay calculation uses the tree-level value $S(M_{\text{SUSY}})$, whereas `NMSSMTools` uses S as extracted from the loop-corrected pole mass matrix. The two choices are equivalent at leading order, and so the numerical difference between the programs is simply a higher order effect. To demonstrate this effect explains much of the remaining differences, the CP even mixing matrix elements have also been set to those of `NMSSMTools` in columns 5 and 6 of Table 4.7.

The other significant difference observed in the partial widths between the default `SoftSusy` results and those of `NMSSMTools` is in the $\gamma\gamma$ channel. By default `SoftSusy` runs α and quark masses, whereas `NMSSMTools` runs α but not the quark masses to calculate the Higgs couplings. The quark masses used by `SoftSusy` for this point are $m_t(m_H) = 144.5\,\text{GeV}$, $m_b(m_H) = 2.40\,\text{GeV}$, $m_c(m_H) = 0.57\,\text{GeV}$ whereas `NMSSMTools` uses $m_t = 170.9\,\text{GeV}$, $m_b = 4.54\,\text{GeV}$, $m_c = 1.40\,\text{GeV}$; meanwhile `SoftSusy` uses $\alpha(m_H) = 7.88 \times 10^{-3}$ whereas `NMSSMTools` obtains $\alpha(m_H) = 7.30 \times 10^{-3}$. The difference in the values of $\alpha(m_H)$ is presumably due to a difference

in the scheme[5]. With the quark masses and α used by `NMSSMTools` inserted into the `SoftSusy` decay code the difference between the two programs is dramatically reduced, with them now showing excellent agreement. This clearly demonstrates that the difference observed is due to different quark masses and coupling constants taken; in particular it is the quark masses which have the largest effect here. The reason for such sensitivity to the masses taken is that for this parameter point there is a large cancellation between the t, W and other loop contributions. The degree of the cancellation is consequently heavily dependent upon the top mass used. With `SoftSusy`'s choices then the real part of the top loop contribution is $\mathcal{R}[I_t] = 8.99 \times 10^{-2}$ and the real part of the W loop contribution $\mathcal{R}[I_W] = -0.114$ whilst the other significant contribution is that of the heaviest chargino $\tilde{W}_2$: $\mathcal{R}[I_{\tilde{W}_2}] = 5.53 \times 10^{-2}$, resulting in significant cancellation such that the total of all the particle loop contributions is $(2.65 - 6.62i) \times 10^{-2}$. With the quark mass choices of `NMSSMTools` instead one obtains $\mathcal{R}[I_t] = 0.135$ and so the total cancellation is much smaller and the total of all the loop contributions is $(7.16 - 7.30i) \times 10^{-2}$, which has a modulus much larger than that obtained using the usual `SoftSusy` choices. Once these are squared this explains the significant discrepancy. Differences seen between the two programs for this channel should be interpreted as an indication of a large theoretical error in the calculation at this order for this parameter point[6].

Figure 4.13 displays the same comparisons of Table 4.7 graphically for ease of reference, with Figure 4.13a presenting the original `SoftSusy` results and Figure 4.13b giving the `SoftSusy` results with the `NMSSMTools` inputs taken. Again the clear improvement in the $H \to bb, cc, \tau\tau, \gamma\gamma$ modes is obvious in Figure 4.13b.

[5] `SoftSusy`, in the version used here, matches at m_Z and then runs α in the full NMSSM at 2-loops. As of `SoftSusy` version 4.1.1 the matching has instead been done at m_t as noted previously [83]. The matching in `NMSSMTools` uses the alternative EFT approach discussed previously as the second approach in Chapter 3.2.1.

[6] Note that our comparisons are carried out against an old version of `NMSSMTools` (`NMSSMTools-4.2.1`) since there only exists an interface between the `SoftSusy` spectrum generator and this version. This allowed the effects of the spectrum generator to be isolated from other differences in the decay calculations for validation.

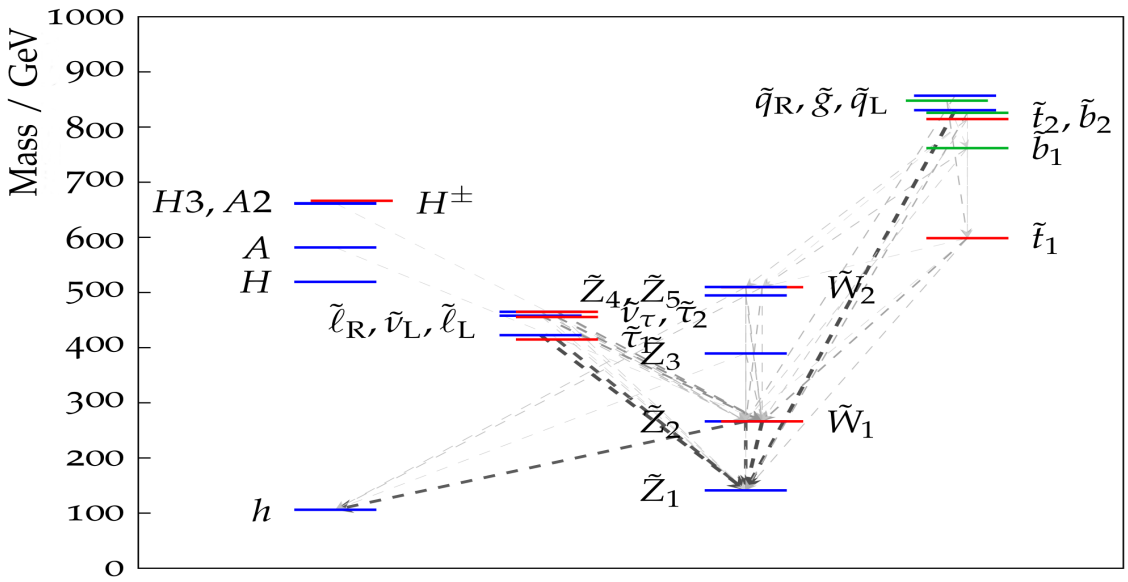

Figure 4.12: Mass spectrum and branching ratios for the constrained NMSSM Z_3 violating parameter point with $m_0 = 400\,\text{GeV}$, $m_{1/2} = 350\,\text{GeV}$, $\tan\beta = 10$, $\text{sign}(\mu) = +1$, $A_0 = -300\,\text{GeV}$, $\lambda = 0.1$, $\kappa = 0.1$, $\lambda\langle S\rangle = 200\,\text{GeV}$ and $\xi_F = 100\,\text{GeV}$ used in Table 4.7. The arrows represent decay modes with branching ratios (BRs) greater than 0.1, with thicker, bolder arrows representing larger BRs. `SoftSusy-4.0` was used for these results. The figure was produced with the aid of `slhaplot-3.0.4` of `pyslha` [186].

`SoftSusy` default		`SoftSusy` with `NMSSMTools` quark masses and running coupling constants		`SoftSusy` with `NMSSMTools` quark masses, running coupling constants and S		`NMSSMTools-4.2.1` with same QCD corrections		mode
PW/GeV	BR	PW/GeV	BR	PW/GeV	BR	PW/GeV	BR	
2.98e-06	9.22e-06	2.99e-06	9.24e-06	3.04e-06	9.22e-06	3.04e-06	9.21e-06	$H \to c\bar{c}$
3.65e-07	1.13e-06	3.67e-07	1.14e-06	4.10e-07	1.24e-06	4.33e-07	1.31e-06	$H \to s\bar{s}$
9.44e-04	2.92e-03	7.73e-04	2.39e-03	8.64e-04	2.62e-03	8.93e-04	2.71e-03	$H \to b\bar{b}$
5.58e-02	1.73e-01	5.58e-02	1.73e-01	5.68e-02	1.72e-01	5.68e-02	1.72e-01	$H \to t\bar{t}$
2.52e-07	7.79e-07	2.68e-07	8.27e-07	2.99e-07	9.06e-07	3.16e-07	9.56e-07	$H \to \mu\mu$
7.75e-05	2.40e-04	7.57e-05	2.34e-04	8.45e-05	2.56e-04	8.92e-05	2.70e-04	$H \to \tau\tau$
1.21e-05	3.73e-05	1.21e-05	3.74e-05	1.33e-05	4.04e-05	1.22e-05	3.70e-05	$H \to \tilde{Z}_1\tilde{Z}_1$
3.25e-05	1.00e-04	3.25e-05	1.01e-04	3.60e-05	1.09e-04	3.44e-05	1.04e-04	$H \to \tilde{Z}_1\tilde{Z}_2$
2.00e-02	6.18e-02	2.00e-02	6.18e-02	2.00e-02	6.06e-02	2.07e-02	6.27e-02	$H \to hh$
9.03e-08	2.97e-07	1.61e-07	4.97e-07	1.62e-07	4.91e-07	1.68e-07	5.09e-07	$H \to \gamma\gamma$
1.47e-04	4.54e-04	1.47e-04	4.54e-04	1.49e-04	4.53e-04	1.53e-04	4.63e-04	$H \to gg$
2.07e-06	6.39e-06	1.93e-06	5.98e-06	2.14e-06	6.47e-06	2.21e-06	6.69e-06	$H \to Z\gamma$
1.67e-01	5.15e-01	1.67e-01	5.15e-01	1.70e-01	5.16e-01	1.70e-01	5.15e-01	$H \to WW$
8.00e-02	2.47e-01	8.00e-02	2.47e-01	8.17e-02	2.48e-01	8.16e-02	2.47e-01	$H \to ZZ$
3.24e-01	1.00e+00	3.23e-01	1.00e+00	3.30e-01	1.00e+00	3.30e-01	1.00e+00	Total

Table 4.7: H decay partial widths and branching ratios as output by `SoftSusy` by default, by `SoftSusy` with the quark masses and coupling constants set to those of `NMSSMTools`, and then with the CP even Higgs mixing matrix (S) additionally set to that of `NMSSMTools`, and finally by `NMSSMTools-4.2.1`. For columns 3 and 4 this meant the main differences are due to setting $m_b = 4.54\,\text{GeV}$ for $H \to b\bar{b}$ compared with the default value `SoftSusy` uses $m_b(\text{pole}) = 4.97\,\text{GeV}$. For $H \to \gamma\gamma$, `SoftSusy` uses $m_t(m_H) = 144.5\,\text{GeV}$, $m_b(m_H) = 2.40\,\text{GeV}$, $m_c(m_H) = 0.57\,\text{GeV}$ whereas `NMSSMTools` has $m_t = 170.9\,\text{GeV}$, $m_b = 4.54\,\text{GeV}$, $m_c = 1.40\,\text{GeV}$. In `SoftSusy` $\alpha(m_H) = 7.88 \times 10^{-3}$ whereas `NMSSMTools` obtains $\alpha(m_H) = 7.30 \times 10^{-3}$. These were therefore input into `SoftSusy` for columns 3 and 4. The CP even mixing matrix (S) was additionally set to that of `NMSSMTools` in columns 5 and 6. `SoftSusy-4.0` was used for these results. This information is presented graphically in Figure 4.13.

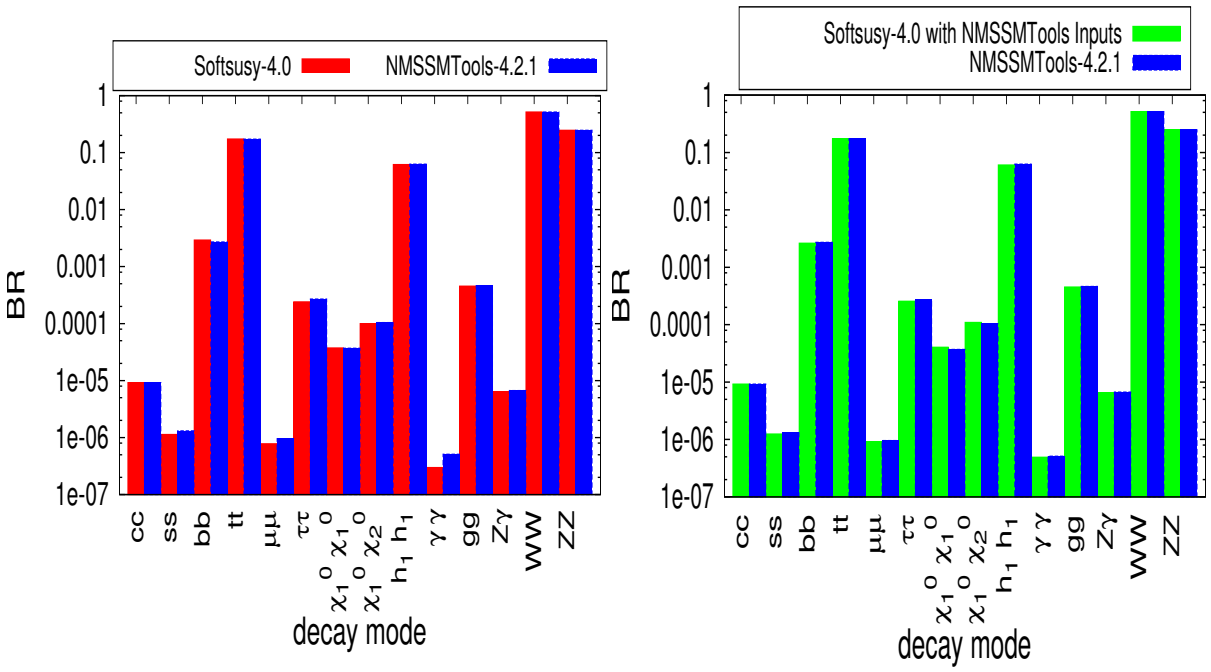

(a) `SoftSusy` (b) `SoftSusy` with `NMSSMTools` Inputs

Figure 4.13: Decays of the second heaviest Higgs of the NMSSM, this is the most singlet-like for this parameter point. The results are those presented in Table 4.7 and demonstrate good agreement between `SoftSusy-4.0` and `NMSSMTools-4.2.1`, particularly after the same inputs are taken in (b), this improves the agreement in the ss, bb, $\mu\mu$, $\tau\tau$ and $\gamma\gamma$ channels. `SoftSusy-4.0` was used for these results.

4.3 NMSSM scan

One advantage that programs such as `SoftSusy` have is that they can calculate the particles masses and couplings for a variety of input parameters, this enables scanning of the parameter spaces of supersymmetric models. With the addition of MSSM and NMSSM supersymmetric and Higgs decays, this scanning may be extended to examining how decay widths (and hence signatures) vary across the parameter spaces of the various supersymmetric models included. Given the inclusion of the NMSSM is rare, and the NMSSM parameter space is enriched via the additional singlet coupling parameters, here we present such a scan for the extended neutralino sector decays of the NMSSM in Figure 4.14. The neutralino singlino components are solid lines in the figure read on the left-hand y-axis and the corresponding neutralino total widths are dashed lines read on the right-hand y-axis . This scan is demonstrative of the analyses which may be performed with `SoftSusy`'s spectrum generator and decay calculator linked together, indicating the improved model examination power of such an all-in-one program package.

As the scan is only for display purposes, we simply take the `nmssmSLHAnoZ3Input` file provided with the `SoftSusy` program and scan λ from 0.001 to 0.25. The data however stop at $\lambda \approx 0.2295$ as at this point the lightest Higgs becomes tachyonic (has negative mass squared) - this is a problem for correct electroweak symmetry breaking so these model points are not valid and the spectrum and decays are not calculated. Referring back to our introduction to the

NMSSM in Chapter 2.4, in equation 2.45 we see that the λ parameter in the extended neutralino sector dictates the coupling of the two Higgsino neutralino gauge eigenstates to the singlino, this ultimately originates in the $\lambda S H_u H_d$ NMSSM superpotential coupling. Therefore we can consider λ as the mixing of the singlino component into the Higgsino like neutralinos. For our setup here the third and fourth heaviest neutralinos are the dominantly Higgsino neutralinos; therefore as we increase λ in Figure 4.14 we observe that their singlino components ($N(3,5)$ and $N(4,5)$) rise most (although those of all the four MSSM neutralino all rise slightly), meanwhile the singlino component of the heaviest neutralino ($N(5,5)$) correspondingly drops as it mixes more with the other neutralinos. As the singlino only interacts with non-Higgs like particles via mixing, we can observe the same effects in the total widths of the neutralinos. At small λ the heaviest neutralino (which is the dominantly singlino one at this stage) has very small total decay width and as λ increases its singlino component reduces and its decay width accordingly increases rapidly as it gains Higgsino neutralino decays. Meanwhile the total width of the fourth heaviest neutralino drops concurrently as it cedes its Higgsino component gradually to the heaviest neutralino. There is also an interesting feature in the singlino components, and in the same manner in the decay widths, at $\lambda \approx 0.1347$; as the Higgsino like neutralinos mix with the singlino, initially it is the fourth heaviest neutralino which mixes most, however as it does so its mass reduces whilst the absolute mass of the third heaviest neutralino increases. Eventually at $\lambda \approx 0.1347$ the third and fourth heaviest neutralinos are relabelled as the absolute values of their masses cross; as a result in our plot we see the $N(3,5)$ and $N(4,5)$ singlino components, and the Γ_3 and Γ_4 total decay width values each interchange.

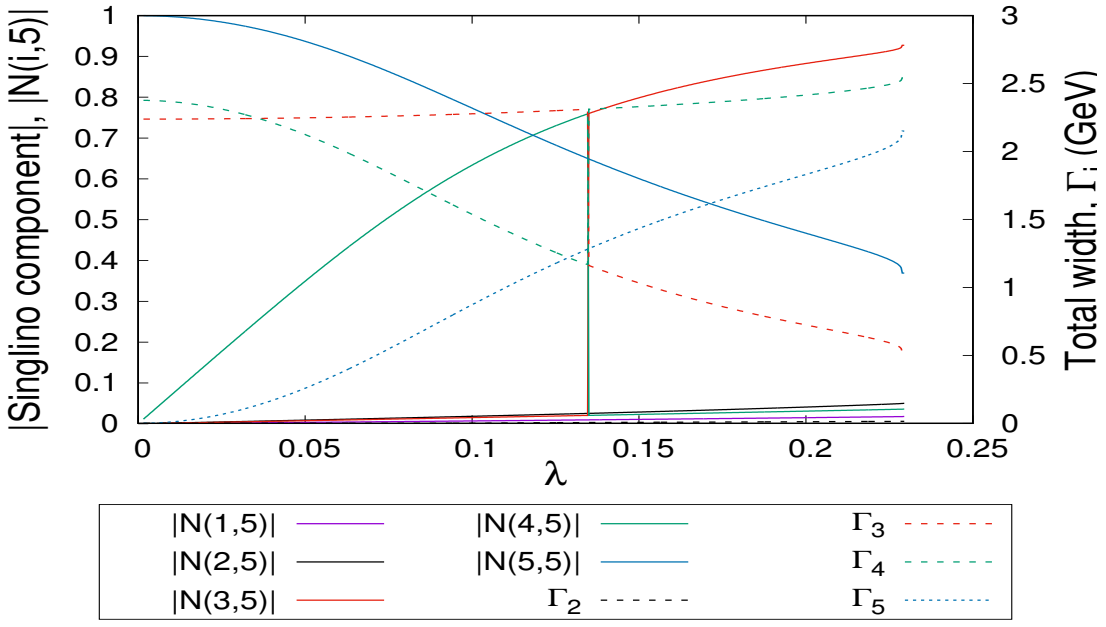

Figure 4.14: A scan of the λ parameter in the NMSSM using `SoftSusy-4.1.4` and the base point `nmssmSLHAnoZ3Input`. The singlino components of each of the 5 physical mass-ordered neutralinos are shown on the left-hand y-axis and are given by the solid lines. This shows that the 3$^{\text{rd}}$ and 4$^{\text{th}}$ heaviest neutralinos, being the dominantly Higgsino neutralinos, mix increasingly with the singlino as λ increases as expected. The dashed lines and right-hand y-axis indicates how the total decay width of each neutralino varies with λ. Increasing/decreasing singlino fraction reduces/increases the total width as expected.

4.3.1 Decay Calculator Processing Performance

In performing such scans the issue is often the program speed; many different parameter points must be evaluated for both their mass spectrum and couplings, and their decay widths. As such, the speed of evaluation of one parameter point is important for allowing such analyses to be easily manageable. Of course, spectrum generator and decay calculator programs are far from the bottleneck in the overall analysis chain (given previously in Figure 3.2), this is in the Monte Carlo event generation for particle production cross-section evaluation. Nonetheless, if investigations include only the spectrum generation and decay calculation we should ensure the decay calculation does not significantly slow the program and thereby make such scans more cumbersome than necessary. Fortunately the decay calculations are not computationally intensive, and our approach to include as many formulae as possible hand-coded and evaluated analytically ensures the decay calculations require minimal time to evaluate. The only modes which may take more significant computational power are the 3-body modes, requiring numerical integration; however even in these cases we have first analytically reduced the integral to one-dimension lessening the computer time required. As a consequence, the decay calculation step adds minimal additional burden to the `SoftSusy` package, typically increasing the evaluation time by only 5% when 3-body modes are included and by only 2% if these are excluded[7]. Although this evaluation time of the decay calculator will increase as further modes, particularly 3-body modes, are added; we still anticipate it taking no more than a fraction of the spectrum calculator computation time, as the spectrum calculator requires an iterative process to be completed until convergence is reached.

4.4 Future Developments

`SoftSusy-4.0` was the first version of many including the decay calculator program and therefore contained only the modes deemed crucial to collider applications. Since then, minor additions and changes have been made in updating the package to the latest `SoftSusy-4.1.4` version; these include the introduction of the chargino to neutralino pion modes described in Chapter 4.2.5 and the addition of a limit to improve the accuracy of predictions for extremely compressed gluino spectra as outlined in Chapter 3.3.5 and elucidated further in Appendix A.4.1, amongst others. We hope the decay calculator aspect will prove of tremendous use for collider search applications, representing a major upgrade of the `SoftSusy` package capabilities. To this end, we plan a program of future developments and improvements to the decay calculator program, building on the foundations we have laid in its first versions. The exact changes, additions and augmentations made and the order of these improvements will be guided by the needs of users, and by data from ATLAS and CMS, nonetheless the following are a selection of those we currently intend to prioritise:

[7]For example, running on my personal laptop with the `lesHouchesInput` file provided with the `SoftSusy` code, I find the mass spectrum generator takes 0.75s, the decay calculator with 3-body modes included takes 0.04s and without 3-body modes included takes 0.01s.

- 3-body sfermion $\tilde{f}$ decays - The current version of `SoftSusy` includes the most phenomenologically relevant 3-body decay modes of the gluinos, charginos and neutralinos; however currently no sfermion 3-body decays are included. These may be particularly relevant for searching compressed spectra regions, for example these are pertinent to spectra with light stop masses[8] such that $m_{\tilde{t}_i} < m_t + m_{\tilde{Z}_1}, m_b + m_{\tilde{W}_1^\pm}$, but $m_{\tilde{t}_i} > m_b + m_W + m_{\tilde{Z}_1}$. These points can arise for light stops due to the larger top mass preventing 2-body decays including tops in the final state. There are also $\tilde{t}_i \to bl\tilde{l}$ decays (where $l\tilde{l}$ are a lepton sneutrino or slepton neutrino pair): these 3-body decays arise where again no 2-body modes are available and sleptons are lighter than squarks, the latter condition often occurring for common GUT scale scalar masses, such as those imposed in mSUGRA. Meanwhile $\tilde{t}_i \to \tilde{b}_i f \bar{f}'$ decays mediated via W bosons or charged Higgses, may be relevant for larger $\tan\beta$ in regions where $\tilde{t}_i - \tilde{b}_i < m_W$. More information on the 3-body decays of third generation squarks is given in [189].

- Further chargino, neutralino and gluino 3-body decays - Whilst the most likely 3-body decays relevant to colliders are included for charginos and neutralinos, there are some rarer candidate decays remaining which may be apposite. These include the chargino or neutralino 3-body modes to gluinos and quark-antiquark pairs, which can easily be incorporated into the program, being the crossing of 3-body gluino modes already included. Also, as of yet, 3-body heaviest chargino to lightest chargino modes plus a fermion-antifermion pair via Higgs, Z or sfermion intermediates are not included, although these are of substantially reduced importance as spectra with the two charginos quasi-degenerate are rare phenomenologically. Concurrently, gluino 3-body decays to stops, a bottom quark and a W boson (or charged Higgs) could also be of relevance in some regions of parameter space, whilst neutralino to neutralino pion modes could also be added, reflecting regions where two neutralinos (particularly the lightest two) are quasi-degenerate

- Loop decay modes - These early versions of the `SoftSusy` decay calculator included only the crucial 1-loop decay modes of Higgs particles, albeit in both the MSSM and NMSSM. However, given we explained briefly in Chapter 3.1 that 1-loop and 3-body modes are ordinarily similarly suppressed, there are radiative decay modes relevant to the compressed spectra regions for which we have included 3-body modes to target. Key examples are the $\tilde{g} \to g\tilde{Z}_i$ and the $\tilde{Z}_j \to \tilde{Z}_i\gamma$ decays, the latter of which can be especially relevant for $\tilde{Z}_2$ decays [190]. In addition, the mode $\tilde{t}_i \to c\tilde{Z}_1$ may be needed for some regions of parameter space, even though it is CKM and loop-suppressed, if no tree-level 2-body modes are available and the phase space for the 3-body modes is small due to the compressed nature of the spectra.

- Further QCD Corrections - To date, the `SoftSusy` decay calculator has only included QCD corrections in the neutral Higgs decays to quarks (at 1-loop) and to gluons (at 2-

[8]The lightest stop is often light as the mixing between the stop eigenstates is proportional to the large top Yukawa and large mixing leads to a large separation of masses between the two stop eigenstates.

loop), although already in both the MSSM and NMSSM, as these are essential to correctly reproducing the branching ratios of the Standard Model-like Higgs. Nonetheless, QCD corrections can have significant impacts on the decays of other supersymmetric particles, in particular the branching ratios of squark and gluino decays. Modes for which QCD corrections will be added include $\tilde{g} \to \tilde{q}\bar{q}$, $\tilde{q} \to \tilde{g}q$, $\tilde{q} \to \tilde{Z}_i q$, $\tilde{q} \to \tilde{W}_i^{\pm} q'$, $\tilde{q}_2 \to \tilde{q}_1 V$ and $\tilde{q}_2 \to \tilde{q}_1 \phi$. More minutiae are given in [134, 191–196], in some regions of parameter space the effects of such SUSY-QCD corrections can be of order 10%.

- Very Compressed Regions - In very compressed regions spectrum generators and decay calculators can lose precision due to two main factors: first of all, decays in such regions are very phase space dominated, and so any small differences in the particle masses determined by the spectrum generator can alter the partial widths significantly by altering the phase space available. Secondly, decay calculators can lose accuracy due to numerical precision in such regions as very fine cancellations frequently arise at the ends of phase space integrals. Whilst the former issue can only be resolved with greater precision in the spectrum generation, the latter can be aided by taking appropriate limits for very compressed regions. This has been performed for the gluino 3-body decays, as described in Chapter 3.3.5 and Appendix A.4.1. This approach could be extended to other very compressed decays.
- NMSSM 3-body decays - Longer term, as we enhance the program with further MSSM 3-body decays, we may also decide to extend this work into incorporating NMSSM 3-body decays. Currently these are less important due to the enlarged parameter space and limited constraints on the NMSSM, nevertheless they may become relevant with time and collider results. A selection of these modes are available in `NMSSMTools`.
- R-parity violation - `SoftSusy` is in limited company as a spectrum generator able to incorporate RPV effects for the MSSM, with only `sPHENO` able to do the same amongst the main programs publicly available (see Table 3.1). Extending this to the decay calculator may therefore offer significant benefits to the community in searching for RPV signatures at colliders, particularly as R-parity conserving models become further restricted by experimental exclusions. Again this would be a longer term development of the program and so is dependent upon the nature of collider results in the interim.

As can be seen, this represents a significant program of development and many opportunities for improvement. We therefore hope and expect this program of research continues considerably into the longer term future.

Chapter 5

Differential Spectra and Resummation

We now take a breath and move onto a different track, describing in this chapter and the next two (Chapters 5-7) the research we have undertaken in the development of the `reSolve` program [2] for transverse momentum resummations and the general production of differential spectra for hadron-hadron processes.

5.1 Precision Physics at the LHC

In our previous discussions of the research performed for the `SoftSusy` decay program in Chapters 2-4, we focused on the search for new physics states via specific model-dependent direct and indirect searches for new particles; through resonances, in loops or via their signatures at the LHC. However, with no clear new discoveries forthcoming from such searches since that of the Higgs boson in 2012 [12, 13], and increasing exclusions on the most minimal Beyond Standard Model parameter spaces, there is a growing endeavour at the LHC and elsewhere to develop efforts in precision physics measurements and searches. In particular, such a lack of observations suggests that new physics may be largely decoupled from the Standard Model at LHC scales and so may only produce small deviations in measured results. In such precision physics analyses, we aim to measure known Standard Model processes to high precision with the objectives being twofold; firstly to further our knowledge and understanding of Standard Model physics, and secondly to look for tiny model-independent deviations of experimental results from precise theoretical predictions as an alternative sign of new physics states. In this vein, differential cross-sections for a variety of processes are being measured at unprecedented precisions during Run II of the LHC and beyond. In order to take advantage of these precise measurements however we need equally precise theoretical predictions. In fact, unlike direct searches which may proceed to a degree without precise theoretical predictions - requiring theoretical predictions largely for the interpretation of new physics results (or lack thereof) in terms of the various model parameter spaces, for precision physics measurements the strategy is fundamentally dependent upon precise theoretical predictions. The calculation of such theoretical predictions for a particularly vital and difficult class of spectra, transverse momentum (p_T) spectra at low p_T, is the target of our work in this area. Transverse momentum spectra are of great importance for the testing of the Standard Model and for the precise measurement of its parameters, including the W mass

and PDFs. The resulting precise determinations of Standard Model parameters allow smaller theoretical uncertainties in many other calculations. In addition, these precise measurements are also able to serve as new physics searches, with any small deviations from the precise Standard Model predictions indicating the potential presence of Beyond Standard Model particles.

Nonetheless, before we embark upon an explanation of the underlying technicalities involved and the functionalities and results of the `reSolve` program we have written to augment efforts in this area through Chapters 6 and 7, we first begin outlining in this chapter some of the basic concepts in collider kinematics, differential spectra and resummation that are required to attain an understanding of this work.

5.2 Collider Kinematics

In this section we are considering production cross-sections of the following form, where h are incoming colliding hadrons, one from each beam, and F is the target measured final state system, whilst X is undetected additional radiation:

$$h(p_1) + h(p_2) \to F + X. \tag{5.1}$$

As the measured final state system F will be two photons, or two Drell-Yan leptons for our applications, here we begin by simplifying and considering the kinematics of $2 \to 2$ processes, we therefore introduce the Lorentz invariant Mandelstam variables s, t, u:

$$s = (p_1 + p_2)^2, \qquad t = (p_1 - p_3)^2, \qquad u = (p_1 - p_4)^2. \tag{5.2}$$

Given these are Lorentz invariant, we may evaluate them in any frame. Considering s in the centre of mass frame of the collision it is clear that $\sqrt{s} = E_{tot}$, i.e. s is the total square centre of mass energy in the collision. s is of particular relevance as it defines the "invariant mass" of a final state system of particles, M^2, or equivalently q^2 (or QQ^2):

$$M^2 = s_{\text{final state}} = m_1^2 + m_2^2 + 2(E_1 E_2 - \mathbf{p}_1 . \mathbf{p}_2). \tag{5.3}$$

However, at a hadron-hadron collider, the incoming beams of colliding partons have a spectrum of longitudinal momenta set by the parton distribution functions; as a result, in general, the centre of mass frame of the parton-parton scattering is boosted along the beam (z) direction. It is therefore useful to classify the 4-momenta in terms of variables which transform straightforwardly under these longitudinal boosts, so rather than describing $p^\mu = (E, p_x, p_y, p_z)$ we choose to describe it in terms of the variables $p^\mu = (E, p_T, \phi, y)$, which are the energy, transverse momentum, angle in the xy plane perpendicular to the beam, and rapidity. We define rapidity by

$$y = \frac{1}{2} \log \left(\frac{E + p_z}{E - p_z} \right). \tag{5.4}$$

Whilst it is clear that the p_T and ϕ angle are invariant under the longitudinal boosts necessary to reach the centre of mass frame, it is not immediately obvious that this is true for rapidity - boosting along z we obtain $E' = \gamma(E - \beta p_z)$, $p'_z = \gamma(-\beta E + p_z)$ and so the rapidity y transforms to:

$$y' = \frac{1}{2}\log\left(\frac{(E-\beta p_z)+(p_z-\beta E)}{(E-\beta p_z)-(p_z-\beta E)}\right) \Longrightarrow y' = y - \tanh^{-1}\beta. \tag{5.5}$$

As a result all rapidities transform with the same additive factor, which is the rapidity of the boost momentum, and so rapidity differences are longitudinal Lorentz boost invariant, as desired.

If we also introduce the "transverse energy" variable[1] defined by:

$$E_T = \sqrt{m^2 + p_T^2} = \sqrt{m^2 + p_x^2 + p_y^2} = \sqrt{E^2 - p_z^2}, \tag{5.6}$$

we may rewrite:

$$E = E_T \cosh y, \qquad p_z = E_T \sinh y. \tag{5.7}$$

So our coordinate change is given by:

$$p^\mu = (E, p_x, p_y, p_z) = (E_T \cosh y, p_T \cos\phi, p_T \sin\phi, E_T \sinh y). \tag{5.8}$$

In practice, in particle phenomenology rapidity, y, is not often used as it relies upon the simultaneous measurement of the energy and longitudinal momentum, instead the "pseudorapidity", η is preferred[2]:

$$\eta = \frac{1}{2}\log\left(\frac{|\mathbf{p}|+p_z}{|\mathbf{p}|-p_z}\right) = \tanh^{-1}\left(\frac{p_z}{|\mathbf{p}|}\right) = \tanh^{-1}(\cos\theta). \tag{5.9}$$

This is clearly equivalent to the rapidity y in the massless limit (as then $E \to |\mathbf{p}|$), however it is preferred as it can be straightforwardly related to the angle to the beam axis θ through

$$\eta = \frac{1}{2}\log\left(\frac{1+\cos\theta}{1-\cos\theta}\right) = -\log(\tan\frac{\theta}{2}). \tag{5.10}$$

The relationship between η and θ is shown in the oft-seen Figure 5.1:

The relationship between rapidity and pseudorapidity can be further elucidated using equation 5.9 and substituting in equations 5.7, which implies after a little algebra that

$$\sinh y = \frac{p_T}{E_T}\sinh\eta. \tag{5.11}$$

[1] Sometimes this is also referred to as transverse mass, however we distinguish here as we also have the experimental definition of transverse mass later in equation 5.15)

[2] Where the penultimate step follows from $\tanh^{-1}(x) = \frac{1}{2}\log\left(\frac{1+x}{1-x}\right)$.

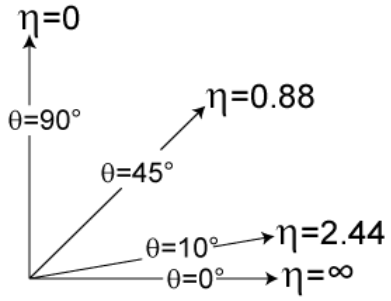

Figure 5.1: The relationship between the pseudorapidity η and the angle to the beam axis θ.

We may then use $\sinh^{-1} z = \log(z + \sqrt{1+z^2})$ to obtain:

$$y = \log\left(\frac{1}{\sqrt{m^2 + p_T^2}}\left(p_T \sinh\eta + \sqrt{m^2 + p_T^2 \cosh^2\eta}\right)\right). \tag{5.12}$$

Finally we can rewrite this as a function of $\chi = \frac{m}{p_T}$ and Taylor expand around $\chi = 0$ (the massless limit):

$$\begin{aligned} y =& \log\left(\frac{\sinh\eta + \sqrt{\cosh^2\eta + \chi^2}}{\sqrt{1+\chi^2}}\right) = \log(\sinh\eta + \cosh\eta) - \frac{\chi^2}{2}\left(1 - \frac{1}{\cosh\eta(\cosh\eta + \sinh\eta)}\right) + \mathcal{O}(\chi^4) \\ =& \frac{1}{2}\log(\exp\eta) - \frac{\chi^2}{2}\tanh\eta + \mathcal{O}(\chi^4) = \eta - \frac{m^2}{2p_T^2}\tanh\eta + \mathcal{O}\left(\frac{m^4}{p_T^4}\right) \end{aligned} \tag{5.13}$$

This makes it further clear that rapidity and pseudorapidity are equivalent in the massless limit.

We also use rapidity and the ϕ angle perpendicular to the beam to determine the angular separation between two final state particles defined by:

$$\Delta R = \sqrt{(\Delta y)^2 + (\Delta\phi)^2} \approx \sqrt{(\Delta\eta)^2 + (\Delta\phi)^2}. \tag{5.14}$$

This is relevant for cuts in the diphoton process, which we consider in Chapter 7.1.2, as two photons with small opening angle may not be distinguished. Furthermore, it may be used to define an "isolation cut" for the photons, in order to reject cases where a QCD parton is too close to the photon, as otherwise distinguishing a photon from a jet containing photons becomes difficult.

Before we move on, we introduce a further variable, the "transverse mass", which has useful properties in particle searches. In experiments often it is the case that one particle in the final state cannot be detected, for example neutrinos produced from W boson decay. As a result the total energy and momentum is often unknown, particularly down the beam-pipe, instead inferring the presence of the additional particle via missing transverse energy and momentum. Consequently, rather than use the transverse energy E_T, the alternative transverse mass m_T^{exp} is often used:

$$m_T^{exp} = \sqrt{(E_T^{(1)} + E_T^{(2)})^2 - (\mathbf{p}_T^{(1)} + \mathbf{p}_T^{(2)})^2} \approx \sqrt{2|\mathbf{p}_T^{(1)}||\mathbf{p}_T^{(2)}| - \mathbf{p}_T^{(1)}.\mathbf{p}_T^{(2)}}. \tag{5.15}$$

The last approximate equality here holds in the limit in which the final state particles are massless. In analogy with the invariant mass given in equation 5.3, we may write this experimental transverse mass[3] as

$$m_T^2 = (E_T^{(1)} + E_T^{(2)})^2 - (\mathbf{p}_T^{(1)} + \mathbf{p}_T^{(2)})^2 = m_1^2 + m_2^2 + 2(E_T^{(1)}E_T^{(2)} - \mathbf{p}_T^{(1)}.\mathbf{p}_T^{(2)}). \tag{5.16}$$

Consider for now the expression for the rapidity difference Δy, for which we may write:

$$\cosh\Delta y = \frac{1}{2}\left[\sqrt{\frac{(E_1 + p_z^{(1)})(E_2 - p_z^{(2)})}{(E_1 - p_z^{(1)})(E_2 + p_z^{(2)})}} + \sqrt{\frac{E_1 - p_z^{(1)})(E_2 + p_z^{(2)})}{(E_1 + p_z^{(1)})(E_2 - p_z^{(2)})}}\right] = \frac{E_1E_2 - p_z^{(1)}p_z^{(2)}}{E_T^{(1)}E_T^{(2)}}. \tag{5.17}$$

Therefore we have

$$E_T^{(1)}E_T^{(2)}\cosh\Delta y - \mathbf{p}_T^{(1)}.\mathbf{p}_T^{(2)} = E_1E_2 - p_z^{(1)}p_z^{(2)} - \mathbf{p}_T^{(1)}.\mathbf{p}_T^{(2)} = E_1E_2 - \mathbf{p}_1.\mathbf{p}_2. \tag{5.18}$$

So we may rewrite the expression for the invariant mass squared as:

$$M^2 = m_1^2 + m_2^2 + 2(E_T^{(1)}E_T^{(2)}\cosh\Delta y - \mathbf{p}_T^{(1)}.\mathbf{p}_T^{(2)}), \tag{5.19}$$

and as $\cosh x \geq 1$ we have the inequality

$$M^2 \geq m_1^2 + m_2^2 + 2(E_T^{(1)}E_T^{(2)} - \mathbf{p}_T^{(1)}.\mathbf{p}_T^{(2)}) = m_T^2, \tag{5.20}$$

where the last equality is from equation 5.15. Therefore if we measure the distribution of transverse masses attained at the LHC for a given final state, then the transverse mass distribution has an upper cut-off at the invariant mass, which will be equal to the mass of the parent intermediate particle producing the two final state particles. This is how the W mass may be measured. Furthermore this endpoint in the transverse mass distribution is achieved when the two final state particles are emitted at the same rapidity so $\Delta y = 0$.

5.3 Production Cross-Sections

Following our brief sojourn into collider kinematics, let us move in the direction of our application and consider the basic theory behind production cross-sections at hadron-hadron colliders. First we begin with a simplification, supposing two fundamental particles (such as two quarks) collide to produce two further particles in a $2 \to 2$ collision; then, following similar calculations we performed for particle decays in Chapter 3.1, it can be shown that the general expression for such a production cross-section is given by[4]:

[3] From now we denote the transverse mass as m_T neglecting the "exp" label which is implied.

[4] In this equation and the next we label the cross-sections as $\hat{\sigma}$ rather than σ to reflect the fact these are cross-sections for the collisions of fundamental objects and so in our context these are the forms of the partonic cross-sections used later.

$$\hat{\sigma}(a+b \to 1+2) = \frac{(2\pi)^4}{4\sqrt{(p_a.p_b)^2 - m_a^2 m_b^2}} \int |M_{fi}|^2 \delta^4(p_a+p_b-p_1-p_2) \frac{d^3\mathbf{p}_1}{2E_1(2\pi)^3} \frac{d^3\mathbf{p}_2}{2E_2(2\pi)^3}. \quad (5.21)$$

Here the prefactor is $(2\pi)^4\mathcal{F}$ where $\mathcal{F}$ is the so-called "Lorentz invariant flux factor"[5]. This general expression is Lorentz invariant and so the cross-section may be evaluated in the centre of mass frame in which the total energy is $\sqrt{s}$ and the initial and outgoing 3-momenta are each net zero. Again, one uses the expression for a delta function of a function of the integration variable in equation 3.7, then in the centre of mass frame:

$$\hat{\sigma}(a+b \to 1+2) = \frac{1}{64\pi^2 s} \frac{p_f^*}{p_i^*} \int |M_{fi}|^2 d\Omega^*, \quad (5.22)$$

where the $*$ indicates these quantities are determined in the centre of mass frame. Performing such phase space integrals is relatively simple when the phase space is complete; however, once cuts are present and the experimental sensitivity is accounted for, it is much more complex. The complexity also grows extremely quickly with the number of particles produced and as beyond leading order contributions are considered. We are however fortunate that at collider scales QCD becomes asymptotically free in its running and so we can treat it perturbatively, allowing the computation of observables such as the total cross-section as a series of Feynman diagrams of growing order and offering increasing precision.

Nevertheless, for precision physics applications we require more than just the total cross-section; instead precise measurements are made of the spectra of particles produced, i.e. we measure cross-sections differential in some experimental variable(s), this adds further complications to the evaluation of the our expressions. From equation 5.22 we can quickly determine the differential cross-section in solid angle in the centre of mass frame $\frac{d\sigma}{d\Omega^*}$, however in general we require either differential cross-sections in the laboratory frame, or in Lorentz invariant variables such as the Mandelstam variable t. This requires changes of coordinates, nonetheless t can be related to scattering angles via equation 5.2 with the 4-momenta in the relevant frame. A pedagogical introduction to cross-sections and differential cross-sections in particle physics is available in [16].

Whilst differential cross-sections in such variables are relatively simply derived, scattering angles are not the most natural variables to measure at hadron-hadron colliders, because the longitudinal boost of the particles produced is unknown. Therefore differential cross-section spectra in terms of longitudinal boost-invariant coordinates p_T, ϕ and y or η are a more natural choice. To obtain differential cross-sections in these variables we again require a change of variables, starting from $d\sigma \propto \frac{d^3\mathbf{p}}{2E(2\pi)^3}$:

[5]This form of the flux factor $\mathcal{F}^{-1} = 4\sqrt{(p_a.p_b)^2 - m_a^2 m_b^2}$ may be unfamiliar, if we assume the particles are travelling in the z-direction only it can be shown this form is equivalent to the alternative common form $\mathcal{F}^{-1} = 4|\epsilon_{\mu 12\nu} p_a^\mu p_b^\nu| = 4|E_b p_a^3 - E_a p_b^3| = 4E_a E_b |v_a - v_b|$. This second form is, in fact, only invariant under boosts along the collision axis (taken to be the z axis) and under general rotations. This must be the case as the cross-section is a space-like area and so must vary with transformations perpendicular to the collision axis. As in the case of particle decays, the non-Lorentz invariance is then all incorporated in this flux factor, ensuring the phase space integral is Lorentz invariant and may be evaluated in any frame.

$$E\frac{d^3\sigma}{dp_x dp_y dp_z} = \frac{E}{p_T}\frac{d^3\sigma}{dp_T d\phi dp_z} = \frac{1}{p_T}\frac{d^3\sigma}{dp_T d\phi dy}. \tag{5.23}$$

In the last step here we have used that:

$$\frac{dy}{dp_z} = \frac{1}{2}\Big[\frac{1}{E+p_z}\Big(1+\frac{dE}{dp_z}\Big) + \frac{1}{E-p_z}\Big(-1+\frac{dE}{dp_z}\Big)\Big] = \frac{1}{E}. \tag{5.24}$$

However, this work so far has been a drastic simplification of the setup at hadron-hadron colliders such as the LHC, indeed the expressions would naturally apply at a lepton-lepton collider. They only apply to the fundamental underlying process at hadron-hadron colliders, which add an additional layer of complication due to the fact the initial and final states are no longer fundamental particles but are hadronised into QCD objects. The colliding quarks or gluons themselves originate as "partons" from the hadrons themselves (protons for the LHC), and therefore carry an unknown fraction of the 4-momentum of the ingoing protons. Therefore whilst our expressions for cross-sections and differential cross-sections so far in this section considered colliding fundamental particles such as quarks, we must generalise to collisions of quarks (or generally partons including gluons) within hadrons. We therefore must make the step from the "partonic cross-sections" we have so far considered to "hadronic cross-sections" reflecting the reality at the LHC. This development adds a myriad of complications and issues. Nevertheless, we begin by introducing the momentum fractions x_1, x_2 of the colliding partons; these are the fractions of the total momenta of their parent hadrons that the colliding partons each have, and may be written in terms of the invariant mass and rapidity as follows. Consider first the 4-momentum of the colliding partons in the hadron-hadron collision centre of mass frame, neglecting their masses as at hadron colliders the energies are much larger than the particle masses, then

$$q = x_1 p_1 + x_2 p_2 = ((x_1+x_2)E, 0, 0, (x_1-x_2)E). \tag{5.25}$$

Therefore we may write the invariant mass squared and transverse energy as[6]:

$$q^2 = ((x_1+x_2)^2 - (x_1-x_2)^2)E^2 = 4x_1x_2E^2 = x_1x_2s, \tag{5.26}$$

$$E_T = \sqrt{E^2 - p_z^2} = 2\sqrt{x_1x_2}E = \sqrt{x_1x_2s} = \sqrt{q^2}. \tag{5.27}$$

Using equation 5.7 we may obtain e^y and then substitute equation 5.27 in to obtain

$$\cosh y = (x_1+x_2)\frac{E}{E_T}, \qquad \sinh y = (x_1-x_2)\frac{E}{E_T}, \qquad \Rightarrow \qquad e^y = \frac{2x_1E}{E_T} = \sqrt{\frac{x_1}{x_2}}, \tag{5.28}$$

therefore finally we reach:

[6]Remember $s = 4E^2$ and note that $E_T = \sqrt{q^2}$ as no momentum transverse to the beam has been taken so $p_z^2 = \mathbf{p}^2$.

$$x_1 = |q|\frac{e^y}{\sqrt{s}}, \qquad x_2 = |q|\frac{e^{-y}}{\sqrt{s}}. \tag{5.29}$$

We now need to convert from our partonic cross-sections, which may be obtained without thought for the detailed QCD non-perturbative dynamics occurring to bind the partons into hadrons, to hadronic cross-sections. To do this we must parametrise our ignorance and create probability distribution functions representing the chance of receiving a parton of given momentum fraction from the protons colliding. "Parton Distribution Functions" (PDFs), $f(x)$, must be defined where $f(x)dx$ represents the probability of obtaining a parton of momentum fraction between x and $x+\delta x$ from a proton; the PDFs are different for each flavour of parton considered due to the QCD dynamics and parton masses. To calculate the required hadronic cross-sections, we then integrate the partonic cross-sections (containing the short distance, high energy physics of the fundamental collision) multiplied by the PDFs for each colliding parton (containing the long distance, low energy physics of the QCD hadronisation) over the total momentum fractions allowed. This "factorisation" of short and long distance physics is key, and not obvious a priori. Our description follows from Feynman's "parton model", which applies at leading-order in QCD up to corrections which reflect various inherent assumptions in this model, including that the separate contributions from each parton may be incoherently summed and do not interact with one another. The QCD improved parton model, incorporating beyond leading order effects of factorisation scale dependence, absorption of collinear singularities and parton splitting is introduced later.

$$\sigma(h_1 + h_2 \to 1 + 2) = \int_0^1 dx_1 \int_0^1 dx_2 \sum_{a,b=-N_f}^{N_f} f_{a/h_1}(x_1) f_{b/h_2}(x_2) \hat{\sigma}(a + b \to 1 + 2). \tag{5.30}$$

In fact, beyond leading-order, the nature of the partonic cross-sections which are summed is also non-trivial, with partonic cross-sections with addition undetected real emissions (X) and loop corrections giving virtual contributions both needing to be summed to obtain the hadronic cross-section for $h_1 + h_2 \to F(= 1 + 2) + X$.

In any case, in this simplified parton model, we convolute the PDFs with the partonic cross-sections to produce the overall hadronic production cross-sections. As a result, as well as the three momentum differentials over which to integrate, we also have the momentum fractions to integrate over, this allows greater flexibility in obtaining differential cross-sections as we may also change variables from the x_1, x_2 to rapidity, invariant mass and other desired variables. For example we may determine the double differential cross-section with respect to rapidity and invariant mass given by equation 5.32 using our expression for the hadronic cross section of equation 5.30 after first determining the Jacobian for the relevant change of variables:

$$\frac{\partial(q^2, y)}{\partial(x_1, x_2)} = \begin{vmatrix} \frac{\partial q^2}{\partial x_1} & \frac{\partial q^2}{\partial x_2} \\ \frac{\partial y}{\partial x_1} & \frac{\partial y}{\partial x_2} \end{vmatrix} = \begin{vmatrix} x_2 s & x_1 s \\ \frac{1}{2x_1} & -\frac{1}{2x_2} \end{vmatrix} = s = \frac{q^2}{x_1 x_2}, \tag{5.31}$$

$$\frac{d^2\sigma}{dq^2dy}(h_1+h_2\to 1+2)=\frac{1}{q^2}\sum_{a,b=-N_f}^{N_f}x_1f_{a/h_1}(x_1)x_2f_{b/h_2}(x_2)\hat{\sigma}(a+b\to 1+2). \tag{5.32}$$

In fact, the partonic cross-section itself was integrated over angular and momentum variables, therefore we can derive higher power differential distributions with respect to further kinematic variables:

$$\frac{d^4\sigma}{dq^2dyd\theta^*d\phi^*}(h_1+h_2\to 1+2)=\frac{1}{q^2}\sum_{a,b=-N_f}^{N_f}x_1f_{a/h_1}(x_1)x_2f_{b/h_2}(x_2)\frac{d^2\hat{\sigma}(a+b\to 1+2)}{d\theta^*d\phi^*}. \tag{5.33}$$

The expression for the double differential distribution with respect to the two angular centre of mass variables is then read from equation 5.22. At Born level, where there can be no net transverse momentum for the outgoing 2 particle system, a 4^{th} order differential distribution is the highest possible as the number of final state independent variables in a $2\to n$ interaction is $3n-4$, plus we have two further from the incoming momentum fractions of the partons.

The evaluation of the integrals over any remaining necessary variables in determining such differential distributions can be significantly more complicated than integrating over the whole phase space to obtain the total cross-section, as more kinematic information is retained. Furthermore this is complicated by arbitrary experimental cuts on different kinematic variables (be it to enhance searches over backgrounds or due to the experiment detector sensitivity itself) which may spoil the analytic form of the integrals. On top of this, to perform analytic integrations we often have to be very "inclusive" in our descriptions in order to avoid problems with un-cancelled singularities, integrating over all possible related final states in a way which does not reflect the exclusive nature of many measurements. Consequently, theoretical tools for performing such calculations typically rely upon Monte Carlo integration, as will our tool `reSolve`.

In Monte Carlo integration, individual "events" corresponding loosely to the events at a collider[7] are generated randomly within the phase space and the cross-section integrand is evaluated for each point. Keeping the information of the individual events calculated one can then sum them, with the sum usually weighted appropriately by a grid describing the error distribution over the phase space, to obtain the total cross-section; or one may sum only in some variables in order to obtain differential distributions, the events can then be binned to produce the desired spectrum. Further details on the Monte Carlo evaluation are given in Appendix B.3.

More specifics and formal background on all the ideas and equations outlined here, and more, including the contents of the rest of the chapter, are given in [14, 17].

[7]The correspondence is not exact due to the effects of higher orders which may produce negative contributions in some applications and as the events produced inherently depend upon any latent assumptions within the theoretical application, such as schemes and other choices.

5.4 Soft and Collinear Divergences

In this section we seek to clarify the IR divergences which were briefly mentioned previously and are the key to the complexity of predictions for transverse momentum spectra at low p_T. In considering an amplitude for an arbitrary process beyond leading order, one must consider all real corrections due to radiating additional particles and all virtual corrections due to additional loops at the order considered. We have seen previously UV divergences arising from arbitrarily high momenta ($k \to \infty$) running in loop integrals; IR divergences on the other hand have their source in low momenta $k \to 0$ integrals, as mentioned in Chapter 1.1.3.

As an example of IR divergences and their cancellations, let us contemplate a general $2 \to 2$ process, at NLO we get real and virtual corrections such as those in Figure 5.2a, amongst other such contributions.

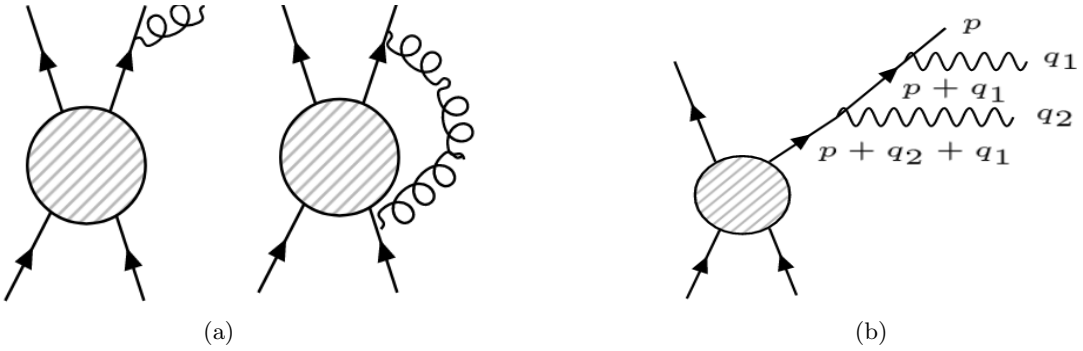

(a) (b)

Figure 5.2: (a) Real (left) and virtual (right) corrections to a generic $2 \to 2$ process, these give additional propagator factors as well as extra vertex gauge coupling factors and photon (for QED) polarisation contractions. (b) Multiple emissions, as have to be summed over for each external state, these emissions are photons in QED.

Each such correction introduces both additional factors of the gauge coupling via the extra vertex, and an additional propagator, the additional propagator is the source of soft and collinear divergences in the infrared in the case of massless propagating particles:

$$\left.\frac{1}{(p+q)^2 - m^2 - i\epsilon}\right|_{q\to 0} = \frac{1}{2p.q} = \frac{1}{2p_0 q_0(1-\cos\theta)} \to 0 \quad \begin{cases} \text{for } q_0 \to 0 \text{ “soft divergence”}, \\ \text{or } \cos\theta \to 1 \text{ “collinear divergence”}. \end{cases} \tag{5.34}$$

In the case of massive propagating particles however, the collinear divergence is regulated by the mass as then $2p.q = 2p_0q_0 - 2|\mathbf{p}|q_0\cos\theta$ which no longer has a divergence as $\cos\theta \to 1$ as $p_0 > |\mathbf{p}|$. Instead logarithmic collinear enhancements appear. Meanwhile, soft divergences cancel between real emissions and virtual corrections, leaving logarithmic soft enhancements. It is these soft and collinear enhancements which may spoil perturbation theory and require resummation.

In order to demonstrate the appearance of such divergences and logarithmic enhancements in the IR, let us consider these divergences in QED, where the structure is simpler. We begin with real emissions, scrutinising first the case of emitting a single soft photon; this is examined

more formally in [14] and [197] (based on [198]). Real emission from a final state particle is shown in the left-hand of Figure 5.2a, nonetheless we will include initial and final state emission in our derivation. For the final state emission case we label the initial momentum as $p+q$ before radiation of a photon of momentum q leaves momentum p on the fermion line[8], this will give an additional factor (dropping the photon polarisation vectors for now) in the amplitude of [9]:

$$[i(2\pi)^4 e(2p^\mu \pm q^\mu)]\left[\frac{-i}{(2\pi)^4}\frac{1}{(p\pm q)^2-m^2-i\epsilon}\right] \xrightarrow[q\to 0]{} \frac{ep^\mu}{\pm p.q - i\epsilon}, \tag{5.35}$$

where the $\pm$ is a "+" for emission in the final state and a "−" for emission in the initial state and we have taken the soft photon limit $q \to 0$. Summing over all n legs off which to emit (4 for us as $2 \to 2$), one obtains an extra factor given in equation 5.36, η_n is ± 1 accordingly for final and initial state real emission:

$$\sum_n \frac{\eta_n e^n p_n^\mu}{p_n.q - i\eta_n\epsilon}. \tag{5.36}$$

However, in reality we must sum over the emission of any number of soft photons, considering two emissions we have a diagram as in Figure 5.2b, as well as the reverse ordering of the photon legs.

The first ordering (given in the figure) and the second ordering give additional factors of:

$$\left[\frac{\eta e p^\mu}{p.q_1 - i\eta\epsilon}\right]\left[\frac{\eta e p^\nu}{p.(q_1+q_2) - i\eta\epsilon}\right], \qquad \left[\frac{\eta e p^\nu}{p.q_2 - i\eta\epsilon}\right]\left[\frac{\eta e p^\mu}{p.(q_1+q_2) - i\eta\epsilon}\right]. \tag{5.37}$$

These may then be summed, and happily factorise into separate analogous factors per emission:

$$\left[\frac{\eta e p^\mu}{p.q_1 - i\eta\epsilon}\right]\left[\frac{\eta e p^\nu}{p.q_2 - i\eta\epsilon}\right]. \tag{5.38}$$

The same applies for any number of photon emissions factoring into separate pieces; this is often referred to as factorisation of dynamics[10] and is explicitly shown in [197] so we do not repeat it here, it is crucial to the ability to resum these emissions via exponentiation as we shall demonstrate. Emitting N soft photons gives an additional factor (neglecting the photon polarisations) of

$$\prod_{r=1}^{N} \frac{\eta_n e_n p_n^\mu}{p.q_r - i\eta_n\epsilon}. \tag{5.39}$$

Each emitted soft photon polarisation then contracts with this extra factor so we obtain

[8] For initial state emission the momentum of the initial fermion is p, it then emits a photon of momentum q leaving momentum $p-q$ on the fermion line so the propagator has an additional relative minus sign.

[9] Here this has been simplified by taking a spin 0 charged particle emitting a photon. In the spin $\frac{1}{2}$ case of real QED the additional factor is instead $\frac{(\not{p}\pm\not{q}+m)}{((p\pm q)^2-m^2)}e\gamma^\mu\epsilon_\mu u(p+q)$, if the $q\to 0$ Eikonal limit is again taken one may commute the relevant γ matrices using the Clifford algebra and use the Dirac equation to obtain the same limit as on the right-hand side of equation 5.35 above. In fact this limiting form is independent of spin, spin 0 was therefore chosen above for simplicity.

[10] This factorisation of dynamics occurs similarly in QCD with the small complication of colour factors.

(where the product is over the number of emissions and the sum is over the number of external states):

$$M_{\text{emissions}} = M_{\text{LO}} \prod_{r=1}^{N} \sum_{n} \frac{\eta_n e_n p_n.\epsilon^*(q_r)}{p_n.q_r}. \tag{5.40}$$

We must square this, sum over helicities $\sum_{h=\pm 1} \epsilon^{\mu}(q,h)\epsilon^{\nu *}(q,h) = -g_{\mu\nu}$ (terms have been dropped here due to charge conservation) and divide by $N!$ as the photons are indistinguishable, and so our differential rate is:

$$d\Gamma_{\text{emissions}}(q_1, q_2, \ldots, q_N) = -\frac{1}{N!}\Gamma_{\text{LO}} \prod_{r=1}^{N} \frac{d^3 q_r}{(2\pi)^3 2|\mathbf{q}|} \sum_{nm} \frac{\eta_n \eta_m e_n e_m (p_n.p_m)}{(p_n.q_r)(p_m.q_r)}. \tag{5.41}$$

Integrating over phase space, which incorporates integrating over the energies and directions of the outgoing photons, we will observe soft divergences and collinear enhancements[11] respectively. First we integrate over the photon directions; for each emitted photon we obtain:

$$-(p_n.p_m) \int \frac{2\pi d\hat{\mathbf{q}}}{(E_n - \hat{\mathbf{q}}.\mathbf{p}_n)(E_m - \hat{\mathbf{q}}.\mathbf{p}_m)} = \frac{2\pi}{\beta_{nm}} \log\left(\frac{1+\beta_{nm}}{1-\beta_{nm}}\right). \tag{5.42}$$

$\hat{\mathbf{q}}$ is the normalised photon momentum and $\beta_{nm} = \sqrt{1 - \frac{m_n^2 m_m^2}{(p_n.p_m)^2}}$ is the relative velocity of particles n and m in each other's rest frames. This demonstrates the collinear enhancements $\log\left(\frac{1+\beta_{nm}}{1-\beta_{nm}}\right)$, which are large when the two intermediate (electron) lines have near collinear momenta as then $\beta_{nm} \to 1$, this occurs when the photon emitted is collinear. However, these are not collinear divergences as the intermediate electrons have mass. If we take the massless limit (which applies for QCD for example as then the charged intermediates can be massless gluons) by taking the mass of one electron line to be zero so $m_1 \to 0$, whilst keeping $\mathbf{p}_1$ fixed, then we can rewrite our collinear logarithmic enhancement:

$$\beta_{1n} = \sqrt{1 - \frac{m_1^2 m_n^2}{(p_1.p_n)^2}} = 1 - \frac{m_1^2 m_n^2}{2(p_1.p_n)^2} + \mathcal{O}(m_1^4), \tag{5.43}$$

so in this limit to first order

$$\log\left(\frac{1+\beta_{nm}}{1-\beta_{nm}}\right) \approx \log\left(\frac{4(p_1.p_n)^2}{m_1^2 m_n^2}\right). \tag{5.44}$$

So, as $m_1 \to 0$ whilst keeping $\mathbf{p}_1$ fixed we have a collinear divergence. We may extract the divergent piece and it is proportional to $\log m_1$, and so it is directly the mass of the charged intermediates which prevent such divergences in QED.

Integrating over all emitted photon momenta leaves the integrals over the photon energies:

[11] QED gives collinear enhancements, rather than divergences, as the electron mass in the propagators regulate the collinear divergences. Nonetheless these enhancements may still be an issue phenomenologically, being potentially large logarithms at all orders in relevant regions of parameter space and so would also have to be resummed in the same way.

$$d\Gamma_{\text{emissions}}(E_1, E_2, \ldots, E_N) = \Gamma_{\text{LO}} \frac{1}{N!} \left[\frac{1}{8\pi^2} \sum_{nm} \frac{e_n e_m \eta_n \eta_m}{\beta_{nm}} \log\left(\frac{1+\beta_{nm}}{1-\beta_{nm}}\right) \right]^N \frac{dE_1}{E_1} \frac{dE_2}{E_2} \cdots \frac{dE_N}{E_N}$$
$$= \Gamma_{\text{LO}} \frac{1}{N!} A^N \frac{dE_1}{E_1} \frac{dE_2}{E_2} \cdots \frac{dE_N}{E_N}, \tag{5.45}$$

where we have defined

$$\begin{aligned} A = \int d^2\Omega A(\hat{\mathbf{q}}) =& -\frac{1}{16\pi^3} \int d^2\Omega \sum_{nm} \frac{e_n e_m \eta_n \eta_m (p_n.p_m)}{(E_n - \hat{\mathbf{q}}.\mathbf{p}_n)(E_m - \hat{\mathbf{q}}.\mathbf{p}_m)} \\ =& \frac{1}{8\pi^2} \sum_{nm} \frac{e_n e_m \eta_n \eta_m}{\beta_{nm}} \log\left(\frac{1+\beta_{nm}}{1-\beta_{nm}}\right), \end{aligned} \tag{5.46}$$

which is raised to power N due to the product over photon emissions.

Now, in integrating over the photon energies, we must introduce an upper bound energy E_d which is the detector threshold energy, below which the photons are undetected and so may be considered "soft" and therefore part of the same final state as the no emissions case, whilst we use an IR cut-off λ to demonstrate the IR divergence:

$$\int_\lambda^{E_d} \frac{dE}{E} = \log \frac{E_d}{\lambda}. \tag{5.47}$$

This soft piece is logarithmically divergent as $\lambda \to 0$. Each emission also produces an extra factor of α from the vertex and so, schematically, for each N we obtain an additional double logarithm factor

$$\frac{1}{N!} \alpha^N \log^N\left(\frac{E_d}{\lambda}\right) \log^N\left(\frac{1+\beta_{nm}}{1-\beta_{nm}}\right). \tag{5.48}$$

As such a term arises for all N, each term in the perturbative expansion in α is enhanced by the double logarithm, with one logarithm from the soft divergence and one from the collinear enhancement; the soft divergence logarithmic enhancement is infinite as the IR cut-off λ is taken to 0:

$$\Gamma_{\text{emissions}} = \Gamma_{\text{LO}} \sum_{N=0}^{\infty} \frac{1}{N!} \alpha^N \log^N\left(\frac{E_d}{\lambda}\right) \log^N\left(\frac{1+\beta_{nm}}{1-\beta_{nm}}\right). \tag{5.49}$$

Formally, this means that if these logarithms are large (the soft logarithm is infinite as $\lambda \to 0$ so they are!) our perturbation theory may break down as each successive order is of the same approximate magnitude as the previous one. This would cause drastic problems for our theoretical predictions. However, we can identify the sum over N as the Taylor series for an exponential and resum this infinite series to obtain:

$$\Gamma_{\text{emissions}} = \Gamma_{\text{LO}} \exp\left[\alpha \log\left(\frac{E_d}{\lambda}\right) \log\left(\frac{1+\beta_{nm}}{1-\beta_{nm}}\right) \right]. \tag{5.50}$$

This resummation via exponentiation is the key to recovering the predictivity of the perturbative

series in the case where the logarithm terms become large. However, our soft divergence still remains (as would our collinear divergence if we had one, as in QCD).

Fortunately, before making any theoretical predictions we must consider all possible degenerate final states, i.e. final states which we cannot distinguish from one another. So far we have considered only the possibility of real emissions below some detector threshold; in addition, physically we cannot distinguish the final state from the loop-corrected final state, and so we must consider the possibility of virtual photons.

Implementing the same analysis for virtual soft photons, for each additional soft photon the additional propagator factor is $\frac{i}{(2\pi)^4}\frac{g_{\mu\nu}}{q^2-i\epsilon}$, and comes along with two additional vertices. As before, we consider an arbitrary number, N, of additional virtual photons and we divide by $2^N N!$ as each propagator can be attached either way around and the ordering is unimportant. Ultimately, the overall matrix element is enhanced by the following factor by possible virtual corrections from photons:

$$\frac{1}{2^N N!}\left[\frac{1}{(2\pi)^4}\sum_{nm} e_n e_m \eta_n \eta_m \int_\lambda^\Lambda \frac{d^4q \quad (ip_n.p_m)}{(q^2 i\epsilon)(p_n.q - i\eta_n\epsilon)(-p_m.q - i\eta_m\epsilon)}\right]^N = \frac{1}{N!}\left[\frac{1}{2}\int_\lambda^\Lambda d^4q[-A(\hat{\mathbf{q}})]\right]^N. \tag{5.51}$$

Unlike the real emissions, this is the extra factor for the matrix element, rather than the transition rate, and so we must square, which removes the superfluous factor of 2. We thus obtain the same integrals as for the real emissions case with different bounds on the photon energies. We integrate the photon energies between the IR cut-off λ as before, and a new upper cut-off Λ which cuts off the integral at large energies as we expect no IR effects once $q \sim \Lambda \sim Q$, where Q is a hard scale - such as the momentum transfer. This Λ cut-off acts to define what is meant by virtual "soft" photons. As a result of the minus sign, once the integral over the photon directions is performed to reveal the same collinear enhancement factor, the integral over the photon energies is:

$$\int_\lambda^\Lambda \frac{-dq}{q} = -\log\frac{\Lambda}{\lambda} = \log\frac{\lambda}{\Lambda}. \tag{5.52}$$

Therefore at the N^{th} order in a perturbative expansion in α the virtual corrections produce an enhancement, again containing a soft divergent piece as $\lambda \to 0$ and a collinear enhancement piece:

$$\frac{1}{N!}\alpha^N \log^N\left(\frac{\lambda}{\Lambda}\right)\log^N\left(\frac{1+\beta_{nm}}{1-\beta_{nm}}\right). \tag{5.53}$$

The virtually corrected rate, Γ_{v}, is therefore as follows, where in the last step we have again resummed via exponentiation, however as for the real emissions case this does not resolve the divergence(s) present:

$$\Gamma_{\text{v}} = \Gamma_{\text{LO}}\sum_{N=0}^{\infty}\frac{1}{N!}\alpha^N \log^N\left(\frac{\lambda}{\Lambda}\right)\log^N\left(\frac{1+\beta_{nm}}{1-\beta_{nm}}\right) = \Gamma_{\text{LO}}\exp\left[\alpha\log\left(\frac{\lambda}{\Lambda}\right)\log\left(\frac{1+\beta_{nm}}{1-\beta_{nm}}\right)\right]. \tag{5.54}$$

We must consider the effect of real emissions and virtual corrections together, multiplying the effects they each have on the leading order rate and combining them at each order:

$$\begin{aligned}\Gamma_{\text{observed}} &= \Gamma_{\text{LO}}\Big[1+\alpha\log\Big(\frac{E_d}{\lambda}\Big)\log\Big(\frac{1+\beta_{nm}}{1-\beta_{nm}}\Big)+\frac{\alpha^2}{2}\log^2\Big(\frac{E_d}{\lambda}\Big)\log^2\Big(\frac{1+\beta_{nm}}{1-\beta_{nm}}\Big)+\dots\Big]\\ &\quad\times\Big[1+\alpha\log\Big(\frac{\lambda}{\Lambda}\Big)\log\Big(\frac{1+\beta_{nm}}{1-\beta_{nm}}\Big)+\frac{\alpha^2}{2}\log^2\Big(\frac{\lambda}{\Lambda}\Big)\log^2\Big(\frac{1+\beta_{nm}}{1-\beta_{nm}}\Big)+\dots\Big]\\ &= 1+\alpha\log\Big(\frac{1+\beta_{nm}}{1-\beta_{nm}}\Big)\log\Big(\frac{E_d}{\Lambda}\Big)+\frac{\alpha^2}{2}\log^2\Big(\frac{1+\beta_{nm}}{1-\beta_{nm}}\Big)\log^2\Big(\frac{E_d}{\Lambda}\Big)+\mathcal{O}(\alpha^3)\end{aligned} \tag{5.55}$$

Therefore the soft divergence as $\lambda \to 0$ cancels out at each order, leaving a soft and a collinear logarithmic enhancement each of the same order in the perturbative series. The overall expression for the rate may then be written:

$$\Gamma_{\text{observed}} = \Gamma_{\text{LO}}\sum_{N=0}^{\infty}\frac{1}{N!}\alpha^N\log^N\left(\frac{E_d}{\Lambda}\right)\log^N\left(\frac{1+\beta_{nm}}{1-\beta_{nm}}\right). \tag{5.56}$$

The logarithmic enhancements may still spoil the perturbative series once $\alpha\log\left(\frac{E_d}{\Lambda}\right)\log\left(\frac{1+\beta_{nm}}{1-\beta_{nm}}\right) \sim 1$, nonetheless we can again identify the sum as the Taylor series for an exponential and resum these potentially dangerous terms to recover the predictivity of the perturbative series:

$$\Gamma_{\text{observed}} = \Gamma_{\text{LO}}\exp\left[\alpha\log\Big(\frac{E_d}{\Lambda}\Big)\log\Big(\frac{1+\beta_{nm}}{1-\beta_{nm}}\Big)\right]. \tag{5.57}$$

We can therefore resum all the logarithmically enhanced pieces arising from the cancelled infrared divergences via exponentiation. This calculation has been schematic so several factors and subtleties have been overlooked but it demonstrates the key physics for resummation associated with IR divergences.

It should be noted at this stage that whilst the soft divergences have cancelled, the collinear logarithms remain the same, however in QED these are not actually divergent as the divergence is regulated by the electron mass, therefore the fact these collinear pieces are unchanged is not an issue as there are no massless QED-charged particles. The IR divergences have therefore cancelled between the real emissions and virtual corrections, as described more rigorously by Block-Nordsieck Theorem for QED [199]. This states that in QED such cancellation of divergences is attained when summing over all possible degenerate final states.

This toy example was given in QED for simplicity, however the same argument can be applied in QCD with a few appropriate changes. First of all $\alpha_s \gg \alpha$, so the logarithmic enhancement in the overall perturbation series for real emissions and virtual corrections is worse, and will ruin the predictivity at smaller ratios of scales than would be required in QED, making the problem all the more pressing. Secondly, whilst we have shown that the soft divergences cancelled, the collinear pieces remained the same; in QCD there is also a collinear divergence arising from the fact that the massless gluons are colour-charged particles and so we also need to cancel these collinear divergences. Fortunately, Block-Nordsieck theorem of QED is replaced with the

Kinoshita-Lee-Nauenberg (KLN) Theorem [200,201], which states that IR divergences (including the collinear divergence) are cancelled in an observable when all possible initial and final states are summed over, with the additional need to sum over initial states arising precisely from the non-Abelian nature of QCD. In fact, when deducing the DGLAP equations in Chapter 5.5, we perform this sum over initial states by allowing parton splittings, causing collinear divergences and absorbing the dependence into PDF running[12].

The need to include all possible real emissions and virtual corrections order-by-order in perturbation theory in order to ensure the cancellation of soft and collinear divergences can be interpreted physically. Any detector could not distinguish between an electron and an electron and a soft photon (or in QCD a quark or gluon and a soft gluon) and similarly any radiation emitted along the fermion line will not be distinguished; both these effects are due to experimental resolution practically. However, here our theoretical understanding of these divergences and the need to be inclusive is actually informing us of something stronger, that regardless of experimental sensitivity any fermion will always be surrounded by a cloud of soft (and collinear) radiation and so this is the physical state of the theory, rather than the single particles we usually think of.

5.5 Scales

Our exposition so far is still not detailed enough to understand the basic fundamentals involved in our research in this area; QCD is full of complications and, in fact, what we have described thus far is itself dependent on various assumptions. Many of these complications arise as a result of the IR and UV divergences present, including the introduction of scales into theoretical predictions. The interested reader can consult any of the vast array of QCD textbooks [17, 202, 203] for more detailed and formal approaches, whilst there are several good reviews [204, 205].

In writing down the hadronic cross-section expression in equation 5.30 we implicitly made the assumption that it is possible to factorise out the long distance, low energy scale physics associated with hadronisation from the details of the short distance, high energy physics associated with the partonic cross-section. Such an assumption need not a priori be true, but separates the physics into our universal (process-independent) PDFs capturing the non-perturbative behaviour, and our process-dependent perturbatively calculable partonic cross sections. This assumption is an example of the "QCD Factorisation Theorem" [206–208], which has been proven for Deep Inelastic Scattering of leptons off hadrons and demonstrated for Drell-Yan, but is typically used as an ansatz for other collider processes [209]. Such factorisations are typically only correct up to a certain order in small corrections, usually of the order $\mathcal{O}(\Lambda_{QCD}/Q)$ due to the assumed independence of physics on the different scales, which adds a degree of approximation on top of the usual perturbative expansion calculation of the partonic cross-section. This sep-

[12]This inclusion of initial state divergences into non-perturbative, universal PDF functions based on QCD factorisation saves us as otherwise KLN would be inapplicable in experimental setups, requiring an initial state as a superposition of all possible degenerate states to be set up.

aration of energy scales itself has an ingrained additional unphysical scale, often termed the "factorisation scale", μ_F, which separates the two regimes. The exact numerical value of this scale choice is somewhat arbitrary, with its order of magnitude guided via other scales in the process; given its arbitrary nature we therefore do not expect any observables to be formally dependent upon it. More rigorously, what is being done is to separate the infrared divergent pieces associated with the long distance physics in the incoming states into PDFs of the incoming hadrons. This removal of the IR divergences comes with a scale (the factorisation scale), and in fact also a scheme choice in the exact same way renormalisation of UV divergences introduces a renormalisation scale and choice. This absorbs the IR divergences associated with the initial state, and so our transverse momentum resummation formalism is left to deal with the remnant initial state soft and collinear enhancements associated with the QCD splittings and additional propagators in virtual corrections[13].

The factorisation scale is only one of three scales introduced in our formulae for the differential spectra determined in the `reSolve` program, with the other two being the "renormalisation scale", μ_R, associated with the removal of UV divergences, and the resummation scale, μ_S, associated with the arbitrariness in our definitions of the logarithms in our b-space resummation formalism or equivalently with the arbitrary division of low and high transverse momentum scales in our resummation formalism. All these scales are artefacts remaining from our theoretical treatment and must drop out of any observable quantities if it were possible to evaluate them to all orders in perturbation theory. In fact, by requiring that any observable quantities are independent of these scales (when summed to all orders) we can absorb divergences into running parameters by writing down Callan-Symanzik style equations, again in an analogous manner to the alternative derivation of the gauge coupling running in Chapter 1.1.4. We take an aside here to outline the first two of these scales, leaving the resummation scale to our discussion in Chapter 6.2.1.

First consider the renormalisation scale arising from the cancellation of UV divergences. Here the additional scale originates from the renormalisation process in the subtraction of infinities via the counter-terms, with the exact scale at which this subtraction is performed translating into a scale dependence for the renormalised quantity. The relevant quantity at some arbitrary scale is related to its value at the renormalisation scale via a renormalisation group equation β function; which, as a solution to the associated differential equations, resums any potential logarithms of the scales considered. For the UV case we absorb the renormalisation scale into the running coupling, $\alpha_s(\mu_R)$, and obtain the renormalisation group equations defining this running given by the β functions.

Next we describe the factorisation scale in more detail; as outlined previously, this arises as a result of IR divergences and leads the PDFs to obtain a factorisation scale dependence. This is where the parton model breaks down, failing to account for initial state radiation giving the "partons" transverse momentum and corresponding collinear divergences, it is replaced by the

[13]Our formalism applies exclusively to final states consisting of non-QCD interacting particles and so there are no final state QCD divergences to deal with.

"QCD Improved Parton Model" with parton splittings and divergences taken into account [203]. For example, following the argument in [210] we may consider the cross-section for a $q\bar{q} \to Zg$ Drell-Yan process with an additional gluon radiation. The squared matrix element then contains a divergence when the gluon emitted becomes collinear to the incoming parton, i.e. as the transverse momentum k_T of the gluon tends to 0

$$|M|^2 \sim \frac{1}{k_T^2} + \mathcal{O}(k_T^0). \tag{5.58}$$

Consequently, the total cross-section will become infinite in the absence of either cut-offs to the integration or regularisation, whilst the transverse momentum spectrum loses predictivity at small values of p_T due to the divergence. To recover the accuracy of the transverse momentum spectrum, we must subtract the divergence at a given scale, which will therefore once more introduce a scale into the problem, this is the factorisation scale μ_F. Now, for the UV divergences and the renormalisation scale, we were able to write down differential equations linking the divergences to the coupling constant via 1-loop diagrams, and so absorb the reference scale at which the subtraction was done into a running of the coupling via the RGEs. We now seek the equivalent absorption of the reference scale for our IR case with the factorisation scale. The collinear divergences we have outlined depend only on the details of QCD and not on the process; specifically they depend on the probabilities of the partons splitting and radiating other partons, which then cause un-cancelled divergences in the collinear limit of the phase space. These are parametrised by the universal Altarelli-Parisi splitting functions $P_{i\leftarrow j}(x)$, which can be found in any QCD textbook and which we list here only at leading order [211]:

$$\begin{aligned} P_{g\leftarrow q}(x) &= C_F\left[\frac{1+(1-x)^2}{x}\right], \quad P_{q\leftarrow q}(x) = C_F\left[\frac{1+x^2}{(1-x)_+} + \frac{3}{2}\delta(1-x)\right], \\ P_{q\leftarrow g}(x) &= \frac{1}{2}\left[x^2+(1-x)^2\right], \quad P_{g\leftarrow g}(x) = 2C_A\left[\frac{x}{[1-x]_+} + \frac{1-x}{x} + x(1-x)\right] + \frac{\beta_0}{2}\delta(1-x). \end{aligned} \tag{5.59}$$

The precise details of these splitting functions are unimportant for now; for reference however here C_A, C_F are different values of the quadratic Casimir of the $SU(3)_c$ QCD group for the adjoint (gluon) and fundamental (quark) representations, and β_0 is the leading order beta function, these are given later in Appendix B.1, whilst x is the momentum fraction of the partons. Meanwhile, the "plus" prescription $[\dots]_+$ removes divergences in the terms at $x = 1$:

$$\int_0^1 \frac{f(z)}{[1-z]_+}dz = \int_0^1 \frac{f(z)-f(1)}{1-z}dz. \tag{5.60}$$

We may then schematically write equation 5.61, assuming only one allowed splitting (the case with multiple splittings linking differential equations is more complicated but does not alter the physics of the divergences we discuss here). This will lead to the advertised logarithmic divergence via ratios of scales upon integration of the gluon transverse momentum as in equation 5.62:

$$d\sigma \sim \frac{\alpha_s}{\pi}\frac{dk_T^2}{k_T^2}dxP_{i\leftarrow j}, \tag{5.61}$$

$$\sigma \sim \sum_j \frac{\alpha_s}{\pi}\log\Big(\frac{Q^2}{\lambda^2}\Big)P_{i\leftarrow j}, \tag{5.62}$$

where Q^2 is a physical scale, such as that of the hard scattering, whilst λ is an IR cut-off to regulate the collinear divergence which occurs as $k_T \to 0$.

Now we seek to absorb these divergences into the parton densities by solving the (coupled) differential equations. This will therefore violate the typical "Bjorken scaling" energy independence of PDFs which arises at leading order, producing scaling violations whereby the parton densities now vary with energy scale; we therefore follow the same procedure as absorbing the UV divergences into the gauge coupling running by requiring independence of the IR cut-off λ. We take our bare PDFs $f(x)$ which are those from the parton model and observe Bjorken scaling and absorb the collinear divergences from the parton splittings into them at a given factorisation scale μ_F. As a result the new renormalised PDFs obtain a factorisation scale dependence due to this subtraction point, the new renormalised PDFs are derived in [17] and can be shown at next-to-leading order to be:

$$f(x,\mu_F^2) = f(x) + \frac{\alpha_s}{\pi}\int_x^1 \frac{dy}{y}f(y)\Big[P(x/y)\log\Big(\frac{\mu_F^2}{\lambda^2}\Big) + C(x/y)\Big]. \tag{5.63}$$

$P(x/y)$ are the QCD splitting functions given previously in equation 5.59 and parametrise how QCD interactions can cause one parton to transform into another (thereby "mixing" the PDFs beyond leading order), where y is the momentum fraction of the initial parton before splitting to give momentum fraction x. Meanwhile, $C(x/y)$ is a finite term added which incorporates how the separation of scales between the low scale non-perturbative hadronic behaviour and the high scale partonic collision is achieved. However, again this has the parton distribution functions dependent on a non-perturbative scale λ - we wish to remove this dependence on the scale and solve the differential equations in order to derive RGEs for the PDFs. Evaluating equation 5.63 at $\mu_F = \lambda$ reveals the bare PDFs are just those evaluated at the non-perturbative scale λ as expected; $f(x,\lambda^2) = f(x)$. Therefore if we require the overall renormalised PDFs $f(x,\mu_F^2)$ are independent of this IR cut-off then we obtain[14]

$$\frac{\partial}{\partial\log\lambda^2}[f(x,\mu_F^2)] = \frac{\partial f(x,\lambda^2)}{\partial\log\lambda^2} - \frac{\alpha_s}{\pi}\int_x^1\frac{dy}{y}f(y,\lambda^2)P(x/y) = 0 \tag{5.64}$$

Rewriting this and writing λ as μ so as to give the PDFs the usual dependence on the energy scale μ at which they are evaluated implies that

$$\frac{\partial f(x,\mu^2)}{\partial\log\mu^2} = \frac{\alpha_s}{\pi}\int_x^1\frac{dy}{y}f(y,\mu^2)P(x/y) \tag{5.65}$$

[14]Here we have neglected the term of $\mathcal{O}(\alpha_s^2)$ arising from the partial derivative acting directly on the $f(y,\lambda^2)$ inside the integral, this is order α_s^2 as the other term tells us $\frac{\partial f(x,\lambda^2)}{\partial\log\lambda^2} \sim \alpha_s$ and there is also the α_s prefactor.

This process thereby absorbs the collinear divergences with λ into a scale dependence of the PDFs. This expression is the general form of the Dokshitzer-Gribov-Lipatov-Altarelli-Parisi (DGLAP) equations [211–214], which in actuality are a set of coupled integro-differential equations due to the nuances of quarks and gluons each splitting into each other. Again we encourage the reader to refer to [17] or [210] for further details. These DGLAP equations are the analogues of the RGEs of the coupling constants, and allow the PDFs to be run between different scales (in the process resumming logarithms of ratios of these scales) once the PDFs have been experimentally extracted at one scale. Different PDF extraction techniques exist, assuming different functional forms, scales, schemes, techniques and methodologies for the $f(x, \lambda^2)$; examples are the MMHT [215], NNPDF [216] and CTEQ [217] extracted PDF sets.

We have seen how these renormalisation and factorisation scales arise out of considerations of divergences in perturbation theory; we have to evaluate the PDFs at a certain factorisation scale and the gauge coupling at a certain renormalisation scale but we expect the effects of these choices to drop out of the overall all-order, formal predictions. Therefore logarithms of these scales will appear in different contributions and at different orders (as we observed) but their effects should cancel out across the summation across all possible contributions and all-orders to make the overall sum renormalisation scale, factorisation scale (and resummation scale) independent. Computing cross-sections and other observables to all orders is however not possible practically; many of the most precise determinations are known only up to NNLO. There are therefore missing higher order corrections and consequently the cancellation of the scale dependence is spoiled, leaving residual scale dependence in the predictions. As we include higher order contributions we expect more of the scale dependences to cancel out, as is verified in all processes currently known for phenomenological applications. This scale dependence therefore introduces a frustrating and somewhat intractable theoretical error which can only be indisputably reduced by incorporating higher orders. There are clearly bad scale choices, scales far from the physical scales of the problem considered will result in large logarithms and so larger higher order corrections would then be expected in such perturbative series; however provided the order of the physical scales is chosen, the size of the logarithms is minimised and little more can be said for the exact value. Nonetheless, as the choices of scales are arbitrary and anthropogenic, we can attempt to exploit our freedom to minimise the dependences on these scales and there are varying approaches about how best to do this [218], which we shall not elucidate here. Furthermore, the scale dependence of predictions may be exploited, with its general reduction order by order indicating the relevant perturbative series are indeed converging. The scale variation may therefore be utilised to estimate the magnitude of the effects of higher order corrections.

5.6 Transverse Momentum Resummation

Large logarithmic terms, such as those observed in the previous section, in general appear in individual contributions in multi-scale physics problems in quantum field theory. For our particular applications we are considering soft and collinear divergences arising in transverse momentum spectra at low q_T[15] and their resummation. First we begin by identifying the intricacies associated with this specific application. Given we revealed the KLN theorem states that soft and collinear logarithmic divergences arising individually in real emission and virtual contributions should cancel in observables when summed over all possible initial and final states, the question quickly arises as to why resummation is necessary for certain differential spectra and other measurements. The resolution is that whilst logarithmic divergences cancel upon integration, they leave logarithmic enhancements in some cases where there may be restrictions on one or more of the phase space integrals which therefore prevents complete cancellation of these logarithms. Viewed alternatively it can be said our observable is not sufficiently inclusive to ensure the complete cancellation, rather the transverse momentum spectrum is a semi-inclusive variable (other examples include shape variables such as the so-called "thrust" of a jet). For the specific case of transverse momentum spectra, whilst it is clear that the integration is performed over the entirety of the phase space for the loop integration in virtual corrections, for real emissions it is less clear. In fact the requirement of conservation of transverse momentum ensures we must incorporate a factor of $\delta^2(\mathbf{q}_T + \mathbf{k}_{T1} + \mathbf{k}_{T2} + \dots)$ into the integrand; this restricts the phase space available for the real emissions, leaving the cancellation of logarithms between real emissions and virtual corrections incomplete. As a result, at each n^{th} order in the perturbative expansion a term known as a "Sudakov double logarithm" [219] appears (as well as sub-leading terms), with one power of the logarithm of square scales from each of the soft and collinear divergences remaining for each power of α_s:

$$\alpha_s^n \log^{2n}\left(\frac{Q^2}{q_T^2}\right). \tag{5.66}$$

Here Q is a hard scale in the problem. Whilst such terms are small for $q_T \sim Q$, ensuring in this large q_T regime the usual perturbative expansion in α_s is justified, once $q_T \ll Q$ the logarithms become large and the perturbative expansion breaks down completely. Therefore these terms must be resummed and factored out of the α_s expansion. In fact, given $\alpha_s(m_Z) = 0.1185$, this occurs once $q_T \sim Q/5$.

Indeed, as an aside in this discussion, the transverse momentum conservation condition increases the complexity further, as it prevents the factorisation of each additional emission piece into a separate factor in the way we saw in our toy calculation in equations 5.38 and 5.39 (and is detailed in [197]) as transverse momentum conservation links emitted states, the kinematics therefore do not factorise in momentum space. This is a problem for the resummation

[15] From this section onwards we refer to transverse momentum (or strictly its magnitude) as q_T rather than p_T as this is the standard in the theoretical formalism we apply.

in the form we saw previously as this factorisation of kinematics was key to how the resummation worked. Fortunately however this factorisation can be recovered by Fourier transforming from transverse momentum $\mathbf{q}_T$ space into impact parameter $\mathbf{b}$ space:

$$\int d^2\mathbf{q}_T \exp(-i\mathbf{b}.\mathbf{q}_T)\delta(\mathbf{q}_T - \sum_i \mathbf{q}_{iT}) = \prod_i \exp(-i\mathbf{b}.\mathbf{q}_{iT}). \tag{5.67}$$

So each additional emission produces an identical separate factor in impact parameter space and we can proceed as before but with the factorisation, and subsequently the resummation (see Chapter 6), now in b-space. The large logarithms at small q_T, $\log(Q^2/q_T^2)$, become large logarithms at large b, $\log(Q^2b^2)$.

Returning to our main discussion, schematically we can understand why the vestiges of the soft and collinear divergences remain in our transverse momentum spectra as follows, this outline follows a more detailed exposition presented in [220, 221] and elsewhere. First we begin considering a general differential distribution $d(X)$ and its cumulative distribution $D(X)$ of some variable of interest X:

$$d(X) = \frac{d\sigma}{dX}, \qquad D(X) = \int_{X_0}^{X} dX' \frac{d\sigma}{dX'} \tag{5.68}$$

For our application $X = p_T$ and the starting point of the integral is $X_0 = 0$; this lower bound is where the singularities arise and also is the Born value. For an observable to be "infrared safe", i.e. to have no remnant singularities, we require it to be unaffected by soft and collinear emission of gluons. We may write our differential distribution $d(X)$ as an integral over the other phase space variables Ω defining the state, with $g(\Omega)$ defining the variable X in terms of the other phase space variables:

$$\frac{d\sigma}{dX} = \int_\Omega \frac{d\sigma}{d\Omega}\delta(X - g(\Omega))d\Omega. \tag{5.69}$$

For IR safety one requires $g(\Omega) \to 0$ for soft and collinear emissions, as if $g(\Omega) \nrightarrow 0$ then it places additional constraints on the form of X in this region in terms of the other phase space variables, thereby constraining the phase space and preventing the complete cancellation of the divergences. Consider the case of real emission of a single gluon, we may write the distribution of our variable X as an integral over the energy and emission angle of the gluon, each normalised, via the variables $\omega = E/E_{\max}$ and $t = 0.5(1 - \cos\theta)$:

$$D_R(X) = \int_0^1 d\omega \int_0^1 dt |\overline{M}|^2(\omega, t)\delta(X - g(w, t)). \tag{5.70}$$

Here $|\overline{M}|^2$ has been integrated over the other phase space variables, such as the azimuthal angle of the gluon emission, and includes summing and averaging over final state and initial states degrees of freedom (colour, helicity). This makes it somewhat clearer that our conditions for IR safety are:

$$g(\omega, t = 0) = 0, \text{ for collinear safety,} \qquad g(\omega = 0, t) = 0, \text{ for soft safety.} \tag{5.71}$$

We can understand this further by expanding our squared matrix element in terms of soft and collinear poles:

$$|\overline{M}|^2(\omega,t) \equiv \frac{\Upsilon(\omega,t)}{\omega t} = \alpha_s \left[\frac{A_1}{\omega t} + \frac{S_1(t)}{\omega} + \frac{C_1(\omega)}{t} + F_1(\omega,t) \right]. \tag{5.72}$$

A_1 then is the coefficient for the part of the square matrix element with soft and collinear singularities and is given by $\Upsilon(0,0)$, $S_1(t)$ is the coefficient for the soft singularity only part and is given by $\frac{\Upsilon(0,t)-\Upsilon(0,0)}{t}$, $C_1(\omega)$ is the coefficient of the collinear singularity only part and is given by $\frac{\Upsilon(\omega,0)-\Upsilon(0,0)}{\omega}$, and $F_1(\omega,t)$ is the finite part of the square amplitude and can be written as $\frac{\Upsilon(\omega,t)-\Upsilon(0,t)-\Upsilon(\omega,0)-\Upsilon(0,0)}{\omega t}$. Then all these coefficient functions are finite by definition as the singularities are factored out. If we integrate this purely real emission process near the borders of the phase space, the expected logarithms then arise in the cumulative distribution:

$$D_R(X) = 1 + \frac{\alpha_s}{\pi}\Big(\tilde{A}_1 \log^2 X + B_1 \log X + r(X) \Big), \tag{5.73}$$

The $\tilde{A}_1$ piece comes from the A_1 coefficient and this term is the leading Sudakov double logarithm piece, the B_1 comes from both the soft S_1 and collinear C_1 pieces separately and is the next-to-leading logarithm contribution, and $r(X)$ is a finite remainder piece of the distribution.

Of course, these logarithms should appear as we have only considered the real emission; if we consider also the virtual corrections, as KLN theorem tells us we must, we obtain the overall distribution

$$D(X) = D_R(X) + D_V(X). \tag{5.74}$$

Then we expect no large logarithms of X appearing near the border of the phase space. So we now add the virtual correction contribution to our integral to obtain equation 5.75; it has no $g(\omega,t)$ part in the second δ function with X as virtual corrections are independent of any radiated gluons:

$$D(X) = R(X) + \alpha_s \int_0^1 d\omega \int_0^1 dt \left[\frac{A_1}{\omega t} + \frac{S_1(t)}{\omega} + \frac{C_1(\omega)}{t} \right] \Big\{ \delta(X - g(\omega,t)) - \delta(X) \Big\}. \tag{5.75}$$

Then for this combined distribution we have IR safety, as from equations 5.71 we have the δ function subtraction piece is 0 where the soft and collinear singularities occur and hence the distribution has no singularities remaining. $R(X)$ is the remaining finite piece.

If however, our setup is such that we constrain the real or virtual pieces, then the conditions in equations 5.71 no longer hold and logarithmically divergent pieces remain as in equation 5.73 as the δ function bracket in equation 5.75 is not zero throughout the integration region. In reality it is the real emissions that are the ones which can be constrained via the $g(\omega,t)$ functions in cases where they do not satisfy equations 5.71.

This is the case for transverse momentum spectra, as transverse momentum conservation restricts the transverse momenta of emitted gluons. The low transverse momentum $q_T \to 0$ region of phase space corresponds to both the soft $q \to 0$ and collinear $\cos\theta \to 1$ regimes and so we retain the double logarithms of the Sudakov form as logarithmic enhancements at each order in the perturbative expansion. We must therefore re-sum these to all orders, as we demonstrated earlier in the chapter in equation 5.57, to recover the predictivity of the perturbative expansion.

In general, when large logarithms remain, the perturbative expansion in the differential cross-section $d\sigma$ will be of the form

$$d\sigma = 1+\alpha_s(L^2+L+1)+\alpha_s^2(L^4+L^3+L^2+L+1)+\alpha_s^3(L^6+L^5+L^4+L^3+L^2+L+1)+\ldots, \quad (5.76)$$

where here we have illustrated the case where double logarithms arise as both soft and collinear logarithms of the scales are present and L are the large logs. In the case of the transverse momentum spectrum $\frac{d\sigma}{dq_T^2}$ we have $L = \log\left(\frac{Q^2}{q_T^2}\right)$ where Q is some high physical scale in the problem. This expansion in α_s may be resummed in an analogous manner to demonstrated previously, but with greater complications (more details of the resummation for our transverse momentum application are given in Chapter 6), to produce an expression of the form:

$$d\sigma = C(\alpha_s)\Sigma(\alpha_s)+R(\alpha_s) = C(\alpha_s)\exp\left[Lg_1(\alpha_s L)+g_2(\alpha_s L)+\alpha_s g_3(\alpha_s L)+\ldots\right]+R(\alpha_s). \quad (5.77)$$

The $C(\alpha_s)$ represents the factorised coefficient function for the hard process and pre-multiplies the resummed contribution, it is a process dependent perturbative expansion in α_s. The $R(\alpha_s)$ is the remainder function, which is also a process dependent expansion in α_s accounting for hard contributions without logarithmic enhancement; it tends to zero in the resummed region but is the dominant contribution in the region where the logs are small, i.e. large q_T for our application. Finally the function $\Sigma(\alpha_s)$ is a universal process-independent function as it depends only on the structure of QCD corrections. It is an exponential and contains the resummed contributions; each of the pieces g_n contain all orders in $\alpha_s L$ resummed but each is suppressed by a power of α_s relative to g_{n-1}. Consequently the exponential is now also a perturbative series in α_s rather than $\alpha_s L$ and we recover predictivity of the perturbative expansion. The first term g_1 therefore offers the largest contributions, and including it incorporates "Leading Logarithms" (LL) in the resummation, i.e. those of the form $\alpha_s^n L^{2n}$ from equation 5.76; the second term g_2 resums "Next-to-Leading Logarithms" (NLL), i.e. those of the form $\alpha_s^n L^{2n-1}$ from equation 5.76; the third term g_3 resums "Next-to-Next-to Leading Logarithms" (NNLL), i.e. those of the form $\alpha_s^n L^{2n-2}$ from equation 5.76; and so on. For our applications we stop at NNLL, which represents the highest precision currently calculated in most processes. The g_i functions will be given later in equations B.1, B.2 and B.3 in Appendix B.1.

There is in fact a subtlety here: whilst if you expand at fixed order and integrate unresolved radiation you obtain the double logarithms and powers $\alpha_s^n L^m$ for $0 \leq m \leq 2n$ in the expansion as in equation 5.76, when you exponentiate and resum, the g_n contain reduced powers of the

logarithms relative to the α_s as any powers $n+2 \leq m \leq 2n$ vanish leaving $\alpha_s^n L^m$ only for $0 \leq m \leq n+1$, so that the g_1 is of order $\alpha_s^n L^{n+1}$, g_2 of order $\alpha_s^n L^n$ and so on as given in equation 5.77[16]. This is detailed further in [222] and originally in [223]. Each additional set of sub-leading logarithms included in the resummation must also be accompanied by an increase in the precision in the finite pieces in order to increase the precision of the prediction; in fact these must be matched to ensure there is no double counting and no inclusion of resummed effects in regions of parameter space where they may cause unphysical contributions. This is discussed briefly in Chapter 5.7. The first term $C(\alpha_s)\Sigma(\alpha_s)$ of equation 5.77 in the formalism we apply in `reSolve`, is called the "resummed part", whilst $R(\alpha_s)$ is called the "finite part". Finally, in order to give an intuitive picture, we mention in passing now that the appearance of an exponential in resummed formulae can be intuitively appreciated by considering the fact it sums an infinite series of Poisson statistics governed emissions, the Sudakov factor then represents a no emission probability.

This section, and the chapter up to this point, has been focused on providing a background for the need for transverse momentum resummation and how it may be performed. Further information is available in a variety of sources including the TASI lectures [204] and the review [224], as well as the original papers which provided the foundations of this work, listed in Chapter 6. The background thus far provided will be built upon and crystallised in Chapter 6, first however we consider the transverse momentum spectrum as a whole.

[16]This apparent difference in orders in the expansion of $d\sigma$ and the exponential is due to the perturbative dynamics and kinematics factorisation. It can be seen that the exponential is able to reproduce all the leading logarithm $\alpha_s^n L^{2n}$ terms by expanding with the functional form of g_1 given later in Appendix B.1 equation B.1, we can set $g_i = 0$ for $i > 1$ as we only need to show it can produce the highest powers of the logarithm. Consider: $\exp[L[1+\log(1-\alpha_s L)/\alpha_s L]]$ which is of the form of $\exp(g_1 L)$, expand first the logarithm in powers of $\alpha_s L$ and then the exponential: $\exp[L+(-\alpha_s L-(\alpha_s L)^2/2-(\alpha_s L)^3/3-\dots)/\alpha_s] = \exp(L-L-\alpha_s L^2/2-\alpha_s^2 L^3/3-\dots) = \exp(-\alpha_s L^2/2-\alpha_s^2 L^3/3-\dots) = (1-\alpha_s L^2/2-(\alpha_s L^2/2)^2/2-(\alpha_s L^2/2)^3/6-\dots)\times(1-\alpha_s^2 L^3/3-(\alpha_s^2 L^3/3)^2/2-\dots) = 1-\alpha_s L^2/2-\alpha_s^2 L^3/3-\alpha_s^2 L^4/8-\alpha_s^3 L^5/6-\alpha_s^3 L^6/48-\dots)$, so the first exponential expansion produces the leading logarithm terms $\alpha_s^n L^{2n}$ as required.

5.7 Transverse Momentum Spectra

The primary aim of our work is the precise prediction of transverse momentum spectra for processes including unresolved radiation. As detailed, this calculation is greatly complicated by the remaining soft and collinear logarithmic enhancements at small q_T requiring resummation. As a result we need to consider the low $q_T \ll Q$ and high $q_T \sim Q$ regions separately, where Q is some natural mass scale in the hard collision, such as the mass of the particle produced or invariant mass of the system of particles. As a result, it is common to decompose the differential q_T spectrum for the partonic cross-section into two regions to make their different behaviour explicit:

$$\frac{d\hat{\sigma}}{dq_T^2} = \frac{d\hat{\sigma}^{\text{res}}}{dq_T^2} + \frac{d\hat{\sigma}^{\text{fin}}}{dq_T^2}. \tag{5.78}$$

Here the "res" part is the resummed contribution dominant at low q_T and is where the majority of the events are produced as the probability of emitting a soft or collinear gluon increases dramatically as the strength of the α_s coupling increases at low energy; this part can be determined to a given logarithmic accuracy in the resummed expansion in α_s. The "fin" part is the usual hard scattering finite contribution, evaluated via truncating the perturbative series in α_s in the standard way at some order, and is dominant at large q_T. Both components are needed to accurately describe the spectrum over the whole region of q_T and their division is arbitrary from a physics perspective, made purely to simplify the theoretical calculation. In order to produce a theoretical prediction at given accuracy, we may truncate each piece at consistent accuracy[17]:

$$\left[\frac{d\hat{\sigma}}{dq_T^2}\right]_{\text{f.o.}} = \left[\frac{d\hat{\sigma}^{\text{res}}}{dq_T^2}\right]_{\text{l.a.}} + \left[\frac{d\hat{\sigma}^{\text{fin}}}{dq_T^2}\right]_{\text{f.o.}}, \tag{5.79}$$

where "f.o." indicates truncation at a fixed order in the usual perturbative expansion, whilst "l.a." indicates truncation of the resummed perturbative expansion at given logarithmic accuracy - i.e. leading logarithm (LL), next-to-leading logarithm (NLL), and higher orders. In fact, we define the fixed order truncation of the finite part of the differential transverse momentum spectrum as the subtraction of the resummed part at fixed order from the overall spectrum, with the resummed part at fixed order being defined as the fixed order truncation of the logarithmic accuracy truncated expansion:

$$\left[\frac{d\hat{\sigma}^{\text{fin}}}{dq_T^2}\right]_{\text{f.o.}} = \left[\frac{d\hat{\sigma}}{dq_T^2}\right]_{\text{f.o.}} - \left[\left[\frac{d\hat{\sigma}^{\text{res}}}{dq_T^2}\right]_{\text{l.a.}}\right]_{\text{f.o}}. \tag{5.80}$$

Any pieces divergent at small q_T are therefore incorporated into the resummed part and so the finite part makes no contribution in the limit $q_T \to 0$; in fact this is imposed order-by-order in perturbation theory. This IR subtraction therefore defines what is meant by the

[17] The notation $\left[d\hat{\sigma}/dq_T^2\right]$ means we truncate the perturbative series for $d\hat{\sigma}/dq_T^2$ at a given order in α_s and any subscripts - "l.a." or "f.o." define how this truncation is done, i.e. to given logarithmic accuracy or given fixed order accuracy.

finite piece. Meanwhile, the finite piece should contain all the contributions at large q_T and so any contributions in this large q_T limit for the resummed piece are unphysical and must be suppressed. In order to achieve this our formalism, which is described in much further detail in Chapter 6 and in [222], imposes a unitarity constraint to constrain the integral over q_T of the resummed part of the differential transverse momentum spectrum at a given logarithmic accuracy to be equal to the corresponding integral truncated at given fixed order:

$$\int_0^\infty dq_T^2 \Big[\frac{d\hat{\sigma}^{\text{res}}}{dq_T^2}\Big]_{\text{l.a.}} = \int_0^\infty dq_T^2 \Big[\frac{d\hat{\sigma}^{\text{res}}}{dq_T^2}\Big]_{\text{f.o.}}. \tag{5.81}$$

This ensures that the integral over the finite and resummed pieces truncated together correctly gives the overall total cross-section evaluated at the same order via standard truncation as indicated in equation 5.82, and particularly constrains the unphysical contributions of the q_T resummed pieces at intermediate q_T;

$$\int_0^\infty dq_T^2 \Big[\frac{d\hat{\sigma}}{dq_T^2}\Big]_{\text{f.o.}} = \int_0^\infty dq_T^2 \Big[\frac{d\hat{\sigma}^{\text{res}}}{dq_T^2}\Big]_{\text{l.a.}} + \int_0^\infty dq_T^2 \Big[\frac{d\hat{\sigma}^{\text{fin}}}{dq_T}\Big]_{\text{f.o.}} = [\hat{\sigma}^{tot}]_{\text{f.o}}. \tag{5.82}$$

This means of putting together the contributions important at either end of the q_T spectrum in a consistent manner is known as "matching". The method described is just one of many that can be used and has the benefit of not having an arbitrary switch-over point between the two regimes, instead interpolating between the two smoothly. Specifically the method described is an "additive matching", which is in some sense more natural - there are also "multiplicative matching" methods which are less well motivated but provide greater numerical stability [225, 226]. In any case, our `reSolve` program in its current, early implementations only determines the resummed part of the spectrum, and so is only relevant at the low q_T end, which nonetheless is where the majority of the total cross-section is produced. From here on we will therefore drop any mention of the finite piece of the differential cross-section, focusing our efforts on the arguably more difficult part of the calculation, and typically the part with the larger contributions, the low q_T resummed part. The need for resummation in this low q_T region can clearly be seen in Figure 5.3, where the leading order contribution without resummation diverges as expected as $q_T \to 0$ whilst the resummation effects cause a Sudakov suppression (essentially by a no-emission probability) at this low transverse momentum end, removing this unphysical divergence.

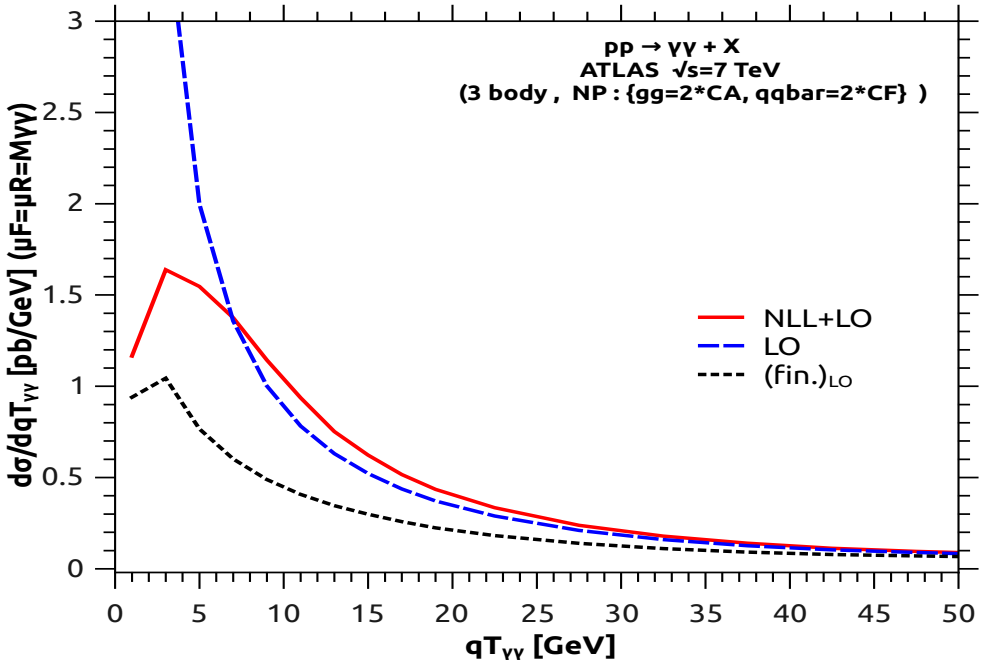

Figure 5.3: The leading order differential transverse momentum spectrum for diphoton production at ATLAS, with the total leading order, finite part leading order, and total leading order + NLL resummation spectra shown. The effects of resummation are clear, removing the unphysical divergence in the theoretical predictions as $q_T \to 0$ seen in the total leading order spectrum. This figure is from the paper [5].

Chapter 6

reSolve Overview

In this chapter we move on to our specific area of research, providing context for different approaches to transverse momentum (q_T) resummation before elaborating on the details of the analytic b-space resummation formalism we apply and its implementation within the `reSolve` program. The diphoton and Drell-Yan production channels included in the current version of `reSolve` are then introduced and a brief catalogue of the advantages of our `reSolve` program implementation of the q_T resummation formalism ends the chapter. Details of the use, validation and results of the `reSolve` program are omitted at this stage, with this left to Chapter 7. The research described in this chapter and the next is based upon that reported in our paper [2].

6.1 Approaches to q_T resummation

As described in Chapter 5, whilst the transverse momentum spectrum for an arbitrary process at colliders is in principle completely derivable in perturbative QCD, at small q_T logarithmic enhancements ruin the perturbativity of the series expansion in the strong coupling α_s, offering large corrections which must first be resummed to all orders before the perturbative expansion can be re-established. This fact has been known for a long time, since at least the 1970s, and several different methods to resum these troubling logarithmic contributions have been developed. In general these can be classified into two distinct types, numerical and analytic resummations. We begin outlining the possibilities available in numerical resummations, before moving onto the analytic resummations of which the formalism in `reSolve` is an example.

Numerical resummations are performed by parton shower programs - these aim to fully exclusively describe the soft and collinear radiation produced in a hard scattering event, rather than simply integrate over it in the way analytic resummations do. They exploit the factorisable and universal nature of QCD splittings in a semi-classical approximation, determining particle splitting probabilities via the Sudakov no-emission probability factors. The basic process of this is to start with the momentum of a hard scattered particle and then randomly choose momenta of emissions, with probabilities guided by the splitting functions, in a Markov Chain Monte Carlo process. Each successive branching particle has the process repeated iteratively until a whole shower of particles, the "parton shower" is produced, with the branching only stopping once a numerical cut-off (usually 1 GeV) of order Λ_{QCD} is reached when hadronisation effects take over. The result is a cascade down in virtuality ($Q^2 = p^2 - m^2$) and momentum fraction space. A full description of the algorithmic procedure adopted for parton shower programs is

presented in [17].

Many of these parton shower programs are incorporated into larger "event generator" programs, which simulate the whole hard scattering process from the hard collision matrix element generation through the showering of each outgoing hard particle and finally to the hadronisation. Well-known examples of such programs include `PYTHIA` [136], `Herwig++` [137, 138] and `Sherpa` [140]. Meanwhile programs like `MC@NLO` [141, 227] and `POWHEG(-BOX)` [228, 229] aim to merge parton showers with NLO QCD corrections from matrix generators using these programs. For further details of the programs' individual capabilities we refer the user to their copious manuals. This start-to-end process involves an array of complications; foremost among them is the "matching" and "merging" of the hard events onto the parton showers. This is done in order to avoid possible double counting as well as dead kinematical regions not populated by events and radiation; this is extensively reviewed in the literature and so we do not describe it here [227, 230–232]. An advantage of such numerical resummations is that they allow the production of explicit "events" with all final state particles exclusively known. This matches the actual events observed at colliders more naturally than the semi-inclusive states needed for analytical resummations, with the large multiplicities of produced events simply intractable for analytic analysis. They also offer the possibility to describe the whole process from hard scatter through to hadronisation including multiple particle interactions and interactions with beam remnants through the overall event generator package. They do however have significant disadvantages relative to analytical resummations; primary amongst these is that they are largely leading order (although this has been extended to NLO via `POWHEG(-BOX)` and `MC@NLO` with the latter using `Herwig`, whilst `MINLO` [233] and `GENEVA` [234] are extending even to NNLO for some simpler processes) meaning leading logarithm resummation is all that is typically included. This occurs as the ability to match parton showers onto hard scatter matrix element generators beyond leading order is far less clear, and so they offer reduced precision relative to analytic resummations. This element is a crucial disadvantage in the context of LHC precision studies.

In any case, numerical resummations are tangential to our research, which has been in analytic resummations in the context of transverse momentum spectra. Before we proceed to the b-space resummation formalism we employ, we first mention that Soft-Collinear Effective field Theory (SCET) is an alternative analytic formalism for developing formulae for transverse momentum resummation. This has become more popular in recent years and is introduced in [235]. The basic idea is to use an effective field theory to separate the high scale (hard scattering process) and low scale (non-perturbative) behaviour. By expanding in the ratio of the scales, the high scale is integrated out and absorbed into the Wilson coefficients of the effective theory at the low scale. By using an effective Lagrangian, rather than perturbative QCD Feynman diagrammatic methods, it can offer a more simple means of maintaining gauge invariance and so may simplify computations otherwise involving cancellations between different diagrams, such as between real emissions and virtual contributions. SCET has been applied to many different resummation problems, including transverse momentum resummation; we refer the reader to references for its application to Drell-Yan [236, 237]. Nonetheless, it has

its disadvantages, connecting less easily with standard Feynman diagrammatic approaches of perturbative QCD (pQCD) expansions.

In our work we utilise the impact parameter b-space analytic transverse momentum resummation formalism which has been developed over a number of years, starting in the 1980s with the development of leading logarithmic resummations [238–240]. This was soon extended to beyond leading logarithm resummation in [241] and further developments summing soft emissions in b-space (typically in the context of $e^+e^- \to A + B + X$) followed [242–244]. The seminal work of the reference [223] then illustrated LL and NLL resummation in the context of Drell-Yan production and considered the connections between low and high transverse momentum regions, setting the foundations for the formalism. Other developments occurring alongside this work are detailed in [245, 246]. Following this early work, the baton was picked up by the group of Catani and collaborators in the work [247], who have led the modern developments in this area. More recently this has borne fruit with the development of NNLL resummation [8, 222, 248, 249] for processes such as Drell-Yan, diphoton and Higgs production. At this stage, the formulae for beyond leading logarithm resummations were written down independently for each process, with collinear factors which were process dependent, and it was simply hoped that this could be developed into a process independent structure. However, it was soon shown [250] that this is not the case and rather a single process dependent hard factor H^F is required to absorb this process dependence (see equation 6.28). This hard factor is purely virtual and so has the same kinematics as the Born, depending upon it in a straightforward manner. As a result, with this hard factor the resummation formalism is made universal, with process independent Sudakovs and collinear factors; this is summarised in the paper [251] and will become clear in our overview of this area later in the chapter. This universality will be key to our development of the `reSolve` program, allowing transverse momentum resummation to be added to any of a given class of processes in an independent manner. As the b-space formalism we apply has developed gradually, there is no over-arching reference - the closest to this are [222] [251], which we will follow for several elements of our description and explanation in Chapter 6.2. We hope our description provides the reader with sufficient clarity to understand this complex area.

We apply this formalism [223, 238–240, 242, 244, 247–249, 251] for transverse momentum resummation to the general class of processes producing colourless measured final states and arbitrary unresolved radiation, focusing our initial efforts on the important diphoton and Drell-Yan channels. `reSolve` nonetheless can be used to add transverse momentum resummation to any such process in principle. There are alternative programs available, including public codes such as `ResBos` [252, 253]. `ResBos` is able to perform transverse momentum resummation for Drell-Yan, diphoton and Higgs processes producing differential spectra in q_T as well as in invariant mass and rapidity; it is therefore similar to `reSolve` in this regard. However it is less modularised to allow adaptation to new processes in the way `reSolve` is and is not parallelisable in the same way. From a theoretical perspective there are also differences in the theoretical approach with the matching done more straightforwardly, switching from low q_T to high q_T at $q_T \sim Q$ rather than using our unitarity constraint of equation 5.81. There are also the largely

private programs of the `2gRes` [5, 6], `HRes` [254, 255], `DYRes` [7, 8] family, of which there is an initial `DYRes` version publicly available. These have acted as a guide in our work and enabled verification of our `reSolve` program, having themselves been used in several experimental works. We hope our work improves on these, being transparently documented, customisable and more straightforwardly implemented via a modularised structure designed to allow general applications, whilst also being completely publicly available. `reSolve` is a completely new program, completely rewritten and developed anew with several advantages over other codes available, whether public or private, which we elucidate throughout our exposition in this chapter and the next and which we summarise in Chapter 6.5. This ensures the `reSolve` program is unique in its area and we hope it will be of great use for future precision studies.

6.2 Theoretical Formalism

We consider hadron-hadron collisions producing only a colourless detected final state F (by which we mean F is made up only of purely colourless particles), accompanied by arbitrary unresolved radiation, X, of the following form, where Ω indicates further final state variables:

$$h(p_1) + h(p_2) \to F(Q^2, q_T^2, y, \Omega) + X. \tag{6.1}$$

Here $\sqrt{s} = (p_1 + p_2) \approx 2p_1.p_2$ is the centre of mass energy of the colliding hadrons and this is pre-multiplied by x_1 and x_2, the momentum fractions of the partons extracted from the PDFs, to obtain the centre of mass energy in the partonic collision $\hat{s} = x_1 x_2 s$. This therefore limits the class of processes for which this is applicable to ones with electroweak gauge bosons, Higgses and leptons in the final state; this nonetheless includes many production channels of great importance to LHC phenomenology, including Drell-Yan, diphoton and Higgs production. There is theoretical work being undertaken to extend this formalism to coloured states [256]; this is more difficult due to the fact the final state then carries colour charge and can interact with initial state radiation and provide additional soft and collinear radiation. The final state F may be made up of several particles, its invariant mass Q^2 is then (as given in equation 5.3) the square sum of the 4-momenta $\{q_1, q_2, \ldots, q_n\}$ of the particles in F, $Q^2 = (q_1 + q_2 + \ldots q_n)^2$. The invariant mass of the system F is not equal to the partonic centre of mass energy in general as the unresolved collinear emissions in X may carry away energy and momentum. The remaining variables to describe the final state system as a whole are its transverse momentum, $\mathbf{q}_T$ and rapidity, y. In addition, further variables Ω are required to fully define the final state configuration in the case it is made up of more than one particle, for example for diphoton production or Drell-Yan production the polar (θ^*) and azimuthal (ϕ^*) angles of one of the two particles in the centre of mass frame are required. Whilst our formalism is targeted at determining the small q_T part of the transverse momentum spectrum, it is fully differential in these final state variables and so may also determine the invariant mass, rapidity and other differential spectra in the same calculation. In general, for most of our purposes we consider the fully differential hadronic cross-section given in equation 6.2; however spectra in further

arbitrary variables such as transverse mass or minimum and maximum transverse momenta of individual components of the final state F may also be determined, and indeed are included in `reSolve`.

$$\frac{d\sigma_F}{d^2\mathbf{q}_T dQ^2 dy d\Omega}(p_1, p_2; \mathbf{q}_T, Q^2, y, \Omega). \tag{6.2}$$

As detailed in Chapter 5.7, we divide the differential cross-section into the resummed contribution important at small q_T and the finite contribution important for large q_T. The resummed contribution contains the logarithmic enhancements and all contributions finite in the $q_T \to 0$ limit and is the focus of our work and of the `reSolve` program. We neglect the remaining finite contribution from here onwards - nonetheless it must be calculated and matched appropriately to the resummed contribution we calculate to determine the q_T spectrum across the full range. This is not available in this first `reSolve` version.

We present a master formula for the whole calculation of the fully differential hadronic cross-section in Chapter 6.2.3; for now however we discuss the key aspects one by one. Coefficients involved in the formalism are gathered in Appendix B.1. We denote the partons extracted from the hadrons in the conventional manner as a and b, not to be confused in the latter case with the impact parameter b, this should however be clear from context. Ultimately, the partons colliding in the hard process are denoted c, $\bar{c}$ to reflect that they must be $q\bar{q}$ or gg - this is true as the final state system F is a made up of particles of no colour charge. These different initiating partons result in different Sudakov form factors (see equation 6.16) but aside from this the Sudakovs show no further, specific process dependence. We use the value of the strong gauge coupling α_s evaluated in the $\overline{MS}$ scheme at the renormalisation scale μ_R.

6.2.1 b-space

Our transverse momentum resummation formalism is crucially dependent upon factorisation of both dynamics and kinematics; therefore we perform a Fourier transform from transverse momentum space to its conjugate variable, impact parameter b-space, as explained in Chapter 5.6. We may then write our transverse momentum spectrum as follows:

$$\begin{aligned}\frac{d\sigma_F^{\text{res}}}{dQ^2 d^2\mathbf{q}_T dy d\Omega}(p_1, p_2, \mathbf{q}_T, Q^2, y, \Omega) &= \int \frac{d^2\mathbf{b}}{(2\pi)^2} \int_{x_1}^1 \frac{dz_1}{z_1} \int_{x_2}^1 \frac{dz_2}{z_2} e^{i\mathbf{b}.\mathbf{q}_T} \mathcal{W}^F(\mathbf{b}, z_1, z_2, Q^2, y, \Omega) \\ &= \int_{x_1}^1 \frac{dz_1}{z_1} \int_{x_2}^1 \frac{dz_2}{z_2} \int_0^\infty db \frac{b}{2\pi} J_0(bq_T) \mathcal{W}^F(b, z_1, z_2, Q^2, y, \Omega).\end{aligned} \tag{6.3}$$

Here z_1 and z_2 are the momentum fractions taken in the collinear splitting, leaving momentum fractions x_1 and x_2 on the colliding partons for the hard scattering, this is clarified by Figure 6.1 later. Note that there is no integral over the momentum fractions x_1 and x_2 of the partons extracted in the PDFs as this formula is fully differential[1]. Transforming into impact parameter

[1]Integrals over x_1 and x_2 arise for cross-sections integrated over invariant mass and rapidity as equation 5.31 illustrates.

space converts our q_T logarithms of the form $\log(Q^2/q_T^2)$ to $\log(Q^2b^2)$ and so low transverse momenta correspond to high impact parameters[2]. In the last step we have assumed that, as for $q\bar{q}$ initiated processes, there is no dependence on the azimuthal angle ϕ_b, where the 0^{th} order Bessel function J_0 is:

$$J_0(x) = \int_0^{2\pi} \frac{d\phi}{2\pi} e^{\pm ix\cos\phi_b}. \tag{6.4}$$

In fact, in the case of gg initiation there is ϕ_b dependence due to the helicities giving azimuthal correlations. In that case the integral is split into a ϕ_b independent piece involving $J_0(bq_T)$, and a ϕ_b dependent piece involving $J_2(bq_T)$ [257]. As a result of this replacement with the 0^{th} order Bessel function, we reduce the number of integrals to be performed from 4 to 3, i.e. over the absolute value of the impact parameter space and the two momentum fractions in collinear splitting z_1, z_2. These integrals are done via an inverse Fourier transform for the b integral, and via a double inverse Mellin transform for z_1 and z_2 (as detailed in the next section and in Appendix B.2). We therefore evaluate the function $\mathcal{W}^F$ in impact parameter space and must inverse Fourier transform back to transverse momentum space at the conclusion of the calculation, this itself offers complications for the numerical use of the formalism as the integrand is a rapidly oscillating function. This problem is overcome in `reSolve` by using a specially designed external integration package, `intde`, using the "double exponential" formula of [258].

The b logarithms however contain divergences: at low b the logarithms become divergent as $\log(Q^2b^2) \to -\infty$ as $b \to 0$, which corresponds to large values of the transverse momentum, where our formulae are not relevant in any case. Therefore we seek to simply cut off the contributions at low b, to do so we shift the argument of the logarithms by 1 so that $\log(Q^2b^2) \to \log(1+Q^2b^2)$, in this case at high b we recover the standard logarithm form as $Q^2b^2 \gg 1$, whilst at low b, $\log(1+Q^2b^2) \to 0$ cutting off these contributions and therefore leaving the finite piece only contributing to the differential cross-section at large q_T. This therefore has the added benefit of ensuring the unitarity constraints of equations 5.81 and 5.82 are implemented by removing the resummed contributions at large q_T where they would be unphysical.

Whilst discussing these logarithms, it is convenient to introduce the resummation scale, μ_S, the third of our three scales after the factorisation scale (present in the PDFs) and the renormalisation scale (present in α_s). As logarithms can always be shifted by a finite piece by rescaling their arguments, the division of logarithmic and finite pieces includes some arbitrariness. The resummation scale is therefore introduced to parametrise this flexibility and enable a quantitative measure of the corresponding theoretical error induced, this can be done through standard scale variation assessments. We therefore rescale the logarithms as follows and define our large logarithms $L = \log(\frac{\mu_S^2 b^2}{b_0^2})$; here $b_0 = 2e^{-\gamma_E}$ and $\gamma_E = 0.5772...$ is the Euler constant:

[2]The way to intuitively see this is to consider the two partons incoming with zero transverse momentum, for a final state with large transverse momentum the outgoing particles are deflected more from those of the incoming beams corresponding to a smaller impact parameter.

$$\log(Q^2b^2) = \log\left(\frac{\mu_S^2 b^2}{b_0^2}\right) + \log\left(\frac{Q^2 b_0^2}{\mu_S^2}\right) = L + \log\left(\frac{Q^2 b_0^2}{\mu_S^2}\right), \tag{6.5}$$

as a result, we have the overall b logarithm

$$b_{log} = \log\left[1 + \frac{\mu_S^2 b^2}{{b_0}^2}\right]. \tag{6.6}$$

The resummation, factorisation and renormalisation scales must all be set to the order of the hard scale in the problem Q as otherwise we reintroduce further large logarithms, these additional unnecessarily large logarithms would then appear at each order in the expansion and so reduce the accuracy of our theoretical prediction made by truncating the series at given order (in both logarithmic accuracy and finite order).

As well as singularities at low b, there are also those present at high b, corresponding to low q_T. These singularities thus arise in the region that our transverse momentum formalism is targeted at and cannot be simply cut off. The singularities arise due to the presence of the Landau pole in QCD; specifically singularities arise as $\lambda = (1/\pi)\beta_0\alpha_s(\mu_S^2)\log(\mu_S^2 b^2/b_0^2) \to 1$ [3], which corresponds to $b \to b_L = (b/\mu_S)\exp[\pi/(2\beta_0\alpha_s(\mu_R^2))] \sim 1/\Lambda_{QCD}$, here β_0 is the lowest order β function coefficient, given later in equation B.7. These divergences are a sign of non-perturbative effects becoming important in these regions corresponding to small $q_T \sim \Lambda_{QCD}$ and must not be ignored as they are of physical relevance and will limit the validity of our calculation. This kind of singularity is a common feature of all-order resummation formulae of soft gluon contributions and has to be regularised. In the current `reSolve` implementation, we follow the standard prescription of reference [259]. We freeze the integration over b below a fixed upper limit via the substitution

$$b \to b_\star = \frac{b}{\sqrt{1 + b^2/b_{\rm lim}^2}}, \tag{6.7}$$

$$b_{\rm lim} = \frac{b_0'}{\sqrt{Q^2}}\exp(1/(2\alpha_s\beta_0)), \qquad \text{and} \quad b_0' = 2\exp(-\gamma_E)\frac{\sqrt{Q^2}}{\mu_S}. \tag{6.8}$$

By replacing b with $b_\star$, at low b we have $b_\star \to b$ as required, whilst at very high b then $b_\star \to b_{\rm lim}$, cutting off the integration before the very high b singularities. We then reintroduce the phenomenological effects at low q_T via non-perturbative functions which smear out the low q_T region:

$$S_{\rm NP} = \exp(-g_{\rm NP}^c b^2), \tag{6.9}$$

these smearing functions pre-multiply the b-space integrand before the inverse Fourier transform is performed and the constants $g_{\rm NP}^c$ parametrise the phenomenological implications of the non-perturbative effects which we cannot calculate. Their values are expected to depend upon if

[3] These singularities arise in the $\bar{g}^{(i)}$ functions given in Appendix B.1 in equations B.1, B.2 and B.3, whilst λ is given in equation B.4.

the process is gg or $q\bar{q}$ initiated ($c = g, q$ respectively). The default values in `reSolve` are $0\,\text{GeV}^2$; nonetheless these can be altered in the `reSolve` input file, and provide an additional source of theoretical error. Generically one might expect $g^q_{\text{NP}} = C_F g_1$ and $g^g_{\text{NP}} = C_A g_2$, however many different values for these parameters are used in the literature. In the validation plots for `reSolve` throughout Chapter 7 we have used values $g^g_{\text{NP}} = 6$, $g^q_{\text{NP}} = \frac{8}{3}$; these are chosen so the quark initiated g^q_{NP} matches that used in the reference [5] (where $g_1 = 2\,\text{GeV}^2$ was seen to provide the best phenomenological match to diphoton data), the gluon-initiated g^g_{NP} was then set by taking arbitrarily that $g_1 = g_2$ which sets $g^g_{\text{NP}} = g^q_{\text{NP}} \times C_A/C_F = 9/4 \times g^q_{\text{NP}} = 6$. There are several other ranges of these g^c_{NP} parameters used and indeed different functional forms of the parametrisation in equation 6.9 in the literature, these are outlined in [8, 222, 260].

All of these complications, and more, are contained within the b-space, double momentum fraction space function $\mathcal{W}^F(b, z_1, z_2, Q^2, y, \Omega)$, whose structure we now examine across the next two sections.

6.2.2 Mellin space

The $\mathcal{W}^F(b, z_1, z_2, Q^2, y, \Omega)$ factor contains the standard "multiplicative" convolutions of the partonic cross-section with the PDFs, however with a great deal of further structure associated with the soft and collinear emissions. By transforming from double momentum fraction space (one integral per ingoing parton) to double Mellin space we convert these convolutions into simple products; this is outlined in Appendix B.2 and follows the work in [222,261]. The double Mellin transform is:

$$W^F_{N_1,N_2}(\mathbf{b}, \ldots) = \int_0^1 \mathrm{d}z_1 z_1^{N_1-1} \int_0^1 \mathrm{d}z_2 z_2^{N_2-1} W^F(\mathbf{b}\,, \ldots), \tag{6.10}$$

z_1, z_2 are the momentum fractions left after the collinear emissions of the ingoing partons. The precise form of the $W^F_{N_1,N_2}$ function is described in great detail in the next chapter.

After evaluating the $W^F_{N_1,N_2}(\mathbf{b}, \ldots)$ Mellin space functions, these must be transformed back to momentum fraction space before the inverse Fourier transform from b-space to q_T is undertaken. As described in Appendix B.2, the inverse of a Mellin transform is an integral over a complex contour in the Mellin space parallel to the imaginary axis (but shifted to avoid poles). In `reSolve` we instead integrate by summing contributions along a contour at 45° to the imaginary axis in the shape of a 'V' rotated anticlockwise; this enhances the convergence without affecting the result to the precision to which we calculate. This prescription is also used in the `2gRes` family of programs. Evaluating the $W^F_{N_1,N_2}(\mathbf{b}, \ldots)$ at each point along this contour adds a further obstacle to the implementation as it requires knowledge of the PDFs in Mellin space[4]. PDF collaborations provide grids of PDF values in momentum fraction space with interpolation between points via the DGLAP evolution equations and the PDFs' functional forms. We determine the PDFs along the contour by fitting the PDFs to an analytic form whose Mellin moments are known. This fit

[4] Any b dependence of the PDFs arises only from the α_s evolution, as the PDFs have no q_T dependence, and therefore is accounted for by the running of α_s.

is done "once and for all" at the start of the `reSolve` program and can be provided to the code by referencing it in the input file. To perform the fit we use the external `minuit` package [262] for minimisation. Further details are supplied in Chapter 7.1.4.

6.2.3 Master Formula

In order to definitively explain the formalism applied in `reSolve`, it is best to give an overall intuitive picture, therefore we start with such a schematic in Figure 6.1, providing also the overall associated "master formula" in equation 6.11. We then spend this section describing how this arises and how it performs the required exponentiation of the soft and collinear logarithms, we follow closely the reference [222] as well as our own `reSolve` paper [2]. We collect many of the basis function expressions involved in Appendix B.1, so as not to obscure the explanation here.

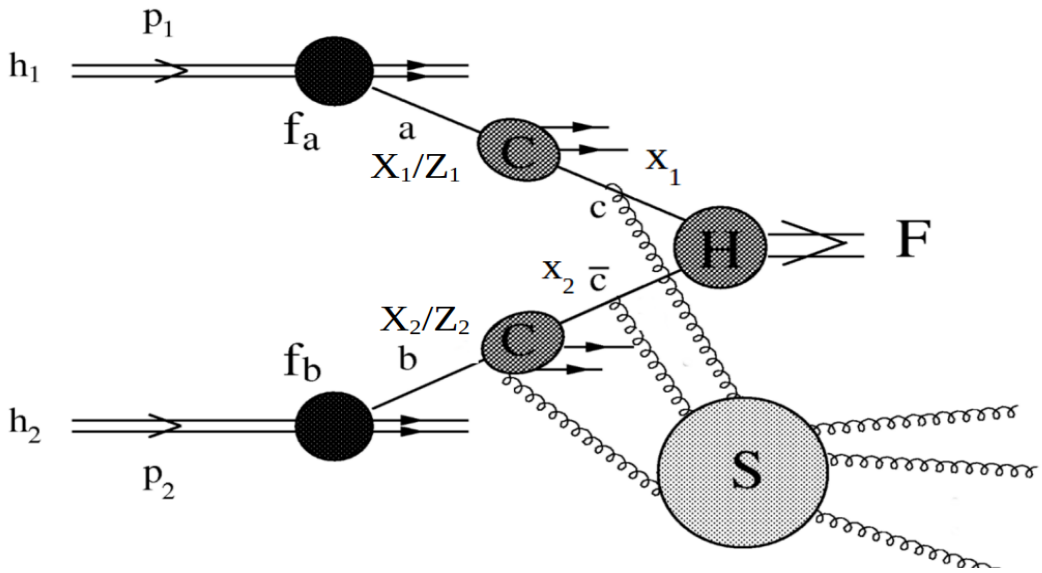

Figure 6.1: Pictorial version of equation 6.11. A parton a of momentum fraction x_1/z_1 is extracted from hadron h_1 in the upper leg with an associated PDF factor, it then splits further to leave momentum fraction x_1 via a collinear partonic sub-process $a \to c$. A specular process happens at the lower leg and so the momenta that enter the hard process H are $x_1 p_1$ and $x_2 p_2$, where $p_{1,2}$ are the momenta of the initial hadrons. Soft partons can be emitted anywhere (except inside H itself) and contribute to the Sudakov form factor S_c. This figure is adapted from [250].

Our master formula [251] for the fully differential cross-section $\mathrm{d}\sigma$ at low q_T for the $h_1 h_2 \to F + X$ process is then:

$$\frac{\mathrm{d}\sigma^F_{res}(p_1, p_2, Q^2, \mathbf{q}_T, y, \mathbf{\Omega})}{\mathrm{d}Q^2 \mathrm{d}^2\mathbf{q}_T \mathrm{d}y \mathrm{d}\mathbf{\Omega}} = \int \frac{\mathrm{d}^2 b}{(2\pi)^2} \int_{x_1}^1 \frac{\mathrm{d}z_1}{z_1} \int_{x_2}^1 \frac{\mathrm{d}z_2}{z_2} W^F(\mathbf{b}, z_1, z_2, \ldots) \equiv \frac{Q^2}{s} \left[\mathrm{d}\hat{\sigma}^{F,\mathrm{LO}}_{c\bar{c}}\right]$$
$$\times \int \frac{\mathrm{d}^2 b}{(2\pi)^2} e^{\mathrm{i}\mathbf{b}\cdot\mathbf{q}_T} S_c(Q^2, b_0^2/b^2) \int_{x_1}^1 \frac{\mathrm{d}z_1}{z_1} \int_{x_2}^1 \frac{\mathrm{d}z_2}{z_2} \left[H^F C_1 C_2\right] f_{a_1/h_1}(x_1/z_1, b_0^2/b^2) f_{a_2/h_2}(x_2/z_2, b_0^2/b^2). \tag{6.11}$$

The master equation contains only the resummed piece, not the finite piece onto which it must be matched, and is therefore valid up to corrections of order $\mathcal{O}(\frac{q_T^2}{Q^2})$, i.e. it is valid at low q_T.

The aim of the resummation formalism is to take the N Mellin moments of the function W^F and write it as an exponential piece containing all the pieces logarithmically divergent as $b \to \infty$, and a separate multiplicative finite piece containing the pieces with no explicit b dependence. As described in the last section, this introduces a resummation scale (μ_S) dependence via the flexibility in the separation of these pieces. We have one Mellin transform for each final leg and so we have N_1 and N_2 Mellin moments:

$$\begin{aligned} W^F_{N_1N_2}(b, Q^2; \alpha_s(\mu_R^2), \mu_R^2, \mu_F^2) = \mathcal{H}^F_{N_1N_2}(Q^2, \alpha_s(\mu_R^2); Q^2/\mu_R^2, Q^2/\mu_F^2, Q^2/\mu_S^2) \\ \times \exp[\mathcal{G}_{N_1N_2}(\alpha_s(\mu_R^2), L; Q^2/\mu_R^2, Q^2/\mu_S^2)]. \end{aligned} \tag{6.12}$$

This form is identical to the first term, representing the resummed piece, of equation 5.77 with $C(\alpha_s)$ now $\mathcal{H}$ and $\Sigma(\alpha_s)$ now $\exp(\mathcal{G})$. We may then expand the exponent $\mathcal{G}$ as a perturbative series in α_s - only powers up to $\alpha_s^n L^{n+1}$ are required as remaining powers are made up in expanding the exponential. The general form of the expression for $\mathcal{G}_N$ is

$$\begin{aligned} \mathcal{G}_{N_1N_2}(\alpha_s(\mu_R^2), L; Q^2/\mu_R^2, Q^2/\mu_S^2) =& Lg^{(1)}(\alpha_s L) + g_N^{(2)}\Big(\alpha_s L; \frac{Q^2}{\mu_R^2}, \frac{Q^2}{\mu_S^2}\Big) \\ &+ \sum_{n=3}^{\infty} \Big(\frac{\alpha_s}{\pi}\Big)^{n-2} g_N^{(n)}\Big(\alpha_s L; \frac{Q^2}{\mu_R^2}, \frac{Q^2}{\mu_S^2}\Big), \end{aligned} \tag{6.13}$$

where the g_N^i are perturbative functions. Meanwhile, as usual we can expand the finite $\mathcal{H}^F_{N_1N_2}$ factor as a series in α_s without issue as it contains no logarithmically divergent terms; $\sigma_F^{(0)}$ is the Born cross-section:

$$\begin{aligned} \mathcal{H}^F_{N_1N_2}(Q^2, \alpha_s(\mu_R^2); Q^2/\mu_R^2, Q^2/\mu_F^2, Q^2/\mu_S^2) = \sigma_F^{(0)}(\alpha_s(\mu_R^2), Q^2)\Bigg[1 + \frac{\alpha_s}{\pi}\mathcal{H}^{F(1)}_{N_1N_2}\Big(\frac{Q^2}{\mu_R^2}, \frac{Q^2}{\mu_F^2}, \frac{Q^2}{\mu_S^2}\Big) \\ + \Big(\frac{\alpha_s}{\pi}\Big)^2 \mathcal{H}^{F(2)}_{N_1N_2}\Big(\frac{Q^2}{\mu_R^2}, \frac{Q^2}{\mu_F^2}, \frac{Q^2}{\mu_S^2}\Big) + \sum_{n=3}^{\infty}\Big(\frac{\alpha_s}{\pi}\Big)^n \mathcal{H}^{F(3)}_{N_1N_2}\Big(\frac{Q^2}{\mu_R^2}, \frac{Q^2}{\mu_F^2}, \frac{Q^2}{\mu_S^2}\Big)\Bigg]. \end{aligned} \tag{6.14}$$

The important things to note at this stage are that $\mathcal{G}_{N_1N_2}$ had no dependence on the process (hence no ^{F} label) or on the factorisation scale, this is due to the universal nature of soft and collinear radiation from QCD partons. All process dependence is contained in the function $\mathcal{H}^F_{N_1N_2}$ which contains the hard scattering cross-section and is proportional to the Born cross-section; therefore it contains only virtual corrections, as one might expect after the factorisation of the real emissions into the exponential. At this stage we can also see why the hard scattering piece (finite piece) must be included up to the same expansion order as the resummation, as they produce the same order in the α_s expansion of the whole expression.

It may then be shown that, in order to perform the all-order resummation of the transverse momentum logarithms, then $\mathcal{H}^F_{N_1N_2}$ becomes a product of the Born cross-section, collinear factors C_{ca} $C_{\bar{c}b}$, hard factor H_c^F and the PDFs f; whilst $\mathcal{G}_{N_1N_2}$ becomes a product of the Sudakov

factor and exponentials from the collinear factor running and PDF running[5]. The explicit required forms of the functions given in these expressions are provided in the rest of this section; as a result the $\mathcal{W}^F_{N_1N_2}$ moments match those listed in our master formula 6.11. This form is crucial to allowing a universal expression for the transverse momentum resummation, which is as process independent as possible [223, 250]:

$$\begin{aligned}\mathcal{W}^F_{N_1N_2} =& \sum_c \sigma^{(0)}_{c,F}(\alpha_s(Q^2), Q^2) H^F_c(\alpha_s(Q^2)) S_c(Q^2, b) \\ &\times \sum_{ab} C_{ca,N_1}(\alpha_s(b_0^2/b^2)) C_{\bar{c}b,N_2}(\alpha_s(b_0^2/b^2)) f_{a/h_1,N_1}(\alpha_s(b_0^2/b^2)) f_{b/h_2,N_2}(\alpha_s(b_0^2/b^2)).\end{aligned} \tag{6.15}$$

It is at this stage we can understand Figure 6.1 in more detail - the two hadrons h_1, h_2 are incoming with momenta p_1, p_2, PDFs f_{a/h_1} and f_{b/h_2} extract partons a and b of momentum fractions x_1/z_1 and x_2/z_2 from the hadrons, collinear emissions on top of the Born process $\sigma^{(0)}_{c,F}$ ensure further z_1 and z_2 fractions of momenta are passed on leaving x_1 and x_2 in each leg before the hard scattering. These transform the parton species to $c\bar{c}$ via factors C_{ca} and $C_{\bar{c}b}$ on each of the respective parton lines. Meanwhile, at any stage the partons may undergo soft emissions which do not change the momentum transfer and can be factored out of the sum over the possible ingoing partons a, b as these depend only on the nature of the final partons $c\bar{c}$, they therefore produce the Sudakov factor, denoted S_c. Finally the partons collide and undergo a hard scattering in the partonic sub-process $c + \bar{c} \to F$ with hard factor H^F_c, which includes possible virtual corrections.

First consider the Sudakov factor, its form is the expected exponential; however as well as a logarithm in the exponent integrand, there is also a non-logarithm piece:

$$S_c(\mu_2^2, \mu_1^2) = \exp\left\{ -\int_{\mu_1^2}^{\mu_2^2} \frac{\mathrm{d}q^2}{q^2} \left[A_c(\alpha_s(q^2)) \log\frac{\mu_2^2}{q^2} + B_c(\alpha_s(q^2)) \right] \right\} , \tag{6.16}$$

where μ_1, μ_2 are any two scales. In our case we have $\mu_1^2 = b_0^2/b^2$ and $\mu_2^2 = Q^2$. This carries out the resummation to all orders via renormalisation group running and exponentiation.

The A_c and B_c functions represent the soft and collinear flavour-conserving radiation respectively, they serve as a basis and are clearly perturbative expansions as each additional emission produces a factor of α_s:

$$A_c(\alpha_s) = \sum_{n=1}^{\infty} \left(\frac{\alpha_s}{\pi}\right)^n A_c^{(n)} , \qquad B_c(\alpha_s) = \sum_{n=1}^{\infty} \left(\frac{\alpha_s}{\pi}\right)^n B_c^{(n)} , \tag{6.17}$$

where we sum over all possible emissions. The coefficients up to $A_c^{(3)}$ and $B_c^{(2)}$ are explicitly

[5]It is these exponentials from the collinear and PDF factors that contribute the Mellin dependence to $\mathcal{G}_N$, the Sudakov is Mellin space independent and so if $\mathcal{G}$ was made up of the Sudakov alone it would have no N dependence.

known; these are those required for NNLL resummation[6]. The expressions for these resummation coefficients, and others, are given in Appendix B.1 so as not to obfuscate the description at this stage.

In order to demonstrate that this Sudakov factor of equation 6.16 does indeed resum the logarithmic contributions to all orders, we can perform the logarithmic q^2 integral in the exponent. This can be done by using the evolution equation for α_s to convert $\alpha_s(q^2)$ to $\alpha_s(Q^2)$ and make its q^2 dependence explicit:

$$\frac{d\log(\alpha_s(q^2))}{d\log q^2} \equiv \beta(\alpha_s(q^2)) \equiv -\sum_{n=0}^{\infty}\beta_n(\alpha_s(q^2))^{n+1}. \tag{6.18}$$

The β_n are the beta function coefficients to the required order, these coefficients are given in Appendix B.1. This means that $\alpha_s(q^2)$ contains an infinite tower of logarithms of q^2 resummed via renormalisation running, where $l = 1 + \beta_0\alpha_s(Q^2)\log(q^2/Q^2)$:

$$\alpha_s(q^2) = \Big(\frac{\alpha_s(Q^2)}{l}\Big) - \Big(\frac{\alpha_s(Q^2)}{l}\Big)^2\frac{\beta_1}{\beta_0}\log l + \dots \quad . \tag{6.19}$$

We may now carry out the integral over $\log q^2$ and gather terms of the same order in $\alpha_s(Q^2)$ to obtain the leading log, next-to-leading log, next-to-next-to leading log terms and more if desired:

$$-\int_{b_0^2/b^2}^{Q^2}\frac{\mathrm{d}q^2}{q^2}\left[A_a(\alpha_s(q^2))\log\frac{Q^2}{q^2} + B_a(\alpha_s(q^2))\right] = \Big(\frac{\alpha_s(Q^2)}{\pi}\Big)^{-1}\bar{g}^{(1)} + \bar{g}^{(2)} + \Big(\frac{\alpha_s(Q^2)}{\pi}\Big)\bar{g}^{(3)} + \dots. \tag{6.20}$$

Finally, if we wished to recover the full tower of $\alpha_s^n L^{2n}$ logarithms in the original expansion we need only expand the exponential. Each of the $\bar{g}^{(n)}$ contain all order contributions of $\alpha_s\log(b^2/b_0^2Q^2)$, now in an expansion in α_s/π; therefore the $\bar{g}^{(1)}$ represent leading logarithmic contributions, the $\bar{g}^{(2)}$ are next-to-leading logarithmic contributions and the $\bar{g}^{(3)}$ are next-to-next-to-leading logarithmic contributions. We include up to NNLL in `reSolve` so we stop our discussion here. The $\bar{g}^{(n)}$ for $n = 1, 2, 3$ are given in Appendix B.1 in equations B.1, B.2, B.3. The leading log $\bar{g}^{(1)}$ depends only on the $A^{(1)}$ coefficient function, the NLL $\bar{g}^{(2)}$ depends on $A^{(2)}$ and $B^{(1)}$, and the NNLL $\bar{g}^{(3)}$ depends on $A^{(3)}$ and $B^{(2)}$.

The PDF factors, like the Sudakov, are universal; nonetheless their form in the master formula requires significant explanation. The PDFs are extracted essentially at the start of the leg in each diagram with momentum fractions $x_1/(z_1z_1')$ and $x_2/(z_2z_2')$ at the factorisation scale at which initial state radiation has been absorbed. In our formalism we require the PDFs at b_0^2/b^2 for the resummation, therefore we may evolve the PDFs using the DGLAP equations to obtain them at this scale with momentum fractions x_1/z_1 and x_2/z_2; as shown at the start of each leg in the master picture in Figure 6.1:

$$f_{a_1/h_1}(x/z, b_0^2/b^2) = \int_x^1\frac{\mathrm{d}z'}{z'}U_{aa_1}(z';\mu_F^2, b_0^2/b^2)f_{a/h_1}(x/zz', \mu_F^2). \tag{6.21}$$

[6]The B coefficients are needed to one order less than the A coefficients as when the expansion is performed the logarithms result in an extra $1/\alpha_s$ for the A terms.

These factors $f_{a_i/h_i}(x_i/z_i, b_0^2/b^2)$ (for $i = 1, 2$) are those appearing in the master formula. As a result of the running of the PDFs between these scales various further logarithms of scales $\alpha_s \log(b^2\mu_F^2/b_0^2)$ arise which are resummed via the kernels $U_{aa_1}(z'; \mu_F^2, b_0^2/b^2)$. The U_{aa_1} evolution kernels are implemented in the program in a dedicated routine and are given by the usual anomalous dimension $\gamma_{aa_1,N}(\alpha_s)$ evolution:

$$\frac{dU_{aa_1,N}(\mu^2, \mu_0^2)}{d\log\mu^2} = \sum_c \gamma_{ac,N}(\alpha_s(\mu^2))U_{ca_1}(\mu^2, \mu_0^2), \tag{6.22}$$

and so we have the usual DGLAP evolution kernels to evolve between energy scales, but in Mellin space:

$$U_N(b_0^2/b^2, Q^2) = \exp\Big[\int_{Q^2}^{b_0^2/b^2} \frac{dq^2}{q^2}\gamma_N(\alpha_s(q^2))\Big] \tag{6.23}$$

These anomalous dimensions are then given by the Mellin moments of the splitting functions $P_{aa_1}(\alpha_s, z)$

$$\gamma_{aa_1,N}(\alpha_s) = \int_0^1 dz z^{N-1} P_{aa_1}(\alpha_s, z) = \sum_{n=1}^{\infty} \Big(\frac{\alpha_s}{\pi}\Big)^n \gamma^{(n)}_{aa_1,N}. \tag{6.24}$$

Next we move onto the hard and collinear factors and the Born factor of equations 6.11 and 6.15, which together contain the process dependence. The Born factor is trivial, with no b dependence as there is no transverse momentum at Born level; to be explicit however, the expression $\Big[\mathrm{d}\hat{\sigma}^{F,\mathrm{LO}}_{c\bar{c}}\Big]$ in equation 6.11 contains additional factors for ease of expression:

$$\Big[\mathrm{d}\hat{\sigma}^{F,\mathrm{LO}}_{c\bar{c}}\Big] = \frac{\mathrm{d}\hat{\sigma}^{F,\mathrm{LO}}_{c\bar{c}}}{Q^2 \mathrm{d}\mathbf{\Omega}}(x_1p_1, x_2p_2, \mathbf{\Omega}, \alpha_s(Q^2)) \,. \tag{6.25}$$

There is further process dependence in the collinear factors C^F_{ca} and $C^F_{\bar{c}b}$; however this dependence is simply on whether the initiating partons are gg or $q\bar{q}$ and nothing further. The collinear factors are then, in some sense universal. We now focus here only on the $q\bar{q}$ case as our diphoton and Drell-Yan processes only involve $q\bar{q}$ initiation for the H^F_c and C^F_{qa} factors as gg only enters in diphoton (and does not enter Drell-Yan) for the first time at NNLO via the gg box diagram of Figure 6.4, whilst H^F_c and C^F_{qa} factors are only required once beyond leading order for a contribution is needed[7]. The $[H^F_c C_1 C_2]_{c\bar{c},a_1a_2}$ part of equation 6.11 is of the form of the corresponding parts of equation 6.15 when written in full. The H^F_c and C^F_{qa} factors then admit perturbative expansions in the usual way:

$$\begin{aligned} H^F_q(x_1p_1, x_2p_2, \mathbf{\Omega}, \alpha_s(M^2), \mu_R) &= 1 + \sum_{n=1}^{\infty} \Big(\frac{\alpha_s}{\pi}\Big)^n H^{F(n)}_q(x_1p_1, x_2p_2, \mathbf{\Omega}, \mu_R), \\ C_{qa}(z, \alpha_s) &= \delta_{qa}\delta(1-z) + \sum_{n=1}^{\infty} \Big(\frac{\alpha_s}{\pi}\Big)^n C^{(n)}_{qa}(z). \end{aligned} \tag{6.26}$$

As we work in the massless quark limit these H^F_q and C_{qa} never obtain dependence on the specific

[7]The structure of the $[H^F_c C_1 C_2]$ piece is more complex for gg initiation due to spin correlations amongst the gluons, see [2] for the expressions.

quark flavour. The collinear factors up to $C_{qa}^{(2)}$ are known and are given in equations B.18 - B.28 in Appendix B.1. We evaluate the collinear factors using α_s at energy scale b_0^2/b^2 in our resummation formalism, and they thereby contribute to the resummation of large logarithms between the factorisation scale at which they are applied and the small scale at which the resummation formalism is implemented b_0^2/b^2. This evolution is done in a way which is general for any function with only implicit dependence on the energy scale through α_s:

$$C_{qa}(z, \alpha_s(b_0^2/b^2)) = C_{qa}(z, \alpha_s(\mu_F^2)) \exp\left[- \int_{b_0^2/b^2}^{\mu_F^2} \frac{\mathrm{d}q^2}{q^2} \beta(\alpha_s(q^2)) \frac{\mathrm{d}\log(C_{qa}(z, \alpha_s(q^2)))}{\mathrm{d}\log(\alpha_s(q^2))} \right]. \quad (6.27)$$

This holds element-by-element for C_{qa}, so that each C_{qa} coefficient is now expressed as a function of α_s at the factorisation scale μ_F^2 and an integral of the same form as in equation 6.16, making it obvious that it contributes to the all-order resummation of the large b logarithms, in addition to the Sudakovs and the PDFs. The C_{ab} factors represent un-cancelled real and virtual contributions due to collinear radiation.

Finally, the H_q^F contain the last explicit process dependence - in fact this hard factor was introduced in [250] in order to absorb as much of the process dependence as possible, enabling our largely process-independent application in `reSolve`. This hard factor is b independent, with all large logarithms absorbed elsewhere in the formalism. The hard factors contain the purely virtual corrections to the $c\bar{c} \to F$ partonic sub-process which occurs after the various emissions. The hard factor H_q^F is the ratio of the square matrix element for the sub-process including virtual corrections to that for the Born process and is therefore

$$H_q^F = \frac{|\tilde{M}_{q\bar{q}\to F}|^2}{|M_{q\bar{q}\to F^{(0)}}|^2}. \quad (6.28)$$

Here $F^{(0)}$ indicates the Born cross-section with no virtual corrections. The matrix element for the virtually corrected amplitude is denoted $\tilde{M}_{q\bar{q}\to F}$, as it must be UV renormalised in the usual way; this is done in the $\overline{MS}$ scheme in `reSolve`. Meanwhile, as described in Chapter 5.4, the virtual correction amplitudes contain IR divergences as well, which normally cancel with those from the real emissions. Therefore given we have separated the real emission and virtual pieces and already accounted for the IR divergences of the real emissions in the rest of the formalism, we must subtract the IR divergences from the virtually corrected matrix element. We use the universal subtraction operator $\tilde{I}_c(\epsilon, Q^2, \mu_R^2)$ to do this:

$$\tilde{M}_{c\bar{c}\to F}(x_1 p_1, x_2 p_2, \Omega, \mu_R) = [1 - \tilde{I}_c(\epsilon, Q^2, \mu_R^2)] M_{q\bar{q}\to F}(x_1 p_1, x_2 p_2, \Omega, \mu_R), \quad (6.29)$$

here the matrix element M in the right-hand side is UV renormalised in the $\overline{MS}$ scheme in the usual manner. $\tilde{M}$ is then the UV-renormalised and IR-regulated matrix element. The explicit expressions for the subtraction operator $\tilde{I}_c(\epsilon, Q^2, \mu_R^2)$ to 1- and 2-loops are given in reference [251]. After cancelling the ϵ poles in this way the renormalised, regularised matrix element for the virtually corrected amplitude $\tilde{M}_{c\bar{c}\to F}$ is finite. A similar relation to equation 6.28

holds for the case of the gg initiation hard factor H_g^F but with the complication of the need to sum over gluon helicities and a similar IR subtraction is then performed. This is yet to be implemented in `reSolve` as the diphoton and Drell-Yan processes have no virtually-corrected contributions from gg initiation as the contributions occur at higher order in α_s than NNLO. The explicit expressions for the subtraction operators are given in [251] and the expressions for the hard factors for the relevant processes are given in Appendix B.1.

Last of all we comment on a further ambiguity in the formalism, additional to the scales introduced via renormalisation, factorisation and resummation, there is a choice of "resummation scheme". This arises from the observation that the equation 6.11 (or equivalently equation 6.15) is invariant under transformation using a perturbative function $h_c(\alpha_s) = 1 + \mathcal{O}(\alpha_s)$ such that:

$$\begin{aligned} H_c^F(\alpha_s) &\to H_c^F(\alpha_s)[h_c(\alpha_s)]^{-1}, \\ B_c(\alpha_s) &\to B_c(\alpha_s) - \beta(\alpha_s)\frac{d\log h_c(\alpha_s)}{d\log\alpha_s}, \\ C_{ab}(\alpha_s, z) &\to C_{ab}(\alpha_s, z)\sqrt{h_c(\alpha_s)}. \end{aligned} \tag{6.30}$$

In order to prove this invariance we begin by deriving how an arbitrary function of α_s, such as $h(\alpha_s)$ evolves between scales, starting from the β function definition in QCD in equation 6.18 we can write:

$$\begin{aligned} \frac{d\log h(\alpha_s(q^2))}{d\log q^2} =& \frac{d\log\alpha_s(q^2)}{d\log q^2}\frac{d\log h(\alpha_s(q^2))}{d\log\alpha_s(q^2)} = \beta(\alpha_s(q^2))\frac{d\log h(\alpha_s(q^2))}{d\log\alpha_s(q^2)} \\ &\Rightarrow \int_{\mu_1^2}^{\mu_2^2} d\log h(\alpha_s(q^2)) = \int_{\mu_1^2}^{\mu_2^2}\frac{dq^2}{q^2}\beta(\alpha_s(q^2))\frac{d\log h(\alpha_s(q^2))}{d\log\alpha_s(q^2)}. \end{aligned} \tag{6.31}$$

So we obtain the general renormalisation group expression (as used in equation 6.27):

$$h(\alpha_s(\mu_1^2)) = h(\alpha_s(\mu_2^2))\exp\left[-\int_{\mu_1^2}^{\mu_2^2}\frac{dq^2}{q^2}\beta(\alpha_s(q^2))\frac{d\log h(\alpha_s(q^2))}{d\log\alpha_s(q^2)}\right]. \tag{6.32}$$

We may now use this expression to consider the invariance of the Sudakovs and the overall master equation under such changes, first take the Sudakov, this changes with $B_c(\alpha_s)$ so that:

$$\begin{aligned} S_c(\mu_2^2,\mu_1^2) \to \exp&\left\{-\int_{\mu_1^2}^{\mu_2^2}\frac{\mathrm{d}q^2}{q^2}\left[A_c(\alpha_s(q^2))\log\frac{\mu_2^2}{q^2} + B_c(\alpha_s(q^2)) - \beta(\alpha_s(q^2))\frac{d\log h(\alpha_s(q^2))}{d\log\alpha_s(q^2)}\right]\right\} \\ &= S_c(\mu_2^2,\mu_1^2)\left[\frac{h(\alpha_s(\mu_1^2))}{h(\alpha_s(\mu_2^2))}\right] = S_c(\mu_2^2,\mu_1^2) + \mathcal{O}(\alpha_s). \end{aligned} \tag{6.33}$$

Where we have substituted in equation 6.32 in the penultimate step, and used the fact that $h(\alpha_s)$ is perturbative in the last stage to show that the change in the Sudakov is of a higher order in α_s. As for the remainder of the master equation, the remaining factor $[H_c^F C_1 C_2]_{c\bar{c},a_1a_2}$ factor is not dependent on the $B_c(\alpha_s)$ basis functions and so its transformation under the resummation

transformation in equation 6.30 is straightforward and the invariance trivial as the $h(\alpha_s)$ factors cancel.

This invariance under resummation scheme transformations of the form in equation 6.30 allows us to make a choice of scheme, and as ever, whilst any choice is equally valid, there are easier and more difficult choices from the point of view of making theoretical predictions. Until the discovered universality of our formalism by Catani et al in [250], essentially applications of this formalism were making the choice $H_c^F = 1$ for each process individually, as there was no such hard factor to absorb process dependence. As a result, the collinear factors (and the $B_c^{(n)}$ factors beyond $n = 1$) were process dependent and non-universal, making the formalism much more difficult to apply in a modular, universal manner to difficult processes of the same class $h_1 + h_2 \to F + X$. This choice is therefore a "bad" one, complicating the theoretical calculations. A common and better choice is the "hard" scheme, where any factors in the flavour off-diagonal parts of the collinear functions $C_{ab}^{(n)}(z)$ which are also singular as $z \to 1$, i.e. which are proportional to $\delta(1-z)$, are removed from the collinear factors. This can be argued to be a "physical" choice in that as $z \to 1$ then there is no longer any collinear radiation as it takes all the momentum and there is no splitting. In fact, as the collinear factors differ depending on the leading order partons which initiate the process, i.e. gg or $q\bar{q}$, an alternative scheme choice can be made by choosing the hard factors in one $q\bar{q}$ initiated process and in one gg initiated process. For example a common choice is to set $H_q^{F(n)} = 0$ and $H_g^{F'(n)} = 0$ for a $q\bar{q}$ initiated final state F and a gg initiated final state F'. Indeed, in `reSolve` we use the "Drell-Yan - Higgs" scheme which sets $H_q^{(n)} = 0$ for Drell-Yan and $H_g^{(n)}$ for Higgs production, simplifying the hard factors for these processes.

The resummation scheme transformations in equation 6.30 can then be used to transform between the hard, collinear and B factors for different processes by replacing the $h_c(\alpha_s)$ with expressions of the form $H^{F\tilde{F}} = H^F/H^{\tilde{F}}$ so that the perturbative function of α_s transforming between schemes is the ratio of the hard factors of different schemes; see [250] for further details.

We can actually offer an intuitive explanation for the resummation scheme independence. It is a real order-by-order invariance of the resummed part alone arising from the fact that some contributions can be moved between the B_c, C_{ab}^F and H_c^F coefficients without affecting the overall combined formula. This ambiguity in the exact nature of each of the pieces can be thought of relating to the method of regulating the IR divergences. The transverse momentum spectrum is not collinear-safe, diverging in perturbation theory; in order to regularise these divergences we must subtract off their effects, however the exact choice to make is not clear and the ambiguity seeps into the definition of the collinear functions C_{ab}, and consequently into the H_c^F and S_c (via the B_c) factors, this effect is also linked to the resummation scale dependence. Again this is explained further in [250, 251].

6.2.4 Phase Space Definition of Final State F

In addition to the theoretical uncertainty already mentioned from scale choices, PDF fitting, Monte Carlo and other sources, there is a further origin of uncertainty. This arises in the definition of the phase space of the final state system F for processes where this is made up of more than one particle, such as the Drell-Yan and diphoton cases implemented in `reSolve`. At leading order in our formalism the final state system F must have zero transverse momentum as the incoming partons have no transverse momentum and there is no radiation against which to recoil. Beyond leading order this is however different as unresolved radiation may have net finite $q_T \neq 0$ and so the final state system F can recoil against this radiation and gain a non-zero transverse momentum itself. Indeed this is crucial in allowing `reSolve`, and the formalism in general, to determine the transverse momentum spectrum; the radiation spreads the delta function in q_T at LO out into a finite q_T distribution peaked near, but just above, 0. However, in the formalism we also factorise out the kinematics into a hard-scattering factor and the Born cross-section from the all-order resummed emissions formally in the limit $q_T \to 0$; fortunately this misalignment only has sizeable effects at large q_T where our resummation formalism is invalid in any case. There is however a further choice to make, these hard scattering and Born cross-sections both require the 4-momenta of the initial incoming partons and of the individual final state particles making up the final state system F. We generate the angles $\Omega = \{\theta_{CM}, \phi_{CM}\}$ via Monte Carlo to define the individual particle momenta of the final state system. However, given the incoming partons have zero net transverse momentum for the Born, the outgoing final state particles in F in this factorisation must also have zero total transverse momentum, producing a contradiction as the resummation gives F non-zero q_T. Therefore to determine the appropriate Born kinematics in our formalism we must choose how to assign the transverse momentum in the initial and final state particles. This includes how to designate the angular variables Ω. This ambiguity disappears if only questions about F, and not the individual particles in F, are asked. However, given we often wish to look at distributions of $p_T^{\text{min/max}}$ in the Drell-Yan case and other similar variables which require assignment of the individual final state particle momenta, we must undertake this assignment consistently and in a physically acceptable manner.

Traditionally there are two approaches to this, which are described further in [5,8]. The first is to neglect this issue, and define the initial state particles with zero net transverse momentum whilst the final state particles still have net $q_T \neq 0$ in order to provide transverse momentum spectra. This therefore builds 4-momentum non-conservation into the implementation of the formalism, which is of course unsatisfactory from a physical point of view and may affect even the transverse momentum spectrum. This is often referred to as the "2-body phase space setup". The second, more physical, approach is that given the final state particles must have net transverse momentum to correctly reproduce the total transverse momentum of the final state system as a whole, we must impose net transverse momentum on the initial state particles to conserve 4-momentum in the Born kinematics. Nonetheless, the exact manner in which to assign this transverse momentum requires specification of a q_T recoil method, with an infinite

number of possibilities. Many applications of the transverse momentum resummation formalism do this in the Collins-Soper rest frame (CS frame) [263], which is the rest frame of the F final state system in which the z-axis bisects the angle between the incoming parton momentum $\mathbf{P}_1$ and minus the other incoming parton momentum $-\mathbf{P}_2$ (now not collinear as there is a net q_T). θ_{CS} is then the angle between the outgoing momentum of one of the final state particles and the z axis and ϕ_{CS} is its angle relative to the net transverse momentum q_T. This therefore absorbs the net transverse momentum of F into the incoming partons. In this frame you may then declare that you will define the (θ_{CM}, ϕ_{CM}) angles of the individual final state particles in the leading order Born distribution (with which we generate the individual final state particle momenta) to be equal to the Collins-Soper angles of the resummed distribution. This is a perfectly valid, adequate, well-defined choice; however it hides the fact that the CS rest frame definition itself is dependent upon the q_T (which is zero for the LO case), so any prescription you declare introduces a dependence on q_T in the angular distribution. Any differences due to this choice of assignment will be $\mathcal{O}(q_T/Q)$ but represent an additional higher order correction which we may wish to estimate.

As characterised in [8], any such prescriptions are one of an infinite class of possibilities for how to assign the incoming parton momenta. There are several properties one desires of such a scheme; the first is that it recovers the standard LO expression of the factorisation for $q_T \to 0$, we also need the energies of the partons to be positive and that their 4-momenta are invariant under longitudinal boosts of the partonic centre of mass frame. Such a method, taken from [8] and adapted in `reSolve`, is given here. The incoming q_T-recoiled 4-momentum of parton 1 is set as:

$$k_1^\mu = \zeta_1 \frac{Q^2}{2Q.P_1} P_1^\mu + k_{1T}^\mu + \frac{\mathbf{k}_{1T}^2}{\zeta_1} \frac{Q.P_1}{Q^2 P_1.P_2} P_2^\mu, \tag{6.34}$$

where

$$\zeta_1 = \frac{Q^2 + 2\mathbf{q}_T.\mathbf{k}_{1T} + \sqrt{(Q^2 + 2\mathbf{q}_T.\mathbf{k}_{1T})^2 - 4M_T^2 \mathbf{k}_{1T}^2}}{2Q^2}. \tag{6.35}$$

We choose k_{1T}^μ as a vector transverse to the 4-momenta of each of the initial incoming hadrons, P_1^μ and P_2^μ, and such that $\mathbf{k}_{1T} \to 0$ as $\mathbf{q}_T \to 0$. This ensures that the LO expression is recovered for $q_T = 0$ and that the $\mathbf{k}_{1T}$ lies in the $\mathbf{q}_T$ plane. Furthermore, $\mathbf{k}_{1T}$ is chosen such that $Q^2 + 2\mathbf{q}_T.\mathbf{k}_{1T} > 2M_T|\mathbf{k}_{1T}|$ so that ζ_1 is real and consequently $k_1^0 > 0$ (then $k_2^0 > 0$ follows as $q_0 > 0$). The definition of k_1^μ in terms of k_{1T}^μ and ζ_1 then ensures that that k_1^μ is invariant under longitudinal hadronic centre of mass boosts. This is useful as it means our definition can be consistently applied regardless of the boosts required to get to the incoming parton frame where we apply the Born kinematics. The other incoming parton 4-momentum is defined via 4-momentum conservation $k_2^\mu = Q^\mu - k_1^\mu$, where Q^μ is the 4-momentum of the final state system F as a whole with non-zero q_T. P_1 and P_2 are the incoming four-momenta of the hadrons. This method is called the "3-body phase space setup", as it assumes recoil against some collective 3$^{\text{rd}}$ particle/system of particles, which physically are the unresolved radiation. In this prescription the $\mathbf{k}_{1T}$ is arbitrary and parametrises the infinite number of possibilities for the assignment of

this transverse momentum, all of which are consistent q_T recoils. Any dependence on this choice of $\mathbf{k}_{1T}$ cancels up to the given order of evaluation in observables inclusive over the individual particles making up the measured final state F, i.e. after integrating over the angular variables in Ω.

It is the latter approach that we use in `reSolve`. Specifically, in this methodology, and in `reSolve`, there are essentially four (sets) of momenta which are to be distinguished. First of all there is the incoming momentum of the hadrons, the $\{P_1^\mu, P_2^\mu\} = (\sqrt{s}/2, 0, 0, \pm\sqrt{s}/2)$ which have zero net transverse momentum. These, along with the parton momentum fractions, set the incoming momenta of the partons, $\{K_1^\mu, K_2^\mu\} = \{x_1 P_1^\mu, x_2 P_2^\mu\}$ which also have zero net transverse momentum. The mismatch and contradiction in the application of the theoretical formalism then comes in matching these with the final state particle momenta, given the final state F has net finite, non-zero q_T. The method we follow, and given above, is to define a q_T recoiled set of incoming parton momenta $\{k_1^\mu, k_2^\mu\}$ given by equation 6.34 which has net non-zero transverse momentum, in fact it has transverse momentum equal to that of F. We then generate the Born dynamics using these incoming parton momenta, transforming to this frame so that there is zero q_T in the rest frame of F before transforming to the frame of the incoming partons with net transverse momentum, so that the formalism is at least physically consistent. As there are infinitely many rest frames of final state systems F depending on the exact Q, q_T, η generated by the Monte Carlo, and any arbitrary 3D rotation gives another rest frame, we have two free parameters in our prescription. These two degrees of freedom correspond to the arbitrary 2D vector $\mathbf{k}_{1T}$, which can be interpreted as a choice in how to spread the 2D vector of transverse momentum between the incoming partons, this is the choice of how to set the $\Omega = \{\theta_{CM}, \phi_{CM}\}$ angles of the individual final state particles. We can then view the relationship between the LO zero net transverse momentum incoming parton momenta K_i^μ and the q_T recoiled k_i^μ as a Lorentz transformation from the hadronic collision frame to the rest frame of the final state (i.e. the rest frame in which the incoming partons actually collided).

In `reSolve` we have $\mathbf{k}_{1T}$ given as in equation 6.36 and with different values of α allowing for the arbitrary nature of the $\mathbf{k}_{1T}$.

$$\mathbf{k}_{1T} = \frac{\mathbf{q}_T}{2}(1+\alpha), \tag{6.36}$$

$\alpha = 0$ is the default choice in the code, corresponding to the Collins-Soper frame, in which case we are equating the angles of the individual particles states $\Omega = \{\theta_{CM}, \phi_{CM}\}$ with those in the Collins-Soper frame. However α, and correspondingly the chosen frame, can be altered should the user wish to investigate the effects of this ambiguity in the phase space definition on distributions of the final state individual particle momenta and associated variables. This may allow an estimate to be made of the higher order corrections and errors associated with this aspect of the resummation formalism.

6.2.5 Crucial Points of the Formalism

The theoretical formalism we have described, and which is applied in `reSolve`, therefore enables the all-order resummation of logarithmically-enhanced contributions at small transverse momenta. Here we summarise the key points of the theoretical formalism applied, for ease of perusal:

- General - The formalism applied is general in nature and can be applied to a wide range of LHC (and other collider) processes, requiring only that the measured final state system is made up of colourless particles.
- Modular - The formalism factorises the different contributions into several different parts; the Born cross-section, Sudakov factor, collinear factors and hard factor are all separate. Therefore it allows a modular application which is customisable so that it can be easily extended to several further processes.
- Universal - It is almost completely universal, as a consequence of QCD factorisation for IR singularities, with process dependence only via the nature of the incoming partons in the LO contribution (for the collinear and Sudakov factors) and the Born cross-section for the hard factor encoding the virtual contributions. The resummation calculation can therefore be applied independently of the hard factor and Born computation and in the same manner for all included processes.
- Fully differential - The setup ensures that, whilst aimed at resumming transverse momentum logarithms in determining the q_T spectra, the differential distributions in a range of other final state variables are automatically generated, including in invariant mass, rapidity and others.
- b-space - The use of b-space allows the factorisation of the kinematics of transverse momentum conservation. Meanwhile the formalism explicitly deals with and controls singularities at high and low impact parameter values.
- Non-perturbative contributions - High b singularities indicating low, non-perturbative q_T values must be cut off and phenomenologically parametrised as a low q_T smearing in the q_T distribution.
- Mellin space - Mellin space converts complex convolution integrals to simple products which can be summed along the inverse Mellin transform contour, as outlined in Appendix B.2.
- Parton level - The resummation is applied at partonic level. PDFs must therefore be evaluated at the factorisation scale.
- Events and cuts - The application of the formalism means that "events" can be generated by Monte Carlo at low q_T with simple interpretation, this means experimental selection cuts can be straightforwardly applied, accurately reflecting experimental setups.

- Perturbative - The formalism recovers the standard predictivity of a perturbative expansion in α_s, all the resummation coefficients are perturbative.
- Standard diagrammatic pQCD - The formalism is based on the standard setup of diagrammatic evaluation in perturbative QCD, which is ubiquitously used throughout particle physics at colliders.
- Known up to NNLO+NNLL - All the necessary resummation coefficients and contributions are known up to at least NNLO with NNLL resummation for all relevant studied processes, although for Higgs production at NNLO+NNLL the final order hard factor coefficients are known only in the large m_t limit. In general, many of the universal factors (such as $A_a^{(4)}$ and $B_a^{(3)}$) are actually known at $\mathrm{N^3LL}$, however the hard factors are not nor are many of the collinear factors. It should be noted however that in this first version `reSolve` only includes the resummed piece, not the matched finite piece. Consequently the vast majority of the results we present in Chapter 7 are only "NNLL"[8]. Nonetheless, whilst they do not include the finite piece they do include some beyond leading order virtual corrections through the hard factors, as seen in equation 6.28. In an upcoming version the matched finite piece will also be included so that the results will then truly be available up to "NNLO+NNLL" including all beyond leading order corrections up to this order.
- NNLO subtraction scheme - Once the hard-virtual factor in the resummation formalism is known one can use the q_T subtraction to define an IR subtracted NNLO fixed order finite term expression.
- Resummation scale - The factorisation of the resummation and the hard factor introduces the resummation scale, representing uncertainties in the theoretical predictions. Its effect and corresponding uncertainty has to be evaluated via scale variation in the same way as is done for the standard factorisation and renormalisation scales.
- Resummation scheme - The resummation scheme choice can simplify the calculation for some processes, for example `reSolve` uses the Drell-Yan - Higgs scheme so extensions from its original diphoton application to Drell-Yan (already completed) and Higgs (future) are simpler than otherwise.
- PDF fitting - Use of Mellin space means PDFs must be fitted to an analytic form of known Mellin transform; this fit provides an additional source of uncertainties into the calculation.
- Final state phase space - Ambiguity in the definition of the momenta of the individual final state particles for observables not inclusive in the final state adds theoretical uncertainty to predictions of differential spectra for these individual final state particle kinematic variables.
- Many integrals - Whilst transforming to b-space and Mellin space for each incoming parton simplifies the formulae analytically, it leaves many nested integrals to be performed.

[8] In fact, as the Born cross-section is included they could be described as "LO+NNLL", we will however refer to them as "NNLL".

6.3 Methodology, Implementation and Structure

Our application of this theoretical formalism is the new `reSolve` program, which is a Monte Carlo differential cross-section parton level event generator written in `C++` and is capable of adding transverse momentum resummation to a range of processes. It is specifically designed to be modular, transparent, easily customisable and extendible, moreover it is clearly commented and comprehensively documented in our paper [2]. It is set up to allow parallelisation of the code (see Chapter 7.1.6) as well as to interface with other codes relatively straightforwardly if desired by the user.

The program works by randomly generating the invariant mass, transverse momentum and rapidity of the final state system F as well as the relative angles of the individual particles in F. This defines an event, for which the 4-momenta of the incoming and outgoing particles are determined and subsequently the Born cross-section is calculated for the given process. In the meantime, completely independently, the resummation is performed in impact parameter space and double Mellin space as the collinear and Sudakov factors are combined with the hard factors. The double Mellin inversion and inverse Fourier transform back to q_T space are then performed to produce the cross-section for each event. This process is repeated, generating separate phase space points and their cross-sections. These events can be weighted according to the approximate value of the integrand for the given phase space point region, this is set by a Monte Carlo grid determined iteration on iteration. Any phase space integration to obtain given spectra is then performed by summing event cross-sections in the integrated variables. The resummation is performed up to NNLL and histograms are automatically produced for the user's desired differential spectra, albeit including only the resummed contribution to the cross-section in the current version.

6.3.1 Program Structure

A key feature of the program is its explicitly modular and carefully constructed structure in order to take maximal advantage of the near universal nature of the resummation formalism. Different aspects of the calculation are divided into different self-contained sections in separate folders in order to make the program as transparent as possible. In principle several of these - Histogrammer, Integral, PDFfit, Resummation and Utility - can be used independently of the main code, this is important for the straightforward extension of the program to additional processes. The details of the calculations in each folder are detailed here, and following this an explanation of how the program works is given in Chapter 6.3.2. This is intended to allow users to understand how the program functions in order to both simplify its use and enable users to add their own processes should they wish.

- Histogrammer - This contains the files required to calculate the cross-section per bin width in the desired differential cross-sections.
- Integral - This contains the files necessary to perform the Monte Carlo phase space in-

tegration. In keeping with the modular and customisable structure there are two Monte Carlo integrators included in `reSolve`: the in-house `k_vegas` integrator (see Appendix B.3 for more information) or the external `Cuba` integrator [264].

- Main - This contains all the general files used to read in the input file, perform pre-processing, post-processing and interface with the Monte Carlo integration routines.
- PDFfit - This contains the routines used to evaluate the fit parameters for the PDF fits, as well as to output them in a form useful for the rest of the program.
- Process - This folder contains any process-specific code, currently these are for the diphoton and Drell-Yan processes.
- Resummation - This folder contains the resummation routines which are process independent. This includes the inverse Fourier and inverse Mellin transforms and the process independent parts of the hard factor calculation, as well as the Sudakov factors.
- User - This is a folder where the user can call additional routines they may write for pre-processing, Monte Carlo or post-processing, as well as to read process-specific input. Currently, it contains the switch between using `k_vegas` or `Cuba` as the Monte Carlo integrator and routines to allow parallelisation of `k_vegas` across multiple cores and multiple machines.
- Utility - This folder contains auxiliary functions necessary for the program; including the `alphaS.f fortran` routine for α_s evolution, the "dumper" routines to output the events in "easy" or "pseudo-lhe" form, routines for the Lorentz algebra, and initialisation routines associated with the PDFs.

This program structure is designed to modularise the program; this enables the straightforward extension of the program into other processes, indeed we intend to perform this further ourselves in the future. In order to add a new process one must simply add a sub-folder in `Process/` with equivalent files to those for diphoton and Drell-Yan for the new process. Depending on the process, additional hard factors may need to be added to the hard function calculation in the resummation and potentially also the different orders included for the $q\bar{q}$ and gg processes as their relative order contributions depend upon the process. Currently, $q\bar{q}$ hard factors are included up to NNLL, whilst gg hard factors are only up to LL; this will be resolved in future versions as we extend the program to additional processes. A detailed guide on how to add a process to the `reSolve` program is given in Chapter 7.1.7. The underlying aim of `reSolve` is to take a Born process and add resummation up to NNLL; this resummed contribution to the total fully differential cross-section must then be consistently matched with the standard fixed order expansion (the "finite piece"), as described in Chapter 5.7, to produce the total fully differential cross-section across the entire q_T range.

By far the most important section of the code, is the unique `Resummation` folder. In here all the theoretical formalism described in Chapter 6.2 is packaged and built into an independently-compilable sub-program which takes the Born cross-section, the PDF fit, and information on the orders at which $q\bar{q}$ and gg initiation contribute in the desired process and on which Born contributions are non-zero. It then determines the resummed part of the differential cross-section

in a process independent manner. The structure of this section of `reSolve` is shown later in Figure 6.3. It consequently knows nearly nothing about the underlying process, with the non-zero Born contributions only specified so as to pragmatically avoid spending time summing over zero contributions.

The program has all necessary external files and codes required for its running explicitly included within it; these include the `minuit` library for function minimisation used for the PDF fits, the `pdffit.f` to perform the PDF fits, `partons.f` to call the PDFs at the required points and interface with the PDF grids, the `fortran` routine `alphaS.f` for evolving the QCD coupling, the `random.f` to generate the random values for the Monte Carlo and the `intde2.cc` code (based on [258]) used to perform the inverse Fourier transform. On top of this, as described, it contains functions to interface with the `Cuba` integrator package [264], which needs to be downloaded separately should the user wish to use it. `Cuba` however is not required as our own `k_vegas` integrator is included within `reSolve` which is based on Lepage's [265] `DGauss` algorithm. As all the separate pieces of the computation in `reSolve` are largely self-contained, passing information via objects, interfacing with other codes or additional calculations should not be difficult to perform, allowing it to be customised, interfaced and extended as the user requires.

6.3.2 Program Flow

We now summarise how the program functions and the different steps performed to undertake the calculation. Figure 6.2 shows in detail the flow of the calculations performed, starting at `main.cc`, Figure 6.3 then illustrates in more detail the crucial resummation aspects of the calculation. The colours of the boxes indicate where in the program structure the various files and routines lie, with the key given in Figure 6.2. The following description and figures are for the diphoton process, but the exact same sequence occurs for the Drell-Yan processes with the appropriate process-specific files in the Process sub-folder interchanged:

1. The calculation begins in `main.cc`, this calls `InputPars.cc` to read in the input file. From here `user.cc` is called to carry out required processing before the Monte Carlo integration.
2. This pre-processing includes calling `resu_preproc.cc`, which carries out various initialisations including those of the inverse Fourier transform, N-independent resummation parameters (via `resu_procindep.cc`), inverse Mellin transform contour and N-dependent resummation parameters (via `mellinspace_fns.cc`). It also calls the PDF fitting routines and calls `pdfmellin.cc` to convert the PDF fits into Mellin space.
3. `User.cc` then moves onto the Monte Carlo aspect of the program, calling `k_vegas_interface.cc` or `cuba_interface.cc` appropriately. These programs call the random generator and pass any points evaluated to the Monte Carlo evaluation programs.
4. The Monte Carlo interface programs themselves then call the process-specific files - first `diphoton_integrand.cc`; this is the integrand of the Monte Carlo integral. It calls `diphoton_ps` to convert the randoms generated into a phase space point; determining qq^2, q_T^2, η, θ_{CM} and ϕ_{CM} - these are the invariant mass squared, transverse momentum

squared and pseudorapidity of the final state system F, and the polar and azimuthal angles of the individual particles in the final state F respectively.

5. `diphoton_integrand.cc` next calls `diphoton_cuts.cc`, this has the task of reading the cut information from the input file and determining whether the current phase space point passes the cuts. Provided the cuts are passed, `diphoton_hard.cc` is called, this evaluates the Born cross-section and other process-specific resummation variables; such as the H_q^1, H_q^2, H_g^1 and H_g^2 hard factors.
6. `reSolve` now moves onto the general resummation routines as `diphoton_integrand.cc` calls resummed in `inv_fourier.cc`. This section of the calculation is shown in more detail in Figure 6.3.
7. First in the resummation routines, `inv_fourier.cc` determines the correction factor required to account for the fact that the PDFs are fit. This factor is the ratio of the LO cross-section calculated directly with standard PDFs to that calculated with the PDF fit. This is all determined in `xsection.cc`.
8. `invbtoqt` is now called to perform the inverse Fourier transform from b-space to q_T space. The routine `invres` is the integrand of this inverse Fourier transform.
9. `invbtoqt` calls `invres` for several points in impact parameter space, usually of the order of 20, depending on the precise details of the convergence. For each b value, `invres` evaluates the double inverse Mellin transform used to perform the resummation via the routine `inversemellin_resummed`.
10. `inversemellin_resummed` in `inv_mellin.cc` organises the double inverse Mellin transform calculation, this calculation is built directly into the code.
11. First, the Sudakov form factors for soft gluon and soft quark emission are calculated by calling `sudakov.cc`. Then `GetResuPars` determines the C_1, C_2, anomalous dimensions and other N-dependent basis functions in Mellin space and evolves them from the resummation scale μ_S to the scale b_0^2/b^2 of the resummed logs.
12. `hard_fns.cc` next determines the hard factors, incorporating the virtual diagram contributions into the resummation.
13. The Sudakovs, hard factors and appropriate weights are used at each of $40 - 88$ points along the contour in Mellin space, with the number of points depending on the rapidities of the two photons; this is done for each inverse Mellin transform. The contributions at each point are then summed along the contours to calculate the double inverse Mellin transform.
14. Putting all this information together gives the inverse Mellin transformations, if these are called for each of around 20 b values this allows the determination of the inverse Fourier transform for each phase space point. Repeating the process for $\mathcal{O}(10^5 - 10^7)$ randomly distributed phase space points and including the effects of the Jacobian transformation between the randoms space volume and the phase space volume, `reSolve` thereby determines the overall cross-section.
15. The total cross-section is printed out after each iteration; meanwhile all the events, their

individual cross-sections and the randoms associated with their phase space points go into output files (one per iteration). This information can be used to re-create the phase space variables and so produce histograms of the differential cross-section in invariant mass (qq), transverse momentum (q_T), rapidity (η), transverse mass (m_T), or minimum and maximum transverse momenta for the two photons ($p_T^{\text{min/max}}$), or alternative user-specified observables.

The Monte Carlo phase space integration selectively refines the grid from which it draws the randoms iteration on iteration so as to maximise the sampling where the integrand is largest; it does this by importance sampling [264] [265], more information on this is given in Appendix B.3. The result is each successive iteration should produce a more accurate estimate. In addition, the number of evaluations per iteration typically increases iteration on iteration (set by `nincrease`) and hence the statistical fluctuations also reduce.

A comprehensive review of how to use the `reSolve` program, its input and output options, parallelisation and other features is presented in Chapter 7.

There are several pragmatic choices made in the `reSolve` program in order to make its application computationally either quicker or simpler. We summarise these here for reference; however they are not of great consequence for using `reSolve` and the list is not exhaustive, with several other differences between the theoretical formalism and its practical computer program implementation in `reSolve` not outlined as they are inconsequential.

Firstly, our summation over Born cross-section contributions in determining the hard factors is process dependent to save time, explicitly not summing over contributions known to be zero. This introduces a process dependence not present in the theoretical framework. This is important as this section of the code is called once per Mellin space point and so is called at least 40 times for each branch of the 2 Mellin inverse transforms. These Mellin transforms are each in turn performed around 20 times for each impact parameter point in the inverse Fourier transform and the inverse Fourier transform is performed for each of the $\mathcal{O}(10^5 - 10^7)$ phase space points. As a result, this section of code may be called $\mathcal{O}(10^{9-11})$ times per program run, and so the speed of this section of the program governs that of the overall calculation. Any time savings which can be made therefore afford significant benefit.

A second difference between the theoretical formalism and the program is that the inverse Mellin transforms are performed over contours at 45 degrees (rather than 90 degrees) to the imaginary axis (displaced from it to avoid poles) to ensure better convergence properties.

Thirdly, problems can arise in regions when b is randomly chosen to be very large, these regions are otherwise uninteresting from the perspective of evaluating the resummed contribution but can nonetheless be reached in the program. In this case the collinear factors in the overall hard factor become very large as there is a large scale difference across which to evolve the relevant factors such as α_s and they are evolved to become close to the Landau pole, whilst the Sudakovs become correspondingly very small as they have the non-perturbative suppression

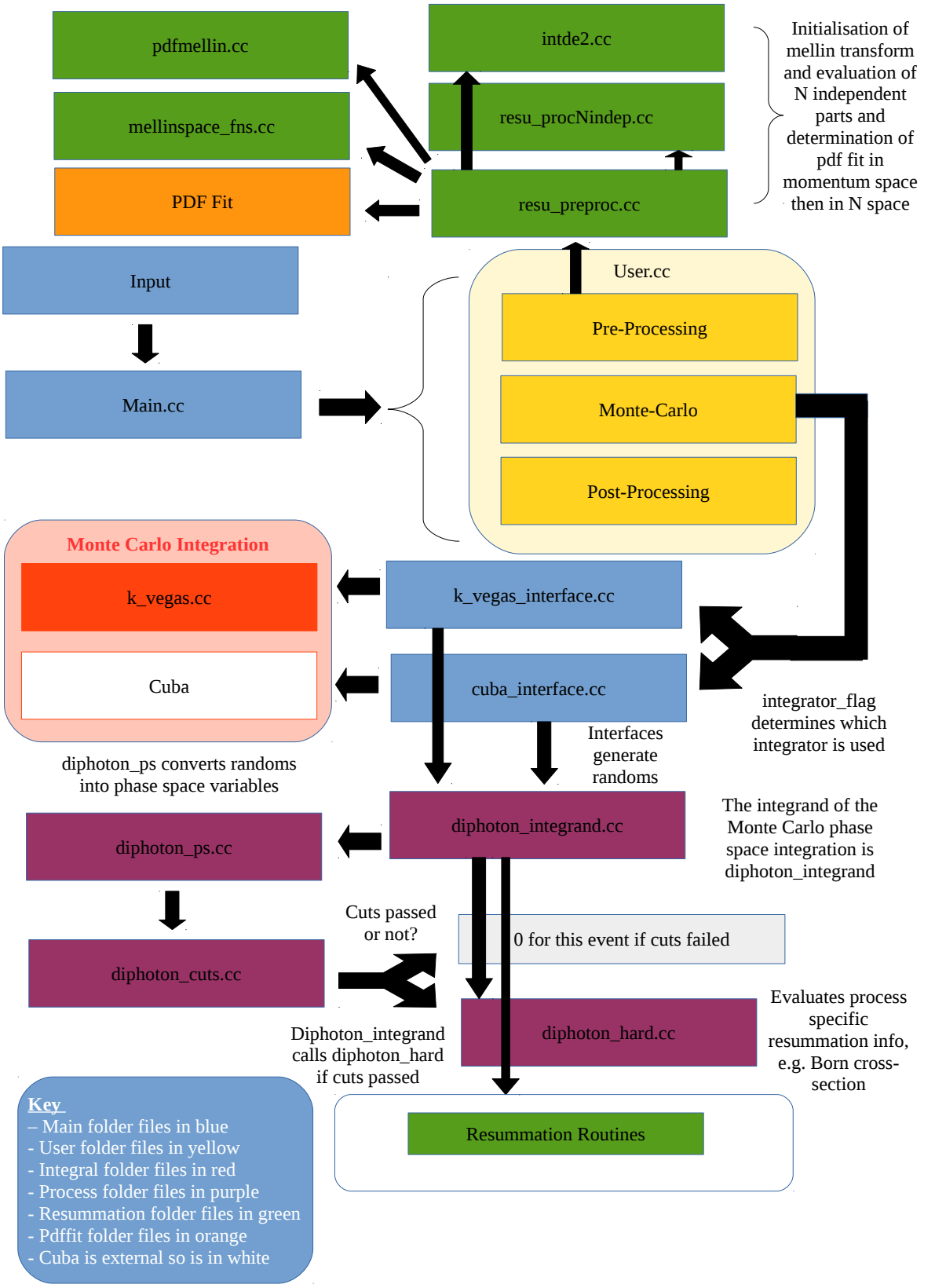

Figure 6.2: A flowchart demonstrating the different aspects included in the program and what is called when in the calculations. The different aspects of the program are coloured differently to indicate where they sit in the program folder structure. A zoom in of the resummation routines at the bottom of the flowchart is given in Figure 6.3. The program functions analogously in the case of Drell-Yan processes.

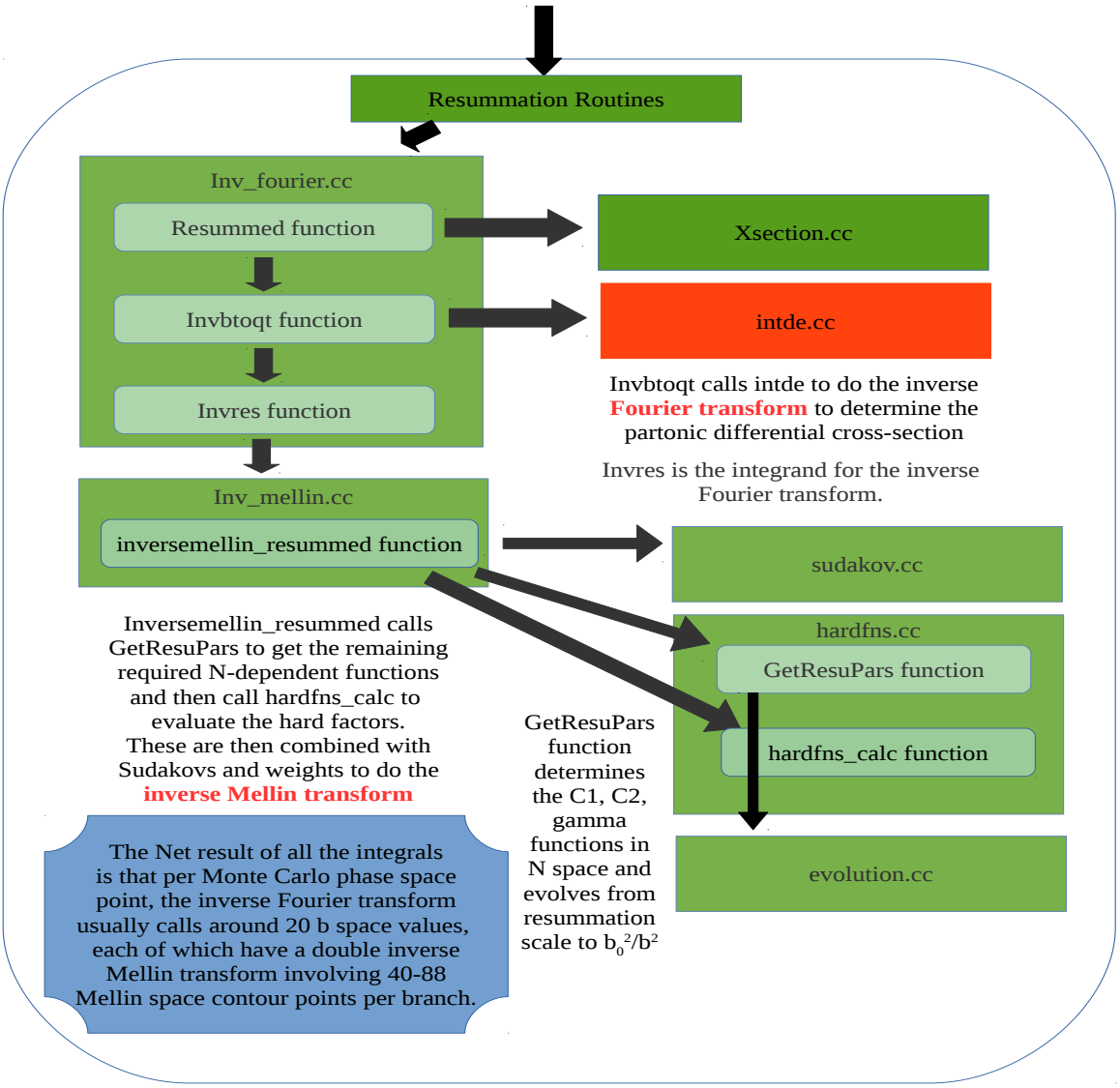

Figure 6.3: A flowchart providing more detail on the resummation aspect of the program, which is the main part of the calculation. This highlights how both the inverse Fourier and double inverse Mellin transforms are performed. This part of the program is process independent.

smearing of $\exp(-g_c^{NP} b^2)$ built-in to the formalism to account for these Landau pole effects. However, at such large b the hard factors can register as infinities, potentially causing problems in determining the inverse Fourier transform. To avoid this, b_{log} as given in equation 6.6 but with b_* in place of b is used in the Sudakovs, whilst b_* is used in the hard factors - this is found to offer greater numerical stability by cutting off particularly large values of b earlier in the formalism. This has no theoretical impact on the numerical output of the `reSolve` calculation, practically it is aimed at ensuring unphysical contributions do not swamp the actual answer and thereby improve the stability of the code if a large b value happens to be chosen by the double exponential inverse Fourier transform function.

Fourthly, to attempt further to avoid such issues, the hard factors and Sudakovs are combined

earlier in the calculation at the level of the Mellin space contour contributions (even though the Sudakov is independent of Mellin space variables), in order to pre-empt the appearance of very large and very small values separately in these factors and improve the accuracy of evaluation.

Finally, there is a difference in the parametrisations of the transverse momentum in the diphoton and Drell-Yan phase space, which has no physical or theoretical impact on the resummed differential cross-sections. In the diphoton phase space, in order to match events against other private codes (such as `2gRes`) used for verification of the `reSolve` program, the transverse momentum is chosen to lie along the x-axis. As a consequence, each event has its xy axes rotated with respect to all others and so individual particle momenta distributions for each of the two photons cannot be deduced directly. For the diphoton case this is not a problem as no such observables are relevant as the two photons cannot be distinguished. For the Drell-Yan case this is not as physically satisfactory, in the case of the $W^{\pm}$ boson production the lepton and neutrino can be distinguished and we may wish for differential distributions in the lepton or neutrino (missing) momenta. We must therefore know the relative orientation of the different events, requiring fixed xy axes; the q_T is therefore defined against fixed axes as $(q_T \cos\phi, q_T \sin\phi)$. Physically, this makes no difference as all observables (even $p_T^{\text{min/max}}$) are rotationally invariant in ϕ.

6.4 Production Channels

The `reSolve` program has been designed to allow the same overall program structure to be extended to many different processes of interest, this can even be performed by the user so they may tailor the program to their own needs. In any case, this process of addition of production channels of experimental and theoretical interest to the program is one the authors expect to continue in the future developments of the program and some of these targeted future additions are given in Chapter 7.3. Currently, only two processes are included, diphoton production and Drell-Yan production, chosen as they are amongst the most important modes at the Large Hadron Collider.

6.4.1 Diphoton Production

Prompt photons are an ideal probe of physics at hadron colliders; both in a theoretical sense due to their lack of QCD interactions, and in an experimental sense as their energies and momenta can be precisely measured in electromagnetic calorimeters and given the diphoton channel has a relatively large production rate. As a result of 4-momentum conservation, quark-antiquark annihilation must produce at least two photons[9] and so diphoton modes are relevant at hadron-hadron colliders. We therefore consider processes $pp \to \gamma\gamma X$ (or $p\bar{p} \to \gamma\gamma X$ for the Tevatron).

As a result of its clean experimental signature, the diphoton decay channel was a golden discovery mode for the Higgs boson at the LHC via $h \to \gamma\gamma$. Therefore hopes of understanding electroweak symmetry breaking and the Higgs boson itself make the diphoton channel a key focus for the LHC in both signal and background. In particular, as the centre of mass energy for collisions at the LHC has increased, higher diphoton invariant masses can be reached and similar resonance searches to those which revealed the Higgs in the diphoton channel can be utilised to search for new physics at higher masses. Many Beyond Standard Model theories, including supersymmetry (as described in Chapters 2-4) via its additional heavier CP even (H) and CP odd (A) neutral Higgs bosons, predict states which lead to resonances in diphoton invariant mass. As a consequence, there has been much experimental and theoretical effort aimed at thoroughly understanding and precisely predicting the Standard Model diphoton backgrounds arising from partonic processes producing diphotons. This enables the analysis of diphoton differential spectra with respect to these precise theoretical predictions and ensures any small deviations can be reliably interpreted as signs of much-coveted new physics states, whilst it also offers an excellent testing ground for perturbative QCD.

[9]Consider the possibility of single photon production, $q\bar{q} \to \gamma$, this is forbidden by energy and momentum conservation as if we Lorentz transform to the centre of mass frame of the colliding quark-antiquark pair they have zero net momentum but non-zero energy, this cannot occur for a photon as it is not possible to transform into its rest frame. Two photons must therefore be produced so that net zero momentum can be produced in the centre of mass frame, therefore diphoton modes are present at colliders, not single photon modes. Meanwhile if one takes the gg channel similar considerations mean two photons must be produced. Similarly the Higgs, as a scalar, must produce two photons rather than one as a result of angular momentum conservation.

We have therefore chosen the diphoton Standard Model background channel as one to include in our first versions of the `reSolve` program. At leading order this production channel is initiated by quark-antiquark annihilation, being a purely electromagnetic process it is $\mathcal{O}(\alpha_s^0)$; at NLO however the $qg \to \gamma\gamma q$ partonic sub-process becomes available which is order $\mathcal{O}(\alpha_s)$; whilst at NNLO the gluon-gluon box initiation process of Figure 6.4 opens up at order $\mathcal{O}(\alpha_s^2)$. This gg box contribution can have a significant impact on the production rate due to the large PDF of the gluon. Consequently, NNLO contributions (and correspondingly NNLL resummations) are known to be of substantial importance for precise theoretical predictions for this mode. We therefore include the diphoton background production process thus far at NNLL and all contributions up to this order are incorporated in `reSolve`, including the important gg box contribution. This includes the majority of the important NNLO corrections through the hard factors containing the virtual corrections but nonetheless will be soon updated to include the matched finite piece at NNLO so that then the diphoton process will be available at NNLO+NNLL. Our work in this area was guided by and verified against the private `2gRes` program [5, 6], as well as experimental data. The results, together with the cuts implemented for the diphoton case, are discussed in greater detail in Chapter 7.2.1. Of these cuts, a standard cut is to require that the larger of the two photon transverse momenta is larger than `pT1cut` and the smaller is larger than `pT2cut` (it must be defined as such as the individual photons cannot be distinguished from one another), whilst a cut on the opening angle between the two photons is required as two highly collimated photons may be interpreted experimentally as a single higher energy photon. This is mentioned here as it has a significant effect on the amplitude of the effects of the beyond LO corrections. At LO, there is no radiation to take away momentum and so the two photons are produced with exactly the same transverse momentum; this means both photons must have momenta greater than the larger transverse momentum cut, i.e. $\mathrm{Max}(q_T^{(\gamma,1)}, q_T^{(\gamma,2)}) = q_T^{(\gamma,1)} = q_T^{(\gamma,2)} >$ pT1cut $>$ pT2cut. Beyond LO however, radiation carries away transverse momentum and so one of the photons can have smaller transverse momentum, greater than the smaller q_T cut so that pT1cut $> \mathrm{Min}(q_T^{(\gamma,1)}, q_T^{(\gamma,2)}) >$ pT2cut is now an allowed non-cut region of phase space. This therefore opens up the phase space available and enhances the effect of NLO corrections. On top of this, an additional effect that ensures beyond LO corrections are large is that new partonic sub-processes open up at each order, thereby adding additional contributions beyond the α_s suppressed additional emissions to the previous order sub-processes [266].

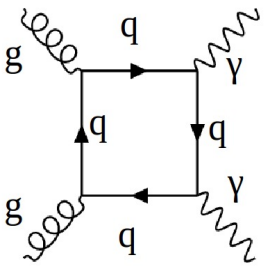

Figure 6.4: Gluon gluon box diagram contribution to diphoton production

Whilst `reSolve` concentrates on the resummed contribution to the diphoton cross-section, several programs are able to compute the finite (non-resummed) part of the differential diphoton cross-section, including `DIPHOX` [267] and `2gammaMC` [268] to NLO, and `MCFM` ("Monte Carlo for FeMtobarn processes") [269] and the private `2gNNLO` program [266] to NNLO. The `ResBos` program [252, 253, 270] includes the finite and resummed contributions up to NNLO+NNLL. Meanwhile, electroweak corrections up to NLO have been analysed in [271]. Many of these programs include the effects of fragmentation, which are not included in `reSolve` - photons may arise from fragmentation of partons, rather than just from the hard scattering partonic subprocess. This however depends on poorly known non-perturbative fragmentation functions for photons, on which there is no consensus in a resummation context. These effects can however be removed by photon isolation cuts, which are often performed at experiments[10].

The validation and results for the diphoton production channel in `reSolve` are presented in Chapter 7.2.1.

6.4.2 Drell-Yan Production

The second process included in the `reSolve` program is Drell-Yan production of lepton pairs [272]. Both neutral current Z on-shell or Z/γ^* off-shell producing a lepton-antilepton pair and charged current $W^{\pm}$, W^+, W^- (again on-shell or off-shell) producing a lepton and neutrino can be calculated in `reSolve` and are included up to NNLL in the resummed piece. The matched finite piece contribution is not yet included however, although it will be in the near future. The formalism naturally includes some beyond leading order corrections through the hard factors which incorporate effects of virtual corrections up to NNLO, however these are not the full NNLO corrections, consequently `reSolve` strictly only calculates the Drell-Yan process up to NNLL currently. Drell-Yan production is a particularly apt channel to include as it has been key to the development of the resummation formalism [7, 8, 223, 238, 239, 273]; its cross-section is largely produced at low transverse momentum with $q_T^2 \ll Q^2$ and so it is a blatant process for which resummation is needed. The Drell-Yan hadroproduction of lepton pairs has been of great importance at many hadron-hadron colliders, and continues to be so at the LHC; its clean signal of lepton pairs may be used as a standard candle due to its experimental and theoretical simplicity arising from the lack of strong interactions of the leptons produced. It also has a large production rate and these features mean it can be used for detector calibration and luminosity measurements. This production channel consequently has a variety of uses, having been the focus of much experimental and theoretical work. Drell-Yan production therefore provides an excellent test of perturbative QCD.

From an experimental point-of-view Drell-Yan production is also of tremendous interest; it is a key input for constraining PDFs, which are crucial to all production processes at hadron colliders. The W^+/W^- rapidity distributions are dependent on the PDFs. At a $p\bar{p}$ collider

[10] `2gRes`, used for the calculations in [5], uses an isolation prescription to mimic the experimental analysis results.

such as the Tevatron, the production of a W^+ is dominated by extracting a u from the proton and a $\bar{d}$ from the antiproton (i.e. $u\bar{d}$ dominates $\bar{d}u$ as the PDFs of the proton/antiproton favour quarks/antiquarks respectively). As the PDFs have larger momentum fraction in up quarks than down quarks in protons (and so more than antidown quarks in antiprotons) the W^+ boson is then dominantly produced along the proton beam direction at positive rapidity. Meanwhile for a W^- it is dominantly produced via $d\bar{u}$ and so is produced along the antiproton beam direction at negative rapidity. This is shown in the LO rapidity distributions for W^+ and W^- produced by `reSolve` in Figure 6.5. Measurements of the rapidity distributions therefore directly depend upon the momentum fractions of the quarks (and antiquarks via the sub-dominant modes) and so these distributions may be used to extract the PDFs for the valence quarks.

The rapidity asymmetries seen at the Tevatron are a direct result of the fact the beam environment is itself asymmetric as the Tevatron was a $p\bar{p}$ collider. At the LHC we have a proton-proton collider and so such rapidity asymmetries are no longer seen in the distributions. However, as both beams are now protons, W^+ are dominantly produced via u and $\bar{d}$ PDFs in the proton and the W^- are dominantly produced via d and $\bar{u}$ PDFs in the proton. Therefore the overall charge asymmetry gives access to the PDFs for the valence and sea quarks. This simplified picture is complicated by detector effects, measurement precision and beyond leading order corrections, nonetheless many of these systematics can be cancelled by considering asymmetries which are ratios or double ratios.

Overall, the Tevatron Drell-Yan production process probed quark PDFs down to momentum fractions $x \sim 10^{-3}$, with fixed target Drell-Yan probing quark and antiquark PDFs at higher x. Meanwhile at the LHC, high precision data on W and Z production is becoming an important part of modern PDF fits, with Z q_T data constraining the PDF of the gluon at intermediate x, which is crucial for Higgs production predictions. The Drell-Yan production process must therefore be accurately theoretically predicted as part of a drive to reduce theoretical uncertainties in both its own predictions and elsewhere.

On the other hand, Drell-Yan is also used to extract the W boson mass - for example from the transverse mass distribution which has an endpoint around m_W (as seen in Figure 7.14), or from the spectrum of the individual lepton transverse momentum which has a "Jacobian peak" at $m_W/2$ (seen also for the Z Drell-Yan as is clear in Figure 7.12). This lepton transverse momentum spectrum method is complicated by the W boson width, as well as QCD effects and experimental precision, and so the shape of the individual lepton transverse momentum distribution, rather than just the peak position, must be used. As the cross-section is dominated by low values of the overall transverse momentum of the lepton-antilepton pair, this shape information can only be accurately predicted once the effects of resummation of large logarithms at small q_T are accounted for. This highlights the importance of being able to accurately predict the transverse momentum spectrum and the need for resummed theoretical predictions of high precision. Indeed, the most precise determinations of m_W are from Drell-Yan at the Tevatron, for which we validate `reSolve` in Chapter 7.2.2. The W mass itself is an important electroweak precision observable for global fits as the close agreement of the values extracted from Drell-Yan

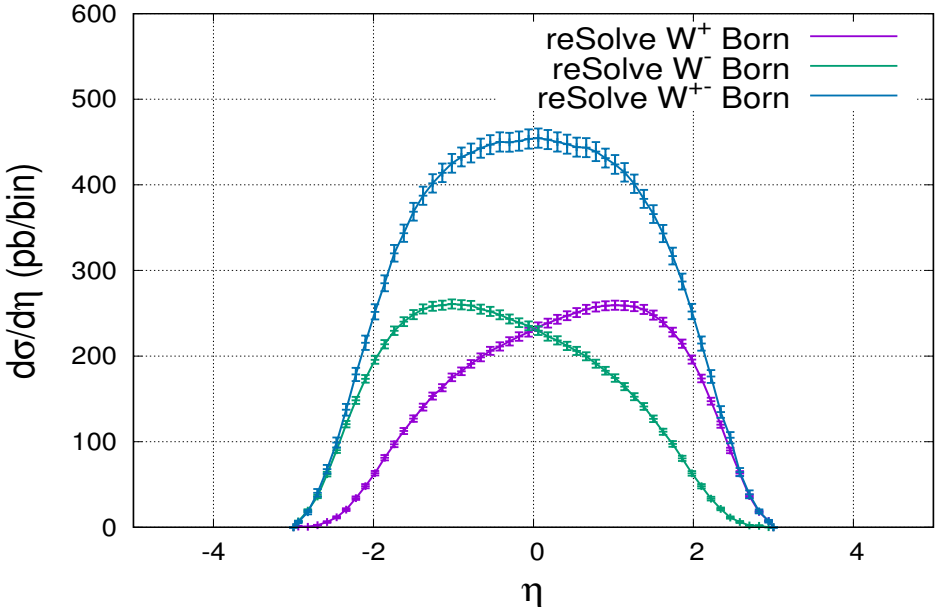

Figure 6.5: The leading order rapidity asymmetries in the W boson Drell-Yan production channel at the Tevatron, as arising from the difference in the momentum fractions carried by the up and down quarks. The W^+ boson follows the direction of the proton beam and the W^- boson follows the direction of the antiproton beam. The effect is averaged out when the W^+ and W^- are considered together. These were calculated by `reSolve`.

and measured indirectly is able to greatly constrain many Beyond Standard Model extensions.

Finally, not only is the Drell-Yan channel important as a test of perturbative QCD and for reducing theoretical errors for other analyses, in and of itself it also allows for the search for Beyond Standard Model extensions, with deviations at high invariant mass potentially indicative of new physics. This further necessitates the development of tools for precise predictions of differential spectra for the Drell-Yan channel. Models including W' and Z' particles would be observable as additional contributions at higher masses to such spectra, such particles arise in a variety of Beyond Standard Model theories: W' and Z' particles occur in $SU(2)^2$ (or indeed $SU(2)^n$ for $n > 1$) gauge groups; whilst Z's materialise from extra dimensional theories, $U(1)$ extensions of the Standard Model and Little Higgs Models [274][11]. Whilst Z' and W' production are not yet included in `reSolve`, the extension to include these modes is not of great difficulty and will be one of several future developments made.

As a result of its general applicability, as well as its comparative experimental and theoretical simplicity, Drell-Yan production is therefore one of the most precisely predicted and measured channels, approaching percent level precision both theoretically and experimentally. In order to produce such high precision theoretical predictions, QCD effects up to NNLO+NNLL have been determined; currently `reSolve` is able to calculate the resummed contribution to this process up to NNLL, whilst the matched finite piece will soon be added to enable NNLO+NNLL predictions to be generated. Furthermore, in order to improve the accuracy from several percent to one

[11] In Little Higgs models the Higgs is regarded as a pseudo-Goldstone boson from the breaking of a global symmetry near the TeV scale or higher.

percent, recent calculations are now including the effects of NLO electroweak corrections [275]. These effects can be important as $\alpha(m_Z) \approx 1/128 \sim \alpha_s^2(m_Z) \approx (0.1178)^2 \approx 1/72$ and so they are of the same order as NNLO QCD corrections. As of yet however, these electroweak corrections are not included in `reSolve`.

`reSolve` calculates only the resummed contribution to the Drell-Yan cross-section, which nonetheless is dominant; several programs determine the finite contribution, including `FEWZ` [275], `MCFM` [269] and many others. `ResBos` [252, 276, 277] and `DYRes` [7, 8], both can calculate the resummed contributions, the former including also the finite contribution and NLO QED effects if desired and the latter being the program against which `reSolve` has been validated. The program `DYNNLO` [278] can be used to compute the finite contribution and matched with the `DYRes` resummed contribution to determine the whole transverse momentum spectrum. Adding the finite contribution and consistently matching it with the resummed contribution in `reSolve` is a priority for both the diphoton and Drell-Yan channels for future developments.

The cuts implemented for the Drell-Yan channel experimentally to reduce backgrounds differ somewhat from those for the diphoton channel as the individual decay products may now be distinguished. These cuts may be applied in `reSolve` and differ between the neutral current and charged current channels due to the presence of an unmeasured neutrino for the W boson case. For the neutral current Z or Z/γ^* both final state leptons are detected, therefore the standard `pT1cut` and `pT2cut` have a different meaning to in the diphoton case, reflecting cuts on the transverse momenta of each of the leptons individually rather than together as they are distinguishable. Similarly, cuts on the rapidities of the produced leptons can also be applied individually for neutral current Drell-Yan. For the case of the charged current, the neutrino produced ensures different cuts must be devised; these are cuts specifically on the rapidity of the charged lepton and on its transverse momentum, `etaecut` and `pTecut` respectively. Cuts on the missing transverse momentum (assigned to the neutrino), `pTmisscut`, and on the transverse mass (as given in equation 5.15), `tmasscut`, may also be administered. Further descriptions of the cuts are given in the explanation of the input files for `reSolve` in Chapter 7.1.2.

The validation and results for the Drell-Yan production channel are detailed in Chapter 7.2.2.

6.5 Advantages of reSolve

Here we finish this section by listing, for ease of perusal, several of the advantages of the `reSolve` program for use in making theoretical predictions including resummation of transverse momentum logarithms.

- Accuracy - As `reSolve` uses the analytic b-space resummation formalism, it offers much greater accuracy than parton shower and other generally applicable programs for resummation, including up to NNLL. Such accuracy is key to precision measurements, which are required to enable the field to maximise the output of the LHC in both testing our understanding of the Standard Model and searching for new physics via small deviations in differential spectra.

- Modularity - `reSolve` has been carefully constructed so as to take maximum advantage of the near-universal nature of the analytic resummation formalism, with the code designed to be modular. As a result, on top of the diphoton and Drell-Yan processes already included, further processes can be added to `reSolve`. In principle its resummation module is generally applicable to a wide range of hadron collider processes producing colourless final states. There are very few such generally applicable and publicly available resummation programs at such accuracy, with public programs either using numerical resummation (parton showers) which is of reduced accuracy, or tending to be focused on specific processes.
- Customisable - The program structure allows the individual program sections to be used independently, should the user wish. This could be used to enable interfacing with other programs, for example with matrix element generators or other Monte Carlo codes.
- Transparent and well documented - A great amount of effort has been made to transparently document all the workings of `reSolve`, both in terms of the theoretical formalism applied and the program structure and flow. We hope this allows the program to be understandable to the user and less opaque. In turn this should enable users to utilise `reSolve` to maximum advantage.
- Parallelisable - The `reSolve` program has been explicitly designed with parallelisation in mind and includes `bash` scripts which enable the parallelisation of the program. This is unique amongst programs in this area and permits a greater number of Monte Carlo evaluations to be performed, reducing this source of theoretical error. A description of the parallelisation is given later in Chapter 7.1.6.
- Works straight out of the box - The `reSolve` program package contains all the necessary files and external programs to work straight out of the box for the user, with simple input and output files (as described in Chapters 7.1.2 and 7.1.3). This should encourage its use in the field and goes hand-in-hand with its transparency and well-documented nature.
- Histogrammer - In keeping with these endeavours to ensure `reSolve` is as usable as possible, `reSolve` immediately produces differential spectra in the desired observables from the events generated. This simplifies the process of making these theoretical predictions, with no further work required outside of the `reSolve` package for the resummed contribution.
- Fully differential - The analytic resummation formalism applied is fully differential; this means that not only the transverse momentum spectrum at which it is aimed, but any arbitrary differential cross-section, can be predicted. It does so by keeping the full event information and the cross-section and weight for all individual events, these may then be combined to compute any differential spectra. Those included in the package are invariant mass, rapidity, minimum and maximum transverse momenta of the individual final state measured particles, and transverse mass; however others can easily be added as described later in Chapter 7.1.8.

Chapter 7

Use and Results of reSolve

In this chapter, we explain the usage and results of the `reSolve` program. We begin by outlining its input and output files and then examine some more specific aspects of its use, including the PDF fits which must be performed, the histogrammer program contained within the package and how to set up `reSolve` for parallelisation. We also present a summary of how new processes and new observables may be added to the program, emphasising its generality of application. Following this, the validation and results for the two production channels included so far, diphoton and Drell-Yan, are examined in detail. Finally we end the chapter with a discussion of the future developments we aim to undertake to `reSolve`, given it is only in its first main version currently. Many of these details have been given previously in our paper [2]. The `reSolve` program itself is provided with this thesis.

7.1 How to use reSolve

The new Monte Carlo parton-level differential cross-section resummation tool `reSolve` is available publicly with both our paper [2] and on `GitHub` at `https://github.com/fkhorad/reSolve`.

7.1.1 Basic Usage

Here we list the steps required to download and use the `reSolve` program:

- Extract the zipped tarball `reSolve.tar.gz` to the desired working directory.
- Enter the makefile, found in `code/src` and adapt any compilation flags as appropriate to your machine. If you wish to use the `Cuba` integrator [264], rather than the built-in `k_vegas` integrator provided with the code, you need to provide the path to its location in your machine. Interface codes for both `k_vegas` (our integrator) and `Cuba` are provided within the program and the relevant interface is automatically used once the integrator chosen is given in the input file, see Chapter 7.1.2.
- Finally run ‘‘`make`’’ to compile the program and produce the `./reSolve.out` executable. `reSolve` is then ready to use.
- Running the program involves simply entering in the terminal `./reSolve.out` {`path to input file`}, e.g. `./reSolve.out input/Wpm_NNLL_Tevatron.dat`.
- The output working directory to which the output is directed is included in the input file. In order to avoid overwriting or corruption of events, `reSolve` will not run if there are already events (or a

file ‘‘reSolve_main_out.dat’’) in the specified folder. To re-run into the same folder either move or delete the event files so the working directory for the output is empty before running.

- The reSolve program will then run and generate events for this setup, with the total cross-section output in reSolve_main_out.dat (or reSolve_main_out_END_ITER.dat for k_vegas parallelised cases). The events are also output into the same specified output folder, along with any specified histogram data files for the desired differential cross-sections, in particular for the q_T spectrum[1].

7.1.2 Input

The input for the reSolve program is read from a single flexibly-styled, customisable input file. This input file is made up of a variety of sections, each dealing with a different type of input information required by the program, and which are described below. There are a plethora of input flags available that allow the user to tailor the program to their needs and we detail many of these here. A sample input file is given in Figure 7.1; this is the Diphoton_NNLL_test_1.dat input file representing the inputs listed later in Table 7.2, and is one of several sample input files presented with the program in the folder "input/", these are summarised later in Table 7.1. The sections making up the input file, which are purely a construction to make them more human-readable, are as follows:

1. Basic - The first section includes general input. These are the process, which is 1 for diphoton resummation or 2 for Drell-Yan resummation - the only processes so far incorporated. If Drell-Yan is selected then one must also chose the specific Drell-Yan process via the DYprocess flag; 1 = W^+, 2 = W^-, 3 = $W^\pm$, 4 = Z only, 5 = Z/γ^*. In addition, the DYnarrowwidthapprox flag allows the calculation of the on-shell only cross-section if it is set to 1. The order flag obviously indicates the order of the calculation (leading order (0), next-to-leading order (1) or next-to-next-to-leading order (2)) and the resum_flag turns the resummation on (1-default) or off (0). pdf_flag allows for the PDFs input into the program to be changed. Currently it is set to 82 indicating the MSTW (Martin-Stirling-Thorne-Watt) 2008 set [279] at NNLO - MSTW is the only set currently incorporated into the program, the program is nonetheless set up to make this easy to change between PDF sets. 80 offers the LO MSTW set and 81 the NLO MSTW PDF set. The MSTW PDF sets are read from ‘‘Grids/’’ in the main program directory. CM_energy indicates the collision energy of the protons/antiprotons in the centre of mass frame in GeV and ih1/2 indicate whether beam 1 and beam 2 are proton (1) or antiproton (-1) beams. save_events is set to 0 if only the total cross-section is required; however to produce differential cross-sections the events must be saved and therefore save_events should be set to 1 to indicate the events will be saved in "easy" form (an output file in "easy" form is given in Figure 7.2) or alternatively to 2 which is a "pseudo-lhe" (i.e. pseudo Les Houches Events) form. Finally workdir sets the working directory to which the events are output.

[1] Histograms are only generated for those variables and binnings specified in the input file in the "Histograms" section, nonetheless histograms can be calculated for previously calculated events using the hist_only mode - see Chapter 7.1.5.

2. Scales - This section sets the three scales involved in the resummation formalism, which were outlined in Chapter 5.5. The factorisation scale `mu_F` (μ_F) encapsulates scale dependence as a result of the factorisation of the input and output processes of the collision - this is the scale from which the PDFs are evolved. The renormalisation scale `mu_R` (μ_R) dependence arises from the scale at which the α_s coupling is evaluated. The resummation scale `mu_S` (μ_S) results from the truncation of the resummed expression at a given perturbative order, parametrising the ambiguity stemming from the precise definition of the logarithmic terms which are being resummed. Should the user wish to set μ_F, μ_R, μ_S directly to fixed values throughout the resummation this is done here; in that case one must ensure that also the flags `muR_flag` and `muF_flag` are set to 0. However, rather than fixed scales one can set the values of μ_F^2, μ_R^2, μ_S^2 to fixed fractions of the Q^2 invariant mass of each generated event. To do this set `muR_flag` and `muF_flag` to 1 and μ_R, μ_F to the desired fraction of Q^2; the resummation scale μ_S will be set to half the renormalisation scale μ_R in this case, as is the convention. Here one may also specify the parameter `mu_min`, which is the starting minimum scale from which the PDF fit factorisation scales are calculated, see Chapter 7.1.4 for more information.

3. Integration - This section deals with the inputs specific to the Monte Carlo phase space integration. `maxeval`, `nstart` and `nincrease` correspond to the approximate maximum number of Monte Carlo evaluations to perform in total across all iterations[2], the number of evaluations to perform in the first iteration, and the number of additional evaluations in each subsequent iteration. Therefore the number of evaluations in the n^{th} iteration is given by $n_{eval} = n_{start} + (n-1)n_{increase}$, and the total number of evaluations across N iterations is $n_{tot} = Nn_{start} + \frac{1}{2}N(N-1)n_{increase}$. The program will stop after a whole number of iterations once this number of evaluations n_{tot} exceeds `maxeval`. The `integrator_flag` determines which integrator algorithm is used - either our own internal `k_vegas` Monte Carlo implementation is used for `integrator_flag`= 1 or an external `Cuba` Monte Carlo implementation [264] is used for `integrator_flag`= 2. Note that `Cuba` will automatically parallelise over the number of cores in the computer used whilst `k_vegas` will not. `multi_machine` sets whether you wish to use parallelisation with `k_vegas`, with 0 indicating not and 1 indicating parallelisation; it allows the user to run different batches on different cores/computers and combine them all after each iteration. `seed` is used to set the seed for the randoms used for the Monte Carlo phase space integration by `k_vegas` or `Cuba`. This can be used to set the seeds for the randoms for the Monte Carlo integration based on time (-1) or a random repeatable set of uniformly distributed seeds (0). If one is using parallelisation with `k_vegas`, one can set -2 to ensure each batch has a different seed, here the seed is set based on the machine tag but is deterministic and repeatable.

[2]This is not true in the `k_vegas` parallelised case, as described in Chapter 7.1.6, here the number of total iterations is set via the number of iterations desired per core and the number of parameter points per core per iteration.

4. Resummation - Here are various process-independent settings for the general resummation implementation, this is the key part of the program. The maximum and minimum values of the invariant mass squared Q^2, transverse momentum squared q_T^2 and rapidity η, are all set here[3] via `QQ_Max`, `QQ_Min`, `QT_Max`, `QT_Min`, `eta_Max` and `eta_Min`. `gqnp` and `ggnp` are factors to account for non-perturbative corrections to the Sudakovs; they factor in uncertainty from very low $q_T \sim \Lambda_{QCD}$ and are given in equation 6.9 in Chapter 6.2.1. In addition, here one may set the variables `en_sec_multiplier` and `PDF_fussiness` which are related to the PDF fit files used. More detail is given later in Chapter 7.1.4. Further PDF fit options are also available; `PDF_fitonly` can be set to 1 to run the code to obtain the PDF fit file without running the whole resummation. This can be useful if running parallel batches, starting without the PDF fit file here causes all batches to attempt to evaluate the fit and this will increase the time taken to run the code (as it will wait for the slowest core to complete the fit). It could also lead to inconsistencies in the fit used.

5. Process Inputs - Penultimately, there are the process-specific inputs.
   (a) Diphoton - We first describe the diphoton process inputs. These include `boxflag`, which allows the user to include (1) or not (0) the $gg \to \gamma\gamma$ box diagram (see Figure 6.4 in Chapter 6.4.1), or even to only have this contribution to the process (`boxflag`= 2). The diphoton cuts are also given here, these are: `crack1/2` which indicate if a crack in the rapidity sensitivity of the detector is present (often 1.37 to 1.56 for the LHC); `etaCut` which should be less than or equal to Min(|`eta_Min`|,|`eta_Max`|); and `pT1cut` and `pT2cut`, which cut based on the q_T of the photons. It is required that Max($q_T^{\gamma_1}, q_T^{\gamma_2}$) >`pT1cut` and Min($q_T^{\gamma_1}, q_T^{\gamma_2}$) >`pT2cut`. Finally `Rcut` is a cut placed on the opening angle of the two photons produced as two highly collimated photons may not be resolved experimentally, we require $\Delta_R = \sqrt{(\eta_1 - \eta_2)^2 + (\phi_1 - \phi_2)^2} >$ `Rcut`.
   (b) Drell-Yan - These process-specific inputs similarly detail possible cuts required. First there are the usual general cuts described for the diphoton section - `crack1/2`. Then there are specific cuts for different Drell-Yan sub-processes; `pT1/2cut` are also available for the neutral current Drell-Yan case, whilst then `eta1cut` and `eta2cut` cut on the rapidity of the produced Drell-Yan leptons. In the case of charged current Drell-Yan, the observables are different as the neutrino is not observed. The standard cuts are `etaecut` - a cut on the rapidity of the produced charged lepton, `pTecut` - a cut on the transverse momentum of the charged lepton produced, `pTmisscut` - a cut on the missing transverse momentum of the event (assumed to be from the (anti-)neutrino), and `tmasscut` - a cut on the transverse mass of the event as defined by $m_T = 2(|p_{T1}||p_{T2}| - p_{T1}.p_{T2})$ (the massless limit of equation 5.15). The cut requirements are $|\eta_e|$ <`etaecut`, $p_T^{(-)\nu}$ >`pTmisscut`, $p_T^{e^\pm}$ >`pTecut` and m_T >`tmasscut`.

[3] It should be noted that the invariant mass, denoted Q or q throughout this thesis, is denoted as QQ in the `reSolve` program.

6. Histogram - Finally, the input file may be supplemented with inputs to the histogrammer, which is incorporated within `reSolve` to determine the histogram files for the desired differential spectra directly. For each differential cross-section desired, one line must be added to the input file of the form "`histo: {variable} {additional info}`" where the variables available are "qT", "qq" (invariant mass), "eta", "mT", "pTmin" or "pTmax" as described in Chapter 7.1.5. The histogrammer can also be used alone on previously generated events using the flag `hist_only:1`.

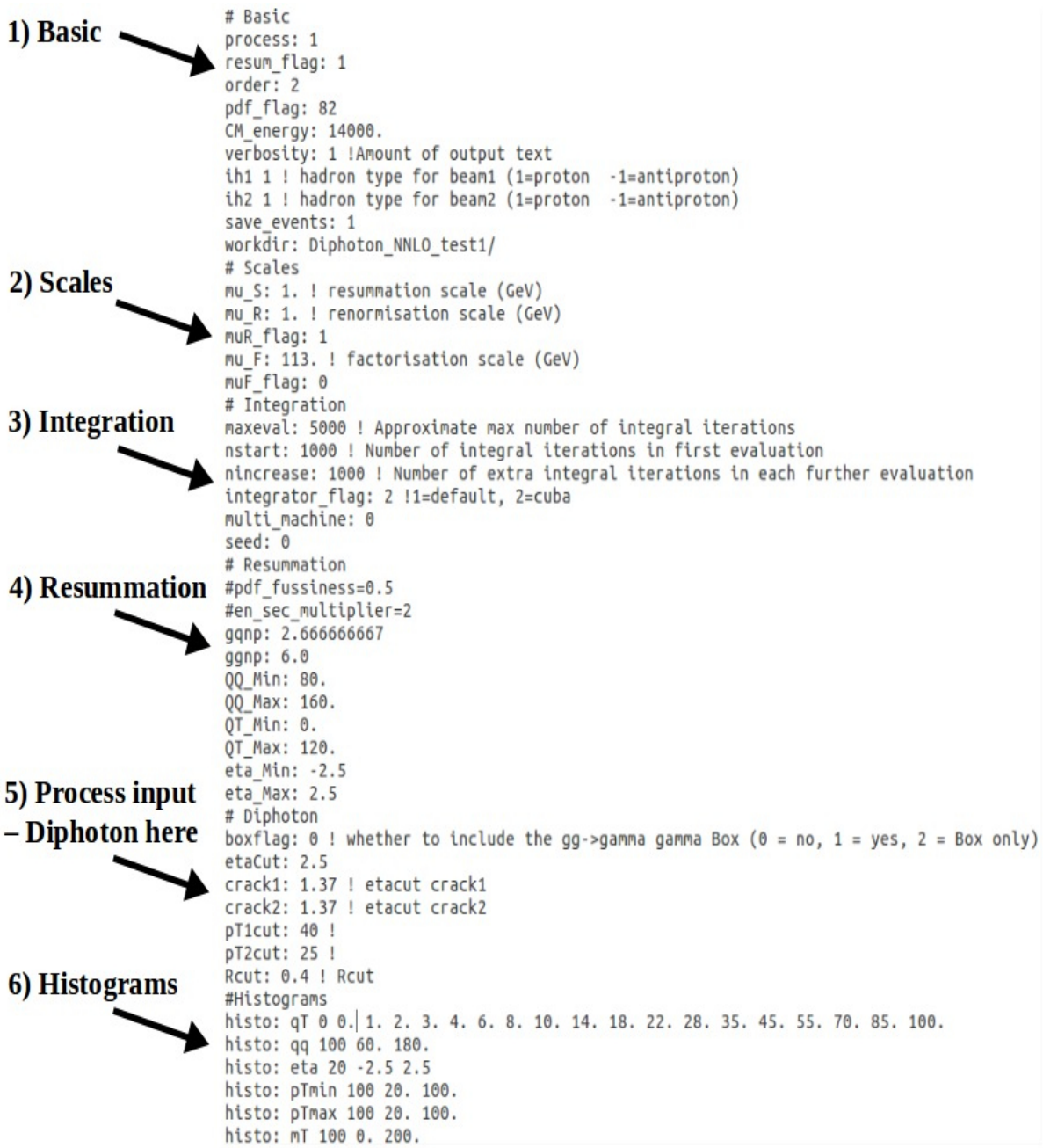

Figure 7.1: Input file for `reSolve`, this file shown is the example file found in `input/Diphoton_NNLL_test_1.dat`. It is split up into appropriate sections - Basic, Scales, Integration, Resummation, Process-specific input (diphoton in this case), and Histograms.

Several input files are provided as part of the `reSolve` package, one for each main use and validation of the program. These are used throughout the validation and results in the remainder of this chapter and are summarised in Table 7.1.

Diphoton Input Files Included	Description
`Diphoton_Born_LHC.dat`	Leading-order diphoton production, LHC 14 TeV
`Diphoton_Born_LHC_parallel.dat`	Leading-order diphoton production, LHC 14 TeV, setup for `k_vegas` parallelisation
`Diphoton_NNLL_test_1.dat`	NNLL diphoton production, LHC 14 TeV
`Diphoton_NNLL_test_1_parallel.dat`	NNLL diphoton production, LHC 14 TeV, setup for `k_vegas` parallelisation on one machine
`Diphoton_NNLL_test_1_parallel_multi.dat`	NNLL diphoton production, LHC 14 TeV, setup for `k_vegas` parallelisation across many machines
`Diphoton_NNLL_test1_twopdffits.dat`	NNLL diphoton production, LHC 14 TeV using two PDF fits at different scales across the invariant mass range
`Diphoton_NNLL_test1_fourpdffits.dat`	NNLL diphoton production, LHC 14 TeV using four PDF fits at different scales across the invariant mass range
`Diphoton_NNLL_test_2.dat`	NNLL diphoton production, LHC 8 TeV
`Diphoton_Atlas_A.dat`	NNLL diphoton production, LHC 8 TeV, setup for experimental comparison
Drell-Yan Input Files Included	**Description**
`Wpm_Born_Tevatron.dat`	Leading-order $W^{\pm}$ production, Tevatron
`Wpm_NLL_Tevatron.dat`	NLL $W^{\pm}$ production, Tevatron
`Wpm_NNLL_Tevatron.dat`	NNLL $W^{\pm}$ production, Tevatron
`yZ_Born_Tevatron.dat`	Leading-order Z/γ^* production, Tevatron
`yZ_Born_Tevatron_parallel.dat`	Leading-order Z/γ^* production, Tevatron, setup for `k_vegas` parallelisation
`yZ_NLL_Tevatron.dat`	NLL Z/γ^* production, Tevatron
`yZ_NNLL_Tevatron.dat`	NNLL Z/γ^* production, Tevatron
`yZ_NNLL_Tevatron_parallel.dat`	NNLL Z/γ^* production, Tevatron, setup for `k_vegas` parallelisation on one machine
`yZ_NNLL_Tevatron_parallel_multi.dat`	NNLL Z/γ^* production, Tevatron, setup for `k_vegas` parallelisation across many machines
`Z_OnShell_Born_LHC.dat`	Leading-order on-shell Z production, LHC
`Z_OnShell_NLL_LHC.dat`	NLL on-shell Z production, LHC
`Z_OnShell_NNLL_LHC.dat`	NNLL on-shell Z production, LHC

Table 7.1: The sample input files included with the `reSolve` program download for the diphoton and Drell-Yan processes, these are used later in the validation of `reSolve` and in results generation, see Chapters 7.2.1 and 7.2.2 for more information on the input files and for the corresponding results and histograms. As emphasised previously, currently `reSolve` calculates only the resummed piece, not the matched finite piece, consequently results are labelled "NLL" and "NNLL" as formally they do not include the full set of finite NLO or NNLO contributions.

7.1.3 Output

The output of the `reSolve` program comes in three parts: the total cross-section, the events, and the histogram binning data for the differential cross-sections. These are all determined from the individual event-by-event cross-sections generated by the program. The events are split into iterations, with the cross-sections used to update the Monte Carlo grid assigning weights to the different parameter space points and refining the grid so that the events are generated where the integrand is largest. The total cross-section estimate is given by the Monte Carlo iteration on iteration, it is output after each iteration to the terminal and is $\frac{1}{N}\sum_i w_i f_i$; here the sum is over the points sampled i, w_i is the weight of each phase space point, N is the total number of samples and f_i is the cross-section estimate for each phase space point. The error estimate meanwhile is given by the square root of the standard variance given in equation 7.1; the factor of $N-1$ ensures we obtain the variance of the mean rather than of the f_i evaluations:

$$\text{Var} = \frac{1}{N-1}\left[\frac{1}{N}\sum_i (f_i^2 w_i^2) - \left(\frac{1}{N}\sum_i (f_i w_i)\right)^2\right]. \tag{7.1}$$

The Monte Carlo cross-section values for the iterations and their error estimates are then combined by weighted average, where the weights are the inverse of the variance estimates. The total cross-section accumulated across all iterations is output into the file ‘‘`reSolve_main_out.dat`’’, or the file ‘‘`reSolve_main_out_END_ITER.dat`’’ if run across many machines. The error given on the cross-section is consequently only approximate and should only be used as a judgement after a few iterations. After each iteration, the grid used to weight the Monte Carlo events is updated; the chi-squared gives an indication of how well the grid approximates the integral, this is estimated via the difference between the weighted events and the cross-section estimate at that iteration (the mean), weighted according to the variance. This chi-squared should be divided by the number of degrees of freedom (which is equal to the iteration number minus 1) to understand how good the estimate is. This is produced as described in [265] and in the `Cuba` package [264], see also Appendix B.3.

In order to generate the histogram differential cross-section data, the events must be saved. By default events are output in the “easy” form into the `workdir` specified; the events are split into a different file for each iteration of the program. A sample output event file (in the “easy” form) is shown in Figure 7.2. Each event details the 4-momenta of the incoming partons, the 2 outgoing particle 4-momenta, the random values used to define the phase space point by the Monte Carlo and finally the event cross-section (in pb) and event weight. The events will all be automatically read by the histogrammer to determine the histograms specified in the input file. To determine the differential cross-sections, the histogrammer performs weighted averaging analogous to that undertaken in the evaluation of the total cross-section, but does so now bin by bin in order to produce a fully differential cross-section in whichever observables are required.

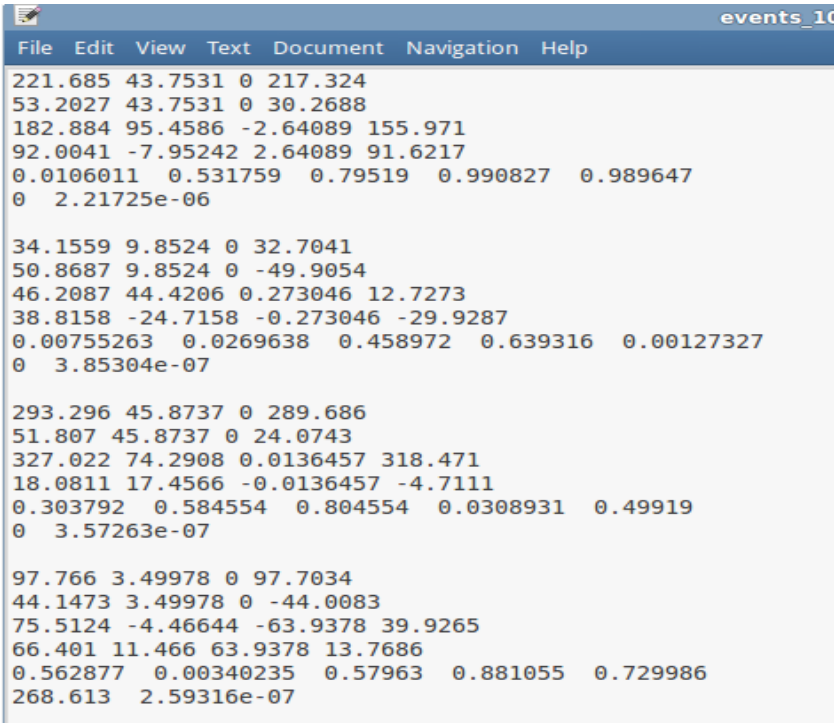

Figure 7.2: Output file of `reSolve`, this file is in the "easy" form. In this form each event is represented by six rows of information and followed by a blank row. The first two rows are the 4-momenta of the incoming partons, the next two rows are the outgoing photon four-momenta, the fifth row is then the set of 5 random values between 0 and 1 used to generate this event and its momenta. These randoms set the invariant mass squared - $Q^2 \equiv qq^2$, the transverse momentum squared - q_T^2, the rapidity - η, and the θ and ϕ opening angles of the two photons in the diphoton centre of mass frame. Finally the last row gives the value of the cross-section (in pb), 0 if cut, and the weight of the event in the Monte Carlo.

7.1.4 PDF Fits

In order to implement the b-space resummation formalism of [251] (and references therein), the PDFs must be defined in Mellin space at generic complex values. This requires that we perform an analytic fit for the PDFs (as a function of x, at fixed scale), which may then be Mellin transformed to obtain the PDFs along the Mellin inversion contour[4]. This PDF fit is done at the very start of the program once and for all. If a fixed scale or a narrow range of invariant masses are used, a PDF fit at a single factorisation scale is satisfactory, indeed this is what is traditionally done in such resummation programs. In this case, the single fit is done at the input fixed factorisation scale μ_F at a momentum fraction set via $x_{\max} = (QQ\_Max/CM\_energy)^2$. However, in cases where the invariant mass squared region considered is broad and one has a dynamical factorisation scale, then one may wish to improve precision by running with multiple PDF fits at various scales in the allowed invariant mass range. This possibility has been built into `reSolve`, in order to do this set `muF_flag` and `mu_F` to 1 and set the variable `en_sec_multiplier` accordingly. It should be noted however that the first version of the program is currently

[4]The PDFs do not need to be Fourier transformed as they have no q_T dependence, they do however gain b dependence from evolution of the PDFs from μ_F to the relevant scales in b-space.

significantly slower for multiple PDF fits[5] therefore we only recommend using this option in particular cases where very wide invariant mass regions are used or if very accurate predictions are required. A precise comparison of the runtime with one and multiple PDF fits is given in Table 7.6, this will be optimised in future versions. The energy scale at which the PDF fits are performed is determined by the invariant mass range and the `en_sec_multiplier` (E_n) variable. The starting scale is taken as QQ_Min, but this can be reset by setting `mu_min` in the input file, the program starts with the scale $Q\_start = \mathrm{Max}(mu\_min, QQ\_min)$. By default the value of `mu_min` is 20 GeV. The setting of the scales for the multiple PDF fits is as follows:

1. To determine the first value of the factorisation scale at which a PDF fit is performed, `reSolve` calculates $QQ\_temp = Q\_start \times E_n$; provided this is less than the QQ_Max then the scale the first PDF fit is performed at is then $QQ\_Min \times \sqrt{E_n}$, i.e. the geometric mean of QQ_Min and the new scale QQ_temp. The program will then go on to perform another PDF fit, see step 3.
2. If however $QQ\_temp > QQ\_Max$ then `reSolve` performs just one fit at the geometric mean of the endpoints of the invariant mass range, $\mu_F = \sqrt{QQ\_Min \times QQ\_Max}$.
3. If in the previous steps, $QQ\_temp < QQ\_Max$, `reSolve` will perform a PDF fit at a further scale. Once more, the program will take the scale of the previous fit and multiply it by E_n giving a new scale $QQ\_tempnew = QQ\_tempprev \times E_n$ and compare this new scale (which in the second fit case would now be $QQ\_Min \times E_n^2$) with QQ_Max. Again if the new scale $QQ\_tempnew < QQ\_Max$ then the PDF fit will be performed at the scale $\mu_F = \sqrt{QQ\_tempprev \times QQ\_tempnew}$. $QQ\_tempnew$ then becomes $QQ\_tempprev$ and we repeat this step 3 until $QQ\_tempnew > QQ\_Max$. Once $QQ\_tempnew > QQ\_Max$, the final fit is performed at $\mu_F = \sqrt{QQ\_tempprev \times QQ\_Max}$.

The process to fit the PDFs can take several minutes depending on the number of fits required. In order to avoid unnecessary fits being made, `PDF_fussiness` allows nearby previously calculated PDF fits in the `pdf_fits` folder to be used, for example setting it to 0.02 will ensure that PDF fits made at a scale within 2% of the desired μ_F are used rather than a timely, completely new fit being performed. By default `PDF_fussiness` will be set to 0.01 if no input is provided. Whether a PDF fit is appropriate is set by the factorisation scale of the fit, the maximum momentum fraction x_{max} (which will be different for the same factorisation scale if the centre of mass energy of the collider is different) and the PDF set used (for now LO, NLO or NNLO MSTW PDFs only are included).

As an aside and to be complete in our description, we comment here that we use the fixed flavour scheme for the PDFs, with a number of active (massless) flavours that can be set from input but is typically set to 5. Meanwhile, the form to which we fit the PDFs is the conventional

[5] Essentially this is an issue of memory access - we have a PDF fit for each beam for each parton (8 corresponding to up valence, down valence, anti-up, anti-down, strange, gluon, charm and bottom), with 8 fit parameters in up to 14 different rapidity regions at each of up to 136 points per branch on the Mellin contour, on top of this we then have a fit for each different fit energy scale where multiple PDF fits are used. This therefore quickly builds up a huge PDF fit grid, which in our crude current implementation can cause slowdown in reading the appropriate values.

form given below which is proportional to a positive power of x and to a positive power of $(1-x)$ to ensure the PDFs correctly go to 0 as $x \to 0, 1$. These are multiplied by a polynomial in $\sqrt{x}$, for which the highest power in the polynomial, aa, can be altered. This conventional form is also used in `2gRes` and `DYRes` and mimics the form of PDF fits performed by MSTW [279]. The form is

$$f = a_1 x^{a_2}(1-x)^{a_3}(1 + a_4 x + a_5 x^{\frac{1}{2}} + a_6 x^{\frac{3}{2}} + a_7 x^2 + a_8 x^{aa}), \tag{7.2}$$

with aa a constant which can be set within `reSolve` in `Utility/constants.h`[6].

For validation plots for running the `reSolve` program with multiple PDF fits please see Chapter 7.2.1.3, Figures 7.7 and 7.8.

7.1.5 Histogrammer

In order to produce the required differential distributions from the event-by-event cross-sections produced by `reSolve`, the cross-sections must be binned in the desired phase space differential variables. In the spirit of making `reSolve` a simple to use and independent package, a histogrammer package is included which can be used to read in the events produced by `reSolve` and bin them to produce the necessary differential cross-section histogram data. In fact, `reSolve` will automatically produce the histogram data if the user includes a few lines in the usual `reSolve` input file detailing the desired histograms and the binning. In the section "Histograms" a line must be added for each desired histogram; begin by indicating this is histogrammer input with "`histo`" at the start of the line, and then follow by the variable for the histogrammer, the number of bins required and the start bin lower bound and final bin upper bound. This will then calculate the events in each bin for the number given of evenly spaced bins across the range specified. The option {`variable`} can be `qT`, `qq`, `eta`, `mT`, `pTmin` or `pTmax` for the transverse momentum spectrum, invariant mass spectrum, rapidity distribution, transverse mass distribution and distribution of the minimum/maximum transverse momentum of the (two) outgoing particles respectively. Further variables for differential spectra can be added by the user, as described in Chapter 7.1.8. To be specific, the form of the lines required in the input file is:

```
histo: {variable} {no. of bins} {start bin lower end} {final bin upper end}.
```

If the user requires unevenly distributed bins, enter a "0." where the number of bins is input, and instead proceed by entering the endpoints of every bin. This is useful in allowing finer bin spacings at the lower end of the transverse momentum spectrum, where resummation is crucial.

Histogram information will only be calculated for each variable specified, therefore if no lines specifying the histogram information to be calculated are included in the input file, the `reSolve` program will produce the events and total cross-section only. These events can then later be used to determine the differential cross-sections required by using the `reSolve` package

[6] In order to compare against the codes `2gRes` and `DYRes` different values of aa must be used, with the former using $aa = 2.5$ and the latter using $aa = 3$. Of course, any differences caused by different aa values and consequent PDF fit differences are a source theoretical error associated with the PDF fit.

in `hist_only` mode. In order to run the histogrammer alone, for example should the user wish to re-bin the events or determine further histograms not initially specified in the input file, one must include the `hist_only` flag set to 1. In `hist_only` mode `reSolve` will assume by default that the event files are in "easy" form corresponding to setting the `save_events` flag to 1 for the initial event generation, if instead the user wishes to read in lhe events then "`save_events: 2`" must also be included in the input file for the `hist_only` run. For either event file form `reSolve` will then read the event files specified in `workdir` and determine the histograms specified by the input lines of the form given earlier in this section. Histogram data files for each of the desired differential distributions are produced; these are "`histo_0_qT.dat`", "`histo_1_qq.dat`", "`histo_2_eta.dat`", "`histo_3_mT.dat`", "`histo_4_pTmin.dat`", "`histo_5_pTmax.dat`". Each of these files lists the centre-points of each bin and the corresponding normalised cross-section in that bin followed by a "0" column (the error in the position of the bin) and a column listing the estimate of the error in that bin. It is important to note that the histogrammer produces the cross-section in each bin normalised by the bin width (rather than the total cross-section in the bin). This ensures the amplitude is independent of the binning used. For many of the validation and results figures in this thesis in Chapter 7.2, the histogram data used is provided with our paper [2].

7.1.6 Parallelisation

The time taken to perform Monte Carlo integration is a bottleneck for all theoretical predictions of this type. Whilst, fortunately, we do not require a very large number of evaluations to reduce the Monte Carlo error down to the size of other theoretical errors, this still increases the time taken to perform such predictions and restricts the reduction in Monte Carlo error. Therefore we have built the `reSolve` program so as to permit straightforward, uncomplicated parallelisation, taking further benefit from the modular and transparent form of the `reSolve` program. As each phase space point undergoes precisely the same calculation to evaluate its cross-section, the total number of phase space points may be divided across many cores and many computers to reduce the physical runtime of the program. The process of parallelisation is, however, somewhat complicated by the need to update the Monte Carlo grid iteration by iteration; as a result all events from each iteration are needed to update the grid before the subsequent iteration may begin. The parallelisation is therefore restricted to within iterations, the program must wait to complete all phase space evaluations in a given iteration before the grid can be updated and the next parallelised iteration begun on the cores and computers available. A schematic of a parallelised run of `reSolve` is given later in Figure 7.3.

The actual use of `reSolve` with parallelisation is as follows. Of the two options for the integrator, the `Cuba` implementation will by default parallelise over the number of cores of the machine used, whilst the `k_vegas` implementation will automatically only use one core. However, the `reSolve` program has been designed to allow `k_vegas` to run batches of events on different cores, and indeed on different machines, and to then combine these batches after each iteration,

before again distributing events in batches across the machines and cores available. This can therefore be used to parallelise across all the cores in the machine used, like `Cuba`, or even to run across multiple machines. This can hasten the process of producing the events required for differential cross-section spectra greatly, depending upon the computer resources available. An example of the reduction in physical runtime needed to produce a theoretical prediction with such parallelisation is given later in Table 7.7.

In order to run batches in parallel across multiple machines/cores using `k_vegas`, one must set up the input file correctly; first turn the `multi_machine` input to 1, as described in Chapter 7.1.2. In addition, in order to avoid producing the same events across multiple cores, one must set `seed` to -2, to allow the randoms' seeds to be set by converting the machine tag into a numerical seed different for each batch (in a deterministic and repeatable manner), or to -1, to set the randoms' seed based on time - which will be marginally different for the batch sent to each machine. For parallel running using `k_vegas`, unlike the standard running or `Cuba` running, the maximum number of iterations is not set by `maxeval` in the input file, rather it is set at the start of the parallelisation script in the variable `max_iter` - this is the number of iterations to run per core. The number of evaluations (phase space points) per iteration per core are set as usual via `nstart` and `nincrease` in the input file. The number of cores per machine is set via `max_cores` at the start of the parallelisation script. In order to parallelise across several of the cores of just one machine, use the built in file `single_machine_parallel`, which in the default form included with `reSolve` parallelises across 4 cores - this number is changed at the top of the script. To run this, type into the terminal the call "`single_machine_parallel {path to input file}`". This terminal call starts the `single_machine_parallel` script included in the `reSolve` package to parallelise the in-built `k_vegas` Monte Carlo implementation across all the cores of a single computer. It is important to note that for parallel runs in the case where one uses the `k_vegas` integrator, whether across the cores of one machine or across many machines, the numbers of integration evaluations at the start and the increase in the number of evaluations from one iteration to the next (`nstart` and `nincrease` in the input file) are then the numbers per core. Therefore each core used in parallel will, in total, undertake $n\_\{\text{tot\_per\_core}\}$ evaluations for a total of n_tot phase space points across all cores:

$$n\_\{\text{tot\_per\_core}\} = [\texttt{max\_iter} * \texttt{nstart} + 0.5 * \texttt{n\_increase} * \texttt{max\_iter} * (\texttt{max\_iter} - 1)], \quad (7.3)$$

$$n\_\text{tot} = \texttt{max\_cores} * [\texttt{max\_iter} * \texttt{nstart} + 0.5 * \texttt{n\_increase} * \texttt{max\_iter} * (\texttt{max\_iter} - 1)]. \quad (7.4)$$

In running the `single_machine_parallel` parallelisation script, the working directory used is filled with event files `events_lhe_{iter_number}.lhe`, each containing all the events from all the cores for that given iteration[7]. In addition, there are `reSolve_main_out__{core_number}.dat` and `reSolve_main_out_END_ITER.dat` files giving the final iteration result and accumulated results for the total cross-section for the specified core and across all cores respectively.

[7] `lhe` here indicates the type of event output selected - `save_events` set to 2 in the input file, the "easy" output form with `save_events` set to 1 also works.

If instead of running across all the cores of one machine, one instead wants to reduce the runtime even further by parallelising across many machines, one must use the integrator option `k_vegas` - setting `integrator_flag` to 1 in the input file. Again `multi_machine` must also be 1. With these settings, one may then use the script `multi_machine_parallel_local` to undertake parallel runs across many computers. This parallelisation script allows the use of multiple machines all of which are accessible via SSH on systems with or without a shared home directory in which to access input files and to output results to. The user must change the `exedir` line to the directory in which the `reSolve` program is installed, unless the script is run from the `reSolve` working directory. To enter which machines to run on, enter the machine names into `machines` at the top of the script. After saving the script, simply typing "`multi_machine_parallel_local {path to input file}`" into the terminal will set off a parallel run across the specified number of cores of all named machines. The information is combined at the end of each iteration to update the grid, before using all machine cores for the subsequent iteration; this continues until all iterations are complete. The maximum number of iterations to be performed is set at the top of the file, as is the number of cores to use per machine, in `max_iter` and `max_cores` respectively. These were also set at the top of the `single_machine_parallel` script. Consequently, for both multiple machine and single machine parallelisation the `maxeval` variable in the input file used for single core `k_vegas` running or `Cuba` running is not relevant. In the working directory for the input file, a file of the form `reSolve_main_out_{machine_name}_{core_number}.dat` is created for each core on each machine used, listing the overall total cross-section for that machine core for both the final iteration and the accumulated results across all iterations. Meanwhile `reSolve_main_out_END_ITER.dat` lists the combined total cross-section across all machines, all cores for the final iteration and then the accumulated result across all machines, all cores and all iterations. The output event files are also output into the input file working directory. A schematic of a parallel run across many machines is given in Figure 7.3.

This capability of the `reSolve` program to parallelise across many machines is unique amongst theoretical computational tools in this area. When `reSolve` is parallelised, histogram data files will be automatically generated by the `reSolve` program as usual. A description of the time taken to run in parallel compared with on one core is given in Chapter 7.2.3.

Sample input files which work with parallelisation, either across many cores of one machine, or across many SSH-accessible cores, are included with the `reSolve` program. These sample parallelisable input files are in the input directory of the `reSolve` program, ready for use, and are called `Diphoton_Born_parallel_LHC.dat`, `yZ_Born_Tevatron_parallel.dat`, `Diphoton_NNLL_test_1__parallel.dat` and `yZ_NNLL_Tevatron_parallel.dat`. These are the same setups of the `Diphoton_Born_LHC.dat`, `yZ_Born_Tevatron.dat`, `Diphoton_NNLL_test_1.dat` and `yZ_NNLL_Tevatron.dat` files (used in the validation of the `reSolve` program in Chapters 7.2.1.1, 7.2.2.1, 7.2.1.2 and 7.2.2.2) except adapted for `k_vegas` parallelisation. The input files included in the `reSolve` package were summarised previously in Table 7.1.

In general, the parallelisation needed depends on the structure of the user's computer network; this varies significantly from one user to another therefore the user may have to make small changes to the scripts as appropriate for their computer resources.

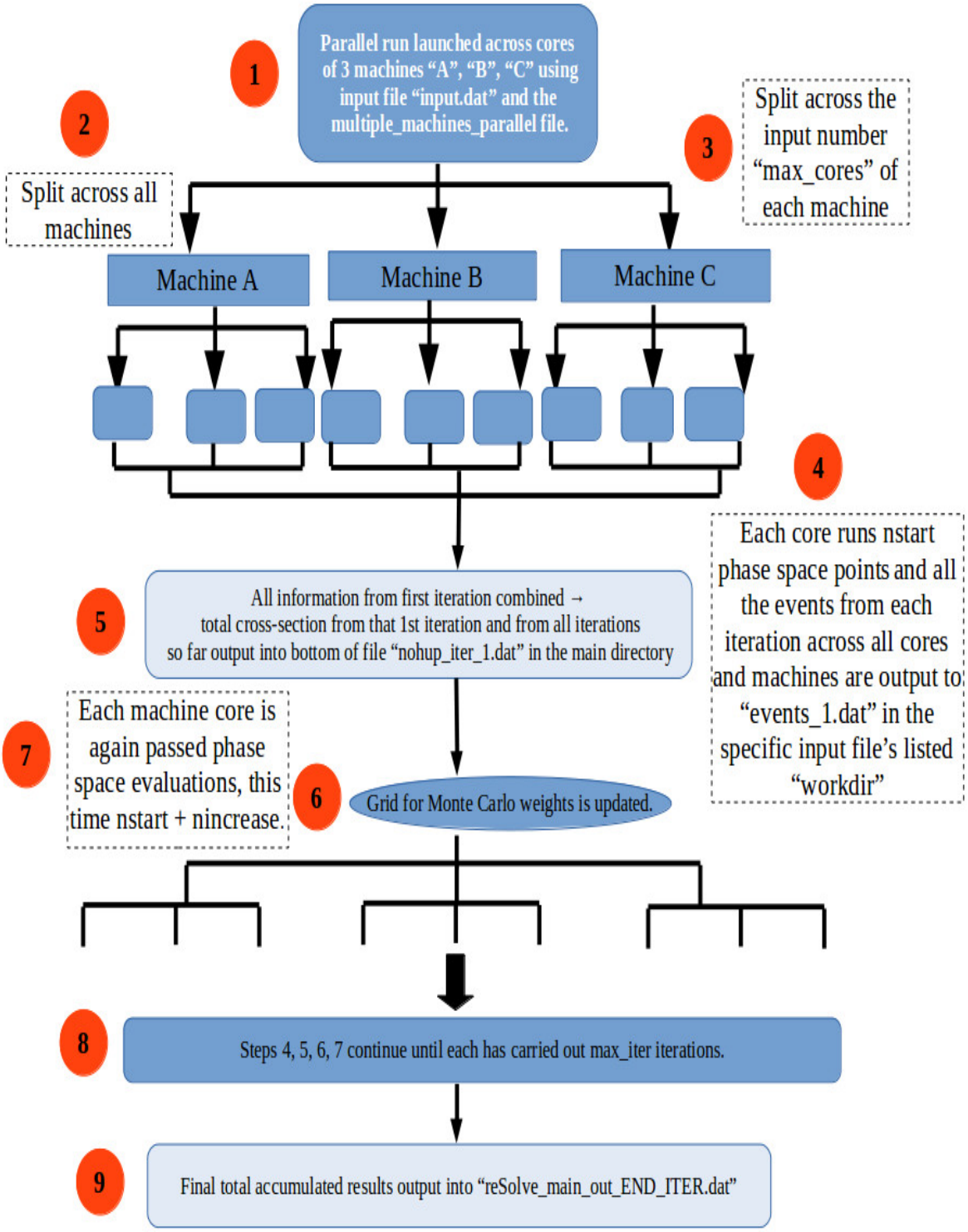

Figure 7.3: Flowchart demonstrating the running of a parallel run across the cores of many machines, the script `multi_machine_parallel_local` may be used to perform this.

7.1.7 Adding a Process

As highlighted extensively in this chapter and previous chapters, a key driver in the development of the `reSolve` program, and a key benefit of the program, is its modularity and near process independence, taking full advantage of the universal nature of the theoretical b-space resummation formalism. This near process independence and modularity has been incorporated to allow flexibility in the use of `reSolve`, whether by enabling the future interfacing of separate stand-alone sections of the code with different programs, or extending the program straightforwardly to meet the user's needs. One set of key extensions of the current program which `reSolve` is specifically designed to enable is the addition of new processes, avoiding the situation in the current literature where separate programs are developed for separate processes. In particular, `reSolve` more generally has been written as a program to add transverse momentum resummation to a generic process of the form $h_1 + h_2 \to F + X$ for a general colourless measured final state F, so as to accurately produce the low q_T part of the spectrum, which is often the technically most-challenging piece. The user must then add this transverse momentum resummed spectrum, produced by `reSolve`, to the usual finite piece and match them appropriately to obtain the complete spectrum over all q_T. `reSolve` is not specifically targeted at the diphoton and Drell-Yan processes, these are no easier to implement in the code than other processes and are simply the first of several processes we have chosen to include.

This exercise of adding a process to `reSolve` is one that we the authors have undertaken ourselves in developing `reSolve` from its β version, which included only the diphoton production channel, to its first main version release which has the Drell-Yan production channels added. The `reSolve` program consequently already includes all the switches and code blocks needed to operate for two separate channels, and many of the sections must simply be copied or extended should further processes be added. The inherently segmented structure of the code means the process dependence is restricted largely to only one module of the program, with the remaining sections functioning exactly as for other processes - including, crucially, the resummation module. The main additions required for any new process are simply the Born cross-section, details in the hard factors (related to the Born cross-section), and the relative orders at which different initiation processes occur. We therefore hope the program, along with its transparent documentation [2], lends itself to generalisation to further processes meeting the users' requirements. To this end we have written a guide to adding a process to `reSolve`, which we reproduce in outline form here; where {`process`} appears in a routine, file or folder name below it is to be replaced by a suitable name for the added process. To add a process to `reSolve` do the following:

1. Set 3 as the process number for the added process and extend `User.cc` to include the new process in its "if ... else if" statement, to do so copy the code section for either diphoton or Drell-Yan to produce the new calls for the new process. This includes calling a new routine {`process`}`_setup` which will be defined in the file "{process}_input.cc", which in turn we will create later in the new sub-folder "Process/{process}_Res/".

2. Enter the Process sub-folder, this contains the process dependent routines. Here there are sub-folders for each process included - currently the diphoton (`Diphoton_Res`) and Drell-Yan (`DrellYan_Res`) production channels. Each process sub-folder contains files and routines {process}_cuts.cc, {process}_hard.cc, {process}_input.cc, {process}_integrand.cc, {process}_ps.cc, and corresponding header files, see Figure 7.4. The goal is to produce appropriate corresponding files for the new process. First create the new process sub-folder {process}_Res.

3. Next, we will begin with the aforementioned process-specific file {process}_input.cc to read the process-specific input from the input file. This contains two parts, first there is the {process}_setup routine which organises the program pre-resummation for the new process. To create this, the form of these files for diphoton or Drell-Yan can be copied. This setup routine will call the second part of the file, the routine {process}_ReadInput, again the basic form of this will be analogous to the diphoton and Drell-Yan cases, with the new relevant cuts for the process under consideration. Create also the corresponding header file, including the class {process}_input used to pass this input information to the cut-checking routine later.

4. Create the {process}_integrand.cc file and corresponding routine. This routine is called from User.cc "if ... else if" segment we have already extended, and coordinates the main calculations for this process. The general form of these files for the diphoton or Drell-Yan case may be copied. First, the routine calls a phase-space generating routine {process}_ps to generate the randoms and phase space for each process event, this is contained in the process-specific file {process}_ps.cc. Next the cuts relevant to the process phase space are checked by calling the {process}_cuts routine in the {process}_cuts.cc file, then the Born-level cross-section is determined via the routine sigmaij{process}calc in the file {process}_hard.cc. The process-independent resummation part of the calculation is then implemented by calling the "resummed" routine contained in inv_fourier.cc. This determines the overall cross-section for each event, including resummation up to NNLL, finally the events are then output in whichever form is indicated in the input file.

5. Therefore the {process}_ps, {process}_cuts and {process}_hard routines and files must be created for the new added process. First consider the phase space generation; this routine reads in randoms generated in the rest of the code and uses them to set the relevant parameters for the process phase space. The Jacobian for the transformation between these random variables, whose values are between 0 and 1, and the phase space variables, is given by "randsjacob". A kinematics routine is then called to determine the 4-momenta and angular separation of the relevant particles (e.g. the two photons for diphoton, two leptons for Z Drell-Yan) in the lab frame in order to allow later application of the cuts. Various other variables such as the factorisation, resummation and renormalisation scales are also set here; this can be copied.

6. The {process}_cuts.cc file may be duplicated from the diphoton and Drell-Yan examples. There are two types of cuts implemented here, first generic kinematical constraints are applied to cut if either $|\eta|$ or q_T become so large that either x_1 or x_2 are too large or that the resummation formalism is no longer valid respectively[8]. These are the "gencuts" and should be kept for all processes. Secondly, there are the process-specific, phase space cuts - "pscuts". These are checked via the PS{process}cuts_1 routine, which will have to be written anew for each added process. The process-specific cut information read in from the input file (via the ReadInput_{process} routine discussed earlier) is passed in via a {process}_input object, whilst the phase space and event information is passed via a "PSpoint" object. With this information, the relevant phase space kinematic parameters can be determined for each event and tested against the process-specific cuts.

7. Finally, the {process}_hard.cc file consists of the sigmaij{process}calc routine, which uses the input process information and event phase space point parameters to determine the Born-level cross-section for the added process. This is then loaded into the sigmaij vector array to be used elsewhere in the code, for example in computation of the hard factors in the resummation. Process-specific hard factors are also calculated here for non-Drell-Yan or Higgs processes, this is unnecessary for Drell-Yan and Higgs production as we employ the DY-Higgs scheme so the hard factors are zero for these processes.

8. It is also necessary to add a new section in the file hardfns.cc in Resummation/; there are sections of code here which detail the contributions from gluon-gluon initiation, quark-gluon initiation and quark-quark initiation to the hard factors. In order to correctly combine contributions with different initialising particles order-by-order, the relative orders in α_s of the leading order quark-quark and gluon-gluon contributions for the new process should be added. In addition, in the interests of the speed of evaluation of the program, only the non-zero hard contributions for each process are explicitly summed, for example for diphoton or neutral current Drell-Yan only $q\bar{q}$ is summed over as the final hard scattering quarks must be the same flavour; whilst for $W^{\pm}$ Drell-Yan the contributions are $q\bar{q}'$ and, as a result of the CKM matrix, can occur with q and q' of different generations, such as $u\bar{s}$. Aside from these differences, one may copy the diphoton and Drell-Yan code here. It is worth noting that the structure of the theoretical formalism here is process-independent, one must just sum over all contributions (including zero contributions) for each process. The small process dependence introduced in reSolve is purely a pragmatic one, to avoid wasting time summing many zero contributions in the time-critical part of the program.

[8]The η general cut comes from equations 5.29, given x_1 and x_2 are each momentum fractions they are bounded to be less than 1, rearranging these equations this occurs if $\eta > -0.5\log(Q^2/s)$, which is the general cut applied.

All of the remainder of the program should remain exactly as it is, the calculation of the hard factors, Sudakovs, determination of the inverse Mellin transforms, the inverse Fourier transform from impact parameter space, the Monte Carlo phase space integration and everything else required will be calculated automatically by the program. In this way `reSolve` takes advantage of the generality of the b-space Mellin-space resummation formalism of [223, 238–240, 242, 244, 247–249, 251].

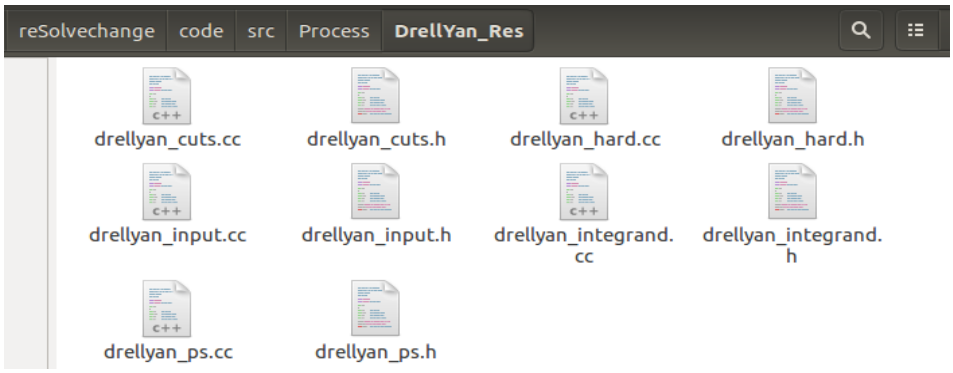

Figure 7.4: The `DrellYan_Res` sub-folder (contained in the Process sub-folder), which contains the Drell-Yan specific routines and links with the generic resummation parts of the `reSolve` program. An analogous sub-folder and routines therein exists for the diphoton process and should be recreated for any processes added.

We intend to undertake this process ourselves in the near future to extend the program to the key Higgs to diphoton signal channel and others, for further information please refer to Chapter 7.3. In the current version only the hard factors for $q\bar{q}$ initiated processes are included up to NNLL, those for gg initiated processes are only included at LL. Therefore processes requiring these hard factors beyond LL will need the additional higher order hard factors to be added, nevertheless we ourselves will add such hard factors for gg in the near future in order to add the Higgs diphoton signal process.

7.1.8 Adding a Differential Observable

A fundamental aspect of the resummation formalism applied in `reSolve` is that it is fully differential, and so further differential spectra above and beyond the theoretically-complicated transverse momentum spectrum at which it is aimed can be produced. Indeed the calculation of differential distributions in invariant mass, rapidity and transverse mass of the final state system F, and maximum and minimum transverse momentum of the individual particles in the final state, are included out-of-the-box in the `reSolve` package. However, given that our Monte Carlo implementation generates a complete description of all the measured particles in each event, and the formalism is fully differential, we may determine arbitrary differential observables for the events. As a result, differential spectra in any physical, measurable quantity can be predicted by `reSolve`. In order to add a new variable for which to evaluate a differential cross-section, minimal changes are required to the `reSolve` code:

1. Enter the `Histogrammer/` folder in the `reSolve` package, and open the `observables.cc` file. At the bottom of the file create a routine "{`variable`}`_obs`" where {`variable`} is replaced by the name of the new desired differential variable and calculate the value of this variable from the event phase space information contained in the `PS` object. This contains the four momenta of the incoming partons and of the individual outgoing final state particles in elements `PS_mom(i)[j]` where i is the particle ($i = 0, 1$ are the incoming partons and $i = 2, 3$ are the outgoing particles as there are two outgoing particles for diphoton and Drell-Yan) and j is the 4-momentum component[9].

2. Remaining in the `observables.cc` file, call the new {`variable`}`_obs` routine from the `obs_values` routine at the top of the file.

3. Including the relevant histogrammer line in the input file will then cause the program to create the histogram data file when `reSolve` is run, producing the differential spectrum in the new variable.

[9]These four momenta are calculated and added to the `PS` object through the `process_PS.cc` files which call `in_state_w_recoil` in `Resummation/resu_PS.cc` to calculate the incoming parton four-momenta including q_T recoil, and `Utility/phase_space.cc/set_PS_twobody` which determines the four-momenta of the outgoing particles.

7.2 Validation and Results

`reSolve` is a completely new program implementation of the b-space resummation formalism, and consequently, as with the development of any new tool, the validation of the results generated is of crucial importance. Only once the code has been thoroughly tested, can it be used to make precise theoretical predictions against which to test experimental data to further our knowledge of the Standard Model and to search for new physics effects. With this in mind, great care and attention was used during the development of `reSolve` to compare the outputs of the various routines enclosed against similar routines and calculations elsewhere in private programs. In addition, extensive physical checks were performed - ensuring the correct events were cut, analysing Sudakovs and hard factors produced and many other elements. Finally, following its completion, a number of further validation comparisons have been undertaken focusing on the results of `reSolve`, comparing against the theoretical predictions of other programs and against experimental data wherever possible. These other programs include the private `2gRes` code (version 2.2), which has been used in the production of results for previous papers in references [5] and [6], and the `DYRes` code (version 1.0) [7, 8]. In this section we provide a selection of these checks, focusing on the results `reSolve` generates. This is undertaken for both the diphoton and Drell-Yan production channels in order to verify the general applicability of `reSolve`. Through this comparison we also verify the ability of the program to use multiple PDF fits at different factorisation scales and we conclude this section by commenting on the speed of the program, which is often a limiting factor for such Monte Carlo reliant programs. In our results in this chapter we do not perform the scale variation to determine the size of theoretical errors as we largely seek to validate against other theoretical results, where we can choose the precise same scales in the calculations we compare against. Throughout this chapter the errors indicated on our results are purely Monte Carlo errors only.

Throughout our validation and the results presented for both the diphoton and Drell-Yan processes, as `reSolve` does not yet include the finite piece, the results presented are the resummed piece only and are therefore described only as "NLL" or "NNLL" rather than "NLO+NLL" or "NNLO+NNLL". In fact, the formalism itself includes in the resummed piece some virtual corrections through the hard factor (as given in equation 6.28) in addition to the logarithmic pieces and so in this sense some "NLO" and "NNLO" pieces are actually included in the resummed piece. By describing as only "NLL" or "NNLL" we wish to distinguish the fact that the finite piece, which contains pieces which are zero in the $q_T \to 0$ limit but which are important at high values of transverse momenta, are not yet included in `reSolve`, therefore the overall total cross-section will be missing a piece beyond leading order. These pieces are only important at large transverse momenta and so do not affect the differential q_T distributions at the low q_T end upon which our resummation is focused. We will seek to add these pieces in future versions, nonetheless for our examples and many others the resummed piece is the dominant one in any

case[10]. The one exception to the rule that we present only resummed pieces in this work is in Figure 7.9 where the matched finite piece has been added from the `2gNNLO` program [266] in order to facilitate a comparison with the ATLAS experimental results.

7.2.1 Diphoton Production Results

For the validation of the program for the diphoton process (process = 1 in the input file), first of all we ensure that the program produces the correct output for the Born-level process by comparison against known results, this is described in Chapter 7.2.1.1. Following this, we compare differential cross-sections in both invariant mass and in transverse momentum, for two main test files, with the private `2gRes` program (version 2.2) in Chapter 7.2.1.2. Finally, in Chapter 7.2.1.3, we demonstrate the validation of `reSolve` for a setup for which we compare against the `2gRes` program and experimental data.

7.2.1.1 Diphoton Born cross-section

The first validation for any process is to confirm the Born cross-section is correctly calculated as this is resummation independent and encodes the key process dependence that is carried into the resummation formalism via the hard factors. Here we compare against known Born cross-section results in a previous resummation paper, in particular against Table 1 in [266]. This reference details the production cross section for diphotons plus jets given a typical set of kinematical cuts applied in ATLAS and CMS analyses [280] [281] for previous Higgs searches. These inputs are $\sqrt{s} = 14\,\text{TeV}$, $2\mu_S = \mu_R = qq$, $\mu_F = 113\,\text{GeV}$, $qq_{\text{min}} = 20\,\text{GeV}$, $qq_{\text{max}} = 250\,\text{GeV}$, $-2.5 < \eta < 2.5$, `etacut`$= 2.5$, no "crack" in the detector, `pT1cut`$= 40\,\text{GeV}$, `pT2cut`$= 25\,\text{GeV}$ and `Rcut`$= 0.4$. Note that as we are at leading order there is no gg box and q_T is unimportant. The input file used is provided with the code as `input/Diphoton_Born_LHC.dat`. We can only use this as a test of the LO result as beyond LO not only the resummed piece of the cross-section is required, but also the finite piece. Nonetheless for LO we obtain a total cross-section of 5.708 ± 0.008pb whilst the value given in the paper was 5.712 ± 0.002pb, we are therefore consistent.

[10]This dominance of the resummed piece can be seen in the results presented, for example later Table 7.4 illustrates that the resummed piece only calculations we have performed beyond leading order for the Drell-Yan processes represent the majority of the known results (which include resummed and finite pieces).

7.2.1.2 Diphoton Differential cross-sections at NNLL

Following the successful verification of the Born process, we now compare the differential cross-sections in invariant mass and transverse momentum as calculated by `reSolve` at with NNLL resummation against results from the private `2gRes` program, which has been used in previous comparisons with experiments. It should be noted that a small error was found in the old `2gRes` code around the Jacobian and subsequently corrected before undertaking this comparison[11]. The test files chosen are the `Diphoton_NNLL_test_1.dat` and `Diphoton_NNLL_test_2.dat` provided with the `reSolve` program. The inputs of these two tests are summarised in Table 7.2. These test files reflect common cuts, invariant mass ranges and transverse momentum ranges used for diphoton measurements, at 14 TeV and 8 TeV for `Diphoton_test_1` and `Diphoton_test_2` respectively. Therefore this comparison is of results produced by the new `reSolve` program in the expected regions of application.

Test file	`Diphoton_test_1`	`Diphoton_test_2`
Process	1	1
Order	2	2
CM_energy (TeV)	14	8
μ_S, μ_R, μ_F (GeV)	$qq/2$, qq, 113	$qq/2$, qq, 85
QQ_Min, QQ_Max (GeV)	80, 160	50, 110
QT_Min, QT_Max (GeV)	0, 120	0, 100
η_Min, η_Max	-2.5, 2.5	-2.37, 2.37
gg box (`boxflag`)	No (0)	No (0)
etaCut	2.5	2.37
crack1, crack2	1.37, 1.37	1.37, 1.37
pT1cut, pT2cut (GeV)	40, 25	40, 30
Rcut	0.4	0.4

Table 7.2: The two test files used for validation for the diphoton process in `reSolve` both against the private code `2gRes` and internally, ensuring different numbers of PDF fits, different integrators and different numbers of iterations all produce consistent results. The files are the `Diphoton_NNLL_test_1.dat` and `Diphoton_NNLL_test_2.dat` provided with the program.

Figure 7.5 shows the comparison between `reSolve` and the previous private program `2gRes` for the `Diphoton_NNLL_test_1.dat` inputs with 500,000 events; with Figure 7.5a showing the invariant mass spectrum and Figure 7.5b showing the transverse momentum spectrum. Excellent agreement is seen in both cases with the two programs agreeing within the errors shown. First of all consider the invariant mass spectrum; the invariant mass region for the `Diphoton_test_1` inputs is $QQ\_Min = 80\,\text{GeV}$ to $QQ\_Max = 160\,\text{GeV}$, this is exactly the region over which we have non-zero cross-section, demonstrating the events are being generated correctly. Meanwhile, the shape of the distribution is as expected, rising sharply above 80 GeV once within the invariant

[11]This error has been known in the past but, being a private program, had not been corrected, essentially the version of `2gRes` we had calculated $H1q = jacob \times H1qYY(costheta)$ and $H2q = jacob \times H2qYY(costheta)$ whereas it should have no Jacobian factors and appropriate factors to cancel out the normalisation differences associated with the k in the resummation coefficients in Appendix B.1, in particular introduced for equation B.6 onwards. Therefore the correction is $H1q = 2 \times H1qYY(costheta)$ and $H2q = 4 \times H2qYY(costheta)$.

mass region and peaking at the lower end of the invariant mass range. This occurs because as the invariant mass increases the phase space for the production of a higher diphoton invariant mass decreases. Meanwhile in Figure 7.5b we obtain the characteristic transverse momentum spectrum shape, with the spectrum approaching zero at $q_T = 0\,\text{GeV}$, peaking sharply just above 0 GeV in the region where transverse momentum resummation is most important, and again reducing as the q_T increases. Furthermore we see a slight rise from 65 GeV peaking around 80 GeV; this is a kinematical effect caused by the q_T cuts applied on each photon being 40 GeV and 25 GeV. This kinematic "shoulder" produced due to the cuts is present in both theoretical predictions and experimental results and was explained in [282][12]. The q_T spectrum is then correctly cut off at the $q_T = 120\,\text{GeV}$ upper bound. For this `Diphoton_NNLL_test_1.dat` input file the total cross-section at NNLL is also in agreement; `reSolve` obtains 7.68 ± 0.03pb, whilst `2gRes` obtains 7.67 ± 0.03pb.

Figure 7.6 illustrates a similar comparison for the `Diphoton_test_2.dat` inputs, again with 500,000 events. Figure 7.6a shows the invariant mass spectrum comparison, whilst Figure 7.6b is the transverse momentum spectrum comparison. For `Diphoton_test_2` the invariant mass range is 50 GeV to 110 GeV as given in Table 7.2 - this region is clearly visible in Figure 7.6a. The transverse momentum spectrum in Figure 7.6b again shows the correct behaviour, going towards 0 at $q_T = 0\,\text{GeV}$, peaking sharply just above 0 and then falling away and cutting off at the edge of the q_T region at 110 GeV. Again the peak around 80 GeV results from an increase in the phase space at this point, due to the cuts applied. Once more the total cross-section at NNLL is also in good agreement between the two programs, with `reSolve` obtaining 2.54 ± 0.01pb and `2gRes` 2.56 ± 0.01pb.

[12]The argument explaining this shoulder in outline is as follows - only when the q_T of the diphoton system is larger than the sum of the individual photon p_T cuts, i.e. only when $q_T > pT1cut + pT2cut$, are all relative angles between the two photons possible. If the q_T of the diphoton system is less than the cuts then the arrangement in which the two photons are parallel is forbidden as it would not pass the cuts. In reality, there is also an angular separation cut, $Rcut$, which requires the two photons to have a minimum angular separation, nonetheless the argument follows through that until q_T reaches some minimum corresponding to the resolved sum of the individual photon momenta at this angular separation, then some angular configurations are forbidden. Moreover, even once q_T surpasses this value more and more contributions for each angular configuration contribute. Therefore as q_T tends to this minimum value and beyond, the phase space allowed by the cuts opens up, causing the kinematic shoulder. In fact for an angular separation of 0.4 radians the minimum q_T which allows all configurations of the two relative photon momenta is given by the cosine rule as $q_T = 64.69\,\text{GeV}$ for cuts $pT1cut = 40\,\text{GeV}$ and $pT2cut = 25\,\text{GeV}$.

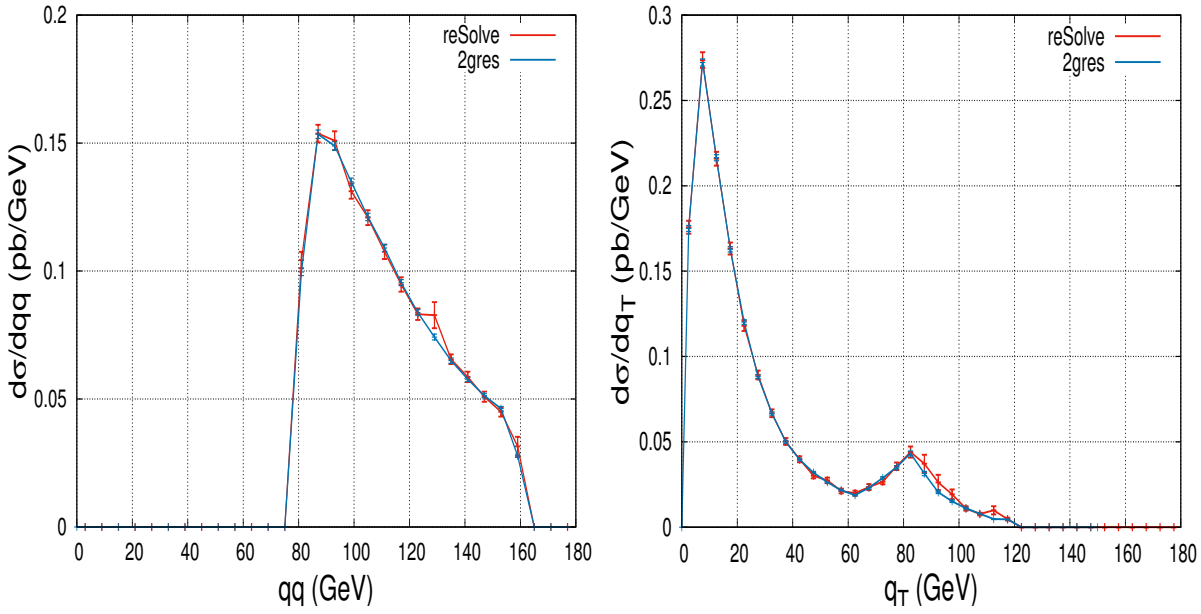

(a) Invariant Mass (b) Transverse Momentum

Figure 7.5: Comparison plots of the diphoton differential cross-sections with invariant mass and transverse momentum for the `Diphoton_test_1` inputs as listed in Table 7.2 using the file `Diphoton_NNLL_test_1.dat` provided with `reSolve`. The comparison is between the `reSolve` program and the previous private program `2gRes`. The comparison here includes only the resummed part of the differential cross-section, not the finite piece, as this is all that is currently available in `reSolve`.

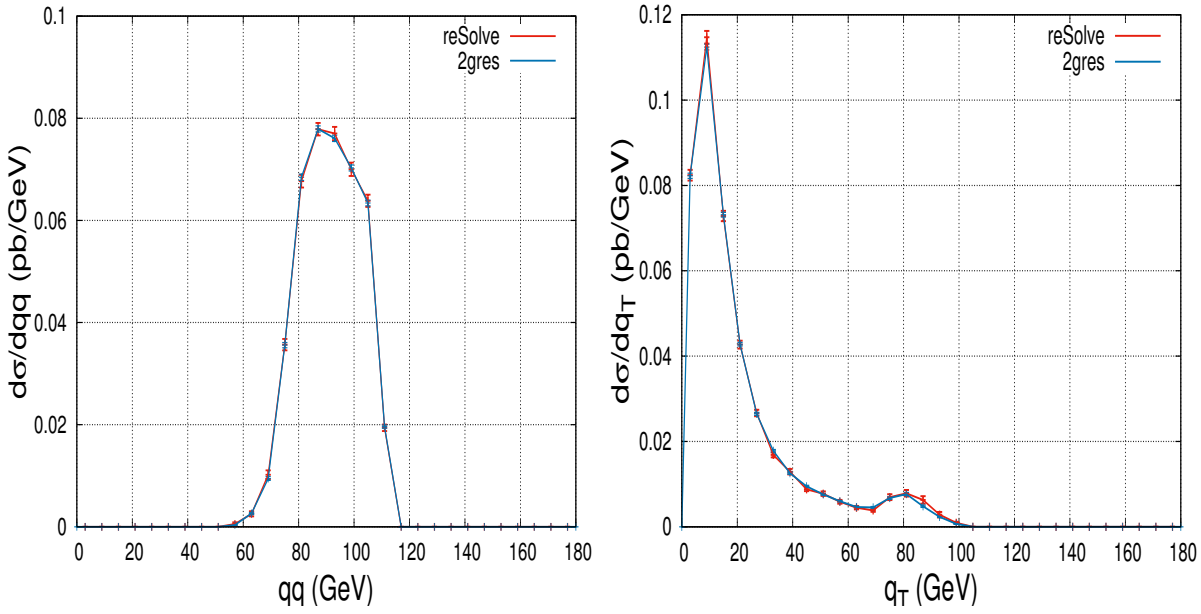

(a) Invariant Mass (b) Transverse Momentum

Figure 7.6: Comparison plots of the diphoton differential cross-sections with invariant mass and transverse momentum for the `Diphoton_test_2` inputs as listed in Table 7.2 using the file `Diphoton_NNLL_test_2.dat` provided with `reSolve`. The comparison is between the `reSolve` program and the previous private program `2gRes`. The comparison includes only the resummed part of the differential cross-section, not the finite piece, as this is all that is currently available in `reSolve`.

7.2.1.3 Diphoton Experimental validation

An additional validation that was performed was to use `reSolve` to reproduce the events and corresponding total cross-section, invariant mass spectrum and transverse momentum spectrum for the inputs listed in [6]. These inputs are provided in the `reSolve` program package in ``input/Diphoton_Atlas_A.dat'' and are: diphoton process at NNLL, MSTW NNLO PDFs (`PDF_flag = 82`), centre of mass energy 8 TeV, pp collisions; $\mu_F^2 = \mu_R^2 = qq^2$ and $\mu_S^2 = \frac{qq^2}{4}$; 2,000,000 iterations with `nstart` = `nincrease` = 10000, $0 < QQ < 500\,\text{GeV}$, $0 < QT < 150\,\text{GeV}$, $-2.37 < \eta < 2.37$, gg box included, `etacut`= 2.37, `crack1`= 1.37, `crack2`= 1.56, `pT1cut`= 40 GeV, `pT2cut`= 30 GeV and `Rcut`= 0.4. As a result of the large invariant mass range considered, 5 PDF fits are used across the allowed range to improve accuracy; this is straightforward to do in `reSolve` by setting `en_sec_multipler` accordingly, whereas when this analysis was performed with `2gRes` the invariant mass region has to be manually split into 5 segments which are run separately and then combined at the end. These comparisons correspondingly also serve as validations for the ability of the `reSolve` program to implement multiple PDF fits across the invariant mass range. For the inputs used in this comparison, the `2gRes` program has been previously validated against experimental data from the ATLAS collaboration [283], with a further comparison performed for the work in [6]. We therefore also validate `reSolve` against these experimental results at the end of this section. In the first parts of the comparison with `2gres` only in Figures 7.7 and 7.8, only the resummed piece is considered so these results are NNLL only. For the later comparison against experimental data in Figure 7.9 the matched finite part from `2gNNLO` [266] is used and so the results are the full NNLO+NNLL, including both resummed and finite pieces.

The total cross-section produced by the `reSolve` program for these inputs was 6.188 ± 0.013pb, compared with 6.18 ± 0.02pb from `2gRes`, this therefore indicates very good agreement. The invariant mass and transverse momentum spectra also are consistent and are given in Figures 7.7 and 7.8 respectively. The q_T plot shows agreement at both the low q_T end and higher q_T end, with the position and height of the peak in the spectrum agreeing within the errors; meanwhile as one increases q_T the differential cross-section reduces as expected. The spectrum peaks again slightly around 80 GeV as a result of increasing phase space available beyond this q_T, as demonstrated in the invariant mass spectrum raising rapidly above 80 GeV. This is a threshold effect caused by the cuts - with cuts on `pT1` and `pT2` of 40 GeV and 30 GeV, invariant masses of less than 80 GeV have fewer angular configurations of the two produced photons allowed, as explained in the previous validations.

As well as validation against just the resummed part of the transverse momentum differential cross-section, we added the finite piece - as previously calculated by `2gNNLO` [266] - in order to validate against the total transverse momentum differential cross-section. We then compared our `reSolve` results with the matched finite piece added (with Monte Carlo error only and only for the resummed part of the differential cross-section) against those of `2gRes` (with errors shown indicating scale variation) and ATLAS experimental results [283]. The compari-

son plot is shown in Figure 7.9. The figure demonstrates the excellent agreement between the `reSolve` program and the data previously calculated with `2gRes`, the main difference coming in the 80 GeV-100 GeV region where we observe the expected kinematic shoulder bump in the resummed cross-section. The difference here is because the previous `2gRes` program (as explained in Chapter 7.2.1.2) had a small bug in the Jacobian which suppressed the effect of the bump. We use the old `2gRes` data to demonstrate its effect - indeed the new `reSolve` program now shows better agreement with the experimental data in this region than the `2gRes` code did previously. There are small differences between the `reSolve` and `2gRes` predictions and the experimental results at intermediate transverse momenta, we expect these are within errors once all errors - including those from the PDF fit, scale variation, Monte Carlo, matching and other sources are taken into account. Given that `reSolve` and `2gRes` agree excellently for the resummed part, and consequently agree when the same matched finite piece is added as is done here, we believe that the underestimate of the diphoton transverse momentum spectrum at intermediate q_T is an effect arising in the finite piece and/or the matching of the resummed and finite contributions. However, given the finite piece calculation and matching were not performed by ourselves as they cannot be undertaken in the current version of `reSolve` it is not possible to pin down the exact source of the difference with respect to the experimental results. We expect to be able to comment further on this matter in the near future once the matching is possible within `reSolve`. In any case the current version of `reSolve` determines only the resummed piece of the differential cross-section and so it is the excellent agreement at low transverse momenta which is the focus of our validation here.

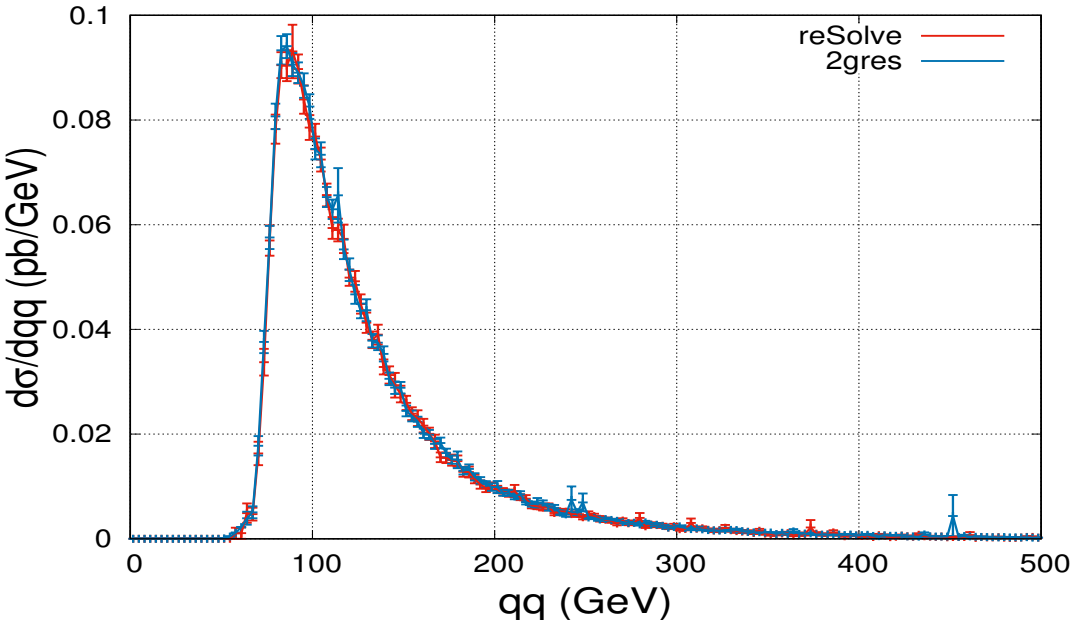

Figure 7.7: Invariant mass spectrum for diphoton production for the `Diphoton_Atlas_A.dat` input file provided with the program, and whose inputs are also listed in the text, as produced by `reSolve` and compared with the previous private program `2gRes` (used in the work in [5] and [6]). 5 PDF fits were used across the invariant mass range. Only the resummed part of the differential cross-section is shown.

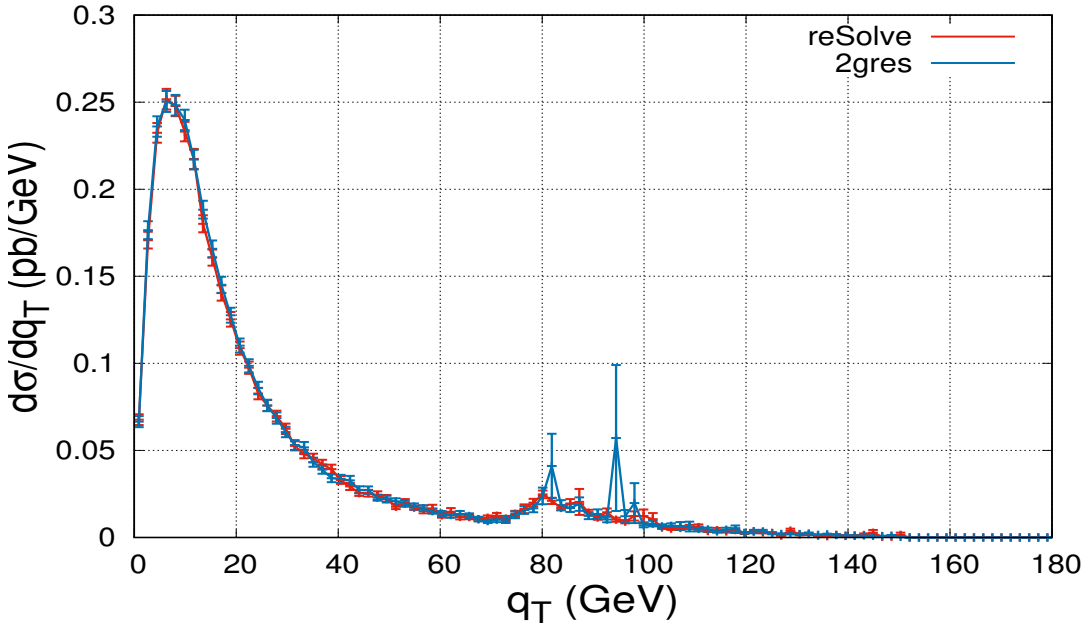

Figure 7.8: Transverse momentum spectrum for diphoton production for the `Diphoton_Atlas_A.dat` input file provided with the program and listed in the text, as produced by `reSolve` and compared with the previous private program `2gRes` (which was used in the work in [5] and [6]). 5 PDF fits were used across the invariant mass range. Only the resummed part of the differential cross-section is shown.

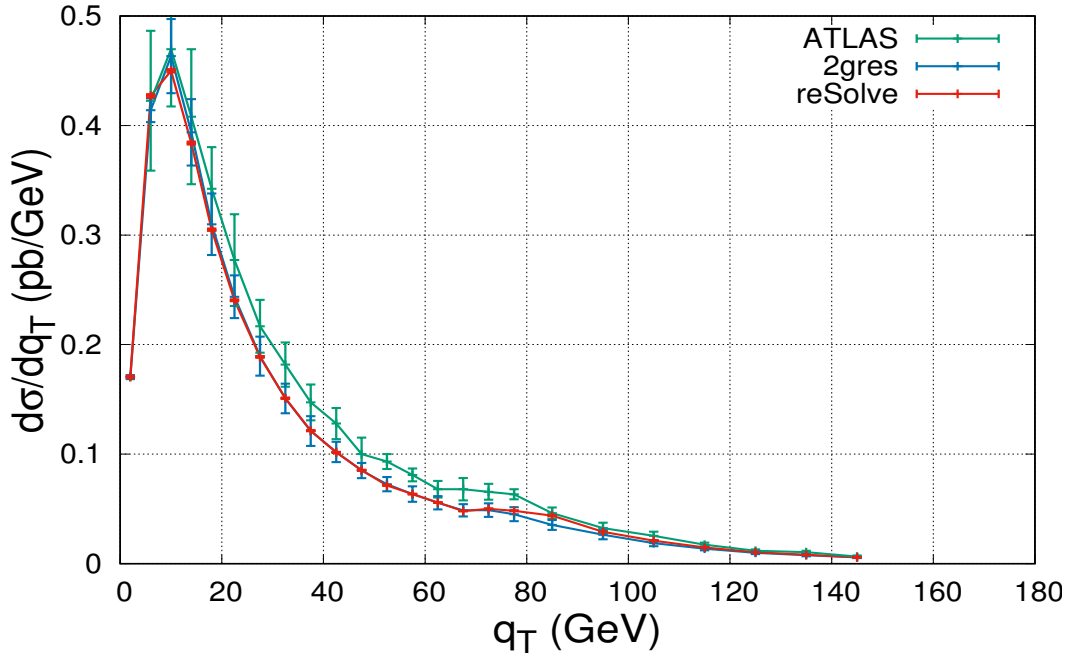

Figure 7.9: Transverse momentum spectrum, including resummed and finite pieces, for diphoton production for the `Diphoton_Atlas_A.dat` input file provided with the program, and whose inputs are also listed in the text. The spectra produced by the `reSolve` program (with finite pieces from `2gNNLO` [266]) and the previous private program `2gRes`, which was used in the work in [5] and [6], are given; also shown are the ATLAS experimental results and corresponding errors [283]. The error bars for `2gRes` show the scale variation error, which is a dominant error. This is not calculable in `reSolve` as we do not include the finite part of the cross-section in this first version of the program, therefore the `reSolve` error bars are the Monte Carlo errors from the resummed part only. Once other sources of theoretical error, including from the PDF fit, scale variation, matching and other sources are accounted for, we expect the theoretical and experimental results would agree within the errors.

7.2.2 Drell-Yan Production Results

The second process included in the `reSolve` program is the historically important Drell-Yan production mode, this continues to be a key process in testing the Standard Model and in probing for new physics extensions at Run II of the LHC and beyond. For this production process there are five different sub-process options (the `DY_process` flag - see Chapter 7.1.2), corresponding to W^+, W^-, $W^\pm$, Z and Z/γ^*, and the possibility of putting any of the intermediate particles on-shell (via the `DYnarrowwidthapprox` flag).

In order to validate the Drell-Yan process, we performed similar checks as for the diphoton case but for all five of these sub-process channels and including the possibility of both on-shell and off-shell intermediate gauge bosons. Again we present only a relatively small collection of these validations here for comparative brevity. We begin in Chapter 7.2.2.1 by verifying the Born cross-section, comparing against known results, and then extend this to comparing results at all included orders. This is followed by a presentation of comparisons against the program `DYRes` (version 1.0) [8] in various differential variables, including the transverse momentum spectrum and rapidity(η) spectrum in Chapter 7.2.2.2; in Chapter 7.2.2.3 we provide further differential plots, comparing the rapidity, transverse mass (m_T), and $p_T^{\text{min/max}}$ distributions against those in [278]. Here further plots of additional differential distributions for the case of $W^\pm$ are also provided in order to confirm the qualitative behaviour of the results is as expected.

It should be noted at this stage that there are several differences between our implementation and `DYRes` which impact upon the answers given. In general, in producing the theoretical predictions beyond leading-order there are a multitude of choices and methodology-linked effects which affect the precise output values of the two programs. In order to produce these comparisons of the `reSolve` and `DYRes` results we have sought to minimise these differences and thereby demonstrate the absolute level of agreement of the codes. In general, results may show larger differences down to the exact choices made in the calculations: from the running of α_s, to the nature of how higher transverse momenta are dealt with - `reSolve` essentially uses a step function by allowing the user to specify a q_T range, whereas `DYRes` gradually reduces the effects of higher q_T values via an arbitrarily-defined "switch" function. There are also differences in the precise generation of phase-space points and how the η range is limited at its extremities, the precise nature of the PDF-fitting function and in many other areas between the two programs. Similarly, there are differences in m_W and G_F numerical values included, where the `reSolve` values for these constants constitute more recent determinations. These choice differences were eliminated as much as possible in the comparisons presented here, nonetheless these effects tend to result in differences of order 5% and so this should be considered the accuracy of the predictions for a generic input[13].

[13]In particular, the effects of the α_s running method and the q_T switch are the largest differences seen and may cause differences themselves of up to 5%, the choices in `DYRes` raise the predictions by around this amount relative to the default choices in `reSolve`.

7.2.2.1 Drell-Yan Born, NLL and NNLL cross-sections

In order to add a new process (in this case all the Drell-Yan processes) to the `reSolve` program, as described in Chapter 7.1.8, we needed mainly to alter the non-resummation part of the code by providing a new Born-level cross-section for the added process. For this reason, the key test to perform to validate the added Drell-Yan process is to confirm it produces the Born cross-sections correctly. With this purpose in mind, `reSolve` was run for three different setups: setup 1 is for Z/γ^* at the Tevatron, setup 2 is for Z on-shell at the 14 TeV LHC, and setup 3 is for $W^{\pm}$ at the Tevatron; the full invariant mass ranges, rapidity ranges, scale and cut setups are listed in Table 7.3. These benchmarks were also used for NLO+NLL and NNLO+NNLL comparisons and plots in later sections (where the `resum_flag` must be changed to 1, the `order` changed accordingly and the `pdf_flag` changed to reflect the order of evaluation of the cross-section). The transverse momentum ranges are therefore given, however note that there is no transverse momentum at Born-level so the q_T range set is unimportant for Born comparisons. These benchmarks were chosen as they reflect the full range of Drell-Yan processes added and there are full results quoted in [278] to compare against, in addition results were also obtained from the `DYRes` (version 1.0) program [8] wherever possible, and from the `MCFM` (version 8.1) program [284–287], for comparison (in the latter case at LO).

With these inputs as listed in Table 7.3, the `reSolve` program obtains the following Born cross-sections: for the Z/γ^* Tevatron setup 1, `reSolve` calculates $\sigma_{\rm LO} = 103.37 \pm 0.06$pb, we may compare this with the results in [278] where $\sigma_{\rm LO} = 103.37 \pm 0.04$pb, whilst `MCFM` [284–287] obtains $\sigma_{\rm LO} = 103.34 \pm 0.04$pb; for the on-shell Z LHC 14 TeV setup 2, `reSolve` calculates $\sigma_{LO} = 1758.9 \pm 1.1$pb, for comparison with $\sigma_{\rm LO} = 1761 \pm 1$pb in [278] and $\sigma_{\rm LO}(pp \to Z \to l^+l^-) = \sigma_{\rm LO}(pp \to Z) \times BR(Z \to l^+l^-) = 1761.1 \pm 0.1$pb from `MCFM`; finally for the $W^{\pm}$ Tevatron setup 3, `reSolve` calculates $\sigma_{\rm LO} = 1160.4 \pm 0.7$pb for comparison with $\sigma_{\rm LO} = 1161 \pm 1$pb in [278], whilst `MCFM` obtains $\sigma_{\rm LO}(p\bar{p} \to W^{\pm}) = 1187.9 \pm 0.4$pb. Therefore there is good agreement for these Born cross-sections between the `reSolve` program and known calculations for all three setups.

Given this incorporates the majority of the process dependence of the formalism used for the `reSolve` program, this indicates the new Drell-Yan processes are functioning correctly in `reSolve`. Nonetheless, we demonstrate further results and validations in the next few sections.

Before any of the differential cross-sections are analysed, first we check that the total cross-sections are sensible for each order beyond the Born - next-to-leading order (NLO) cross-section with next-to-leading logarithm (NLL) resummation, and next-to-next-to-leading order (NNLO) with next-to-next-to-leading logarithm (NNLL) resummation. For the moment, `reSolve`, as mentioned, only includes the resummed piece of the differential cross-section and so produces only "NLL" and "NNLL" results. The input files used are those for the 3 benchmark setups of Table 7.3 adapted to each of the orders and they are provided with the `reSolve` program; including the Born input files used for the Born comparison already described they are: `yZ_Born_Tevatron.dat`, `yZ_NLL_Tevatron.dat`, `yZ_NNLL_Tevatron.dat`;

Test file	setup 1	setup 2	setup 3
Process	2	2	2
resum_flag	0	0	0
DYProcess	5	4	3
DYnarrowwidthapprox	0	1	0
Order	0	0	0
pdf_flag	80	80	80
CM_energy (GeV)	1960	14000	1960
ih1	1	1	1
ih2	-1	1	-1
μ_S, μ_R, μ_F (GeV)	All $m_Z = 91.187$	All $m_Z = 91.187$	All $m_W = 80.398$
QQ_Min, QQ_Max (GeV)	70, 110	70, 110	0, 200
QT_Min, QT_Max (GeV)	0, 200	0, 200	0, 200
η_Min, η_Max	-3, 3	-10, 10	-3, 3
crack1, crack2	1.37, 1.37	1.37, 1.37	1.37, 1.37
pT1cut, pT2cut (GeV)	20, 20	0, 0	N.A., N.A.
eta1Cut = eta2cut	2	10	N.A.
pTecut (GeV)	N.A.	N.A.	20
pTmisscut (GeV)	N.A	N.A.	25
etaecut	N.A	N.A.	2
tmasscut (GeV)	N.A	N.A.	0

Table 7.3: The three test files used for validation of the Born cross-section for the Drell-Yan processes in `reSolve` against the results in [278] and results from the program `MCFM` [284–287], as well as against those of `DYRes` [8]. The PDF set used is MSTW2008 LO PDFs, therefore pdf_flag = 80. The files used are `yZ_Born_Tevatron.dat`, `Z_OnShell_Born_LHC.dat` and `Wpm_Born_Tevatron.dat`, and similar inputs were used for the NLL and NNLL tests, all these files are also provided with the `reSolve` program.

`Z_OnShell_Born_LHC.dat`, `Z_OnShell_NLL_LHC.dat`, `Z_OnShell_NNLL_LHC.dat`; and `Wpm_Born_Tevatron.dat`, `Wpm_NLL_Tevatron.dat` and `Wpm_NNLL_Tevatron.dat`. The results obtained from `reSolve` are compared with known results calculated in [278], the difference being that, as-of-yet, `reSolve` does not include the finite part of the cross-section, just the resummed part; therefore we expect our beyond LO results to be lower than in [278] but showing the same trend with NNLL > NLL > LO. For this reason, we also present the resummed only total cross-section contributions calculated in `DYRes` in Chapter 7.2.2.2 for the NNLL case. The results are summarised in Table 7.4, those for LO were also given in the previous section. The agreement shown at leading-order is good for all three benchmark setups with the known results. Meanwhile, comparing the `reSolve` NLL and NNLL predictions with known results for NLO+NLL and NNLO+NNLL, the predictions behave as expected, with each successive order increasing the total cross-section as more contributions are added, whilst still being smaller than the known results which include the additional finite contributions. Moreover, the increases in the total cross-section are significant in going from LO to NLL but much smaller upon going to NNLL, exactly as seen in the known results order by order. Also, as is well known, the resummed contributions constitute the majority of the cross-section for Drell-Yan, as is seen in our results here. Meanwhile, as reported and expanded in the next section, it is clear the resummed only contributions of `reSolve` and `DYRes` show good agreement at the level of the total cross-section.

		reSolve	Known Result	DYRes	MCFM
Z/γ^* setup 1	LO	103.37 ± 0.06	103.37 ± 0.04	-	103.34 ± 0.04
	NLO(+NLL)	130.37 ± 0.10	140.43 ± 0.07	-	-
	NNLO(+NNLL)	130.40 ± 0.10	143.86 ± 0.12	130.30 ± 1.20	-
Z On-shell setup 2	LO	1758.9 ± 1.1	1761 ± 1	-	1761.1 ± 0.1
	NLO(+NLL)	2009.1 ± 0.5	2030 ± 1	-	-
	NNLO(+NNLL)	2056.2 ± 3.0	2089 ± 3	2050.5 ± 2.1	-
$W^{\pm}$ setup 3	LO	1160.4 ± 0.7	1161 ± 1	-	1187.9 ± 0.4
	NLO(+NLL)	1438.6 ± 1.2	1550 ± 1	-	-
	NNLO(+NNLL)	1465.4 ± 1.3	1586 ± 1	1487 ± 10	-

Table 7.4: Summary of the total cross-sections in pb calculated by reSolve and compared with known results [278] for the three setups of Table 7.3, the DYRes resummed only NNLL contributions calculated for Chapter 7.2.2.2 are given for further verification, as are MCFM Born results for completeness. The agreement is good between reSolve and the known results at LO and the behaviour beyond LO is as expected. reSolve results beyond leading order are smaller than the known results as reSolve only includes the resummed part of the total cross-section (i.e. NLL and NNLL), which is nonetheless the dominant contribution as seen, not the finite part which is important at larger transverse momentum. The beyond LO results of reSolve agree well with the resummed piece only calculations of DYRes. The errors indicated are Monte Carlo errors only and so those for DYRes are larger as it is slower than reSolve.

7.2.2.2 Validation of reSolve against DYRes code

The aim of the reSolve program is, of course, to produce differential cross-sections not total cross-sections. Therefore we must validate the differential cross-section results for the Drell-Yan process in reSolve and we do so by comparison again with the program DYRes. This is from the same series of programs as the 2gRes program against which we compared the diphoton, and crucially for our validation it allows for the calculation of the resummed contribution only.

First we consider the Z/γ^* Tevatron case of setup 1 (given previously in Table 7.3). DYRes produces data for the transverse momentum spectrum and rapidity distribution, amongst others, so we may compare these directly with these distributions as produced by reSolve. The comparison plots are shown below in Figures 7.10a and 7.10b respectively; both figures show the NNLL spectra and demonstrate very good agreement with the DYRes program, thereby validating reSolve for this process. As given in Table 7.4, the total cross-section also agrees well, reSolve obtains 130.4 ± 0.1pb whilst DYRes (for the resummed piece only) obtains 130.3 ± 1.2pb.

Similar comparisons can be performed for the on-shell Z LHC 14 TeV case of setup 2 (given previously in Table 7.3). Figure 7.11a demonstrates the agreement in the NLL and NNLL transverse momentum spectra between reSolve and DYRes. The total cross-sections, again given in Table 7.4, are also in agreement between reSolve and DYRes with the programs obtaining 2056.2 ± 3.0pb and 2050.5 ± 2.1pb respectively for the resummed pieces only.

Finally, similar comparisons may be undertaken for the $W^{\pm}$ channel, and are shown for the transverse momentum spectrum with NNLL resummation in Figure 7.11b, indicating excellent agreement once more. The overall resummed piece only NNLL results for reSolve and DYRes are 1465.4 ± 1.3pb and 1487 ± 10pb, this agrees at the 2% level.

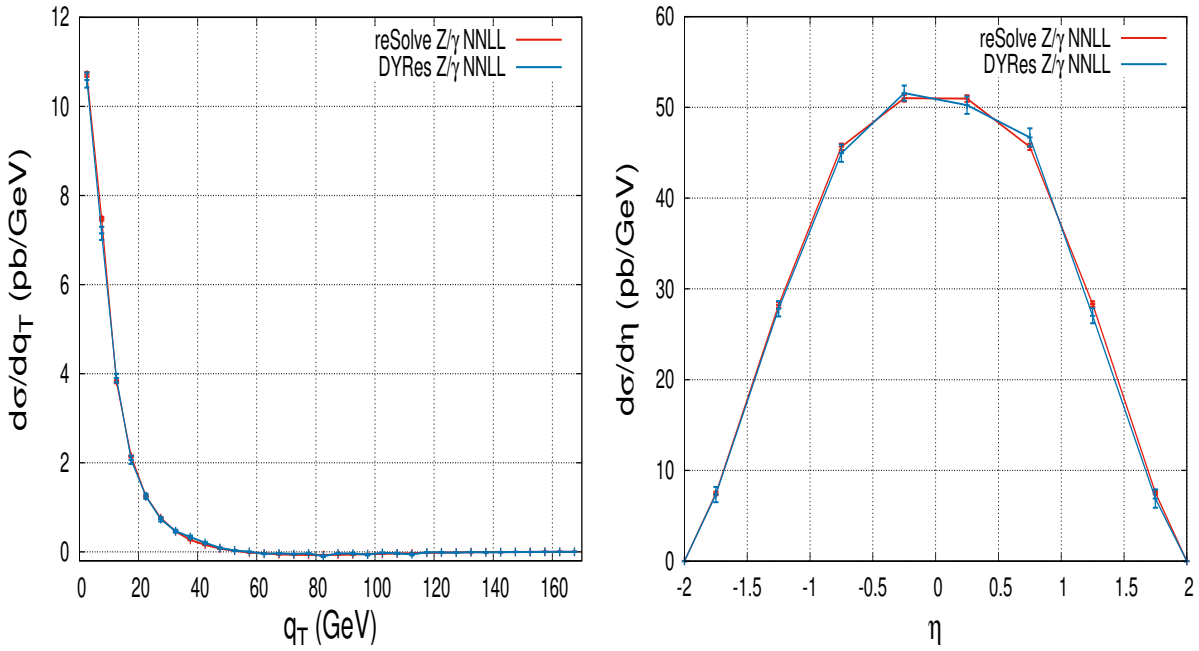

(a) Transverse Momentum (b) Rapidity

Figure 7.10: (a) Transverse momentum spectrum and (b) rapidity spectrum, including only the resummed piece, for Drell-Yan production via neutral current Z or γ^* at NNLL for the setup 1 benchmark, as given in Table 7.3. The agreement between the two programs is excellent, validating `reSolve`. The error bars are the Monte Carlo errors from the resummed part only and are largely a reflection of the length of the runs performed.

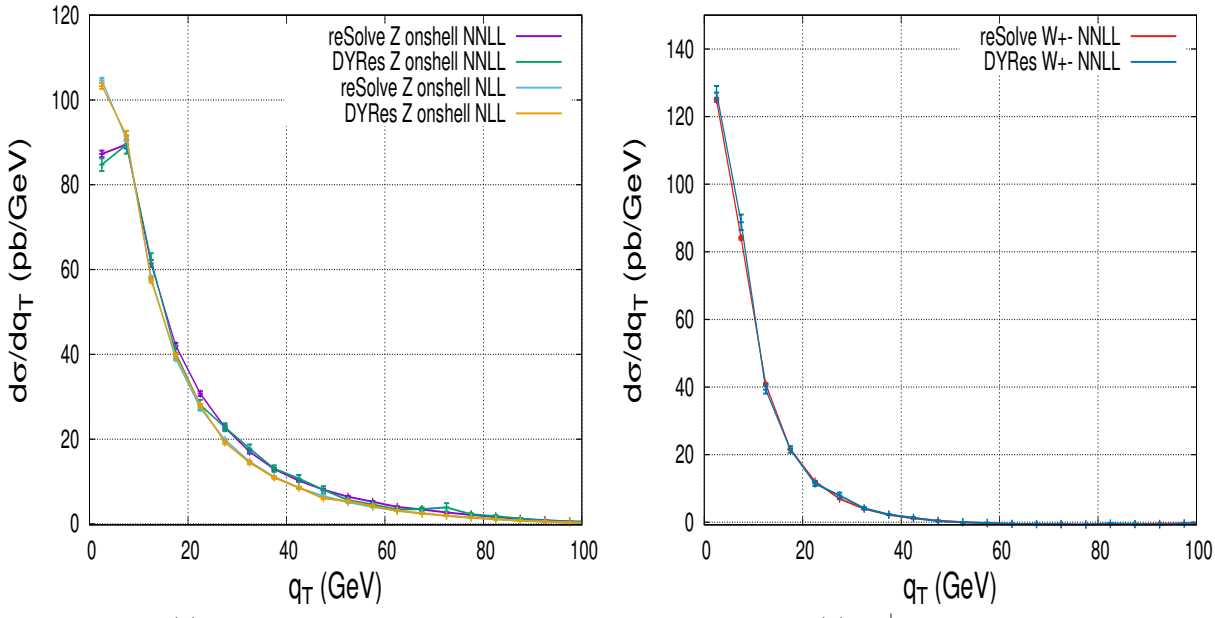

(a) Z on-shell q_T spectrum (b) $W^{\pm}$ q_T spectrum

Figure 7.11: (a) Transverse momentum spectrum, including only the resummed piece, for Drell-Yan production via neutral current Z on-shell for the setup 2 benchmark, as given in Table 7.3. (b) Transverse momentum spectrum, including only the resummed piece, for Drell-Yan production via charged current $W^{\pm}$ for the setup 3 benchmark, as given in Table 7.3. In both cases the agreement between the two programs is good, further validating `reSolve`. The error bars are the Monte Carlo errors from the resummed part only and are largely a reflection of the length of the runs performed.

At this stage it should be noted that the transverse momentum spectra in Figures 7.10a, 7.11a and 7.11b do not show the expected behaviour of the differential cross-section tending to zero at zero transverse momentum solely because of the binning (set to match `DYRes`), Figure 7.15a in Chapter 7.2.2.3 demonstrates this expected behaviour in reSolve for the $W^{\pm}$ case of setup 3, where finer binning has been used for the low q_T end of the spectrum to demonstrate this behaviour.

7.2.2.3 Further Drell-Yan Differential Spectra

Finally, we provide several spectra obtained for each of the three setups to demonstrate the agreement with the corresponding figures provided in [278] and to illustrate that the qualitative behaviour of the reSolve program is as expected. Again, the figures in [278] include the finite contribution as well as the resummed contribution, and so we expect the same behaviour in our `reSolve` results but with mildly reduced cross-sections as we calculate only the resummed part.

First again consider the case of Z/γ^* in our benchmark setup 1, the $p_T^{\min}$ and $p_T^{\max}$ distributions for this setup were given in Figure 2 of [278]. The corresponding spectrum, as produced by the new `reSolve` program, is provided below in Figure 7.12 - we provide only the NLL and NNLL spectra as the transverse momentum of the system at LO is zero within our formalism. The qualitative agreement between the `reSolve` spectra and the previous spectra is good, meanwhile the behaviour of the spectra is exactly as expected with the NNLL spectrum having a fractionally harder peak than the NLL. Both the $p_T^{\min}$ and $p_T^{\max}$ distributions cut off at 20 GeV due to the applied p_T cut; the $p_T^{\min}$ spectrum peaks just below $\frac{m_Z}{2}$ and the $p_T^{\max}$ spectrum at just above $\frac{m_Z}{2}$. The $p_T^{\min}$ spectrum also cuts-off at 55 GeV as the q_T range had an upper limit of 110 GeV whilst the $p_T^{\max}$ spectrum continues above 55 GeV, all this behaviour is exactly as expected.

For the on-shell Z case of benchmark setup 2, Figure 1 of [278] provides the rapidity distribution; the corresponding distribution calculated by `reSolve` is given below in our Figure 7.13, the agreement between the two is excellent, with the effects of the resummation beyond LO significantly increasing the cross-section between LO and NLL, with NNLL only offering a small additional correction.

For the case of $W^{\pm}$ in our benchmark setup 3, the differential distribution provided in [278] is the transverse mass distribution in their Figure 3, compare this with the same transverse mass distribution produced by `reSolve` in Figure 7.14. Again, there is good agreement between the results, the leading order m_T distribution turns on at 50 GeV because the $W^{\pm}$ is produced at zero net transverse momentum, so without any additional radiation we require $p_T^{lepton} = p_T^{miss}$ therefore the p_T^{miss} cut of 25 GeV sets the lower limit of the LO m_T distribution to 50 GeV. Of course, this limit is not a hard limit beyond LO as additional radiation can carry away transverse momentum. For LO, NLL and NNLL the m_T distribution peaks just below the W mass at around 80 GeV as expected.

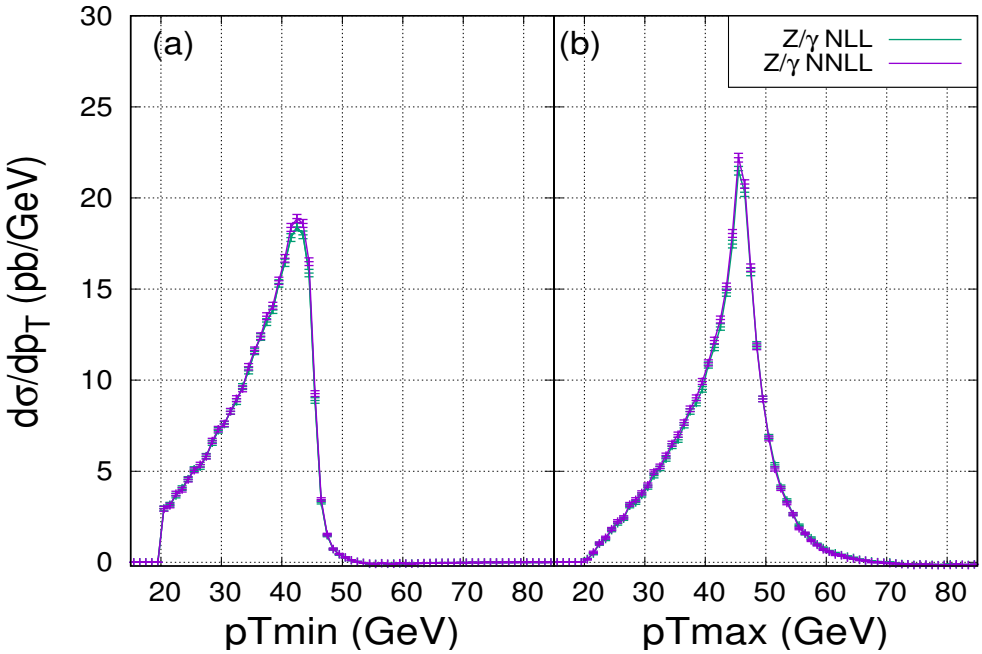

Figure 7.12: Minimum and maximum transverse momenta spectra produced by `reSolve` for the two outgoing leptons produced, including only the resummed piece, for Drell-Yan production via neutral current Z or γ^* for the setup 1 benchmark, as given in Table 7.3. This figure should be compared with Figure 2 of [278], the agreement between the two results is good, with slight differences arising due to the implementation of the formalism, as well as the lack of finite piece in `reSolve`. The error bars are the Monte Carlo errors from the resummed part only and are largely a reflection of the length of the runs performed.

Lastly, to demonstrate further validation and results in the $W^{\pm}$ channel, Figure 7.15 exhibits the transverse momentum spectrum (Figure 7.15a) and rapidity spectrum (Figure 7.15b) of the intermediate $W^{\pm}$ boson in charged current Drell-Yan production. As before, the features of both differential spectra are as expected, the $W^{\pm}$ transverse momentum going to zero at zero q_T, peaking sharply at low transverse momentum and tailing towards zero once more as q_T is increased; whilst the rapidity spectrum is symmetric (indicating W^+ and W^- are treated equally) and is zero outside the range $-3 < \eta < 3$ set in the input file. The rapidity spectrum also indicates the large increase in cross-section between LO and NLL, with a much smaller further increase up to NNLL, as anticipated and as revealed in the total cross-sections in Table 7.4.

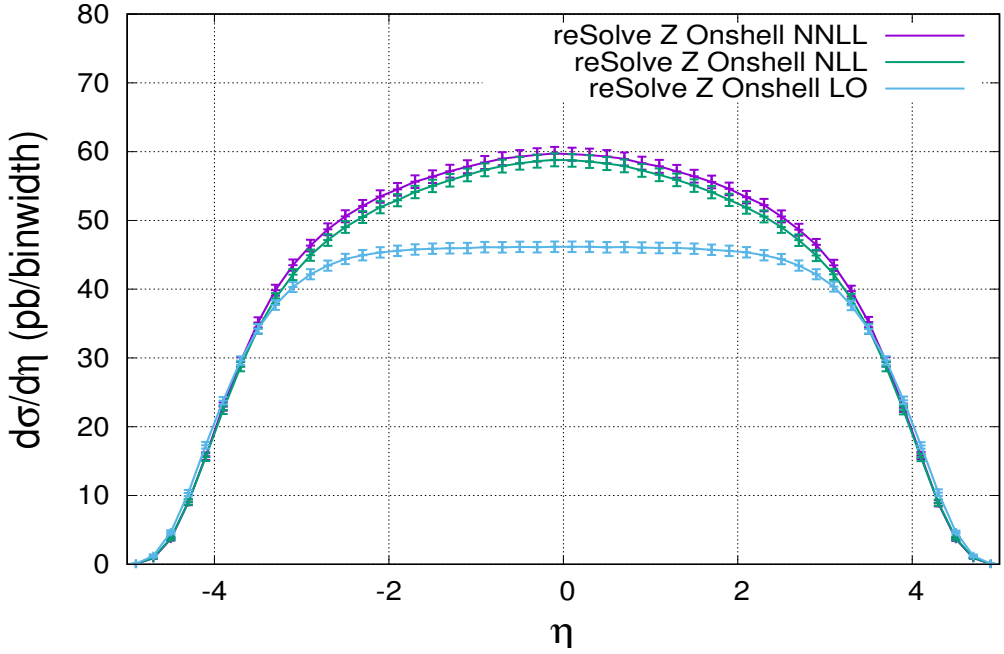

Figure 7.13: Rapidity distribution for the two outgoing leptons produced by the on-shell Z boson, including only the resummed piece, for Drell-Yan production via neutral current Z on-shell for the setup 2 benchmark, as given in Table 7.3. This figure should be compared with Figure 1 of [278], the agreement between the two results is excellent. The LO includes no resummation, whilst for beyond LO resummation is included, so the results are at NLL and NNLL. The error bars are the Monte Carlo errors from the resummed part only and are largely a reflection of the length of the runs performed.

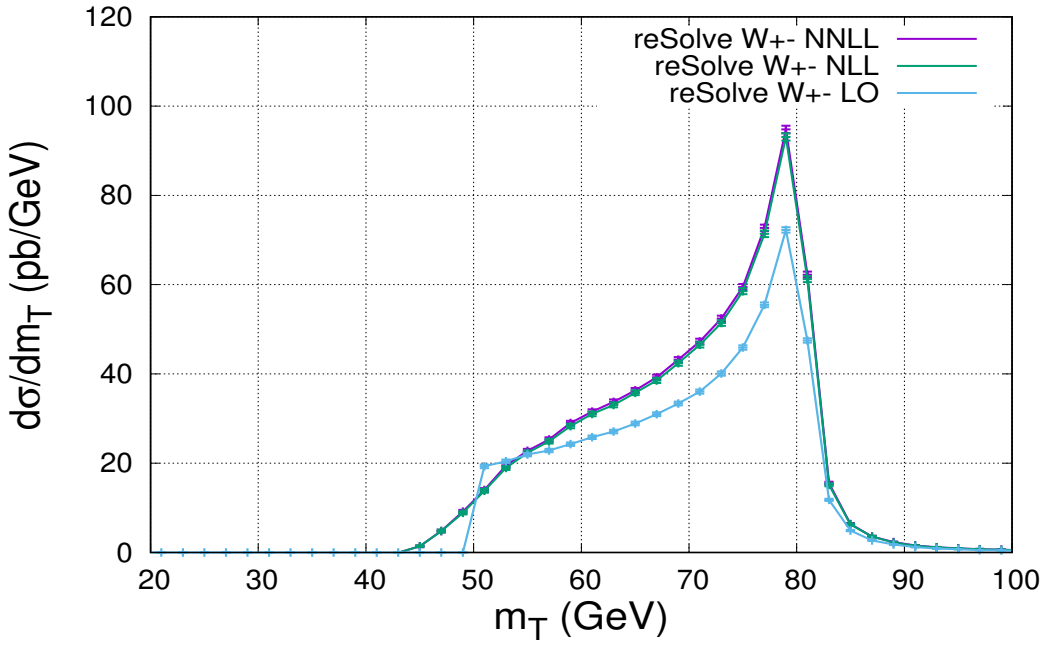

Figure 7.14: Transverse mass distribution for the $W^{\pm}$ case of the setup 3 benchmark, including only the resummed piece, as given in Table 7.3. This figure should be compared with Figure 3 of [278], the agreement between the two results is good, with the results of `reSolve` marginally smaller due to the lack of finite piece. The LO includes no resummation, whilst beyond LO inclues resummation, so the results are at NLL and NNLL. The error bars are the Monte Carlo errors from the resummed part only and are largely a reflection of the length of the runs performed.

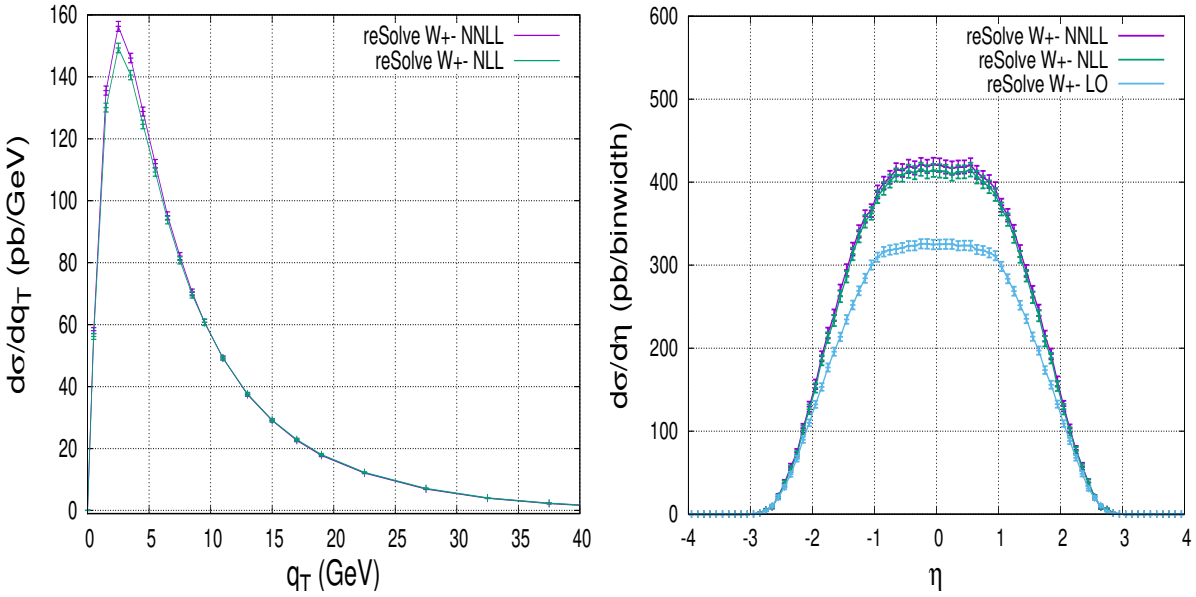

(a) Transverse Momentum (b) Rapidity

Figure 7.15: (a) Transverse momentum spectrum and (b) rapidity spectrum, including only the resummed piece, for Drell-Yan production via charged current W^+ or W^- up to NNLL for the setup 3 benchmark, as given in Table 7.3. The addition of resummation and the additional virtual corrections in going from leading order to NLL (with virtual corrections up to next-to-leading order also included via the hard factors) significantly increases the amplitude of the rapidity distribution and correspondingly also the total cross-section, contrastingly however the increase between NLL and NNLL is insignigicant. The error bars are the Monte Carlo errors from the resummed part only and are largely a reflection of the length of the runs performed.

7.2.3 `reSolve` Performance

Given the number of Monte Carlo iterations it is necessary to perform for the phase space integral to produce the desired accuracy, and the fact that for each phase space point an inverse Fourier transform and double inverse Mellin transform is required - each of which require at least around 20, 50 and 50 points respectively, speed can be very important for transverse momentum resummation programs in this formalism. As a demonstration, for 1,000,000 phase space points parts of the resummation code (parts of `inverse_mellinresummed.cc` and `hardfns.cc`) will be called $1,000,000 \times 20 \times 50 \times 50 = 5 \times 10^{10}$ times. Therefore particular care has been taken, even within this first main version of the code, to ensure it runs quickly. The run time naturally varies significantly depending upon the input file; certain points require more b points to be evaluated in the inverse Fourier transform, large η values have more points on each Mellin contour, and different processes require different numbers of non-zero contributions to the cross-section to be summed. Nevertheless we seek here to give a guide as to the speed of this first main version of the `reSolve` program. In particular, in Table 7.5 we compare it against the private code `2gRes` used also for the validations in Chapter 7.2.1, again for the `Diphoton_test_1` and `Diphoton_test_2` inputs at NNLL listed in Table 7.2 with 550,000 phase space points. As demonstrated, the `reSolve` program is consistently almost twice as quick as the previous `2gRes`

program, completing the same run in 53% of the time. This speed up is important, allowing a greater number of evaluations to be performed and thereby attaining a greater accuracy with the same computer resources.

Program	Diphoton_NNLL_test_1		Diphoton_NNLL_test_2	
	σ(pb)	time(min:s)	σ(pb)	time(min:s)
`reSolve`	7.68 ± 0.03	1678m:22s	2.536 ± 0.009	1370m:11s
`2gRes`	7.68 ± 0.03	3178m:35s	2.556 ± 0.008	2763m:46s

Table 7.5: Comparison of the time taken to evaluate 550,000 phase space points in the new public code `reSolve` and the old private code `2gRes`. The times listed are total core times, summing those across all cores. The total cross-sections are also given, demonstrating good consistency between the programs. Note that `reSolve` here used one PDF fit, as that is all that was available in the previous `2gRes` program, and the integrator `Cuba` was used by both programs to allow a fair comparison. The test files are the `Diphoton_NNLL_test_1` and `Diphoton_NNLL_test_2` files used previously and listed in Table 7.2.

Running with multiple PDF fits will slow down the running of the `reSolve` program; multiple PDF fits therefore should only be used for cases with a dynamical factorisation scale (i.e. which varies event by event) and a wide invariant mass range, where the adoption of multiple PDF fits at different scales through the invariant mass range may offer increased precision. In order to demonstrate this slowdown, Table 7.6 provides the run-times of the `reSolve` program using 1, 2 and 4 PDF fit files respectively, once more for the `Diphoton_NNLL_test_1` inputs listed previously, although with a dynamical factorisation scale for the cases of 2 and 4 PDF fits. Again the specific input files are available with the `reSolve` program already set up for 1, 2 and 4 PDF fits as `Diphoton_NNLL_test_1.dat`, `Diphoton_NNLL_test1_twopdffits.dat` and `Diphoton_NNLL_test1_fourpdffits.dat`. The invariant mass and transverse momentum spectra for these runs show excellent agreement as the number of PDF fits used is varied however here we give only the comparison of the total cross section in Table 7.6 for brevity. The comparison demonstrates that, as one might expect, the runtime is significantly longer for multiple PDF fits, indeed it is more than twice as long. Nonetheless, between 2 and 4 PDF fits the runtime does not increase, demonstrating that the main difference comes when one starts to use multiple PDF fits. Note however that even with multiple PDF fits, the `reSolve` program is not dissimilar in speed to the private `2gRes` program, which only uses one PDF fit.

Many of these issues of the time taken to evaluate the phase space points required are further ameliorated by the ability of the `reSolve` program to allow parallelisation across many cores in many machines. A comparison of the physical time elapsed when running more than 500,000 phase space points on one core, on 4 cores with `Cuba`, and on many cores on many machines with `k_vegas` is provided in Table 7.7. The run-times clearly demonstrate how much physical time may be saved using the parallelisation option in `reSolve`. The results obtained are for the `Diphoton_NNLL_test_1` inputs used previously and were also consistent with those provided in Table 7.5, with the 12 cores parallelisation across 3 machines obtaining 7.67 ± 0.08pb. Note that the error is however larger here as the same number of total iterations were performed in smaller batches. Also it should be noted that, as in its current form the `reSolve` program

when parallelised using `k_vegas` waits for all cores to be complete at a given iteration, the speed of the program will be governed by the slowest core - this is why the core time in the parallelised setup is longer than for the unparallelised or `Cuba` parallelised over one machine implementations. This is necessary so that after each iteration the overall grid of points and weights for the Monte Carlo integration is updated and used by all cores for the next iteration. We therefore recommend parallelising across cores and machines of similar speeds. We intend to develop the parallelisation scripts in the future to reduce this effect.

Number of PDF fits	Diphoton_NNLL_test_1	
	σ(pb)	time(min:s)
1	7.68 ± 0.03	1678m:22s
2	7.67 ± 0.03	3636m:35s
4	7.63 ± 0.03	3617m:52s

Table 7.6: Comparison of the time taken to evaluate 550,000 phase space points in the `reSolve` program for different numbers of PDF fits. Again the times listed are total core times, summing those across all cores. It should be noted that the time listed does not include producing the fits as the PDF fit files were provided here. The total cross-sections are also given, demonstrating consistency between the fits. As expected multiple PDF fits take much longer, however 4 PDF fits took no longer than 2 PDF fits. The test files used were the `Diphoton_NNLL_test_1.dat`, `Diphoton_NNLL_test1_twopdffits.dat` and `Diphoton_NNLL_test1_fourpdffits.dat` provided with the `reSolve` program. The general inputs for this setup were listed in Table 7.2 in the case of 1 PDF fit.

Time elapsed(min:s)					
One Core		4 cores (1 machine) `Cuba`		12 cores (3 machines) `k_vegas`	
Core time	Physical time	Core time	Physical time	Core time	Physical time
∼1678m:22s	∼1678m:22s	1678m:22s	474m:34s	2756m:12s	229m:41s

Table 7.7: The time taken to evaluate over 500,000 phase space points in the `reSolve` program with different degrees of parallelisation and using the `Diphoton_NNLL_test_1` inputs given in Table 7.2. "One Core" indicates either `k_vegas` or `Cuba` used with one core only, the second column shows `Cuba` used parallelising across the 4 cores of the machine used as standard, finally the time taken parallelising across 12 cores across 3 machines using the `k_vegas` parallelisation routine `multi_machine_parallel_local` provided with `reSolve` is given. Note that the time given here for one core is approximate as this test was not run, it is an indication based on extrapolation from 4 cores on the same machine.

7.3 Future Developments

This version of the `reSolve` program is the first main version of many; we intend to optimise and extend the program further, undertaking an ongoing development program. There are many areas for improvement in the program, a few of those we consider the most important are listed here:

- Add the finite parts for the diphoton and Drell-Yan spectra. Given the program currently only includes the resummed (i.e. low q_T) part of the transverse momentum differential cross-section, the obvious extension is to add the finite piece which is dominant at high q_T. This will require matching of the low and high q_T pieces at intermediate q_T using the matching procedure outlined in [222] and Chapter 5.7.
- Extend to additional processes such as Higgs production. This will require addition of the gg initiation hard factors beyond LO. With this extension the program will include both signal and background (diphoton) for the Higgs and signal-background interference could be examined [6].
- Beyond Standard Model contributions in cases such as Z' could be added to study how to use the transverse momentum spectrum as a new tool with which to probe new physics at the LHC. Addition of Z', and W', would not constitute a great amount of additional effort as the hard factors are similar to those already incorporated in `reSolve` for the Drell-Yan electroweak gauge bosons.
- Currently the PDFs are fitted and used at given scales, and whilst `reSolve` allows multiple scales to be used and thereby enables the reduction of this source of error, as an initial step we would like to examine the possibility of interpolating and using them directly at the scale desired.
- The only PDF sets currently available to use are the MSTW PDFs [279], in future versions we will broaden to allow any PDF set to be used. In order to do so we will allow Les Houches Accord PDF formats [288] to be read in.
- The need for the PDFs in Mellin space is a weak point of the application of the formalism, as it requires the PDF fit to be made with corresponding theoretical uncertainties engrained in its application due to the fit form. We could attempt to avoid the need to fit the PDFs altogether by taking the PDFs out of Mellin space. This perhaps could be done with the addition of two further Monte Carlo integration variables with a potential ensuing slowdown of the program. In addition, several evaluations would then correspond to a single "event" losing some physical interpretation. Nonetheless the uncertainty from this aspect of the code could be more easily gauged as it would then contribute a Monte Carlo error rather than a difficult to measure, systematic theoretical error.
- There is substantial scope to further speed up the program, the speed of the program is currently hampered by memory considerations which constitute a slowdown of around 20%, this could be reduced substantially. Furthermore, this memory slowdown is largely associated with the PDF fit in Mellin space, and would be eliminated if the need to fit

the PDF is removed. In addition, the parallelisation will be developed so that it is not held up by the slowest core. This can be done by distributing further events to cores as they finish their previous events, this will allow faster cores to calculate more events and so reduce the time spent waiting for the slowest core to finish.

- The formalism could be relatively easily adapted to allow the implementation of a jet veto, which may be of interest in certain applications. Associated with this is that in the diphoton case photon isolation requirements could be implemented.
- The formalism and `reSolve` program can be extended to QED resummation.
- There is also interest in extending the application of this resummation formalism to larger final states, perhaps $WW\gamma$ even if only at NLL; `reSolve`, with its general implementation of the formalism in a process-independent manner, is ideally placed to allow such studies.
- A further area of theoretical uncertainty is in the non-perturbative effects, which are currently cut off at very large b (equivalent to very small $q_T \sim \Lambda_{QCD}$) and then modelled by exponential factors smearing the low q_T peak. It would be compelling to analyse if there is a better means of modelling such effects phenomenologically, perhaps guided by experimental measurements or observations.

Beyond these short to medium-term objectives, the universality of the formalism applied within `reSolve`, along with the program's clearly-designed modularity, allow the potential to interface the code with existing more general packages in order to allow their extension to higher accuracy. This could incorporate interfacing with existing Matrix Element generators for automatic generation of resummed spectra for a much wider class of processes, for example NLO Matrix Element generators could be interfaced to allow semi-automatic production of differential spectra at next-to-next-to-leading order with next-to-next-to-leading logarithm resummation. From a theoretical perspective, there is also substantial interest in extending the formalism to coloured states [256] and also separately perhaps even to $\mathrm{N^3LL}$, although much work remains in this approximations may be possible in the shorter term and `reSolve` would be well placed to incorporate any such extensions to the formalism. In any case, whichever the precise longer-term direction taken, the properties of the `reSolve` transverse momentum resummation program mean it can form a key part of current and future tools for precise theoretical predictions for collider processes.

Chapter 8

Summary and Conclusions

In this thesis we have focused our attention on the development of theoretical computational tools for particle physics phenomenology. With the increasing amounts of data generated at colliders such as the LHC, as well as the complicated nature of the theoretical calculations associated with these experiments, this area of computational tools is of growing importance and will act as a key driver of discoveries and improvements of our understanding into the future.

With the lack of obvious, compelling new physics signals at the Large Hadron Collider at Run I and Run II so far, the particle physics community is in a position of searching for ways by which to both probe our understanding and reveal new unknown physics contributions at experiments. In this thesis we present two programs offering complementary means of doing just this. The first, the `SoftSusy` decay calculator, explicitly calculates and predicts the forms of signals for the Beyond Standard Model class of supersymmetric theories, focusing directly on new physics at the LHC. The second, the `reSolve` transverse momentum resummation program, takes a different approach instead concentrating on making precise predictions of known Standard Model processes and their differential distributions in a variety of collider variables. This allows the careful measurement of such spectra at the LHC to have the potential to reveal small discrepancies relative to these theoretical predictions. These differences may then challenge our current understanding of particle physics and offer insights into Beyond Standard Model particles and their contributions. Both approaches are complementary, offering different levers by which to attempt to find the path to a more detailed knowledge of particle physics.

We therefore began this thesis with an overview of the Standard Model, itself a tremendous success of particle physics in the latter part of the 20^{th} century, and its problems and oversights. We used this to motivate the need for new physics beyond the Standard Model. In Chapter 2.1.1 we introduced such a possible solution to many of these problems, and for a long period one of the most favoured Beyond Standard Model theories, supersymmetry. We detailed its minimal and next-to-minimal models, the MSSM and NMSSM, as well as various properties and motivations, before moving onto to directly consider supersymmetric decays as a means to detect supersymmetry at the LHC in Chapter 3. As part of this effort we have developed the `SoftSusy` decay calculator, which is the subject of the research presented in the first half of the thesis.

Following this synopsis of the decay calculator program incorporated into `SoftSusy`, we proceeded to describe the great number of decay modes incorporated as well as the validation and results generated using the program. In particular, we provided results for each class of included decay channels, including Higgs loop decays, 3-body supersymmetric decays and

NMSSM decays. We also illustrated how the combination of the spectrum generator and decay calculator of `SoftSusy` can be used to scan the supersymmetric parameter space and examine the decay behaviour. A detailed and full list of all modes included in the program, as well as their partial width formulae as implemented, is indexed in Appendix A.

Chapter 5 began the second half of the thesis, and the second major project undertaken, which focuses on differential spectra and precision physics theoretical predictions, specifically for the transverse momentum spectrum. It was made clear at this stage why this presents a theoretical challenge, with the presence of un-cancelled logarithmically enhanced terms which ruin the usual perturbative expansion in α_s at low values of transverse momentum. These terms must be resummed in order to recover predictivity. In this chapter we acquainted ourselves with the background of this area of precision physics and resummation.

After this introduction, in Chapter 6 a meticulous narration of the b-space Mellin space theoretical formalism chosen for our work in this area was presented, including the master formula and a variety of included factors and their individual expressions. A summary was also given of further pertinent points about the formalism which are crucial to its general application in the new `reSolve` program, which is the centrepiece of our work in this subject. We proceeded to describe the methodology and implementation of the transverse momentum resummation formalism in `reSolve` and the carefully designed modular structure of the program, which is key to its applications. We ended the chapter by exploring the two production channels thus far included in the program, diphoton and Drell-Yan production, and their importance for experimental searches and phenomenology. We culminated our description of our work on `reSolve` in Chapter 7 with an explanation of the validation carried out as a vital part of the program development; and we presented the results of the `reSolve` program, comparing against other programs, known results and experimental data wherever possible. Details of the exact resummation coefficients of the formalism, and further explanations of the Monte Carlo integration method and of the use of Mellin space, are left to Appendix B.

Finally, for both the `SoftSusy` and `reSolve` programs we envisage our efforts to this point as part of a continuing development of the programs, which will be guided by theoretical and experimental motivations into the future. We have therefore summarised our work in each section with an outline of potential extensions to the programs in both the short and long term.

The work presented in this thesis therefore represents a contribution to the ongoing global effort of theoretical and phenomenological work associated with the LHC, which offers a tremendous opportunity to further our knowledge of fundamental particle physics. The mystery of the need for Beyond Standard Model physics so far remains unsolved and will only be unlocked by detailed examination of the Standard Model and its potential extensions. By confronting these with experimental data we can hope to guide our theoretical developments. With the LHC set to continue for many more years, there is much further we can hope to learn. Computational tools for theoretical predictions for LHC phenomenology, such as the two presented in this work, will be crucial to any advances made. We therefore hope `SoftSusy` and `reSolve` can play a role in extending our knowledge of fundamental particles physics at the LHC and beyond.

Appendix A

SoftSusy Decay Formulae

A.1 Glossary - Reference Tables for Decay Formulae

We begin by listing the various decay modes included in `SoftSusy` along with equation numbers for ease of reference. We group the listings into several tables: 2-body MSSM tree-level decays are in Table A.1, Table A.2 contains MSSM Higgs boson decays, Table A.3 has MSSM 3-body decays, decays to gravitinos are in Table A.4, whilst Table A.5 and Table A.6 list the additional NMSSM decays of neutralinos and Higgses.

Gluino Decays		**Slepton of first 2 generations decays**	
$\tilde{g} \to q\tilde{q}_{L/R}, q\tilde{q}_{1/2}$	A.4, A.5	$\tilde{l}_L \to l\tilde{Z}_i$	A.30
Squark of first 2 generations decays		$\tilde{l}_R \to l\tilde{Z}_i$	A.31
$\tilde{q}_L \to \tilde{Z}_i q$	A.12	$\tilde{\nu}_l \to \nu_l \tilde{Z}_i$	A.32
$\tilde{q}_{L/R} \to q\tilde{g}$	A.6	$\tilde{l}_L \to \nu_l \tilde{W}_j^-$	A.33
$\tilde{q}_L \to q^{'}\tilde{W}_{1/2}^-$	A.8	$\tilde{\nu}_l \to l\tilde{W}_j^+$	A.34
$\tilde{q}_R \to \tilde{Z}_i q$	A.13		
Squark of 3$^{\mathrm{rd}}$ generation decays			
$\tilde{q}_{1/2} \to q\tilde{g}$	A.7	**Slepton of 3$^{\mathrm{rd}}$ generation decays**	
$\tilde{b}_{1/2} \to \tilde{W}_j^- t$	A.9	$\tilde{\tau}_{1/2} \to \tau\tilde{Z}_i$	A.35
$\tilde{t}_{1/2} \to \tilde{W}_j^+ b$	A.10	$\tilde{\tau}_{1/2} \to \nu_\tau \tilde{W}_j^-$	A.39
$\tilde{t}_{1/2} \to \tilde{Z}_i t$	A.14	$\tilde{\nu}_\tau \to \tau\tilde{W}_j^+$	A.40
$\tilde{b}_{1/2} \to \tilde{Z}_i b$	A.17	$\tilde{\tau}_{1/2} \to \tilde{\nu}_\tau H^-$	A.41
$\tilde{t}_{1/2} \to \tilde{b}_{1/2} W^+$	A.20	$\tilde{\tau}_{1/2} \to \tilde{\nu}_\tau W^-$	A.42
$\tilde{t}_{1/2} \to \tilde{b}_{1/2} H^+$	A.21	$\tilde{\nu}_\tau \to \tilde{Z}_i \nu_\tau$	A.32
$\tilde{t}_2 \to \phi\tilde{t}_1$	A.23	$\tilde{\nu}_\tau \to \tilde{\tau}_{1/2} W^+$	A.42
$\tilde{b}_2 \to \phi\tilde{b}_1$	A.26	$\tilde{\nu}_\tau \to \tilde{\tau}_{1/2} H^+$	A.41
$\tilde{q}_2 \to Z\tilde{q}_1$	A.29	$\tilde{\tau}_2 \to \tilde{\tau}_1 Z$	A.43
Chargino decays		$\tilde{\tau}_2 \to \tilde{\tau}_1 \phi$	A.44
$\tilde{W}_i^+ \to \bar{q}\tilde{q}'_L$	A.47	**Neutralino decays**	
$\tilde{W}_i^+ \to \bar{b}\tilde{t}_{1/2}$	A.48	$\tilde{Z}_i \to \bar{q}\tilde{q}_L/R$	A.75
$\tilde{W}_i^+ \to \bar{t}\tilde{b}_{1/2}$	A.51	$\tilde{Z}_i \to \bar{l}\tilde{l}_L/R$	A.77
$\tilde{W}_i^+ \to \bar{l}\tilde{l}_L$	A.55	$\tilde{Z}_i \to \bar{t}\tilde{t}_{1/2}$	A.79
$\tilde{W}_i^+ \to \bar{\tau}\tilde{\nu}_\tau$	A.57	$\tilde{Z}_i \to \bar{b}\tilde{b}_{1/2}$	A.83
$\tilde{W}_i^+ \to \bar{\tilde{\tau}}_{1/2}\nu_\tau$	A.60	$\tilde{Z}_i \to \bar{\tau}\tilde{\tau}_{1/2}$	A.86
$\tilde{W}_1^+ \to W\tilde{Z}_j$	A.62	$\tilde{Z}_i \to W\tilde{W}_{1/2}$	A.90
$\tilde{W}_1^+ \to H^-\tilde{Z}_j$	A.64	$\tilde{Z}_j \to H^+\tilde{W}_{1/2}$	A.92
$\tilde{W}_2 \to Z\tilde{W}_1$	A.67	$\tilde{Z}_i \to Z\tilde{Z}_j$	A.93
$\tilde{W}_2 \to \phi\tilde{W}_1$	A.69	$\tilde{Z}_i \to h\tilde{Z}_j$	A.94
$\tilde{W}_1^+ \to \pi^+\tilde{Z}_1$	A.72	$\tilde{Z}_i \to A\tilde{Z}_j$	A.96

Table A.1: MSSM 2-body decays included in the `SoftSusy` decay program, the references for the formulae in the appendices are given. ϕ here is $h/H/A$ i.e. any of the neutral Higgs bosons.

CP Even Higgs decays		**CP Odd Higgs decays**	
$h/H \to f\bar{f}$	A.98, A.1003	$A \to f\bar{f}$	A.100, A.1005
$h/H \to \tilde{Z}_i\tilde{Z}_j$	A.102	$A \to \tilde{Z}_i\tilde{Z}_j$	A.103
$h/H \to AZ$	A.112	$A \to hZ$	A.113
$h \to AA$	A.108	$A \to \tilde{f}_i\tilde{f}_j^*$	A.129
$H \to hh$	A.109	**CP Even/Odd Higgs decays**	
$H \to AA$	A.110	$\phi \to \tilde{W}_i^+\tilde{W}_i^-$	A.104
$H \to H^+H^-$	A.111	$\phi \to \tilde{W}_i^+\tilde{W}_j^-$	A.106
$h \to \tilde{q}_{L/R}\tilde{q}_{L/R}^*$	A.114	$\phi \to \gamma\gamma$	A.150
$H \to \tilde{q}_{L/R}\tilde{q}_{L/R}^*$	A.116	$\phi \to gg$	A.195, A.1011, A.1012
$h \to \tilde{l}_{L/R}\tilde{l}_{L/R}^*$	A.118	$\phi \to Z\gamma$	A.196
$h \to \tilde{t}_i\tilde{t}_j^*$	A.120	**Charged Higgs decays**	
$h \to \tilde{b}_i\tilde{b}_j^*$	A.123	$H^+ \to f\bar{f}'$	A.131
$h \to \tilde{\tau}_i\tilde{\tau}_j^*$	A.126	$H^+ \to \tilde{Z}_i\tilde{W}_j$	A.132
$h/H \to ZZ^*, ZZ$	A.144, A.149	$H^+ \to W^+h$	A.139
$h/H \to WW^*, WW$	A.145, A.148	$H^+ \to \tilde{f}_{L/R}\tilde{f'}_{L/R}$	A.140
		$H^+ \to \tilde{f}_i\tilde{f'}_j$	A.142

Table A.2: Higgs decays included in the `SoftSusy` decay program, the references for the formulae in the appendices are given. The same references may be given for different decays in cases where the underlying formulae are the same and the necessary replacements for different outgoing particles are described with the formulae. Multiple references are given for decays where QCD corrections are included, the first reference is the non-QCD corrected decay and the remainder are once QCD corrections are included.

Gluino 3-body decays		**Neutralino 3-body decays**	
$\tilde{g} \to q\bar{q}\tilde{Z}_i$	A.205	$\tilde{Z}_i \to \tilde{Z}_j f\bar{f}$	A.262
$\tilde{g} \to t\bar{t}\tilde{Z}_i$	A.217	$\tilde{Z}_i \to \tilde{W}_j f'\bar{f}$	A.393
$\tilde{g} \to b\bar{b}\tilde{Z}_i$	A.217	**Chargino 3-body decays**	
$\tilde{g} \to q\bar{q}'\tilde{W}_i^-$	A.235	$\tilde{W}_j \to \tilde{Z}_i\bar{f}'f$	A.393
$\tilde{g} \to t\bar{b}\tilde{W}_i^-$	A.235	$\tilde{W}_1^+ \to \pi^0\pi^+\tilde{Z}_1$	A.796

Table A.3: 3-body decays included in the `SoftSusy` decay program, the references for the formulae in the appendices are given. Not all 3-body decays are included as they are naturally suppressed with respect to the 2-body tree level decays. For this reason we have aimed only to incorporate the most phenomenologically relevant 3-body decays, however more may be added in future versions. The same reference is given for neutralino decays to a chargino, fermion and antifermion as for the "reverse" decays of a chargino to a neutralino, fermion and antifermion as this just results in minus signs in several places in the partial width formulae, which are given in the appendix.

Gravitino Decays			
$\tilde{g} \to g\tilde{G}$	A.799	$\tilde{q} \to q\tilde{G}$	A.800
$\tilde{Z}_i \to \gamma\tilde{G}$	A.801	$\tilde{l} \to l\tilde{G}$	A.800
$\tilde{Z}_i \to \phi\tilde{G}$	A.803	$\tilde{Z}_i \to Z\tilde{G}$	A.802

Table A.4: The Next-to-Lightest Susy Particle (NLSP) decays to gravitinos included in the program along with the appendix references for their formulae.

Neutralino Decays		**Decays into Neutralinos**	
$\tilde{Z}_i \to \tilde{q}_{L/R}\bar{q}$	A.959	$\tilde{q}_{L/R} \to q\tilde{Z}_i$	A.984
$\tilde{Z}_i \to \tilde{t}_{1/2}\bar{t}$	A.963	$\tilde{t}_{1/2} \to t\tilde{Z}_i$	A.987
$\tilde{Z}_i \to \tilde{b}_{1/2}\bar{b}$	A.966	$\tilde{b}_{1/2} \to b\tilde{Z}_i$	A.990
$\tilde{Z}_i \to \tilde{\tau}_{1/2}\bar{\tau}$	A.969	$\tilde{\tau}_{1/2} \to \tau\tilde{Z}_i$	A.993
$\tilde{Z}_i \to W\tilde{W}_{1/2}$	A.972	$\tilde{\nu}_{\tau_{1/2}} \to \nu_\tau\tilde{Z}_i$	A.996
$\tilde{Z}_i \to H^\pm\tilde{W}_{1/2}$	A.975	$\tilde{W}_1 \to H^\pm\tilde{Z}_j$	A.997
$\tilde{Z}_i \to Z\tilde{Z}_j$	A.978	$\tilde{W}_1 \to W\tilde{Z}_j$	A.1000
$\tilde{Z}_i \to h_k\tilde{Z}_j$	A.980		
$\tilde{Z}_i \to A_k\tilde{Z}_j$	A.982		

Table A.5: The NMSSM decays involving neutralinos that are included in the `SoftSusy` decay program. Note that any decays not involving neutralinos or neutral Higgs bosons are the same as in the MSSM.

CP Even Higgs Decays		**CP Odd Higgs Decays**	
$h_i \to f\bar{f}$	A.805, A.1003	$A_i \to f\bar{f}$	A.903, A.1005
$h_i \to \tilde{f}_{L/R}\tilde{f}_{L/R}$	A.807	$A_i \to \tilde{f}_L\tilde{f}_R$	A.905
$h_i \to \tilde{f}_{L/R}\tilde{f}_{R/L}$	A.810	$A_i \to \tilde{Z}_j\tilde{Z}_k$	A.907
$h_i \to \tilde{t}_j\tilde{t}_j$	A.812	$A_i \to \tilde{W}_j\tilde{W}_j$	A.909
$h_i \to \tilde{t}_1\tilde{t}_2$	A.814	$A_i \to \tilde{W}_1\tilde{W}_2$	A.911
$h_i \to \tilde{b}_j\tilde{b}_j$	A.812	$A_i \to h_jZ$	A.914
$h_i \to \tilde{b}_1\tilde{b}_2$	A.814	$A_i \to H^\pm W$	A.916
$h_i \to \tilde{\tau}_j\tilde{\tau}_k$	A.818	$A_i \to \gamma\gamma$	A.920
$h_i \to \tilde{W}_j\tilde{W}_j$	A.822	$A_i \to Z\gamma$	A.926
$h_i \to \tilde{W}_1\tilde{W}_2$	A.824	$A_i \to gg$	A.933, A.1019
$h_i \to \tilde{Z}_j\tilde{Z}_k$	A.827	**Decays into Higgs bosons**	
$h_i \to A_jA_k$	A.829	$\tilde{b}_2 \to \tilde{b}_1h_i$	A.937
$h_i \to A_jZ$	A.831	$\tilde{t}_2 \to \tilde{t}_1h_i$	A.941
$h_i \to H^+H^-$	A.833	$\tilde{\tau}_2 \to \tilde{\tau}_1h_i$	A.945
$h_i \to W^+H^-$	A.835	$\tilde{b}_2 \to \tilde{b}_1A_i$	A.949
$h_i \to ZZ^*$	A.842	$\tilde{t}_2 \to \tilde{t}_1A_i$	A.949
$h_i \to WW^*$	A.843	$\tilde{\tau}_2 \to \tilde{\tau}_1A_i$	A.949
$h_i \to ZZ$	A.842	$\tilde{W}_2 \to \tilde{W}_1h_i$	A.953
$h_i \to WW$	A.843	$\tilde{W}_2 \to \tilde{W}_1A_i$	A.956
$h_i \to \gamma\gamma$	A.851	$h_i \to h_jh_k$	A.836
$h_i \to gg$	A.890 A.1016	$h_i \to h_jh_k$	A.836
$h_i \to Z\gamma$	A.878	$A_2 \to Ah_i$	A.917

Table A.6: The NMSSM decays involving neutral Higgs bosons that are included in the `SoftSusy` decay program, the references for the formulae in the appendices are given, where two references are given the first is for the leading order case and the second for the QCD-corrected case. Note that any decays not involving neutralinos or neutral Higgs bosons are the same as in the MSSM.

A.2 Kinematic Functions

Here we begin the list of partial width expressions used in calculating the decay branching ratios in `SoftSusy`, we hope this provides a useful reference. With the exception of the 3-body decays, the majority of these widths were re-derived as a form of validation. First we list commonly occurring functions that arise from the kinematics of the decays: $\tilde{\lambda}^{1/2}$ appears as a result of the phase space integration:

$$\tilde{\lambda}^{1/2}(m_1, m_2, m_3) = \sqrt{\left(1 - (\frac{m_2 + m_3}{m_1})^2\right)\left(1 - (\frac{m_2 - m_3}{m_1})^2\right)}. \tag{A.1}$$

For loop integrals the real and imaginary parts of the loop give the following kinetic factor, where $\tau_a = 4(\frac{m_a}{m_{h_i}})^2$:

$$f(\tau) = \begin{cases} [\sin^{-1}(\frac{1}{\sqrt{\tau}})]^2, \text{for} & \tau \geq 1, \\ -\frac{1}{4}[\ln(\frac{1+\sqrt{1-\tau}}{1-\sqrt{1-\tau}}) - i\pi]^2, \text{for} & \tau < 1, \end{cases} \tag{A.2}$$

For the $Z\gamma$ decay loops, the kinetic factor $g(\tau)$ also occurs:

$$g(\tau) = \begin{cases} \sqrt{\tau - 1}\sin^{-1}(\frac{1}{\sqrt{\tau}}), \text{for} & \tau \geq 1, \\ \frac{1}{2}\sqrt{1-\tau}[\ln\left(\frac{1+\sqrt{1-\tau}}{1-\sqrt{1-\tau}}\right) - i\pi], \text{for} & \tau < 1. \end{cases} \tag{A.3}$$

A.3 MSSM Two Body Decay Formulae

Here we list for ease of reference the formulae for the partial widths of each of the $1 \to 2$ decay modes incorporated into the decay calculator `SoftSusy`. The $1 \to 2$ decay widths were all re-derived, the book by Baer and Tata [65] was used as a guide, however differences exist relative to their formulae. The formulae provided in `SUSYHIT` [84, 131, 132, 134] also provided a useful check.

A.3.1 Gluinos

The partial widths for the decays of the gluinos to squarks and quarks are[1]:

$$\Gamma(\tilde{g} \to q\tilde{q}_{L/R}) = \frac{\alpha_S}{4}\frac{1}{2m_{\tilde{g}}}(1 + \frac{m_q^2}{m_{\tilde{g}}^2} - \frac{m_{\tilde{q}_{L/R}}^2}{m_{\tilde{g}}^2})\tilde{\lambda}^{1/2}(m_{\tilde{g}}, m_q, m_{\tilde{q}_{L/R}}), \tag{A.4}$$

$$\Gamma(\tilde{g} \to q\tilde{q}_{1/2}) = \frac{\alpha_S}{4}\frac{1}{2m_{\tilde{g}}}[1 + \frac{m_q^2}{m_{\tilde{g}}^2} - \frac{m_{\tilde{q}_{L/R}}^2}{m_{\tilde{g}}^2} \mp 2\sin 2\theta_q \frac{m_q}{m_{\tilde{g}}}]\tilde{\lambda}^{1/2}(m_{\tilde{g}}, m_q, m_{\tilde{q}_{L/R}}). \tag{A.5}$$

A.3.2 Squarks

The partial widths for the decays of the squarks to quarks are[1]:

$$\Gamma(\tilde{q}_{L/R} \to q\tilde{g}) = \frac{4\alpha_S}{3}\frac{1}{2m_{\tilde{q}_{L/R}}}(1 - \frac{m_q^2}{m_{\tilde{q}_{L/R}^2}} - \frac{m_{\tilde{g}}^2}{m_{\tilde{q}_{L/R}^2}})\tilde{\lambda}^{1/2}(m_{\tilde{q}_{L,R}}, m_q, m_{\tilde{g}}), \tag{A.6}$$

$$\Gamma(\tilde{q}_{1/2} \to q\tilde{g}) = \frac{4\alpha_S}{3}\frac{1}{2m_{\tilde{q}_{1/2}}}(1 - \frac{m_q^2}{m_{\tilde{q}_{1/2}^2}} - \frac{m_{\tilde{g}}^2}{m_{\tilde{q}_{1/2}^2}} \pm 2\sin 2\theta_q \frac{m_q m_{\tilde{g}}}{m_{\tilde{q}_{1,2}}^2})\tilde{\lambda}^{1/2}(m_{\tilde{q}_{1,2}}, m_q, m_{\tilde{g}}), \tag{A.7}$$

[1] In both cases labelled the minus/plus sign applies for $\tilde{q}_1/\tilde{q}_2$ respectively.

$$\Gamma(\tilde{q}_L \to q^{'}\tilde{W}_1^-) = \frac{g^2}{\sin\theta^2_{L/R}}\frac{m_{\tilde{q}_L}}{16\pi}(1 - \frac{m^2_{\tilde{W}_1^-}}{m^2_{\tilde{q}_L}} - \frac{m^2_q}{m^2_{\tilde{q}_L}})\tilde{\lambda}^{1/2}(m_{\tilde{q}_L}, m_q, m_{\tilde{W}_1^-}). \tag{A.8}$$

Here the $'$ indicates that the quark produced is the opposite type to the squark (so $\tilde{d}_L$ produces an up quark for example), meanwhile θ_L and θ_R are for when up-type quarks (i.e. up or charm) or down-type quarks (i.e. down or strange) are produced respectively. The expression (A.8) applies for the first two generations of quarks as no mixing has been accounted for. The formula for decay to $\tilde{W}_2^-$ is similar but $\sin\theta_{L/R} \to \cos\theta_{L/R}$). The expressions with sfermion mixing, for the third generation of squarks, are:

$$\begin{aligned}\Gamma(\tilde{b}_1 \to \tilde{W}_1^- t) =& \frac{m_{\tilde{b}_1}}{16\pi}\Big[\{(-g\sin\theta_L\cos\theta_b + f_b\cos\theta_L\sin\theta_b)^2 + (-f_t\cos\theta_R\cos\theta_b)^2\}(1 - \frac{m^2_{\tilde{W}_1}}{m^2_{\tilde{b}_1}} - \frac{m^2_t}{m^2_{\tilde{b}_1}}) \\ &+ 4\frac{m_t m_{\tilde{W}_1}}{m^2_{\tilde{b}_1}}(-g\sin\theta_L\cos\theta_b + f_b\cos\theta_L\sin\theta_b)(-f_t\cos\theta_R\cos\theta_b)\Big]\tilde{\lambda}^{1/2}(m_{\tilde{b}_1}, m_t, m_{\tilde{W}_1}),\end{aligned} \tag{A.9}$$

$$\begin{aligned}\Gamma(\tilde{t}_1 \to \tilde{W}_1^+ b) =& \frac{m_{\tilde{t}_1}}{16\pi}\Big[\{(-g\sin\theta_R\cos\theta_t + f_t\cos\theta_R\sin\theta_t)^2 + (-f_b\cos\theta_L\cos\theta_t)^2\}(1 - \frac{m^2_{\tilde{W}_1}}{m^2_{\tilde{t}_1}} - \frac{m^2_b}{m^2_{\tilde{t}_1}}) \\ &+ 4\frac{m_b m_{\tilde{W}_1}}{m^2_{\tilde{t}_1}}(-g\sin\theta_R\cos\theta_t + f_t\cos\theta_R\sin\theta_t)(-f_b\cos\theta_L\cos\theta_t)\Big]\tilde{\lambda}^{1/2}(m_{\tilde{t}_1}, b, m_{\tilde{W}_1}),\end{aligned} \tag{A.10}$$

where

$$f_t = \frac{g m_t^{run}}{\sqrt{2} m_W \sin\beta}, \qquad f_b = \frac{g m_b^{run}}{\sqrt{2} m_W \cos\beta}. \tag{A.11}$$

(For decays of stops and sbottoms to $\tilde{W}_2^+$, $\sin\theta_{L/R} \to \cos\theta_{L/R}$ and $\cos\theta_{L/R} \to -\sin\theta_{L/R}$, and for decays of $\tilde{b}_2$ and $\tilde{t}_2$, $\sin\theta_{t/b} \to \cos\theta_{t/b}$ and $\cos\theta_{t/b} \to -\sin\theta_{t/b}$.) The squark decays to neutralinos are given by:

$$\Gamma(\tilde{q}_L \to \tilde{Z}_i q) = \frac{1}{2}(\pm g N_{2i} + \frac{g'}{3}N_{1i})^2 \frac{m_{\tilde{q}_L}}{16\pi}(1 - \frac{m^2_{\tilde{Z}_i}}{m^2_{\tilde{q}_L}} - \frac{m^2_q}{m^2_{\tilde{q}_L}})\tilde{\lambda}^{1/2}(m_{\tilde{q}_L}, m_q, m_{\tilde{Z}_i}), \tag{A.12}$$

$$\Gamma(\tilde{q}_R \to \tilde{Z}_i q) = \frac{1}{2}(\frac{a}{3}g' N_{1i})^2 \frac{m_{\tilde{q}_R}}{16\pi}(1 - \frac{m^2_{\tilde{Z}_i}}{m^2_{\tilde{q}_R}} - \frac{m^2_q}{m^2_{\tilde{q}_R}})\tilde{\lambda}^{1/2}(m_{\tilde{q}_R}, m_q, m_{\tilde{Z}_i}), \tag{A.13}$$

where $a = 4$ for up type squarks and $a = -2$ for down type squarks. N_{ji} are neutralino mixing matrix elements. Decays of $\tilde{t}_1$, $\tilde{b}_1$, $\tilde{t}_2$ and $\tilde{b}_2$ are similar except the mixing of the L and R parts gives a linear combination of the two pre-factors involving the elements N_{ji} with weights which are sines and cosines of the mixing angle $\theta_{t/b}$. In addition the Higgsino components of the neutralinos become important:

$$\Gamma(\tilde{t}_1 \to \tilde{Z}_i t) = \frac{m_{\tilde{t}_1}}{8\pi}\tilde{\lambda}^{1/2}(m_{\tilde{t}_1}, m_t, m_{\tilde{Z}_i})\Big[\frac{1}{2}\{a^2(1 - (\frac{m_t + m_{\tilde{Z}_i}}{m_{\tilde{t}_1}})^2) + b^2(1 - (\frac{m_t - m_{\tilde{Z}_i}}{m_{\tilde{t}_1}})^2)\}\Big], \tag{A.14}$$

$$a = \frac{1}{2}\left[\frac{1}{\sqrt{2}}\cos\theta_t[-gN_{2i} - \frac{g'}{3}N_{1i}] - f_u\sin\theta_t N_{4i} + \frac{4}{3\sqrt{2}}g' N_{1i} sin\theta_t - f_u N_{4i}\cos\theta_t\right], \tag{A.15}$$

$$b = \frac{1}{2}\left[\frac{1}{\sqrt{2}}\cos\theta_t[-gN_{2i} - \frac{g'}{3}N_{1i}] - f_u\sin\theta_t N_{4i} - \frac{4}{3\sqrt{2}}g' N_{1i}\sin\theta_t + f_u N_{4i}\cos\theta_t\right]. \tag{A.16}$$

Whilst

$$\Gamma(\tilde{b}_1 \to \tilde{Z}_i b) = \frac{m_{\tilde{b}_1}}{8\pi}\tilde{\lambda}^{1/2}(m_{\tilde{b}_1}, m_b, m_{\tilde{Z}_i})\left[a^2(1 - (\frac{m_{\tilde{Z}_i} + m_b}{m_{\tilde{b}_1}})^2) + b^2(1 - (\frac{m_{\tilde{Z}_i} - m_b}{m_{\tilde{b}_1}})^2)\right], \tag{A.17}$$

$$a = \frac{1}{2}\left[\frac{1}{\sqrt{2}}(\cos\theta_b[-N_{1i}\frac{g'}{3} + N_{3i}g)] - \sin\theta_b N_{3i} f_d - \frac{2}{3\sqrt{2}}\sin\theta_b N_{1i} g' - \cos\theta_b f_d N_{3i}\right], \tag{A.18}$$

$$b = \frac{1}{2}\left[\frac{1}{\sqrt{2}}(\cos\theta_b[-N_{1i}\frac{g'}{3} + N_{3i}g)] - \sin\theta_b N_{3i} f_d + \frac{2}{3\sqrt{2}}\sin\theta_b N_{1i} g' + \cos\theta_b f_d N_{3i}\right]. \tag{A.19}$$

As usual if we instead consider $\tilde{q}_2$, make the changes $m_{q_1} \to m_{q_2}$, $\cos\theta_q \to \sin\theta_q$ and $\sin\theta_q \to -\cos\theta_q$.

$$\Gamma(\tilde{t}_1 \to \tilde{b}_1 W^+) = \frac{g^2}{32\pi}\frac{m_{\tilde{t}_1}^3}{m_W^2}\tilde{\lambda}^{3/2}(m_{\tilde{t}_1}, m_W, m_{\tilde{b}_1})\cos^2\theta_t \cos^2\theta_b. \tag{A.20}$$

For $\tilde{t}_2$, $\cos\theta_t \to \sin\theta_t$, whereas for $\tilde{b}_2$ then $\cos\theta_b \to \sin\theta_b$. If the sbottoms are the initial states and stops are in the final state then exchange $m_{\tilde{t}_i}$ and $m_{\tilde{b}_i}$. For the decays to charged Higgs bosons:

$$\Gamma(\tilde{t}_1 \to \tilde{b}_1 H^+) = \frac{g^2}{32\pi m_{\tilde{t}_1} m_W^2} A^2 \tilde{\lambda}^{1/2}(m_{\tilde{t}_1}, m_{H^+}, m_{\tilde{b}_1}), \tag{A.21}$$

$$\begin{aligned} A =& m_t m_b(\tan\beta + \cot\beta)\sin\theta_t \sin\theta_b + m_t(\mu + A_t\cot\beta)\sin\theta_t\cos\theta_b + m_b(\mu + A_b\tan\beta)\sin\theta_b\cos\theta_t \\ &+ (m_b^2\tan\beta + m_t^2\cot\beta - m_W^2\sin 2\beta)\cos\theta_t\cos\theta_b. \end{aligned} \tag{A.22}$$

If instead we have $\tilde{t}_2$ then $\cos\theta_t \to \sin\theta_t$ and if we have $\tilde{b}_2$ then $\cos\theta_b \to \sin\theta_b$ and again if the sbottoms are the initial states and the stops are the final state then exchange $m_{\tilde{t}_i}$ and $m_{\tilde{b}_i}$.

$$\Gamma(\tilde{t}_2 \to \phi\tilde{t}_1) = \frac{A_\phi^2}{16\pi m_{\tilde{t}_2}}\tilde{\lambda}^{1/2}(m_{\tilde{t}_2}, m_\phi, m_{\tilde{t}_1}), \tag{A.23}$$

$$A_h = \frac{g m_W}{4}\sin(\beta+\alpha)\Big[1 - \frac{5}{3}\frac{g'^2}{g^2}\Big]\sin 2\theta_t + \frac{g m_t}{2 m_W \sin\beta}\cos 2\theta_t(A_t\cos\alpha + \mu\sin\alpha), \tag{A.24}$$

A_H is similar but we must transform $\cos\alpha \to -\sin\alpha$ and $\sin\alpha \to \cos\alpha$, whilst

$$A_A = \frac{g m_t}{2 m_W}(A_t\cot\beta + \mu). \tag{A.25}$$

For $\tilde{b}_2$ decaying to a Higgs and $\tilde{b}_1$:

$$\Gamma(\tilde{b}_2 \to \phi\tilde{b}_1) = \frac{B_\phi^2}{16\pi m_{\tilde{b}_2}}\tilde{\lambda}^{1/2}(m_{\tilde{b}_2}, m_\phi, m_{\tilde{b}_1}), \tag{A.26}$$

$$B_h = g m_W \sin(\alpha+\beta)\frac{1}{4}[-1 + \frac{1}{3}\frac{g'^2}{g^2}\sin 2\theta_b] + g m_b \cos 2\theta_b \frac{1}{2 m_W\cos\beta}[-A_b\sin\alpha - \mu\cos\alpha], \tag{A.27}$$

B_H is similar but again we must transform $\cos\alpha \to -\sin\alpha$ and $\sin\alpha \to \cos\alpha$, whilst

$$B_A = \frac{g m_b}{2 m_W}(A_b\tan\beta + \mu). \tag{A.28}$$

For third generation squark decays to Z bosons we have the following[2]:

$$\Gamma(\tilde{q}_2 \to Z\tilde{q}_1) = \frac{g^2 m_{\tilde{q}_2}^3}{64\pi m_Z^2\cos^2\theta_W}\tilde{\lambda}^{3/2}(m_{\tilde{q}_2}, m_{\tilde{q}_1}, m_Z)\cos^2\theta_q \sin^2\theta_q. \tag{A.29}$$

[2]Note that the amplitude is proportional to the sine squared of the mixing so this does not occur for the first two generations.

A.3.3 Sleptons

$$\Gamma(\tilde{l}_L \to l\tilde{Z}_i) = \frac{1}{2}[gN_{2i} + g'N_{1i}]^2 \frac{m_{\tilde{l}_L}}{16\pi}(1 - \frac{m^2_{\tilde{Z}_i}}{m^2_{\tilde{l}_L}} - \frac{m^2_l}{m^2_{\tilde{l}_L}})\tilde{\lambda}^{1/2}(m_{\tilde{l}_L}, m_l, m_{\tilde{Z}_i}). \tag{A.30}$$

$$\Gamma(\tilde{l}_R \to l\tilde{Z}_i) = \frac{1}{2}[g'N_{1i}]^2 \frac{m_{\tilde{l}_R}}{16\pi}(1 - \frac{m^2_{\tilde{Z}_i}}{m^2_{\tilde{l}_R}} - \frac{m^2_l}{m^2_{\tilde{l}_R}})\tilde{\lambda}^{1/2}(m_{\tilde{l}_R}, m_l, m_{\tilde{Z}_i}). \tag{A.31}$$

$$\Gamma(\tilde{\nu}_l \to \nu_l\tilde{Z}_i) = \frac{1}{2}[gN_{2i} - g'N_{1i}]^2 \frac{m_{\tilde{\nu}_l}}{16\pi}(1 - \frac{m^2_{\tilde{Z}_i}}{m^2_{\tilde{\nu}_l}})^2. \tag{A.32}$$

$$\Gamma(\tilde{l}_L \to \nu_l\tilde{W}_1^-) = \frac{g^2 \sin^2\theta_L}{16\pi} m_{\tilde{l}_L}(1 - \frac{m^2_{\tilde{W}_1}}{m^2_{\tilde{l}_L}})^2. \tag{A.33}$$

For decays to $\tilde{W}_2$ make the replacement $\sin\theta_L \to \cos\theta_L$.

$$\Gamma(\tilde{\nu}_l \to l\tilde{W}_1^+) = \frac{g^2 \sin^2\theta_R}{16\pi} m_{\tilde{\nu}_l}(1 - \frac{m^2_{\tilde{W}_1}}{m^2_{\tilde{\nu}_l}} - \frac{m^2_l}{m^2_{\tilde{\nu}_l}})^2 \tilde{\lambda}^{1/2}(m_{\tilde{\nu}_l}, m_l, m_{\tilde{W}_1}). \tag{A.34}$$

For decays to $\tilde{W}_2$ make the replacement $\sin\theta_R \to \cos\theta_R$.

$$\Gamma(\tilde{\tau}_1 \to \tau\tilde{Z}_i) = \frac{m_{\tilde{\tau}_1}}{8\pi}\left[a^2(1 - (\frac{m_\tau + m_{\tilde{Z}_i}}{m_{\tilde{\tau}_1}})^2) + b^2(1 - (\frac{m_\tau - m_{\tilde{Z}_i}}{m_{\tilde{\tau}_1}})^2)\right]\tilde{\lambda}^{1/2}(m_{\tilde{\tau}_1}, m_\tau, m_{\tilde{Z}_i}), \tag{A.35}$$

where

$$a = \frac{1}{2}\left[\frac{1}{\sqrt{2}}\sin\theta_\tau(gN_{2i} + g'N_{1i}) + f_\tau N_{3i}\cos\theta\tau - \sqrt{2}g'N_{1i}\cos\theta\tau + f_\tau N_{3i}\sin\theta\tau\right], \tag{A.36}$$

$$b = \frac{1}{2}\left[\frac{1}{\sqrt{2}}\sin\theta_\tau(gN_{2i} + g'N_{1i}) + f_\tau N_{3i}\cos\theta\tau + \sqrt{2}g'N_{1i}\cos\theta\tau + f_\tau N_{3i}\sin\theta\tau\right], \tag{A.37}$$

$$f_\tau = \frac{gm_\tau}{\sqrt{2}m_W\cos\beta}. \tag{A.38}$$

For $\tilde{\tau}_2$ decaying replace $m_{\tilde{\tau}_1} \to m_{\tilde{\tau}_2}$, $\cos\theta_\tau \to \sin\theta_\tau$ and $\sin\theta\tau \to -\cos\theta\tau$.

$$\Gamma(\tilde{\tau}_1 \to \nu_\tau\tilde{W}_1^-) = [-g\sin\theta_L\sin\theta_\tau - f_\tau\cos\theta_L\cos\theta_\tau]^2 m_{\tilde{\tau}_1}(1 - \frac{m^2_{\tilde{W}_1}}{m^2_{\tilde{\tau}_1}})^2. \tag{A.39}$$

For decays to $\tilde{W}_2$ make the replacements $m_{\tilde{W}_1} \to m_{\tilde{W}_2}$, $\sin\theta_L \to \cos\theta_L$ and $\cos\theta_L \to -\sin\theta_L$, meanwhile for $\tilde{\tau}_2$ decays change $m_{\tilde{\tau}_1} \to m_{\tilde{\tau}_2}$, $\cos\theta_\tau \to \sin\theta_\tau$ and $\sin\theta_\tau \to -\cos\theta_\tau$.

$$\begin{aligned}\Gamma(\tilde{\nu}_\tau \to \tau\tilde{W}_1^+) = \frac{m_{\tilde{\nu}_\tau}}{16\pi}\Big[&(g^2\sin^2\theta_R + f_\tau^2\cos^2\theta_L)(1 - \frac{m_{\tilde{W}_1}}{m^2_{\tilde{\nu}_\tau}} - \frac{m^2_\tau}{m^2_{\tilde{\nu}_\tau}}) \\ &- 4\frac{m_\tau m_{\tilde{W}_1}}{m^2_{\tilde{\nu}_\tau}} g\sin\theta_R f_\tau\cos\theta_L\Big]\tilde{\lambda}^{1/2}(m_{\tilde{\nu}_\tau}, m_\tau, m_{\tilde{W}_1}).\end{aligned} \tag{A.40}$$

For decays to $\tilde{W}_2$ then make the replacements $m_{\tilde{W}_1} \to m_{\tilde{W}_2}$, $\sin\theta_R \to \cos\theta_R$ and $\cos\theta_L \to -\sin\theta_L$.

$$\Gamma(\tilde{\tau}_1 \to \tilde{\nu}_\tau H^-) = \frac{g^2}{32\pi m^2_W m_{\tilde{\tau}_1}}\Big[m^2_\tau\tan\beta\sin\theta_\tau - m_\tau(\mu + A_\tau\tan\beta)\cos\theta_\tau\Big]^2\tilde{\lambda}^{1/2}(m_{\tilde{\tau}_1}, m_{\tilde{\nu}_\tau}, m^-_H). \tag{A.41}$$

For $\tilde{\tau}_2$ decays then one must make the changes $m_{\tilde{\tau}_1} \to m_{\tilde{\tau}_2}$, $\cos\theta_\tau \to \sin\theta_\tau$ and $\sin\theta_\tau \to -\cos\theta_\tau$ as usual.

$$\Gamma(\tilde{\tau}_1 \to \tilde{\nu}_\tau W^-) = \frac{g^2 \sin^2\theta_\tau m^3_{\tilde{\tau}_1}}{32\pi m_W^2} \tilde{\lambda}^{3/2}(m_{\tilde{\tau}_1}, m_{\tilde{\nu}_\tau}, m_W). \tag{A.42}$$

The equations for $\tilde{\tau}_{1/2} \to \tilde{\nu}_\tau W^-$ and $\tilde{\tau}_{1/2} \to \tilde{\nu}_\tau H^-$ can be used for $\tilde{\nu}_\tau \to \tilde{\tau}_{1/2} W^-$ and $\tilde{\nu}_\tau \to \tilde{\tau}_{1/2} H^-$ by interchanging the $m_{\tilde{\tau}_{1/2}} \leftrightarrow m_{\tilde{\nu}_\tau}$.

$$\Gamma(\tilde{\tau}_2 \to \tilde{\tau}_1 Z) = \frac{g^2 \sin^2\theta_\tau \cos^2\theta_\tau m^3_{\tilde{\tau}_2}}{64\pi m_Z^2 \cos^2\theta_W} \tilde{\lambda}^{3/2}(m_{\tilde{\tau}_2}.m_{\tilde{\tau}_1}, m_Z), \tag{A.43}$$

$$\Gamma(\tilde{\tau}_2 \to \tilde{\tau}_1 \phi) = \frac{\tilde{A}^2_\phi}{16\pi m_{\tilde{\tau}_2}} \tilde{\lambda}^{1/2}(m_{\tilde{\tau}_2}, m_{\tilde{\tau}_1}, m_\phi), \tag{A.44}$$

$$\tilde{A}_h = \frac{-g m_w}{4} \sin(\alpha+\beta) \sin 2\theta_\tau \Big[-1 + 3\frac{g'^2}{g^2} \Big] + \frac{g m_\tau}{2 m_W \cos\beta} \cos 2\theta_\tau (\mu \cos\alpha + A_\tau \sin\alpha), \tag{A.45}$$

$\tilde{A}_H$ is the same as $\tilde{A}_h$ but with the changes $\cos\alpha \to -\sin\alpha$ and $\sin\alpha \to \cos\alpha$, meanwhile $\tilde{A}_A$ is:

$$\tilde{A}_A = \frac{g m_\tau}{2 m_W} (\mu + A_\tau \tan\beta). \tag{A.46}$$

A.3.4 Charginos

$$\Gamma(\tilde{W}_1 \to \bar{q}\tilde{q}'_L) = \frac{3 m_{\tilde{W}_1}}{32\pi} (g^2 \sin^2\theta_{L/R}) (1 - \frac{m^2_{\tilde{q}_L}}{m^2_{\tilde{W}_1}} + \frac{{m_q}^2}{m^2_{\tilde{W}_1}}) \tilde{\lambda}^{1/2}(m_{\tilde{W}_1}, m_q, m_{\tilde{q}_L}). \tag{A.47}$$

Here the ' on the squark indicates it's of the opposite $SU(2)_L$ type to the quark, e.g. if the quark is an up then the squark is a $\tilde{d}_L$. Also note that θ_L occurs when up-type quarks (i.e. up or charm) are produced and θ_R is when down-type quarks are produced (i.e. down or strange). The formula for decay of $\tilde{W}_2^-$ is similar but we must change $\sin\theta_{L/R} \to \cos\theta_{L/R}$.

$$\Gamma(\tilde{W}_1^+ \to \bar{b}\tilde{t}_1) = \frac{3 m_{\tilde{W}_1}}{32\pi} \left[(\mathcal{A}^2 + C^2 \sin^2\theta_t)(1 - \frac{m^2_{\tilde{t}_1}}{m^2_{\tilde{W}_1}} + \frac{m^2_b}{m^2_{\tilde{W}_1}}) + 4\mathcal{A}C \sin\theta_t \frac{m_b}{m_{\tilde{W}_1}} \right] \tilde{\lambda}^{1/2}(m_{\tilde{W}_1}, m_b, m_{\tilde{t}_1}), \tag{A.48}$$

where

$$\mathcal{A} = g \sin\theta_R \cos\theta_t - f_u \cos\theta_R \sin\theta_t, \tag{A.49}$$

$$C = -f_d \cos\theta_L. \tag{A.50}$$

For $\tilde{t}_2$ take $\cos\theta_t \to \sin\theta_t$, $\sin\theta_t \to -\cos\theta_t$ and $m_{\tilde{t}_1} \to m_{\tilde{t}_2}$ and for $\tilde{W}_2$ take $\cos\theta_R \to -\sin\theta_R$, $\cos\theta_L \to -\sin\theta_L$ and $\sin\theta_R \to \cos\theta_R$, and also $m_{\tilde{W}_1} \to m_{\tilde{W}_2}$.

$$\Gamma(\tilde{W}_1^+ \to \bar{t}\tilde{b}_1) = \frac{3 m_{\tilde{W}_1}}{32\pi} \left[(\mathcal{A}^2 + C^2 \cos^2\theta_b)(1 - \frac{m^2_{\tilde{b}_1}}{m^2_{\tilde{W}_1}} + \frac{m^2_t}{m^2_{\tilde{W}_1}}) + 4\mathcal{A}C \cos\theta_b \frac{m_t}{m_{\tilde{W}_1}} \right] \tilde{\lambda}^{1/2}(m_{\tilde{W}_1}, m_t, m_{\tilde{b}_1}), \tag{A.51}$$

where now

$$\mathcal{A} = -g \sin\theta_L \cos\theta_b + f_d \cos\theta_L \sin\theta_b, \tag{A.52}$$

$$C = f_u \cos\theta_R, \tag{A.53}$$

$$f_t = \frac{g m_t^{run}}{\sqrt{2} m_W \sin\beta}, \qquad f_b = \frac{g m_b^{run}}{\sqrt{2} m_W \cos\beta}. \tag{A.54}$$

For $\tilde{b}_2$ take $\cos\theta_b \to \sin\theta_b$, $\sin\theta_b \to -\cos\theta_b$ and o $m_{\tilde{b}_1} \to m_{\tilde{b}_2}$. For $\tilde{W}_2$ take $\cos\theta_R \to -\sin\theta_R$,

$\cos\theta_L \to -\sin\theta_L$ and $\sin\theta_L \to \cos\theta_L$, and also $m_{\tilde{W}_1} \to m_{\tilde{W}_2}$.

$$\Gamma(\tilde{W}_i^+ \to \bar{l}\tilde{l}_L) = \frac{m_{\tilde{W}_i}}{32\pi} A^2 (1 - \frac{m_{\tilde{l}_L}^2}{m_{\tilde{W}_i}^2} + \frac{m_l^2}{m_{\tilde{W}_i}^2}) \tilde{\lambda}^{1/2}(m_{\tilde{W}_i}, m_l, m_{\tilde{l}_L}), \tag{A.55}$$

where

$$A = \begin{cases} -g \sin\theta_{L/R}, & \text{for } \tilde{W}_1. \\ -g \cos\theta_{L/R}, & \text{for } \tilde{W}_2. \end{cases} \tag{A.56}$$

θ_L is used for decays to ν_l and θ_R for decays to $\tilde{\nu}_{l_L}$.

$$\Gamma(\tilde{W}_i^+ \to \bar{\tau}\tilde{\nu}_\tau) = \frac{m_{\tilde{W}_i}}{32\pi} \left[(A^2 + B^2)(1 - \frac{m_{\tilde{\nu}_\tau}^2}{m_{\tilde{W}_i}^2} + \frac{m_\tau^2}{m_{\tilde{W}_i}^2}) + 4AB \frac{m_\tau}{m_{\tilde{W}_i}} \right] \tilde{\lambda}^{1/2}(m_{\tilde{W}_i}, m_\tau, m_{\tilde{\nu}_\tau}), \tag{A.57}$$

$$A = \begin{cases} g \sin\theta_R, & \text{for } \tilde{W}_1, \\ g \cos\theta_R, & \text{for } \tilde{W}_2, \end{cases} \tag{A.58}$$

$$B = \begin{cases} -f_\tau \cos\theta_L, & \text{for } \tilde{W}_1, \\ f_\tau \sin\theta_L, & \text{for } \tilde{W}_2, \end{cases} \tag{A.59}$$

and f_τ has been given before in (A.38).

$$\Gamma(\tilde{W}_i^+ \to \bar{\tilde{\tau}}_1 \nu_\tau) = \frac{m_{\tilde{W}_i}}{32\pi} \mathcal{A}^2 (1 - \frac{m_{\tilde{\tau}_1}^2}{m_{\tilde{W}_i}^2})^2, \tag{A.60}$$

where

$$\mathcal{A} = -g \sin\theta_L \sin\theta_\tau - f_\tau \cos\theta_L \cos\theta_\tau. \tag{A.61}$$

For $\tilde{W}_2$ make the replacements $\cos\theta_L \to -\sin\theta_L$, $\sin\theta_L \to \cos\theta_L$ and $m_{\tilde{W}_1} \to m_{\tilde{W}_2}$. For $\tilde{\tau}_2$ make the replacements $\cos\theta_\tau \to \sin\theta_\tau$, $\sin\theta_\tau \to -\cos\theta_\tau$ and $m_{\tilde{\tau}_1} \to m_{\tilde{\tau}_2}$.

$$\begin{aligned} \Gamma(\tilde{W}_1^+ \to W\tilde{Z}_j) = \frac{g^2}{16\pi |m_{\tilde{W}_1}|} \tilde{\lambda}^{1/2}(m_{\tilde{W}_1}, m_W, m_{\tilde{Z}_j}) \Big[(X^2 + Y^2) \Big(m_{\tilde{W}_1}^2 + m_{\tilde{Z}_j}^2 - m_W^2 \\ + \frac{1}{m_W^2} \{ (m_{\tilde{W}_1}^2 - m_{\tilde{Z}_j}^2)^2 - m_W^4 \} \Big) - 6(X^2 - Y^2) m_{\tilde{W}_1} m_{\tilde{Z}_j}) \Big], \end{aligned} \tag{A.62}$$

$$X = \frac{1}{2} [\cos\theta_R N_{4j} \frac{1}{\sqrt{2}} - \sin\theta_R N_{2j} - \cos\theta_L N_{3j} \frac{1}{\sqrt{2}} - \sin\theta_L N_{2j}]. \tag{A.63}$$

Y is the same as X except the first two terms change sign. For $\tilde{W}_2$ transform $\cos\theta_L \to -\sin\theta_L$, $\sin\theta_L \to \cos\theta_L$, $\cos\theta_R \to -\sin\theta_R$, $\sin\theta_R \to \cos\theta_R$ and change $m_{\tilde{W}_1} \to m_{\tilde{W}_2}$.

$$\begin{aligned} \Gamma(\tilde{W}_1^+ \to H^+ \tilde{Z}_j) = \frac{1}{16\pi |m_{\tilde{W}_1}|} \tilde{\lambda}^{1/2}(m_{\tilde{W}_1}, m_{H^-}, m_{\tilde{Z}_j}) [(a^2 + b^2)(m_{\tilde{W}_1}^2 + m_{\tilde{Z}_j}^2 - m_{H^-}^2) \\ + 2(a^2 - b^2) m_{\tilde{W}_1} m_{\tilde{Z}_j}], \end{aligned} \tag{A.64}$$

where

$$\begin{aligned} a &= \frac{1}{2}(-\cos\beta A_2 + \sin\beta A_4), \\ b &= \frac{1}{2}(-\cos\beta A_2 - \sin\beta A_4), \end{aligned} \tag{A.65}$$

$$A_2 = -\frac{1}{\sqrt{2}}[gN_{2j} + g'N_{1j}]\cos\theta_R - gN_{4j}\sin\theta_R,$$
$$A_4 = -\frac{1}{\sqrt{2}}[gN_{2j} + g'N_{1j}]\cos\theta_L + gN_{3j}\sin\theta_L. \tag{A.66}$$

For $\tilde{W}_2$ change $\cos\theta_L \to -\sin\theta_L$, $\sin\theta_L \to \cos\theta_L$, $\cos\theta_R \to -\sin\theta_R$, $\sin\theta_R \to \cos\theta_R$ and $m_{\tilde{W}_1} \to m_{\tilde{W}_2}$.

$$\Gamma(\tilde{W}_2 \to Z\tilde{W}_1) = \frac{1}{64\pi m_{\tilde{W}_2}}\tilde{\lambda}^{1/2}(m_{\tilde{W}_2}, m_Z, m_{\tilde{W}_1})\frac{(gg')^2}{g^2+g'^2}\Big[(\frac{g}{g'}+\frac{g'}{g})^2[(x^2+y^2)\Big(m^2_{\tilde{W}_2}+m^2_{\tilde{W}_1}-m^2_Z + \frac{1}{m^2_{\tilde{W}}}((m^2_{\tilde{W}_1}-m^2_{\tilde{W}_2})^2-m^4_Z)\Big) + 6(x^2-y^2)m_{\tilde{W}_1}m_{\tilde{W}_2}\Big], \tag{A.67}$$

where

$$x = \frac{1}{2}(\sin\theta_L\cos\theta_L - \sin\theta_R\cos\theta_R), \tag{A.68}$$

and y is the same as x except the second term changes sign.

$$\Gamma(\tilde{W}_2 \to \phi\tilde{W}_1) = \frac{g^2}{32\pi m_{\tilde{W}_2}}\tilde{\lambda}^{1/2}(m_{\tilde{W}_2}, m_\phi, m_{\tilde{W}_1})\Big[(S^2_\phi + P^2_\phi)(m^2_{\tilde{W}_2}+m^2_{\tilde{W}_1}-m^2_\phi) + 2(S^2_\phi - P^2_\phi)m_{\tilde{W}_1}m_{\tilde{W}_2}\Big], \tag{A.69}$$

$$S_h = \frac{1}{2}(-\sin\theta_R\sin\theta_L\sin\alpha - \cos\theta_L\cos\theta_R\cos\alpha + \sin\theta_L\sin\theta_R\cos\alpha + \cos\theta_L\cos\theta_R\sin\alpha), \tag{A.70}$$

P_h is the same as S_h except the first and second terms gain an extra minus sign (become +). S_H , P_H are the same as S_h and P_h if you take $\sin\alpha \to -\cos\alpha$ and $\cos\alpha \to \sin\alpha$.

$$S_A = \frac{1}{2}(\sin\theta_R\sin\theta_L\sin\beta - \cos\theta_L\cos\theta_R\cos\beta - \sin\theta_L\sin\theta_R\cos\beta + \cos\theta_L\cos\theta_R\sin\beta). \tag{A.71}$$

Again P_A is the same as S_A except the first two terms gain an additional minus sign.

For the case when the lightest chargino and the lightest neutralino are quasi-degenerate and ignoring decays to kaons (whose decays are Cabbibo suppressed by a factor of 20 or so), the partial width of the lightest chargino decaying into a pion and the lightest neutralino reads [289][3]:

$$\begin{aligned}\Gamma(\tilde{W}_1^+ \to \tilde{Z}_1\pi^+) &= \frac{f_\pi^2 G_F^2}{4\pi}\frac{\lambda(m_{\tilde{W}_1},\ m_{\tilde{Z}_1},\ m_{\pi^+})}{m_{\tilde{W}_1}}\Big\{(O^L_{11}+O^R_{11})^2\left[(m^2_{\tilde{W}_1}-m^2_{\tilde{Z}_1})^2 - m^2_{\pi^+}(m_{\tilde{Z}_1}-m_{\tilde{W}_1})^2\right] \\ &\quad +(O^R_{11}-O^L_{11})^2\left[(m^2_{\tilde{W}_1}-m^2_{\tilde{Z}_1})^2 - m^2_{\pi^+}(m_{\tilde{W}_1}+m_{\tilde{Z}_1})^2\right]\Big\},\end{aligned} \tag{A.72}$$

where $f_\pi \approx 93\,\text{MeV}$ is the pion decay constant and, noting that $\Theta(x)$ is the Heaviside theta function of x, we have:

$$O^L_{11} = (-i)^{1-\Theta(M_{\tilde{Z}_1})}(-i)^{1-\Theta(M_{\tilde{W}_1})}\left(-\frac{1}{\sqrt{2}}N_{14}\sin\theta_L + N_{12}\cos\theta_L\right), \tag{A.73}$$

$$O^R_{11} = i^{1-\Theta(M_{\tilde{Z}_1})}i^{1-\Theta(M_{\tilde{W}_1})}\left(\frac{1}{\sqrt{2}}N_{13}\sin\theta_R + N_{12}\cos\theta_R\right), \tag{A.74}$$

which account for the wino content of the lightest chargino and the lightest neutralino.

[3]Note that in Eq. A.72 we have switched conventions $O^L_{11} \leftrightarrow O^R_{11}$ with respect to Ref. [289].

A.3.5 Neutralinos

$$\Gamma(\tilde{Z}_i \to \bar{u}\tilde{u}_L/R) = \frac{3C^2|m_{\tilde{Z}_i}|}{32\pi}\tilde{\lambda}^{1/2}(m_{\tilde{Z}_i}, m_u, m_{\tilde{u}_{L/R}})(1 + \frac{m_u^2}{m_{\tilde{Z}_i}^2} - \frac{m_{\tilde{u}_{L/R}}^2}{m_{\tilde{Z}_i}^2}), \tag{A.75}$$

where

$$C = \begin{cases} \frac{1}{\sqrt{2}}(-gN_{2i} - \frac{g'}{3}N_{1i}), & \text{for } \tilde{u}_L, \\ \frac{-4}{3\sqrt{2}}g'N_{1i}, & \text{for } \tilde{u}_R. \end{cases} \tag{A.76}$$

Neutralino decays to charm and $\tilde{c}_{L/R}$ have a similar expression. For decays to down and $\tilde{d}_{L/R}$ or to strange and $\tilde{s}_{L/R}$ then C for the L component is the same as above except $g \to -g$ and C for the R component has a factor of 2 rather than -4 in the numerator of the pre-factor. The masses must also be changed appropriately. Note that the difference between the left-handed (LH) and right-handed (RH) squark comes from the LH squark coupling to both the zino and wino components of the neutralinos whereas the RH squark couples only to the zino components.

$$\Gamma(\tilde{Z}_i \to \bar{l}\tilde{l}_L/R) = \frac{C^2|m_{\tilde{Z}_i}|}{32\pi}\tilde{\lambda}^{1/2}(m_{\tilde{Z}_i}, m_l, m_{\tilde{l}_{L/R}})(1 + \frac{m_l^2}{m_{\tilde{Z}_i}^2} - \frac{m_{\tilde{l}_{L/R}}^2}{m_{\tilde{Z}_i}^2}), \tag{A.77}$$

$$C = \begin{cases} \frac{1}{\sqrt{2}}(gN_{2i} + g'N_{1i}), & \text{for } \tilde{l}_L, \\ \sqrt{2}g'N_{1i}, & \text{for } \tilde{l}_R. \end{cases} \tag{A.78}$$

Again the difference here between the L and R sleptons is due to the L sleptons coupling to the wino and zino components of the neutralinos whilst the R sleptons couple only to the zino components.

$$\Gamma(\tilde{Z}_i \to \bar{t}\tilde{t}_1) = \frac{3|m_{\tilde{Z}_i}|}{16\pi}\tilde{\lambda}^{1/2}(m_{\tilde{Z}_i}, m_t, m_{\tilde{t}_1}) \left[a^2\{(1 + \frac{m_t}{m_{\tilde{Z}_i}})^2 - (\frac{m_{\tilde{t}_1}}{m_{\tilde{Z}_i}})^2\} + b^2\{(1 - \frac{m_t}{m_{\tilde{Z}_i}})^2 - (\frac{m_{\tilde{t}_1}}{\tilde{Z}_i})^2\}\right], \tag{A.79}$$

$$a = \frac{1}{2}(\alpha + \beta), \qquad b = \frac{1}{2}(\alpha - \beta), \tag{A.80}$$

$$\alpha = \cos\theta_t \frac{1}{\sqrt{2}}[-gN_{2i} - \frac{g'}{3}N_{1i}] - f_t \sin\theta_t N_{4i}, \tag{A.81}$$

$$\beta = \frac{4}{3\sqrt{2}}g'N_{1i}\sin\theta_t - f_t\cos\theta_t N_{4i}. \tag{A.82}$$

For $\tilde{t}_2$ take $\cos\theta_t \to \sin\theta_t$, $\sin\theta_t \to -\cos\theta_t$ and $m_{\tilde{t}_1} \to m_{\tilde{t}_2}$.

$$\Gamma(\tilde{Z}_i \to \bar{b}\tilde{b}_1) = \frac{3|m_{\tilde{Z}_i}|}{16\pi}\tilde{\lambda}^{1/2}(m_{\tilde{Z}_i}, m_b, m_{\tilde{b}_1}) \left[a^2\{(1 + \frac{m_b}{m_{\tilde{Z}_i}})^2 - (\frac{m_{\tilde{b}_1}}{m_{\tilde{Z}_i}})^2\} + b^2\{(1 - \frac{m_b}{m_{\tilde{Z}_i}})^2 - (\frac{m_{\tilde{b}_1}}{\tilde{Z}_i})^2\}\right], \tag{A.83}$$

where a and b are as before but the α and β are different:

$$\alpha = \cos\theta_b \frac{1}{\sqrt{2}}[-\frac{g'}{3}N_{1i} + gN_{2i}] - f_b \sin\theta_b N_{3i}, \tag{A.84}$$

$$\beta = -\sin\theta_b \frac{2}{3\sqrt{2}}g'N_{1i} - \cos\theta_b f_b N_{3i}. \tag{A.85}$$

For $\tilde{b}_2$ take $\cos\theta_b \to \sin\theta_b$, $\sin\theta_b \to -\cos\theta_b$ and $m_{\tilde{b}_1} \to m_{\tilde{b}_2}$.

$$\Gamma(\tilde{Z}_i \to \bar{\tau}\tilde{\tau}_1) = \frac{|m_{\tilde{Z}_i}|}{16\pi}\tilde{\lambda}^{1/2}(m_{\tilde{Z}_i}, m_\tau, m_{\tilde{\tau}_1})\left[a^2\{(1-(\frac{m_\tau + m_{\tilde{\tau}_1}}{m_{\tilde{Z}_i}})^2\} + b^2\{(1-(\frac{m_\tau - m_{\tilde{\tau}_1}}{m_{\tilde{Z}_i}})^2\}\right], \quad \text{(A.86)}$$

$$a = \frac{1}{2}(\alpha+\beta), \qquad b = \frac{1}{2}(\beta-\alpha), \quad \text{(A.87)}$$

$$\alpha = \frac{1}{\sqrt{2}}\sin\theta_\tau[gN_{2i} + g'N_{1i}] + f_\tau N_{3i}\cos\theta_\tau, \quad \text{(A.88)}$$

$$\beta = -\sqrt{2}g'N_{1i}\cos\theta_\tau + f_\tau N_{3i}\sin\theta_\tau. \quad \text{(A.89)}$$

For $\tilde{\tau}_2$ make the replacements $\cos\theta_\tau \to \sin\theta_\tau$, $\sin\theta_\tau \to -\cos\theta_\tau$ and $m_{\tilde{\tau}_1} \to m_{\tilde{\tau}_2}$.

$$\begin{aligned}\Gamma(\tilde{Z}_i \to W\tilde{W}_1) =& \frac{g^2}{16\pi|m_{\tilde{Z}_i}|}\tilde{\lambda}^{1/2}(m_{\tilde{Z}_i}, m_W, m_{\tilde{W}_1})\Big[(X^2+Y^2)\times \\ & \Big(m^2_{\tilde{Z}_i} + m^2_{\tilde{W}_1} - m^2_W + \frac{1}{m^2_W}\{(m^2_{\tilde{Z}_i} - m^2_{\tilde{W}_1})^2 - m^4_W\}\Big) - 6(X^2-Y^2)m_{\tilde{Z}_i}m_{\tilde{W}_1}\Big],\end{aligned} \quad \text{(A.90)}$$

$$X = \frac{1}{2}[\cos\theta_R N_{4i}\frac{1}{\sqrt{2}} - \sin\theta_R N_{2i} - \cos\theta_L N_{3i}\frac{1}{\sqrt{2}} - \sin\theta_L N_{2i}], \quad \text{(A.91)}$$

and Y is the same as X except the first two terms get an extra minus sign. For $\tilde{W}_2$ change $\cos\theta_L \to -\sin\theta_L$, $\sin\theta_L \to \cos\theta_L$, $\cos\theta_R \to -\sin\theta_R$, $\sin\theta_R \to \cos\theta_R$ and $m_{\tilde{W}_1} \to m_{\tilde{W}_2}$.

$$\Gamma(\tilde{Z}_j \to H^+\tilde{W}_1) = \frac{1}{16\pi|m_{\tilde{Z}_i}|}\tilde{\lambda}^{1/2}(m_{\tilde{Z}_j}, m_{H^+}, m_{\tilde{W}_1})\Big[(a^2+b^2)(m^2_{\tilde{Z}_j} + m^2_{\tilde{W}_1} - m^2_{H^+}) + 2(a^2-b^2)m_{\tilde{Z}_j}m_{\tilde{W}_1}\Big], \quad \text{(A.92)}$$

where a and b and then A_2 and A_4 are exactly as given for the decay $\tilde{W}_1 \to H^+ Z_j$ in (A.64).

$$\begin{aligned}\Gamma(\tilde{Z}_i \to Z\tilde{Z}_j) = & \frac{g^2+g'^2}{64\pi|m_{\tilde{Z}_i}|}\tilde{\lambda}^{1/2}(m_{\tilde{Z}_{ij}}, m_Z, m_{\tilde{Z}_j})\{N_{4i}N_{4j} - N_{3i}N_{3j}\}^2 \\ & \times\left[m^2_{\tilde{Z}_i} + m^2_{\tilde{Z}_j} - m^2_Z + \frac{1}{m^2_Z}[(m^2_{\tilde{Z}_i} - m^2_{\tilde{Z}_j})^2 - m^4_Z] + 6m_{\tilde{Z}_i}m_{\tilde{Z}_j}\right].\end{aligned} \quad \text{(A.93)}$$

$$\Gamma(\tilde{Z}_i \to h\tilde{Z}_j) = \frac{(X^h_{ij} + X^h_{ji})^2}{16\pi|m_{\tilde{Z}_i}|}\tilde{\lambda}^{1/2}(m_{\tilde{Z}_{ij}}, m_h, m_{\tilde{Z}_j})[m^2_{\tilde{Z}_i} + m^2_{\tilde{Z}_j} - m^2_h + 2m_{\tilde{Z}_i}m_{\tilde{Z}_j}], \quad \text{(A.94)}$$

$$X^h_{ij} = \frac{1}{2}[N_{3i}\sin\alpha + N_{4i}\cos\alpha](-gN_{2j} + g'N_{1j}), \quad \text{(A.95)}$$

For $\tilde{Z}_i \to H\tilde{Z}_j$ the formula is the same except one must change $\sin\alpha \to -\cos\alpha$, $\cos\alpha \to \sin\alpha$ and $m_h \to m_H$.

$$\Gamma(\tilde{Z}_i \to A\tilde{Z}_j) = \frac{(X^A_{ij} + X^A_{ji})^2}{16\pi|m_{\tilde{Z}_i}|}\tilde{\lambda}^{1/2}(m_{\tilde{Z}_{ij}}, m_A, m_{\tilde{Z}_j})[m^2_{\tilde{Z}_i} + m^2_{\tilde{Z}_j} - m^2_A - 2m_{\tilde{Z}_i}m_{\tilde{Z}_j}], \quad \text{(A.96)}$$

$$X^A_{ij} = \frac{1}{2}[N_{3i}\sin\beta - N_{4i}\cos\beta](-gN_{2j} + g'N_{1j}). \quad \text{(A.97)}$$

A.3.6 Higgs Sector

Once more, the partial widths for all of the Higgs decays incorporated into `SoftSusy` were re-derived, including for the 3-body and 1-loop decays, however the majority of them can also be found in "The Higgs Hunter's Guide" [102].

$$\Gamma(h \to q\bar{q}) = \frac{3g^2 m_h}{32\pi}\Big(\frac{m_q}{m_W}\Big)^2 (1 - 4\frac{m_q^2}{m_h^2})^{\frac{3}{2}} \mathcal{J}^2, \tag{A.98}$$

where

$$\mathcal{J} = \begin{cases} \frac{\cos\alpha}{\sin\beta}, & \text{for up type quarks (u,c,t),} \\ \frac{\sin\alpha}{\cos\beta}, & \text{for down type quarks (d,s,b).} \end{cases} \tag{A.99}$$

The same formulae apply for the decays to leptons, however without the factor of 3 which arises due to colour. This is similar for $H \to qq$ except we must make the replacements $\sin\alpha \to -\cos\alpha$, $\cos\alpha \to \sin\alpha$ and $m_h \to m_H$.

With regards to the `SoftSusy` spectrum generator, when the mixing parameter is set to -1 it considers only third family Yukawa couplings to be non zero. This would mean no $h \to \mu\mu$ decay, which may be important phenomenologically in spite of its small branching ratio. In this case, for the decay, we use the pole muon mass to calculate the branching ratio.

$$\Gamma(A \to q\bar{q}) = \frac{3g^2 \mathcal{J}_A^2}{32\pi}\Big(\frac{m_q}{m_W}\Big)^2 m_A \sqrt{1 - 4(\frac{m_q}{m_A})^2}), \tag{A.100}$$

where

$$\mathcal{J}_A = \begin{cases} 1/(\tan\beta), & \text{for up type quarks (u,c,t),} \\ \tan\beta, & \text{for down type quarks (d,s,b).} \end{cases} \tag{A.101}$$

Again, the same formulae apply for the decays to leptons, however without the factor of 3 due to colour:

$$\Gamma(h \to \tilde{Z}_i \tilde{Z}_j) = \frac{|m_h|}{8\pi}(X_{ij}^h + X_{ji}^h)^2 \tilde{\lambda}^{\frac{1}{2}}(m_h, m_{\tilde{Z}_i}, m_{\tilde{Z}_j})\Big(1 - (\frac{m_{\tilde{Z}_i} + m_{\tilde{Z}_j}}{m_h})^2\Big), \tag{A.102}$$

with an extra pre-factor of $\frac{1}{2}$ if $i = j$ (as the above formula includes a pre-factor of 2 from $\tilde{Z}_i\tilde{Z}_j$ being indistinguishable from $\tilde{Z}_j\tilde{Z}_i$). Here X_{ij}^h is as in Eq. (A.95) and X_{ji}^h is the same but with $i \leftrightarrow j$. Again similar formulae exist for $H \to \tilde{Z}_i\tilde{Z}_j$ except we transform $\sin\alpha \to -\cos\alpha$, $\cos\alpha \to \sin\alpha$ and $m_h \to m_H$.

$$\Gamma(A \to \tilde{Z}_i \tilde{Z}_j) = \frac{|m_A|}{8\pi}(X_{ij}^A + X_{ji}^A)^2 \tilde{\lambda}^{\frac{1}{2}}(m_A, m_{\tilde{Z}_i}, m_{\tilde{Z}_j})\Big(1 - (\frac{m_{\tilde{Z}_i} + m_{\tilde{Z}_j}}{m_A})^2\Big), \tag{A.103}$$

here X_{ij}^A is as given in Eq. (A.97) and X_{ji}^A is the same but with $i \leftrightarrow j$.

$$\Gamma(\phi \to \tilde{W}_i^+ \tilde{W}_i^-) = \frac{g^2|m_\phi|}{4\pi} S^2 \tilde{\lambda}^a(m_\phi, m_{\tilde{W}_i}, m_{\tilde{W}_i}), \tag{A.104}$$

where $a = 3/2$ for $\phi = h, H$ or $a = 1/2$ for A and S is given by:

$$S = \begin{cases} \frac{1}{2}(-\sin\alpha\sin\theta_R\cos\theta_L + \cos\alpha\sin\theta_L\cos\theta_R), & \text{for: } h \to \tilde{W}_1\tilde{W}_1, \\ \frac{1}{2}(\sin\alpha\cos\theta_R\sin\theta_L - \cos\alpha\cos\theta_L\sin\theta_R), & \text{for: } h \to \tilde{W}_2\tilde{W}_2, \\ \frac{1}{2}(\cos\alpha\sin\theta_R\cos\theta_L + \sin\alpha\sin\theta_L\cos\theta_R), & \text{for: } H \to \tilde{W}_1\tilde{W}_1, \\ -\frac{1}{2}(\cos\alpha\cos\theta_R\sin\theta_L + \sin\alpha\cos\theta_L\sin\theta_R), & \text{for: } H \to \tilde{W}_2\tilde{W}_2, \\ \frac{1}{2}(\sin\beta\sin\theta_R\cos\theta_L + \cos\beta\sin\theta_L\cos\theta_R), & \text{for: } A \to \tilde{W}_1\tilde{W}_1, \\ -\frac{1}{2}(\sin\beta\cos\theta_R\sin\theta_L + \cos\beta\cos\theta_L\sin\theta_R), & \text{for: } A \to \tilde{W}_2\tilde{W}_2. \end{cases} \tag{A.105}$$

$$\Gamma(\phi \to \tilde{W}_i^+\tilde{W}_j^-) = \frac{g^2}{16\pi|m_\phi|}\tilde{\lambda}^{\frac{1}{2}}(m_\phi, m_{\tilde{W}_i}, m_{\tilde{W}_j})\left[S^2(1 - (\frac{m_{\tilde{W}_i} + m_{\tilde{W}_j}}{m_\phi})^2) + P^2(1 - (\frac{m_{\tilde{W}_i} - m_{\tilde{W}_j}}{m_\phi})^2)\right], \tag{A.106}$$

where

$$S = \begin{cases} \frac{1}{2}(\sin\alpha\sin\theta_R\sin\theta_L + \cos\alpha\cos\theta_L\cos\theta_R - \sin\theta_L\sin\theta_R\cos\alpha - \cos\theta_L\cos\theta_R\sin\alpha), & \text{for: } \phi = h, \\ \frac{1}{2}(-\cos\alpha\sin\theta_R\sin\theta_L + \sin\alpha\cos\theta_L\cos\theta_R - \sin\theta_L\sin\theta_R\sin\alpha + \cos\theta_L\cos\theta_R\cos\alpha), & \text{for: } \phi = H, \\ \frac{1}{2}(-\sin\beta\sin\theta_R\sin\theta_L + \cos\beta\cos\theta_L\cos\theta_R + \sin\theta_L\sin\theta_R\cos\beta - \cos\theta_L\cos\theta_R\sin\beta), & \text{for: } \phi = A. \end{cases} \tag{A.107}$$

P is the same as S except the signs of the first two terms are reversed.

$$\Gamma(h \to AA) = \frac{g^2 m_W^2}{128\pi|m_h|\cos^4(\theta_W)}\tilde{\lambda}^{\frac{1}{2}}(m_h, m_A, m_A)\sin^2(\alpha+\beta)\cos^2 2\beta. \tag{A.108}$$

$$\Gamma(H \to hh) = \frac{g^2 m_W^2}{128\pi|m_H|\cos^4(\theta_W)}\tilde{\lambda}^{\frac{1}{2}}(m_H, m_h, m_h)\Big[\cos 2\alpha\cos(\alpha+\beta) - 2\sin 2\alpha\sin(\alpha+\beta)\Big]^2. \tag{A.109}$$

$$\Gamma(H \to AA) = \frac{g^2 m_W^2}{128\pi|m_H|\cos^4(\theta_W)}\tilde{\lambda}^{\frac{1}{2}}(m_H, m_A, m_A)\cos^2 2\beta\cos^2(\alpha+\beta). \tag{A.110}$$

$$\Gamma(H \to H^+H^-) = \frac{g^2 m_W^2}{16\pi|m_H|}\tilde{\lambda}^{\frac{1}{2}}(m_H, m_{H^+}, m_{H^-})\left[\cos(\beta-\alpha) - \frac{\cos(\alpha+\beta)\cos 2\beta}{2\cos^2\theta_W}\right]^2. \tag{A.111}$$

$$\Gamma(h \to AZ) = \frac{g^2|m_h^3|\cos^2(\beta-\alpha)}{64\pi\cos^2\theta_w m_Z^2}\tilde{\lambda}^{\frac{3}{2}}(m_h, m_Z, m_A). \tag{A.112}$$

The decay $H \to AZ$ follows the same formula but with the changes $\cos(\beta-\alpha) \to \sin(\beta-\alpha)$ and $m_h \to m_H$.

$$\Gamma(A \to hZ) = \frac{g^2|m_A^3|\cos^2(\beta-\alpha)}{64\pi\cos^2\theta_w m_Z^2}\tilde{\lambda}^{\frac{3}{2}}(m_A, m_Z, m_h). \tag{A.113}$$

The decay $A \to HZ$ is not included as it's largely ruled out by SUSY mass constraints.

$$\Gamma(h \to \tilde{q}_{L/R}\tilde{q}^*_{L/R}) = \frac{3}{16\pi m_h}\tilde{\lambda}^{1/2}(m_h, m_{\tilde{q}_{L/R}}, m_{\tilde{q}_{L/R}})\mathcal{C}^2_{h\tilde{q}_{L/R}\tilde{q}_{L/R}}, \tag{A.114}$$

where

$$\mathcal{C}_{h\tilde{q}_{L/R}\tilde{q}_{L/R}} = \begin{cases} g\Big[m_W(\frac{1}{2} - \frac{1}{6}\frac{g'^2}{g^2})\sin(\beta+\alpha) - \frac{m_u^2\cos\alpha}{m_W\sin\beta}\Big], & \text{for: } \tilde{u}_L\bar{\tilde{u}}_L, \\ g\Big[m_W(-\frac{1}{2} - \frac{1}{6}\frac{g'^2}{g^2})\sin(\beta+\alpha) + \frac{m_d^2\sin\alpha}{m_W\cos\beta}\Big], & \text{for: } \tilde{d}_L\bar{\tilde{d}}_L, \\ g\Big[\frac{2}{3}m_W\frac{g'^2}{g^2}\sin(\beta+\alpha) - \frac{m_u^2\cos\alpha}{m_W\sin\beta}\Big], & \text{for: } \tilde{u}_R\bar{\tilde{u}}_R, \\ g\Big[\frac{-m_W}{3}\frac{g'^2}{g^2}\sin(\beta+\alpha) + \frac{m_d^2\sin\alpha}{m_W\cos\beta}\Big], & \text{for: } \tilde{d}_R\bar{\tilde{d}}_R, \\ \frac{gm_u}{2m_W\sin\beta}(\mu\sin\alpha + A_u\cos\alpha), & \text{for: } \tilde{u}_L\bar{\tilde{u}}_R \text{ or } \tilde{u}_R\bar{\tilde{u}}_L, \\ \frac{gm_d}{2m_W\cos\beta}(-\mu\cos\alpha - A_d\sin\alpha), & \text{for: } \tilde{d}_L\bar{\tilde{d}}_R \text{ or } \tilde{d}_R\bar{\tilde{d}}_L. \end{cases} \tag{A.115}$$

$$\Gamma(H \to \tilde{q}_{L/R}\tilde{q}^*_{L/R}) = \frac{3}{16\pi m_H}\tilde{\lambda}^{1/2}(m_H, m_{\tilde{q}_{L/R}}, m_{\tilde{q}_{L/R}})\mathcal{C}^2_{H\tilde{q}_{L/R}\tilde{q}_{L/R}}, \tag{A.116}$$

where

$$\mathcal{C}_{H\tilde{q}_{L/R}\tilde{q}_{L/R}} = \begin{cases} g\Big[-m_W(\frac{1}{2} - \frac{1}{6}\frac{g'^2}{g^2})\cos(\beta+\alpha) - \frac{m_u^2\sin\alpha}{m_W\sin\beta}\Big], & \text{for: } \tilde{u}_L\bar{\tilde{u}}_L, \\ g\Big[m_W(\frac{1}{2} + \frac{1}{6}\frac{g'^2}{g^2})\cos(\beta+\alpha) - \frac{m_d^2\cos\alpha}{m_W\cos\beta}\Big], & \text{for: } \tilde{d}_L\bar{\tilde{d}}_L, \\ g\Big[\frac{-2m_W}{3}\frac{g'^2}{g^2}\cos(\beta+\alpha) - \frac{m_u^2\sin\alpha}{m_W\cos\beta}\Big], & \text{for: } \tilde{u}_R\bar{\tilde{u}}_R, \\ g\Big[\frac{m_W}{3}\frac{g'^2}{g^2}\cos(\beta+\alpha) - \frac{m_d^2\cos\alpha}{m_W\cos\beta}\Big], & \text{for: } \tilde{d}_R\bar{\tilde{d}}_R, \\ \frac{gm_u}{2m_W\sin\beta}(-\mu\cos\alpha + A_u\sin\alpha), & \text{for: } \tilde{u}_L\bar{\tilde{u}}_R \text{ or } \tilde{u}_R\bar{\tilde{u}}_L, \\ \frac{gm_d}{2m_W\cos\beta}(-\mu\sin\alpha + A_d\cos\alpha), & \text{for: } \tilde{d}_L\bar{\tilde{d}}_R \text{ or } \tilde{d}_R\bar{\tilde{d}}_L. \end{cases} \tag{A.117}$$

$$\Gamma(h \to \tilde{l}_{L/R}\bar{\tilde{l}}_{L/R}) = \frac{1}{16\pi m_h}\tilde{\lambda}^{1/2}(m_h, m_{\tilde{l}_{L/R}}, m_{\tilde{l}_{L/R}})\mathcal{C}^2_{h\tilde{l}_{L/R}\tilde{l}_{L/R}}, \tag{A.118}$$

where

$$\mathcal{C}_{h\tilde{l}_{L/R}\tilde{l}_{L/R}} = \begin{cases} g\Big[m_W(\frac{1}{2} + \frac{1}{2}\frac{g'^2}{g^2})\Big]\sin(\beta+\alpha), & \text{for } \tilde{\nu}_L\tilde{\nu}^*_L, \\ g\Big[m_W(-\frac{1}{2} + \frac{1}{2}\frac{g'^2}{g^2})\sin(\alpha+\beta) + \frac{m^2_{\tilde{e}_L}\sin\alpha}{m_W\cos\beta}\Big], & \text{for } \tilde{e}_L\tilde{e}^*_L, \\ g\Big[-m_W\frac{g'^2}{g^2}\sin(\alpha+\beta) + \frac{m^2_{\tilde{e}_L}\sin\alpha}{m_W\cos\beta}\Big], & \text{for } \tilde{e}_R\tilde{e}^*_R, \\ \frac{gm_{\tilde{e}_L}}{2m_W\cos\beta}(-\mu\cos\alpha - A_e\sin\alpha), & \text{for } \tilde{e}_L\tilde{e}^*_R \text{ or } \tilde{e}_R\tilde{e}^*_L. \end{cases} \tag{A.119}$$

For third generation sfermions, the formulae are more complicated as a result of sfermion mixing and Yukawa coupling effects:

$$\Gamma(h \to \tilde{t}_i\tilde{t}^*_j) = \frac{3}{16\pi m_h}\tilde{\lambda}^{1/2}(m_h, m_{\tilde{t}_i}, m_{\tilde{t}_j})\mathcal{C}^2_{h\tilde{t}_i\tilde{t}_j}, \tag{A.120}$$

where here i and j can each be 1 or 2 independently of each other. The coupling depends on i and j, for $\tilde{t}_1\tilde{t}^*_1$ (i.e. $i = j = 1$):

$$\mathcal{C}_{h\tilde{t}_1\tilde{t}_1} = \cos^2\theta_t\mathcal{C}_{h\tilde{t}_L\tilde{t}_L} + \sin^2\theta_t\mathcal{C}_{h\tilde{t}_R\tilde{t}_R} - 2\sin\theta_t\cos\theta_t\mathcal{C}_{h\tilde{t}_L\tilde{t}_R}, \tag{A.121}$$

where $\mathcal{C}_{h\tilde{t}_L\tilde{t}_L}$, $\mathcal{C}_{h\tilde{t}_R\tilde{t}_R}$ and $\mathcal{C}_{h\tilde{t}_L\tilde{t}_R}$ are the corresponding couplings of $\tilde{u}_L\bar{\tilde{u}}_L$, $\tilde{u}_R\bar{\tilde{u}}_R$ and $\tilde{u}_L\bar{\tilde{u}}_R$, respectively with the changes $m_u \to m_t$ and $A_u \to A_t$. For $\tilde{t}_2\tilde{t}^*_2$ make the replacements $\cos\theta_t \to \sin\theta_t$, $\sin\theta_t \to$

$-\cos\theta_t$, $m_{\tilde{t}_1} \to m_{\tilde{t}_2}$. For $\tilde{t}_1\tilde{t}_2^*$ or $\tilde{t}_2\tilde{t}_1^*$:

$$\mathcal{C}_{h\tilde{t}_1\tilde{t}_2} = (\mathcal{C}_{h\tilde{t}_L\tilde{t}_L} - \mathcal{C}_{h\tilde{t}_R\tilde{t}_R})\cos\theta_t \sin\theta_t + \mathcal{C}_{h\tilde{t}_L\tilde{t}_R}\cos 2\theta_t. \tag{A.122}$$

For $H \to \tilde{t}_i\tilde{t}_j^*$ everything is as above but one must transform $\sin\alpha \to -\cos\alpha$ and $\cos\alpha \to \sin\alpha$ and $m_h \to m_H$.

$$\Gamma(h \to \tilde{b}_i\tilde{b}_j^*) = \frac{3}{16\pi m_h}\tilde{\lambda}^{1/2}(m_h, m_{\tilde{b}_i}, m_{\tilde{b}_j})\mathcal{C}^2_{h\tilde{b}_i\tilde{b}_j}. \tag{A.123}$$

For $\tilde{b}_1\tilde{b}_1^*$, i.e. $i = j = 1$:

$$\mathcal{C}_{h\tilde{b}_1\tilde{b}_1} = \mathcal{C}_{h\tilde{b}_L\tilde{b}_L}\cos^2\theta_b + \mathcal{C}_{h\tilde{b}_R\tilde{b}_R}\sin^2\theta_b - 2\cos\theta_b\sin\theta_b\mathcal{C}_{h\tilde{b}_L\tilde{b}_R}, \tag{A.124}$$

where $\mathcal{C}_{h\tilde{b}_L\tilde{b}_L}$, $\mathcal{C}_{h\tilde{b}_R\tilde{b}_R}$ and $\mathcal{C}_{h\tilde{b}_L\tilde{b}_R}$ correspond to the couplings for $\tilde{d}_L\bar{\tilde{d}}_L$, $\tilde{d}_R\bar{\tilde{d}}_R$ and $\tilde{d}_L\bar{\tilde{d}}_R$ with the changes $m_d \to m_b$ and $A_d \to A_b$. For $\tilde{b}_2\tilde{b}_2^*$ one must change $\cos\theta_b \to \sin\theta_b$, $\sin\theta_b \to -\cos\theta_b$, $m_{\tilde{b}_1} \to m_{\tilde{b}_2}$.

For $\tilde{b}_1\tilde{b}_2^*$ or $\tilde{b}_2\bar{\tilde{b}}_1$:

$$\mathcal{C}_{h\tilde{b}_1\tilde{b}_2} = (\mathcal{C}_{h\tilde{b}_L\tilde{b}_L} - \mathcal{C}_{h\tilde{b}_R\tilde{b}_R})\sin\theta_b\cos\theta_b + \mathcal{C}_{h\tilde{b}_L\tilde{b}_R}\cos 2\theta_b. \tag{A.125}$$

For $H \to \tilde{b}_i\tilde{b}_j^*$ everything is as above with the replacements $\sin\alpha \to -\cos\alpha$ and $\cos\alpha \to \sin\alpha$ and $m_h \to m_H$.

$$\Gamma(h \to \tilde{\tau}_1\tilde{\tau}_1^*) = \frac{1}{16\pi m_h}\tilde{\lambda}^{\frac{1}{2}}\mathcal{C}^2_{h\tilde{\tau}_1\tilde{\tau}_1}, \tag{A.126}$$

where

$$\mathcal{C}_{h\tilde{\tau}_1\tilde{\tau}_1} = \mathcal{C}_{h\tilde{\tau}_L\tilde{\tau}_L}\sin^2\theta_\tau + \mathcal{C}_{h\tilde{\tau}_R\tilde{\tau}_R}\cos^2\theta_\tau + 2\cos\theta_\tau\sin\theta_\tau\mathcal{C}_{h\tilde{\tau}_L\tilde{\tau}_R}. \tag{A.127}$$

$h \to \tilde{\tau}_2\tilde{\tau}_2^*$ is the same with the replacements $\cos\theta_\tau \to \sin\theta_\tau$, $\sin\theta_\tau \to -\cos\theta_\tau$ and $m_{\tilde{\tau}_1} \to m_{\tilde{\tau}_2}$. For $h \to \tilde{\tau}_1\tilde{\tau}_2^*$ or $\tilde{\tau}_2\tilde{\tau}_1^*$ the coupling is instead given by:

$$\mathcal{C}_{h\tilde{\tau}_1\tilde{\tau}_2} = (\mathcal{C}_{h\tilde{\tau}_R\tilde{\tau}_R} - \mathcal{C}_{h\tilde{\tau}_L\tilde{\tau}_L})\cos\theta_\tau\sin\theta_\tau + \mathcal{C}_{h\tilde{\tau}_L\tilde{\tau}_R}\cos 2\theta_\tau. \tag{A.128}$$

$\mathcal{C}_{h\tilde{\tau}_L\tilde{\tau}_L}$, $\mathcal{C}_{h\tilde{\tau}_R\tilde{\tau}_R}$ and $\mathcal{C}_{h\tilde{\tau}_L\tilde{\tau}_R}$ are identical to the corresponding couplings of $\tilde{e}_L\tilde{e}_L^*$, $\tilde{e}_R\tilde{e}_R^*$ and $\tilde{e}_L\tilde{e}_R^*$ respectively, with the expected replacements.

For $H \to \tilde{\tau}_i\tilde{\tau}_j^*$ everything is as above with the changes $\sin\alpha \to -\cos\alpha$, $\cos\alpha \to \sin\alpha$ and $m_h \to m_H$.

$$\Gamma(A \to \tilde{f}_i\tilde{f}_j^*) = \frac{N_c}{16\pi m_A}\tilde{\lambda}^{1/2}\mathcal{C}^2_{A\tilde{f}_i\tilde{f}_j}, \tag{A.129}$$

note that $i \neq j$ by CP conservation, and N_c is 3 for squarks and 1 for sleptons. The coupling is given by:

$$\mathcal{C}_{A\tilde{f}_i\tilde{f}_j} = \begin{cases} \frac{gm_f}{2m_W}(\mu + A_f\cot\beta), \text{ for} & u\text{-type sfermions } \tilde{u}, \tilde{c}, \tilde{t}, \tilde{\nu}, \\ \frac{gm_f}{2m_W}(\mu + A_f\tan\beta), \text{ for} & d\text{-type sfermions } \tilde{d}, \tilde{s}, \tilde{b}, \tilde{l}. \end{cases} \tag{A.130}$$

$$\Gamma(H^+ \to q\bar{q}') = \frac{3g^2CKM^2}{32\pi m_W^2 m_{H^+}}\tilde{\lambda}^{1/2}(m_{H^+}, m_{q_1}, m_{q_2})\Big\{[m_{q_1}^2\tan^2\beta + \frac{m_{q_2}^2}{\tan^2\beta}](m_{H^+}^2 - m_{q_1}^2 - m_{q_2}^2) - 4m_{q_1}^2 m_{q_2}^2\Big\}, \tag{A.131}$$

here m_{q_1} is the mass of the u-type quark and m_{q_2} is the mass of the d-type quark.

$$\Gamma(H^+ \to \tilde{Z}_i\tilde{W}_j) = \frac{1}{8\pi m_{H^+}}\tilde{\lambda}^{1/2}(m_{H^+}, m_{\tilde{Z}_i}, m_{\tilde{W}_j})\left[(a^2+b^2)(m_{H^+}^2 - m_{\tilde{Z}_i}^2 - m_{\tilde{W}_j}^2) - 2(a^2-b^2)m_{\tilde{Z}_i}m_{\tilde{W}_j}\right], \tag{A.132}$$

where for $j = 1$ i.e. $\tilde{W}_1$:

$$a = \frac{1}{2}(-\cos\beta A_2 + \sin\beta A_4), \qquad b = \frac{1}{2}(-\cos\beta A_2 - \sin\beta A_4), \tag{A.133}$$

for $j = 2$ i.e. $\tilde{W}_2$:

$$a = \frac{1}{2}(-\cos\beta A_1 + \sin\beta A_3), \qquad b = \frac{1}{2}(-\cos\beta A_1 - \sin\beta A_3). \tag{A.134}$$

The A_i are:

$$A_1 = \frac{1}{\sqrt{2}}[gN_{2i} + g'N_{1i}]\sin\theta_R - gN_{4i}\cos\theta_R, \tag{A.135}$$

$$A_2 = \frac{1}{\sqrt{2}}[-gN_{2i} - g'N_{1i}]\cos\theta_R - gN_{4i}\sin\theta_R, \tag{A.136}$$

$$A_3 = \frac{1}{\sqrt{2}}[gN_{2i} + g'N_{1i}]\sin\theta_L + gN_{3i}\cos\theta_L, \tag{A.137}$$

$$A_4 = \frac{1}{\sqrt{2}}[-gN_{2i} - g'N_{1i}]\cos\theta_L + gN_{3i}\sin\theta_L. \tag{A.138}$$

$$\Gamma(H^+ \to W^+ h) = \frac{g^2\cos^2(\beta-\alpha)m_{H^+}^3}{64\pi m_W^2}\tilde{\lambda}^{3/2}(m_{H^+}, m_W, m_h). \tag{A.139}$$

$$\Gamma(H^+ \to \tilde{q}_{L/R}\tilde{q'}_{L/R}) = \frac{3B}{16\pi m_{H^+}}\tilde{\lambda}^{1/2}(m_{H^+}, m_{\tilde{q}_{L/R}}, m_{\tilde{q'}_{L/R}}), \tag{A.140}$$

where B is the coupling and is given by:

$$B = \begin{cases} \frac{g}{\sqrt{2}}\Big[-m_W\sin 2\beta + \frac{1}{m_W}(m_d^2\tan\beta + m_u\cot\beta)\Big], & \text{for } \tilde{u}_L\tilde{d}_L, \\ g m_u m_d(\tan\beta + \cot\beta)\frac{1}{\sqrt{2}m_W}, & \text{for } \tilde{u}_R\tilde{d}_R, \\ \frac{-gm_d}{\sqrt{2}m_W}(A_d\tan\beta + \mu), & \text{for } \tilde{u}_L\tilde{d}_R, \\ \frac{-gm_u}{\sqrt{2}m_W}(A_u\cot\beta + \mu) & \text{for } \tilde{u}_R\tilde{d}_L. \end{cases} \tag{A.141}$$

$$\Gamma(H^+ \to \tilde{q}_i\tilde{q'}_j) = \frac{3}{16\pi m_{H^+}}\tilde{\lambda}^{1/2}(m_{H^+}, m_{\tilde{q}_i}, m_{\tilde{q}_j})C^2, \tag{A.142}$$

note that q is the top squark and q' the bottom squark; for $i = j = 1$ we have $\tilde{t}_1\tilde{b}_1$ and:

$$C = \cos\theta_t\cos\theta_b B_{\tilde{u}_L\tilde{d}_L} + \sin\theta_t\sin\theta_b B_{\tilde{u}_R\tilde{d}_R} - \cos\theta_t\sin\theta_b B_{\tilde{u}_L\tilde{d}_R} - \sin\theta_t\cos\theta_b B_{\tilde{u}_R\tilde{d}_L}, \tag{A.143}$$

for a $\tilde{b}_2$ take $\cos\theta_b \to \sin\theta_b$, $\sin\theta_b \to -\cos\theta_b$; for a $\tilde{t}_2$ take $\cos\theta_t \to \sin\theta_t$, $\sin\theta_t \to -\cos\theta_t$. The same formulae as in Eq.s (A.140) and (A.142) can be used for $H^\pm$ decays to sleptons, but for staus one must use $\theta_\tau - \pi/2$, so the replacements $\cos\theta_\tau \to \sin\theta_\tau$ and $\sin\theta_\tau \to -\cos\theta_\tau$ are necessary in C in Eq. (A.143).

Decays to two vector bosons are somewhat more complicated. Included in `SoftSusy` are the cases both where the Higgs has mass $m_{h/H} > 2m_V$, and so decays to two on-shell vector bosons, and also the case where the Higgs has mass $m_V < m_{h/H} < 2m_V$, so that it may only undergo a decay to one on-shell vector boson and one off-shell vector boson, which then decays into a fermion-antifermion pair, i.e. $h/H \to ZZ^* \to Zf\bar{f}$ or $h/H \to WW^* \to Wf'\bar{f}$. This is technically a 3-body decay but is included here as it is computed exactly without the need for numerical integration, unlike the 3-body decays listed later. To obtain the formulae for $h/H \to VV^*$, one therefore sums over all possible outgoing $f^{(\prime)}\bar{f}$

into which the V^* may decay. First consider the case where $m_V < m_{h/H} < 2m_V$ so we have decays $h/H \to WW^* \to Wf'\bar{f}$ and $h/H \to ZZ^* \to Zf\bar{f}$, this is how the SM-like lightest Higgs, h, will decay:

$$\Gamma(h/H \to ZZ^*) = \frac{G_F^2 m_{h/H} m_W^4 c_{h/HVV}^2}{64\pi^3 \cos^4\theta_W} F(\epsilon_Z)\left[7 - \frac{40}{3}\sin^2\theta_W + \frac{160}{9}\sin^4\theta_W\right], \tag{A.144}$$

$$\Gamma(h/H \to WW^*) = \frac{3G_F^2 m_W^4 m_{h/H} c_{h/HVV}^2}{16\pi^3} F(\epsilon_W), \tag{A.145}$$

here

$$\epsilon_V = \frac{m_V}{m_{h/H}}, \qquad c_{hVV} = \sin(\beta-\alpha), \qquad c_{HVV} = \cos(\beta-\alpha), \tag{A.146}$$

and

$$F(\epsilon_V) = \frac{3(1-8\epsilon_V^2+20\epsilon_V^4)}{\sqrt{4\epsilon_V^2-1}}\cos^{-1}\left[\frac{3\epsilon_V^2-1}{2\epsilon_V^3}\right] - (1-\epsilon_V^2)\left(\frac{47}{2}\epsilon_V^2 - \frac{13}{2} + \frac{1}{\epsilon_V^2}\right) - 3(1-6\epsilon_V^2+4\epsilon_V^4)\log(\epsilon_V). \tag{A.147}$$

If however $m_{h/H} > 2m_V$ then the decay to two on-shell vector bosons occurs instead and the formulae are:

$$\Gamma(h/H \to WW) = \frac{G_F m_{h/H}^3}{8\pi\sqrt{2}}\tilde{\lambda}^{\frac{1}{2}}(m_{h/H}, m_W, m_W)(1 - r^2 + \frac{3}{4}r^4)c_{h/HWW}^2, \tag{A.148}$$

$$\Gamma(h/H \to ZZ) = \frac{G_F m_{h/H}^3}{16\pi\sqrt{2}}\tilde{\lambda}^{\frac{1}{2}}(m_{h/H}, m_Z, m_Z)(1 - r^2 + \frac{3}{4}r^4)c_{h/HZZ}^2, \tag{A.149}$$

where $r = 2\frac{m_V}{m_{h/H}}$.

Throughout many of the decay formulae there is some ambiguity at tree-level about whether one should use $\frac{g^2}{8m_W^2}$ or $\frac{G_F}{\sqrt{2}}$, whilst these are formally equivalent they are not at a given order of calculation as $\frac{G_F}{\sqrt{2}}$ is a measured value, thereby containing many higher order vertex corrections. In general throughout the program we use $\frac{G_F}{\sqrt{2}}$ as this is found to give better agreement where higher order calculations are available. For example in the diboson decays comparing with `HDECAY-3.4`, which includes higher orders and finite width effects, we find that our agreement is improved using $\frac{G_F}{\sqrt{2}}$.

One loop decays to $\gamma\gamma$:

The function $f(\tau)$ appears, it is given previously in Eq. (A.2),

$$\Gamma(\phi \to \gamma\gamma) = \frac{G_F \alpha_{em}^2(m_\phi) m_\phi^3}{128\pi^3\sqrt{2}} ||\Sigma I_{loop}^\phi|^2, \tag{A.150}$$

where the I_{loop}^ϕ are the amplitudes of the contributions of different particles in the loop to the decay $\phi \to \gamma\gamma$. The top contributions are:

$$I_t^h = \frac{4}{3}\frac{\cos\alpha}{\sin\beta}\Big[-2\tau\{1 + (1-\tau)f(\tau)\}\Big], \tag{A.151}$$

$$I_t^H = \frac{4}{3}\frac{\sin\alpha}{\sin\beta}\Big[-2\tau\{1 + (1-\tau)f(\tau)\}\Big], \tag{A.152}$$

$$I_t^A = -\frac{8}{3}\tau f(\tau)\cot\beta. \tag{A.153}$$

The stop contributions for $h \to \gamma\gamma$ are:

$$I_{\tilde{t}_1}^h = \frac{4}{3}\tau(1-\tau f(\tau))\Big[R_{\tilde{t}_L\tilde{t}_L}^1 \cos^2\theta_t + R_{\tilde{t}_R\tilde{t}_R}^1 \sin^2\theta_t - 2R_{\tilde{t}_L\tilde{t}_R}^1 \cos\theta_t \sin\theta_t\Big], \tag{A.154}$$

$$I^h_{\tilde{t}_2} = \frac{4}{3}\tau(1-\tau f(\tau))\Big[R^2_{\tilde{t}_L\tilde{t}_L}\sin^2\theta_t + R^2_{\tilde{t}_R\tilde{t}_R}\cos^2\theta_t + 2R^2_{\tilde{t}_L\tilde{t}_R}\cos\theta_t\sin\theta_t\Big], \tag{A.155}$$

where

$$R^i_{\tilde{t}_L\tilde{t}_L} = R_{\tilde{t}_L}\frac{m_W}{gm_{\tilde{t}_i}} = \left[m_W(\frac{1}{2} - \frac{1}{6}\tan^2\theta_W)\sin(\alpha+\beta) - \frac{m_t^2\cos\alpha}{m_W\sin\beta}\right]\frac{m_W}{m_{\tilde{t}_i}}, \tag{A.156}$$

$$R^i_{\tilde{t}_R\tilde{t}_R} = R_{\tilde{t}_R}\frac{m_W}{gm_{\tilde{t}_i}} = \left[m_W\frac{2}{3}\tan^2\theta_W\sin(\alpha+\beta) - \frac{m_t^2\cos\alpha}{m_W\sin\beta}\right]\frac{m_W}{m_{\tilde{t}_i}}, \tag{A.157}$$

$$R^i_{\tilde{t}_L\tilde{t}_R} = R_{\tilde{t}_L\tilde{t}_R}\frac{m_W}{gm_{\tilde{t}_i}} = \frac{m_t}{2m_W\sin\beta}(\mu\sin\alpha + A_t\cos\alpha)\frac{m_W}{m_{\tilde{t}_i}}. \tag{A.158}$$

The stop contributions for H are the same but the $R^i_{\tilde{t}_L\tilde{t}_L}$, $R^i_{\tilde{t}_R\tilde{t}_R}$, $R^i_{\tilde{t}_L\tilde{t}_R}$ are different:

$$R^i_{\tilde{t}_L\tilde{t}_L} = \frac{m_W}{m_{\tilde{t}_i}}\left[-m_W(\frac{1}{2} - \frac{1}{6}\tan^2\theta_W)\cos(\alpha+\beta) - \frac{m_t^2\sin\alpha}{m_W\sin\beta}\right], \tag{A.159}$$

$$R^i_{\tilde{t}_R\tilde{t}_R} = \frac{m_W}{m_{\tilde{t}_i}}\left[-m_W\frac{2}{3}\tan^2\theta_W\cos(\alpha+\beta) - \frac{m_t^2\sin\alpha}{m_W\sin\beta}\right], \tag{A.160}$$

$$R^i_{\tilde{t}_L\tilde{t}_R} = \frac{m_W}{m_{\tilde{t}_i}}\frac{m_t}{2m_W\sin\beta}(-\mu\cos\alpha + A_t\sin\alpha). \tag{A.161}$$

$A \to \gamma\gamma$ has no stop loop contribution by CP conservation, i.e. $I^A_{\tilde{t}_{1/2}} = 0$. The bottom contributions are:

$$I^h_b = -\frac{1}{3}\Big[-2\tau\{1+(1-\tau)f(\tau)\}\Big]\frac{\sin\alpha}{\cos\beta}, \tag{A.162}$$

$$I^H_b = \frac{1}{3}\Big[-2\tau\{1+(1-\tau)f(\tau)\}\Big]\frac{\cos\alpha}{\cos\beta}, \tag{A.163}$$

$$I^A_b = -\frac{1}{3}\{2\tau f(\tau)\}\tan\beta. \tag{A.164}$$

The sbottom contributions to $h \to \gamma\gamma$ are as follows:

$$I^h_{\tilde{b}_1} = \frac{1}{3}\tau\{1-\tau f(\tau)\}\left[R^1_{\tilde{b}_L\tilde{b}_L}\cos^2\theta_b + R^1_{\tilde{b}_R\tilde{b}_R}\sin^2\theta_b - 2\sin\theta_b\cos\theta_b R^1_{\tilde{b}_L\tilde{b}_R}\right], \tag{A.165}$$

$$I^h_{\tilde{b}_2} = \frac{1}{3}\tau\{1-\tau f(\tau)\}\left[R^2_{\tilde{b}_L\tilde{b}_L}\sin^2\theta_b + R^2_{\tilde{b}_R\tilde{b}_R}\cos^2\theta_b + 2\sin\theta_b\cos\theta_b R^2_{\tilde{b}_L\tilde{b}_R}\right], \tag{A.166}$$

where here

$$R^i_{\tilde{b}_L\tilde{b}_L} = \frac{m_W}{m_{\tilde{b}_i}}\left[m_W(-\frac{1}{2} - \frac{1}{6}\tan^2\theta_W)\sin(\alpha+\beta) + \frac{m_b^2\sin\alpha}{m_W\cos\beta}\right], \tag{A.167}$$

$$R^i_{\tilde{b}_R\tilde{b}_R} = \frac{m_W}{m_{\tilde{b}_i}}\left[-\frac{1}{3}m_W\tan^2\theta_W\sin(\alpha+\beta) + \frac{m_b^2\sin\alpha}{m_W\cos\beta}\right], \tag{A.168}$$

$$R^i_{\tilde{b}_L\tilde{b}_R} = \frac{m_W}{m_{\tilde{b}_i}}\frac{m_b}{2m_W\cos\beta}(-\mu\cos\alpha - A_b\sin\alpha). \tag{A.169}$$

For $H \to \gamma\gamma$ the sbottom contributions are the same except the $R^i_{\tilde{b}_L\tilde{b}_L}$, $R^i_{\tilde{b}_R\tilde{b}_R}$, $R^i_{\tilde{b}_L\tilde{b}_R}$ change:

$$R^i_{\tilde{b}_L\tilde{b}_L} = \frac{m_W}{g m_{\tilde{b}_i}} g \left[m_W (\frac{1}{2} + \frac{1}{6}\tan^2\theta_W)\cos(\alpha+\beta) - \frac{m_b^2 \cos\alpha}{m_W \cos\beta} \right], \tag{A.170}$$

$$R^i_{\tilde{b}_R\tilde{b}_R} = \frac{m_W}{g m_{\tilde{b}_i}} g \left[m_W (\frac{1}{3}\tan^2\theta_W)\cos(\alpha+\beta) - \frac{m_b^2 \cos\alpha}{m_W \cos\beta} \right], \tag{A.171}$$

$$R^i_{\tilde{b}_L\tilde{b}_R} = \frac{m_W}{g m_{\tilde{b}_i}} g \frac{m_b}{2 m_W \cos\beta} [-\mu \sin\alpha + A_b \cos\alpha]. \tag{A.172}$$

$A \to \gamma\gamma$ has no sbottom loop contribution because of CP conservation, i.e. $I^A_{\tilde{b}_{1/2}} = 0$. The charm loop contributions are given by:

$$I^h_c = \frac{4}{3}\Big[-2\tau\{1 + (1-\tau) f(\tau)\}\Big] \frac{\cos\alpha}{\sin\beta}, \tag{A.173}$$

$$I^H_c = \frac{4}{3}\Big[-2\tau\{1 + (1-\tau) f(\tau)\}\Big] \frac{\sin\alpha}{\sin\beta}, \tag{A.174}$$

$$I^A_c = -\frac{4}{3}(2\tau f(\tau)) \cot\beta. \tag{A.175}$$

τ loop contributions are given by:

$$I^h_\tau = 2\tau[1 + (1-\tau) f(\tau)] \frac{\sin\alpha}{\cos\beta}, \tag{A.176}$$

$$I^H_\tau = -2\tau[1 + (1-\tau) f(\tau)] \frac{\cos\alpha}{\cos\beta}, \tag{A.177}$$

$$I^A_\tau = -2\tau f(\tau) \tan\beta. \tag{A.178}$$

$\tilde{\tau}_i$ contributions to $h \to \gamma\gamma$ are:

$$I_{\tilde{\tau}_1} = \tau\{1 - \tau f(\tau)\} \left[R^1_{\tilde{\tau}_L\tilde{\tau}_L} \sin^2\theta_\tau + R^1_{\tilde{\tau}_R\tilde{\tau}_R} \cos^2\theta_\tau + 2\sin\theta_\tau \cos\theta_\tau R^1_{\tilde{\tau}_L\tilde{\tau}_R} \right], \tag{A.179}$$

$$I_{\tilde{\tau}_2} = \tau\{1 - \tau f(\tau)\} \left[R^2_{\tilde{\tau}_L\tilde{\tau}_L} \cos^2\theta_\tau + R^2_{\tilde{\tau}_R\tilde{\tau}_R} \sin^2\theta_\tau - 2\sin\theta_\tau \cos\theta_\tau R^2_{\tilde{\tau}_L\tilde{\tau}_R} \right], \tag{A.180}$$

here

$$R^i_{\tilde{\tau}_L\tilde{\tau}_L} = \frac{m_W}{m_{\tilde{\tau}_i}} \left[m_W (-\frac{1}{2} + \frac{1}{2}\tan^2\theta_W)\sin(\alpha+\beta) + \frac{m_\tau^2 \sin\alpha}{m_W \cos\beta} \right], \tag{A.181}$$

$$R^i_{\tilde{\tau}_R\tilde{\tau}_R} = \frac{m_W}{m_{\tilde{\tau}_i}} \left[-m_W \tan^2\theta_W \sin(\alpha+\beta) + \frac{m_\tau^2 \sin\alpha}{m_W \cos\beta} \right], \tag{A.182}$$

$$R^i_{\tilde{\tau}_L\tilde{\tau}_R} = \frac{m_W}{m_{\tilde{\tau}_i}} \frac{m_\tau}{2 m_W \cos\beta} (-\mu \cos\alpha - A_\tau \sin\alpha). \tag{A.183}$$

For $H \to \gamma\gamma$ via $\tilde{\tau}_i$ it's the same except the $R^i_{\tilde{\tau}_L\tilde{\tau}_L}$, $R^i_{\tilde{\tau}_R\tilde{\tau}_R}$, $R^i_{\tilde{\tau}_L\tilde{\tau}_R}$ differ:

$$R^i_{\tilde{\tau}_L\tilde{\tau}_L} = \frac{m_W}{m_{\tilde{\tau}_i}} \left[m_W (\frac{1}{2} - \frac{1}{2}\tan^2\theta_W)\cos(\alpha+\beta) - \frac{m_\tau^2 \cos\alpha}{m_W \cos\beta} \right], \tag{A.184}$$

$$R^i_{\tilde{\tau}_R\tilde{\tau}_R} = \frac{m_W}{m_{\tilde{\tau}_i}} \left[m_W \tan^2\theta_W \cos(\alpha+\beta) - \frac{m_\tau^2 \cos\alpha}{m_W \cos\beta} \right], \tag{A.185}$$

$$R^i_{\tilde{\tau}_L\tilde{\tau}_R} = \frac{m_W}{m_{\tilde{\tau}_i}} \frac{m_\tau}{2 m_W \cos\beta} (-\mu \sin\alpha + A_\tau \cos\alpha). \tag{A.186}$$

$A \to \gamma\gamma$ has no stau loop contribution because of CP conservation, i.e. $I^A_{\tilde{\tau}_{1/2}} = 0$. The W loop contribu-

tions are:

$$I_W^h = \Big[2 + 3\tau + 3\tau(2-\tau)f(\tau)\Big]\sin(\beta-\alpha), \tag{A.187}$$

$$I_W^H = \Big[2 + 3\tau + 3\tau(2-\tau)f(\tau)\Big]\cos(\beta-\alpha). \tag{A.188}$$

$A \to \gamma\gamma$ has no W loop contribution because of CP conservation, i.e. $I_W^A = 0$. H^+ loop contributions are:

$$I_{H^+}^h = \tau\{1-\tau f(\tau)\}\frac{m_W^2}{m_{H^+}^2}\left[\sin(\beta-\alpha) + \frac{\cos 2\beta \sin(\beta+\alpha)}{2\cos^2\theta_W}\right], \tag{A.189}$$

$$I_{H^+}^H = \tau\{1-\tau f(\tau)\}\frac{m_W^2}{m_{H^+}^2}\left[\cos(\beta-\alpha) + \frac{\cos 2\beta \cos(\beta+\alpha)}{2\cos^2\theta_W}\right]. \tag{A.190}$$

$A \to \gamma\gamma$ has no H^+ loop contribution because of CP conservation, i.e. $I_{H^+}^A = 0$. $\tilde{W}_i^+$ loop contributions are:

$$I_{\tilde{W}_1^+}^h = [-2\tau\{1+(1-\tau)f(\tau)\}]\,\frac{m_W}{m_{\tilde{W}_1^+}}\sqrt{2}(-\sin\alpha\sin\theta_R\cos\theta_L + \cos\alpha\sin\theta_L\cos\theta_R), \tag{A.191}$$

$$I_{\tilde{W}_2^+}^h = [-2\tau\{1+(1-\tau)f(\tau)\}]\,\frac{m_W}{m_{\tilde{W}_2^+}}\sqrt{2}(\sin\alpha\cos\theta_R\sin\theta_L - \cos\alpha\cos\theta_L\sin\theta_R). \tag{A.192}$$

For $\tilde{W}_i^+$ contributions to H make replacements $\cos\alpha \to \sin\alpha$ and $\sin\alpha \to -\cos\alpha$, whilst for A the $\tilde{W}_i^+$ contributions are:

$$I_{\tilde{W}_1^+}^A = -2\tau f(\tau)\frac{m_W}{m_{\tilde{W}_1^+}}\sqrt{2}(\sin\theta_R\cos\theta_L\sin\beta + \sin\theta_L\cos\theta_R\cos\beta), \tag{A.193}$$

$$I_{\tilde{W}_2^+}^A = 2\tau f(\tau)\frac{m_W}{m_{\tilde{W}_2^+}}\sqrt{2}(\cos\theta_R\sin\theta_L\sin\beta + \cos\theta_L\sin\theta_R\cos\beta). \tag{A.194}$$

One loop decays to gg

The coloured particle loop contributions for $\phi \to gg$ are exactly the same, except the pre-factor changes and the b and $\tilde{b}$ contributions get multiplied by 4 in their amplitudes. There can be no uncoloured particles in the loop so there are no W, $H^\pm$, $\tilde{W}_i$, l or $\tilde{l}$ contributions; only q and $\tilde{q}$ loop contributions:

$$\Gamma(\phi \to gg) = \frac{\alpha_s^2(m_\phi)G_F m_\phi^3}{128\pi^3\sqrt{2}}\frac{9}{8}\Sigma|I_{loop}^\phi|^2, \tag{A.195}$$

with the $I_b^\phi \to 4I_b^\phi$, $I_{\tilde{b}_i}^\phi \to 4I_{\tilde{b}_i}^\phi$ and the remaining I_{loop}^ϕ as in the $\phi \to \gamma\gamma$ decays.

One Loop decays to $Z\gamma$: Throughout the function $g(\tau)$ appears, it is given previously in Eq. (A.3),

$$\Gamma(\phi \to Z\gamma) = \frac{m_\phi^3\alpha_{em}^2(m_\phi)}{64\pi^3}\frac{G_F}{\sqrt{2}}\left(1 - \frac{{m_Z}^2}{m_\phi}\right)^3\Sigma|I_{loop}^\phi|^2. \tag{A.196}$$

$I_1(\tau_a, \tau_{aZ})$ and $I_2(\tau_a, \tau_{aZ})$ also occur frequently, where $\tau_{aZ} = 4(\frac{m_a}{m_Z})^2$ in comparison with $\tau_a = 4(\frac{m_a}{m_{h_i}})^2$, they are as follows:

$$I_1(\tau_a, \tau_{aZ}) = \frac{\tau_a\tau_{aZ}}{2(\tau_a - \tau_{aZ})} + \frac{\tau_a^2\tau_{aZ}^2}{2(\tau_a-\tau_{aZ})^2}[f(\tau_a) - f(\tau_{aZ})] + \frac{\tau_a^2\tau_{aZ}}{(\tau_a-\tau_{aZ})^2}[g(\tau_a) - g(\tau_{aZ})], \tag{A.197}$$

$$I_2(\tau_a, \tau_{aZ}) = -\frac{\tau_a\tau_{aZ}}{2(\tau_a - \tau_{aZ})}[f(\tau_a) - f(\tau_{aZ})]. \tag{A.198}$$

The fermion loop contributions are:

$$I_t^h = 3\frac{\cos\alpha}{\sin\beta}\frac{-\frac{4}{3}(\frac{1}{2}-\frac{4}{3}\sin^2\theta_W)}{\sin\theta_W\cos\theta_W}\Big(I_1(\tau_t,\tau_{tZ})-I_2(\tau_t,\tau_{tZ})\Big), \tag{A.199}$$

$$I_b^h = -3\frac{\sin\alpha}{\cos\beta}\frac{\frac{2}{3}(-\frac{1}{2}+\frac{2}{3}\sin^2\theta_W)}{\sin\theta_w\cos\theta_W}\Big(I_1(\tau_b,\tau_{bZ})-I_2(\tau_b,\tau_{bZ})\Big), \tag{A.200}$$

For the I_f^H transform $\cos\alpha\to\sin\alpha$, $\sin\alpha\to-\cos\alpha$.

$$I_t^A = 3\cot\beta\frac{\frac{4}{3}(\frac{1}{2}-\frac{4}{3}\sin^2\theta_W)}{\sin\theta_W\cos\theta_W}I_2(\tau_t,\tau_{tZ}), \tag{A.201}$$

$$I_b^A = -3\tan\beta\frac{\frac{2}{3}(-\frac{1}{2}+\frac{2}{3}\sin^2\theta_W)}{\sin\theta_w\cos\theta_W}I_2(\tau_b,\tau_{bZ}). \tag{A.202}$$

I_c^h, I_s^h, I_c^A, I_s^A are analogous to I_t^h, I_b^h, I_t^A and I_b^A respectively.

The W loop contributions are given by:

$$I_W^h = -\frac{\sin(\beta-\alpha)}{\tan\theta_W}\left[4(3-\tan^2\theta_W)I_2(\tau_W,\tau_{WZ})+\{(1+\frac{2}{\tau_W})\tan^2\theta_W-(5+\frac{2}{\tau_W})\}I_1(\tau_W,\tau_{WZ})\right]. \tag{A.203}$$

I_W^H is the same but with the change $\sin(\beta-\alpha)\to\cos(\beta-\alpha)$. $I_W^A=0$ by CP conservation.

H^+ contributions are:

$$I_{H^+}^h = \left[\sin(\beta-\alpha)+\frac{\cos2\beta\sin(\beta+\alpha)}{2\cos^2\theta_W}\right]\frac{(1-2\sin^2\theta_W)}{\cos\theta_W\sin\theta_W}I_1(\tau_{H^+},\tau_{H^+Z})\frac{m_W^2}{m_{H^+}^2}. \tag{A.204}$$

For H, the $I_{H^+}^H$ are the same except the replacements $\sin(\beta-\alpha)\to\cos(\beta-\alpha)$ and $\sin(\beta+\alpha)\to-\cos(\beta+\alpha)$. Meanwhile $I_{H^+}^A=0$ by CP conservation.

A.4 MSSM Three Body Decay Formulae

The following decay modes are included in `SoftSusy`:

1. $h\to WW^*\to Wf'\bar{f}$
2. $h\to ZZ^*\to Zf\bar{f}$
3. $\tilde{g}\to\tilde{Z}_iq\bar{q}$
4. $\tilde{g}\to\tilde{W}_iq\bar{q}'$
5. $\tilde{Z}_i\to\tilde{Z}_jf\bar{f}$ where $i>j$
6. $\tilde{Z}_i\to\tilde{W}_jf\bar{f}'$
7. $\tilde{W}_j\to\tilde{Z}_if\bar{f}'$

The modes included are the most phenomenologically relevant modes, the formulae used were not re-derived although are written in our notation and are restructured to match the calculations performed in `SoftSusy`. The formulae are as provided in `sPHENO-3.3.8` [3,4], which were based on the calculations in [177,178].

$\underline{h\to VV*\to Vf\bar{f}}$ Detailed previously, see equations A.145 and A.144.

A.4.1 Gluino 3-body Decays

$\underline{\tilde{g} \to \tilde{Z}_i q \bar{q}}$

First the formulae for the decays to a neutralino and a quark-antiquark pair of the first two generations; here the Yukawa coupling contributions, squark mixing effects and final state quark masses have been neglected as they are negligible. The formulae later for the third generation quarks include all such effects.

$$\Gamma(\tilde{g} \to q\bar{q}\tilde{Z}_i) = \frac{\alpha_s}{8\pi^2}\Big[|A^q_{\tilde{Z}_i}|^2(\psi_L \pm \phi_L) + |B^q_{\tilde{Z}_i}|^2(\psi_R \pm \phi_R)\Big]. \tag{A.205}$$

Here which of the $\pm$ signs to take depends on the signs of the neutralino and gluino masses; the '+' sign applies for the case when both masses have the same sign so $m_{\tilde{Z}_i} > 0$ and $m_{\tilde{g}} > 0$ (or when they are both less than 0) and the '$-$' sign applies when one (but not both) of $m_{\tilde{Z}_i}$ and $m_{\tilde{g}}$ are negative. The signs essentially account for the fact that the couplings should become complex as the masses become negative. Here the $\psi_{L/R}$ and $\phi_{L/R}$ are integrals related to the $\tilde{\psi}$ and $\tilde{\phi}$ integrals given later in Eq.s (A.291) and (A.295) by:

$$\psi_{L/R} = \frac{1}{\pi^2 m_{\tilde{g}}}\tilde{\psi}(m_{\tilde{g}}, m_{\tilde{q}_{L/R}}, m_{\tilde{q}_{L/R}}, m_{\tilde{Z}_i}). \tag{A.206}$$

$$\phi_{L/R} = \frac{1}{\pi^2 m_{\tilde{g}}}\tilde{\phi}(m_{\tilde{g}}, m_{\tilde{q}_{L/R}}, m_{\tilde{q}_{L/R}}, m_{\tilde{Z}_i}). \tag{A.207}$$

The $A^q_{\tilde{Z}_i}$ and $B^q_{\tilde{Z}_i}$ are couplings which depend upon if the quarks are "up-type" or "down-type" in $SU(2)_L$:

$$A^q_{\tilde{Z}_i} = \begin{cases} \frac{1}{\sqrt{2}}(-gN_{2i} - \frac{g'}{3}N_{1i}), \text{ for "up-type" quarks,} \\ \frac{1}{\sqrt{2}}(gN_{2i} - \frac{g'}{3}N_{1i}), \text{ for "down-type" quarks,} \end{cases} \tag{A.208}$$

$$B^q_{\tilde{Z}_i} = \begin{cases} \frac{-4}{3\sqrt{2}}g'N_{1i}, \text{ for "up-type" quarks,} \\ \frac{2}{3\sqrt{2}}g'N_{1i}, \text{ for "down-type" quarks.} \end{cases} \tag{A.209}$$

As described in Section 3.3.5, in some circumstances we may have very compressed mass spectra, and in this limit the formulae provided here demonstrate numerical precision issues due to fine cancellation. In particular, in the ϕ integral it is seen that the terms $-[E_{\bar{f}}(max) - E_{\bar{f}}(min)]$ and $-\frac{m^2_{\tilde{Z}_j} - m^2_f + 2|m_{\tilde{Z}_i}|E_f - m^2_{\tilde{f}_2}}{2|m_{\tilde{Z}_i}|}\log Z(m_{\tilde{f}_2})$ of equation A.295 may cancel to such a degree that numerical precision (particularly in $\log Z$) affects the output of the integral. In general this may lead to the "partial widths" calculated being incorrect as they are purely a reflection of integrating a series of positive and negative numbers randomly distributed and reflecting numerical precision. Fortunately however, such fine cancellations only occur for extremely (a few hundred MeV) compressed spectra, which are naturally very phase-space suppressed. These modes are therefore only important to the phenomenology of the parent particles and the sparticle spectrum when they are the only modes available and so dictate the lifetime of the decaying particle. In the case of the gluino here, this occurs when the gluino is only a few hundred MeV larger in mass than the neutralino LSP ($\tilde{Z}_1$), in which case the decay to the first generation quark and antiquark pairs set the total width and lifetime of this near degenerate gluino. We therefore must attempt to circumvent numerical precision issues in this case to accurately reflect the phenomenology of such ultra-compressed spectra. In order to do so we therefore focus on the fine cancellation and expand in the limit of very compressed spectra in order to carry out any cancellation analytically, the formula remaining then contains only the remainder piece and so can be evaluated by `SoftSusy` accurately to give the partial widths and overall gluino lifetime relevant for these cases.

Consider the $\tilde{\phi}(m_{\tilde{g}}, m_{\tilde{q}_{L/R}}, m_{\tilde{q}_{L/R}}, m_{\tilde{Z}})$ integrand, which we call here $g(\tilde{\phi})$:

$$g(\tilde{\phi}) = \frac{-0.5\pi^2 |m_{\tilde{g}}||m_{\tilde{Z}}|}{m_{\tilde{g}}^2 + m_q^2 - 2|m_{\tilde{g}}|E_f - m_{\tilde{q}_{L/R}}^2} \Big[[E_{\bar{q}}(max) - E_{\bar{q}}(min)] + \frac{m_{\tilde{Z}}^2 - m_q^2 + 2|m_{\tilde{g}}|E_q - m_{\tilde{q}_{L/R}}^2}{2|m_{\tilde{g}}|} \log Z(m_{\tilde{q}_{L/R}}) \Big]. \tag{A.210}$$

The fine cancellation issues arise in the square brackets between the term $[E_{\bar{q}}(max) - E_{\bar{q}}(min)]$ and the final term, specifically the numerical precision issues often arise in the log as Z is given by:

$$Z(m_{\tilde{q}_{L/R}}) = \frac{m_{\tilde{g}}^2 + m_q^2 - 2|m_{\tilde{g}}|E_{\bar{q}}(max) - m_{\tilde{q}_{L/R}}^2}{m_{\tilde{g}}^2 + m_q^2 - 2|m_{\tilde{g}}|E_{\bar{q}}(min) - m_{\tilde{q}_{L/R}}^2}, \tag{A.211}$$

where $E_{\bar{q}}(max/min)$ are given in equation A.300. If the spectrum is very compressed, $E_{\bar{q}}(max)$ and $E_{\bar{q}}(min)$ are very close as their difference is given by:

$$E_{\bar{q}}(max) - E_{\bar{q}}(min) = p_q \frac{\sqrt{\zeta^2 - 4m_q^2(m_{\tilde{g}}^2 + m_q^2 - 2|m_{\tilde{g}}|E_q|)}}{m_{\tilde{g}}^2 + m_q^2 - 2|m_{\tilde{g}}|E_q}, \tag{A.212}$$

where $p_q = \sqrt{E_q^2 - m_q^2}$ and $\zeta = 2m_q^2 + m_{\tilde{g}}^2 - m_{\tilde{Z}}^2 - 2|m_{\tilde{g}}|E_q$ and the limits on the E_q integration run from $m_q \to (m_{\tilde{g}}^2 - 2m_q|m_{\tilde{Z}}| - m_{\tilde{Z}}^2)/(2|m_{\tilde{g}}|)$ which for very compressed spectra is of order a few times m_q. Consequently $p_q \sim m_q$ and $E_{\bar{q}}(max) - E_{\bar{q}}(min) \ll |m_{\tilde{g}}|$. In this limit, Z is very close to 1 and so the logarithm is very small, causing issues with numerical precision. The same behaviour also arises in the limit the intermediate squarks are much heavier than the initial and final state particles, i.e. when $m_{\tilde{q}_{L/R}} \gg m_{\tilde{g}}$. In this case, the same limit and expression we shall derive also applies. First we rewrite Z to make this closeness to 1 more explicit and Taylor expand the logarithm, taking the first term in this expansion:

$$Z(m_{\tilde{q}_{L/R}}) = 1 - \frac{2|m_{\tilde{g}}|(E_{\bar{q}}(max) - E_{\bar{q}}(min))}{m_{\tilde{g}}^2 + m_q^2 - 2|m_{\tilde{g}}|E_{\bar{q}}(min) - m_{\tilde{q}_{L/R}}^2}, \tag{A.213}$$

$$\log Z(m_{\tilde{q}_{L/R}}) = -\frac{2|m_{\tilde{g}}|(E_{\bar{q}}(max) - E_{\bar{q}}(min))}{m_{\tilde{g}}^2 + m_q^2 - 2|m_{\tilde{g}}|E_{\bar{q}}(min) - m_{\tilde{q}_{L/R}}^2} + \dots, \tag{A.214}$$

where we have neglected higher order terms. It is at this point that the limit $(E_{\bar{q}}(max) - E_{\bar{q}}(min)) \ll m_{\tilde{g}}$ or $m_{\tilde{g}} \ll m_{\tilde{q}_{L/R}}$ is taken. With this limit then we may rewrite our $g(\tilde{\phi})$ integrand as follows, where in the second line we explicitly perform the cancellation analytically in order to leave the remainder piece to be evaluated by `SoftSusy` without the issues of numerical precision:

$$\begin{aligned} g(\tilde{\phi}) &= \frac{0.5\pi^2 |m_{\tilde{g}}||m_{\tilde{Z}}|[E_{\bar{q}}(max) - E_{\bar{q}}(min)]}{m_{\tilde{g}}^2 + m_q^2 - 2|m_{\tilde{g}}|E_f - m_{\tilde{q}_{L/R}}^2} \Big[-1 + \frac{m_{\tilde{Z}}^2 - m_q^2 + 2|m_{\tilde{g}}|E_q - m_{\tilde{q}_{L/R}}^2}{m_{\tilde{g}}^2 + m_q^2 - 2|m_{\tilde{g}}|E_{\bar{q}}(min) - m_{\tilde{q}_{L/R}}^2} \Big] \\ &= \frac{0.5\pi^2 |m_{\tilde{g}}||m_{\tilde{Z}}|[E_{\bar{q}}(max) - E_{\bar{q}}(min)]}{m_{\tilde{g}}^2 + m_q^2 - 2|m_{\tilde{g}}|E_f - m_{\tilde{q}_{L/R}}^2} \Big[-1 + 1 + \frac{m_{\tilde{Z}}^2 - 2m_q^2 + 2|m_{\tilde{g}}|E_q + 2|m_{\tilde{g}}|E_{\bar{q}}(min) - m_{\tilde{g}}^2}{m_{\tilde{g}}^2 + m_q^2 - 2|m_{\tilde{g}}|E_{\bar{q}}(min) - m_{\tilde{q}_{L/R}}^2} \Big]. \end{aligned} \tag{A.215}$$

Consequently, in the limit of a very compressed spectrum or very large intermediate squark masses, we may improve numerical precision and avoid fine cancellations by instead evaluating:

$$g(\tilde{\phi}) = \frac{0.5\pi^2 |m_{\tilde{g}}||m_{\tilde{Z}}|[E_{\bar{q}}(max) - E_{\bar{q}}(min)]}{m_{\tilde{g}}^2 + m_q^2 - 2|m_{\tilde{g}}|E_f - m_{\tilde{q}_{L/R}}^2} \Big[\frac{m_{\tilde{Z}}^2 - 2m_q^2 + 2|m_{\tilde{g}}|E_q + 2|m_{\tilde{g}}|E_{\bar{q}}(min) - m_{\tilde{g}}^2}{m_{\tilde{g}}^2 + m_q^2 - 2|m_{\tilde{g}}|E_{\bar{q}}(min) - m_{\tilde{q}_{L/R}}^2} \Big]. \tag{A.216}$$

As this situation is only of importance where these modes are the only modes available (as otherwise they will be completely swamped by less phase space suppressed modes), we currently apply this only to the cases of gluino decays to the lightest neutralino and the first generation quarks ($\tilde{g} \to \tilde{Z}_i u\bar{u}$ or $\tilde{g} \to \tilde{Z}_i d\bar{d}$). The limiting formula Eq. A.216 is taken when $p_t < 10 m_{\tilde{g}}$ or $m_{\tilde{q}_{L/R}} < 5 m_{\tilde{g}}$ (these choices are somewhat arbitrary and can be changed by the user). We leave an investigation of the precise points to change between the two formulae, and to whether similar limits may be taken for other very compressed 3-body decays (such as those of neutralinos and charginos) to future study.

For the more complicated case of decays to third generation quarks; the Yukawa coupling contributions, squark-mixing effects and final state quark masses are all included as they can have significant effects. The decay is mediated by either $\tilde{t}_1$ or $\tilde{t}_2$ in the t or u channel, giving 4 Feynman diagrams (2 shown below as $j = 1, 2$) and 6 (i.e. ${}^4C_2$) interferences. The six interferences can be split into 2 "diagonal" contributions ($\tilde{t}_1$ t - $\tilde{t}_1$ u interference and $\tilde{t}_2$ t - $\tilde{t}_2$ u interference) and 4 "non-diagonal" contributions ($\tilde{t}_1$ t - $\tilde{t}_2$ t, $\tilde{t}_1$ t - $\tilde{t}_2$ u, $\tilde{t}_1$ u - $\tilde{t}_2$ t and $\tilde{t}_1$ u - $\tilde{t}_2$ u interferences). The possibility of negative neutralino masses (which can be absorbed into imaginary couplings) is also included. The formulae are adopted from `sPHENO`, it should be noted that differences exit between these formulae and those present in Baer and Tata's book [65].

(a) channel a (b) channel b

Figure A.1: Feynman diagrams for the 3-body decay of a gluino into a neutralino and a top-antitop pair, as mediated by stops $\tilde{t}_{1/2}$. $i = 1, 2, 3, 4$ and $j = 1, 2$.

The formulae for the case of $\tilde{g} \to \tilde{Z}_i t\bar{t}$ are given, from this decays to other quarks can be obtained by making the appropriate replacements.

$$\Gamma(\tilde{g} \to t\bar{t}\tilde{Z}_i) = \frac{\alpha_s}{8\pi^4 m_{\tilde{g}}}[\Gamma_{\tilde{t}_1} + \Gamma_{\tilde{t}_2} + \Gamma_{\tilde{t}_1\tilde{t}_2}]. \tag{A.217}$$

The $\Gamma_{\tilde{t}_1}$, $\Gamma_{\tilde{t}_2}$, $\Gamma_{\tilde{t}_1\tilde{t}_2}$ can be split up into different contributions:

$$\Gamma_{\tilde{t}_1} = \Gamma_{LL}(\tilde{t}_1)\cos^2\theta_t + \Gamma_{RR}(\tilde{t}_1)\sin^2\theta_t - \sin\theta_t\cos\theta_t\Big[\Gamma_{L_1R_1}(\tilde{t}_1) + \Gamma_{L_1R_2}(\tilde{t}_1) + \Gamma_{L_2R_1}(\tilde{t}_1) + \Gamma_{L_2R_2}(\tilde{t}_1)\Big]. \tag{A.218}$$

$$\Gamma_{\tilde{t}_2} = \Gamma_{LL}(\tilde{t}_2)\sin^2\theta_t + \Gamma_{RR}(\tilde{t}_2)\cos^2\theta_t + \sin\theta_t\cos\theta_t\Big[\Gamma_{L_1R_1}(\tilde{t}_2) + \Gamma_{L_1R_2}(\tilde{t}_2) + \Gamma_{L_2R_1}(\tilde{t}_2) + \Gamma_{L_2R_2}(\tilde{t}_2)\Big]. \tag{A.219}$$

$$\Gamma_{\tilde{t}_1\tilde{t}_2} = \Big[\Gamma_{LL}(\tilde{t}_1,\tilde{t}_2) + \Gamma_{RR}(\tilde{t}_1,\tilde{t}_2)\Big]\sin\theta_t\cos\theta_t + \Gamma_{LR}(\tilde{t}_1,\tilde{t}_2)\cos^2\theta_t + \Gamma_{RL}(\tilde{t}_1,\tilde{t}_2)\sin^2\theta_t. \tag{A.220}$$

The moduli of the complex couplings are as follows:

$$|\alpha_1^{\tilde{t}_1}| = \tilde{A}^t_{\tilde{Z}_i}\cos\theta_t - f_t N_{4i}\sin\theta_t, \qquad |\beta_1^{\tilde{t}_1}| = f_t N_{4i}\cos\theta_t + \tilde{B}^t_{\tilde{Z}_i}\sin\theta_t, \tag{A.221}$$

$$|\alpha_1^{\tilde{t}_2}| = \tilde{A}^t_{\tilde{Z}_i}\sin\theta_t + f_t N_{4i}\cos\theta_t, \qquad |\beta_1^{\tilde{t}_2}| = f_t N_{4i}\sin\theta_t - \tilde{B}^t_{\tilde{Z}_i}\cos\theta_t, \tag{A.222}$$

where

$$\tilde{A}^t_{\tilde{Z}_i} = -\frac{g}{\sqrt{2}}N_{2i} - \frac{g^{'}}{3\sqrt{2}}N_{1i}, \qquad \text{(A.223)} \qquad \tilde{B}^t_{\tilde{Z}_i} = -\frac{4}{3}\frac{g^{'}}{\sqrt{2}}N_{1i}, \qquad \text{(A.224)}$$

$$f_t = \frac{g m_t^{run}}{\sqrt{2} M_W \sin\beta}. \qquad \text{(A.225)}$$

The overall couplings are complex and depend upon the sign of the corresponding neutralino's mass. They are of the form (a, b), where this represents the complex number $a + bi$. For positive masses they are:

$$a^{\tilde{t}_1} = (|\alpha_1^{\tilde{t}_1}|, 0), \qquad b^{\tilde{t}_1} = (|\beta_1^{\tilde{t}_1}|, 0), \qquad a^{\tilde{t}_2} = (|\alpha_1^{\tilde{t}_2}|, 0), \qquad b^{\tilde{t}_2} = (|\beta_1^{\tilde{t}_2}|, 0). \qquad \text{(A.226)}$$

Meanwhile, for negative neutralino masses the effect of our field redefinition is to multiply the corresponding row of the neutralino mixing matrix by $-i$ therefore the couplings are then:

$$a^{\tilde{t}_1} = (0, -|\alpha_1^{\tilde{t}_1}|), \qquad b^{\tilde{t}_1} = (0, -|\beta_1^{\tilde{t}_1}|), \qquad a^{\tilde{t}_2} = (0, -|\alpha_1^{\tilde{t}_2}|), \qquad b^{\tilde{t}_2} = (0, -|\beta_1^{\tilde{t}_2}|). \qquad \text{(A.227)}$$

In addition to account for differences in interactions for positive and negative neutralino masses as a result of this coupling difference and the extra associated γ_5 matrices we must also include factors of:

$$(-1)^{\theta_i} = \begin{cases} +1, \text{ for positive neutralino masses,} \\ -1, \text{ for negative neutralino masses.} \end{cases} \qquad \text{(A.228)}$$

The formula we use for $\Gamma_{\tilde{t}_1}$ and $\Gamma_{\tilde{t}_2}$ are:

$$\begin{aligned}
\Gamma_{\tilde{t}_1} =& (-1)^{\theta_i}\Big[(a^{\tilde{t}_1{}^2} + b^{\tilde{t}_1{}^2})\tilde{\psi}(m_{\tilde{g}}, m_{\tilde{t}_1}, m_{\tilde{t}_1}, m_{\tilde{Z}_i}) + 4a^{\tilde{t}_1} b^{\tilde{t}_1} m_t m_{\tilde{Z}_i} \tilde{\chi}(m_{\tilde{g}}, m_{\tilde{t}_1}, m_{\tilde{t}_1}, m_{\tilde{Z}_i}) \\
&- 4\sin\theta_t \cos\theta_t (a^{\tilde{t}_1{}^2} + b^{\tilde{t}_1{}^2}) m_{\tilde{g}} m_t X(m_{\tilde{g}}, m_{\tilde{t}_1}, m_{\tilde{t}_1}, m_{\tilde{Z}_i}) \\
&- 8\sin\theta_t \cos\theta_t a^{\tilde{t}_1} b^{\tilde{t}_1} m_{\tilde{g}} m_t^2 m_{\tilde{Z}_i} \zeta(m_{\tilde{g}}, m_{\tilde{t}_1}, m_{\tilde{t}_1}, m_{\tilde{Z}_i}) \\
&- 2\sin\theta_t \cos\theta_t a^{\tilde{t}_1} b^{\tilde{t}_1} Y(m_{\tilde{g}}, m_{\tilde{t}_1}, m_{\tilde{t}_1}, m_{\tilde{Z}_i}) + \{a^{\tilde{t}_1{}^2}\cos^2\theta_t + b^{\tilde{t}_1{}^2}\sin^2\theta_t\}\tilde{\phi}(m_{\tilde{g}}, m_{\tilde{t}_1}, m_{\tilde{t}_1}, m_{\tilde{Z}_i}) \\
&- 2m_t^2 \sin\theta_t \cos\theta_t a^{\tilde{t}_1} b^{\tilde{t}_1} \xi(m_{\tilde{g}}, m_{\tilde{t}_1}, m_{\tilde{t}_1}, m_{\tilde{Z}_i}) + m_{\tilde{g}} m_t a^{\tilde{t}_1} b^{\tilde{t}_1} \xi(m_{\tilde{g}}, m_{\tilde{t}_1}, m_{\tilde{t}_1}, m_{\tilde{Z}_i}) \\
&- m_{\tilde{g}} m_t a^{\tilde{t}_1} b^{\tilde{t}_1} m_{\tilde{Z}_i}^2 \tilde{\rho}(m_{\tilde{g}}, m_{\tilde{t}_1}, m_{\tilde{t}_1}, m_{\tilde{Z}_i}) + m_{\tilde{g}} m_t^2 m_{\tilde{Z}_i} \{a^{\tilde{t}_1{}^2}\sin^2\theta_t + b^{\tilde{t}_1{}^2}\cos^2\theta_t\}\tilde{\rho}(m_{\tilde{g}}, m_{\tilde{t}_1}, m_{\tilde{t}_1}, m_{\tilde{Z}_i}) \\
&- (a^{\tilde{t}_1{}^2} + b^{\tilde{t}_1{}^2})\{m_{\tilde{Z}_i} m_t \sin\theta_t \cos\theta_t m_{\tilde{g}}^2 \tilde{\rho}(m_{\tilde{g}}, m_{\tilde{t}_1}, m_{\tilde{t}_1}, m_{\tilde{Z}_i}) \\
&- m_{\tilde{Z}_i} m_t \sin\theta_t \cos\theta_t \xi(m_{\tilde{g}}, m_{\tilde{t}_1}, m_{\tilde{t}_1}, m_{\tilde{Z}_i})\}\Big].
\end{aligned} \qquad \text{(A.229)}$$

$$\begin{aligned}
\Gamma_{\tilde{t}_2} =& (-1)^{\theta_i}\Big[(a^{\tilde{t}_2{}^2} + b^{\tilde{t}_2{}^2})\tilde{\psi}(m_{\tilde{g}}, m_{\tilde{t}_2}, m_{\tilde{t}_2}, m_{\tilde{Z}_i}) + 4a^{\tilde{t}_2} b^{\tilde{t}_2} m_t m_{\tilde{Z}_i} \tilde{\chi}(m_{\tilde{g}}, m_{\tilde{t}_2}, m_{\tilde{t}_2}, m_{\tilde{Z}_i}) \\
&+ 4m_{\tilde{g}} m_t \sin\theta_t \cos\theta_t (a^{\tilde{t}_2{}^2} + b^{\tilde{t}_2{}^2}) X(m_{\tilde{g}}, m_{\tilde{t}_2}, m_{\tilde{t}_2}, m_{\tilde{Z}_i}) \\
&+ 8\sin\theta_t \cos\theta_t a^{\tilde{t}_2} b^{\tilde{t}_2} m_{\tilde{g}} m_t^2 m_{\tilde{Z}_i} \zeta(m_{\tilde{g}}, m_{\tilde{t}_2}, m_{\tilde{t}_2}, m_{\tilde{Z}_i}) + 2\sin\theta_t \cos\theta_t a^{\tilde{t}_2} b^{\tilde{t}_2} Y(m_{\tilde{g}}, m_{\tilde{t}_2}, m_{\tilde{t}_2}, m_{\tilde{Z}_i}) \\
&+ \{a^{\tilde{t}_2{}^2}\sin^2\theta_t + \cos^2\theta_t b^{\tilde{t}_2{}^2}\}\tilde{\phi}(m_{\tilde{g}}, m_{\tilde{t}_2}, m_{\tilde{t}_2}, m_{\tilde{Z}_i}) + 2m_t^2 \sin\theta_t \cos\theta_t a^{\tilde{t}_2} b^{\tilde{t}_2} \xi(m_{\tilde{g}}, m_{\tilde{t}_2}, m_{\tilde{t}_2}, m_{\tilde{Z}_i}) \\
&+ m_{\tilde{g}} m_t a^{\tilde{t}_2} b^{\tilde{t}_2} \xi(m_{\tilde{g}}, m_{\tilde{t}_2}, m_{\tilde{t}_2}, m_{\tilde{Z}_i}) - m_{\tilde{g}} m_t m_{\tilde{Z}_i}^2 a^{\tilde{t}_2} b^{\tilde{t}_2} \tilde{\rho}(m_{\tilde{g}}, m_{\tilde{t}_2}, m_{\tilde{t}_2}, m_{\tilde{Z}_i}) \\
&+ m_{\tilde{g}} m_{\tilde{Z}_i} m_t^2 \{a^{\tilde{t}_2{}^2}\cos^2\theta_t + b^{\tilde{t}_2{}^2}\sin^2\theta_t\}\tilde{\rho}(m_{\tilde{g}}, m_{\tilde{t}_2}, m_{\tilde{t}_2}, m_{\tilde{Z}_i}) \\
&- (a^{\tilde{t}_2{}^2} + b^{\tilde{t}_2{}^2})\{m_{\tilde{Z}_i} m_t \sin\theta_t \cos\theta_t \xi(m_{\tilde{g}}, m_{\tilde{t}_2}, m_{\tilde{t}_2}, m_{\tilde{Z}_i}) \\
&- m_{\tilde{g}}^2 m_{\tilde{Z}_i} m_t \sin\theta_t \cos\theta_t \tilde{\rho}(m_{\tilde{g}}, m_{\tilde{t}_2}, m_{\tilde{t}_2}, m_{\tilde{Z}_i})\}\Big].
\end{aligned} \qquad \text{(A.230)}$$

For $\Gamma_{\tilde{t}_1\tilde{t}_2}$, our formula, again extracted from `sPHENO-3.3.8`, is:

$$\begin{aligned}\Gamma_{\tilde{t}_1\tilde{t}_2} = (-1)^{\theta_i}\Big[&4m_{\tilde{g}}m_t(\cos^2\theta_t - \sin^2\theta_t)(a^{\tilde{t}_1}a^{\tilde{t}_2} + b^{\tilde{t}_1}b^{\tilde{t}_2})X(m_{\tilde{g}}, m_{\tilde{t}_1}, m_{\tilde{t}_2}, m_{\tilde{Z}_i})\\ &+ 4m_{\tilde{g}}m_t^2 m_{\tilde{Z}_i}(a^{\tilde{t}_1}b^{\tilde{t}_2} + b^{\tilde{t}_1}a^{\tilde{t}_2})(\cos^2\theta_t - \sin^2\theta_t)\zeta(m_{\tilde{g}}, m_{\tilde{t}_1}, m_{\tilde{t}_2}, m_{\tilde{Z}_i})\\ &+ 2\{b^{\tilde{t}_1}a^{\tilde{t}_1}\cos^2\theta_t - \sin^2\theta_t b^{\tilde{t}_2}a^{\tilde{t}_1}\}Y(m_{\tilde{g}}, m_{\tilde{t}_1}, m_{\tilde{t}_2}, m_{\tilde{Z}_i})\\ &+ 2\sin\theta_t\cos\theta_t(a^{\tilde{t}_1}a^{\tilde{t}_2} - b^{\tilde{t}_1}b^{\tilde{t}_2})\tilde{\phi}(m_{\tilde{g}}, m_{\tilde{t}_1}, m_{\tilde{t}_2}, m_{\tilde{Z}_i})\\ &+ 2m_t m_{\tilde{Z}_i}(a^{\tilde{t}_1}a^{\tilde{t}_2} - b^{\tilde{t}_1}b^{\tilde{t}_2})\chi^{'}(m_{\tilde{g}}, m_{\tilde{t}_1}, m_{\tilde{t}_2}, m_{\tilde{Z}_i})\\ &+ 2m_t^2\{\cos^2\theta_t a^{\tilde{t}_1}b^{\tilde{t}_2} - \sin^2\theta_t b^{\tilde{t}_1}a^{\tilde{t}_2}\}\xi(m_{\tilde{g}}, m_{\tilde{t}_1}, m_{\tilde{t}_2}, m_{\tilde{Z}_i})\\ &+ 2m_{\tilde{g}}m_t^2 m_{\tilde{Z}_i}(b^{\tilde{t}_1}b^{\tilde{t}_2} - a^{\tilde{t}_1}a^{\tilde{t}_2})\sin\theta_t\cos\theta_t\tilde{\rho}(m_{\tilde{g}}, m_{\tilde{t}_1}, m_{\tilde{t}_2}, m_{\tilde{Z}_i})\\ &- 4\sin\theta_t\cos\theta_t m_{\tilde{g}}m_t(a^{\tilde{t}_1}b^{\tilde{t}_2} - b^{\tilde{t}_1}a^{\tilde{t}_2})\chi^{'}(m_{\tilde{g}}, m_{\tilde{t}_1}, m_{\tilde{t}_2}, m_{\tilde{Z}_i})\\ &- 2\sin\theta_t\cos\theta_t m_{\tilde{g}}m_t(a^{\tilde{t}_1}b^{\tilde{t}_2} - b^{\tilde{t}_1}a^{\tilde{t}_2})\xi(m_{\tilde{g}}, m_{\tilde{t}_1}, m_{\tilde{t}_2}, m_{\tilde{Z}_i})\\ &+ 2m_t m_{\tilde{Z}_i}\{\sin^2\theta_t a^{\tilde{t}_1}a^{\tilde{t}_2} - \cos^2\theta_t b^{\tilde{t}_1}b^{\tilde{t}_2}\}\xi(m_{\tilde{g}}, m_{\tilde{t}_1}, m_{\tilde{t}_2}, m_{\tilde{Z}_i})\\ &+ 2m_{\tilde{g}}^3 m_t(a^{\tilde{t}_1}b_1^{\tilde{t}_2} - b^{\tilde{t}_2}a^{\tilde{t}_2})\sin\theta_t\cos\theta_t\tilde{\rho}(m_{\tilde{g}}, m_{\tilde{t}_1}, m_{\tilde{t}_2}, m_{\tilde{Z}_i})\\ &- 2m_{\tilde{g}}^2 m_t m_{\tilde{Z}_i}\{\sin^2\theta_t a^{\tilde{t}_1}a^{\tilde{t}_2} - \cos^2\theta_t b^{\tilde{t}_1}b^{\tilde{t}_2}\}\tilde{\rho}(m_{\tilde{g}}, m_{\tilde{t}_1}, m_{\tilde{t}_2}, m_{\tilde{Z}_i})\Big].\end{aligned} \tag{A.231}$$

For the 3-body decay of $\tilde{g} \to \tilde{Z}_i b\bar{b}$ then the formulae are exactly as above but with the replacements: $m_{\tilde{t}_i} \to m_{\tilde{b}_i}$, $\tilde{A}^t_{\tilde{Z}_i} \to \tilde{A}^b_{\tilde{Z}_i}$, $\tilde{B}^t_{\tilde{Z}_i} \to \tilde{B}^b_{\tilde{Z}_i}$, $f_t \to f_b$, $N_{4i} \to N_{3i}$, $\theta_t \to \theta_b$, $m_t \to m_b$. In our program both the $\tilde{g} \to \tilde{Z}_i t\bar{t}$ and $\tilde{g} \to \tilde{Z}_i b\bar{b}$ decays are implemented in the same function, just depending on whether its decaying to tops or bottoms different couplings are used as described above.

$$\tilde{A}^b_{\tilde{Z}_i} = \frac{g}{\sqrt{2}}N_{2i} - \frac{g^{'}}{3\sqrt{2}}N_{1i}, \tag{A.232}$$

$$\tilde{B}^b_{\tilde{Z}_i} = \frac{2}{3}\frac{g^{'}}{\sqrt{2}}N_{1i}, \tag{A.233}$$

$$f_b = \frac{g m_b^{run}}{\sqrt{2}M_W\cos\beta}. \tag{A.234}$$

Note that the integrals used in these equations, $\tilde{\psi}$, $\tilde{\chi}$, X, ζ, $\tilde{\phi}$, ξ, $\tilde{\rho}$, Y, $\chi^{'}$ are given below in Eq: (A.291), (A.292), (A.293), (A.294), (A.295), (A.296), (A.297) (A.298), (A.299) respectively, when the formulae for $\tilde{Z}_i \to \tilde{Z}_j f\bar{f}$ are given.

$\underline{\tilde{g} \to \tilde{W}_i q\bar{q}'}$

The decay of a gluino into a chargino, quark(q) and antiquark($\bar{q}'$) can occur via intermediate squarks of either the q or q', therefore there are four possible intermediates in the case where intra-generational squark mixing effects are included. For example, $\tilde{g} \to \tilde{W}_j t\bar{b}$ may proceed via $\tilde{t}_1$, $\tilde{t}_2$, $\tilde{b}_1$ or $\tilde{b}_2$. Again there are both t and u channel contributions which may contribute to $\tilde{g} \to \tilde{W}_j t\bar{b}$ or $\tilde{g} \to \tilde{W}_j b\bar{t}$. The 8 diagrams are therefore shown as a set of 4 ($k = 1, 2$ for each intermediate shown) in Fig A.2. There are 4 squared contributions to each of $t\bar{b}$ and $b\bar{t}$ as well as $\tilde{t}_1\tilde{t}_1$, $\tilde{t}_1\tilde{t}_2$, $\tilde{t}_2\tilde{t}_2$, $\tilde{b}_1\tilde{b}_1$, $\tilde{b}_1\tilde{b}_2$, $\tilde{b}_2\tilde{b}_2$, $\tilde{t}_1\tilde{b}_1$, $\tilde{t}_1\tilde{b}_2$, $\tilde{t}_2\tilde{b}_1$ and $\tilde{t}_2\tilde{b}_2$ interferences. Note that "diagonal" interferences such as $\tilde{t}_1\tilde{t}_1$ are included with non-interference squared terms into the $\Gamma_{\tilde{t}_1}$ type contributions. In the formulae, the Yukawa couplings, intra-generational squark mixing and final state fermion masses are all accounted for; however whilst the bottom quark mass m_b is included in the phase space, it is neglected from the squared matrix element, this drops any $\tilde{b}_k\tilde{b}_l$ interferences as these are proportional to m_b. The approach used follows Baer and Tata's book *'Weak Scale Supersymmetry'* [65] with the formulae we use taken from `sPHENO` [3, 4], based on the calculations in reference [178]. The formulae used, as in `sPHENO`, differ in a few places from those in Baer and Tata.

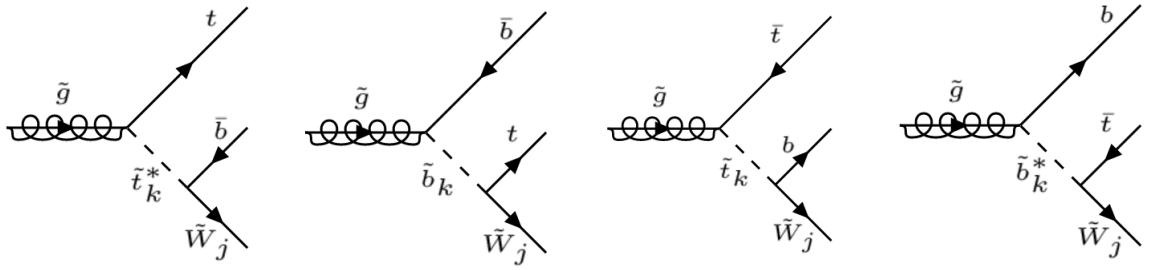

(a) (b) (c) (d)

Figure A.2: Feynman diagrams for the 3-body decay of a gluino into a chargino and a top-bottom pair, as mediated by stops $\tilde{t}_{1/2}$ and sbottoms $\tilde{t}_{1/2}$. $j, k = 1, 2$.

$$\Gamma(\tilde{g} \to t\bar{b}\tilde{W}_i^-) = \frac{\alpha_s}{16\pi^2 m_{\tilde{g}}}(\Gamma_{\tilde{t}_1} + \Gamma_{\tilde{t}_2} + \Gamma_{\tilde{t}_1\tilde{t}_2} + \Gamma_{\tilde{b}_1} + \Gamma_{\tilde{b}_2} + \Gamma_{\tilde{t}_1\tilde{b}_1} + \Gamma_{\tilde{t}_1\tilde{b}_2} + \Gamma_{\tilde{t}_2\tilde{b}_1} + \Gamma_{\tilde{t}_2\tilde{b}_2}). \tag{A.235}$$

The $chargino - quark - squark$ couplings are given below, remember we have the chargino mixing angle θ_L and θ_R pre-transformed so that $\theta_{L/R} \to -\theta_{L/R} + \pi/2$ in order to use the convention where the lightest mass chargino eigenstate $\tilde{W}_1$ appears first in the multiplet:

$$\begin{aligned}
\alpha^{\tilde{t}_1}_{\tilde{W}_1} &= -g\sin\theta_L\cos\theta_t + f_t\cos\theta_R\sin\theta_t, \quad \beta^{\tilde{t}_1}_{\tilde{W}_1} = -f_b\cos\theta_L\cos\theta_t,\\
\alpha^{\tilde{b}_1}_{\tilde{W}_1} &= -g\sin\theta_L\cos\theta_b + f_b\cos\theta_L\sin\theta_b, \quad \beta^{\tilde{b}_1}_{\tilde{W}_1} = -f_t\cos\theta_R\cos\theta_b,\\
\alpha^{\tilde{t}_1}_{\tilde{W}_2} &= -g\cos\theta_L\cos\theta_t - f_t\sin\theta_R\sin\theta_t, \quad \beta^{\tilde{t}_1}_{\tilde{W}_2} = f_b\sin\theta_L\cos\theta_t,\\
\alpha^{\tilde{b}_1}_{\tilde{W}_2} &= -g\cos\theta_L\cos\theta_b - f_b\sin\theta_L\sin\theta_b, \quad \beta^{\tilde{b}_1}_{\tilde{W}_2} = f_t\sin\theta_R\cos\theta_b.
\end{aligned} \tag{A.236}$$

We obtain the couplings for $\tilde{t}_2$ and $\tilde{b}_2$ by changing $\cos\theta_q \to \sin\theta_q$ and $\sin\theta_q \to -\cos\theta_q$. The $\tilde{W}_2$ couplings are obtained from those of $\tilde{W}_1$ by making the replacements $\cos\theta_{L/R} \to -\sin\theta_{L/R}$ and $\sin\theta_{L/R} \to \cos\theta_{L/R}$.

The contributions in (A.235) are as follows:

$$\Gamma_{\tilde{t}_1} = [(\alpha^{\tilde{t}_1}_{\tilde{W}_i})^2 + (\beta^{\tilde{t}_1}_{\tilde{W}_i})^2]\left[G_1(m_{\tilde{g}}, m_{\tilde{t}_1}, m_{\tilde{W}_i}) - \sin 2\theta_t G_8(m_{\tilde{g}}, m_{\tilde{t}_1}, m_{\tilde{t}_1}, m_{\tilde{W}_i})\right], \tag{A.237}$$

$$\Gamma_{\tilde{t}_2} = [(\alpha^{\tilde{t}_2}_{\tilde{W}_i})^2 + (\beta^{\tilde{t}_2}_{\tilde{W}_i})^2]\left[G_1(m_{\tilde{g}}, m_{\tilde{t}_2}, m_{\tilde{W}_i}) + \sin 2\theta_t G_8(m_{\tilde{g}}, m_{\tilde{t}_2}, m_{\tilde{t}_2}, m_{\tilde{W}_i})\right], \tag{A.238}$$

$$\Gamma_{\tilde{b}_1} = [(\alpha^{\tilde{b}_1}_{\tilde{W}_i})^2 + (\beta^{\tilde{b}_1}_{\tilde{W}_i})^2]G_2(m_{\tilde{g}}, m_{\tilde{b}_1}, m_{\tilde{W}_i}) + \alpha^{\tilde{b}_1}_{\tilde{W}_i}\beta^{\tilde{b}_1}_{\tilde{W}_i}G_3(m_{\tilde{g}}, m_{\tilde{b}_1}, m_{\tilde{W}_i}), \tag{A.239}$$

$$\Gamma_{\tilde{b}_2} = [(\alpha^{\tilde{b}_2}_{\tilde{W}_i})^2 + (\beta^{\tilde{b}_2}_{\tilde{W}_i})^2]G_2(m_{\tilde{g}}, m_{\tilde{b}_2}, m_{\tilde{W}_i}) + \alpha^{\tilde{b}_2}_{\tilde{W}_i}\beta^{\tilde{b}_2}_{\tilde{W}_i}G_3(m_{\tilde{g}}, m_{\tilde{b}_2}, m_{\tilde{W}_i}), \tag{A.240}$$

$$\Gamma_{\tilde{t}_1\tilde{t}_2} = 2(\alpha^{\tilde{t}_1}_{\tilde{W}_i}\alpha^{\tilde{t}_2}_{\tilde{W}_i} + \beta^{\tilde{t}_1}_{\tilde{W}_i}\beta^{\tilde{t}_2}_{\tilde{W}_i})\cos 2\theta_t G_8(m_{\tilde{g}}, m_{\tilde{t}_1}, m_{\tilde{t}_2}, m_{\tilde{W}_i}), \tag{A.241}$$

$$\Gamma_{\tilde{t}_1\tilde{b}_1} = (\cos\theta_t\sin\theta_b\alpha^{\tilde{b}_1}_{\tilde{W}_i}\beta^{\tilde{t}_1}_{\tilde{W}_i} + \sin\theta_t\cos\theta_b\beta^{\tilde{b}_1}_{\tilde{W}_i}\alpha^{\tilde{t}_1}_{\tilde{W}_i})G_6(m_{\tilde{g}}, m_{\tilde{t}_1}, m_{\tilde{b}_1}, m_{\tilde{W}_i}) \tag{A.242}$$

$$- (\cos\theta_t\cos\theta_b\alpha^{\tilde{b}_1}_{\tilde{W}_i}\alpha^{\tilde{t}_1}_{\tilde{W}_i} + \sin\theta_t\sin\theta_b\beta^{\tilde{b}_1}_{\tilde{W}_i}\beta^{\tilde{t}_1}_{\tilde{W}_i})G_4(m_{\tilde{g}}, m_{\tilde{t}_1}, m_{\tilde{b}_1}, m_{\tilde{W}_i}) \tag{A.243}$$

$$- (\cos\theta_t\cos\theta_b\beta^{\tilde{b}_1}_{\tilde{W}_i}\alpha^{\tilde{t}_1}_{\tilde{W}_i} + \sin\theta_t\sin\theta_b\alpha^{\tilde{b}_1}_{\tilde{W}_i}\beta^{\tilde{t}_1}_{\tilde{W}_i})G_5(m_{\tilde{g}}, m_{\tilde{t}_1}, m_{\tilde{b}_1}, m_{\tilde{W}_i}) \tag{A.244}$$

$$- (\cos\theta_t\sin\theta_b\beta^{\tilde{b}_1}_{\tilde{W}_i}\beta^{\tilde{t}_1}_{\tilde{W}_i} + \sin\theta_t\cos\theta_b\alpha^{\tilde{b}_1}_{\tilde{W}_i}\alpha^{\tilde{t}_1}_{\tilde{W}_i})G_7(m_{\tilde{g}}, m_{\tilde{t}_1}, m_{\tilde{b}_1}, m_{\tilde{W}_i}), \tag{A.245}$$

$$\Gamma_{\tilde{t}_1\tilde{b}_2} = (-\cos\theta_t\cos\theta_b\alpha^{\tilde{b}_1}_{\tilde{W}_i}\beta^{\tilde{t}_1}_{\tilde{W}_i} + \sin\theta_t\sin\theta_b\beta^{\tilde{b}_1}_{\tilde{W}_i}\alpha^{\tilde{t}_1}_{\tilde{W}_i})G_6(m_{\tilde{g}}, m_{\tilde{t}_1}, m_{\tilde{b}_1}, m_{\tilde{W}_i}) \tag{A.246}$$

$$- (\cos\theta_t\sin\theta_b\alpha^{\tilde{b}_1}_{\tilde{W}_i}\alpha^{\tilde{t}_1}_{\tilde{W}_i} - \sin\theta_t\cos\theta_b\beta^{\tilde{b}_1}_{\tilde{W}_i}\beta^{\tilde{t}_1}_{\tilde{W}_i})G_4(m_{\tilde{g}}, m_{\tilde{t}_1}, m_{\tilde{b}_1}, m_{\tilde{W}_i}) \tag{A.247}$$

$$- (\cos\theta_t\sin\theta_b\beta^{\tilde{b}_1}_{\tilde{W}_i}\alpha^{\tilde{t}_1}_{\tilde{W}_i} - \sin\theta_t\cos\theta_b\alpha^{\tilde{b}_1}_{\tilde{W}_i}\beta^{\tilde{t}_1}_{\tilde{W}_i})G_5(m_{\tilde{g}}, m_{\tilde{t}_1}, m_{\tilde{b}_1}, m_{\tilde{W}_i}) \tag{A.248}$$

$$- (-\cos\theta_t\cos\theta_b\beta^{\tilde{b}_1}_{\tilde{W}_i}\beta^{\tilde{t}_1}_{\tilde{W}_i} + \sin\theta_t\sin\theta_b\alpha^{\tilde{b}_1}_{\tilde{W}_i}\alpha^{\tilde{t}_1}_{\tilde{W}_i})G_7(m_{\tilde{g}}, m_{\tilde{t}_1}, m_{\tilde{b}_1}, m_{\tilde{W}_i}), \tag{A.249}$$

$$\begin{aligned}\Gamma_{\tilde{t}_2\tilde{b}_1} =&(\sin\theta_t\sin\theta_b\alpha^{\tilde{b}_1}_{\tilde{W}_i}\beta^{\tilde{t}_1}_{\tilde{W}_i} - \cos\theta_t\cos\theta_b\beta^{\tilde{b}_1}_{\tilde{W}_i}\alpha^{\tilde{t}_1}_{\tilde{W}_i})G_6(m_{\tilde{g}}, m_{\tilde{t}_1}, m_{\tilde{b}_1}, m_{\tilde{W}_i})\\ &-(\sin\theta_t\cos\theta_b\alpha^{\tilde{b}_1}_{\tilde{W}_i}\alpha^{\tilde{t}_1}_{\tilde{W}_i} - \cos\theta_t\sin\theta_b\beta^{\tilde{b}_1}_{\tilde{W}_i}\beta^{\tilde{t}_1}_{\tilde{W}_i})G_4(m_{\tilde{g}}, m_{\tilde{t}_1}, m_{\tilde{b}_1}, m_{\tilde{W}_i})\\ &-(\sin\theta_t\cos\theta_b\beta^{\tilde{b}_1}_{\tilde{W}_i}\alpha^{\tilde{t}_1}_{\tilde{W}_i} - \cos\theta_t\sin\theta_b\alpha^{\tilde{b}_1}_{\tilde{W}_i}\beta^{\tilde{t}_1}_{\tilde{W}_i})G_5(m_{\tilde{g}}, m_{\tilde{t}_1}, m_{\tilde{b}_1}, m_{\tilde{W}_i})\\ &-(\sin\theta_t\sin\theta_b\beta^{\tilde{b}_1}_{\tilde{W}_i}\beta^{\tilde{t}_1}_{\tilde{W}_i} - \cos\theta_t\cos\theta_b\alpha^{\tilde{b}_1}_{\tilde{W}_i}\alpha^{\tilde{t}_1}_{\tilde{W}_i})G_7(m_{\tilde{g}}, m_{\tilde{t}_1}, m_{\tilde{b}_1}, m_{\tilde{W}_i}),\end{aligned} \tag{A.250}$$

$$\begin{aligned}\Gamma_{\tilde{t}_2\tilde{b}_2} =&-(\sin\theta_t\cos\theta_b\alpha^{\tilde{b}_1}_{\tilde{W}_i}\beta^{\tilde{t}_1}_{\tilde{W}_i} + \cos\theta_t\sin\theta_b\beta^{\tilde{b}_1}_{\tilde{W}_i}\alpha^{\tilde{t}_1}_{\tilde{W}_i})G_6(m_{\tilde{g}}, m_{\tilde{t}_1}, m_{\tilde{b}_1}, m_{\tilde{W}_i})\\ &-(\sin\theta_t\sin\theta_b\alpha^{\tilde{b}_1}_{\tilde{W}_i}\alpha^{\tilde{t}_1}_{\tilde{W}_i} + \cos\theta_t\cos\theta_b\beta^{\tilde{b}_1}_{\tilde{W}_i}\beta^{\tilde{t}_1}_{\tilde{W}_i})G_4(m_{\tilde{g}}, m_{\tilde{t}_1}, m_{\tilde{b}_1}, m_{\tilde{W}_i})\\ &-(\sin\theta_t\sin\theta_b\beta^{\tilde{b}_1}_{\tilde{W}_i}\alpha^{\tilde{t}_1}_{\tilde{W}_i} + \cos\theta_t\cos\theta_b\alpha^{\tilde{b}_1}_{\tilde{W}_i}\beta^{\tilde{t}_1}_{\tilde{W}_i})G_5(m_{\tilde{g}}, m_{\tilde{t}_1}, m_{\tilde{b}_1}, m_{\tilde{W}_i})\\ &+(\sin\theta_t\cos\theta_b\beta^{\tilde{b}_1}_{\tilde{W}_i}\beta^{\tilde{t}_1}_{\tilde{W}_i} + \cos\theta_t\sin\theta_b\alpha^{\tilde{b}_1}_{\tilde{W}_i}\alpha^{\tilde{t}_1}_{\tilde{W}_i})G_7(m_{\tilde{g}}, m_{\tilde{t}_1}, m_{\tilde{b}_1}, m_{\tilde{W}_i}).\end{aligned} \tag{A.251}$$

The integrals G_1 to G_8 are given by the following, where $s_t = m^2_{\tilde{g}} + m^2_t - 2E_t m_{\tilde{g}}$ and $s_b = m^2_{\tilde{g}} + m^2_b - 2E_b m_{\tilde{g}}$:

$$G_1(m_{\tilde{g}}, m_{\tilde{t}_k}, m_{\tilde{W}_i}) = m_{\tilde{g}} \int \frac{dE_t p_t E_t (s_t - m^2_{\tilde{W}_i})^2}{(s_t - m^2_{\tilde{t}_k})^2 s_t}, \tag{A.252}$$

$$G_2(m_{\tilde{g}}, m_{\tilde{b}_k}, m_{\tilde{W}_i}) = m_{\tilde{g}} \int dE_b E_b^2 \lambda^{\frac{1}{2}}(s_b, m^2_{\tilde{W}_i}, m^2_t) \frac{s_b - m^2_t - m^2_{\tilde{W}_i}}{(s_b^2 - m^2_{\tilde{b}_k})^2 s_b}, \tag{A.253}$$

$$G_3(m_{\tilde{g}}, m_{\tilde{b}_k}, m_{\tilde{W}_i}) = \int dE_b E_b^2 \lambda^{\frac{1}{2}}(s_b, m^2_{\tilde{W}_i}, m^2_t) \frac{4 m_{\tilde{g}} m_{\tilde{W}_i} m_t}{(s_b^2 - m^2_{\tilde{b}_k})^2 s_b}, \tag{A.254}$$

$$G_4(m_{\tilde{g}}, m_{\tilde{t}_j}, m_{\tilde{b}_k}, m_{\tilde{W}_i}) = m_{\tilde{g}} m_{\tilde{W}_i} \int \frac{dE_t}{s_t - m^2_{\tilde{t}_j}} \left[E_b(max) - E_b(min) - \frac{m^2_{\tilde{b}_j} + m^2_t + 2E_t m_{\tilde{g}} - m^2_{\tilde{W}_i}}{2m_{\tilde{g}}} \log X \right], \tag{A.255}$$

$$G_5(m_{\tilde{g}}, m_{\tilde{t}_j}, m_{\tilde{b}_k}, m_{\tilde{W}_i}) = \frac{m_t}{2} \int dE_t \frac{s_t - m^2_{\tilde{W}_i}}{s_t - m^2_{\tilde{t}_j}} \log X, \tag{A.256}$$

$$G_6(m_{\tilde{g}}, m_{\tilde{t}_j}, m_{\tilde{b}_k}, m_{\tilde{W}_i}) = \frac{1}{2} \int \frac{dE_t}{s_t - m^2_{\tilde{t}_j}} \left\{ [m_{\tilde{g}}(s_t - m^2_{\tilde{W}_i}) + \frac{m^2_{\tilde{b}_k} - m^2_{\tilde{g}}}{m_{\tilde{g}}} s_t] \log X - 2 s_t [E_b(max) - E_b(min)] \right\}, \tag{A.257}$$

$$G_7(m_{\tilde{g}}, m_{\tilde{t}_j}, m_{\tilde{b}_k}, m_{\tilde{W}_i}) = \frac{1}{2} m_{\tilde{W}_i} m_t \int \frac{dE_t}{s_t - m^2_{\tilde{t}_j}} \left\{ 2[E_b(max) - E_b(min)] - \frac{m^2_{\tilde{b}_k} - m^2_{\tilde{g}}}{m_{\tilde{g}}} \log X \right\}, \tag{A.258}$$

$$G_8(m_{\tilde{g}}, m_{\tilde{t}_1}, m_{\tilde{t}_2}, m_{\tilde{W}_i}) = m_{\tilde{g}} m_t \int dE_t \frac{(s_t - m^2_{\tilde{W}_i})[E_b(max) - E_b(min)]}{(s_t - m^2_{\tilde{t}_1})(s_t - m^2_{\tilde{t}_2})}. \tag{A.259}$$

The limits of integration here are m_t to $(m^2_{\tilde{g}} + m^2_t - (m_{\tilde{W}_i} + m_b)^2)/(2m_{\tilde{g}})$ for the E_t integrals, and m_b to $(m^2_{\tilde{g}} - (m_t + m_{\tilde{W}_i})^2)/(2m_{\tilde{g}})$ for the E_b integrals. Here $p_t = \sqrt{E_t^2 - m_t^2}$, $E_b(max/min)$ and X are given by:

$$E_b(max/min) = \frac{(s_t + m^2_b - m^2_{\tilde{W}_i})(m_{\tilde{g}} - E_t) \pm \lambda^{\frac{1}{2}}(s_t, m^2_b, m^2_{\tilde{W}_i})}{2 s_t}, \tag{A.260}$$

$$X = \frac{m^2_{\tilde{b}_j} + 2E_b(max) m_{\tilde{g}} - m^2_{\tilde{g}}}{m^2_{\tilde{b}_j} + 2E_b(min) m_{\tilde{g}} - m^2_{\tilde{g}}}. \tag{A.261}$$

The formulae for the first and second generation quarks can be obtained from those for the third generation straightforwardly, in fact they are simpler as the Yukawa coupling can often be neglected.

A.4.2 Neutralino 3-body Decays

$\underline{\tilde{Z}_i \to \tilde{Z}_j f \bar{f}}$

For the 3-body decay of a neutralino into a lighter neutralino and a fermion-antifermion pair there are three types of contribution, as illustrated in the Feynman diagrams in Fig A.3; Z boson exchange, neutral Higgs boson exchange and sfermion exchange. The effects of Yukawa couplings, sfermion mixing and finite non-zero quark masses in the final state have been included. Similarly, the effects of negative neutralino masses in initial or final states are included. However, we have taken the approach of Baer et al in references [65, 178]; whilst we have included the effects of the quark mass in the phase space, the quark mass has been approximated as zero in the squared matrix element. This approximation is justified on the basis that the fermion-antifermion pair may not be a $t\bar{t}$ pair as the decay calculator only evaluates the 3-body decays when 2-body decays are absent, given the dominance of 2-body modes over 3-body modes in branching ratios. Whenever the 3-body mode $\tilde{Z}_i \to \tilde{Z}_j t\bar{t}$ is available then so are the 2-body modes $\tilde{Z}_i \to \tilde{Z}_j Z$ and $\tilde{Z}_i \to \tilde{Z}_j h$, which will make the 3-body modes negligible. It is however crucial to include the effects of the non-zero quark masses in the phase space, as has been done, as often the phase space available to these decays is limited (e.g. for compressed spectra) and so the reduction in phase space caused by the finite quark masses is important. Similarly, with non-zero quark masses the Higgs intermediate contributions are allowed. Nonetheless the effect of the approximation is just to remove the Higgs boson - Z interferences and CP even - CP odd Higgs boson interferences, which are generally necessarily small compared to other contributions. The formulae for the included contributions themselves are all taken from `sPHENO`, as for the other 3-body modes. It should also be noted that the calculation in `sPHENO` was done in the Feynman gauge so a Goldstone contribution, corresponding to the longitudinal component of the Z boson, is required. The included contributions are therefore the squared Z (including Goldstone), ϕ and $\tilde{f}$ contributions as well as hH, $Z\tilde{f}$, $\phi\tilde{f}$ and ZA interferences.[4]

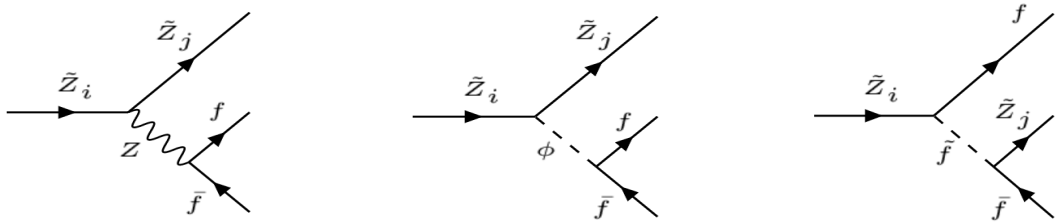

Figure A.3: Feynman diagrams for the 3-body decay of a neutralino into a lighter neutralino and a fermion-antifermion pair, as mediated by Z bosons, Higgs bosons $\phi = h, H, A$, or sfermions $\tilde{f}_{1/2}$. $i > j$ and $i, j \in 1, 2, 3, 4$.

$$\Gamma(\tilde{Z}_i \to \tilde{Z}_j f \bar{f}) = \frac{N_c}{512\pi^3 |m_{\tilde{Z}_i}|^3} (\Gamma_Z + \Gamma_h + \Gamma_H + \Gamma_A + \Gamma_{hH} + \Gamma_{\tilde{f}} - 4\Gamma_{h\tilde{f}_1} - 4\Gamma_{h\tilde{f}_2} - 4\Gamma_{H\tilde{f}_1} - 4\Gamma_{H\tilde{f}_2} - 4\Gamma_{A\tilde{f}_1} - 4\Gamma_{A\tilde{f}_2} + 4\Gamma_{Z\tilde{f}_1} - 4\Gamma_{Z\tilde{f}_2} - 4\Gamma_{ZA} + \Gamma_G + 2\Gamma_{GA} - 4\Gamma_{ZG} - 4\Gamma_{G\tilde{f}_1} - 4\Gamma_{G\tilde{f}_2}). \tag{A.262}$$

G indicates the Goldstone contribution. In the following contributions we again account for negative neutralino masses via factors of -1 corresponding to the effects of absorbing factors of $-i\gamma_5$ into the couplings for negative mass neutralinos:

$$(-1)^{\theta_i} = \begin{cases} 1, \text{ for } m_{\tilde{Z}_i} > 0, \\ -1, \text{ for } m_{\tilde{Z}_i} < 0. \end{cases} \tag{A.263}$$

[4] Differential decay rate calculations for this mode using a different approach are available in reference [177].

The contributions are as follows:

$$\Gamma_h = 2(X^h_{ij} + X^h_{ji})^2 f_q^2 t^2_{\alpha_h} \Big[I^h_4 - 2m_f^2 I^h_3 + 2(-1)^{\theta_j} |m_{\tilde{Z}_i}||m_{\tilde{Z}_j}| I^h_2 - 4(-1)^{\theta_j} |m_{\tilde{Z}_i}||m_{\tilde{Z}_j}| m_f^2 I^h_1 \Big], \quad \text{(A.264)}$$

where

$$s = m^2_{\tilde{Z}_i} + m^2_{\tilde{Z}_j} - 2|m_{\tilde{Z}_i}|E, \quad \text{(A.265)}$$

$$E_{max} = \frac{m^2_{\tilde{Z}_i} + m^2_{\tilde{Z}_j} - 4m_f^2}{2|m_{\tilde{Z}_i}|}, \quad \text{(A.266)}$$

$$I^h_1 = \int_{|m_{\tilde{Z}_j}|}^{E_{max}} dE \frac{2|m_{\tilde{Z}_i}|\sqrt{s - 4m_f^2}\sqrt{E^2 - m^2_{\tilde{Z}_j}}\, 2|m_{\tilde{Z}_i}|}{\sqrt{s}(s - m_h^2)^2}, \quad \text{(A.267)}$$

$$I^h_2 = \int_{|m_{\tilde{Z}_j}|}^{E_{max}} dE \frac{2|m_{\tilde{Z}_i}|\sqrt{s - 4m_f^2}\sqrt{E^2 - m^2_{\tilde{Z}_j}}\, 2|m_{\tilde{Z}_i}|(s - 2m_f^2)}{\sqrt{s}(s - m_h^2)^2}, \quad \text{(A.268)}$$

$$I^h_3 = \int_{|m_{\tilde{Z}_j}|}^{E_{max}} dE \frac{2|m_{\tilde{Z}_i}|\sqrt{s - 4m_f^2}\sqrt{E^2 - m^2_{\tilde{Z}_j}}\, 2|m_{\tilde{Z}_i}|2|m_{\tilde{Z}_i}|E}{\sqrt{s}(s - m_h^2)^2}, \quad \text{(A.269)}$$

$$I^h_4 = \int_{|m_{\tilde{Z}_j}|}^{E_{max}} dE \frac{2|m_{\tilde{Z}_i}|\sqrt{s - 4m_f^2}\sqrt{E^2 - m^2_{\tilde{Z}_j}}\, 2|m_{\tilde{Z}_i}|(s - 2m_f^2)2|m_{\tilde{Z}_i}|E}{\sqrt{s}(s - m_h^2)^2}. \quad \text{(A.270)}$$

$$\Gamma_H = 2(X^H_{ij} + X^H_{ji})^2 f_q^2 t^2_{\alpha_H} \Big[I^H_4 - 2m_f^2 I^H_3 + 2(-1)^{\theta_j} |m_{\tilde{Z}_i}||m_{\tilde{Z}_j}| I^H_2 - 4(-1)^{\theta_j} |m_{\tilde{Z}_i}||m_{\tilde{Z}_j}| m_f^2 I^H_1 \Big]. \quad \text{(A.271)}$$

where the $I^H_{1,2,3,4}$ are exactly the same as the $I^h_{1,2,3,4}$ with the change $m_h \to m_H$.

$$\begin{aligned}\Gamma_Z = 64 g^2 \sin^2\theta_W W^2_{ij} \Big[& 4(-1)^{\theta_j} |m_{\tilde{Z}_i}||m_{\tilde{Z}_j}| m_f^2 (\alpha_f^2 - \beta_f^2) I^Z_4 + m_f^2(\alpha_f^2 - \beta_f^2) I^Z_3 \\ & + (-1)^{\theta_i}(-1)^{\theta_j} |m_{\tilde{Z}_i}||m_{\tilde{Z}_j}| (\alpha_f^2 + \beta_f^2) I^Z_2 + \frac{1}{2}(\alpha_f^2 + \beta_f^2) I^Z_1 \Big],\end{aligned} \quad \text{(A.272)}$$

where the integrals I^Z_i are:

$$\begin{aligned} I^Z_1 = \int_{4m_f^2}^{(|m_{\tilde{Z}_i}| - |m_{\tilde{Z}_j}|)^2} ds \Big[& \frac{1}{3s^2(s - m_Z^2)^2} \{ -2s^4 + (m^2_{\tilde{Z}_i} + m^2_{\tilde{Z}_j} + 2m_f^2)s^3 + [(m^2_{\tilde{Z}_i} - m^2_{\tilde{Z}_j})^2 \\ & - 2(m^2_{\tilde{Z}_i} + m^2_{\tilde{Z}_j})2m_f^2]s^2 + 2m_f^2(m^2_{\tilde{Z}_i} - m^2_{\tilde{Z}_j})^2 s \} \frac{1}{s} \\ & \times \sqrt{(s - (|m_{\tilde{Z}_i}| - |m_{\tilde{Z}_j}|)^2)((s - (|m_{\tilde{Z}_i}| + |m_{\tilde{Z}_j}|)^2)} \sqrt{s(s - 4m_f^2)} \Big], \end{aligned} \quad \text{(A.273)}$$

$$\begin{aligned} I^Z_2 = \int_{4m_f^2}^{(|m_{\tilde{Z}_i}| - |m_{\tilde{Z}_j}|)^2} ds \Big[& \frac{1}{s(s - m_Z^2)^2}(s - 2m_f^2) \sqrt{(s - (|m_{\tilde{Z}_i}| - |m_{\tilde{Z}_j}|)^2)((s - (|m_{\tilde{Z}_i}| + |m_{\tilde{Z}_j}|)^2)} \\ & \times \sqrt{s(s - 4m_f^2)} \Big], \end{aligned} \quad \text{(A.274)}$$

$$\begin{aligned} I^Z_3 = \int_{4m_f^2}^{(|m_{\tilde{Z}_i}| - |m_{\tilde{Z}_j}|)^2} ds \Big[& \frac{1}{s(s - m_Z^2)^2}(m^2_{\tilde{Z}_i} + m^2_{\tilde{Z}_j} - s) \sqrt{(s - (|m_{\tilde{Z}_i}| - |m_{\tilde{Z}_j}|)^2)((s - (|m_{\tilde{Z}_i}| + |m_{\tilde{Z}_j}|)^2)} \\ & \times \sqrt{s(s - 4m_f^2)} \Big], \end{aligned} \quad \text{(A.275)}$$

$$I^Z_4 = \int_{4m_f^2}^{(|m_{\tilde{Z}_i}| - |m_{\tilde{Z}_j}|)^2} ds \Big[\frac{1}{s(s - m_Z^2)^2} \sqrt{(s - (|m_{\tilde{Z}_i}| - |m_{\tilde{Z}_j}|)^2)((s - (|m_{\tilde{Z}_i}| + |m_{\tilde{Z}_j}|)^2)} \sqrt{s(s - 4m_f^2)} \Big]. \quad \text{(A.276)}$$

$$\Gamma_A = (X^A_{ij} + X^A_{ji})^2 A_q^2 \Big[I^A_4 + 2m_f^2 I^A_3 - 2(-1)^{\theta_i}(-1)^{\theta_j}|m_{\tilde{Z}_i}||m_{\tilde{Z}_j}|I^A_2 - 4(-1)^{\theta_i}(-1)^{\theta_j} m_f^2 |m_{\tilde{Z}_i}||m_{\tilde{Z}_j}| I^A_1 \Big], \tag{A.277}$$

where the integrals I^A_i are:

$$I^A_1 = \int_{|m_{\tilde{Z}_j}|}^{E_{max}} dE \sqrt{E^2 - m^2_{\tilde{Z}_j}} \sqrt{s - 4m_f^2} \frac{4m^2_{\tilde{Z}_i}}{\sqrt{s}(s - m_A^2)^2}, \tag{A.278}$$

$$I^A_2 = \int_{|m_{\tilde{Z}_j}|}^{E_{max}} dE \sqrt{E^2 - m^2_{\tilde{Z}_j}} \sqrt{s - 4m_f^2} \frac{4m^2_{\tilde{Z}_i}(s - 2m_f^2)}{\sqrt{s}(s - m_A^2)^2}, \tag{A.279}$$

$$I^A_3 = \int_{|m_{\tilde{Z}_j}|}^{E_{max}} dE \sqrt{E^2 - m^2_{\tilde{Z}_j}} \sqrt{s - 4m_f^2} \frac{4m^2_{\tilde{Z}_i} 2|m_{\tilde{Z}_i}|E}{\sqrt{s}(s - m_A^2)^2}, \tag{A.280}$$

$$I^A_4 = \int_{|m_{\tilde{Z}_j}|}^{E_{max}} dE \sqrt{E^2 - m^2_{\tilde{Z}_j}} \sqrt{s - 4m_f^2} \frac{4m^2_{\tilde{Z}_i} 2|m_{\tilde{Z}_i}|E(s - 2m_f^2)}{\sqrt{s}(s - m_A^2)^2}, \tag{A.281}$$

$$\begin{aligned}\Gamma_{hH} = 4(X^h_{ij} + X^h_{ji})(X^H_{ij} + X^H_{ji}) f_q^2 t_{\alpha_h} t_{\alpha_H} \Big[& I^{hH}_4 - 2m_f^2 I^{hH}_3 + 2(-1)^{\theta_i}(-1)^{\theta_j}|m_{\tilde{Z}_i}||m_{\tilde{Z}_j}| I^{hH}_2 \\ & - 4(-1)^{\theta_i}(-1)^{\theta_j}|m_{\tilde{Z}_i}||m_{\tilde{Z}_j}| m_f^2 I^{hH}_1 \Big],\end{aligned} \tag{A.282}$$

where:

$$I^{hH}_1 = \int_{|m_{\tilde{Z}_j}|}^{E_{max}} dE \Big[2|m_{\tilde{Z}_i}| \sqrt{s - 4m_f^2} \sqrt{E^2 - m^2_{\tilde{Z}_j}} \frac{2|m_{\tilde{Z}_i}|}{\sqrt{s}(s - m_h^2)(s - m_H^2)} \Big], \tag{A.283}$$

$$I^{hH}_2 = \int_{|m_{\tilde{Z}_j}|}^{E_{max}} dE \Big[2|m_{\tilde{Z}_i}| \sqrt{s - 4m_f^2} \sqrt{E^2 - m^2_{\tilde{Z}_j}} \frac{2|m_{\tilde{Z}_i}|(s - 2m_f^2)}{\sqrt{s}(s - m_h^2)(s - m_H^2)} \Big], \tag{A.284}$$

$$I^{hH}_3 = \int_{|m_{\tilde{Z}_j}|}^{E_{max}} dE \Big[2|m_{\tilde{Z}_i}| \sqrt{s - 4m_f^2} \sqrt{E^2 - m^2_{\tilde{Z}_j}} \frac{4m^2_{\tilde{Z}_i} E}{\sqrt{s}(s - m_h^2)(s - m_H^2)} \Big], \tag{A.285}$$

$$I^{hH}_4 = \int_{|m_{\tilde{Z}_j}|}^{E_{max}} dE \Big[2|m_{\tilde{Z}_i}| \sqrt{s - 4m_f^2} \sqrt{E^2 - m^2_{\tilde{Z}_j}} \frac{4m^2_{\tilde{Z}_i} E(s - 2m_f^2)}{\sqrt{s}(s - m_h^2)(s - m_H^2)} \Big]. \tag{A.286}$$

$$\Gamma_{\tilde{f}} = 2\Gamma^{diag}_{\tilde{f}_1\tilde{f}_1} + 2\Gamma^{diag}_{\tilde{f}_2\tilde{f}_2} + 2\Gamma^{nondiag}_{\tilde{f}\tilde{f}} + \Gamma^{tu}_{\tilde{f}_1\tilde{f}_1} + \Gamma^{tu}_{\tilde{f}_2\tilde{f}_2} + 2\Gamma^{tu}_{\tilde{f}_1\tilde{f}_2}, \tag{A.287}$$

There are many sfermion contributions included here, they are as follows:

$$\begin{aligned}\Gamma^{diag}_{\tilde{f}_1\tilde{f}_1} = & \frac{8m^2_{\tilde{Z}_i}}{\pi^2}(\alpha^{\tilde{Z}_i\,2}_{\tilde{f}_1} + \beta^{\tilde{Z}_i\,2}_{\tilde{f}_1}) \Big[(\alpha^{\tilde{Z}_j\,2}_{\tilde{f}_1} + \beta^{\tilde{Z}_j\,2}_{\tilde{f}_1}) \tilde{\psi}(\tilde{Z}_i, \tilde{f}_1, \tilde{f}_1, \tilde{Z}_j) + 4(-1)^{\theta_j} \alpha^{\tilde{Z}_j}_{\tilde{f}_1} \beta^{\tilde{Z}_j}_{\tilde{f}_1} m_f |m_{\tilde{Z}_j}| \tilde{\chi}(\tilde{Z}_i, \tilde{f}_1, \tilde{f}_1, \tilde{Z}_j) \Big] \\ & - \frac{32m^2_{\tilde{Z}_i}}{\pi^2}(-1)^{\theta_i}(\alpha^{\tilde{Z}_j\,2}_{\tilde{f}_1} + \beta^{\tilde{Z}_j\,2}_{\tilde{f}_1}) \alpha^{\tilde{Z}_i}_{\tilde{f}_1} \beta^{\tilde{Z}_i}_{\tilde{f}_1} m_f |m_{\tilde{Z}_i}| X(\tilde{Z}_i, \tilde{f}_1, \tilde{f}_1, \tilde{Z}_j) \\ & - \frac{64m^2_{\tilde{Z}_i}}{\pi^2}(-1)^{\theta_i}(-1)^{\theta_j} \alpha^{\tilde{Z}_i}_{\tilde{f}_1} \beta^{\tilde{Z}_i}_{\tilde{f}_1} \alpha^{\tilde{Z}_j}_{\tilde{f}_1} \beta^{\tilde{Z}_j}_{\tilde{f}_1} |m_{\tilde{Z}_i}| m_f^2 |m_{\tilde{Z}_j}| \zeta(\tilde{Z}_i, \tilde{f}_1, \tilde{f}_1, \tilde{Z}_j),\end{aligned} \tag{A.288}$$

$$\begin{aligned}\Gamma^{diag}_{\tilde{f}_2\tilde{f}_2} = & \frac{8m^2_{\tilde{Z}_i}}{\pi^2}(\alpha^{\tilde{Z}_i\,2}_{\tilde{f}_2} + \beta^{\tilde{Z}_i\,2}_{\tilde{f}_2}) \Big[(\alpha^{\tilde{Z}_j\,2}_{\tilde{f}_2} + \beta^{\tilde{Z}_j\,2}_{\tilde{f}_2}) \tilde{\psi}(\tilde{Z}_i, \tilde{f}_2, \tilde{f}_2, \tilde{Z}_j) + 4(-1)^{\theta_j} \alpha^{\tilde{Z}_j}_{\tilde{f}_2} \beta^{\tilde{Z}_j}_{\tilde{f}_2} m_f |m_{\tilde{Z}_j}| \tilde{\chi}(\tilde{Z}_i, \tilde{f}_2, \tilde{f}_2, \tilde{Z}_j) \Big] \\ & - \frac{32m^2_{\tilde{Z}_i}}{\pi^2}(-1)^{\theta_i}(\alpha^{\tilde{Z}_j\,2}_{\tilde{f}_2} + \beta^{\tilde{Z}_j\,2}_{\tilde{f}_2}) \alpha^{\tilde{Z}_i}_{\tilde{f}_2} \beta^{\tilde{Z}_i}_{\tilde{f}_2} m_f |m_{\tilde{Z}_i}| X(\tilde{Z}_i, \tilde{f}_2, \tilde{f}_2, \tilde{Z}_j) \\ & - \frac{64m^2_{\tilde{Z}_i}}{\pi^2}(-1)^{\theta_i}(-1)^{\theta_j} \alpha^{\tilde{Z}_i}_{\tilde{f}_2} \beta^{\tilde{Z}_i}_{\tilde{f}_2} \alpha^{\tilde{Z}_j}_{\tilde{f}_2} \beta^{\tilde{Z}_j}_{\tilde{f}_2} |m_{\tilde{Z}_i}| m_f^2 |m_{\tilde{Z}_j}| \zeta(\tilde{Z}_i, \tilde{f}_2, \tilde{f}_2, \tilde{Z}_j),\end{aligned} \tag{A.289}$$

where the $\tilde{\psi}$, $\tilde{\chi}$, X, ζ integrals have been used before for the gluino 3-body decays and are:

$$E_f^{max} = \frac{m^2_{\tilde{Z}_i} - 2m_f|m_{\tilde{Z}_j} - m^2_{\tilde{Z}_j}}{2|m_{\tilde{Z}_i}|}, \tag{A.290}$$

$$\tilde{\psi}(m_{\tilde{Z}_i}, m_{\tilde{f}_1}, m_{\tilde{f}_2}, m_{\tilde{Z}_j}) = \pi^2 m_{\tilde{Z}_i} \int_{m_f}^{E_f^{max}} dE_f \sqrt{{E_f}^2 - m_f^2} E_f \frac{\lambda^{\frac{1}{2}}(s, m_f^2, m_{\tilde{Z}_j}^2)}{s} \frac{m_{\tilde{Z}_i}^2 - m_{\tilde{Z}_j}^2 - 2m_{\tilde{Z}_i} E_f}{(s - m_{\tilde{f}_1}^2)(s - m_{\tilde{f}_2}^2)}, \tag{A.291}$$

$$\tilde{\chi}(m_{\tilde{Z}_i}, m_{\tilde{f}_1}, m_{\tilde{f}_2}, m_{\tilde{Z}_j}) = \pi^2 m_{\tilde{Z}_i} \int_{m_f}^{E_f^{max}} dE_f \sqrt{{E_f}^2 - m_f^2} E_f \frac{\lambda^{\frac{1}{2}}(s, m_f^2, m_{\tilde{Z}_j}^2)}{s} \frac{1}{(s - m_{\tilde{f}_1}^2)(s - m_{\tilde{f}_2}^2)}, \tag{A.292}$$

$$X(m_{\tilde{Z}_i}, m_{\tilde{f}_1}, m_{\tilde{f}_2}, m_{\tilde{Z}_j}) = \frac{\pi^2}{2} \int_{m_f}^{E_f^{max}} dE_f \sqrt{{E_f}^2 - m_f^2} \frac{m_{\tilde{Z}_i}^2 - m_{\tilde{Z}_j}^2 - 2m_{\tilde{Z}_i} E_f}{m_{\tilde{Z}_i}^2 + m_f^2 - 2m_{\tilde{Z}_i} E_f} \frac{\lambda^{\frac{1}{2}}(s, m_f^2, m_{\tilde{Z}_j}^2)}{(s - m_{\tilde{f}_1}^2)(s - m_{\tilde{f}_2}^2)}, \tag{A.293}$$

$$\zeta(m_{\tilde{Z}_i}, m_{\tilde{f}_1}, m_{\tilde{f}_2}, m_{\tilde{Z}_j}) = \pi^2 \int_{m_f}^{E_f^{max}} dE_f \frac{[E_{\bar{f}}(max) - E_{\bar{f}}(min)]}{(s - m_{\tilde{f}_1}^2)(s - m_{\tilde{f}_2}^2)}. \tag{A.294}$$

Later the following integrals will also be required, where $Z(m_{\tilde{f}_2}) = \frac{m_{\tilde{Z}_i}^2 + m_f^2 - 2|m_{\tilde{Z}_i}|E_{\bar{f}}(max) - m_{\tilde{f}_2}^2}{m_{\tilde{Z}_i}^2 + m_f^2 - 2|m_{\tilde{Z}_i}|E_{\bar{f}}(min) - m_{\tilde{f}_2}^2}$:

$$\tilde{\phi}(m_{\tilde{Z}_i}, m_{\tilde{f}_1}, m_{\tilde{f}_2}, m_{\tilde{Z}_j}) = \frac{1}{2}\pi^2 |m_{\tilde{Z}_i}||m_{\tilde{Z}_j}| \int_{m_f}^{E_f^{max}} dE_f \frac{1}{s - m_{\tilde{f}_1}^2} \Big[- [E_{\bar{f}}(max) - E_{\bar{f}}(min)] - \frac{m_{\tilde{Z}_j}^2 - m_f^2 + 2|m_{\tilde{Z}_i}|E_f - m_{\tilde{f}_2}^2}{2|m_{\tilde{Z}_i}|} \log Z(m_{\tilde{f}_2}) \Big], \tag{A.295}$$

$$\xi(m_{\tilde{Z}_i}, m_{\tilde{f}_1}, m_{\tilde{f}_2}, m_{\tilde{Z}_j}) = \frac{1}{2}\pi^2 \int_{m_f}^{E_f^{max}} dE_f \frac{1}{s - m_{\tilde{f}_1}^2} \Big[[E_{\bar{f}}(max) - E_{\bar{f}}(min)] - \frac{m_{\tilde{Z}_i}^2 - m_f^2 - 2|m_{\tilde{Z}_i}|E_f + m_{\tilde{f}_2}^2}{2|m_{\tilde{Z}_i}|} \log Z(m_{\tilde{f}_2}) \Big], \tag{A.296}$$

$$\tilde{\rho}(m_{\tilde{Z}_i}, m_{\tilde{f}_1}, m_{\tilde{f}_2}, m_{\tilde{Z}_j}) = -\frac{\pi^2}{2|m_{\tilde{Z}_i}|} \int_{m_f}^{E_f^{max}} dE_f \frac{1}{s - m_{\tilde{f}_1}^2} \log Z(m_{\tilde{f}_2}), \tag{A.297}$$

$$Y(m_{\tilde{Z}_i}, m_{\tilde{f}_1}, m_{\tilde{f}_2}, m_{\tilde{Z}_j}) = \frac{\pi^2}{2} \int_{m_f}^{E_f^{max}} dE_f \frac{1}{s - m_{\tilde{f}_1}^2} \Big[[E_{\bar{f}}(max) - E_{\bar{f}}(min)]s + \frac{1}{2|m_{\tilde{Z}_i}|}(m_{\tilde{Z}_i}^2 m_{\tilde{Z}_j}^2 - m_{\tilde{Z}_i}^2 m_{\tilde{f}_2}^2 + m_f^4 + 2|m_{\tilde{Z}_i}|E_f m_{\tilde{f}_2}^2 - m_{\tilde{f}_2}^2 m_f^2) \log Z(m_{\tilde{f}_2}) \Big], \tag{A.298}$$

$$\chi^{'}(m_{\tilde{Z}_i}, m_{\tilde{f}_1}, m_{\tilde{f}_2}, m_{\tilde{Z}_j}) = \frac{-\pi^2}{2} \int_{m_f}^{E_f^{max}} \frac{dE_f E_f}{s - m_{\tilde{f}_2}^2} \log Z(m_{\tilde{f}_1}), \tag{A.299}$$

where here

$$E_{\bar{f}}(max/min) = \frac{(s + m_f^2 - m_{\tilde{Z}_j}^2)(|m_{\tilde{Z}_i}| - E_f) \pm \sqrt{(E_f^2 - m_f^2)(s + m_f^2 - m_{\tilde{Z}_j}^2)^2 - 4(E_f^2 - m_f^2)m_f^2 s}}{2s}. \tag{A.300}$$

$$\begin{aligned}\Gamma_{\tilde{f}\tilde{f}}^{nondiag} =& \frac{16m_{\tilde{Z}_i}^2}{\pi^2} \Big[(\beta_{\tilde{f}_1}^{\tilde{Z}_i}\beta_{\tilde{f}_2}^{\tilde{Z}_i} + \alpha_{\tilde{f}_1}^{\tilde{Z}_i}\alpha_{\tilde{f}_2}^{\tilde{Z}_i})(\alpha_{\tilde{f}_1}^{\tilde{Z}_j}\alpha_{\tilde{f}_2}^{\tilde{Z}_j} + \beta_{\tilde{f}_2}^{\tilde{Z}_j}\beta_{\tilde{f}_2}^{\tilde{Z}_j})\tilde{\psi}(\tilde{Z}_i, \tilde{f}_1, \tilde{f}_2, \tilde{Z}_j) \\ &+ 2(-1)^{\theta_j}(\beta_{\tilde{f}_1}^{\tilde{Z}_i}\beta_{\tilde{f}_2}^{\tilde{Z}_i} + \alpha_{\tilde{f}_1}^{\tilde{Z}_i}\alpha_{\tilde{f}_2}^{\tilde{Z}_i})(\alpha_{\tilde{f}_2}^{\tilde{Z}_j}\beta_{\tilde{f}_1}^{\tilde{Z}_j} + \alpha_{\tilde{f}_1}^{\tilde{Z}_j}\beta_{\tilde{f}_2}^{\tilde{Z}_j})m_f|m_{\tilde{Z}_j}|\tilde{\chi}(\tilde{Z}_i, \tilde{f}_1, \tilde{f}_2, \tilde{Z}_j) \\ &- 2(-1)^{\theta_i}(\alpha_{\tilde{f}_1}^{\tilde{Z}_i}\beta_{\tilde{f}_2}^{\tilde{Z}_i} + \alpha_{\tilde{f}_2}^{\tilde{Z}_i}\beta_{\tilde{f}_1}^{\tilde{Z}_i})(\alpha_{\tilde{f}_1}^{\tilde{Z}_j}\alpha_{\tilde{f}_2}^{\tilde{Z}_j} + \beta_{\tilde{f}_2}^{\tilde{Z}_j}\beta_{\tilde{f}_1}^{\tilde{Z}_j})|m_{\tilde{Z}_i}|m_f X(\tilde{Z}_i, \tilde{f}_1, \tilde{f}_2, \tilde{Z}_j) \\ &- 2(-1)^{\theta_i}(-1)^{\theta_j}(\alpha_{\tilde{f}_1}^{\tilde{Z}_i}\beta_{\tilde{f}_2}^{\tilde{Z}_i} + \alpha_{\tilde{f}_2}^{\tilde{Z}_i}\beta_{\tilde{f}_1}^{\tilde{Z}_i})(\alpha_{\tilde{f}_2}^{\tilde{Z}_j}\beta_{\tilde{f}_1}^{\tilde{Z}_j} + \alpha_{\tilde{f}_1}^{\tilde{Z}_j}\beta_{\tilde{f}_2}^{\tilde{Z}_j})m_f^2|m_{\tilde{Z}_i}||m_{\tilde{Z}_j}|\zeta(\tilde{Z}_i, \tilde{f}_1, \tilde{f}_2, \tilde{Z}_j) \Big],\end{aligned} \tag{A.301}$$

$$\begin{aligned}\Gamma^{tu}_{\tilde{f}_1\tilde{f}_1} = -2\Big\{&8(\alpha^{\tilde{Z}_i}_{\tilde{f}_1}\beta^{\tilde{Z}_i}_{\tilde{f}_1}\beta^{\tilde{Z}_j}_{\tilde{f}_1}\alpha^{\tilde{Z}_j}_{\tilde{f}_1} + \beta^{\tilde{Z}_i}_{\tilde{f}_1}\alpha^{\tilde{Z}_i}_{\tilde{f}_1}\alpha^{\tilde{Z}_j}_{\tilde{f}_1}\beta^{\tilde{Z}_j}_{\tilde{f}_1})m^2_{\tilde{Z}_i}\pi^2(-1)^{\theta_i}Y(\tilde{Z}_i,\tilde{f}_1,\tilde{f}_1,\tilde{Z}_j)\\
&-(\alpha^{\tilde{Z}_i}_{\tilde{f}_1}{}^2\alpha^{\tilde{Z}_j}_{\tilde{f}_1}{}^2 + \beta^{\tilde{Z}_i}_{\tilde{f}_1}{}^2\beta^{\tilde{Z}_j}_{\tilde{f}_1}{}^2)8m^2_{\tilde{Z}_i}\pi^2(-1)^{\theta_i}(-1)^{\theta_j}\tilde{\phi}(\tilde{Z}_i,\tilde{f}_1,\tilde{f}_1,\tilde{Z}_j)\\
&+(\alpha^{\tilde{Z}_i}_{\tilde{f}_1}\beta^{\tilde{Z}_i}_{\tilde{f}_1}\alpha^{\tilde{Z}_j}_{\tilde{f}_1}\beta^{\tilde{Z}_j}_{\tilde{f}_1} + \alpha^{\tilde{Z}_i}_{\tilde{f}_1}\beta^{\tilde{Z}_i}_{\tilde{f}_1}\alpha^{\tilde{Z}_j}_{\tilde{f}_1}\beta^{\tilde{Z}_j}_{\tilde{f}_1})m^2_f\frac{8m^2_{\tilde{Z}_i}}{\pi^2}(-1)^{\theta_i}\xi(\tilde{Z}_i,\tilde{f}_1,\tilde{f}_1,\tilde{Z}_j)\\
&-\{(\alpha^{\tilde{Z}_i}_{\tilde{f}_1}{}^2\alpha^{\tilde{Z}_j}_{\tilde{f}_1}\beta^{\tilde{Z}_j}_{\tilde{f}_1} + \beta^{\tilde{Z}_i}_{\tilde{f}_1}{}^2\alpha^{\tilde{Z}_j}_{\tilde{f}_1}\beta^{\tilde{Z}_j}_{\tilde{f}_1})|m_{\tilde{Z}_i}|m_f\}\Big[\frac{8m^2_{\tilde{Z}_i}}{\pi^2}\xi(\tilde{Z}_i,\tilde{f}_1,\tilde{f}_1,\tilde{Z}_j)\\
&-\frac{4m^2_{\tilde{Z}_i}}{\pi^2}(m^2_{\tilde{Z}_i}+m^2_{\tilde{Z}_j})(-1)^{\theta_i}\tilde{\rho}(\tilde{Z}_i,\tilde{f}_1,\tilde{f}_1,\tilde{Z}_j) + \frac{8m^2_{\tilde{Z}_i}}{\pi^2}\chi'(\tilde{Z}_i,\tilde{f}_1,\tilde{f}_1,\tilde{Z}_j)\Big]\\
&+|m_{\tilde{Z}_j}|(-1)^{\theta_j}m_f(\alpha^{\tilde{Z}_i}_{\tilde{f}_1}\beta^{\tilde{Z}_i}_{\tilde{f}_1}\alpha^{\tilde{Z}_j}_{\tilde{f}_1}{}^2 + \alpha^{\tilde{Z}_i}_{\tilde{f}_1}\beta^{\tilde{Z}_i}_{\tilde{f}_1}\beta^{\tilde{Z}_j}_{\tilde{f}_1}{}^2)\Big[\frac{-8m^2_{\tilde{Z}_i}}{\pi^2}\xi(\tilde{Z}_i,\tilde{f}_1,\tilde{f}_1,\tilde{Z}_j)\\
&+\frac{8m^4_{\tilde{Z}_i}}{\pi^2}(-1)^{\theta_i}\tilde{\rho}(\tilde{Z}_i,\tilde{f}_1,\tilde{f}_1,\tilde{Z}_j) - \frac{8m^2_{\tilde{Z}_i}}{\pi^2}\chi'(\tilde{Z}_i,\tilde{f}_1,\tilde{f}_1,\tilde{Z}_j)\Big]\\
&-(\beta^{\tilde{Z}_i}_{\tilde{f}_1}{}^2\beta^{\tilde{Z}_j}_{\tilde{f}_1}\alpha^{\tilde{Z}_j}_{\tilde{f}_1} + \alpha^{\tilde{Z}_i}_{\tilde{f}_1}{}^2\alpha^{\tilde{Z}_j}_{\tilde{f}_1}\beta^{\tilde{Z}_j}_{\tilde{f}_1})|m_{\tilde{Z}_i}|(-1)^{\theta_i}m_f\Big[\frac{4m^2_{\tilde{Z}_i}}{\pi^2}(m^2_{\tilde{Z}_i}-m^2_{\tilde{Z}_j})\tilde{\rho}(\tilde{Z}_i,\tilde{f}_1,\tilde{f}_1,\tilde{Z}_j)\\
&-\frac{8m^2_{\tilde{Z}_i}}{\pi^2}\chi'(\tilde{Z}_i,\tilde{f}_1,\tilde{f}_1,\tilde{Z}_j)\Big]\\
&+(\alpha^{\tilde{Z}_i}_{\tilde{f}_1}\beta^{\tilde{Z}_i}_{\tilde{f}_1}\alpha^{\tilde{Z}_j}_{\tilde{f}_1}{}^2 + \alpha^{\tilde{Z}_i}_{\tilde{f}_1}\beta^{\tilde{Z}_i}_{\tilde{f}_1}\beta^{\tilde{Z}_j}_{\tilde{f}_1}{}^2)m_f|m_{\tilde{Z}_j}|\frac{8m^2_{\tilde{Z}_i}}{\pi^2}(-1)^{\theta_i}(-1)^{\theta_j}\chi'(\tilde{Z}_i,\tilde{f}_1,\tilde{f}_1,\tilde{Z}_j)\\
&-2(\beta^{\tilde{Z}_i}_{\tilde{f}_1}{}^2\alpha^{\tilde{Z}_j}_{\tilde{f}_1}{}^2 + \alpha^{\tilde{Z}_i}_{\tilde{f}_1}{}^2\beta^{\tilde{Z}_j}_{\tilde{f}_1}{}^2)m^2_f(-1)^{\theta_i}(-1)^{\theta_j}|m_{\tilde{Z}_i}||m_{\tilde{Z}_j}|\frac{4m^2_{\tilde{Z}_i}}{\pi^2}\tilde{\rho}(\tilde{Z}_i,\tilde{f}_1,\tilde{f}_1,\tilde{Z}_j)\Big\}.\end{aligned} \tag{A.302}$$

$\Gamma^{tu}_{\tilde{f}_2\tilde{f}_2}$ is as above but with $\tilde{f}_1 \to \tilde{f}_2$ everywhere including in the masses and integrals.

$$\begin{aligned}\Gamma^{tu}_{\tilde{f}_1\tilde{f}_2} = -2\Big\{&8(\alpha^{\tilde{Z}_i}_{\tilde{f}_1}\beta^{\tilde{Z}_i}_{\tilde{f}_2}\beta^{\tilde{Z}_j}_{\tilde{f}_1}\alpha^{\tilde{Z}_j}_{\tilde{f}_2} + \beta^{\tilde{Z}_i}_{\tilde{f}_1}\alpha^{\tilde{Z}_i}_{\tilde{f}_2}\alpha^{\tilde{Z}_j}_{\tilde{f}_1}\beta^{\tilde{Z}_j}_{\tilde{f}_2})m^2_{\tilde{Z}_i}\pi^2Y(\tilde{Z}_i,\tilde{f}_1,\tilde{f}_2,\tilde{Z}_j)\\
&-(\alpha^{\tilde{Z}_i}_{\tilde{f}_1}\alpha^{\tilde{Z}_i}_{\tilde{f}_2}\alpha^{\tilde{Z}_j}_{\tilde{f}_1}\alpha^{\tilde{Z}_j}_{\tilde{f}_2} + \beta^{\tilde{Z}_i}_{\tilde{f}_1}\beta^{\tilde{Z}_i}_{\tilde{f}_2}\beta^{\tilde{Z}_j}_{\tilde{f}_1}\beta^{\tilde{Z}_j}_{\tilde{f}_2})8m^2_{\tilde{Z}_i}\pi^2(-1)^{\theta_i}(-1)^{\theta_j}\tilde{\phi}(\tilde{Z}_i,\tilde{f}_1,\tilde{f}_2,\tilde{Z}_j)\\
&+(\alpha^{\tilde{Z}_i}_{\tilde{f}_2}\beta^{\tilde{Z}_i}_{\tilde{f}_1}\alpha^{\tilde{Z}_j}_{\tilde{f}_2}\beta^{\tilde{Z}_j}_{\tilde{f}_1} + \alpha^{tildeZ_i}_{\tilde{f}_1}\beta^{\tilde{Z}_i}_{\tilde{f}_2}\alpha^{\tilde{Z}_j}_{\tilde{f}_1}\beta^{\tilde{Z}_j}_{\tilde{f}_2})m^2_f\frac{8m^2_{\tilde{Z}_i}}{\pi^2}(-1)^{\theta_i}\xi(\tilde{Z}_i,\tilde{f}_1,\tilde{f}_2,\tilde{Z}_j)\\
&-\{(\alpha^{\tilde{Z}_i}_{\tilde{f}_1}\alpha^{\tilde{Z}_i}_{\tilde{f}_2}\alpha^{\tilde{Z}_j}_{\tilde{f}_2}\beta^{\tilde{Z}_j}_{\tilde{f}_1} + \beta^{\tilde{Z}_i}_{\tilde{f}_1}\beta^{\tilde{Z}_i}_{\tilde{f}_2}\alpha^{\tilde{Z}_j}_{\tilde{f}_1}\beta^{\tilde{Z}_j}_{\tilde{f}_2})|m_{\tilde{Z}_i}|m_f\}\Big[\frac{8m^2_{\tilde{Z}_i}}{\pi^2}\xi(\tilde{Z}_i,\tilde{f}_1,\tilde{f}_2,\tilde{Z}_j)\\
&-\frac{4m^2_{\tilde{Z}_i}}{\pi^2}(m^2_{\tilde{Z}_i}+m^2_{\tilde{Z}_j})(-1)^{\theta_i}\tilde{\rho}(\tilde{Z}_i,\tilde{f}_1,\tilde{f}_2,\tilde{Z}_j) + \frac{8m^2_{\tilde{Z}_i}}{\pi^2}\chi'(\tilde{Z}_i,\tilde{f}_1,\tilde{f}_2,\tilde{Z}_j)\Big]\\
&+|m_{\tilde{Z}_j}|(-1)^{\theta_j}m_f(\alpha^{\tilde{Z}_i}_{\tilde{f}_2}\beta^{\tilde{Z}_i}_{\tilde{f}_1}\alpha^{\tilde{Z}_j}_{\tilde{f}_1}\alpha^{\tilde{Z}_j}_{\tilde{f}_2} + \alpha^{\tilde{Z}_i}_{\tilde{f}_1}\beta^{\tilde{Z}_i}_{\tilde{f}_2}\beta^{\tilde{Z}_j}_{\tilde{f}_1}\beta^{\tilde{Z}_j}_{\tilde{f}_2})\Big[\frac{-8m^2_{\tilde{Z}_i}}{\pi^2}\xi(\tilde{Z}_i,\tilde{f}_1,\tilde{f}_2,\tilde{Z}_j)\\
&+\frac{8m^4_{\tilde{Z}_i}}{\pi^2}(-1)^{\theta_i}\tilde{\rho}(\tilde{Z}_i,\tilde{f}_1,\tilde{f}_2,\tilde{Z}_j) - \frac{8m^2_{\tilde{Z}_i}}{\pi^2}\chi'(\tilde{Z}_i,\tilde{f}_1,\tilde{f}_2,\tilde{Z}_j)\Big]\\
&-(\beta^{\tilde{Z}_i}_{\tilde{f}_1}\beta^{\tilde{Z}_i}_{\tilde{f}_2}\beta^{\tilde{Z}_j}_{\tilde{f}_1}\alpha^{\tilde{Z}_j}_{\tilde{f}_2} + \alpha^{\tilde{Z}_i}_{\tilde{f}_1}\alpha^{\tilde{Z}_i}_{\tilde{f}_2}\alpha^{\tilde{Z}_j}_{\tilde{f}_1}\beta^{\tilde{Z}_j}_{\tilde{f}_2})|m_{\tilde{Z}_i}|(-1)^{\theta_i}m_f\Big[\frac{4m^2_{\tilde{Z}_i}}{\pi^2}(m^2_{\tilde{Z}_i}-m^2_{\tilde{Z}_j})\tilde{\rho}(\tilde{Z}_i,\tilde{f}_1,\tilde{f}_2,\tilde{Z}_j)\\
&-\frac{8m^2_{\tilde{Z}_i}}{\pi^2}\chi'(\tilde{Z}_i,\tilde{f}_1,\tilde{f}_2,\tilde{Z}_j))\Big]\\
&+(\alpha^{\tilde{Z}_i}_{\tilde{f}_1}\beta^{\tilde{Z}_i}_{\tilde{f}_2}\alpha^{\tilde{Z}_j}_{\tilde{f}_1}\alpha^{\tilde{Z}_j}_{\tilde{f}_2} + \alpha^{\tilde{Z}_i}_{\tilde{f}_2}\beta^{\tilde{Z}_i}_{\tilde{f}_1}\beta^{\tilde{Z}_j}_{\tilde{f}_1}\beta^{\tilde{Z}_i}_{\tilde{f}_2}m_f(-1)^{\theta_j}|m_{\tilde{Z}_j}|)\frac{8m^2_{\tilde{Z}_i}}{\pi^2}\chi'(\tilde{Z}_i,\tilde{f}_1,\tilde{f}_2,\tilde{Z}_j)\\
&-2(\beta^{\tilde{Z}_i}_{\tilde{f}_1}\beta^{\tilde{Z}_i}_{\tilde{f}_2}\alpha^{\tilde{Z}_j}_{\tilde{f}_1}\alpha^{\tilde{Z}_j}_{\tilde{f}_2} + \alpha^{\tilde{Z}_i}_{\tilde{f}_1}\alpha^{\tilde{Z}_i}_{\tilde{f}_2}\beta^{\tilde{Z}_j}_{\tilde{f}_1}\beta^{\tilde{Z}_j}_{\tilde{f}_2})m^2_f(-1)^{\theta_i}(-1)^{\theta_j}|m_{\tilde{Z}_i}||m_{\tilde{Z}_j}|\frac{4m^2_{\tilde{Z}_i}}{\pi^2}\tilde{\rho}(\tilde{Z}_i,\tilde{f}_1,\tilde{f}_2,\tilde{Z}_j)\Big\}.\end{aligned} \tag{A.303}$$

As for the Z sfermion interferences:

$$\Gamma_{Z\tilde{f}_1} = (-1)^{\theta_i}(C_1^{Z\tilde{f}_1}I_1^{Z\tilde{f}_1} + C_2^{Z\tilde{f}_1}I_2^{Z\tilde{f}_1} + C_3^{Z\tilde{f}_1}I_3^{Z\tilde{f}_1} + C_4^{Z\tilde{f}_1}I_4^{Z\tilde{f}_1} + C_5^{Z\tilde{f}_1}I_5^{Z\tilde{f}_1} + C_6^{Z\tilde{f}_1}I_6^{Z\tilde{f}_1} + C_7^{Z\tilde{f}_1}I_7^{Z\tilde{f}_1} + C_8^{Z\tilde{f}_1}I_8^{Z\tilde{f}_1}), \tag{A.304}$$

where

$$C_1^{Z\tilde{f}_1} = -4W_{ij}g\sin\theta_W[-\alpha_{\tilde{f}_1}^{\tilde{Z}_i}(\alpha_f - \beta_f)\beta_{\tilde{f}_1}^{\tilde{Z}_j} + \beta_{\tilde{f}_1}^{\tilde{Z}_i}(\alpha_f + \beta_f)\alpha_{\tilde{f}_1}^{\tilde{Z}_j}]m_f|m_{\tilde{Z}_i}|, \tag{A.305}$$

$$C_2^{Z\tilde{f}_1} = -4(-1)^{\theta_i}(-1)^{\theta_j}W_{ij}g\sin\theta_W[-\alpha_{\tilde{f}_1}^{\tilde{Z}_i}(\alpha_f + \beta_f)\beta_{\tilde{f}_1}^{\tilde{Z}_j} + \beta_{\tilde{f}_1}^{\tilde{Z}_i}(\alpha_f - \beta_f)\alpha_{\tilde{f}_1}^{\tilde{Z}_j}]m_f|m_{\tilde{Z}_j}|, \tag{A.306}$$

$$C_3^{Z\tilde{f}_1} = -4(-1)^{\theta_i}W_{ij}g\sin\theta_W[\beta_{\tilde{f}_1}^{\tilde{Z}_i}(\alpha_f + \beta_f)\beta_{\tilde{f}_1}^{\tilde{Z}_j} - \alpha_{\tilde{f}_1}^{\tilde{Z}_i}(\alpha_f - \beta_f)\alpha_{\tilde{f}_1}^{\tilde{Z}_j}], \tag{A.307}$$

$$C_4^{Z\tilde{f}_1} = -8W_{ij}g\sin\theta_W[-\alpha_{\tilde{f}_1}^{\tilde{Z}_i}(\alpha_f + \beta_f)\beta_{\tilde{f}_1}^{\tilde{Z}_j} + \beta_{\tilde{f}_1}^{\tilde{Z}_i}(\alpha_f - \beta_f)\alpha_{\tilde{f}_1}^{\tilde{Z}_j}]|m_{\tilde{Z}_i}|m_f, \tag{A.308}$$

$$C_5^{Z\tilde{f}_1} = -8(-1)^{\theta_i}(-1)^{\theta_j}W_{ij}g\sin\theta_W[-\alpha_{\tilde{f}_1}^{\tilde{Z}_i}(\alpha_f - \beta_f)\beta_{\tilde{f}_1}^{\tilde{Z}_j} + \beta_{\tilde{f}_1}^{\tilde{Z}_i}(\alpha_f + \beta_f)\alpha_{\tilde{f}_1}^{\tilde{Z}_j}]|m_{\tilde{Z}_j}|m_f, \tag{A.309}$$

$$C_6^{Z\tilde{f}_1} = -4(-1)^{\theta_j}W_{ij}g\sin\theta_W[\beta_{\tilde{f}_1}^{\tilde{Z}_i}(\alpha_f + \beta_f)\beta_{\tilde{f}_1}^{\tilde{Z}_j} - \alpha_{\tilde{f}_1}^{\tilde{Z}_i}(\alpha_f - \beta_f)\alpha_{\tilde{f}_1}^{\tilde{Z}_j}]|m_{\tilde{Z}_i}||m_{\tilde{Z}_j}|, \tag{A.310}$$

$$C_7^{Z\tilde{f}_1} = -4(-1)^{\theta_i}W_{ij}g\sin\theta_W[\beta_{\tilde{f}_1}^{\tilde{Z}_i}(\alpha_f - \beta_f)\beta_{\tilde{f}_1}^{\tilde{Z}_j} - \alpha_{\tilde{f}_1}^{\tilde{Z}_i}(\alpha_f + \beta_f)\alpha_{\tilde{f}_1}^{\tilde{Z}_j}]m_f^2, \tag{A.311}$$

$$C_8^{Z\tilde{f}_1} = -16(-1)^{\theta_j}W_{ij}g\sin\theta_W[\beta_{\tilde{f}_1}^{\tilde{Z}_i}(\alpha_f - \beta_f)\beta_{\tilde{f}_1}^{\tilde{Z}_j} - \alpha_{\tilde{f}_1}^{\tilde{Z}_i}(\alpha_f + \beta_f)\alpha_{\tilde{f}_1}^{\tilde{Z}_j}]m_f^2|m_{\tilde{Z}_i}||m_{\tilde{Z}_j}|. \tag{A.312}$$

The upper limit for the integrals here is $E_{upper} = \frac{(m_{\tilde{Z}_i}^2 + m_{\tilde{Z}_j}^2 - 4m_f^2)}{2|m_{\tilde{Z}_i}|}$. The argument of the logarithm in these integrals is as follows:

$$L = [|m_{\tilde{Z}_i}|(E_Q + Q') - \mu^2]/[|m_{\tilde{Z}_i}|(E_Q - Q') - \mu^2], \tag{A.313}$$

In these expressions, $E_Q = \frac{s + m_{\tilde{Z}_i}^2 - m_{\tilde{Z}_j}^2}{2|m_{\tilde{Z}_i}|}$, $Q' = \sqrt{E_Q^2 - s}\sqrt{1 - 4m_f^2/s}$ and $\mu^2 = s + m_{\tilde{f}_1}^2 - m_{\tilde{Z}_j}^2 - m_q^2$, where $s = m_{\tilde{Z}_i}^2 + m_{\tilde{Z}_j}^2 - 2|m_{\tilde{Z}_i}|E$. The necessary integrals are given by:

$$I_1^{Z\tilde{f}_1} = 2|m_{\tilde{Z}_i}|\int_{|m_{\tilde{Z}_j}|}^{E_{upper}} dE \frac{1}{s - m_Z^2}\Big[-2|m_{\tilde{Z}_i}|\sqrt{1 - 4m_q^2/s}\sqrt{E^2 - m_{\tilde{Z}_j}^2} - (m_{\tilde{f}_1}^2 - m_f^2 + m_{\tilde{Z}_j}^2 - 2|m_{\tilde{Z}_i}|E)\log L\Big], \tag{A.314}$$

$$I_2^{Z\tilde{f}_1} = 2|m_{\tilde{Z}_i}|\int_{|m_{\tilde{Z}_j}|}^{E_{upper}} dE \frac{1}{s - m_Z^2}\left[2|m_{\tilde{Z}_i}|\sqrt{1 - 4m_q^2/s}\sqrt{E^2 - m_{\tilde{Z}_j}^2} + (m_{\tilde{f}_1}^2 + m_{\tilde{Z}_i}^2 - 2|m_{\tilde{Z}_i}|E - m_f^2)\log L\right], \tag{A.315}$$

$$\begin{aligned} I_3^{Z\tilde{f}_1} =& 2|m_{\tilde{Z}_i}|\int_{|m_{\tilde{Z}_j}|}^{E_{upper}} dE \frac{1}{s - m_Z^2}\Big[\{m_{\tilde{Z}_i}^2 + 2m_f^2 + m_{\tilde{Z}_j}^2 - \frac{3}{2}m_{\tilde{f}_1}^2 - \frac{1}{2}(m_f^2 + |m_{\tilde{Z}_i}|E \\ &+ |m_{\tilde{Z}_i}|\sqrt{1 - 4m_f^2/s}\sqrt{E^2 - m_{\tilde{Z}_j}^2}\ )\}(m_f^2 + |m_{\tilde{Z}_i}|E + |m_{\tilde{Z}_i}|\sqrt{1 - 4m_f^2/s}\sqrt{E^2 - m_{\tilde{Z}_j}^2} - m_{\tilde{f}_1}^2) \\ &- \{m_{\tilde{Z}_i}^2 + 2m_f^2 + m_{\tilde{Z}_j}^2 - \frac{3}{2}m_{\tilde{f}_1}^2 - \frac{1}{2}(m_f^2 + |m_{\tilde{Z}_i}|E - |m_{\tilde{Z}_i}|\sqrt{1 - 4m_f^2/s}\sqrt{E^2 - m_{\tilde{Z}_j}^2}\ ) \\ &\times (m_f^2 + |m_{\tilde{Z}_i}|E - |m_{\tilde{Z}_i}|\sqrt{1 - 4m_f^2/s}\sqrt{E^2 - m_{\tilde{Z}_j}^2}\ ) - m_{\tilde{f}_1}^2\} \\ &+ (m_{\tilde{Z}_i}^2 + m_f^2 - m_{\tilde{f}_1}^2)(m_{\tilde{f}_1}^2 - m_f^2 - m_{\tilde{Z}_j}^2)\log L\Big], \end{aligned} \tag{A.316}$$

$$I_4^{Z\tilde{f}_1} = 2|m_{\tilde{Z}_i}|\int_{|m_{\tilde{Z}_j}|}^{E_{upper}} dE \frac{1}{s - m_Z^2}\left[2|m_{\tilde{Z}_i}|\sqrt{1 - 4m_f^2/s}\sqrt{E^2 - m_{\tilde{Z}_j}^2} + (m_{\tilde{f}_1}^2 - m_f^2 - m_{\tilde{Z}_j}^2)\log L\right], \tag{A.317}$$

$$I_5^{Z\tilde{f}_1} = 2|m_{\tilde{Z}_i}|\int_{|m_{\tilde{Z}_j}|}^{E_{upper}} dE \frac{-1}{s - m_Z^2}\left[2|m_{\tilde{Z}_i}|\sqrt{1 - 4m_f^2/s}\sqrt{E^2 - m_{\tilde{Z}_j}^2} + (m_{\tilde{f}_1}^2 - m_f^2 - m_{\tilde{Z}_i}^2)\log L\right], \tag{A.318}$$

$$I_6^{Z\tilde{f}_1} = 2|m_{\tilde{Z}_i}| \int_{|m_{\tilde{Z}_j}|}^{E_{upper}} dE \frac{1}{s - m_Z^2}(s - 2m_f^2) \log L, \tag{A.319}$$

$$I_7^{Z\tilde{f}_1} = 2|m_{\tilde{Z}_i}| \int_{|m_{\tilde{Z}_j}|}^{E_{upper}} dE \frac{1}{s - m_Z^2} 2|m_{\tilde{Z}_i}| E \log L, \tag{A.320}$$

$$I_8^{Z\tilde{f}_1} = 2|m_{\tilde{Z}_i}| \int_{|m_{\tilde{Z}_j}|}^{E_{upper}} dE \frac{1}{s - m_Z^2} \log L. \tag{A.321}$$

$\Gamma_{Z\tilde{f}_2}$ is exactly the same as $\Gamma_{Z\tilde{f}_1}$ but with the change $\tilde{f}_1 \to \tilde{f}_2$ throughout to get the couplings $C_{1,\ldots,8}^{Z\tilde{f}_2}$ and the integrals $I_{1,\ldots,8}^{Z\tilde{f}_2}$.

$$\Gamma_{h\tilde{f}_1} = C_1^{h\tilde{f}_1} I_1^{h\tilde{f}_1} + C_2^{h\tilde{f}_1} I_2^{h\tilde{f}_1} + C_3^{h\tilde{f}_1} I_3^{h\tilde{f}_1} + C_4^{h\tilde{f}_1} I_4^{h\tilde{f}_1} + C_5^{h\tilde{f}_1} I_5^{h\tilde{f}_1} + C_6^{h\tilde{f}_1} I_6^{h\tilde{f}_1} + C_7^{h\tilde{f}_1} I_7^{h\tilde{f}_1} + C_8^{h\tilde{f}_1} I_8^{h\tilde{f}_1}, \tag{A.322}$$

where here the couplings are:

$$C_1^{h\tilde{f}_1} = -\frac{1}{2}(-1)^{\theta_i}(-1)^{\theta_j}(X_{ij}^h + X_{ji}^h)\frac{f_q}{\sqrt{2}} t_{\alpha_h}(\alpha_{\tilde{f}_1}^{\tilde{Z}_i}\beta_{\tilde{f}_1}^{\tilde{Z}_j} + \beta_{\tilde{f}_1}^{\tilde{Z}_i}\alpha_{\tilde{f}_1}^{\tilde{Z}_j}), \tag{A.323}$$

$$C_2^{h\tilde{f}_1} = -(-1)^{\theta_j}(X_{ij}^h + X_{ji}^h)\frac{f_q}{\sqrt{2}} t_{\alpha_h}(\beta_{\tilde{f}_1}^{\tilde{Z}_i}\beta_{\tilde{f}_1}^{\tilde{Z}_j} + \alpha_{\tilde{f}_1}^{\tilde{Z}_i}\alpha_{\tilde{f}_1}^{\tilde{Z}_j})|m_{\tilde{Z}_i}|m_f, \tag{A.324}$$

$$C_3^{h\tilde{f}_1} = (-1)^{\theta_i}(X_{ij}^h + X_{ji}^h)\frac{f_q}{\sqrt{2}} t_{\alpha_h}(\beta_{\tilde{f}_1}^{\tilde{Z}_i}\beta_{\tilde{f}_1}^{\tilde{Z}_j} + \alpha_{\tilde{f}_1}^{\tilde{Z}_i}\alpha_{\tilde{f}_1}^{\tilde{Z}_j})|m_{\tilde{Z}_j}|m_f, \tag{A.325}$$

$$C_4^{h\tilde{f}_1} = -(-1)^{\theta_j}(X_{ij}^h + X_{ji}^h)\frac{f_q}{\sqrt{2}} t_{\alpha_h}(-\beta_{\tilde{f}_1}^{\tilde{Z}_i}\beta_{\tilde{f}_1}^{\tilde{Z}_j} - \alpha_{\tilde{f}_1}^{\tilde{Z}_i}\alpha_{\tilde{f}_1}^{\tilde{Z}_j})|m_{\tilde{Z}_i}|m_f, \tag{A.326}$$

$$C_5^{h\tilde{f}_1} = -(-1)^{\theta_i}(X_{ij}^h + X_{ji}^h)\frac{f_q}{\sqrt{2}} t_{\alpha_h}(\beta_{\tilde{f}_1}^{\tilde{Z}_i}\beta_{\tilde{f}_1}^{\tilde{Z}_j} + \alpha_{\tilde{f}_1}^{\tilde{Z}_i}\alpha_{\tilde{f}_1}^{\tilde{Z}_j})|m_{\tilde{Z}_j}|m_f, \tag{A.327}$$

$$C_6^{h\tilde{f}_1} = (X_{ij}^h + X_{ji}^h)\frac{f_q}{\sqrt{2}} t_{\alpha_h}(-\alpha_{\tilde{f}_1}^{\tilde{Z}_i}\beta_{\tilde{f}_1}^{\tilde{Z}_j} - \beta_{\tilde{f}_1}^{\tilde{Z}_i}\alpha_{\tilde{f}_1}^{\tilde{Z}_j})|m_{\tilde{Z}_i}||m_{\tilde{Z}_j}|, \tag{A.328}$$

$$C_7^{h\tilde{f}_1} = (-1)^{\theta_i}(-1)^{\theta_j}(X_{ij}^h + X_{ji}^h)\frac{f_q}{\sqrt{2}} t_{\alpha_h}(\alpha_{\tilde{f}_1}^{\tilde{Z}_i}\beta_{\tilde{f}_1}^{\tilde{Z}_j} + \beta_{\tilde{f}_1}^{\tilde{Z}_i}\alpha_{\tilde{f}_1}^{\tilde{Z}_j})m_f^2, \tag{A.329}$$

$$C_8^{h\tilde{f}_1} = 2(X_{ij}^h + X_{ji}^h)\frac{f_q}{\sqrt{2}} t_{\alpha_h}(\alpha_{\tilde{f}_1}^{\tilde{Z}_i}\beta_{\tilde{f}_1}^{\tilde{Z}_j} + \beta_{\tilde{f}_1}^{\tilde{Z}_i}\alpha_{\tilde{f}_1}^{\tilde{Z}_j})|m_{\tilde{Z}_i}|m_f^2|m_{\tilde{Z}_j}|. \tag{A.330}$$

The necessary integrals are:

$$I_1^{h\tilde{f}_1} = 2|m_{\tilde{Z}_i}| \int_{|m_{\tilde{Z}_j}|}^{E_{upper}} dE \frac{2}{s - m_h^2} \left[2s|m_{\tilde{Z}_i}|\sqrt{E^2 - m_{\tilde{Z}_j}^2}\sqrt{1 - 4m_f^2/s} + \{m_{\tilde{f}_1}^2 s - m_f^2(m_{\tilde{Z}_i}^2 + m_{\tilde{Z}_j}^2)\}\log L\right], \tag{A.331}$$

$$I_2^{h\tilde{f}_1} = -2|m_{\tilde{Z}_i}| \int_{|m_{\tilde{Z}_j}|}^{E_{upper}} dE \frac{1}{s - m_h^2} \left[2|m_{\tilde{Z}_i}|\sqrt{E^2 - m_{\tilde{Z}_j}^2}\sqrt{1 - 4m_f^2/s} + (m_{\tilde{f}_1}^2 - m_f^2 + m_{\tilde{Z}_j}^2 - 2m_{\tilde{Z}_i}E)\log L\right], \tag{A.332}$$

$$I_3^{h\tilde{f}_1} = 2|m_{\tilde{Z}_i}| \int_{|m_{\tilde{Z}_j}|}^{E_{upper}} dE \frac{1}{s - m_h^2} \left[2|m_{\tilde{Z}_i}|\sqrt{E^2 - m_{\tilde{Z}_j}^2}\sqrt{1 - 4m_f^2/s} + (m_{\tilde{f}_1}^2 - m_f^2 + m_{\tilde{Z}_i}^2 - 2m_{\tilde{Z}_i}E)\log L\right], \tag{A.333}$$

$$I_4^{h\tilde{f}_1} = 2|m_{\tilde{Z}_i}| \int_{|m_{\tilde{Z}_j}|}^{E_{upper}} dE \frac{1}{s - m_h^2} \left[2|m_{\tilde{Z}_i}|\sqrt{E^2 - m_{\tilde{Z}_j}^2}\sqrt{1 - 4m_f^2/s} + (m_{\tilde{f}_1}^2 - m_f^2 + m_{\tilde{Z}_j}^2)\log L\right], \tag{A.334}$$

$$I_5^{h\tilde{f}_1} = -2|m_{\tilde{Z}_i}| \int_{|m_{\tilde{Z}_j}|}^{E_{upper}} dE \frac{1}{s - m_h^2} \left[2|m_{\tilde{Z}_i}| \sqrt{E^2 - m_{\tilde{Z}_j}^2} \sqrt{1 - 4m_f^2/s} + (m_{\tilde{f}_1}^2 - m_f^2 + m_{\tilde{Z}_i}^2) \log L \right], \tag{A.335}$$

$$I_6^{h\tilde{f}_1} = -2|m_{\tilde{Z}_i}| \int_{|m_{\tilde{Z}_j}|}^{E_{upper}} dE \frac{1}{s - m_h^2} (s - 2m_f^2) \log L, \tag{A.336}$$

$$I_7^{h\tilde{f}_1} = -2|m_{\tilde{Z}_i}| \int_{|m_{\tilde{Z}_j}|}^{E_{upper}} dE \frac{1}{s - m_h^2} (2|m_{\tilde{Z}_i}|E) \log L, \tag{A.337}$$

$$I_8^{h\tilde{f}_1} = -2|m_{\tilde{Z}_i}| \int_{|m_{\tilde{Z}_j}|}^{E_{upper}} dE \frac{1}{s - m_h^2} \log L. \tag{A.338}$$

Note that $\Gamma_{h\tilde{f}_2}$ is exactly the same as $\Gamma_{h\tilde{f}_1}$ but with the replacement $\tilde{f}_1 \to \tilde{f}_2$ throughout to get the couplings $C_{1,\ldots,8}^{h\tilde{f}_2}$ and the integrals $I_{1,\ldots,8}^{h\tilde{f}_2}$. Similarly, one can obtain the $\Gamma_{H\tilde{f}_1}$ from $\Gamma_{h\tilde{f}_1}$ by replacing h by H throughout all the couplings, masses and integrals; therefore the changes $X_{ij}^h + X_{ji}^h \to X_{ij}^H + X_{ji}^H$ and $t_{\alpha_h} \to t_{\alpha_H}$ are made. One can then obtain $\Gamma_{H\tilde{f}_2}$ again by changing $\tilde{f}_1 \to \tilde{f}_2$ throughout the couplings, masses and integrals.

$$\Gamma_{A\tilde{f}_1} = C_1^{A\tilde{f}_1} I_1^{A\tilde{f}_1} + C_2^{A\tilde{f}_1} I_2^{A\tilde{f}_1} + C_3^{A\tilde{f}_1} I_3^{A\tilde{f}_1} + C_4^{A\tilde{f}_1} I_4^{A\tilde{f}_1} + C_5^{A\tilde{f}_1} I_5^{A\tilde{f}_1} + C_6^{A\tilde{f}_1} I_6^{A\tilde{f}_1} + C_7^{A\tilde{f}_1} I_7^{A\tilde{f}_1} + C_8^{A\tilde{f}_1} I_8^{A\tilde{f}_1}, \tag{A.339}$$

here we have:

$$C_1^{A\tilde{f}_1} = \frac{1}{2}(-1)^{\theta_i}(X_{ij}^A + X_{ji}^A) \frac{A_q}{2} (\alpha_{\tilde{f}_1}^{\tilde{Z}_i} \beta_{\tilde{f}_1}^{\tilde{Z}_j} + \beta_{\tilde{f}_1}^{\tilde{Z}_i} \alpha_{\tilde{f}_1}^{\tilde{Z}_j}), \tag{A.340}$$

$$C_2^{A\tilde{f}_1} = -(X_{ij}^A + X_{ji}^A) \frac{A_q}{2} |m_{\tilde{Z}_i}| m_f (\beta_{\tilde{f}_1}^{\tilde{Z}_i} \beta_{\tilde{f}_1}^{\tilde{Z}_j} + \alpha_{\tilde{f}_1}^{\tilde{Z}_i} \alpha_{\tilde{f}_1}^{\tilde{Z}_j}), \tag{A.341}$$

$$C_3^{A\tilde{f}_1} = (-1)^{\theta_i}(-1)^{\theta_j}(X_{ij}^A + X_{ji}^A) \frac{A_q}{2} |m_{\tilde{Z}_j}| m_f (\beta_{\tilde{f}_1}^{\tilde{Z}_i} \beta_{\tilde{f}_1}^{\tilde{Z}_j} + \alpha_{\tilde{f}_1}^{\tilde{Z}_i} \alpha_{\tilde{f}_1}^{\tilde{Z}_j}), \tag{A.342}$$

$$C_4^{A\tilde{f}_1} = -(X_{ij}^A + X_{ji}^A) \frac{A_q}{2} |m_{\tilde{Z}_i}| m_f (\beta_{\tilde{f}_1}^{\tilde{Z}_i} \beta_{\tilde{f}_1}^{\tilde{Z}_j} + \alpha_{\tilde{f}_1}^{\tilde{Z}_i} \alpha_{\tilde{f}_1}^{\tilde{Z}_j}), \tag{A.343}$$

$$C_5^{A\tilde{f}_1} = (-1)^{\theta_i}(-1)^{\theta_j}(X_{ij}^A + X_{ji}^A) \frac{A_q}{2} |m_{\tilde{Z}_j}| m_f (\beta_{\tilde{f}_1}^{\tilde{Z}_i} \beta_{\tilde{f}_1}^{\tilde{Z}_j} + \alpha_{\tilde{f}_1}^{\tilde{Z}_i} \alpha_{\tilde{f}_1}^{\tilde{Z}_j}), \tag{A.344}$$

$$C_6^{A\tilde{f}_1} = -(-1)^{\theta_j}(X_{ij}^A + X_{ji}^A) \frac{A_q}{2} |m_{\tilde{Z}_i}| |m_{\tilde{Z}_j}| (\alpha_{\tilde{f}_1}^{\tilde{Z}_i} \beta_{\tilde{f}_1}^{\tilde{Z}_j} + \beta_{\tilde{f}_1}^{\tilde{Z}_i} \alpha_{\tilde{f}_1}^{\tilde{Z}_j}), \tag{A.345}$$

$$C_7^{A\tilde{f}_1} = (-1)^{\theta_i}(X_{ij}^A + X_{ji}^A) \frac{A_q}{2} m_f^2 (\alpha_{\tilde{f}_1}^{\tilde{Z}_i} \beta_{\tilde{f}_1}^{\tilde{Z}_j} + \beta_{\tilde{f}_1}^{\tilde{Z}_i} \alpha_{\tilde{f}_1}^{\tilde{Z}_j}), \tag{A.346}$$

$$C_8^{A\tilde{f}_1} = -(-1)^{\theta_j}(X_{ij}^A + X_{ji}^A) A_q m_f^2 |m_{\tilde{Z}_i}| |m_{\tilde{Z}_j}| (\alpha_{\tilde{f}_1}^{\tilde{Z}_i} \beta_{\tilde{f}_1}^{\tilde{Z}_j} + \beta_{\tilde{f}_1}^{\tilde{Z}_i} \alpha_{\tilde{f}_1}^{\tilde{Z}_j}). \tag{A.347}$$

The $I_i^{A\tilde{f}_1}$ are exactly as the $I_i^{h\tilde{f}_1}$ but with the change $m_h \to m_A$.

$$\Gamma_{ZA} = 2C_1^{ZA} I_1^{ZA} + 2C_2^{ZA} I_2^{ZA}, \tag{A.348}$$

where

$$C_1^{ZA} = -4(-1)^{\theta_i}(-1)^{\theta_j} W_{ij} (X_{ij}^A + X_{ji}^A) A_q g \sin\theta_W \beta_f |m_{\tilde{Z}_j}| m_f, \tag{A.349}$$

$$C_2^{ZA} = 4W_{ij} (X_{ij}^A + X_{ji}^A) A_q g \sin\theta_W \beta_f |m_{\tilde{Z}_i}| m_f. \tag{A.350}$$

The integrals included here are:

$$I_1^{ZA} = 2|m_{\tilde{Z}_i}| \int_{|m_{\tilde{Z}_j}|}^{E_{upper}} d_E \frac{1}{(s-m_z^2)(s-m_A^2)} 2|m_{\tilde{Z}_i}| \sqrt{E^2 - m_{\tilde{Z}_j}^2} \sqrt{1-4m_f^2/s} \, \{m_{\tilde{Z}_i}^2 - |m_{\tilde{Z}_i}|E\}, \quad \text{(A.351)}$$

$$I_2^{ZA} = -2|m_{\tilde{Z}_i}| \int_{|m_{\tilde{Z}_j}|}^{E_{upper}} d_E \frac{1}{(s-m_z^2)(s-m_A^2)} 2|m_{\tilde{Z}_i}| \sqrt{E^2 - m_{\tilde{Z}_j}^2} \sqrt{1-4m_f^2/s} \, \{m_{\tilde{Z}_j}^2 - |m_{\tilde{Z}_i}|E\}. \quad \text{(A.352)}$$

The Goldstone contribution is:

$$\Gamma_G = 4c_{G\tilde{Z}_i\tilde{Z}_j}^2 c_{Gff}^2 \left[I_4^G + 2m_f^2 I_3^G - 2(-1)^{\theta_i}(-1)^{\theta_j}|m_{\tilde{Z}_i}||m_{\tilde{Z}_j}|I_2^G - 4(-1)^{\theta_i}(-1)^{\theta_j} m_f^2 |m_{\tilde{Z}_i}||m_{\tilde{Z}_j}| I_1^G \right]. \quad \text{(A.353)}$$

The Goldstone interferences with fermions are given by:

$$\Gamma_{G\tilde{f}_1} = C_1^{G\tilde{f}_1} I_1^{G\tilde{f}_1} + C_2^{G\tilde{f}_1} I_2^{G\tilde{f}_1} + C_3^{G\tilde{f}_1} I_3^{G\tilde{f}_1} + C_4^{G\tilde{f}_1} I_4^{G\tilde{f}_1} + C_5^{G\tilde{f}_1} I_5^{G\tilde{f}_1} + C_6^{G\tilde{f}_1} I_6^{G\tilde{f}_1} + C_7^{G\tilde{f}_1} I_7^{G\tilde{f}_1} + C_8^{G\tilde{f}_1} I_8^{G\tilde{f}_1}, \quad \text{(A.354)}$$

where

$$C_1^{G\tilde{f}_1} = \frac{1}{2} c_{G\tilde{Z}_i\tilde{Z}_j} c_{Gff} (\alpha_{\tilde{f}_1}^{\tilde{Z}_i} \beta_{\tilde{f}_1}^{\tilde{Z}_j} + \beta_{\tilde{f}_1}^{\tilde{Z}_i} \alpha_{\tilde{f}_1}^{\tilde{Z}_j}), \quad \text{(A.355)}$$

$$C_2^{G\tilde{f}_1} = -(-1)^{\theta_i} m_f |m_{\tilde{Z}_i}| c_{G\tilde{Z}_i\tilde{Z}_j} c_{Gff} (\beta_{\tilde{f}_1}^{\tilde{Z}_i} \beta_{\tilde{f}_1}^{\tilde{Z}_j} + \alpha_{\tilde{f}_1}^{\tilde{Z}_i} \alpha_{\tilde{f}_1}^{\tilde{Z}_j}), \quad \text{(A.356)}$$

$$C_3^{G\tilde{f}_1} = (-1)^{\theta_j} m_f |m_{\tilde{Z}_j}| c_{G\tilde{Z}_i\tilde{Z}_j} c_{Gff} (\alpha_{\tilde{f}_1}^{\tilde{Z}_i} \alpha_{\tilde{f}_1}^{\tilde{Z}_j} + \beta_{\tilde{f}_1}^{\tilde{Z}_i} \beta_{\tilde{f}_1}^{\tilde{Z}_j}), \quad \text{(A.357)}$$

$$C_4^{G\tilde{f}_1} = -(-1)^{\theta_i} m_f |m_{\tilde{Z}_i}| c_{G\tilde{Z}_i\tilde{Z}_j} c_{Gff} (\alpha_{\tilde{f}_1}^{\tilde{Z}_i} \alpha_{\tilde{f}_1}^{\tilde{Z}_j} + \beta_{\tilde{f}_1}^{\tilde{Z}_i} \beta_{\tilde{f}_1}^{\tilde{Z}_j}), \quad \text{(A.358)}$$

$$C_5^{G\tilde{f}_1} = (-1)^{\theta_j} |m_{\tilde{Z}_i}| m_f c_{G\tilde{Z}_i\tilde{Z}_j} c_{Gff} (\alpha_{\tilde{f}_1}^{\tilde{Z}_i} \alpha_{\tilde{f}_1}^{\tilde{Z}_j} + \beta_{\tilde{f}_1}^{\tilde{Z}_i} \beta_{\tilde{f}_1}^{\tilde{Z}_j}), \quad \text{(A.359)}$$

$$C_6^{G\tilde{f}_1} = -(-1)^{\theta_i}(-1)^{\theta_j} |m_{\tilde{Z}_i}||m_{\tilde{Z}_j}| c_{G\tilde{Z}_i\tilde{Z}_j} c_{Gff} (\alpha_{\tilde{f}_1}^{\tilde{Z}_i} \beta_{\tilde{f}_1}^{\tilde{Z}_j} + \beta_{\tilde{f}_1}^{\tilde{Z}_i} \alpha_{\tilde{f}_1}^{\tilde{Z}_j}), \quad \text{(A.360)}$$

$$C_7^{G\tilde{f}_1} = m_f^2 c_{G\tilde{Z}_i\tilde{Z}_j} c_{Gff} (\alpha_{\tilde{f}_1}^{\tilde{Z}_i} \beta_{\tilde{f}_1}^{\tilde{Z}_j} + \beta_{\tilde{f}_1}^{\tilde{Z}_i} \alpha_{\tilde{f}_1}^{\tilde{Z}_j}), \quad \text{(A.361)}$$

$$C_8^{G\tilde{f}_1} = -2(-1)^{\theta_i}(-1)^{\theta_j} m_f^2 |m_{\tilde{Z}_i}||m_{\tilde{Z}_j}| c_{G\tilde{Z}_i\tilde{Z}_j} c_{Gff} (\alpha_{\tilde{f}_1}^{\tilde{Z}_i} \beta_{\tilde{f}_1}^{\tilde{Z}_j} + \beta_{\tilde{f}_1}^{\tilde{Z}_i} \alpha_{\tilde{f}_1}^{\tilde{Z}_j}). \quad \text{(A.362)}$$

The $I_{1,\ldots,8}^{G\tilde{f}_1}$ integrals are the same as the $I_{1,\ldots,8}^{h\tilde{f}_1}$ but with the replacement $m_h \to m_Z$ as the mass of the Goldstone is the Z mass as it represents the longitudinal component of the Z boson. Similar changes apply to the $I_{1,\ldots,8}^{G\tilde{f}_2}$, whilst in the couplings we apply the replacement $\tilde{f}_1 \to \tilde{f}_2$ throughout. The Z-Goldstone interference contribution is:

$$\Gamma_{ZG} = 2C_1^{ZG} I_1^{ZG} + 2C_2^{ZG} I_2^{ZG}, \quad \text{(A.363)}$$

where

$$C_1^{ZG} = -8W_{ij}(-1)^{\theta_j} m_f |m_{\tilde{Z}_j}| c_{Gff} c_{G\tilde{Z}_i\tilde{Z}_j} g \sin\theta_W \beta_f, \quad \text{(A.364)}$$

$$C_2^{ZG} = 8W_{ij}(-1)^{\theta_i} m_f |m_{\tilde{Z}_i}| c_{Gff} c_{G\tilde{Z}_i\tilde{Z}_j} g \sin\theta_W \beta_f. \quad \text{(A.365)}$$

The $I_{1,2}^{ZG}$ are the same as the $I_{1,2}^{ZA}$ but with the expected change $m_A \to m_Z$.

$$\Gamma_{GA} = C_1^{GA} C_3^{GA} I_4^{GA} - 2C_1^{GA} C_4^{GA} m_f^2 I_3^{GA} + 2C_2^{GA} C_3^{GA} |m_{\tilde{Z}_i}||m_{\tilde{Z}_j}| I_2^{GA} - 4C_2^{GA} C_4^{GA} m_f^2 |m_{\tilde{Z}_i}||m_{\tilde{Z}_j}| I_1^{GA}, \quad \text{(A.366)}$$

where here

$$C_1^{GA} = -2(-1)^{\theta_i} c_{G\tilde{Z}_i\tilde{Z}_j} (X_{ij}^A + X_{ji}^A), \quad \text{(A.367)}$$

$$C_2^{GA} = 2(-1)^{\theta_j} c_{G\tilde{Z}_i\tilde{Z}_j}(X_{ij}^A + X_{ji}^A), \tag{A.368}$$

$$C_3^{GA} = -A_q c_{Gff}, \tag{A.369}$$

$$C_4^{GA} = A_q c_{Gff}. \tag{A.370}$$

The integrals are:

$$I_1^{GA} = 2|m_{\tilde{Z}_i}| \int_{|m_{\tilde{Z}_j}|}^{E_{max}} dE \frac{2|m_{\tilde{Z}_i}|\sqrt{E^2 - m_{\tilde{Z}_j}^2}\sqrt{1 - 4m_f^2/s}}{(s - m_Z^2)(s - m_A^2)}, \tag{A.371}$$

$$I_2^{GA} = 2|m_{\tilde{Z}_i}| \int_{|m_{\tilde{Z}_j}|}^{E_{max}} dE \frac{2|m_{\tilde{Z}_i}|(s - 2m_f^2)\sqrt{E^2 - m_{\tilde{Z}_j}^2}\sqrt{1 - 4m_f^2/s}}{(s - m_Z^2)(s - m_A^2)}, \tag{A.372}$$

$$I_3^{GA} = 2|m_{\tilde{Z}_i}| \int_{|m_{\tilde{Z}_j}|}^{E_{max}} dE \frac{4|m_{\tilde{Z}_i}|^2 E\sqrt{E^2 - m_{\tilde{Z}_j}^2}\sqrt{1 - 4m_f^2/s}}{(s - m_Z^2)(s - m_A^2)}, \tag{A.373}$$

$$I_4^{GA} = 2|m_{\tilde{Z}_i}| \int_{|m_{\tilde{Z}_j}|}^{E_{max}} dE \frac{4|m_{\tilde{Z}_i}|^2 E(s - 2m_f^2)\sqrt{E^2 - m_{\tilde{Z}_j}^2}\sqrt{1 - 4m_f^2/s}}{(s - m_Z^2)(s - m_A^2)}. \tag{A.374}$$

Now the list of the couplings used is:

$$W_{ij} = 0.25\sqrt{g^2 + g'^2}(N_{4i}N_{4j} - N_{3i}N_{3j}). \tag{A.375}$$

The X_{ij}^{ϕ} couplings are:

$$X_{ij}^h = -\frac{1}{2}(-1)^{\theta_i}(-1)^{\theta_j}[-N_{3i}\sin\alpha - N_{4i}\cos\alpha](-gN_{2j} + g'N_{1j}), \tag{A.376}$$

$$X_{ij}^H = -\frac{1}{2}(-1)^{\theta_i}(-1)^{\theta_j}[N_{3i}\cos\alpha - N_{4i}\sin\alpha](-gN_{2j} + g'N_{1j}), \tag{A.377}$$

$$X_{ij}^A = \frac{1}{2}(-1)^{\theta_i}(-1)^{\theta_j}[N_{3i}\sin\beta - N_{4i}\cos\beta](-gN_{2j} + g'N_{1j}). \tag{A.378}$$

$$f_q = \begin{cases} \frac{gm_q^{run}}{\sqrt{2}m_W\sin\beta}, \text{ for } u\text{-type quarks}, \\ \frac{gm_q^{run}}{\sqrt{2}m_W\cos\beta}, \text{ for } d\text{-type quarks}, \\ 0, \text{ for neutrinos } \nu, \\ \frac{gm_l^{run}}{\sqrt{2}m_W\cos\beta}, \text{ for charged leptons}. \end{cases} \tag{A.379}$$

$$A_q = \begin{cases} \frac{gm_q^{run}}{m_W\tan\beta}, \text{ for } u\text{-type quarks}, \\ \frac{gm_q^{run}\tan\beta}{m_W}, \text{ for } d\text{-type quarks}, \\ 0, \text{ for neutrinos } \nu, \\ \frac{gm_l^{run}\tan\beta}{m_W}, \text{ for charged leptons}. \end{cases} \tag{A.380}$$

$$t_{\alpha_h} = \begin{cases} \cos\alpha, \text{ for } u\text{-type quarks}, \\ -\sin\alpha, \text{ for } d\text{-type quarks}, \\ \cos\alpha, \text{ for neutrinos } \nu, \\ -\sin\alpha, \text{ for charged leptons}. \end{cases} \tag{A.381}$$

$$t_{\alpha_H} = \begin{cases} \sin\alpha, \text{ for } u\text{-type quarks}, \\ \cos\alpha, \text{ for } d\text{-type quarks}, \\ \sin\alpha, \text{ for neutrinos } \nu, \\ \cos\alpha, \text{ for charged leptons}. \end{cases} \tag{A.382}$$

$$\alpha_f = \begin{cases} -\frac{5g'p}{12g} + \frac{g}{4g'}, \text{ for } u\text{-type quarks}, \\ \frac{g'p}{12g} - \frac{g}{4g'}, \text{ for } d\text{-type quarks}, \\ \frac{1}{4}(\frac{g'}{g} + \frac{g}{g'}), \text{ for neutrinos } \nu, \\ \frac{3}{4}\frac{g'}{g} - \frac{g}{4g'}, \text{ for charged leptons}. \end{cases} \tag{A.383}$$

$$\beta_f = \begin{cases} -\frac{1}{4}(\frac{g'}{g} + \frac{g}{g'}), \text{ for } u\text{-type quarks}, \\ \frac{1}{4}(\frac{g'}{g} + \frac{g}{g'}), \text{ for } d\text{-type quarks}, \\ -\frac{1}{4}(\frac{g'}{g} + \frac{g}{g'}), \text{ for neutrinos } \nu, \\ \frac{1}{4}(\frac{g'}{g} + \frac{g}{g'}), \text{ for charged leptons}. \end{cases} \tag{A.384}$$

$$\alpha_{\tilde{f}_1}^{\tilde{Z}_i} = \begin{cases} A_{\tilde{Z}_i}\cos\theta_q - f_q N_{4i}\sin\theta_q, \text{ for } u\text{-type quarks}, \\ A_{\tilde{Z}_i}\cos\theta_q - f_q N_{3i}\sin\theta_q, \text{ for } d\text{-type quarks}, \\ A_{\tilde{Z}_i}\cos\theta_q, \text{ for neutrinos } \nu, \\ A_{\tilde{Z}_i}\sin\theta_q + f_q N_{3i}\cos\theta_q, \text{ for charged leptons}. \end{cases} \tag{A.385}$$

$$\alpha_{\tilde{f}_2}^{\tilde{Z}_i} = \begin{cases} A_{\tilde{Z}_i}\sin\theta_q + f_q N_{4i}\cos\theta_q, \text{ for } u\text{-type quarks}, \\ A_{\tilde{Z}_i}\sin\theta_q + f_q N_{3i}\cos\theta_q, \text{ for } d\text{-type quarks}, \\ A_{\tilde{Z}_i}\sin\theta_q, \text{ for neutrinos } \nu, \\ -A_{\tilde{Z}_i}\cos\theta_q + f_q N_{3i}\sin\theta_q, \text{ for charged leptons}. \end{cases} \tag{A.386}$$

$$\beta_{\tilde{f}_1}^{\tilde{Z}_i} = \begin{cases} f_q N_{4i}\cos\theta_q + B_{\tilde{Z}_i}\sin\theta_q, \text{ for } u\text{-type quarks}, \\ f_q N_{3i}\cos\theta_q + B_{\tilde{Z}_i}\sin\theta_q, \text{ for } d\text{-type quarks}, \\ 0, \text{ for neutrinos } \nu, \\ f_q N_{3i}\sin\theta_q - B_{\tilde{Z}_i}\cos\theta_q, \text{ for charged leptons}. \end{cases} \tag{A.387}$$

$$\beta_{\tilde{f}_2}^{\tilde{Z}_i} = \begin{cases} f_q N_{4i}\sin\theta_q - B_{\tilde{Z}_i}\cos\theta_q, \text{ for } u\text{-type quarks}, \\ f_q N_{3i}\sin\theta_q - B_{\tilde{Z}_i}\cos\theta_q, \text{ for } d\text{-type quarks}, \\ 0, \text{ for neutrinos } \nu, \\ -f_q N_{3i}\cos\theta_q - B_{\tilde{Z}_i}\sin\theta_q, \text{ for charged leptons}. \end{cases} \tag{A.388}$$

$$A_{\tilde{Z}_i} = \begin{cases} -\frac{g}{\sqrt{2}}N_{2i} - \frac{g'}{3\sqrt{2}}N_{1i}, \text{ for } u\text{-type quarks}, \\ \frac{g}{\sqrt{2}}N_{2i} - \frac{g'}{3\sqrt{2}}N_{1i}, \text{ for } d\text{-type quarks}, \\ -\frac{g}{\sqrt{2}}N_{2i} + \frac{g'}{3\sqrt{2}}N_{1i}, \text{ for neutrinos } \nu, \\ \frac{g}{\sqrt{2}}N_{2i} + \frac{g'}{3\sqrt{2}}N_{1i}, \text{ for charged leptons}. \end{cases} \tag{A.389}$$

$$B_{\tilde{Z}_i} = \begin{cases} -\frac{4g'}{3\sqrt{2}}N_{1i}, \text{ for } u\text{-type quarks}, \\ \frac{2g'}{3\sqrt{2}}N_{1i}, \text{ for } d\text{-type quarks}, \\ 0, \text{ for neutrinos } \nu, \\ \sqrt{2}g' N_{1i}, \text{ for charged leptons}. \end{cases} \tag{A.390}$$

$$c_{Gff} = \begin{cases} \frac{-f_q\sin\beta}{\sqrt{2}}, \text{ for } u\text{-type quarks}, \\ \frac{f_q\cos\beta}{\sqrt{2}}, \text{ for } d\text{-type quarks}, \\ 0, \text{ for neutrinos } \nu, \\ \frac{f_q\cos\beta}{\sqrt{2}}, \text{ for charged leptons}. \end{cases} \tag{A.391}$$

$$c_{G\tilde{Z}_i\tilde{Z}_j} = \frac{1}{2}\left[(g^{'}N_{1i} - gN_{2i})(N_{3j}\cos\beta + N_{j4}\sin\beta) + (g^{'}N_{1j} - gN_{2j})(N_{3i}\cos\beta + N_{4i}\sin\beta)\right]. \tag{A.392}$$

$\underline{\tilde{Z}_i \to \tilde{W}_j f' \bar{f}}$

We turn now onto the 3-body decays of a neutralino into a chargino, fermion and antifermion. As for all the other 3-body modes included, this mode is only calculated if no 2-body modes are kinematically accessible. There are 4 main contributions to these decays, with W boson, $H^{\pm}$, $\tilde{f'}_k$ and $\tilde{f}_k$ intermediates, the Feynman diagrams for these are shown in Figure A.4. Therefore there are nominally 6 squared contributions and 15 interferences; however, as the calculation is again done in Feynman gauge, the Goldstone boson corresponding to the longitudinal components of the W boson must be added, adding a further squared contribution and its 6 interferences.

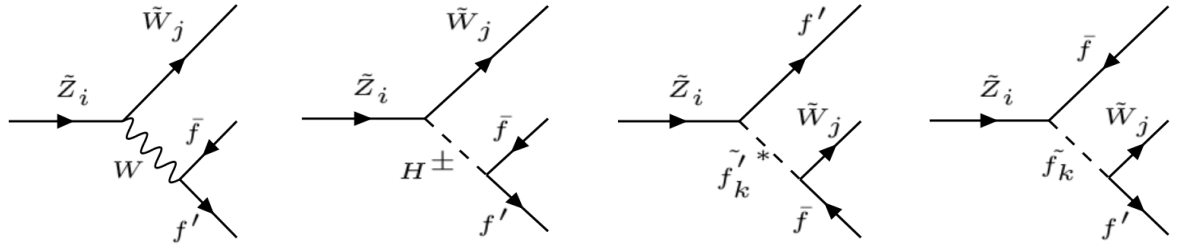

(a) W (b) $H^{\pm}$ (c) $\tilde{f'}_k$ (d) $\tilde{f}_k$

Figure A.4: W, $H^{\pm}$, $\tilde{f'}_k$, $\tilde{f}_k$ contributions to the $\tilde{Z}_i \to \tilde{W}_j f' \bar{f}$ decay. $i = 1, 2, 3, 4$, $j = 1, 2$, $k = 1, 2$. There are then also interferences between all these contributions.

For this decay mode, and the "reverse" decay mode $\tilde{W}_j \to \tilde{Z}_i f' \bar{f}$, the formulae used are extracted from the `sPHENO` code, based on the work in references [65, 178]. Note that f', f are fermions with third components of weak isospin $\frac{1}{2}$ and $-\frac{1}{2}$ respectively. A difference relative to these references is that, following the formulae of `sPHENO`, the expressions given do not neglect m_f in the Dirac algebra of the squared matrix element (whereas in [65, 178] it is neglected here, but of course included in the phase space). As a result there is also $WH^{\pm}$ interference which is not present if m_f is neglected in the Dirac algebra. The possibilities of positive and negative neutralino and chargino masses are included via $(-1)^{\theta_i}$ and $(-1)^{\theta_j}$ factors. Similarly the fermion Yukawa couplings are included and the formulae themselves allow for mixing of the fermions. However in our program, mixing is only considered for the third generation of sfermions and here this 3-body mode $\tilde{Z}_i \to \tilde{W}_j t \bar{b}$ is not calculated as the 2-body modes $\tilde{Z}_i \to W \tilde{W}_j$ and $\tilde{Z}_i \to h \tilde{W}_j$ are then kinematically available and will dominate the branching ratios. The overall expression for the partial width is:

$$\begin{aligned}\Gamma =& \frac{N_c}{512\pi^3 |m_{Z_i}|^3}\Big[\Gamma_W + \Gamma_{\tilde{f}_1} + \Gamma_{\tilde{f}_2} + \Gamma_{\tilde{f'}_1} + \Gamma_{\tilde{f'}_2} - 2\Gamma_{\tilde{f'}_1\tilde{f}_1} - 2\Gamma_{\tilde{f'}_1\tilde{f}_2} - 2\Gamma_{\tilde{f'}_2\tilde{f}_1} - 2\Gamma_{\tilde{f'}_2\tilde{f}_2} + 2\Gamma_{WH^{\pm}} \\ &+ 2\Gamma_{WG} + \Gamma_{H^{\pm}} + \Gamma_G - 2\Gamma_{W\tilde{f'}_1} - 2\Gamma_{W\tilde{f'}_2} - 2\Gamma_{W\tilde{f}_1} - 2\Gamma_{W\tilde{f}_2} + 2\Gamma_{H^{\pm}G} - 2\Gamma_{G\tilde{f'}_1} \\ &- 2\Gamma_{G\tilde{f'}_2} - 2\Gamma_{G\tilde{f}_1} - 2\Gamma_{G\tilde{f}_2} - 2\Gamma_{H^{\pm}\tilde{f'}_1} - 2\Gamma_{H^{\pm}\tilde{f'}_2} - 2\Gamma_{H^{\pm}\tilde{f}_1} - 2\Gamma_{H^{\pm}\tilde{f}_2} + 2\Gamma_{\tilde{f'}_1\tilde{f'}_2} + 2\Gamma_{\tilde{f}_1\tilde{f}_2}\Big].\end{aligned} \tag{A.393}$$

Here G refers to the Goldstone contribution which is the longitudinal component of the W and so has mass equal to the W boson mass. Here the following variables and couplings are used:

$$N_c = \begin{cases} 3, \text{ for } f' \ \bar{f} \text{ quarks,} \\ 1, \text{ for } f' \ \bar{f} \text{ charged leptons or neutrinos.} \end{cases} \tag{A.394}$$

There are several factors of (-1) depending on whether the neutralino or chargino have negative masses, and also there are factors of (-1) if the decay chargino $\to$ neutralino $f' \ \bar{f}$ is being considered rather than

neutralino $\to$ chargino $f'\ \bar{f}$.

$$(-1)^{\theta_i} = \begin{cases} 1, \text{ for } m_{\tilde{Z}_i} > 0, \\ -1, \text{ for } m_{\tilde{Z}_i} < 0. \end{cases} \quad \text{(A.395)} \qquad (-1)^{\theta_j} = \begin{cases} 1, \text{ for } m_{\tilde{W}_j} > 0, \\ -1, \text{ for } m_{\tilde{W}_j} < 0. \end{cases} \quad \text{(A.396)}$$

$$(-1)^{\theta_c} = \begin{cases} 1, \text{ for neutralino decaying to chargino,} \\ -1, \text{ for chargino decaying to neutralino.} \end{cases} \quad \text{(A.397)}$$

The following couplings are used:

$$f_u = \frac{g m_{q'}^{run}}{\sqrt{2}\sin\beta m_W}, \quad \text{(A.398)} \qquad f_d = \frac{g m_q^{run}}{\sqrt{2}\cos\beta m_W}. \quad \text{(A.399)}$$

For $\tilde{W}_1^+$, i.e. the lightest chargino ($j = 1$), and where i is the index of the neutralino:

$$\mathcal{C}^L_{\tilde{W}\tilde{Z}W} = g\left(\sin\theta_L N_{2i} + \frac{\cos\theta_L N_{3i}}{\sqrt{2}}\right), \quad \text{(A.400)} \qquad \mathcal{C}^R_{\tilde{W}\tilde{Z}W} = g\left(\sin\theta_R N_{2i} - \frac{\cos\theta_R N_{4i}}{\sqrt{2}}\right), \quad \text{(A.401)}$$

$$\mathcal{C}^L_{\tilde{W}\tilde{Z}H+} = g\sin\theta_R N_{4i} + \frac{\cos\theta_R}{\sqrt{2}}(g' N_{1i} + g N_{2i}), \quad \text{(A.402)}$$

$$\mathcal{C}^R_{\tilde{W}\tilde{Z}H+} = g\sin\theta_L N_{3i} - \frac{\cos\theta_L}{\sqrt{2}})(g' N_{1i} + g N_{2i}), \quad \text{(A.403)}$$

$$\alpha^{\tilde{W}_1}_{\tilde{f'}_1} = -g\sin\theta_R\cos\theta_{q'} + f_u\cos\theta_R\sin\theta_{q'}, \quad \text{(A.404)} \qquad \beta^{\tilde{W}_1}_{\tilde{f'}_1} = -f_d\cos\theta_L\cos\theta_{q'}(-1)^{\theta_c}, \quad \text{(A.405)}$$

$$\alpha^{\tilde{W}_1}_{\tilde{f}_1} = -g\sin\theta_L\cos\theta_q + f_d\cos\theta_L\sin\theta_q(-1)^{\theta_c}, \quad \text{(A.406)} \qquad \beta^{\tilde{W}_1}_{\tilde{f}_1} = -f_u\cos\theta_R\cos\theta_q, \quad \text{(A.407)}$$

$$\alpha^{\tilde{W}_1}_{\tilde{f'}_2} = g\sin\theta_R\sin\theta_{q'}(-1)^{\theta_c} - f_u\cos\theta_R\cos\theta_{q'}, \quad \text{(A.408)} \qquad \beta^{\tilde{W}_1}_{\tilde{f'}_2} = -f_d\cos\theta_L\sin\theta_{q'}(-1)^{\theta_c}, \quad \text{(A.409)}$$

$$\alpha^{\tilde{W}_1}_{\tilde{f}_2} = -f_d\cos\theta_L\cos\theta_q + g\sin\theta_L\sin\theta_q, \quad \text{(A.410)} \qquad \beta^{\tilde{W}_1}_{\tilde{f}_2} = -f_u\cos\theta_R\sin\theta_q. \quad \text{(A.411)}$$

Note that because of the conventions adopted, if the fermions considered are τ and ν_τ, so that the intermediates are $\tilde{\tau}_1$ and $\tilde{\tau}_2$, then the mixing angles in the formulae for this 3-body decay must be rotated so that one must take $\cos\theta_\tau \to \sin\theta_\tau$ and $\sin\theta_\tau \to -\cos\theta_\tau$ in the formulae listed for the $\tilde{Z}_i \to \tilde{W}_j f' \bar{f}$ and for the reverse decay $\tilde{W}_j \to \tilde{Z}_i f' \bar{f}$. Note that in this case where the fermions are τ and ν_τ, then θ_q would be the mixing angle for the $\tilde{\tau}$, whilst $\theta_{q'} = 0$ as there is no mixing for $\tilde{\nu_\tau}$.

For $\tilde{W}_2^+$, i.e. the heaviest chargino ($j = 2$), where i is the index of the neutralino:

$$\mathcal{C}^L_{\tilde{W}\tilde{Z}W} = g\left(\cos\theta_L N_{2i} - \frac{\sin\theta_L N_{3i}}{\sqrt{2}}\right), \quad \text{(A.412)}$$

$$\mathcal{C}^R_{\tilde{W}\tilde{Z}W} = g\left(\cos\theta_R N_{2i} + \frac{\sin\theta_R N_{4i}}{\sqrt{2}}\right), \quad \text{(A.413)}$$

$$\mathcal{C}^L_{\tilde{W}\tilde{Z}H+} = g\cos\theta_R N_{4i} - \frac{\sin\theta_R}{\sqrt{2}}(g' N_{1i} + g N_{2i}), \quad \text{(A.414)}$$

$$\mathcal{C}^R_{\tilde{W}\tilde{Z}H+} = g\cos\theta_L N_{3i} + \frac{\sin\theta_L}{\sqrt{2}}(g' N_{1i} + g N_{2i}), \quad \text{(A.415)}$$

$$\alpha^{\tilde{W}_2}_{\tilde{f'}_1} = -g\cos\theta_R\cos\theta_{q'} - f_u\sin\theta_R\sin\theta_{q'}, \quad \text{(A.416)} \qquad \beta^{\tilde{W}_2}_{\tilde{f'}_1} = f_d\sin\theta_L\cos\theta_{q'}(-1)^{\theta_c}, \quad \text{(A.417)}$$

$$\alpha^{\tilde{W}_2}_{\tilde{f}_1} = -g\cos\theta_L\cos\theta_q - f_d\sin\theta_L\sin\theta_q(-1)^{\theta_c}, \quad \text{(A.418)} \qquad \beta^{\tilde{W}_2}_{\tilde{f}_1} = f_u\sin\theta_R\cos\theta_q, \quad \text{(A.419)}$$

$$\alpha^{\tilde{W}_2}_{\tilde{f}'_2} = g\cos\theta_R \sin\theta_{q'}(-1)^{\theta_c} + f_u \sin\theta_R \cos\theta_{q'}, \quad (A.420) \qquad \beta^{\tilde{W}_2}_{\tilde{f}'_2} = f_d \sin\theta_L \sin\theta_{q'}(-1)^{\theta_c}, \quad (A.421)$$

$$\alpha^{\tilde{W}_2}_{\tilde{f}_2} = f_d \sin\theta_L \cos\theta_q + g\cos\theta_L \sin\theta_q, \quad (A.422) \qquad \beta^{\tilde{W}_2}_{\tilde{f}_2} = f_u \sin\theta_R \sin\theta_q. \quad (A.423)$$

There are also the neutralino couplings to the f' $\bar{f}$ pair and these depend upon whether they are quarks(q) or leptons(l) and whether they are "u-type" or "d-type" (i.e. third component of weak isospin being $+\frac{1}{2}$ or $-\frac{1}{2}$ respectively). For quarks:

$$A^u_{\tilde{Z}_i} = -\frac{g}{\sqrt{2}}N_{2i} - \frac{g'}{3\sqrt{2}}N_{1i}, \quad (A.424) \qquad B^u_{\tilde{Z}_i} = -\frac{4g'}{3\sqrt{2}}N_{1i}, \quad (A.425)$$

$$A^d_{\tilde{Z}_i} = \frac{g}{\sqrt{2}}N_{2i} - \frac{g'}{3\sqrt{2}}N_{1i}, \quad (A.426) \qquad B^d_{\tilde{Z}_i} = \frac{2g'}{3\sqrt{2}}N_{1i}, \quad (A.427)$$

$$\alpha^u_{\tilde{Z}_i\tilde{f}_1} = -A^u_{\tilde{Z}_i}\cos\theta_{q'}(-1)^{\theta_j}(-1)^{\theta_i}(-1)^{\theta_c} - f_u N_{4i}\sin\theta_{q'}, \quad (A.428)$$

$$\beta^u_{\tilde{Z}_i\tilde{f}_1} = f_u N_{4i}\cos\theta_{q'}(-1)^{\theta_c} - B^u_{\tilde{Z}_i}\sin\theta_{q'}, \quad (A.429)$$

$$\alpha^u_{\tilde{Z}_i\tilde{f}_2} = -f_u N_{4i}\cos\theta_{q'}(-1)^{\theta_i} + A^u_{\tilde{Z}_i}\sin\theta_{q'}(-1)^{\theta_c}, \quad (A.430)$$

$$\beta^u_{\tilde{Z}_i\tilde{f}_2} = B^u_{\tilde{Z}_i}\cos\theta_{q'}(-1)^{\theta_j}(-1)^{\theta_i}(-1)^{\theta_c} + f_u N_{4i}\sin\theta_{q'}. \quad (A.431)$$

$$\alpha^d_{\tilde{Z}_i\tilde{f}_1} = -A^d_{\tilde{Z}_i}\cos\theta_q(-1)^{\theta_j}(-1)^{\theta_i}(-1)^{\theta_c} - f_d N_{4i}\sin\theta_q, \quad (A.432)$$

$$\beta^d_{\tilde{Z}_i\tilde{f}_1} = f_d N_{3i}\cos\theta_q(-1)^{\theta_c} - B^d_{\tilde{Z}_i}\sin\theta_q(-1)^{\theta_i}, \quad (A.433)$$

$$\alpha^d_{\tilde{Z}_i\tilde{f}_2} = f_d N_{3i}\cos\theta_q(-1)^{\theta_c} - (-1)^{\theta_c}(-1)^{\theta_i}A^d_{\tilde{Z}_i}\sin\theta_q, \quad (A.434)$$

$$\beta^d_{\tilde{Z}_i\tilde{f}_2} = B^d_{\tilde{Z}_i}\cos\theta_q(-1)^{\theta_j}(-1)^{\theta_i}(-1)^{\theta_c} + f_d N_{4i}\sin\theta_q. \quad (A.435)$$

Again, remember for the case of τ and ν_τ as f and f' respectively then one must take $\cos\theta_\tau \to \sin\theta_\tau$ and $\sin\theta_\tau \to -\cos\theta_\tau$ in the formulae listed for this decay mode.

For leptons instead the neutralino couplings are:

$$A^u_{\tilde{Z}_i} = -\frac{g}{\sqrt{2}}N_{2i} + \frac{g'}{\sqrt{2}}N_{1i}, \quad (A.436) \qquad B^u_{\tilde{Z}_i} = 0, \quad (A.437)$$

$$A^d_{\tilde{Z}_i} = \frac{g}{\sqrt{2}}N_{2i} + \frac{g'}{\sqrt{2}}N_{1i}, \quad (A.438) \qquad B^d_{\tilde{Z}_i} = \sqrt{2}g' N_{1i}. \quad (A.439)$$

The α and β couplings are as before except $\alpha^u_{\tilde{Z}_i\tilde{f}_2} = 0$ and $\beta^u_{\tilde{Z}_i\tilde{f}_2} = 0$ as there are no RH sneutrinos. Note that in `SoftSusy` we use the same function for a neutralino decaying to a chargino as a chargino decaying to a neutralino, in general the changes required are $m_{\tilde{Z}_i} \leftrightarrow m_{\tilde{W}_j}$, $m_{f'} \leftrightarrow m_f$ and $m_{\tilde{f}'} \leftrightarrow m_{\tilde{f}}$, in some places there are further effects on the integrals or couplings, where this occurs it's listed in the following formulae.

Now we list the contributions to this mode one by one:

$\underline{\Gamma_W}$

The upper limit of integration here is:

$$\mathcal{T} = \frac{1}{2|m_{\tilde{Z}_i}|}(m^2_{\tilde{Z}_i} + m^2_{\tilde{W}_j} - m^2_f - m^2_{f'} - 2m_f m_{f'}), \quad (A.440)$$

We also use s and λ given by:

$$s = m^2_{\tilde{Z}_i} + m^2_{\tilde{W}_j} - 2|m_{\tilde{Z}_i}|E, \tag{A.441}$$

$$\lambda = \sqrt{(s-(m_f+m_{f'})^2)(s-(m_f-m_{f'})^2)}. \tag{A.442}$$

The necessary integrals are:

$$\begin{aligned} I^1_W = 2|m_{\tilde{Z}_i}| \int_{|m_{\tilde{W}_j}|}^{\mathcal{T}} dE \frac{2|m_{\tilde{Z}_i}|}{s} \lambda \sqrt{E^2 - m^2_{\tilde{W}_j}} \Big[&-2s^4 + ((m^2_{\tilde{Z}_i} + m^2_{\tilde{W}_j} + m^2_f + m^2_{f'}))s^3 \\ &+ ((m^2_{\tilde{Z}_i} - m^2_{\tilde{W}_j})^2 + (m^2_f - m^2_{f'})^2 - 2(m^2_{\tilde{Z}_i} + m^2_{\tilde{W}_j})^2(m^2_f + m^2_{f'})s^2 \\ &+ ((m^2_{\tilde{Z}_i} + m^2_{\tilde{W}_j})(m^2_f - m^2_{f'})^2 + (m^2_f + m^2_{f'})(m^2_{\tilde{Z}_i} - m^2_{\tilde{W}_j})^2)s \\ &- 2(m^2_{\tilde{Z}_i} - m^2_{\tilde{W}_j})^2(m^2_f + m^2_{f'})^2 \Big] \frac{1}{3s^2} \frac{1}{(s-m^2_W)^2}, \end{aligned} \tag{A.443}$$

$$I^2_W = 2|m_{\tilde{Z}_i}| \int_{|m_{\tilde{W}_j}|}^{\mathcal{T}} dE \frac{2|m_{\tilde{Z}_i}|}{s} \lambda \sqrt{E^2 - m^2_{\tilde{W}_j}} (s - m^2_f - m^2_{f'}) \frac{1}{(s-m^2_W)^2}. \tag{A.444}$$

Then

$$\Gamma_W = -8\mathcal{C}^L_{\tilde{W}\tilde{Z}W}\mathcal{C}^R_{\tilde{W}\tilde{Z}W} \frac{g^2}{2} |m_{\tilde{Z}_i}||m_{\tilde{W}_j}| I^2_W (-1)^{\theta_i}(-1)^{\theta_j} + 2(\mathcal{C}^L_{\tilde{W}\tilde{Z}W}{}^2 + \mathcal{C}^R_{\tilde{W}\tilde{Z}W}{}^2) \frac{g^2}{2} I^1_W. \tag{A.445}$$

$$\frac{\Gamma_{H^\pm}}{} \omega^L_{H^+\tilde{W}^+\tilde{Z}} = \mathcal{C}^L_{\tilde{W}\tilde{Z}H+} \cos\beta, \tag{A.446}$$

$$\omega^R_{H^+\tilde{W}^+\tilde{Z}} = \mathcal{C}^R_{\tilde{W}\tilde{Z}H+} \sin\beta, \tag{A.447}$$

$$\mathcal{C}^u_{H^+ff'} = f_u \cos\beta, \tag{A.448}$$

$$\mathcal{C}^d_{H^+ff'} = f_d \sin\beta, \tag{A.449}$$

The relevant combinations of these couplings for this contribution are:

$$\mathcal{V}^{(1)}_{H+} = \omega^L_{H^+\tilde{W}^+\tilde{Z}}{}^2 + \omega^R_{H^+\tilde{W}^+\tilde{Z}}{}^2, \tag{A.450}$$

$$\mathcal{V}^{(2)}_{H+} = \omega^L_{H^+\tilde{W}^+\tilde{Z}} \omega^R_{H^+\tilde{W}^+\tilde{Z}} (-1)^{\theta_i}, \tag{A.451}$$

$$\mathcal{V}^{(3)}_{H+} = \mathcal{C}^u_{H^+ff'}{}^2 + \mathcal{C}^d_{H^+ff'}{}^2, \tag{A.452}$$

$$\mathcal{V}^{(4)}_{H+} = \mathcal{C}^u_{H^+ff'} \mathcal{C}^d_{H^+ff'}. \tag{A.453}$$

The integrals are:

$$I^1_{H^\pm} = 2|m_{\tilde{Z}_i}| \int_{|m_{\tilde{W}_j}|}^{\mathcal{T}} dE \frac{2|m_{\tilde{Z}_i}|}{s} \sqrt{(s-(m_{f'}+m_f)^2)(s-(m_{f'}-m_f)^2)} \sqrt{E^2 - m^2_{\tilde{W}_j}} \frac{1}{(s-m^2_{H^\pm})^2}, \tag{A.454}$$

$$\begin{aligned} I^2_{H^\pm} = 2|m_{\tilde{Z}_i}| \int_{|m_{\tilde{W}_j}|}^{\mathcal{T}} dE \Big[&\frac{2|m_{\tilde{Z}_i}|}{s} \sqrt{(s-(m_{f'}+m_f)^2)(s-(m_{f'}-m_f)^2)} \sqrt{E^2 - m^2_{\tilde{W}_j}} \\ &\times (s - m^2_f - m^2_{f'}) \frac{1}{(s-m^2_{H^\pm})^2} \Big], \end{aligned} \tag{A.455}$$

$$I^3_{H^\pm} = 2|m_{\tilde{Z}_i}| \int_{|m_{\tilde{W}_j}|}^{\mathcal{T}} dE \Big[\frac{2|m_{\tilde{Z}_i}|}{s} \sqrt{(s-(m_{f'}+m_f)^2)(s-(m_{f'}-m_f)^2)} \sqrt{E^2 - m^2_{\tilde{W}_j}} \frac{2|m_{\tilde{Z}_i}|E}{(s-m^2_{H^\pm})^2} \Big], \tag{A.456}$$

$$\begin{aligned} I^4_{H^\pm} = 2|m_{\tilde{Z}_i}| \int_{|m_{\tilde{W}_j}|}^{\mathcal{T}} dE \Big[&\frac{2|m_{\tilde{Z}_i}|}{s} \sqrt{(s-(m_{f'}+m_f)^2)(s-(m_{f'}-m_f)^2)} \sqrt{E^2 - m^2_{\tilde{W}_j}} \\ &\times 2|m_{\tilde{Z}_i}|E(s - m^2_f - m^2_{f'}) \frac{1}{(s-m^2_{H^\pm})^2} \Big]. \end{aligned} \tag{A.457}$$

The overall contribution is then:

$$\begin{aligned}\Gamma_{H^\pm} =&\mathcal{V}^{(1)}_{H+}\mathcal{V}^{(3)}_{H+}I^4_{H^\pm} - 4\mathcal{V}^{(1)}_{H+}\mathcal{V}^{(4)}_{H+}I^3_{H^\pm}m_f m_{f'} + 4\mathcal{V}^{(2)}_{H+}\mathcal{V}^{(3)}_{H+}I^2_{H^\pm}|m_{\tilde{Z}_i}||m_{\tilde{W}_j}|(-1)^{\theta_j}\\ &- 16\mathcal{V}^{(2)}_{H+}\mathcal{V}^{(4)}_{H+}I^1_{H^\pm}m_f m_{f'}|m_{\tilde{Z}_i}||m_{\tilde{W}_j}|(-1)^{\theta_j}.\end{aligned} \tag{A.458}$$

$\underline{\Gamma_G}$

Here G refers to the Goldstone contribution which is the longitudinal component of the W and so has mass equal to the W boson mass. The couplings used are:

$$\omega^L_{G\tilde{W}\tilde{Z}} = \mathcal{C}^L_{\tilde{W}\tilde{Z}H+}\sin\beta, \tag{A.459}$$
$$\omega^R_{G\tilde{W}\tilde{Z}} = -\mathcal{C}^R_{\tilde{W}\tilde{Z}H+}\cos\beta, \tag{A.460}$$
$$\mathcal{C}^u_{Gff'} = f_u\sin\beta, \tag{A.461}$$
$$\mathcal{C}^d_{Gff'} = -f_d\cos\beta, \tag{A.462}$$

$$\mathcal{V}^{(1)}_G = {\omega^L_{G\tilde{W}\tilde{Z}}}^2 + {\omega^R_{G\tilde{W}\tilde{Z}}}^2, \tag{A.463}$$
$$\mathcal{V}^{(2)}_G = \omega^L_{G\tilde{W}\tilde{Z}}\omega^R_{G\tilde{W}\tilde{Z}}(-1)^{\theta_i}, \tag{A.464}$$
$$\mathcal{V}^{(3)}_G = {\mathcal{C}^u_{Gff'}}^2 + {\mathcal{C}^d_{Gff'}}^2, \tag{A.465}$$
$$\mathcal{V}^{(4)}_G = \mathcal{C}^u_{Gff'}\mathcal{C}^d_{Gff'}. \tag{A.466}$$

The integrals here I^1_G etc are exactly the same as those for $H^\pm$ but with the change $m_{H^\pm} \to m_W$.

$$\begin{aligned}\Gamma_G =&\mathcal{V}^{(1)}_G\mathcal{V}^{(3)}_G I^4_G - 4\mathcal{V}^{(1)}_G\mathcal{V}^{(4)}_G I^3_G m_f m_{f'} + 4\mathcal{V}^{(2)}_G\mathcal{V}^{(3)}_G I^2_G|m_{\tilde{Z}_i}||m_{\tilde{W}_j}|(-1)^{\theta_j}\\ &- 16\mathcal{V}^{(2)}_G\mathcal{V}^{(4)}_G I^1_G m_f m_{f'}|m_{\tilde{Z}_i}||m_{\tilde{W}_j}|(-1)^{\theta_j}.\end{aligned} \tag{A.467}$$

$\underline{\Gamma_{\tilde{f'}_1}}$

$$\mathcal{V}^{(1)}_{\tilde{f'}_1} = {\alpha^u_{\tilde{Z}_i\tilde{f}_1}}^2 + {\beta^u_{\tilde{Z}_i\tilde{f}_1}}^2, \tag{A.468}$$
$$\mathcal{V}^{(2)}_{\tilde{f'}_1} = -{\alpha^u_{\tilde{Z}_i\tilde{f}_1}}^2{\beta^u_{\tilde{Z}_i\tilde{f}_1}}^2(-1)^{\theta_i}, \tag{A.469}$$
$$\mathcal{V}^{(3)}_{\tilde{f'}_1} = {\alpha^{\tilde{W}}_{\tilde{f'}_1}}^2 + {\beta^{\tilde{W}}_{\tilde{f'}_1}}^2, \tag{A.470}$$
$$\mathcal{V}^{(4)}_{\tilde{f'}_1} = -\alpha^{\tilde{W}}_{\tilde{f'}_1}\beta^{\tilde{W}}_{\tilde{f'}_1}. \tag{A.471}$$

Now the integrals $I^{1,2,3,4}_{\tilde{f'}_1}$ are exactly as the $I^{1,2,3,4}_{H^\pm}$ integrals in (A.454) to (A.457) but with lower limit $m_{f'}$, upper limit of integration $E_{upper} = \frac{1}{2|m_{\tilde{Z}_1}|}(m^2_{\tilde{Z}_i} + m^2_{f'} - m^2_f - m^2_{\tilde{Z}_j} - 2m_f|m_{\tilde{W}_j}|)$ and the replacements $m_{H^\pm} \to m_{\tilde{f'}_1}$, $|m_{\tilde{W}_j}| \to m_{f'}$ and $m_{f'} \to |m_{\tilde{W}_j}|$. Then:

$$\begin{aligned}\Gamma_{\tilde{f'}_1} =&\mathcal{V}^{(1)}_{\tilde{f'}_1}\mathcal{V}^{(3)}_{\tilde{f'}_1}I^4_{\tilde{f'}_1} - 4\mathcal{V}^{(1)}_{\tilde{f'}_1}\mathcal{V}^{(4)}_{\tilde{f'}_1}m_f|m_{\tilde{W}_j}|I^3_{\tilde{f'}_1} + 4\mathcal{V}^{(2)}_{\tilde{f'}_1}\mathcal{V}^{(3)}_{\tilde{f'}_1}|m_{\tilde{Z}_i}|m_{f'}I^2_{\tilde{f'}_1}\\ &- 16\mathcal{V}^{(2)}_{\tilde{f'}_1}\mathcal{V}^{(4)}_{\tilde{f'}_1}|m_{\tilde{Z}_i}||m_{\tilde{W}_j}|m_{f'}m_f I^1_{\tilde{f'}_1}.\end{aligned} \tag{A.472}$$

$\underline{\Gamma_{\tilde{f'}_2}}$

Everything for $\Gamma_{\tilde{f'}_2}$ is exactly as for $\Gamma_{\tilde{f'}_1}$ but with the change $m_{\tilde{f'}_1} \to m_{\tilde{f'}_2}$ and the coupling combinations:

$$\mathcal{V}^{(1)}_{\tilde{f'}_2} = {\alpha^u_{\tilde{Z}_i\tilde{f}_2}}^2 + {\beta^u_{\tilde{Z}_i\tilde{f}_2}}^2, \tag{A.473}$$
$$\mathcal{V}^{(2)}_{\tilde{f'}_2} = {\alpha^u_{\tilde{Z}_i\tilde{f}_2}}^2{\beta^u_{\tilde{Z}_i\tilde{f}_2}}^2, \tag{A.474}$$
$$\mathcal{V}^{(3)}_{\tilde{f'}_2} = {\alpha^{\tilde{W}}_{\tilde{f'}_2}}^2 + {\beta^{\tilde{W}}_{\tilde{f'}_2}}^2, \tag{A.475}$$
$$\mathcal{V}^{(4)}_{\tilde{f'}_2} = \alpha^{\tilde{W}}_{\tilde{f'}_2}\beta^{\tilde{W}}_{\tilde{f'}_2}. \tag{A.476}$$

The contribution is then:

$$\begin{aligned}\Gamma_{\tilde{f'}_2} =&\mathcal{V}^{(1)}_{\tilde{f'}_2}\mathcal{V}^{(3)}_{\tilde{f'}_2}I^4_{\tilde{f'}_2} - 4\mathcal{V}^{(1)}_{\tilde{f'}_2}\mathcal{V}^{(4)}_{\tilde{f'}_2}m_f|m_{\tilde{W}_j}|I^3_{\tilde{f'}_2}(-1)^{\theta_c} + 4\mathcal{V}^{(2)}_{\tilde{f'}_2}\mathcal{V}^{(3)}_{\tilde{f'}_2}|m_{\tilde{Z}_i}|m_{f'}I^2_{\tilde{f'}_2}(-1)^{\theta_c}\\ &- 16\mathcal{V}^{(2)}_{\tilde{f'}_2}\mathcal{V}^{(4)}_{\tilde{f'}_2}|m_{\tilde{Z}_i}||m_{\tilde{W}_j}|m_{f'}m_f I^1_{\tilde{f'}_2}.\end{aligned} \tag{A.477}$$

$\underline{\Gamma_{\tilde{f}_1}}$

The coupling combinations are now:

$$\mathcal{V}^{(1)}_{\tilde{f}_1} = {\alpha^d_{\tilde{Z}_i\tilde{f}_1}}^2 + {\beta^d_{\tilde{Z}_i\tilde{f}_1}}^2, \tag{A.478}$$
$$\mathcal{V}^{(2)}_{\tilde{f}_1} = -(-1)^{\theta_i}\alpha^d_{\tilde{Z}_i\tilde{f}_1}\beta^d_{\tilde{Z}_i\tilde{f}_1}, \tag{A.479}$$

$$\mathcal{V}^{(3)}_{\tilde{f}_1} = {\alpha^{\tilde{W}}_{\tilde{f}_1}}^2 + {\beta^{\tilde{W}}_{\tilde{f}_1}}^2, \quad \text{(A.480)} \qquad \mathcal{V}^{(4)}_{\tilde{f}_1} = -\alpha^{\tilde{W}}_{\tilde{f}_1}\beta^{\tilde{W}}_{\tilde{f}_1}(-1)^{\theta_j}. \quad \text{(A.481)}$$

The integrals are are exactly as the $I^{1,2,3,4}_{H^\pm}$ integrals in (A.454) to (A.457) but the lower limit is now m_f, the upper limit is $E_{upper2} = \frac{1}{2|m_{\tilde{Z}_i}|}[m^2_{\tilde{Z}_i} + m^2_f - m^2_{\tilde{W}_j} - m^2_{f'} - 2m_{f'}|m_{\tilde{W}_j}|]$ and in general relative to the $H^\pm$ integrals we must make the changes $m_{H^\pm} \to m_{\tilde{f}_1}$, $|m_{\tilde{W}_j}| \to m_f$ and $m_f \to |m_{\tilde{W}_j}|$.

$$\begin{aligned}\Gamma_{\tilde{f}_1} =& \mathcal{V}^{(1)}_{\tilde{f}_1}\mathcal{V}^{(3)}_{\tilde{f}_1} I^4_{\tilde{f}_1} - 4\mathcal{V}^{(1)}_{\tilde{f}_1}\mathcal{V}^{(4)}_{\tilde{f}_1} m_{f'}|m_{\tilde{W}_j}| I^3_{\tilde{f}_1}(-1)^{\theta_c}(-1)^{\theta_j} + 4\mathcal{V}^{(2)}_{\tilde{f}_1}\mathcal{V}^{(3)}_{\tilde{f}_1}|m_{\tilde{Z}_i}| m_f I^2_{\tilde{f}_1}(-1)^{\theta_c} \\ & - 16\mathcal{V}^{(2)}_{\tilde{f}_1}\mathcal{V}^{(4)}_{\tilde{f}_1}|m_{\tilde{Z}_i}||m_{\tilde{W}_j}| m_f m_{f'}(-1)^{\theta_j} I^1_{\tilde{f}_1}.\end{aligned} \quad \text{(A.482)}$$

$\underline{\Gamma_{\tilde{f}_2}}$

Nominally $\Gamma_{\tilde{f}_2}$ has the same expression as $\Gamma_{\tilde{f}_1}$ with the replacement $\tilde{f}_1 \to \tilde{f}_2$, however differences in expressions for couplings mean we have slight differences; the coupling combinations are now:

$$\mathcal{V}^{(1)}_{\tilde{f}_2} = {\alpha^d_{\tilde{Z}_i\tilde{f}_2}}^2 + {\beta^d_{\tilde{Z}_i\tilde{f}_2}}^2, \quad \text{(A.483)} \qquad \mathcal{V}^{(2)}_{\tilde{f}_2} = \alpha^d_{\tilde{Z}_i\tilde{f}_2}\beta^d_{\tilde{Z}_i\tilde{f}_2}, \quad \text{(A.484)}$$

$$\mathcal{V}^{(3)}_{\tilde{f}_2} = {\alpha^{\tilde{W}}_{\tilde{f}_2}}^2 + {\beta^{\tilde{W}}_{\tilde{f}_2}}^2, \quad \text{(A.485)} \qquad \mathcal{V}^{(4)}_{\tilde{f}_2} = \alpha^{\tilde{W}}_{\tilde{f}_2}\beta^{\tilde{W}}_{\tilde{f}_2}(-1)^{\theta_c}. \quad \text{(A.486)}$$

Therefore the contribution is given by:

$$\begin{aligned}\Gamma_{\tilde{f}_2} =& \mathcal{V}^{(1)}_{\tilde{f}_2}\mathcal{V}^{(3)}_{\tilde{f}_2} I^4_{\tilde{f}_2} - 4\mathcal{V}^{(1)}_{\tilde{f}_2}\mathcal{V}^{(4)}_{\tilde{f}_2} m_{f'}|m_{\tilde{W}_j}| I^3_{\tilde{f}_2}(-1)^{\theta_c} + 4\mathcal{V}^{(2)}_{\tilde{f}_2}\mathcal{V}^{(3)}_{\tilde{f}_2}|m_{\tilde{Z}_i}| m_f I^2_{\tilde{f}_2}(-1)^{\theta_c} \\ & - 16\mathcal{V}^{(2)}_{\tilde{f}_2}\mathcal{V}^{(4)}_{\tilde{f}_2}|m_{\tilde{Z}_i}||m_{\tilde{W}_j}| m_f m_{f'} I^1_{\tilde{f}_2}.\end{aligned} \quad \text{(A.487)}$$

$\underline{\Gamma_{\tilde{f'}_1\tilde{f}_1}}$

Here the coupling combinations differ significantly depending on which way around the decay is being considered, i.e. neutralino to chargino or chargino to neutralino. The following are fixed regardless of this:

$$\mathcal{V}^{(1)}_{\tilde{f'}_1\tilde{f}_1} = \frac{1}{2}\left[\alpha^u_{\tilde{Z}_i\tilde{f}_1}\beta^d_{\tilde{Z}_i\tilde{f}_1}\beta^{\tilde{W}}_{\tilde{f'}_1}\alpha^{\tilde{W}}_{\tilde{f}_1}(-1)^{\theta_i} + \beta^u_{\tilde{Z}_i\tilde{f}_1}\alpha^d_{\tilde{Z}_i\tilde{f}_1}\alpha^{\tilde{W}}_{\tilde{f'}_1}\beta^{\tilde{W}}_{\tilde{f}_1}\right](-1)^{\theta_j}, \quad \text{(A.488)}$$

$$\mathcal{V}^{(2)}_{\tilde{f'}_1\tilde{f}_1} = -|m_{\tilde{Z}_i}||m_{\tilde{W}_j}|\left[(-1)^{\theta_i}\alpha^u_{\tilde{Z}_i\tilde{f}_1}\alpha^d_{\tilde{Z}_i\tilde{f}_1}\alpha^{\tilde{W}}_{\tilde{f'}_1}\alpha^{\tilde{W}}_{\tilde{f}_1} + \beta^u_{\tilde{Z}_i\tilde{f}_1}\beta^d_{\tilde{Z}_i\tilde{f}_1}\beta^{\tilde{W}}_{\tilde{f'}_1}\beta^{\tilde{W}}_{\tilde{f}_1}\right](-1)^{\theta_j}, \quad \text{(A.489)}$$

$$\mathcal{V}^{(3)}_{\tilde{f'}_1\tilde{f}_1} = -m_f m_{f'}\left[\beta^u_{\tilde{Z}_i\tilde{f}_1}\alpha^d_{\tilde{Z}_i\tilde{f}_1}\beta^{\tilde{W}}_{\tilde{f'}_1}\alpha^{\tilde{W}}_{\tilde{f}_1} + (-1)^{\theta_i}\alpha^u_{\tilde{Z}_i\tilde{f}_1}\beta^d_{\tilde{Z}_i\tilde{f}_1}\alpha^{\tilde{W}}_{\tilde{f}_1}\beta^{\tilde{W}}_{\tilde{f}_1}\right](-1)^{\theta_j}(-1)^{\theta_c}, \quad \text{(A.490)}$$

$$\mathcal{V}^{(8)}_{\tilde{f'}_1\tilde{f}_1} = -2|m_{\tilde{Z}_i}||m_{\tilde{W}_j}| m_f m_{f'}\left[\beta^u_{\tilde{Z}_i\tilde{f}_1}\beta^d_{\tilde{Z}_i\tilde{f}_1}\alpha^{\tilde{W}}_{\tilde{f}'}\alpha^{\tilde{W}}_{\tilde{f}_1} + (-1)^{\theta_i}\alpha^u_{\tilde{Z}_i\tilde{f}_1}\alpha^d_{\tilde{Z}_i\tilde{f}_1}\beta^{\tilde{W}}_{\tilde{f}'}\beta^{\tilde{W}}_{\tilde{f}_1}\right](-1)^{\theta_j}(-1)^{\theta_c}. \quad \text{(A.491)}$$

Meanwhile, if the decay is neutralino to chargino:

$$\mathcal{V}^{(4)}_{\tilde{f'}_1\tilde{f}_1} = -|m_{\tilde{Z}_i}| m_f\left[(-1)^{\theta_i}\alpha^u_{\tilde{Z}_i\tilde{f}_1}\alpha^d_{\tilde{Z}_i\tilde{f}_1}\beta^{\tilde{W}}_{\tilde{f}'}\alpha^{\tilde{W}}_{\tilde{f}_1} + \beta^u_{\tilde{Z}_i\tilde{f}_1}\beta^d_{\tilde{Z}_i\tilde{f}_1}\alpha^{\tilde{W}}_{\tilde{f}'}\beta^{\tilde{W}}_{\tilde{f}_1}\right], \quad \text{(A.492)}$$

$$\mathcal{V}^{(5)}_{\tilde{f'}_1\tilde{f}_1} = m_{f'}|m_{\tilde{W}_j}|\left[\beta^u_{\tilde{Z}_i\tilde{f}_1}\alpha^d_{\tilde{Z}_i\tilde{f}_1}\alpha^{\tilde{W}}_{\tilde{f'}_1}\alpha^{\tilde{W}}_{\tilde{f}_1} + (-1)^{\theta_i}\alpha^u_{\tilde{Z}_i\tilde{f}_1}\beta^d_{\tilde{Z}_i\tilde{f}_1}\beta^{\tilde{W}}_{\tilde{f'}_1}\beta^{\tilde{W}}_{\tilde{f}_1}\right](-1)^{\theta_j}, \quad \text{(A.493)}$$

$$\mathcal{V}^{(6)}_{\tilde{f'}_1\tilde{f}_1} = -|m_{\tilde{Z}_i}| m_{f'}\left[\beta^u_{\tilde{Z}_i\tilde{f}_1}\beta^d_{\tilde{Z}_i\tilde{f}_1}\beta^{\tilde{W}}_{\tilde{f}'}\alpha^{\tilde{W}}_{\tilde{f}_1} + (-1)^{\theta_i}\alpha^u_{\tilde{Z}_i\tilde{f}_1}\alpha^d_{\tilde{Z}_i\tilde{f}_1}\alpha^{\tilde{W}}_{\tilde{f'}_1}\beta^{\tilde{W}}_{\tilde{f}_1}\right], \quad \text{(A.494)}$$

$$\mathcal{V}^{(7)}_{\tilde{f'}_1\tilde{f}_1} = |m_{\tilde{W}_j}| m_f\left[(-1)^{\theta_i}\alpha^u_{\tilde{Z}_i\tilde{f}_1}\beta^d_{\tilde{Z}_i\tilde{f}_1}\alpha^{\tilde{W}}_{\tilde{f'}_1}\alpha^{\tilde{W}}_{\tilde{f}_1} + \beta^u_{\tilde{Z}_i\tilde{f}_1}\alpha^d_{\tilde{Z}_i\tilde{f}_1}\beta^{\tilde{W}}_{\tilde{f'}_1}\beta^{\tilde{W}}_{\tilde{f}_1}\right](-1)^{\theta_j}. \quad \text{(A.495)}$$

Whilst if the decay is instead chargino to neutralino:

$$\mathcal{V}^{(4)}_{\tilde{f}'_1\tilde{f}_1} = |m_{\tilde{Z}_i}|m_f\left[\alpha^{\tilde{W}}_{\tilde{f}'_1}\alpha^{\tilde{W}}_{\tilde{f}_1}\beta^{u}_{\tilde{Z}_i\tilde{f}_1}\alpha^{d}_{\tilde{Z}_i\tilde{f}_1} + \beta^{\tilde{W}}_{\tilde{f}'_1}\beta^{\tilde{W}}_{\tilde{f}_1}\alpha^{u}_{\tilde{Z}_i\tilde{f}_1}\beta^{d}_{\tilde{Z}_i\tilde{f}_1}\right](-1)^{\theta_j}, \tag{A.496}$$

$$\mathcal{V}^{(5)}_{\tilde{f}'_1\tilde{f}_1} = -|m_{\tilde{W}_j}|m_{f'}\left[\alpha^{\tilde{W}}_{\tilde{f}_1}\beta^{\tilde{W}}_{\tilde{f}'_1}\alpha^{u}_{\tilde{Z}_i\tilde{f}_1}\alpha^{d}_{\tilde{Z}_i\tilde{f}_1} + \alpha^{\tilde{W}}_{\tilde{f}'_1}\beta^{\tilde{W}}_{\tilde{f}_1}\beta^{u}_{\tilde{Z}_i\tilde{f}_1}\beta^{d}_{\tilde{Z}_i\tilde{f}_1}\right](-1)^{\theta_j}, \tag{A.497}$$

$$\mathcal{V}^{(6)}_{\tilde{f}'_1\tilde{f}_1} = -|m_{\tilde{Z}_i}|m_{f'}\left[\beta^{\tilde{W}}_{\tilde{f}'_1}\beta^{\tilde{W}}_{\tilde{f}_1}\beta^{u}_{\tilde{Z}_i\tilde{f}_1}\alpha^{d}_{\tilde{Z}_i\tilde{f}_1} + \alpha^{\tilde{W}}_{\tilde{f}'_1}\alpha^{\tilde{W}_1}_{\tilde{f}_1}\alpha^{u}_{\tilde{Z}_i\tilde{f}_1}\beta^{d}_{\tilde{Z}_i\tilde{f}_1}\right](-1)^{\theta_j}, \tag{A.498}$$

$$\mathcal{V}^{(7)}_{\tilde{f}'_1\tilde{f}_1} = |m_{\tilde{W}_j}|m_f\left[\alpha^{\tilde{W}}_{\tilde{f}'_1}\beta^{\tilde{W}}_{\tilde{f}_1}\alpha^{u}_{\tilde{Z}_i\tilde{f}_1}\alpha^{d}_{\tilde{Z}_i\tilde{f}_1} + \beta^{\tilde{W}}_{\tilde{f}'_1}\alpha^{\tilde{W}}_{\tilde{f}_1}\beta^{u}_{\tilde{Z}_i\tilde{f}_1}\beta^{d}_{\tilde{Z}_i\tilde{f}_1}\right](-1)^{\theta_j}. \tag{A.499}$$

We also need the following integrals with:

$$s = m^2_{\tilde{Z}_i} + m^2_{f'} - 2|m_{\tilde{Z}_i}|E, \tag{A.500}$$

$$\lambda = \sqrt{(s-(m_f+m_{\tilde{W}})^2)(s-(m_f-m_{\tilde{W}})^2)}, \tag{A.501}$$

$$A = \left[m^2_f + m^2_{\tilde{W}_j} + 2|m_{\tilde{Z}_i}|E + (m^2_{\tilde{Z}_i} - m^2_{f'})(m^2_{\tilde{W}} - m^2_f)\frac{1}{s} + 2|m_{\tilde{Z}_i}|\lambda\frac{1}{s}\sqrt{E^2 - m^2_{f'}} - 2m^2_{\tilde{f}_1}\right], \tag{A.502}$$

$$B = \left[m^2_f + m^2_{\tilde{W}_j} + 2|m_{\tilde{Z}_i}|E + (m^2_{\tilde{Z}_i} - m^2_{f'})(m^2_{\tilde{W}} - m^2_f)\frac{1}{s} - 2|m_{\tilde{Z}_i}|\lambda\frac{1}{s}\sqrt{E^2 - m^2_{f'}} - 2m^2_{\tilde{f}_1}\right], \tag{A.503}$$

$$I^1_{\tilde{f}'_1\tilde{f}_1} = 4|m_{\tilde{Z}_i}|\int_{m_{f'}}^{E_{upper}} dE \frac{[2|m_{\tilde{Z}_i}|\lambda\sqrt{E^2 - m^2_{f'}} + (m^2_{\tilde{f}_1}s - m^2_{\tilde{Z}_i}m^2_{\tilde{W}_j} - m^2_f m^2_{f'})\log(A/B)]}{s - m^2_{\tilde{f}'_1}}, \tag{A.504}$$

$$I^2_{\tilde{f}'_1\tilde{f}_1} = -2|m_{\tilde{Z}_i}|\int_{m_{f'}}^{E_{upper}} dE \frac{[2|m_{\tilde{Z}_i}|\lambda\frac{1}{s}\sqrt{E^2 - m^2_{f'}} + (m^2_{\tilde{f}_1} - 2|m_{\tilde{Z}_i}E + m^2_{f'} - m^2_{\tilde{W}_j})\log(A/B)]}{s - m^2_{\tilde{f}'_1}}, \tag{A.505}$$

$$I^3_{\tilde{f}'_1\tilde{f}_1} = 2|m_{\tilde{Z}_i}|\int_{m_{f'}}^{E_{upper}} dE \frac{[2|m_{\tilde{Z}_i}|\lambda\frac{1}{s}\sqrt{E^2 - m^2_{f'}} + (m^2_{\tilde{f}_1} - 2|m_{\tilde{Z}_i}E + m^2_{\tilde{Z}_i} - m^2_f)\log(A/B)]}{s - m^2_{\tilde{f}'_1}}, \tag{A.506}$$

$$I^4_{\tilde{f}'_1\tilde{f}_1} = 2|m_{\tilde{Z}_i}|\int_{m_{f'}}^{E_{upper}} dE \frac{[2|m_{\tilde{Z}_i}|\lambda\frac{1}{s}\sqrt{E^2 - m^2_{f'}} + (m^2_{\tilde{f}_1} - m^2_{\tilde{W}_j} - m^2_{f'})\log(A/B)]}{s - m^2_{\tilde{f}'_1}}, \tag{A.507}$$

$$I^5_{\tilde{f}'_1\tilde{f}_1} = 2|m_{\tilde{Z}_i}|\int_{m_{f'}}^{E_{upper}} dE \frac{[2|m_{\tilde{Z}_i}|\lambda\frac{1}{s}\sqrt{E^2 - m^2_{f'}} + (m^2_{\tilde{f}_1} - m^2_{\tilde{Z}_i} - m^2_f)\log(A/B)]}{s - m^2_{\tilde{f}'_1}}, \tag{A.508}$$

$$I^6_{\tilde{f}'_1\tilde{f}_1} = 2|m_{\tilde{Z}_i}|\int_{m_{f'}}^{E_{upper}} dE \frac{\log(A/B)(s - m^2_f - m^2_{\tilde{W}_j})}{s - m^2_{\tilde{f}'_1}}, \tag{A.509}$$

$$I^7_{\tilde{f}'_1\tilde{f}_1} = 2|m_{\tilde{Z}_i}|\int_{m_{f'}}^{E_{upper}} dE \frac{\log(A/B)2|m_{\tilde{Z}_i}|E}{s - m^2_{\tilde{f}'_1}}, \tag{A.510}$$

$$I^8_{\tilde{f}'_1\tilde{f}_1} = 2|m_{\tilde{Z}_i}|\int_{m_{f'}}^{E_{upper}} dE \frac{\log(A/B)}{s - m^2_{\tilde{f}'_1}}. \tag{A.511}$$

The $\Gamma_{\tilde{f}'_1\tilde{f}_1}$ contribution is then given by:

$$\begin{aligned}\Gamma_{\tilde{f}'_1\tilde{f}_1} =& \mathcal{V}^{(1)}_{\tilde{f}'_1\tilde{f}_1}I^1_{\tilde{f}'_1\tilde{f}_1} + \mathcal{V}^{(2)}_{\tilde{f}'_1\tilde{f}_1}I^2_{\tilde{f}'_1\tilde{f}_1} + \mathcal{V}^{(3)}_{\tilde{f}'_1\tilde{f}_1}I^3_{\tilde{f}'_1\tilde{f}_1} + \mathcal{V}^{(4)}_{\tilde{f}'_1\tilde{f}_1}I^4_{\tilde{f}'_1\tilde{f}_1} \\ &+ \mathcal{V}^{(5)}_{\tilde{f}'_1\tilde{f}_1}I^5_{\tilde{f}'_1\tilde{f}_1} + \mathcal{V}^{(6)}_{\tilde{f}'_1\tilde{f}_1}I^6_{\tilde{f}'_1\tilde{f}_1} + \mathcal{V}^{(7)}_{\tilde{f}'_1\tilde{f}_1}I^7_{\tilde{f}'_1\tilde{f}_1} + \mathcal{V}^{(8)}_{\tilde{f}'_1\tilde{f}_1}I^8_{\tilde{f}'_1\tilde{f}_1}.\end{aligned} \tag{A.512}$$

The $\Gamma_{\tilde{f}'_1\tilde{f}_2}$, $\Gamma_{\tilde{f}'_2\tilde{f}_1}$ and $\Gamma_{\tilde{f}'_2\tilde{f}_2}$ contributions follow analogously, they are given here as slight differences in the expressions for couplings complicated the expressions.

$\underline{\Gamma_{\tilde{f'}_1\tilde{f}_2}}$

$$\mathcal{V}^{(1)}_{\tilde{f'}_1\tilde{f}_2} = -\frac{1}{2}\left[\alpha^u_{\tilde{Z}_i\tilde{f}_1}\beta^d_{\tilde{Z}_i\tilde{f}_2}\beta^{\tilde{W}}_{\tilde{f'}_1}\alpha^{\tilde{W}}_{\tilde{f}_2} + \beta^u_{\tilde{Z}_i\tilde{f}_1}\alpha^d_{\tilde{Z}_i\tilde{f}_2}\alpha^{\tilde{W}}_{\tilde{f'}_1}\beta^{\tilde{W}}_{\tilde{f}_2}\right](-1)^{\theta_i}, \tag{A.513}$$

$$\mathcal{V}^{(2)}_{\tilde{f'}_1\tilde{f}_2} = |m_{\tilde{Z}_i}||m_{\tilde{W}_j}|\left[(-1)^{\theta_i}\alpha^u_{\tilde{Z}_i\tilde{f}_1}\alpha^d_{\tilde{Z}_i\tilde{f}_2}\alpha^{\tilde{W}}_{\tilde{f'}_1}\alpha^{\tilde{W}}_{\tilde{f}_2} + \beta^u_{\tilde{Z}_i\tilde{f}_1}\beta^d_{\tilde{Z}_i\tilde{f}_2}\beta^{\tilde{W}}_{\tilde{f'}_1}\beta^{\tilde{W}}_{\tilde{f}_2}\right], \tag{A.514}$$

$$\mathcal{V}^{(3)}_{\tilde{f'}_1\tilde{f}_2} = (-1)^{\theta_i}m_f m_{f'}\left[\beta^u_{\tilde{Z}_i\tilde{f}_1}\alpha^d_{\tilde{Z}_i\tilde{f}_2}\beta^{\tilde{W}}_{\tilde{f'}_1}\alpha^{\tilde{W}}_{\tilde{f}_2} - (-1)^{\theta_c}\alpha^u_{\tilde{Z}_i\tilde{f}_1}\beta^d_{\tilde{Z}_i\tilde{f}_2}\alpha^{\tilde{W}}_{\tilde{f}_1}\beta^{\tilde{W}}_{\tilde{f}_2}\right], \tag{A.515}$$

$$\mathcal{V}^{(8)}_{\tilde{f'}_1\tilde{f}_2} = 2|m_{\tilde{Z}_i}||m_{\tilde{W}_j}|m_f m_{f'}\left[(-1)^{\theta_i}\beta^u_{\tilde{Z}_i\tilde{f}_1}\beta^d_{\tilde{Z}_i\tilde{f}_2}\alpha^{\tilde{W}}_{\tilde{f'}_1}\alpha^{\tilde{W}}_{\tilde{f}_2} + \alpha^u_{\tilde{Z}_i\tilde{f}_1}\alpha^d_{\tilde{Z}_i\tilde{f}_2}\beta^{\tilde{W}}_{\tilde{f'}_1}\beta^{\tilde{W}}_{\tilde{f}_2}\right]. \tag{A.516}$$

If the decay is neutralino to chargino:

$$\mathcal{V}^{(4)}_{\tilde{f'}_1\tilde{f}_2} = (-1)^{\theta_i}|m_{\tilde{Z}_i}|m_f\left[\alpha^u_{\tilde{Z}_i\tilde{f}_1}\alpha^d_{\tilde{Z}_i\tilde{f}_2}\beta^{\tilde{W}}_{\tilde{f}'}\alpha^{\tilde{W}}_{\tilde{f}_2} - \beta^u_{\tilde{Z}_i\tilde{f}_1}\beta^d_{\tilde{Z}_i\tilde{f}_2}\alpha^{\tilde{W}}_{\tilde{f'}_1}\beta^{\tilde{W}}_{\tilde{f}_2}\right], \tag{A.517}$$

$$\mathcal{V}^{(5)}_{\tilde{f'}_1\tilde{f}_2} = m_{f'}|m_{\tilde{W}_j}|\left[(-1)^{\theta_i}\beta^u_{\tilde{Z}_i\tilde{f}_1}\alpha^d_{\tilde{Z}_i\tilde{f}_2}\alpha^{\tilde{W}}_{\tilde{f'}_1}\alpha^{\tilde{W}}_{\tilde{f}_2} + \alpha^u_{\tilde{Z}_i\tilde{f}_1}\beta^d_{\tilde{Z}_i\tilde{f}_2}\beta^{\tilde{W}}_{\tilde{f'}_1}\beta^{\tilde{W}}_{\tilde{f}_2}\right](-1)^{\theta_j}, \tag{A.518}$$

$$\mathcal{V}^{(6)}_{\tilde{f'}_1\tilde{f}_2} = -(-1)^{\theta_i}|m_{\tilde{Z}_i}|m_{f'}\left[-\beta^u_{\tilde{Z}_i\tilde{f}_1}\beta^d_{\tilde{Z}_i\tilde{f}_2}\beta^{\tilde{W}}_{\tilde{f'}_1}\alpha^{\tilde{W}}_{\tilde{f}_2} + \alpha^u_{\tilde{Z}_i\tilde{f}_1}\alpha^d_{\tilde{Z}_i\tilde{f}_2}\alpha^{\tilde{W}}_{\tilde{f'}_1}\beta^{\tilde{W}}_{\tilde{f}_2}\right], \tag{A.519}$$

$$\mathcal{V}^{(7)}_{\tilde{f'}_1\tilde{f}_2} = |m_{\tilde{W}_j}|m_f\left[(-1)^{\theta_i}\alpha^u_{\tilde{Z}_i\tilde{f}_1}\beta^d_{\tilde{Z}_i\tilde{f}_2}\alpha^{\tilde{W}}_{\tilde{f'}_1}\alpha^{\tilde{W}}_{\tilde{f}_2} + \beta^u_{\tilde{Z}_i\tilde{f}_1}\alpha^d_{\tilde{Z}_i\tilde{f}_2}\beta^{\tilde{W}}_{\tilde{f'}_1}\beta^{\tilde{W}}_{\tilde{f}_2}\right](-1)^{\theta_j}. \tag{A.520}$$

Whilst if the decay is instead chargino to neutralino:

$$\mathcal{V}^{(4)}_{\tilde{f'}_1\tilde{f}_2} = |m_{\tilde{Z}_i}|m_f\left[(-1)^{\theta_j}\alpha^{\tilde{W}}_{\tilde{f'}_1}\alpha^{\tilde{W}}_{\tilde{f}_2}\beta^u_{\tilde{Z}_i\tilde{f}_1}\alpha^d_{\tilde{Z}_i\tilde{f}_2} - \beta^{\tilde{W}}_{\tilde{f'}_1}\beta^{\tilde{W}}_{\tilde{f}_2}\alpha^u_{\tilde{Z}_i\tilde{f}_1}\beta^d_{\tilde{Z}_i\tilde{f}_2}\right], \tag{A.521}$$

$$\mathcal{V}^{(5)}_{\tilde{f'}_1\tilde{f}_2} = -|m_{\tilde{W}_j}|m_{f'}\left[\alpha^{\tilde{W}}_{\tilde{f}_2}\beta^{\tilde{W}}_{\tilde{f'}_1}\alpha^u_{\tilde{Z}_i\tilde{f}_1}\alpha^d_{\tilde{Z}_i\tilde{f}_2} - (-1)^{\theta_j}\alpha^{\tilde{W}}_{\tilde{f'}_1}\beta^{\tilde{W}}_{\tilde{f}_2}\beta^u_{\tilde{Z}_i\tilde{f}_1}\beta^d_{\tilde{Z}_i\tilde{f}_2}\right], \tag{A.522}$$

$$\mathcal{V}^{(6)}_{\tilde{f'}_1\tilde{f}_2} = |m_{\tilde{Z}_i}|m_{f'}\left[-\beta^{\tilde{W}}_{\tilde{f'}_1}\beta^{\tilde{W}}_{\tilde{f}_2}\beta^u_{\tilde{Z}_i\tilde{f}_1}\alpha^d_{\tilde{Z}_i\tilde{f}_2} - \alpha^{\tilde{W}}_{\tilde{f'}_1}\alpha^{\tilde{W}_1}_{\tilde{f}_2}\alpha^u_{\tilde{Z}_i\tilde{f}_1}\beta^d_{\tilde{Z}_i\tilde{f}_2}\right], \tag{A.523}$$

$$\mathcal{V}^{(7)}_{\tilde{f'}_1\tilde{f}_2} = |m_{\tilde{W}_j}|m_f\left[-\alpha^{\tilde{W}}_{\tilde{f'}_1}\beta^{\tilde{W}}_{\tilde{f}_2}\alpha^u_{\tilde{Z}_i\tilde{f}_1}\alpha^d_{\tilde{Z}_i\tilde{f}_2} + (-1)^{\theta_j}\beta^{\tilde{W}}_{\tilde{f'}_1}\alpha^{\tilde{W}}_{\tilde{f}_2}\beta^u_{\tilde{Z}_i\tilde{f}_1}\beta^d_{\tilde{Z}_i\tilde{f}_2}\right]. \tag{A.524}$$

The integrals are as in the $\tilde{f'}_1\tilde{f}_1$ case, with the appropriate mass replacements. Similarly, $\Gamma_{\tilde{f'}_1\tilde{f}_2}$ is just the product of each coupling combination $\mathcal{V}^{(k)}_{\tilde{f'}_1\tilde{f}_2}$ with each corresponding integral $I^k_{\tilde{f'}_1\tilde{f}_2}$.

$\underline{\Gamma_{\tilde{f'}_2\tilde{f}_1}}$

$$\mathcal{V}^{(8)}_{\tilde{f'}_2\tilde{f}_1} = |m_{\tilde{Z}_i}||m_{\tilde{W}_j}|m_f m_{f'}(-1)^{\theta_i}(-1)^{\theta_c}\left[\beta^u_{\tilde{Z}_i\tilde{f}_2}\beta^d_{\tilde{Z}_i\tilde{f}_1}\alpha^{\tilde{W}}_{\tilde{f'}_2}\alpha^{\tilde{W}}_{\tilde{f}_1} - \alpha^u_{\tilde{Z}_i\tilde{f}_2}\alpha^d_{\tilde{Z}_i\tilde{f}_1}\beta^{\tilde{W}}_{\tilde{f'}_2}\beta^{\tilde{W}}_{\tilde{f}_1}\right]. \tag{A.525}$$

If the decay is neutralino to chargino:

$$\mathcal{V}^{(1)}_{\tilde{f'}_2\tilde{f}_1} = \frac{1}{2}(-1)^{\theta_i}\left[-\alpha^u_{\tilde{Z}_i\tilde{f}_2}\beta^d_{\tilde{Z}_i\tilde{f}_1}\beta^{\tilde{W}}_{\tilde{f'}_2}\alpha^{\tilde{W}}_{\tilde{f}_1} + \beta^u_{\tilde{Z}_i\tilde{f}_2}\alpha^d_{\tilde{Z}_i\tilde{f}_1}\alpha^{\tilde{W}}_{\tilde{f'}_2}\beta^{\tilde{W}}_{\tilde{f}_1}\right], \tag{A.526}$$

$$\mathcal{V}^{(2)}_{\tilde{f'}_2\tilde{f}_1} = -|m_{\tilde{Z}_i}||m_{\tilde{W}_j}|\left[\alpha^u_{\tilde{Z}_i\tilde{f}_2}\alpha^d_{\tilde{Z}_i\tilde{f}_1}\alpha^{\tilde{W}}_{\tilde{f'}_2}\alpha^{\tilde{W}}_{\tilde{f}_1} - \beta^u_{\tilde{Z}_i\tilde{f}_2}\beta^d_{\tilde{Z}_i\tilde{f}_1}\beta^{\tilde{W}}_{\tilde{f'}_2}\beta^{\tilde{W}}_{\tilde{f}_1}\right], \tag{A.527}$$

$$\mathcal{V}^{(3)}_{\tilde{f'}_2\tilde{f}_1} = (-1)^{\theta_i}m_f m_{f'}\left[-\beta^u_{\tilde{Z}_i\tilde{f}_2}\alpha^d_{\tilde{Z}_i\tilde{f}_1}\beta^{\tilde{W}}_{\tilde{f'}_2}\alpha^{\tilde{W}}_{\tilde{f}_1} + \alpha^u_{\tilde{Z}_i\tilde{f}_2}\beta^d_{\tilde{Z}_i\tilde{f}_1}\alpha^{\tilde{W}}_{\tilde{f}_2}\beta^{\tilde{W}}_{\tilde{f}_1}\right], \tag{A.528}$$

$$\mathcal{V}^{(4)}_{\tilde{f'}_2\tilde{f}_1} = |m_{\tilde{Z}_i}|m_f\left[\alpha^u_{\tilde{Z}_i\tilde{f}_2}\alpha^d_{\tilde{Z}_i\tilde{f}_1}\beta^{\tilde{W}}_{\tilde{f'}_2}\alpha^{\tilde{W}}_{\tilde{f}_1} + (-1)^{\theta_i}\beta^u_{\tilde{Z}_i\tilde{f}_2}\beta^d_{\tilde{Z}_i\tilde{f}_1}\alpha^{\tilde{W}}_{\tilde{f'}_2}\beta^{\tilde{W}}_{\tilde{f}_1}\right], \tag{A.529}$$

$$\mathcal{V}^{(5)}_{\tilde{f'}_2\tilde{f}_1} = (-1)^{\theta_i}m_{f'}|m_{\tilde{W}_j}|\left[\beta^u_{\tilde{Z}_i\tilde{f}_2}\alpha^d_{\tilde{Z}_i\tilde{f}_1}\alpha^{\tilde{W}}_{\tilde{f'}_2}\alpha^{\tilde{W}}_{\tilde{f}_1} - \alpha^u_{\tilde{Z}_i\tilde{f}_2}\beta^d_{\tilde{Z}_i\tilde{f}_1}\beta^{\tilde{W}}_{\tilde{f'}_2}\beta^{\tilde{W}}_{\tilde{f}_1}\right](-1)^{\theta_j}, \tag{A.530}$$

$$\mathcal{V}^{(6)}_{\tilde{f'}_2\tilde{f}_1} = -(-1)^{\theta_i}|m_{\tilde{Z}_i}|m_{f'}\left[-\beta^u_{\tilde{Z}_i\tilde{f}_2}\beta^d_{\tilde{Z}_i\tilde{f}_1}\beta^{\tilde{W}}_{\tilde{f'}_2}\alpha^{\tilde{W}}_{\tilde{f}_1} + (-1)^{\theta_i}\alpha^u_{\tilde{Z}_i\tilde{f}_2}\alpha^d_{\tilde{Z}_i\tilde{f}_1}\alpha^{\tilde{W}}_{\tilde{f'}_2}\beta^{\tilde{W}}_{\tilde{f}_1}\right], \tag{A.531}$$

$$\mathcal{V}^{(7)}_{\tilde{f'}_2\tilde{f}_1} = -|m_{\tilde{W}_j}|m_f\left[\alpha^u_{\tilde{Z}_i\tilde{f}_2}\beta^d_{\tilde{Z}_i\tilde{f}_1}\alpha^{\tilde{W}}_{\tilde{f'}_2}\alpha^{\tilde{W}}_{\tilde{f}_1} + (-1)^{\theta_i}\beta^u_{\tilde{Z}_i\tilde{f}_2}\alpha^d_{\tilde{Z}_i\tilde{f}_1}\beta^{\tilde{W}}_{\tilde{f'}_2}\beta^{\tilde{W}}_{\tilde{f}_1}\right](-1)^{\theta_j}. \tag{A.532}$$

Whilst if the decay is instead chargino to neutralino:

$$\mathcal{V}^{(1)}_{\tilde{f'}_2\tilde{f}_1} = \frac{1}{2}\left[\alpha^u_{\tilde{Z}_i\tilde{f}_2}\beta^d_{\tilde{Z}_i\tilde{f}_1}\beta^{\tilde{W}}_{\tilde{f'}_2}\alpha^{\tilde{W}}_{\tilde{f}_1} + \beta^u_{\tilde{Z}_i\tilde{f}_2}\alpha^d_{\tilde{Z}_i\tilde{f}_1}\alpha^{\tilde{W}}_{\tilde{f'}_2}\beta^{\tilde{W}}_{\tilde{f}_1}\right](-1)^{\theta_i}, \tag{A.533}$$

$$\mathcal{V}^{(2)}_{\tilde{f'}_2\tilde{f}_1} = |m_{\tilde{Z}_i}||m_{\tilde{W}_j}|(-1)^{\theta_i}\left[\alpha^u_{\tilde{Z}_i\tilde{f}_2}\alpha^d_{\tilde{Z}_i\tilde{f}_1}\alpha^{\tilde{W}}_{\tilde{f'}_2}\alpha^{\tilde{W}}_{\tilde{f}_1} + \beta^u_{\tilde{Z}_i\tilde{f}_2}\beta^d_{\tilde{Z}_i\tilde{f}_1}\beta^{\tilde{W}}_{\tilde{f'}_2}\beta^{\tilde{W}}_{\tilde{f}_1}\right], \tag{A.534}$$

$$\mathcal{V}^{(3)}_{\tilde{f'}_2\tilde{f}_1} = -m_f m_{f'}\left[\beta^u_{\tilde{Z}_i\tilde{f}_2}\alpha^d_{\tilde{Z}_i\tilde{f}_1}\beta^{\tilde{W}}_{\tilde{f'}_2}\alpha^{\tilde{W}}_{\tilde{f}_1} + \alpha^u_{\tilde{Z}_i\tilde{f}_2}\beta^d_{\tilde{Z}_i\tilde{f}_1}\alpha^{\tilde{W}}_{\tilde{f}_2}\beta^{\tilde{W}}_{\tilde{f}_1}\right], \tag{A.535}$$

$$\mathcal{V}^{(4)}_{\tilde{f'}_2\tilde{f}_1} = -|m_{\tilde{Z}_i}|m_f\left[\alpha^{\tilde{W}}_{\tilde{f'}_2}\alpha^{\tilde{W}}_{\tilde{f}_1}\beta^u_{\tilde{Z}_i\tilde{f}_2}\alpha^d_{\tilde{Z}_i\tilde{f}_1} + \beta^{\tilde{W}}_{\tilde{f'}_2}\beta^{\tilde{W}}_{\tilde{f}_1}\alpha^u_{\tilde{Z}_i\tilde{f}_2}\beta^d_{\tilde{Z}_i\tilde{f}_1}\right], \tag{A.536}$$

$$\mathcal{V}^{(5)}_{\tilde{f'}_2\tilde{f}_1} = |m_{\tilde{W}_j}|m_{f'}\left[\alpha^{\tilde{W}}_{\tilde{f}_1}\beta^{\tilde{W}}_{\tilde{f'}_2}\alpha^u_{\tilde{Z}_i\tilde{f}_2}\alpha^d_{\tilde{Z}_i\tilde{f}_1} + \alpha^{\tilde{W}}_{\tilde{f'}_2}\beta^{\tilde{W}}_{\tilde{f}_1}\beta^u_{\tilde{Z}_i\tilde{f}_2}\beta^d_{\tilde{Z}_i\tilde{f}_1}\right], \tag{A.537}$$

$$\mathcal{V}^{(6)}_{\tilde{f'}_2\tilde{f}_1} = |m_{\tilde{Z}_i}|m_{f'}\left[\beta^{\tilde{W}}_{\tilde{f'}_2}\beta^{\tilde{W}}_{\tilde{f}_1}\beta^u_{\tilde{Z}_i\tilde{f}_2}\alpha^d_{\tilde{Z}_i\tilde{f}_1} + \alpha^{\tilde{W}}_{\tilde{f'}_2}\alpha^{\tilde{W}_1}_{\tilde{f}_1}\alpha^u_{\tilde{Z}_i\tilde{f}_2}\beta^d_{\tilde{Z}_i\tilde{f}_1}\right], \tag{A.538}$$

$$\mathcal{V}^{(7)}_{\tilde{f'}_2\tilde{f}_1} = -|m_{\tilde{W}_j}|m_f\left[\alpha^{\tilde{W}}_{\tilde{f'}_2}\beta^{\tilde{W}}_{\tilde{f}_1}\alpha^u_{\tilde{Z}_i\tilde{f}_2}\alpha^d_{\tilde{Z}_i\tilde{f}_1} + \beta^{\tilde{W}}_{\tilde{f'}_2}\alpha^{\tilde{W}}_{\tilde{f}_1}\beta^u_{\tilde{Z}_i\tilde{f}_2}\beta^d_{\tilde{Z}_i\tilde{f}_1}\right]. \tag{A.539}$$

Again, the integrals are as in the $\tilde{f'}_1\tilde{f}_1$ case with the obvious mass replacements. $\Gamma_{\tilde{f'}_2\tilde{f}_1}$ is just the product of each coupling combination $\mathcal{V}^{(k)}_{\tilde{f'}_2\tilde{f}_1}$ with each corresponding integral $I^k_{\tilde{f'}_2\tilde{f}_1}$.

$\underline{\Gamma_{\tilde{f'}_2\tilde{f}_2}}$

$$\mathcal{V}^{(8)}_{\tilde{f'}_2\tilde{f}_2} = -|m_{\tilde{Z}_i}||m_{\tilde{W}_j}|m_f m_{f'}(-1)^{\theta_i}(-1)^{\theta_j}\left[\beta^u_{\tilde{Z}_i\tilde{f}_2}\beta^d_{\tilde{Z}_i\tilde{f}_2}\alpha^{\tilde{W}}_{\tilde{f'}_2}\alpha^{\tilde{W}}_{\tilde{f}_2} - \alpha^u_{\tilde{Z}_i\tilde{f}_2}\alpha^d_{\tilde{Z}_i\tilde{f}_2}\beta^{\tilde{W}}_{\tilde{f'}_2}\beta^{\tilde{W}}_{\tilde{f}_2}\right]. \tag{A.540}$$

If the decay is neutralino to chargino:

$$\mathcal{V}^{(1)}_{\tilde{f'}_2\tilde{f}_2} = \frac{1}{2}(-1)^{\theta_j}\left[-\alpha^u_{\tilde{Z}_i\tilde{f}_2}\beta^d_{\tilde{Z}_i\tilde{f}_2}\beta^{\tilde{W}}_{\tilde{f'}_2}\alpha^{\tilde{W}}_{\tilde{f}_2} + (-1)^{\theta_i}\beta^u_{\tilde{Z}_i\tilde{f}_2}\alpha^d_{\tilde{Z}_i\tilde{f}_2}\alpha^{\tilde{W}}_{\tilde{f'}_2}\beta^{\tilde{W}}_{\tilde{f}_2}\right], \tag{A.541}$$

$$\mathcal{V}^{(2)}_{\tilde{f'}_2\tilde{f}_2} = |m_{\tilde{Z}_i}||m_{\tilde{W}_j}|(-1)^{\theta_j}\left[\alpha^u_{\tilde{Z}_i\tilde{f}_2}\alpha^d_{\tilde{Z}_i\tilde{f}_2}\alpha^{\tilde{W}}_{\tilde{f'}_2}\alpha^{\tilde{W}}_{\tilde{f}_2} - \beta^u_{\tilde{Z}_i\tilde{f}_2}\beta^d_{\tilde{Z}_i\tilde{f}_2}\beta^{\tilde{W}}_{\tilde{f'}_2}\beta^{\tilde{W}}_{\tilde{f}_2}\right], \tag{A.542}$$

$$\mathcal{V}^{(3)}_{\tilde{f'}_2\tilde{f}_2} = -m_f m_{f'}\left[-(-1)^{\theta_i}\beta^u_{\tilde{Z}_i\tilde{f}_2}\alpha^d_{\tilde{Z}_i\tilde{f}_2}\beta^{\tilde{W}}_{\tilde{f'}_2}\alpha^{\tilde{W}}_{\tilde{f}_2} + \alpha^u_{\tilde{Z}_i\tilde{f}_2}\beta^d_{\tilde{Z}_i\tilde{f}_2}\alpha^{\tilde{W}}_{\tilde{f}_2}\beta^{\tilde{W}}_{\tilde{f}_2}\right], \tag{A.543}$$

$$\mathcal{V}^{(4)}_{\tilde{f'}_2\tilde{f}_2} = -|m_{\tilde{Z}_i}|m_f(-1)^{\theta_j}\left[\alpha^u_{\tilde{Z}_i\tilde{f}_2}\alpha^d_{\tilde{Z}_i\tilde{f}_2}\beta^{\tilde{W}}_{\tilde{f'}_2}\alpha^{\tilde{W}}_{\tilde{f}_2} - (-1)^{\theta_i}\beta^u_{\tilde{Z}_i\tilde{f}_2}\beta^d_{\tilde{Z}_i\tilde{f}_2}\alpha^{\tilde{W}}_{\tilde{f'}_2}\beta^{\tilde{W}}_{\tilde{f}_2}\right], \tag{A.544}$$

$$\mathcal{V}^{(5)}_{\tilde{f'}_2\tilde{f}_2} = -m_{f'}|m_{\tilde{W}_j}|\left[(-1)^{\theta_i}(-1)^{\theta_j}\beta^u_{\tilde{Z}_i\tilde{f}_2}\alpha^d_{\tilde{Z}_i\tilde{f}_2}\alpha^{\tilde{W}}_{\tilde{f'}_2}\alpha^{\tilde{W}}_{\tilde{f}_2} + \alpha^u_{\tilde{Z}_i\tilde{f}_2}\beta^d_{\tilde{Z}_i\tilde{f}_2}\beta^{\tilde{W}}_{\tilde{f'}_2}\beta^{\tilde{W}}_{\tilde{f}_2}\right], \tag{A.545}$$

$$\mathcal{V}^{(6)}_{\tilde{f'}_2\tilde{f}_2} = |m_{\tilde{Z}_i}|m_{f'}\left[(-1)^{\theta_i}\beta^u_{\tilde{Z}_i\tilde{f}_2}\beta^d_{\tilde{Z}_i\tilde{f}_2}\beta^{\tilde{W}}_{\tilde{f'}_2}\alpha^{\tilde{W}}_{\tilde{f}_2} - \alpha^u_{\tilde{Z}_i\tilde{f}_2}\alpha^d_{\tilde{Z}_i\tilde{f}_2}\alpha^{\tilde{W}}_{\tilde{f'}_2}\beta^{\tilde{W}}_{\tilde{f}_2}\right], \tag{A.546}$$

$$\mathcal{V}^{(7)}_{\tilde{f'}_2\tilde{f}_2} = |m_{\tilde{W}_j}|m_f\left[\alpha^u_{\tilde{Z}_i\tilde{f}_2}\beta^d_{\tilde{Z}_i\tilde{f}_2}\alpha^{\tilde{W}}_{\tilde{f'}_2}\alpha^{\tilde{W}}_{\tilde{f}_2} - \beta^u_{\tilde{Z}_i\tilde{f}_2}\alpha^d_{\tilde{Z}_i\tilde{f}_2}\beta^{\tilde{W}}_{\tilde{f'}_2}\beta^{\tilde{W}}_{\tilde{f}_2}\right](-1)^{\theta_j}. \tag{A.547}$$

Whilst if the decay is instead chargino to neutralino:

$$\mathcal{V}^{(1)}_{\tilde{f'}_2\tilde{f}_2} = -\frac{1}{2}\left[(-1)^{\theta_j}\alpha^u_{\tilde{Z}_i\tilde{f}_2}\beta^d_{\tilde{Z}_i\tilde{f}_2}\beta^{\tilde{W}}_{\tilde{f'}_2}\alpha^{\tilde{W}}_{\tilde{f}_2} - \beta^u_{\tilde{Z}_i\tilde{f}_2}\alpha^d_{\tilde{Z}_i\tilde{f}_2}\alpha^{\tilde{W}}_{\tilde{f'}_2}\beta^{\tilde{W}}_{\tilde{f}_2}\right], \tag{A.548}$$

$$\mathcal{V}^{(2)}_{\tilde{f'}_2\tilde{f}_2} = -|m_{\tilde{Z}_i}||m_{\tilde{W}_j}(-1)^{\theta_i}|\left[(-1)^{\theta_j}\alpha^u_{\tilde{Z}_i\tilde{f}_2}\alpha^d_{\tilde{Z}_i\tilde{f}_2}\alpha^{\tilde{W}}_{\tilde{f'}_2}\alpha^{\tilde{W}}_{\tilde{f}_2} - \beta^u_{\tilde{Z}_i\tilde{f}_2}\beta^d_{\tilde{Z}_i\tilde{f}_2}\beta^{\tilde{W}}_{\tilde{f'}_2}\beta^{\tilde{W}}_{\tilde{f}_2}\right], \tag{A.549}$$

$$\mathcal{V}^{(3)}_{\tilde{f'}_2\tilde{f}_2} = m_f m_{f'}\left[-(-1)^{\theta_j}\beta^u_{\tilde{Z}_i\tilde{f}_2}\alpha^d_{\tilde{Z}_i\tilde{f}_2}\beta^{\tilde{W}}_{\tilde{f'}_2}\alpha^{\tilde{W}}_{\tilde{f}_2} - \alpha^u_{\tilde{Z}_i\tilde{f}_2}\beta^d_{\tilde{Z}_i\tilde{f}_2}\alpha^{\tilde{W}}_{\tilde{f}_2}\beta^{\tilde{W}}_{\tilde{f}_2}\right], \tag{A.550}$$

$$\mathcal{V}^{(4)}_{\tilde{f'}_2\tilde{f}_2} = |m_{\tilde{Z}_i}|m_f(-1)^{\theta_j}\left[\alpha^{\tilde{W}}_{\tilde{f'}_2}\alpha^{\tilde{W}}_{\tilde{f}_2}\beta^u_{\tilde{Z}_i\tilde{f}_2}\alpha^d_{\tilde{Z}_i\tilde{f}_2} + \beta^{\tilde{W}}_{\tilde{f'}_2}\beta^{\tilde{W}}_{\tilde{f}_2}\alpha^u_{\tilde{Z}_i\tilde{f}_2}\beta^d_{\tilde{Z}_i\tilde{f}_2}\right], \tag{A.551}$$

$$\mathcal{V}^{(5)}_{\tilde{f'}_2\tilde{f}_2} = |m_{\tilde{W}_j}|m_{f'}\left[\alpha^{\tilde{W}}_{\tilde{f}_2}\beta^{\tilde{W}}_{\tilde{f'}_2}\alpha^u_{\tilde{Z}_i\tilde{f}_2}\alpha^d_{\tilde{Z}_i\tilde{f}_2} - \alpha^{\tilde{W}}_{\tilde{f'}_2}\beta^{\tilde{W}}_{\tilde{f}_2}\beta^u_{\tilde{Z}_i\tilde{f}_2}\beta^d_{\tilde{Z}_i\tilde{f}_2}\right], \tag{A.552}$$

$$\mathcal{V}^{(6)}_{\tilde{f'}_2\tilde{f}_2} = (-1)^{\theta_j}|m_{\tilde{Z}_i}|m_{f'}\left[\beta^{\tilde{W}}_{\tilde{f'}_2}\beta^{\tilde{W}}_{\tilde{f}_2}\beta^u_{\tilde{Z}_i\tilde{f}_2}\alpha^d_{\tilde{Z}_i\tilde{f}_2} + \alpha^{\tilde{W}}_{\tilde{f'}_2}\alpha^{\tilde{W}_1}_{\tilde{f}_2}\alpha^u_{\tilde{Z}_i\tilde{f}_2}\beta^d_{\tilde{Z}_i\tilde{f}_2}\right], \tag{A.553}$$

$$\mathcal{V}^{(7)}_{\tilde{f'}_2\tilde{f}_2} = |m_{\tilde{W}_j}|m_f\left[-\alpha^{\tilde{W}}_{\tilde{f'}_2}\beta^{\tilde{W}}_{\tilde{f}_2}\alpha^u_{\tilde{Z}_i\tilde{f}_2}\alpha^d_{\tilde{Z}_i\tilde{f}_2} + \beta^{\tilde{W}}_{\tilde{f'}_2}\alpha^{\tilde{W}}_{\tilde{f}_2}\beta^u_{\tilde{Z}_i\tilde{f}_2}\beta^d_{\tilde{Z}_i\tilde{f}_2}\right]. \tag{A.554}$$

The integrals are again as in the $\tilde{f'}_1\tilde{f}_1$ case with the obvious mass replacements and $\Gamma_{\tilde{f'}_2\tilde{f}_2}$ is just the product of each coupling combination $\mathcal{V}^{(k)}_{\tilde{f'}_2\tilde{f}_2}$ with each corresponding integral $I^k_{\tilde{f'}_2\tilde{f}_2}$.

$\underline{\Gamma_{WH^\pm}}$

For this contribution the relevant coupling combinations are:

$$\mathcal{V}^{(1)}_{WH^\pm} = -(\mathcal{C}^R_{\tilde{W}\tilde{Z}W}\omega^R_{H^+\tilde{W}^+\tilde{Z}} + \mathcal{C}^L_{\tilde{W}\tilde{Z}W}\omega^L_{H^+\tilde{W}^+\tilde{Z}})\frac{g}{\sqrt{2}}\mathcal{C}^u_{H^+ff'}|m_{\tilde{W}_j}|m_{f'}(-1)^{\theta_c}, \tag{A.555}$$

$$\mathcal{V}^{(2)}_{WH^\pm} = (\mathcal{C}^L_{\tilde{W}\tilde{Z}W}\omega^R_{H^+\tilde{W}^+\tilde{Z}} + \mathcal{C}^R_{\tilde{W}\tilde{Z}W}\omega^L_{H^+\tilde{W}^+\tilde{Z}})\frac{g}{\sqrt{2}}\mathcal{C}^d_{H^+ff'}|m_{\tilde{Z}_i}|m_f(-1)^{\theta_i}(-1)^{\theta_j}(-1)^{\theta_c}, \tag{A.556}$$

$$\mathcal{V}^{(3)}_{WH^\pm} = (\mathcal{C}^R_{\tilde{W}\tilde{Z}W}\omega^R_{H^+\tilde{W}^+\tilde{Z}} + \mathcal{C}^L_{\tilde{W}\tilde{Z}W}\omega^L_{H^+\tilde{W}^+\tilde{Z}})\frac{g}{\sqrt{2}}\mathcal{C}^d_{H^+ff'}|m_{\tilde{W}_j}|m_f(-1)^{\theta_c}, \tag{A.557}$$

$$\mathcal{V}^{(4)}_{WH^\pm} = -(\mathcal{C}^L_{\tilde{W}\tilde{Z}W}\omega^R_{H^+\tilde{W}^+\tilde{Z}} + \mathcal{C}^R_{\tilde{W}\tilde{Z}W}\omega^L_{H^+\tilde{W}^+\tilde{Z}})\frac{g}{\sqrt{2}}\mathcal{C}^u_{H^+ff'}|m_{\tilde{Z}_i}|m_{f'}(-1)^{\theta_i}(-1)^{\theta_j}(-1)^{\theta_c}. \tag{A.558}$$

The integrals are as follows with the following variables:

$$E_{upper3} = \frac{1}{2|m_{\tilde{Z}_i}|}(m^2_{\tilde{Z}_i} + m^2_{\tilde{W}_j} - m^2_f - m^2_{f'} - 2m_f m_{f'}), \tag{A.559}$$

$$s = m^2_{\tilde{Z}_i} + m^2_{\tilde{W}_j} - 2|m_{\tilde{Z}_i}|E, \tag{A.560}$$

$$\lambda = \sqrt{(s-(m_f+m_{f'})^2)(s-(m_f-m_{f'})^2)}, \tag{A.561}$$

$$\mathcal{A} = 2|m_{\tilde{Z}_i}E + m^2_f + m^2_{f'} - (m^2_{\tilde{Z}_i} - m^2_{\tilde{W}_j})(m^2_f - m^2_{f'})/s, \tag{A.562}$$

$$\mathcal{B} = \frac{2|m_{\tilde{Z}_i}|}{s}\lambda\sqrt{E^2 - m^2_{\tilde{W}_j}}, \tag{A.563}$$

$$I^1_{WH^\pm} = 2|m_{\tilde{Z}_i}|\int_{|m_{\tilde{W}_j}|}^{E_{upper3}} dE \frac{-\frac{1}{2}\mathcal{A}\mathcal{B} + (m^2_{\tilde{Z}_i} + m^2_f)\mathcal{B}}{(s-m^2_W)(s-m^2_{H^\pm})}, \tag{A.564}$$

$$I^2_{WH^\pm} = 2|m_{\tilde{Z}_i}|\int_{|m_{\tilde{W}_j}|}^{E_{upper3}} dE \frac{\frac{1}{2}\mathcal{A}\mathcal{B} - (m^2_{\tilde{W}_j} + m^2_{f'})\mathcal{B}}{(s-m^2_W)(s-m^2_{H^\pm})}, \tag{A.565}$$

$$I^3_{WH^\pm} = 2|m_{\tilde{Z}_i}|\int_{|m_{\tilde{W}_j}|}^{E_{upper3}} dE \frac{-\frac{1}{2}\mathcal{A}\mathcal{B} + (m^2_{\tilde{Z}_i} - 2|m_{\tilde{Z}_i}|E - m^2_f)\mathcal{B}}{(s-m^2_W)(s-m^2_{H^\pm})}, \tag{A.566}$$

$$I^4_{WH^\pm} = 2|m_{\tilde{Z}_i}|\int_{|m_{\tilde{W}_j}|}^{E_{upper3}} dE \frac{-\frac{1}{2}\mathcal{A}\mathcal{B} - (m^2_{\tilde{Z}_j} - 2|m_{\tilde{Z}_i}| - m^2_{f'})\mathcal{B}}{(s-m^2_W)(s-m^2_{H^\pm})}, \tag{A.567}$$

So overall:

$$\Gamma_{WH^\pm} = \mathcal{V}^{(1)}_{WH^\pm}I^1_{WH^\pm}(-1)^{\theta_c}(-1)^{\theta_j} + \mathcal{V}^{(2)}_{WH^\pm}I^2_{WH^\pm}(-1)^{\theta_c}(-1)^{\theta_j} + \mathcal{V}^{(3)}_{WH^\pm}I^3_{WH^\pm} + \mathcal{V}^{(4)}_{WH^\pm}I^4_{WH^\pm}. \tag{A.568}$$

$\underline{\Gamma_{WG}}$

Here everything is as above but in the coupling combinations we must make the appropriate replacements $\omega^{L/R}_{H^+\tilde{W}^+\tilde{Z}} \to \omega^{L/R}_{G\tilde{W}\tilde{Z}}$, whilst in the integrals we make the change $m_{H^\pm} \to m_{Goldstone} = m_W$. However because of subtle differences in the definitions of the couplings, the overall contribution here is given by:

$$\Gamma_{WG} = \mathcal{V}^{(1)}_{WG}I^1_{WG} + \mathcal{V}^{(2)}_{WG}I^2_{WG} + \mathcal{V}^{(3)}_{WG}I^3_{WG} + \mathcal{V}^{(4)}_{WG}I^4_{WG}. \tag{A.569}$$

$\underline{\Gamma_{W\tilde{f}'_1}}$

The coupling combinations are:

$$\mathcal{V}^{(1)}_{W\tilde{f}'_1} = -2\mathcal{C}^L_{\tilde{W}\tilde{Z}W}\alpha^u_{\tilde{Z}_i\tilde{f}_1}\frac{g}{\sqrt{2}}\beta^{\tilde{W}_j}_{\tilde{f}'_1}|m_{\tilde{Z}_i}|m_f(-1)^{\theta_j}, \tag{A.570}$$

$$\mathcal{V}^{(2)}_{W\tilde{f}'_1} = -2\mathcal{C}^L_{\tilde{W}\tilde{Z}W}\beta_{\tilde{Z}_i\tilde{f}_1}\frac{g}{\sqrt{2}}\alpha^{\tilde{W}_j}_{\tilde{f}_1}m_{f'}|m_{\tilde{W}_j}|(-1)^{\theta_c}, \tag{A.571}$$

$$\mathcal{V}^{(3)}_{W\tilde{f}'_1} = 2\mathcal{C}^R_{\tilde{W}\tilde{Z}W}\alpha^u_{\tilde{Z}_i\tilde{f}_1}\frac{g}{\sqrt{2}}\alpha^{\tilde{W}_j}_{\tilde{f}'_1}(-1)^{\theta_i}(-1)^{\theta_j}(-1)^{\theta_c}, \tag{A.572}$$

$$\mathcal{V}^{(4)}_{W\tilde{f}'_1} = (-1)^{\theta_i}4\mathcal{C}^R_{\tilde{W}\tilde{Z}W}\beta^u_{\tilde{Z}_i\tilde{f}_1}\frac{g}{\sqrt{2}}\alpha^{\tilde{W}_j}_{\tilde{f}'_1}|m_{\tilde{Z}_i}|m_{f'}(-1)^{\theta_c}, \tag{A.573}$$

$$\mathcal{V}^{(5)}_{W\tilde{f}'_1} = 4\mathcal{C}^R_{\tilde{W}\tilde{Z}W}\alpha^u_{\tilde{Z}_i\tilde{f}_1}\frac{g}{\sqrt{2}}\beta^{\tilde{W}_j}_{\tilde{f}'_1}m_f|m_{\tilde{W}_j}|(-1)^{\theta_i}, \tag{A.574}$$

$$\mathcal{V}^{(6)}_{W\tilde{f}'_1} = -2\mathcal{C}^L_{\tilde{W}\tilde{Z}W}\alpha^u_{\tilde{Z}_i\tilde{f}_1}\frac{g}{\sqrt{2}}\alpha^{\tilde{W}_j}_{\tilde{f}'_1}|m_{\tilde{Z}_i}||m_{\tilde{W}_j}|(-1)^{\theta_c}, \tag{A.575}$$

$$\mathcal{V}^{(7)}_{W\tilde{f}'_1} = -2\mathcal{C}^L_{\tilde{W}\tilde{Z}W}\beta^u_{\tilde{Z}_i\tilde{f}_1}\frac{g}{\sqrt{2}}\beta^{\tilde{W}_f}_{\tilde{f}'_1}m_{f'}m_f, \tag{A.576}$$

$$\mathcal{V}^{(8)}_{W\tilde{f}'_1} = 8\mathcal{C}^R_{\tilde{W}\tilde{Z}W}\beta^u_{\tilde{Z}_i\tilde{f}_1}\frac{g}{\sqrt{2}}\beta^{\tilde{W}_1}_{\tilde{f}'_1}|m_{\tilde{Z}_i}|m_{f'}m_f|m_{\tilde{W}_j}|(-1)^{\theta_i}(-1)^{\theta_j}. \tag{A.577}$$

The integrals are as follows with:

$$s = m^2_{\tilde{Z}_i} + m^2_{\tilde{W}_j} - 2|m_{\tilde{Z}_i}|E, \tag{A.578}$$

$$\lambda = \sqrt{(s-(m_{f'}+m_f)^2)(s-(m_{f'}-m_f)^2)}, \tag{A.579}$$

$$A = m^2_{f'} + m^2_f + 2|m_{\tilde{Z}_i}|E + (m^2_{\tilde{Z}_i} - m^2_{\tilde{W}_j})(m^2_f - m^2_{f'})/s, \tag{A.580}$$

$$B = 2|m_{\tilde{Z}_i}|\lambda\sqrt{E^2 - m^2_{\tilde{W}_j}}, \tag{A.581}$$

$$Z = \frac{A + B - 2m^2_{\tilde{f}'_1}}{A - B - 2m^2_{\tilde{f}'_1}}. \tag{A.582}$$

$$I^1_{W\tilde{f}'_1} = -2|m_{\tilde{Z}_i}|\int_{|m_{\tilde{W}_j}|}^{E_{upper3}} dE\frac{B + (m^2_{\tilde{f}'_1} + m^2_{\tilde{W}_j} - 2|m_{\tilde{Z}_i}|E - m^2_f)\log(Z)}{s - m^2_W}, \tag{A.583}$$

$$I^2_{W\tilde{f}'_1} = 2|m_{\tilde{Z}_i}|\int_{|m_{\tilde{W}_j}|}^{E_{upper3}} dE\frac{B + (m^2_{\tilde{f}'_1} + m^2_{\tilde{Z}_i} - 2|m_{\tilde{Z}_i}|E - m^2_{f'})\log(Z)}{s - m^2_W}, \tag{A.584}$$

$$\begin{aligned} I^3_{W\tilde{f}'_1} = 2|m_{\tilde{Z}_i}|\int_{|m_{\tilde{W}_j}|}^{E_{upper3}} dE\Big[&\{m^2_{\tilde{Z}_i} + m^2_f + m^2_{f'} + m^2_{\tilde{W}_j} - 1.5m^2_{\tilde{f}'_1} - 0.25(A+B)\}(\frac{1}{2}(A+B) - m^2_{\tilde{f}'_1} \\ &- (m^2_{\tilde{Z}_i} + m^2_f + m^2_{f'} + m^2_{\tilde{W}_j} - 1.5m^2_{\tilde{f}'_1} - 0.25(A-B))(\frac{1}{2}(A-B) - m^2_{\tilde{f}'_1}) \\ &+ (m^2_{\tilde{Z}_i} + m^2_{f'} - m^2_{\tilde{f}'_1})(m^2_{\tilde{f}'_1} - m^2_f - m^2_{\tilde{W}_j})\log(Z)\Big]\frac{1}{s - m^2_W}, \end{aligned} \tag{A.585}$$

$$I^4_{W\tilde{f}'_1} = 2|m_{\tilde{Z}_i}|\int_{|m_{\tilde{W}_j}|}^{E_{upper3}} dE\frac{B + (m^2_{\tilde{f}'} - m^2_f - m^2_{\tilde{W}_j})\log(Z)}{s - m^2_W}, \tag{A.586}$$

$$I^5_{W\tilde{f}'_1} = -2|m_{\tilde{Z}_i}|\int_{|m_{\tilde{W}_j}|}^{E_{upper3}} dE\frac{B + (m^2_{\tilde{f}'_1} - m^2_{\tilde{Z}_i} - m^2_{f'})\log(Z)}{s - m^2_W}, \tag{A.587}$$

$$I^6_{W\tilde{f'}_1} = 2|m_{\tilde{Z}_i}| \int_{|m_{\tilde{W}_j}|}^{E_{upper3}} dE \frac{(s - m^2_{f'} - m^2_f)\log(Z)}{s - m^2_W}, \tag{A.588}$$

$$I^7_{W\tilde{f'}_1} = 2|m_{\tilde{Z}_i}| \int_{|m_{\tilde{W}_j}|}^{E_{upper3}} dE \frac{2|m_{\tilde{Z}_i}|E\log(Z)}{s - m^2_W}, \tag{A.589}$$

$$I^8_{W\tilde{f'}_1} = 2|m_{\tilde{Z}_i}| \int_{|m_{\tilde{W}_j}|}^{E_{upper3}} dE \frac{\log(Z)}{s - m^2_W}. \tag{A.590}$$

Therefore the overall contribution is:

$$\begin{aligned}\Gamma_{W\tilde{f'}_1} =& \mathcal{V}^{(1)}_{W\tilde{f'}_1} I^1_{W\tilde{f'}_1} + \mathcal{V}^{(2)}_{W\tilde{f'}_1} I^2_{W\tilde{f'}_1} + \mathcal{V}^{(3)}_{W\tilde{f'}_1} I^3_{W\tilde{f'}_1} + \mathcal{V}^{(4)}_{W\tilde{f'}_1} I^4_{W\tilde{f'}_1} \\ &+ \mathcal{V}^{(5)}_{W\tilde{f'}_1} I^5_{W\tilde{f'}_1} + \mathcal{V}^{(6)}_{W\tilde{f'}_1} I^6_{W\tilde{f'}_1} + \mathcal{V}^{(7)}_{W\tilde{f'}_1} I^7_{W\tilde{f'}_1} + \mathcal{V}^{(8)}_{W\tilde{f'}_1} I^8_{W\tilde{f'}_1}.\end{aligned} \tag{A.591}$$

$\underline{\Gamma_{W\tilde{f'}_2}}$

The coupling combinations here are:

$$\mathcal{V}^{(1)}_{W\tilde{f'}_2} = 2\mathcal{C}^L_{\tilde{W}\tilde{Z}W}\alpha^u_{\tilde{Z}_i\tilde{f}_2}\frac{g}{\sqrt{2}}\beta^{\tilde{W}_j}_{\tilde{f'}_2}|m_{\tilde{Z}_i}|m_f(-1)^{\theta_j}(-1)^{\theta_c}, \tag{A.592}$$

$$\mathcal{V}^{(2)}_{W\tilde{f'}_2} = 2\mathcal{C}^L_{\tilde{W}\tilde{Z}W}\beta^u_{\tilde{Z}_i\tilde{f}_2}\frac{g}{\sqrt{2}}\alpha^{\tilde{W}_j}_{\tilde{f'}_2}m_{f'}|m_{\tilde{W}_j}|(-1)^{\theta_i}(-1)^{\theta_j}, \tag{A.593}$$

$$\mathcal{V}^{(3)}_{W\tilde{f'}_2} = 2\mathcal{C}^R_{\tilde{W}\tilde{Z}W}\alpha^u_{\tilde{Z}_i\tilde{f}_2}\frac{g}{\sqrt{2}}\alpha^{\tilde{W}_j}_{\tilde{f'}_2}(-1)^{\theta_i}, \tag{A.594}$$

$$\mathcal{V}^{(4)}_{W\tilde{f'}_2} = -4\mathcal{C}^R_{\tilde{W}\tilde{Z}W}\beta^u_{\tilde{Z}_i\tilde{f}_2}\frac{g}{\sqrt{2}}\alpha^{\tilde{W}_j}_{\tilde{f'}_2}|m_{\tilde{Z}_i}|m_{f'}, \tag{A.595}$$

$$\mathcal{V}^{(5)}_{W\tilde{f'}_2} = -4\mathcal{C}^R_{\tilde{W}\tilde{Z}W}\alpha^u_{\tilde{Z}_i\tilde{f}_2}\frac{g}{\sqrt{2}}\beta^{\tilde{W}_j}_{\tilde{f'}_2}m_f|m_{\tilde{W}_j}|(-1)^{\theta_i}(-1)^{\theta_c}, \tag{A.596}$$

$$\mathcal{V}^{(6)}_{W\tilde{f'}_2} = -2\mathcal{C}^L_{\tilde{W}\tilde{Z}W}\alpha^u_{\tilde{Z}_i\tilde{f}_2}\frac{g}{\sqrt{2}}\alpha^{\tilde{W}_j}_{\tilde{f'}_2}|m_{\tilde{Z}_i}||m_{\tilde{W}_j}|(-1)^{\theta_j}, \tag{A.597}$$

$$\mathcal{V}^{(7)}_{W\tilde{f'}_2} = -2\mathcal{C}^L_{\tilde{W}\tilde{Z}W}\beta^u_{\tilde{Z}_i\tilde{f}_2}\frac{g}{\sqrt{2}}\beta^{\tilde{W}_j}_{\tilde{f'}_2}m_{f'}m_f(-1)^{\theta_i}(-1)^{\theta_j}(-1)^{\theta_c}, \tag{A.598}$$

$$\mathcal{V}^{(8)}_{W\tilde{f'}_2} = 8\mathcal{C}^R_{\tilde{W}\tilde{Z}W}\beta^u_{\tilde{Z}_i\tilde{f}_2}\frac{g}{\sqrt{2}}\beta^{\tilde{W}_j}_{\tilde{f'}_2}|m_{\tilde{Z}_i}|m_{f'}m_f|m_{\tilde{W}_j}|(-1)^{\theta_c}. \tag{A.599}$$

The integrals here are exactly as for $W\tilde{f'}_1$ with the change $m_{\tilde{f'}_1} \to m_{\tilde{f'}_2}$. As above $\Gamma_{W\tilde{f'}_2}$ is then the sum of the products of coupling combinations, $\mathcal{V}^{(i)}$ and integrals, $I^i_{W\tilde{f'}_2}$.

$\underline{\Gamma_{W\tilde{f}_1}}$

Here the coupling combinations required are:

$$\mathcal{V}^{(6)}_{W\tilde{f}_1} = -2\mathcal{C}^R_{\tilde{W}\tilde{Z}W}\alpha^d_{\tilde{Z}_i\tilde{f}_1}\frac{g}{\sqrt{2}}\alpha^{\tilde{W}_j}_{\tilde{f}_1}|m_{\tilde{Z}_i}||m_{\tilde{W}_j}|(-1)^{\theta_c}, \tag{A.600}$$

$$\mathcal{V}^{(7)}_{W\tilde{f}_1} = -2\mathcal{C}^R_{\tilde{W}\tilde{Z}W}\beta^d_{\tilde{Z}_i\tilde{f}_1}\frac{g}{\sqrt{2}}\beta^{\tilde{W}_j}_{\tilde{f}_1}m_f m_{f'}, \tag{A.601}$$

$$\mathcal{V}^{(8)}_{W\tilde{f}_1} = 8\mathcal{C}^L_{\tilde{W}\tilde{Z}W}\beta^d_{\tilde{Z}_i\tilde{f}_1}\frac{g}{\sqrt{2}}\beta^{\tilde{W}_j}_{\tilde{f}_1}|m_{\tilde{Z}_i}|m_f m_{f'}|m_{\tilde{W}_j}|(-1)^{\theta_i}(-1)^{\theta_j}. \tag{A.602}$$

The other coupling combinations depend upon if it is a neutralino decaying into a chargino or a chargino decaying into a neutralino, for a neutralino decaying:

$$\mathcal{V}^{(1)}_{W\tilde{f}_1} = -2\mathcal{C}^R_{\tilde{W}\tilde{Z}W}\alpha^d_{\tilde{Z}_i\tilde{f}_1}\frac{g}{\sqrt{2}}\beta^{\tilde{W}_j}_{\tilde{f}_1}|m_{\tilde{Z}_i}|m_{f'}, \tag{A.603}$$

$$\mathcal{V}^{(2)}_{W\tilde{f}_1} = -2\mathcal{C}^R_{\tilde{W}\tilde{Z}W}\beta^d_{\tilde{Z}_i\tilde{f}_1}\frac{g}{\sqrt{2}}\alpha^{\tilde{W}_j}_{\tilde{f}_1}m_f|m_{\tilde{W}_j}|(-1)^{\theta_j}, \tag{A.604}$$

$$\mathcal{V}^{(3)}_{W\tilde{f}_1} = 2\mathcal{C}^R_{\tilde{W}\tilde{Z}W}\alpha^d_{\tilde{Z}_i\tilde{f}_1}\frac{g}{\sqrt{2}}\alpha^{\tilde{W}_j}_{\tilde{f}_1}, \tag{A.605}$$

$$\mathcal{V}^{(4)}_{W\tilde{f}_1} = 4\mathcal{C}^L_{\tilde{W}\tilde{Z}W}\beta^d_{\tilde{Z}_i\tilde{f}_1}\frac{g}{\sqrt{2}}\alpha^{\tilde{W}_j}_{\tilde{f}_1}|m_{\tilde{Z}_i}|m_f(-1)^{\theta_i}, \tag{A.606}$$

$$\mathcal{V}^{(5)}_{W\tilde{f}_1} = 4\mathcal{C}^L_{\tilde{W}\tilde{Z}W}\alpha^d_{\tilde{Z}_i\tilde{f}_1}\frac{g}{\sqrt{2}}\beta^{\tilde{W}_j}_{\tilde{f}_1}m_{f'}|m_{\tilde{W}_j}|(-1)^{\theta_i}(-1)^{\theta_j}, \tag{A.607}$$

whilst if it's a chargino decaying:

$$\mathcal{V}^{(1)}_{W\tilde{f}_1} = 2\mathcal{C}^R_{\tilde{W}\tilde{Z}W}\beta^d_{\tilde{Z}_i\tilde{f}_1}\alpha^{\tilde{W}_j}_{\tilde{f}_1}\frac{g}{\sqrt{2}}|m_{\tilde{Z}_i}|m_{f'}(-1)^{\theta_i}, \tag{A.608}$$

$$\mathcal{V}^{(2)}_{W\tilde{f}_1} = -2\mathcal{C}^R_{\tilde{W}\tilde{Z}W}\alpha^d_{\tilde{Z}_i\tilde{f}_1}\beta^{\tilde{W}_j}_{\tilde{f}_1}\frac{g}{\sqrt{2}}m_f|m_{\tilde{W}_j}|, \tag{A.609}$$

$$\mathcal{V}^{(3)}_{W\tilde{f}_1} = -2\mathcal{C}^L_{\tilde{W}\tilde{Z}W}\alpha^d_{\tilde{Z}_i\tilde{f}_1}\alpha^{\tilde{W}_j}_{\tilde{f}_1}\frac{g}{\sqrt{2}}(-1)^{\theta_i}(-1)^{\theta_j}, \tag{A.610}$$

$$\mathcal{V}^{(4)}_{W\tilde{f}_1} = 4\mathcal{C}^L_{\tilde{W}\tilde{Z}W}\alpha^d_{\tilde{Z}_i\tilde{f}_1}\beta^{\tilde{W}_j}_{\tilde{f}_1}\frac{g}{\sqrt{2}}|m_{\tilde{Z}_i}|m_f(-1)^{\theta_i}(-1)^{\theta_j}, \tag{A.611}$$

$$\mathcal{V}^{(5)}_{W\tilde{f}_1} = -4\mathcal{C}^L_{\tilde{W}\tilde{Z}W}\beta^d_{\tilde{Z}_i\tilde{f}_1}\alpha^{\tilde{W}_j}_{\tilde{f}_1}\frac{g}{\sqrt{2}}m_{f'}|m_{\tilde{W}_j}|(-1)^{\theta_j}. \tag{A.612}$$

Then the integrals are exactly as for $W\tilde{f'}_1$ but with the changes $m_{f'} \leftrightarrow m_f$, $m_{\tilde{f'}_1} \to m_{\tilde{f}_1}$. $\Gamma_{W\tilde{f}_1}$ is, as above, just the sum of the products of coupling combinations and corresponding integrals.

$\underline{\Gamma_{W\tilde{f}_2}}$

The coupling combinations now are:

$$\mathcal{V}^{(6)}_{W\tilde{f}_2} = 2\mathcal{C}^R_{\tilde{W}\tilde{Z}W}\alpha^d_{\tilde{Z}_i\tilde{f}_2}\frac{g}{\sqrt{2}}\alpha^{\tilde{W}_j}_{\tilde{f}_2}|m_{\tilde{Z}_i}||m_{\tilde{W}_j}|(-1)^{\theta_j}(-1)^{\theta_c}, \tag{A.613}$$

$$\mathcal{V}^{(7)}_{W\tilde{f}_2} = -2\mathcal{C}^R_{\tilde{W}\tilde{Z}W}\beta^d_{\tilde{Z}_i\tilde{f}_2}\frac{g}{\sqrt{2}}\beta^{\tilde{W}_j}_{\tilde{f}_2}m_f m_{f'}(-1)^{\theta_c}, \tag{A.614}$$

$$\mathcal{V}^{(8)}_{W\tilde{f}_2} = 8\mathcal{C}^L_{\tilde{W}\tilde{Z}W}\beta^d_{\tilde{Z}_i\tilde{f}_2}\frac{g}{\sqrt{2}}\beta_{\tilde{f}_2}|m_{\tilde{Z}_i}|m_f m_{f'}|m_{\tilde{W}_j}|(-1)^{\theta_i}(-1)^{\theta_j}(-1)^{\theta_c}. \tag{A.615}$$

Again, here some of the coupling combinations depend upon which way around the decay occurs, i.e. neutralino to chargino or chargino to neutralino, for the neutralino decaying:

$$\mathcal{V}^{(1)}_{W\tilde{f}_2} = -2\mathcal{C}^R_{\tilde{W}\tilde{Z}W}\alpha^d_{\tilde{Z}_i\tilde{f}_2}\frac{g}{\sqrt{2}}\beta^{\tilde{W}_j}_{\tilde{f}_2}|m_{\tilde{Z}_i}|m_{f'}, \tag{A.616}$$

$$\mathcal{V}^{(2)}_{W\tilde{f}_2} = 2\mathcal{C}^R_{\tilde{W}\tilde{Z}W}\beta^d_{\tilde{Z}_i\tilde{f}_2}\frac{g}{\sqrt{2}}\alpha^{\tilde{W}_j}_{\tilde{f}_2}m_f|m_{\tilde{W}_j}|(-1)^{\theta_j}, \tag{A.617}$$

$$\mathcal{V}^{(3)}_{W\tilde{f}_2} = -2\mathcal{C}^R_{\tilde{W}\tilde{Z}W}\alpha^d_{\tilde{Z}_i\tilde{f}_2}\frac{g}{\sqrt{2}}\alpha^{\tilde{W}_j}_{\tilde{f}_2}, \tag{A.618}$$

$$\mathcal{V}^{(4)}_{W\tilde{f}_2} = -4\mathcal{C}^L_{\tilde{W}\tilde{Z}W}\beta^d_{\tilde{Z}_i\tilde{f}_2}\frac{g}{\sqrt{2}}\alpha^{\tilde{W}_j}_{\tilde{f}_2}|m_{\tilde{Z}_i}|m_f(-1)^{\theta_i}, \tag{A.619}$$

$$\mathcal{V}^{(5)}_{W\tilde{f}_2} = 4\mathcal{C}^L_{\tilde{W}\tilde{Z}W}\alpha^d_{\tilde{Z}_i\tilde{f}_2}\frac{g}{\sqrt{2}}\beta^{\tilde{W}_j}_{\tilde{f}_2}m_{f'}|m_{\tilde{W}_j}|(-1)^{\theta_i}(-1)^{\theta_j}, \tag{A.620}$$

whilst if it's a chargino decaying:

$$\mathcal{V}^{(1)}_{W\tilde{f}_2} = -2\mathcal{C}^R_{\tilde{W}\tilde{Z}W}\beta^d_{\tilde{Z}_i\tilde{f}_2}\alpha^{\tilde{W}_j}_{\tilde{f}_2}\frac{g}{\sqrt{2}}|m_{\tilde{Z}_i}|m_{f'}(-1)^{\theta_i}(-1)^{\theta_j}(-1)^{\theta_c}, \tag{A.621}$$

$$\mathcal{V}^{(2)}_{W\tilde{f}_2} = 2\mathcal{C}^R_{\tilde{W}\tilde{Z}W}\alpha^d_{\tilde{Z}_i\tilde{f}_2}\beta^{\theta W_j}_{\tilde{f}_2}\frac{g}{\sqrt{2}}m_f|m_{\tilde{W}_j}|(-1)^{\theta_c}, \tag{A.622}$$

$$\mathcal{V}^{(3)}_{W\tilde{f}_2} = -2\mathcal{C}^L_{\tilde{W}\tilde{Z}W}\alpha^d_{\tilde{Z}_i\tilde{f}_2}\alpha^{\tilde{W}_j}_{\tilde{f}_2}\frac{g}{\sqrt{2}}(-1)^{\theta_i}(-1)^{\theta_c}, \tag{A.623}$$

$$\mathcal{V}^{(4)}_{W\tilde{f}_2} = -4\mathcal{C}^L_{\tilde{W}\tilde{Z}W}\alpha^d_{\tilde{Z}_i\tilde{f}_2}\beta^{\tilde{W}_j}_{\tilde{f}_2}\frac{g}{\sqrt{2}}|m_{\tilde{Z}_i}|m_f(-1)^{\theta_i}(-1)^{\theta_j}(-1)^{\theta_c}, \tag{A.624}$$

$$\mathcal{V}^{(5)}_{W\tilde{f}_2} = 4\mathcal{C}^L_{\tilde{W}\tilde{Z}W}\beta^d_{\tilde{Z}_i\tilde{f}_2}\alpha^{\tilde{W}_j}_{\tilde{f}_2}\frac{g}{\sqrt{2}}m_{f'}|m_{\tilde{W}_j}|(-1)^{\theta_c}. \tag{A.625}$$

Then the integrals, and indeed the overall expression for $\Gamma_{W\tilde{f}_2}$, are just like that for $W\tilde{f}_1$ but with the expected replacement $m_{\tilde{f}_1} \to m_{\tilde{f}_2}$.

$\underline{\Gamma_{H^\pm G}}$

The coupling combinations are:

$$\mathcal{V}^{(1)}_{H^\pm G} = \omega^L_{G\tilde{W}\tilde{Z}}\omega^L_{H^+\tilde{W}^+\tilde{Z}} + \omega^R_{G\tilde{W}\tilde{Z}}\omega^R_{H^+\tilde{W}^+\tilde{Z}}, \tag{A.626}$$

$$\mathcal{V}^{(2)}_{H^\pm G} = (\omega^R_{G\tilde{W}\tilde{Z}}\omega^L_{H^+\tilde{W}^+\tilde{Z}} + \omega^L_{G\tilde{W}\tilde{Z}}\omega^R_{H^+\tilde{W}^+\tilde{Z}})(-1)^{\theta_i}(-1)^{\theta_j}, \tag{A.627}$$

$$\mathcal{V}^{(3)}_{H^\pm G} = \mathcal{C}^u_{Gff'}\mathcal{C}^u_{H^+ff'} + \mathcal{C}^d_{Gff'}\mathcal{C}^d_{H^+ff'}, \tag{A.628}$$

$$\mathcal{V}^{(4)}_{H^\pm G} = \mathcal{C}^d_{Gff'}\mathcal{C}^u_{H^+ff'} + \mathcal{C}^u_{Gff'}\mathcal{C}^d_{H^+ff'}, \tag{A.629}$$

and the integrals with $s = m^2_{\tilde{Z}_i} + m^2_{\tilde{W}_j} - 2|m_{\tilde{Z}_i}|E$, $\lambda = \sqrt{(s-(m_f+m_{f'})^2)(s-(m_f-m_{f'})^2)}$ are:

$$I^1_{H^\pm G} = 2|m_{\tilde{Z}_i}|\int_{|m_{\tilde{W}_j}|}^{E_{upper3}} dE \frac{\lambda\sqrt{E^2 - m^2_{\tilde{W}_j}}}{s(s-m^2_W)(s-m^2_{H^\pm})}, \tag{A.630}$$

$$I^2_{H^\pm G} = 2|m_{\tilde{Z}_i}|\int_{|m_{\tilde{W}_j}|}^{E_{upper3}} dE \frac{2|m_{\tilde{Z}_i}|\lambda\sqrt{E^2 - m^2_{\tilde{W}_j}}(s-m^2_f-m^2_{f'})}{s(s-m^2_W)(s-m^2_{H^\pm})}, \tag{A.631}$$

$$I^3_{H^\pm G} = 2|m_{\tilde{Z}_i}|\int_{|m_{\tilde{W}_j}|}^{E_{upper3}} dE \frac{2|m_{\tilde{Z}_i}|\lambda\sqrt{E^2 - m^2_{\tilde{W}_j}}2|m_{\tilde{Z}_i}|E}{s(s-m^2_W)(s-m^2_{H^\pm})}, \tag{A.632}$$

$$I^4_{H^\pm G} = 2|m_{\tilde{Z}_i}|\int_{|m_{\tilde{W}_j}|}^{E_{upper3}} dE \frac{2|m_{\tilde{Z}_i}|\lambda\sqrt{E^2 - m^2_{\tilde{W}_j}}(s-m^2_f-m^2_{f'})2|m_{\tilde{Z}_i}|E}{s(s-m^2_W)(s-m^2_{H^\pm})}. \tag{A.633}$$

The overall contribution is then:

$$\begin{aligned}\Gamma_{H^\pm G} =& \mathcal{V}^{(1)}_{H^\pm G}\mathcal{V}^{(3)}_{H^\pm G}I^4_{H^\pm G} - 2\mathcal{V}^{(1)}_{H^\pm G}\mathcal{V}^{(4)}_{H^\pm G}m_f m_{f'}I^3_{H^\pm G} + 2\mathcal{V}^{(2)}_{H^\pm G}\mathcal{V}^{(3)}_{H^\pm G}|m_{\tilde{Z}_i}||m_{\tilde{W}_j}|I^2_{H^\pm G} \\ & - 4\mathcal{V}^{(2)}_{H^\pm G}\mathcal{V}^{(4)}_{H^\pm G}|m_{\tilde{Z}_i}||m_{\tilde{W}_j}|m_f m_{f'}I^1_{H^\pm G}(-1)^{\theta_j}.\end{aligned} \tag{A.634}$$

$\underline{\Gamma_{G\tilde{f}'_1}}$

Here the required coupling combinations are dependent on whether it's neutralino to chargino or chargino to neutralino. For a neutralino decaying:

$$\mathcal{V}^{(1)}_{G\tilde{f}'_1} = \frac{1}{2}(\omega^R_{G\tilde{W}\tilde{Z}}\alpha^u_{\tilde{Z}_i\tilde{f}_1}\mathcal{C}^d_{Gff'}\beta^{\tilde{W}_j}_{\tilde{f}'_1} + \omega^L_{G\tilde{W}\tilde{Z}}\beta^u_{\tilde{Z}_i\tilde{f}_1}\mathcal{C}^u_{Gff'}\alpha^{\tilde{W}_j}_{\tilde{f}'_1}), \tag{A.635}$$

$$\mathcal{V}^{(2)}_{G\tilde{f}'_1} = -(\omega^R_{G\tilde{W}\tilde{Z}}\beta^u_{\tilde{Z}_i\tilde{f}_1}\mathcal{C}^u_{Gff'}\beta^{\tilde{W}_j}_{\tilde{f}'_1} + \omega^L_{G\tilde{W}\tilde{Z}}\alpha^u_{\tilde{Z}_i\tilde{f}_1}\mathcal{C}^d_{Gff'}\alpha^{\tilde{W}_j}_{\tilde{f}'_1})m_f|m_{\tilde{Z}_i}|, \tag{A.636}$$

$$\mathcal{V}^{(3)}_{G\tilde{f}'_1} = (\omega^L_{G\tilde{W}\tilde{Z}}\beta^u_{\tilde{Z}_i\tilde{f}_1}\mathcal{C}^d_{Gff'}\beta^{\tilde{W}_j}_{\tilde{f}'_1} + \omega^R_{G\tilde{W}\tilde{Z}}\alpha^u_{\tilde{Z}_i\tilde{f}_1}\mathcal{C}^u_{Gff'}\alpha^{\tilde{W}_j}_{\tilde{f}'_1})(-1)^{\theta_i}m_{f'}|m_{\tilde{W}_j}|, \tag{A.637}$$

$$\mathcal{V}^{(4)}_{G\tilde{f}'_1} = (\omega^R_{G\tilde{W}\tilde{Z}}\beta^u_{\tilde{Z}_i\tilde{f}_1}\mathcal{C}^d_{Gff'}\beta^{\tilde{W}_j}_{\tilde{f}'_1} + \omega^L_{G\tilde{W}\tilde{Z}}\alpha^u_{\tilde{Z}_i\tilde{f}_1}\mathcal{C}^u_{Gff'}\alpha^{\tilde{W}_j}_{\tilde{f}'_1})m_{f'}|m_{\tilde{Z}_i}|, \tag{A.638}$$

$$\mathcal{V}^{(5)}_{G\tilde{f}'_1} = (\omega^L_{G\tilde{W}\tilde{Z}}\beta^u_{\tilde{Z}_i\tilde{f}_1}\mathcal{C}^u_{Gff'}\beta^{\tilde{W}_j}_{\tilde{f}'_1} - (-1)^{\theta_i}\omega^R_{G\tilde{W}\tilde{Z}}\alpha^u_{\tilde{Z}_i\tilde{f}_1}\mathcal{C}^d_{Gff'}\alpha^{\tilde{W}_j}_{\tilde{f}'_1})m_f|m_{\tilde{W}_j}|, \tag{A.639}$$

$$\mathcal{V}^{(6)}_{G\tilde{f}'_1} = (-1)^{\theta_i}(\omega^L_{G\tilde{W}\tilde{Z}}\alpha^u_{\tilde{Z}_i\tilde{f}_1}\mathcal{C}^d_{Gff'}\beta^{\tilde{W}_j}_{\tilde{f}'_1} + \omega^R_{G\tilde{W}\tilde{Z}}\beta^u_{\tilde{Z}_i\tilde{f}_1}\mathcal{C}^u_{Gff'}\alpha^{\tilde{W}_j}_{\tilde{f}'_1})|m_{\tilde{Z}_i}||m_{\tilde{W}_j}|, \tag{A.640}$$

$$\mathcal{V}^{(7)}_{G\tilde{f}'_1} = -(\omega^R_{G\tilde{W}\tilde{Z}}\alpha^u_{\tilde{Z}_i\tilde{f}_1}\mathcal{C}^u_{Gff'}\beta^{\tilde{W}_j}_{\tilde{f}'_1} + \omega^L_{G\tilde{W}\tilde{Z}}\beta^u_{\tilde{Z}_i\tilde{f}_1}\mathcal{C}^d_{Gff'}\alpha^{\tilde{W}_j}_{\tilde{f}'_1})m_{f'}m_f, \tag{A.641}$$

$$\mathcal{V}^{(8)}_{G\tilde{f}'_1} = 2(\omega^L_{G\tilde{W}\tilde{Z}}\alpha^u_{\tilde{Z}_i\tilde{f}_1}\mathcal{C}^u_{Gff'}\beta^{\tilde{W}_j}_{\tilde{f}'_1} + (-1)^{\theta_i}\omega^R_{G\tilde{W}\tilde{Z}}\beta^u_{\tilde{Z}_i\tilde{f}_1}\mathcal{C}^d_{Gff'}\alpha^{\tilde{W}_j}_{\tilde{f}'_1})|m_{\tilde{Z}_i}|m_{f'}m_f|m_{\tilde{W}_j}|. \tag{A.642}$$

For a chargino decaying:

$$\mathcal{V}^{(1)}_{G\tilde{f}'_1} = -\frac{1}{2}(\omega^L_{G\tilde{W}\tilde{Z}}\alpha^u_{\tilde{Z}_i\tilde{f}_1}\mathcal{C}^u_{Gff'}\beta^{\tilde{W}_j}_{\tilde{f}'_1} + (-1)^{\theta_f}\omega^R_{G\tilde{W}\tilde{Z}}\beta^u_{\tilde{Z}_i\tilde{f}_1}\mathcal{C}^d_{Gff'}\alpha^{\tilde{W}_j}_{\tilde{f}'_1}), \tag{A.643}$$

$$\mathcal{V}^{(2)}_{G\tilde{f}'_1} = (\omega^L_{G\tilde{W}\tilde{Z}}\alpha^u_{\tilde{Z}_i\tilde{f}_1}\mathcal{C}^d_{Gff'}\alpha^{\tilde{W}_j}_{\tilde{f}'_1} + (-1)^{\theta_j}\omega^R_{G\tilde{W}\tilde{Z}}\beta^u_{\tilde{Z}_i\tilde{f}_1}\mathcal{C}^u_{Gff'}\beta^{\tilde{W}_j}_{\tilde{f}'_1})m_{f'}|m_{\tilde{Z}_i}|, \tag{A.644}$$

$$\mathcal{V}^{(3)}_{G\tilde{f}'_1} = -(\omega^R_{G\tilde{W}\tilde{Z}}\alpha^u_{\tilde{Z}_i\tilde{f}_1}\mathcal{C}^u_{Gff'}\alpha^{\tilde{W}_j}_{\tilde{f}'_1} + (-1)^{\theta_j}\omega^L_{G\tilde{W}\tilde{Z}}\beta^u_{\tilde{Z}_i\tilde{f}_1}\mathcal{C}^d_{Gff'}\beta^{\tilde{W}_j}_{\tilde{f}'_1})(-1)^{\theta_j}m_f|m_{\tilde{W}_j}|, \tag{A.645}$$

$$\mathcal{V}^{(4)}_{G\tilde{f}'_1} = -(\omega^L_{G\tilde{W}\tilde{Z}}\alpha^u_{\tilde{Z}_i\tilde{f}_1}\mathcal{C}^u_{Gff'}\alpha^{\tilde{W}_j}_{\tilde{f}'_1} + (-1)^{\theta_j}\omega^R_{G\tilde{W}\tilde{Z}}\beta^u_{\tilde{Z}_i\tilde{f}_1}\mathcal{C}^d_{Gff'}\beta^{\tilde{W}_j}_{\tilde{f}'_1})m_f|m_{\tilde{Z}_i}|, \tag{A.646}$$

$$\mathcal{V}^{(5)}_{G\tilde{f}'_1} = ((-1)^{\theta_j}\omega^R_{G\tilde{W}\tilde{Z}}\alpha^u_{\tilde{Z}_i\tilde{f}_1}\mathcal{C}^d_{Gff'}\alpha^{\tilde{W}_j}_{\tilde{f}'_1} + \omega^L_{G\tilde{W}\tilde{Z}}\beta^u_{\tilde{Z}_i\tilde{f}_1}\mathcal{C}^u_{Gff'}\beta^{\tilde{W}_j}_{\tilde{f}'_1})m_{f'}|m_{\tilde{W}_j}|, \tag{A.647}$$

$$\mathcal{V}^{(6)}_{G\tilde{f}'_1} = -((-1)^{\theta_j}\omega^R_{G\tilde{W}\tilde{Z}}\alpha^u_{\tilde{Z}_i\tilde{f}_1}\mathcal{C}^u_{Gff'}\beta^{\tilde{W}_j}_{\tilde{f}'_1} + \omega^L_{G\tilde{W}\tilde{Z}}\beta^u_{\tilde{Z}_i\tilde{f}_1}\mathcal{C}^d_{Gff'}\alpha^{\tilde{W}_j}_{\tilde{f}'_1})|m_{\tilde{Z}_i}||m_{\tilde{W}_j}|, \tag{A.648}$$

$$\mathcal{V}^{(7)}_{G\tilde{f}'_1} = (\omega^L_{G\tilde{W}\tilde{Z}}\alpha^u_{\tilde{Z}_i\tilde{f}_1}\mathcal{C}^d_{Gff'}\beta^{\tilde{W}_j}_{\tilde{f}'_1} + (-1)^{\theta_j}\omega^R_{G\tilde{W}\tilde{Z}}\beta^u_{\tilde{Z}_i\tilde{f}_1}\mathcal{C}^u_{Gff'}\alpha^{\tilde{W}_j}_{\tilde{f}'_1})m_{f'}m_f, \tag{A.649}$$

$$\mathcal{V}^{(8)}_{G\tilde{f}'_1} = 2((-1)^{\theta_j}\omega^R_{G\tilde{W}\tilde{Z}}\alpha^u_{\tilde{Z}_i\tilde{f}_1}\mathcal{C}^d_{Gff'}\beta^{\tilde{W}_j}_{\tilde{f}'_1} + \omega^L_{G\tilde{W}\tilde{Z}}\beta^u_{\tilde{Z}_i\tilde{f}_1}\mathcal{C}^u_{Gff'}\alpha^{\tilde{W}_j}_{\tilde{f}'_1})|m_{\tilde{Z}_i}|m_{f'}m_f|m_{\tilde{W}_j}|. \tag{A.650}$$

The integrals necessary are, for neutralino decaying with $s = m^2_{\tilde{Z}_i} + m^2_{\tilde{W}_j} - 2|m_{\tilde{Z}_i}|E$, $\lambda = \sqrt{(s-(m_{f'}+m_f)^2)(s-(m_{f'}-m_f)^2)}$, $A = m^2_f + m^2_{f'} + 2|m_{\tilde{Z}_i}|E + (m^2_{\tilde{Z}_i} - m^2_{\tilde{W}_j})(m^2_f - m^2_{f'})/s$, $B = 2|m_{\tilde{Z}_i}|\lambda/s\sqrt{E^2 - m^2_{\tilde{W}_j}}$, $Z = \frac{(\frac{1}{2}(A+B)-m^2_{\tilde{f}'_1})}{(\frac{1}{2}(A-B)-m^2_{\tilde{f}'_1})}$, given by:

$$I^1_{G\tilde{f}'_1} = 2|m_{\tilde{Z}_i}| \int_{|m_{\tilde{W}_j}|}^{E_{upper3}} dE \frac{2[sB + (m^2_{\tilde{f}'_1} s - m^2_{\tilde{Z}_i} m^2_f - m^2_{f'} m^2_{\tilde{W}_j}) \log(Z)]}{s - m^2_W}, \tag{A.651}$$

$$I^2_{G\tilde{f}'_1} = -2|m_{\tilde{Z}_i}| \int_{|m_{\tilde{W}_j}|}^{E_{upper3}} dE \frac{[B + (m^2_{\tilde{f}'_1} + m^2_{\tilde{W}_j} - 2|m_{\tilde{Z}_i}|E - m^2_f) \log(Z)]}{s - m^2_W}, \tag{A.652}$$

$$I^3_{G\tilde{f}'_1} = 2|m_{\tilde{Z}_i}| \int_{|m_{\tilde{W}_j}|}^{E_{upper3}} dE \frac{[B + (m^2_{\tilde{f}'_1} + m^2_{\tilde{Z}_i} - 2|m_{\tilde{Z}_i}|E - m^2_{f'}) \log(Z)]}{s - m^2_W}, \tag{A.653}$$

$$I^4_{G\tilde{f}'_1} = 2|m_{\tilde{Z}_i}| \int_{|m_{\tilde{W}_j}|}^{E_{upper3}} dE \frac{[B + (m^2_{\tilde{f}'_1} - m^2_f - m^2_{\tilde{W}_j}) \log(Z)]}{s - m^2_W}, \tag{A.654}$$

$$I^5_{G\tilde{f}'_1} = -2|m_{\tilde{Z}_i}| \int_{|m_{\tilde{W}_j}|}^{E_{upper3}} dE \frac{[B + (m^2_{\tilde{f}'_1} - m^2_{\tilde{Z}_i} - m^2_{f'}) \log(Z)]}{s - m^2_W}, \tag{A.655}$$

$$I^6_{G\tilde{f}'_1} = 2|m_{\tilde{Z}_i}| \int_{|m_{\tilde{W}_j}|}^{E_{upper3}} dE \frac{(s - m^2_{f'} - m^2_f) \log(Z)}{s - m^2_W}, \tag{A.656}$$

$$I^7_{G\tilde{f}'_1} = 2|m_{\tilde{Z}_i}| \int_{|m_{\tilde{W}_j}|}^{E_{upper3}} dE \frac{2|m_{\tilde{Z}_i}|E \log(Z)}{s - m^2_W}, \tag{A.657}$$

$$I^8_{G\tilde{f}'_1} = 2|m_{\tilde{Z}_i}| \int_{|m_{\tilde{W}_j}|}^{E_{upper3}} dE \frac{\log(Z)}{s - m^2_W}. \tag{A.658}$$

For a chargino decaying the integrals have the same expressions but one must swap integrals 2 and 4 and integrals 3 and 5. The overall contribution is the product of each coupling combination with the corresponding integral:

$$\begin{aligned}\Gamma_{G\tilde{f}'_1} =& \mathcal{V}^{(1)}_{G\tilde{f}'_1} I^1_{G\tilde{f}'_1} + \mathcal{V}^{(2)}_{G\tilde{f}'_1} I^2_{G\tilde{f}'_1} + \mathcal{V}^{(3)}_{G\tilde{f}'_1} I^3_{G\tilde{f}'_1} + \mathcal{V}^{(4)}_{G\tilde{f}'_1} I^4_{G\tilde{f}'_1} \\ &+ \mathcal{V}^{(5)}_{G\tilde{f}'_1} I^5_{G\tilde{f}'_1} + \mathcal{V}^{(6)}_{G\tilde{f}'_1} I^6_{G\tilde{f}'_1} + \mathcal{V}^{(7)}_{G\tilde{f}'_1} I^7_{G\tilde{f}'_1} + \mathcal{V}^{(8)}_{G\tilde{f}'_1} I^8_{G\tilde{f}'_1}.\end{aligned} \tag{A.659}$$

$\underline{\Gamma_{G\tilde{f}'_2}}$

Again here the coupling combinations depend upon if we are considering neutralino to chargino or chargino to neutralino, for neutralino decaying:

$$\mathcal{V}^{(1)}_{G\tilde{f}'_2} = -\frac{1}{2}(-1)^{\theta_i}[-(-1)^{\theta_i} \omega^R_{G\tilde{W}\tilde{Z}} \alpha^u_{\tilde{Z}_i \tilde{f}_2} \mathcal{C}^d_{Gff'} \beta^{\tilde{W}_j}_{\tilde{f}'_2} + \omega^L_{G\tilde{W}\tilde{Z}} \beta^u_{\tilde{Z}_i \tilde{f}_2} \mathcal{C}^u_{Gff'} \alpha^{\tilde{W}_j}_{\tilde{f}'_2}], \tag{A.660}$$

$$\mathcal{V}^{(2)}_{G\tilde{f}'_2} = (-1)^{\theta_i}(\omega^R_{G\tilde{W}\tilde{Z}} \beta^u_{\tilde{Z}_i \tilde{f}_2} \mathcal{C}^u_{Gff'} \beta^{\tilde{W}_j}_{\tilde{f}'_2} - \omega^L_{G\tilde{W}\tilde{Z}} \alpha^u_{\tilde{Z}_i \tilde{f}_2} \mathcal{C}^d_{Gff'} \alpha^{\tilde{W}_j}_{\tilde{f}'_2}) |m_{\tilde{Z}_i}| m_f, \tag{A.661}$$

$$\mathcal{V}^{(3)}_{G\tilde{f}'_2} = -(\omega^L_{G\tilde{W}\tilde{Z}} \beta^u_{\tilde{Z}_i \tilde{f}_2} \mathcal{C}^d_{Gff'} \beta^{\tilde{W}_j}_{\tilde{f}'_2} - \omega^R_{G\tilde{W}\tilde{Z}} \alpha^u_{\tilde{Z}_i \tilde{f}_2} \mathcal{C}^u_{Gff'} \alpha^{\tilde{W}_j}_{\tilde{f}'_2}) m_{f'} |m_{\tilde{W}_j}| (-1)^{\theta_j}, \tag{A.662}$$

$$\mathcal{V}^{(4)}_{G\tilde{f}'_2} = -(\omega^R_{G\tilde{W}\tilde{Z}} \beta^u_{\tilde{Z}_i \tilde{f}_2} \mathcal{C}^d_{Gff'} \beta^{\tilde{W}_j}_{\tilde{f}'_2} - (-1)^{\theta_i} \omega^L_{G\tilde{W}\tilde{Z}} \alpha^u_{\tilde{Z}_i \tilde{f}_2} \mathcal{C}^u_{Gff'} \alpha^{\tilde{W}_j}_{\tilde{f}'_2}) |m_{\tilde{Z}_i}| m_{f'}, \tag{A.663}$$

$$\mathcal{V}^{(5)}_{G\tilde{f}'_2} = (\omega^L_{G\tilde{W}\tilde{Z}} \beta^u_{\tilde{Z}_i \tilde{f}_2} \mathcal{C}^u_{Gff'} \beta^{\tilde{W}_j}_{\tilde{f}'_2} + \omega^R_{G\tilde{W}\tilde{Z}} \alpha^u_{\tilde{Z}_i \tilde{f}_2} \mathcal{C}^d_{Gff'} \alpha^{\tilde{W}_j}_{\tilde{f}'_2}) m_f |m_{\tilde{W}_j}| (-1)^{\theta_j}, \tag{A.664}$$

$$\mathcal{V}^{(6)}_{G\tilde{f}'_1} = [\omega^L_{G\tilde{W}\tilde{Z}} \alpha^u_{\tilde{Z}_i \tilde{f}_2} \mathcal{C}^d_{Gff'} \beta^{\tilde{W}_j}_{\tilde{f}'_2} - (-1)^{\theta_i} \omega^R_{G\tilde{W}\tilde{Z}} \beta^u_{\tilde{Z}_i \tilde{f}_2} \mathcal{C}^u_{Gff'} \alpha^{\tilde{W}_j}_{\tilde{f}'_2}] |m_{\tilde{Z}_i}| |m_{\tilde{W}_j}|, \tag{A.665}$$

$$\mathcal{V}^{(7)}_{G\tilde{f}'_2} = [-(-1)^{\theta_i} \omega^R_{G\tilde{W}\tilde{Z}} \alpha^u_{\tilde{Z}_i \tilde{f}_2} \mathcal{C}^u_{Gff'} \beta^{\tilde{W}_j}_{\tilde{f}'_2} + \omega^L_{G\tilde{W}\tilde{Z}} \beta^u_{\tilde{Z}_i \tilde{f}_2} \mathcal{C}^d_{Gff'} \alpha^{\tilde{W}_j}_{\tilde{f}'_2}] m_{f'} m_f, \tag{A.666}$$

$$\mathcal{V}^{(8)}_{G\tilde{f}'_2} = 2[-\omega^L_{G\tilde{W}\tilde{Z}} \alpha^u_{\tilde{Z}_i \tilde{f}_2} \mathcal{C}^u_{Gff'} \beta^{\tilde{W}_j}_{\tilde{f}'_2} + (-1)^{\theta_i} \omega^R_{G\tilde{W}\tilde{Z}} \beta^u_{\tilde{Z}_i \tilde{f}_2} \mathcal{C}^d_{Gff'} \alpha^{\tilde{W}_j}_{\tilde{f}'_2}] |m_{\tilde{Z}_i}| m_{f'} m_f |m_{\tilde{W}_j}|, \tag{A.667}$$

whilst if it's a chargino decaying into a neutralino:

$$\mathcal{V}^{(1)}_{G\tilde{f}'_2} = \frac{1}{2}[\omega^L_{G\tilde{W}\tilde{Z}}\beta^{\tilde{W}_j}_{\tilde{f}'_2}\mathcal{C}^u_{Gff'}\alpha^u_{\tilde{Z}_i\tilde{f}_2}(-1)^{\theta_j} + \omega^R_{G\tilde{W}\tilde{Z}}\alpha^{\tilde{W}_j}_{\tilde{f}'_2}\mathcal{C}^d_{Gff'}\beta^u_{\tilde{Z}_i\tilde{f}_2}], \tag{A.668}$$

$$\mathcal{V}^{(2)}_{G\tilde{f}'_2} = -((-1)^{\theta_j}\omega^L_{G\tilde{W}\tilde{Z}}\alpha^{\tilde{W}_j}_{\tilde{f}'_2}\mathcal{C}^d_{Gff'}\alpha^u_{\tilde{Z}_i\tilde{f}_2} + \omega^R_{G\tilde{W}\tilde{Z}}\beta^{\tilde{W}_j}_{\tilde{f}'_2}\mathcal{C}^u_{Gff'}\beta^u_{\tilde{Z}_i\tilde{f}_2})|m_{\tilde{Z}_i}|m_{f'}, \tag{A.669}$$

$$\mathcal{V}^{(3)}_{G\tilde{f}'_2} = (\omega^R_{G\tilde{W}\tilde{Z}}\alpha^{\tilde{W}_j}_{\tilde{f}'_2}\mathcal{C}^u_{Gff'}\alpha^u_{\tilde{Z}_i\tilde{f}_2} + (-1)^{\theta_j}\omega^L_{G\tilde{W}\tilde{Z}}\beta^{\tilde{W}_j}_{\tilde{f}'_2}\mathcal{C}^d_{Gff'}\beta^u_{\tilde{Z}_i\tilde{f}_2})m_f|m_{\tilde{W}_j}|, \tag{A.670}$$

$$\mathcal{V}^{(4)}_{G\tilde{f}'_2} = ((-1)^{\theta_j}\omega^L_{G\tilde{W}\tilde{Z}}\alpha^{\tilde{W}_j}_{\tilde{f}'_2}\mathcal{C}^u_{Gff'}\alpha^u_{\tilde{Z}_i\tilde{f}_2} + \omega^R_{G\tilde{W}\tilde{Z}}\beta^{\tilde{W}_j}_{\tilde{f}'_2}\mathcal{C}^d_{Gff'}\beta^u_{\tilde{Z}_i\tilde{f}_2})|m_{\tilde{Z}_i}|m_f, \tag{A.671}$$

$$\mathcal{V}^{(5)}_{G\tilde{f}'_2} = -(\omega^R_{G\tilde{W}\tilde{Z}}\alpha^{\tilde{W}_j}_{\tilde{f}'_2}\mathcal{C}^d_{Gff'}\alpha^u_{\tilde{Z}_i\tilde{f}_2} + (-1)^{\theta_j}\omega^L_{G\tilde{W}\tilde{Z}}\beta^{\tilde{W}_j}_{\tilde{f}'_2}\mathcal{C}^u_{Gff'}\beta^u_{\tilde{Z}_i\tilde{f}_2})m_{f'}|m_{\tilde{W}_j}|, \tag{A.672}$$

$$\mathcal{V}^{(6)}_{G\tilde{f}'_2} = [\omega^R_{G\tilde{W}\tilde{Z}}\beta^{\tilde{W}_j}_{\tilde{f}'_2}\mathcal{C}^u_{Gff'}\alpha^u_{\tilde{Z}_i\tilde{f}_2} + (-1)^{\theta_j}\omega^L_{G\tilde{W}\tilde{Z}}\alpha^{\tilde{W}_j}_{\tilde{f}'_2}\mathcal{C}^d_{Gff'}\beta^u_{\tilde{Z}_i\tilde{f}_2}]|m_{\tilde{W}_j}||m_{\tilde{Z}_i}|, \tag{A.673}$$

$$\mathcal{V}^{(7)}_{G\tilde{f}'_2} = -[(-1)^{\theta_j}\omega^L_{G\tilde{W}\tilde{Z}}\beta^{\tilde{W}_j}_{\tilde{f}'_2}\mathcal{C}^d_{Gff'}\alpha^u_{\tilde{Z}_i\tilde{f}_2} + \omega^R_{G\tilde{W}\tilde{Z}}\alpha^{\tilde{W}_j}_{\tilde{f}'_2}\mathcal{C}^u_{Gff'}\beta^u_{\tilde{Z}_i\tilde{f}_2}]m_f m_{f'}, \tag{A.674}$$

$$\mathcal{V}^{(8)}_{G\tilde{f}'_2} = -2[\omega^R_{G\tilde{W}\tilde{Z}}\beta^{\tilde{W}_j}_{\tilde{f}'_2}\mathcal{C}^d_{Gff'}\alpha^u_{\tilde{Z}_i\tilde{f}_2} + (-1)^{\theta_j}\omega^L_{G\tilde{W}\tilde{Z}}\alpha^{\tilde{W}_j}_{\tilde{f}'_2}\mathcal{C}^u_{Gff'}\beta^u_{\tilde{Z}_i\tilde{f}_2}]m_f m_{f'}|m_{\tilde{W}_j}|m_{\tilde{Z}_i}|. \tag{A.675}$$

The integrals are exactly as for $G\tilde{f}'_1$ but with the change $m_{\tilde{f}'_1} \to m_{\tilde{f}'_2}$, and similar changes produce the overall expression for $\Gamma_{G\tilde{f}'_2}$.

$\underline{\Gamma_{H^\pm\tilde{f}'_1}}$

Here the couplings required are dependent again on which particle is initial state and which final state, for the neutralino as the decaying (i.e. initial state) particle:

$$\mathcal{V}^{(1)}_{H^\pm\tilde{f}'_1} = -\frac{1}{2}[(-1)^{\theta_i}\omega^R_{H^+\tilde{W}^+\tilde{Z}}\alpha^u_{\tilde{Z}_i\tilde{f}_1}\mathcal{C}^d_{H^+ff'}\beta^{\tilde{W}_j}_{\tilde{f}'_1} + \omega^L_{H^+\tilde{W}^+\tilde{Z}}\beta^u_{\tilde{Z}_i\tilde{f}_1}\mathcal{C}^u_{H^+ff'}\alpha^{\tilde{W}_j}_{\tilde{f}'_1}], \tag{A.676}$$

$$\mathcal{V}^{(2)}_{H^\pm\tilde{f}'_1} = -(\omega^R_{H^+\tilde{W}^+\tilde{Z}}\beta^u_{\tilde{Z}_i\tilde{f}_1}\mathcal{C}^u_{H^+ff'}\beta^{\tilde{W}_j}_{\tilde{f}'_1} + \omega^L_{H^+\tilde{W}^+\tilde{Z}}\alpha^u_{\tilde{Z}_i\tilde{f}_1}\mathcal{C}^d_{H^+ff'}\alpha^{\tilde{W}_j}_{\tilde{f}'_1})|m_{\tilde{Z}_i}|m_f, \tag{A.677}$$

$$\mathcal{V}^{(3)}_{H^\pm\tilde{f}'_1} = (\omega^L_{H^+\tilde{W}^+\tilde{Z}}\beta^u_{\tilde{Z}_i\tilde{f}_1}\mathcal{C}^d_{H^+ff'}\beta^{\tilde{W}_j}_{\tilde{f}'_1} + \omega^R_{H^+\tilde{W}^+\tilde{Z}}\alpha^u_{\tilde{Z}_i\tilde{f}_1}\mathcal{C}^u_{H^+ff'}\alpha^{\tilde{W}_j}_{\tilde{f}'_1})m_{f'}|m_{\tilde{W}_j}|(-1)^{\theta_i}, \tag{A.678}$$

$$\mathcal{V}^{(4)}_{H^\pm\tilde{f}'_1} = -[(-1)^{\theta_i}\omega^R_{H^+\tilde{W}^+\tilde{Z}}\beta^u_{\tilde{Z}_i\tilde{f}_1}\mathcal{C}^d_{H^+ff'}\beta^{\tilde{W}_j}_{\tilde{f}'_1} - \omega^L_{H^+\tilde{W}^+\tilde{Z}}\alpha^u_{\tilde{Z}_i\tilde{f}_1}\mathcal{C}^u_{H^+ff'}\alpha^{\tilde{W}_j}_{\tilde{f}'_1}]|m_{\tilde{Z}_i}|m_{f'}, \tag{A.679}$$

$$\mathcal{V}^{(5)}_{H^\pm\tilde{f}'_1} = -(\omega^L_{H^+\tilde{W}^+\tilde{Z}}\beta^u_{\tilde{Z}_i\tilde{f}_1}\mathcal{C}^u_{H^+ff'}\beta^{\tilde{W}_1}_{\tilde{f}'_1} + \omega^R_{H^+\tilde{W}^+\tilde{Z}}\alpha^u_{\tilde{Z}_i\tilde{f}_1}\mathcal{C}^d_{H^+ff'}\alpha^{\tilde{W}_j}_{\tilde{f}'_1})m_f|m_{\tilde{W}_j}|(-1)^{\theta_i}, \tag{A.680}$$

$$\mathcal{V}^{(6)}_{H^\pm\tilde{f}'_1} = (-1)^{\theta_i}[\omega^L_{H^+\tilde{W}^+\tilde{Z}}\alpha^u_{\tilde{Z}_i\tilde{f}_1}\mathcal{C}^d_{H^+ff'}\beta^{\tilde{W}_j}_{\tilde{f}'_1} + \omega^R_{H^+\tilde{W}^+\tilde{Z}}\beta^u_{\tilde{Z}_i\tilde{f}_1}\mathcal{C}^u_{H^+ff'}\alpha^{\tilde{W}_j}_{\tilde{f}'_1}]|m_{\tilde{Z}_i}||m_{\tilde{W}_j}|, \tag{A.681}$$

$$\mathcal{V}^{(7)}_{H^\pm\tilde{f}'_1} = -(\omega^R_{H^+\tilde{W}^+\tilde{Z}}\alpha^u_{\tilde{Z}_i\tilde{f}_1}\mathcal{C}^u_{H^+ff'}\beta^{\tilde{W}_j}_{\tilde{f}'_1} + \omega^L_{H^+\tilde{W}^+\tilde{Z}}\beta^u_{\tilde{Z}_i\tilde{f}_1}\mathcal{C}^d_{H^+ff'}\alpha^{\tilde{W}_j}_{\tilde{f}'_1})m_{f'}m_f, \tag{A.682}$$

$$\mathcal{V}^{(8)}_{H^\pm\tilde{f}'_1} = -2(-1)^{\theta_i}[\omega^L_{H^+\tilde{W}^+\tilde{Z}}\alpha^u_{\tilde{Z}_i\tilde{f}_1}\mathcal{C}^u_{H^+ff'}\beta^{\tilde{W}_j}_{\tilde{f}'_1} + \omega^R_{H^+\tilde{W}^+\tilde{Z}}\beta^u_{\tilde{Z}_i\tilde{f}_1}\mathcal{C}^d_{H^+ff'}\alpha^{\tilde{W}_j}_{\tilde{f}'_1}]|m_{\tilde{Z}_i}||m_{\tilde{W}_j}|m_{f'}m_f. \tag{A.683}$$

If the initial state is a chargino:

$$\mathcal{V}^{(1)}_{H^\pm\tilde{f}'_1} = \frac{1}{2}(-1)^{\theta_j}[\omega^L_{H^+\tilde{W}^+\tilde{Z}}\beta^{\tilde{W}_j}_{\tilde{f}'_1}\mathcal{C}^u_{H^+ff'}\alpha^u_{\tilde{Z}_i\tilde{f}_1} + (-1)^{\theta_j}\omega^R_{H^+\tilde{W}^+\tilde{Z}}\alpha^{\tilde{W}_j}_{\tilde{f}'_1}\mathcal{C}^d_{H^+ff'}\beta^u_{\tilde{Z}_i\tilde{f}_1}], \tag{A.684}$$

$$\mathcal{V}^{(2)}_{H^\pm\tilde{f}'_1} = [\omega^L_{H^+\tilde{W}^+\tilde{Z}}\alpha^{\tilde{W}_j}_{\tilde{f}'_1}\mathcal{C}^d_{H^+ff'}\alpha^u_{\tilde{Z}_i\tilde{f}_1} + (-1)^{\theta_j}\omega^R_{H^+\tilde{W}^+\tilde{Z}}\beta^{\tilde{W}_j}_{\tilde{f}'_1}\mathcal{C}^u_{H^+ff'}\beta^u_{\tilde{Z}_i\tilde{f}_1}]|m_{\tilde{Z}_i}|m_{f'}, \tag{A.685}$$

$$\mathcal{V}^{(3)}_{H^\pm\tilde{f}'_1} = -[(-1)^{\theta_j}\omega^R_{H^+\tilde{W}^+\tilde{Z}}\alpha^{\tilde{W}_j}_{\tilde{f}'_1}\mathcal{C}^u_{H^+ff'}\alpha^u_{\tilde{Z}_i\tilde{f}_1} + \omega^L_{H^+\tilde{W}^+\tilde{Z}}\beta^{\tilde{W}_j}_{\tilde{f}'_1}\mathcal{C}^d_{H^+ff'}\beta^u_{\tilde{Z}_i\tilde{f}_1}]m_f|m_{\tilde{W}_j}|, \tag{A.686}$$

$$\mathcal{V}^{(4)}_{H^\pm\tilde{f}'_1} = -[\omega^L_{H^+\tilde{W}^+\tilde{Z}}\alpha^{\tilde{W}_j}_{\tilde{f}'_1}\mathcal{C}^u_{H^+ff'}\alpha^u_{\tilde{Z}_i\tilde{f}_1} + (-1)^{\theta_j}\omega^R_{H^+\tilde{W}^+\tilde{Z}}\beta^{\tilde{W}_j}_{\tilde{f}'_1}\mathcal{C}^d_{H^+ff'}\beta^u_{\tilde{Z}_i\tilde{f}_1}]|m_{\tilde{Z}_i}|m_f, \tag{A.687}$$

$$\mathcal{V}^{(5)}_{H^\pm\tilde{f}'_1} = [(-1)^{\theta_j}\omega^R_{H^+\tilde{W}^+\tilde{Z}}\alpha^{\tilde{W}_j}_{\tilde{f}'_1}\mathcal{C}^d_{H^+ff'}\alpha^u_{\tilde{Z}_i\tilde{f}_1} + \omega^L_{H^+\tilde{W}^+\tilde{Z}}\beta^{\tilde{W}_j}_{\tilde{f}'_1}\mathcal{C}^u_{H^+ff'}\beta^u_{\tilde{Z}_i\tilde{f}_1}]m_{f'}|m_{\tilde{W}_j}|, \tag{A.688}$$

$$\mathcal{V}^{(6)}_{H^\pm\tilde{f}'_1} = [\omega^R_{H^+\tilde{W}^+\tilde{Z}}\beta^{\tilde{W}_j}_{\tilde{f}'_1}\mathcal{C}^u_{H^+ff'}\alpha^u_{\tilde{Z}_i\tilde{f}_1} + (-1)^{\theta_j}\omega^L_{H^+\tilde{W}^+\tilde{Z}}\alpha^{\tilde{W}_j}_{\tilde{f}'_1}\mathcal{C}^d_{H^+ff'}\beta^u_{\tilde{Z}_i\tilde{f}_1}]|m_{\tilde{W}_j}||m_{\tilde{Z}_i}|, \tag{A.689}$$

$$\mathcal{V}^{(7)}_{H^\pm\tilde{f}'_1} = -[(-1)^{\theta_j}\omega^L_{H^+\tilde{W}^+\tilde{Z}}\beta^{\tilde{W}_j}_{\tilde{f}'_1}\mathcal{C}^d_{H^+ff'}\alpha^u_{\tilde{Z}_i\tilde{f}_1} + \omega^R_{H^+\tilde{W}^+\tilde{Z}}\alpha^{\tilde{W}_j}_{\tilde{f}'_1}\mathcal{C}^u_{H^+ff'}\beta^u_{\tilde{Z}_i\tilde{f}_1}]m_f m_{f'}, \tag{A.690}$$

$$\mathcal{V}^{(8)}_{H^\pm\tilde{f}'_1} = -2[\omega^R_{H^+\tilde{W}^+\tilde{Z}}\beta^{\tilde{W}_j}_{\tilde{f}'_1}\mathcal{C}^d_{H^+ff'}\alpha^u_{\tilde{Z}_i\tilde{f}_1} + (-1)^{\theta_j}\omega^L_{H^+\tilde{W}^+\tilde{Z}}\alpha^{\tilde{W}_j}_{\tilde{f}'_1}\mathcal{C}^u_{H^+ff'}\beta^u_{\tilde{Z}_i\tilde{f}_1}]m_f m_{f'}|m_{\tilde{W}_j}||m_{\tilde{Z}_i}|. \tag{A.691}$$

The integrals required are exactly as in the $G\tilde{f'}_1$ but with the expected change $m_W \to m_{H^\pm}$. $\Gamma_{H^\pm \tilde{f'}_1}$ is then given exactly as $\Gamma_{G\tilde{f'}_1}$.

$\underline{\Gamma_{H^\pm \tilde{f'}_2}}$

The coupling combinations now are, if it's a neutralino decaying:

$$\mathcal{V}^{(1)}_{H^\pm \tilde{f'}_2} = -\frac{1}{2}[(-1)^{\theta_i}\omega^R_{H^+\tilde{W}^+\tilde{Z}}\alpha^u_{\tilde{Z}_i\tilde{f}_2}\mathcal{C}^d_{H^+ff'}\beta^{\tilde{W}_j}_{\tilde{f'}_2} + \omega^L_{H^+\tilde{W}^+\tilde{Z}}\beta^u_{\tilde{Z}_i\tilde{f}_2}\mathcal{C}^u_{H^+ff'}\alpha^{\tilde{W}_j}_{\tilde{f'}_2}], \tag{A.692}$$

$$\mathcal{V}^{(2)}_{H^\pm \tilde{f'}_2} = (\omega^R_{H^+\tilde{W}^+\tilde{Z}}\beta^u_{\tilde{Z}_i\tilde{f}_2}\mathcal{C}^u_{H^+ff'}\beta^{\tilde{W}_j}_{\tilde{f'}_2} - \omega^L_{H^+\tilde{W}^+\tilde{Z}}\alpha^u_{\tilde{Z}_i\tilde{f}_2}\mathcal{C}^d_{H^+ff'}\alpha^{\tilde{W}_j}_{\tilde{f'}_2})m_f|m_{\tilde{Z}_i}|(-1)^{\theta_i}, \tag{A.693}$$

$$\mathcal{V}^{(3)}_{H^\pm \tilde{f'}_2} = -[(-1)^{\theta_i}\omega^L_{H^+\tilde{W}^+\tilde{Z}}\beta^u_{\tilde{Z}_i\tilde{f}_2}\mathcal{C}^d_{H^+ff'}\beta^{\tilde{W}_j}_{\tilde{f'}_2} + \omega^R_{H^+\tilde{W}^+\tilde{Z}}\alpha^u_{\tilde{Z}_i\tilde{f}_2}\mathcal{C}^u_{H^+ff'}\alpha^{\tilde{W}_j}_{\tilde{f'}_2}]m_{f'}|m_{\tilde{W}_j}|, \tag{A.694}$$

$$\mathcal{V}^{(4)}_{H^\pm \tilde{f'}_2} = -[(-1)^{\theta_i}\omega^R_{H^+\tilde{W}^+\tilde{Z}}\beta^u_{\tilde{Z}_i\tilde{f}_2}\mathcal{C}^d_{H^+ff'}\beta^{\tilde{W}_j}_{\tilde{f'}_2} + \omega^L_{H^+\tilde{W}^+\tilde{Z}}\alpha^u_{\tilde{Z}_i\tilde{f}_2}\mathcal{C}^u_{H^+ff'}\alpha^{\tilde{W}_j}_{\tilde{f'}_2}]|m_{\tilde{Z}_i}|m_{f'}, \tag{A.695}$$

$$\mathcal{V}^{(5)}_{H^\pm \tilde{f'}_2} = (\omega^L_{H^+\tilde{W}^+\tilde{Z}}\beta^u_{\tilde{Z}_i\tilde{f}_2}\mathcal{C}^u_{H^+ff'}\beta^{\tilde{W}_j}_{\tilde{f'}_2} - \omega^R_{H^+\tilde{W}^+\tilde{Z}}\alpha^u_{\tilde{Z}_i\tilde{f}_2}\mathcal{C}^d_{H^+ff'}\alpha^{\tilde{W}_j}_{\tilde{f'}_2})m_f|m_{\tilde{W}_j}|(-1)^{\theta_j}, \tag{A.696}$$

$$\mathcal{V}^{(6)}_{H^\pm \tilde{f'}_2} = [\omega^L_{H^+\tilde{W}^+\tilde{Z}}\alpha^u_{\tilde{Z}_i\tilde{f}_2}\mathcal{C}^d_{H^+ff'}\beta^{\tilde{W}_j}_{\tilde{f'}_2} - (-1)^{\theta_i}\omega^R_{H^+\tilde{W}^+\tilde{Z}}\beta^u_{\tilde{Z}_i\tilde{f}_2}\mathcal{C}^u_{H^+ff'}\alpha^{\tilde{W}_j}_{\tilde{f'}_2}]|m_{\tilde{Z}_i}||m_{\tilde{W}_j}|, \tag{A.697}$$

$$\mathcal{V}^{(7)}_{H^\pm \tilde{f'}_2} = [-(-1)^{\theta_i}\omega^R_{H^+\tilde{W}^+\tilde{Z}}\alpha^u_{\tilde{Z}_i\tilde{f}_2}\mathcal{C}^u_{H^+ff'}\beta^{\tilde{W}_j}_{\tilde{f}'} + \omega^L_{H^+\tilde{W}^+\tilde{Z}}\beta^u_{\tilde{Z}_i\tilde{f}_2}\mathcal{C}^d_{H^+ff'}\alpha^{\tilde{W}_j}_{\tilde{f'}_2}]m_{f'}m_f, \tag{A.698}$$

$$\mathcal{V}^{(8)}_{H^\pm \tilde{f'}_2} = 2(-1)^{\theta_i}[-\omega^L_{H^+\tilde{W}^+\tilde{Z}}\alpha^u_{\tilde{Z}_i\tilde{f}_2}\mathcal{C}^u_{H^+ff'}\beta^{\tilde{W}_j}_{\tilde{f'}_2} + \omega^R_{H^+\tilde{W}^+\tilde{Z}}\beta^u_{\tilde{Z}_i\tilde{f}_2}\mathcal{C}^d_{H^+ff'}\alpha^{\tilde{W}_j}_{\tilde{f'}_2}]|m_{\tilde{Z}_i}||m_{\tilde{W}_j}|m_{f'}m_f. \tag{A.699}$$

Whilst if it's a chargino decaying:

$$\mathcal{V}^{(1)}_{H^\pm \tilde{f'}_2} = \frac{1}{2}[(-1)^{\theta_j}\omega^L_{H^+\tilde{W}^+\tilde{Z}}\beta^{\tilde{W}_j}_{\tilde{f'}_2}\mathcal{C}^u_{H^+ff'}\alpha^u_{\tilde{Z}_i\tilde{f}_2} + \omega^R_{H^+\tilde{W}^+\tilde{Z}}\alpha^{\tilde{W}_j}_{\tilde{f'}_2}\mathcal{C}^d_{H^+ff'}\beta^u_{\tilde{Z}_i\tilde{f}_2}], \tag{A.700}$$

$$\mathcal{V}^{(2)}_{H^\pm \tilde{f'}_2} = -[(-1)^{\theta_j}\omega^L_{H^+\tilde{W}^+\tilde{Z}}\alpha^{\tilde{W}_j}_{\tilde{f'}_2}\mathcal{C}^d_{H^+ff'}\alpha^u_{\tilde{Z}_i\tilde{f}_2} + \omega^R_{H^+\tilde{W}^+\tilde{Z}}\beta^{\tilde{W}_j}_{\tilde{f'}_2}\mathcal{C}^u_{H^+ff'}\beta^u_{\tilde{Z}_i\tilde{f}_2}]|m_{\tilde{Z}_i}|m_{f'}, \tag{A.701}$$

$$\mathcal{V}^{(3)}_{H^\pm \tilde{f'}_2} = (\omega^R_{H^+\tilde{W}^+\tilde{Z}}\alpha^{\tilde{W}_j}_{\tilde{f'}_2}\mathcal{C}^u_{H^+ff'}\alpha^u_{\tilde{Z}_i\tilde{f}_2} + (-1)^{\theta_j}\omega^L_{H^+\tilde{W}^+\tilde{Z}}\beta^{\tilde{W}_j}_{\tilde{f'}_2}\mathcal{C}^d_{H^+ff'}\beta^u_{\tilde{Z}_i\tilde{f}_2})m_f|m_{\tilde{W}_j}|, \tag{A.702}$$

$$\mathcal{V}^{(4)}_{H^\pm \tilde{f'}_2} = [(-1)^{\theta_j}\omega^L_{H^+\tilde{W}^+\tilde{Z}}\alpha^{\tilde{W}_j}_{\tilde{f'}_2}\mathcal{C}^u_{H^+ff'}\alpha^u_{\tilde{Z}_i\tilde{f}_2} + \omega^R_{H^+\tilde{W}^+\tilde{Z}}\beta^{\tilde{W}_j}_{\tilde{f'}_2}\mathcal{C}^d_{H^+ff'}\beta^u_{\tilde{Z}_i\tilde{f}_2}]|m_{\tilde{Z}_i}|m_f, \tag{A.703}$$

$$\mathcal{V}^{(5)}_{H^\pm \tilde{f'}_2} = -[\omega^R_{H^+\tilde{W}^+\tilde{Z}}\alpha^{\tilde{W}_j}_{\tilde{f'}_2}\mathcal{C}^d_{H^+ff'}\alpha^u_{\tilde{Z}_i\tilde{f}_2} + (-1)^{\theta_j}\omega^L_{H^+\tilde{W}^+\tilde{Z}}\beta^{\tilde{W}_j}_{\tilde{f'}_2}\mathcal{C}^u_{H^+ff'}\beta^u_{\tilde{Z}_i\tilde{f}_2}]m_{f'}|m_{\tilde{W}_j}|, \tag{A.704}$$

$$\mathcal{V}^{(6)}_{H^\pm \tilde{f'}_2} = (\omega^R_{H^+\tilde{W}^+\tilde{Z}}\beta^{\tilde{W}_j}_{\tilde{f'}_2}\mathcal{C}^u_{H^+ff'}\alpha^u_{\tilde{Z}_i\tilde{f}_2} + (-1)^{\theta_j}\omega^L_{H^+\tilde{W}^+\tilde{Z}}\alpha^{\tilde{W}_j}_{\tilde{f'}_2}\mathcal{C}^d_{H^+ff'}\beta^u_{\tilde{Z}_i\tilde{f}_2})|m_{\tilde{W}_j}||m_{\tilde{Z}_i}|, \tag{A.705}$$

$$\mathcal{V}^{(7)}_{H^\pm \tilde{f'}_2} = -[(-1)^{\theta_j}\omega^L_{H^+\tilde{W}^+\tilde{Z}}\beta^{\tilde{W}_j}_{\tilde{f'}_2}\mathcal{C}^d_{H^+ff'}\alpha^u_{\tilde{Z}_i\tilde{f}_2} + \omega^R_{H^+\tilde{W}^+\tilde{Z}}\alpha^{\tilde{W}_j}_{\tilde{f'}_2}\mathcal{C}^u_{H^+ff'}\beta^u_{\tilde{Z}_i\tilde{f}_2}]m_fm_{f'}, \tag{A.706}$$

$$\mathcal{V}^{(8)}_{H^\pm \tilde{f'}_2} = -2[\omega^R_{H^+\tilde{W}^+\tilde{Z}}\beta^{\tilde{W}_j}_{\tilde{f'}_2}\mathcal{C}^d_{H^+ff'}\alpha^u_{\tilde{Z}_i\tilde{f}_2} + (-1)^{\theta_j}\omega^L_{H^+\tilde{W}^+\tilde{Z}}\alpha^{\tilde{W}_j}_{\tilde{f'}_2}\mathcal{C}^u_{H^+ff'}\beta^u_{\tilde{Z}_i\tilde{f}_2}]m_fm_{f'}|m_{\tilde{W}_j}||m_{\tilde{Z}_i}|. \tag{A.707}$$

The required integrals are as for $G\tilde{f'}_2$ but with with the mass change $m_W \to m_{H^\pm}$. Similarly, $\Gamma_{H^\pm \tilde{f'}_2}$ is given analogously.

$\underline{\Gamma_{G\tilde{f}_1}}$

The coupling combinations here again depend upon if it's a neutralino decaying or chargino decaying, if it's a neutralino decaying:

$$\mathcal{V}^{(1)}_{G\tilde{f}_1} = -\frac{1}{2}[\omega^R_{G\tilde{W}\tilde{Z}}\beta^d_{\tilde{f}_1\tilde{Z}_i}\mathcal{C}^d_{Gff'}\alpha^{\tilde{W}_j}_{\tilde{f}_1} + (-1)^{\theta_i}\omega^L_{G\tilde{W}\tilde{Z}}\alpha^d_{\tilde{f}_1\tilde{Z}_i}\mathcal{C}^u_{Gff'}\beta^{\tilde{W}_j}_{\tilde{f}_1}], \tag{A.708}$$

$$\mathcal{V}^{(2)}_{G\tilde{f}_1} = -(\omega^R_{G\tilde{W}\tilde{Z}}\alpha^d_{\tilde{f}_1\tilde{Z}_i}\mathcal{C}^u_{Gff'}\alpha^{\tilde{W}_j}_{\tilde{f}_1} + (-1)^{\theta_i}\omega^L_{G\tilde{W}\tilde{Z}}\beta^d_{\tilde{f}_1\tilde{Z}_i}\mathcal{C}^d_{Gff'}\beta^{\tilde{W}_j}_{\tilde{f}_1})|m_{\tilde{Z}_i}|m_{f'}, \tag{A.709}$$

$$\mathcal{V}^{(3)}_{G\tilde{f}_1} = [(-1)^{\theta_i}\omega^L_{G\tilde{W}\tilde{Z}}\alpha^d_{\tilde{f}_1\tilde{Z}_i}\mathcal{C}^d_{Gff'}\alpha^{\tilde{W}_j}_{\tilde{f}_1} + \omega^R_{G\tilde{W}\tilde{Z}}\beta^d_{\tilde{f}_1\tilde{Z}_i}\mathcal{C}^u_{Gff'}\beta^{\tilde{W}_j}_{\tilde{f}_1}]m_f|m_{\tilde{W}_j}|, \tag{A.710}$$

$$\mathcal{V}^{(4)}_{G\tilde{f}_1} = (\omega^R_{G\tilde{W}\tilde{Z}}\alpha^d_{\tilde{f}_1\tilde{Z}_i}\mathcal{C}^d_{Gff'}\alpha^{\tilde{W}_j}_{\tilde{f}_1} - (-1)^{\theta_i}\omega^L_{G\tilde{W}\tilde{Z}}\beta^d_{\tilde{f}_1\tilde{Z}_i}\mathcal{C}^u_{Gff'}\beta^{\tilde{W}_j}_{\tilde{f}_1})|m_{\tilde{Z}_i}|m_f, \tag{A.711}$$

$$\mathcal{V}^{(5)}_{G\tilde{f}_1} = -[(-1)^{\theta_i}\omega^L_{G\tilde{W}\tilde{Z}}\alpha^d_{\tilde{f}_1\tilde{Z}_i}\mathcal{C}^u_{Gff'}\alpha^{\tilde{W}_j}_{\tilde{f}_1} + \omega^R_{G\tilde{W}\tilde{Z}}\beta^d_{\tilde{f}_1\tilde{Z}_i}\mathcal{C}^d_{Gff'}\beta^{\tilde{W}_j}_{\tilde{f}_1}]m_{f'}|m_{\tilde{W}_j}|, \tag{A.712}$$

$$\mathcal{V}^{(6)}_{G\tilde{f}_1} = -[(-1)^{\theta_i}\omega^L_{G\tilde{W}\tilde{Z}}\beta^d_{\tilde{f}_1\tilde{Z}_i}\mathcal{C}^d_{Gff'}\alpha^{\tilde{W}_j}_{\tilde{f}_1} - \omega^R_{G\tilde{W}\tilde{Z}}\alpha^d_{\tilde{f}_1\tilde{Z}_i}\mathcal{C}^u_{Gff'}\beta^{\tilde{W}_j}_{\tilde{f}_1}]|m_{\tilde{Z}_i}||m_{\tilde{W}_j}|, \tag{A.713}$$

$$\mathcal{V}^{(7)}_{G\tilde{f}_1} = -(\omega^R_{G\tilde{W}\tilde{Z}}\beta^d_{\tilde{f}_1\tilde{Z}_i}\mathcal{C}^u_{Gff'}\alpha^{\tilde{W}_j}_{\tilde{f}_1} - (-1)^{\theta_i}\omega^L_{G\tilde{W}\tilde{Z}}\alpha^d_{\tilde{f}_1\tilde{Z}_i}\mathcal{C}^d_{Gff'}\beta^{\tilde{W}_j}_{\tilde{f}_1})m_{f'}m_f, \tag{A.714}$$

$$\mathcal{V}^{(8)}_{G\tilde{f}_1} = -2[(-1)^{\theta_i}\omega^L_{G\tilde{W}\tilde{Z}}\beta^d_{\tilde{f}_1\tilde{Z}_i}\mathcal{C}^u_{Gff'}\alpha^{\tilde{W}_j}_{\tilde{f}_1} + \omega^R_{G\tilde{W}\tilde{Z}}\alpha^d_{\tilde{f}_1\tilde{Z}_i}\mathcal{C}^d_{Gff'}\beta^{\tilde{W}_j}_{\tilde{f}_1}]|m_{\tilde{Z}_i}||m_{\tilde{W}_j}|m_{f'}m_f. \tag{A.715}$$

On the other hand, if it's instead a chargino decaying to neutralino:

$$\mathcal{V}^{(1)}_{G\tilde{f}_1} = \frac{1}{2}[(-1)^{\theta_j}\omega^L_{G\tilde{W}\tilde{Z}}\beta^{\tilde{W}_j}_{\tilde{f}_1}\mathcal{C}^u_{Gff'}\alpha^d_{\tilde{f}_1\tilde{Z}_i} + \omega^R_{G\tilde{W}\tilde{Z}}\alpha^{\tilde{W}_j}_{\tilde{f}_1}\mathcal{C}^d_{Gff'}\beta^d_{\tilde{f}_1\tilde{Z}_i}], \tag{A.716}$$

$$\mathcal{V}^{(2)}_{G\tilde{f}_1} = [(-1)^{\theta_j}\omega^L_{G\tilde{W}\tilde{Z}}\alpha^{\tilde{W}_j}_{\tilde{f}_1}\mathcal{C}^d_{Gff'}\alpha^d_{\tilde{f}_1\tilde{Z}_i} + \omega^R_{G\tilde{W}\tilde{Z}}\beta^{\tilde{W}_j}_{\tilde{f}_1}\mathcal{C}^u_{Gff'}\beta^d_{\tilde{f}_1\tilde{Z}_i}]|m_{\tilde{Z}_i}|m_f, \tag{A.717}$$

$$\mathcal{V}^{(3)}_{G\tilde{f}_1} = -(\omega^R_{G\tilde{W}\tilde{Z}}\alpha^{\tilde{W}_j}_{\tilde{f}_1}\mathcal{C}^u_{Gff'}\alpha^d_{\tilde{f}_1\tilde{Z}_i} + (-1)^{\theta_j}\omega^L_{G\tilde{W}\tilde{Z}}\beta^{\tilde{W}_j}_{\tilde{f}_1}\mathcal{C}^d_{Gff'}\beta^d_{\tilde{f}_1\tilde{Z}_i})m_{f'}|m_{\tilde{W}_j}|, \tag{A.718}$$

$$\mathcal{V}^{(4)}_{G\tilde{f}_1} = -[(-1)^{\theta_j}\omega^L_{G\tilde{W}\tilde{Z}}\alpha^{\tilde{W}_j}_{\tilde{f}_1}\mathcal{C}^u_{Gff'}\alpha^d_{\tilde{f}_1\tilde{Z}_i} + \omega^R_{G\tilde{W}\tilde{Z}}\beta^{\tilde{W}_j}_{\tilde{f}_1}\mathcal{C}^d_{Gff'}\beta^d_{\tilde{f}_1\tilde{Z}_i}]|m_{\tilde{Z}_i}|m_{f'}, \tag{A.719}$$

$$\mathcal{V}^{(5)}_{G\tilde{f}_1} = (\omega^R_{G\tilde{W}\tilde{Z}}\alpha^{\tilde{W}_j}_{\tilde{f}_1}\mathcal{C}^d_{Gff'} + (-1)^{\theta_j}\omega^L_{G\tilde{W}\tilde{Z}}\beta^{\tilde{W}_j}_{\tilde{f}_1}\mathcal{C}^u_{Gff'}\beta^d_{\tilde{f}_1\tilde{Z}_i})m_f|m_{\tilde{W}_j}|, \tag{A.720}$$

$$\mathcal{V}^{(6)}_{G\tilde{f}_1} = (\omega^R_{G\tilde{W}\tilde{Z}}\beta^{\tilde{W}_j}_{\tilde{f}_1}\mathcal{C}^u_{Gff'}\alpha^d_{\tilde{f}_1\tilde{Z}_i} + (-1)^{\theta_j}\omega^L_{G\tilde{W}\tilde{Z}}\alpha^{\tilde{W}_j}_{\tilde{f}_1}\mathcal{C}^d_{Gff'}\beta^d_{\tilde{f}_1\tilde{Z}_i})|m_{\tilde{W}_j}||m_{\tilde{Z}_i}|, \tag{A.721}$$

$$\mathcal{V}^{(7)}_{G\tilde{f}_1} = -[(-1)^{\theta_j}\omega^L_{G\tilde{W}\tilde{Z}}\beta^{\tilde{W}_j}_{\tilde{f}_1}\mathcal{C}^d_{Gff'}\alpha^d_{\tilde{f}_1\tilde{Z}_i} + \omega^R_{G\tilde{W}\tilde{Z}}\alpha^{\tilde{W}_j}_{\tilde{f}_1}\mathcal{C}^u_{Gff'}\beta^d_{\tilde{f}_1\tilde{Z}_i}]m_f m_{f'}, \tag{A.722}$$

$$\mathcal{V}^{(8)}_{G\tilde{f}_1} = -2[\omega^R_{G\tilde{W}\tilde{Z}}\beta^{\tilde{W}_j}_{\tilde{f}_1}\mathcal{C}^d_{Gff'}\alpha^d_{\tilde{f}_1\tilde{Z}_i} + (-1)^{\theta_j}\omega^L_{G\tilde{W}\tilde{Z}}\alpha^{\tilde{W}_j}_{\tilde{f}_1}\mathcal{C}^u_{Gff'}\beta^d_{\tilde{f}_1\tilde{Z}_i}]m_f m_{f'}|m_{\tilde{W}_j}||m_{\tilde{Z}_i}|. \tag{A.723}$$

The integrals are exactly as for $G\tilde{f}'_1$ except you must swap $m_{f'} \leftrightarrow m_f$ and $m_{\tilde{f}'_1} \leftrightarrow m_{\tilde{f}_1}$. As for $G\tilde{f}'_1$, for the case of a chargino decaying to a neutralino you must relabel integrals such that integrals 2 and 4 are swapped as are integrals 3 and 5. The $\Gamma_{G\tilde{f}_1}$ is then given analogously to $\Gamma_{G\tilde{f}'_1}$ as the sum of the products of the coupling combinations with corresponding integrals.

$\underline{\Gamma_{G\tilde{f}_2}}$

Here the coupling combinations are, if a neutralino is decaying:

$$\mathcal{V}^{(1)}_{G\tilde{f}_2} = -\frac{1}{2}[\omega^R_{G\tilde{W}\tilde{Z}}\beta^d_{\tilde{f}_2\tilde{Z}_i}\mathcal{C}^d_{Gff'}\alpha^{\tilde{W}_j}_{\tilde{f}_2} + (-1)^{\theta_i}\omega^L_{G\tilde{W}\tilde{Z}}\alpha^d_{\tilde{f}_2\tilde{Z}_i}\mathcal{C}^u_{Gff'}\beta^{\tilde{W}_j}_{\tilde{f}_2}], \tag{A.724}$$

$$\mathcal{V}^{(2)}_{G\tilde{f}_2} = [\omega^R_{G\tilde{W}\tilde{Z}}\alpha^d_{\tilde{f}_2\tilde{Z}_i}\mathcal{C}^u_{Gff'}\alpha^{\tilde{W}_j}_{\tilde{f}_2} + (-1)^{\theta_i}\omega^L_{G\tilde{W}\tilde{Z}}\beta^d_{\tilde{f}_2\tilde{Z}_i}\mathcal{C}^d_{Gff'}\beta^{\tilde{W}_j}_{\tilde{f}_2}]|m_{\tilde{Z}_i}|m_{f'}, \tag{A.725}$$

$$\mathcal{V}^{(3)}_{G\tilde{f}_2} = -((-1)^{\theta_i}\omega^L_{G\tilde{W}\tilde{Z}}\alpha^d_{\tilde{f}_2\tilde{Z}_i}\mathcal{C}^d_{Gff'}\alpha^{\tilde{W}_j}_{\tilde{f}_2} + \omega^R_{G\tilde{W}\tilde{Z}}\beta^d_{\tilde{f}_2\tilde{Z}_i}\mathcal{C}^u_{Gff'}\beta^{\tilde{W}_j}_{\tilde{f}_2})m_f|m_{\tilde{W}_j}|, \tag{A.726}$$

$$\mathcal{V}^{(4)}_{G\tilde{f}_2} = -[\omega^R_{G\tilde{W}\tilde{Z}}\alpha^d_{\tilde{f}_2\tilde{Z}_i}\mathcal{C}^d_{Gff'}\alpha^{\tilde{W}_j}_{\tilde{f}_2} + (-1)^{\theta_i}\omega^L_{G\tilde{W}\tilde{Z}}\beta^d_{\tilde{f}_2\tilde{Z}_i}\mathcal{C}^u_{Gff'}\beta^{\tilde{W}_j}_{\tilde{f}_2}]|m_{\tilde{Z}_i}|m_f, \tag{A.727}$$

$$\mathcal{V}^{(5)}_{G\tilde{f}_2} = [(-1)^{\theta_i}\omega^L_{G\tilde{W}\tilde{Z}}\alpha^d_{\tilde{f}_2\tilde{Z}_i}\mathcal{C}^u_{Gff'}\alpha^{\tilde{W}_j}_{\tilde{f}_2} + \omega^R_{G\tilde{W}\tilde{Z}}\beta^d_{\tilde{f}_2\tilde{Z}_i}\mathcal{C}^d_{Gff'}\beta^{\tilde{W}_j}_{\tilde{f}_2}]m_{f'}|m_{\tilde{W}_j}|, \tag{A.728}$$

$$\mathcal{V}^{(6)}_{G\tilde{f}_2} = -((-1)^{\theta_i}\omega^L_{G\tilde{W}\tilde{Z}}\beta^d_{\tilde{f}_2\tilde{Z}_i}\mathcal{C}^d_{Gff'}\alpha^{\tilde{W}_j}_{\tilde{f}_2} + \omega^R_{G\tilde{W}\tilde{Z}}\alpha^d_{\tilde{f}_2\tilde{Z}_i}\mathcal{C}^u_{Gff'}\beta^{\tilde{W}_j}_{\tilde{f}_2})|m_{\tilde{Z}_i}||m_{\tilde{W}_j}|(-1)^{\theta_j}, \tag{A.729}$$

$$\mathcal{V}^{(7)}_{G\tilde{f}_2} = [\omega^R_{G\tilde{W}\tilde{Z}}\beta^d_{\tilde{f}_2\tilde{Z}_i}\mathcal{C}^u_{Gff'}\alpha^{\tilde{W}_j}_{\tilde{f}_2} + (-1)^{\theta_i}\omega^L_{G\tilde{W}\tilde{Z}}\alpha^d_{\tilde{f}_2\tilde{Z}_i}\mathcal{C}^d_{Gff'}\beta^{\tilde{W}_j}_{\tilde{f}_2}]m_{f'}m_f, \tag{A.730}$$

$$\mathcal{V}^{(8)}_{G\tilde{f}_2} = 2[(-1)^{\theta_i}\omega^L_{G\tilde{W}\tilde{Z}}\beta^d_{\tilde{f}_2\tilde{Z}_i}\mathcal{C}^u_{Gff'}\alpha^{\tilde{W}_j}_{\tilde{f}_2} + \omega^R_{G\tilde{W}\tilde{Z}}\alpha^d_{\tilde{f}_2\tilde{Z}_i}\mathcal{C}^d_{Gff'}\beta^{\tilde{W}_j}_{\tilde{f}_2}]|m_{\tilde{Z}_i}|m_{f'}m_f|m_{\tilde{W}_j}|(-1)^{\theta_j}. \tag{A.731}$$

If it's a chargino decaying:

$$\mathcal{V}^{(1)}_{G\tilde{f}_2} = -\frac{1}{2}(-1)^{\theta_j}[\omega^L_{G\tilde{W}\tilde{Z}}\beta^{\tilde{W}_j}_{\tilde{f}_2}\mathcal{C}^u_{Gff'}\alpha^d_{\tilde{f}_2\tilde{Z}_i} - \omega^R_{G\tilde{W}\tilde{Z}}\alpha^{\tilde{W}_j}_{\tilde{f}_2}\mathcal{C}^d_{Gff'}\beta^d_{\tilde{f}_2\tilde{Z}_i}], \tag{A.732}$$

$$\mathcal{V}^{(2)}_{G\tilde{f}_2} = -[\omega^L_{G\tilde{W}\tilde{Z}}\alpha^{\tilde{W}_j}_{\tilde{f}_2}\mathcal{C}^d_{Gff'}\alpha^d_{\tilde{f}_2\tilde{Z}_i} - (-1)^{\theta_j}\omega^R_{G\tilde{W}\tilde{Z}}\beta^{\tilde{W}_j}_{\tilde{f}_2}\mathcal{C}^u_{Gff'}\beta^d_{\tilde{f}_2\tilde{Z}_i}]|m_{\tilde{Z}_i}|m_f, \tag{A.733}$$

$$\mathcal{V}^{(3)}_{G\tilde{f}_2} = [(-1)^{\theta_j}\omega^R_{G\tilde{W}\tilde{Z}}\alpha^{\tilde{W}_j}_{\tilde{f}_2}\mathcal{C}^u_{Gff'}\alpha^d_{\tilde{f}_2\tilde{Z}_i} - \omega^L_{G\tilde{W}\tilde{Z}}\beta^{\tilde{W}_j}_{\tilde{f}_2}\mathcal{C}^d_{Gff'}\beta^d_{\tilde{f}_2\tilde{Z}_i}]m_{f'}|m_{\tilde{W}_j}|, \tag{A.734}$$

$$\mathcal{V}^{(4)}_{G\tilde{f}_2} = (\omega^L_{G\tilde{W}\tilde{Z}}\alpha^{\tilde{W}_j}_{\tilde{f}_2}\mathcal{C}^u_{Gff'}\alpha^d_{\tilde{f}_2\tilde{Z}_i} + (-1)^{\theta_j}\omega^R_{G\tilde{W}\tilde{Z}}\beta^{\tilde{W}_j}_{\tilde{f}_2}\mathcal{C}^d_{Gff'}\beta^d_{\tilde{f}_2\tilde{Z}_i})|m_{\tilde{Z}_i}|m_{f'}, \tag{A.735}$$

$$\mathcal{V}^{(5)}_{G\tilde{f}_2} = -[(-1)^{\theta_j}\omega^R_{G\tilde{W}\tilde{Z}}\alpha^{\tilde{W}_j}_{\tilde{f}_2}\mathcal{C}^d_{Gff'}\alpha^d_{\tilde{f}_2\tilde{Z}_i} + \omega^L_{G\tilde{W}\tilde{Z}}\beta^{\tilde{W}_j}_{\tilde{f}_2}\mathcal{C}^u_{Gff'}\beta^d_{\tilde{f}_2\tilde{Z}_i}]m_f|m_{\tilde{W}_j}|, \tag{A.736}$$

$$\mathcal{V}^{(6)}_{G\tilde{f}_2} = [\omega^R_{G\tilde{W}\tilde{Z}}\beta^{\tilde{W}_j}_{\tilde{f}_2}\mathcal{C}^u_{Gff'}\alpha^d_{\tilde{f}_2\tilde{Z}_i} + \omega^L_{G\tilde{W}\tilde{Z}}\alpha^{\tilde{W}_j}_{\tilde{f}_2}\mathcal{C}^d_{Gff'}\beta^d_{\tilde{f}_2\tilde{Z}_i}]|m_{\tilde{W}_j}||m_{\tilde{Z}_i}|, \tag{A.737}$$

$$\mathcal{V}^{(7)}_{G\tilde{f}_2} = -(-1)^{\theta_j}[\omega^L_{G\tilde{W}\tilde{Z}}\beta^{\tilde{W}_j}_{\tilde{f}_2}\mathcal{C}^d_{Gff'}\alpha^d_{\tilde{f}_2\tilde{Z}_i} + \omega^R_{G\tilde{W}\tilde{Z}}\alpha^{\tilde{W}_j}_{\tilde{f}_2}\mathcal{C}^u_{Gff'}\beta^d_{\tilde{f}_2\tilde{Z}_i}]m_f m_{f'}, \tag{A.738}$$

$$\mathcal{V}^{(8)}_{G\tilde{f}_2} = 2[(-1)^{\theta_j}\omega^R_{G\tilde{W}\tilde{Z}}\beta^{\tilde{W}_j}_{\tilde{f}_2}\mathcal{C}^d_{Gff'}\alpha^d_{\tilde{f}_2\tilde{Z}_i} + \omega^L_{G\tilde{W}\tilde{Z}}\alpha^{\tilde{W}_j}_{\tilde{f}_2}\mathcal{C}^u_{Gff'}\beta^d_{\tilde{f}_2\tilde{Z}_i}]m_f m_{f'}|m_{\tilde{W}_j}||m_{\tilde{Z}_i}|. \tag{A.739}$$

The integrals are exactly as for $G\tilde{f}'_2$ except you must swap $m_{f'} \leftrightarrow m_f$ and $m_{\tilde{f}'_2} \leftrightarrow m_{\tilde{f}_2}$. As for $G\tilde{f}'_2$, for the case of a chargino decaying to a neutralino you must relabel integrals such that integrals 2 and 4 are swapped as are integrals 3 and 5. The $\Gamma_{G\tilde{f}_2}$ is then given analogously to $\Gamma_{G\tilde{f}'_2}$ as the sum of the products of the coupling combinations with corresponding integrals.

$\underline{\Gamma_{H^\pm\tilde{f}_1}}$

Again couplings depend upon which direction the decay occurs, if it is a neutralino decaying the couplings are:

$$\mathcal{V}^{(1)}_{H^\pm\tilde{f}_1} = \frac{1}{2}[\omega^R_{H^+\tilde{W}^+\tilde{Z}}\beta^d_{\tilde{Z}_i\tilde{f}_1}\mathcal{C}^d_{H^+ff'}\alpha^{\tilde{W}_j}_{\tilde{f}_1} + \omega^L_{H^+\tilde{W}^+\tilde{Z}}\alpha^d_{\tilde{Z}_i\tilde{f}_1}\mathcal{C}^u_{H^+ff'}\beta^{\tilde{W}_j}_{\tilde{f}_1}], \tag{A.740}$$

$$\mathcal{V}^{(2)}_{H^\pm\tilde{f}_1} = -[\omega^R_{H^+\tilde{W}^+\tilde{Z}}\alpha^d_{\tilde{Z}_i\tilde{f}_1}\mathcal{C}^u_{H^+ff'}\alpha^{\tilde{W}_j}_{\tilde{f}_1} + \omega^L_{H^+\tilde{W}^+\tilde{Z}}\beta^d_{\tilde{Z}_i\tilde{f}_1}\mathcal{C}^d_{H^+ff'}\beta^{\tilde{W}_j}_{\tilde{f}_1}]|m_{\tilde{Z}_i}|m_{f'}, \tag{A.741}$$

$$\mathcal{V}^{(3)}_{H^\pm\tilde{f}_1} = (\omega^L_{H^+\tilde{W}^+\tilde{Z}}\alpha^d_{\tilde{Z}_i\tilde{f}_1}\mathcal{C}^d_{H^+ff'}\alpha^{\tilde{W}_j}_{\tilde{f}_1} + \omega^R_{H^+\tilde{W}^+\tilde{Z}}\beta^d_{\tilde{Z}_i\tilde{f}_1}\mathcal{C}^u_{H^+ff'}\beta^{\tilde{W}_j}_{\tilde{f}_1})m_f|m_{\tilde{W}_j}|(-1)^{\theta_i}, \tag{A.742}$$

$$\mathcal{V}^{(4)}_{H^\pm\tilde{f}_1} = (\omega^R_{H^+\tilde{W}^+\tilde{Z}}\alpha^d_{\tilde{Z}_i\tilde{f}_1}\mathcal{C}^d_{H^+ff'}\alpha^{\tilde{W}_j}_{\tilde{f}_1} + \omega^L_{H^+\tilde{W}^+\tilde{Z}}\beta^d_{\tilde{Z}_i\tilde{f}_1}\mathcal{C}^u_{H^+ff'}\beta^{\tilde{W}_j}_{\tilde{f}_1})|m_{\tilde{Z}_i}|m_f, \tag{A.743}$$

$$\mathcal{V}^{(5)}_{H^\pm\tilde{f}_1} = -[(-1)^{\theta_i}\omega^L_{H^+\tilde{W}^+\tilde{Z}}\alpha^d_{\tilde{Z}_i\tilde{f}_1}\mathcal{C}^u_{H^+ff'}\alpha^{\tilde{W}_j}_{\tilde{f}_1} + \omega^R_{H^+\tilde{W}^+\tilde{Z}}\beta^d_{\tilde{Z}_i\tilde{f}_1}\mathcal{C}^d_{H^+ff'}\beta^{\tilde{W}_j}_{\tilde{f}_1}]m_{f'}|m_{\tilde{W}_j}|, \tag{A.744}$$

$$\mathcal{V}^{(6)}_{H^\pm\tilde{f}_1} = [(-1)^{\theta_i}\omega^L_{H^+\tilde{W}^+\tilde{Z}}\beta^d_{\tilde{Z}_i\tilde{f}_1}\mathcal{C}^d_{H^+ff'}\alpha^{\tilde{W}_j}_{\tilde{f}_1} - \omega^R_{H^+\tilde{W}^+\tilde{Z}}\alpha^d_{\tilde{Z}_i\tilde{f}_1}\mathcal{C}^u_{H^+ff'}\beta^{\tilde{W}_j}_{\tilde{f}_1}]|m_{\tilde{Z}_i}||m_{\tilde{W}_j}|, \tag{A.745}$$

$$\mathcal{V}^{(7)}_{H^\pm\tilde{f}_1} = -[\omega^R_{H^+\tilde{W}^+\tilde{Z}}\beta^d_{\tilde{Z}_i\tilde{f}_1}\mathcal{C}^u_{H^+ff'}\alpha^{\tilde{W}_j}_{\tilde{f}_1} - (-1)^{\theta_i}\omega^L_{H^+\tilde{W}^+\tilde{Z}}\alpha^d_{\tilde{Z}_i\tilde{f}_1}\mathcal{C}^d_{H^+ff'}\beta^{\tilde{W}_j}_{\tilde{f}_1}]m_{f'}m_f, \tag{A.746}$$

$$\mathcal{V}^{(8)}_{H^\pm\tilde{f}_1} = -2[(-1)^{\theta_i}\omega^L_{H^+\tilde{W}^+\tilde{Z}}\beta^d_{\tilde{Z}_i\tilde{f}_1}\mathcal{C}^u_{H^+ff'}\alpha^{\tilde{W}_j}_{\tilde{f}_1} - \omega^R_{H^+\tilde{W}^+\tilde{Z}}\alpha^d_{\tilde{Z}_i\tilde{f}_1}\mathcal{C}^d_{H^+ff'}\beta^{\tilde{W}_j}_{\tilde{f}_1}]|m_{\tilde{Z}_i}||m_{\tilde{W}_j}|m_{f'}m_f. \tag{A.747}$$

Whilst if it's a chargino decaying:

$$\mathcal{V}^{(1)}_{H^\pm\tilde{f}_1} = \frac{1}{2}[(-1)^{\theta_j}\omega^L_{H^+\tilde{W}^+\tilde{Z}}\beta^{\tilde{W}_j}_{\tilde{f}_1}\mathcal{C}^u_{H^+ff'}\alpha^d_{\tilde{Z}_i\tilde{f}_1} + \omega^R_{H^+\tilde{W}^+\tilde{Z}}\alpha^{\tilde{W}_j}_{\tilde{f}_1}\mathcal{C}^d_{H^+ff'}\beta^d_{\tilde{Z}_i\tilde{f}_1}], \tag{A.748}$$

$$\mathcal{V}^{(2)}_{H^\pm\tilde{f}_1} = [(-1)^{\theta_j}\omega^L_{H^+\tilde{W}^+\tilde{Z}}\alpha^{\tilde{W}_j}_{\tilde{f}_1}\mathcal{C}^d_{H^+ff'}\alpha^d_{\tilde{Z}_i\tilde{f}_1} + \omega^R_{H^+\tilde{W}^+\tilde{Z}}\beta^{\tilde{W}_j}_{\tilde{f}_1}\mathcal{C}^u_{H^+ff'}\beta^d_{\tilde{Z}_i\tilde{f}_1}]|m_{\tilde{Z}_i}|m_f, \tag{A.749}$$

$$\mathcal{V}^{(3)}_{H^\pm\tilde{f}_1} = -[\omega^R_{H^+\tilde{W}^+\tilde{Z}}\alpha^{\tilde{W}_j}_{\tilde{f}_1}\mathcal{C}^u_{H^+ff'}\alpha^d_{\tilde{Z}_i\tilde{f}_1} + (-1)^{\theta_j}\omega^L_{H^+\tilde{W}^+\tilde{Z}}\beta^{\tilde{W}_j}_{\tilde{f}_1}\mathcal{C}^d_{H^+ff'}\beta^d_{\tilde{Z}_i\tilde{f}_1}]m_{f'}|m_{\tilde{W}_j}|, \tag{A.750}$$

$$\mathcal{V}^{(4)}_{H^\pm\tilde{f}_1} = -[(-1)^{\theta_j}\omega^L_{H^+\tilde{W}^+\tilde{Z}}\alpha^{\tilde{W}_j}_{\tilde{f}_1}\mathcal{C}^u_{H^+ff'}\alpha^d_{\tilde{Z}_i\tilde{f}_1} + \omega^R_{H^+\tilde{W}^+\tilde{Z}}\beta^{\tilde{W}_j}_{\tilde{f}_1}\mathcal{C}^d_{H^+ff'}\beta^d_{\tilde{Z}_i\tilde{f}_1}]|m_{\tilde{Z}_i}|m_{f'}, \tag{A.751}$$

$$\mathcal{V}^{(5)}_{H^\pm\tilde{f}_1} = (\omega^R_{H^+\tilde{W}^+\tilde{Z}}\alpha^{\tilde{W}_j}_{\tilde{f}_1}\mathcal{C}^d_{H^+ff'}\alpha^d_{\tilde{Z}_i\tilde{f}_1} + (-1)^{\theta_j}\omega^L_{H^+\tilde{W}^+\tilde{Z}}\beta^{\tilde{W}_j}_{\tilde{f}_1}\mathcal{C}^u_{H^+ff'}\beta^d_{\tilde{Z}_i\tilde{f}_1})m_f|m_{\tilde{W}_j}|, \tag{A.752}$$

$$\mathcal{V}^{(6)}_{H^\pm\tilde{f}_1} = (\omega^R_{H^+\tilde{W}^+\tilde{Z}}\beta^{\tilde{W}_j}_{\tilde{f}_1}\mathcal{C}^u_{H^+ff'}\alpha^d_{\tilde{Z}_i\tilde{f}_1} + (-1)^{\theta_j}\omega^L_{H^+\tilde{W}^+\tilde{Z}}\alpha^{\tilde{W}_j}_{\tilde{f}_1}\mathcal{C}^d_{H^+ff'}\beta^d_{\tilde{Z}_i\tilde{f}_1})|m_{\tilde{W}_j}||m_{\tilde{Z}_i}|, \tag{A.753}$$

$$\mathcal{V}^{(7)}_{H^\pm\tilde{f}_1} = -[(-1)^{\theta_j}\omega^L_{H^+\tilde{W}^+\tilde{Z}}\beta^{\tilde{W}_j}_{\tilde{f}_1}\mathcal{C}^d_{H^+ff'}\alpha^d_{\tilde{Z}_i\tilde{f}_1} + \omega^R_{H^+\tilde{W}^+\tilde{Z}}\alpha^{\tilde{W}_j}_{\tilde{f}_1}\mathcal{C}^u_{H^+ff'}\beta^d_{\tilde{Z}_i\tilde{f}_1}]m_f m_{f'}, \tag{A.754}$$

$$\mathcal{V}^{(8)}_{H^\pm\tilde{f}_1} = -2[\omega^R_{H^+\tilde{W}^+\tilde{Z}}\beta^{\tilde{W}_j}_{\tilde{f}_1}\mathcal{C}^d_{H^+ff'}\alpha^d_{\tilde{Z}_i\tilde{f}_1} + (-1)^{\theta_j}\omega^L_{H^+\tilde{W}^+\tilde{Z}}\alpha^{\tilde{W}_j}_{\tilde{f}_1}\mathcal{C}^u_{H^+ff'}\beta^d_{\tilde{Z}_i\tilde{f}_1}]m_f m_{f'}|m_{\tilde{W}_j}||m_{\tilde{Z}_i}|. \tag{A.755}$$

The integrals and overall contribution are given exactly as for $H^{\pm}\tilde{f'}_1$ but $m_{\tilde{f'}_1} \to m_{\tilde{f}_1}$. Remember the integrals' labelling depends on whether it's a neutralino decaying (to a chargino) or a chargino decaying (to a neutralino).

$\underline{\Gamma_{H^{\pm}\tilde{f}_2}}$

The coupling combinations again depend upon which way around the decay is occurring, for a neutralino decaying the coupling combinations are:

$$\mathcal{V}^{(1)}_{H^{\pm}\tilde{f}_2} = -\frac{1}{2}[\omega^R_{H^+\tilde{W}^+\tilde{Z}}\beta^d_{\tilde{f}_2\tilde{Z}_i}\mathcal{C}^d_{H^+ff'}\alpha^{\tilde{W}_j}_{\tilde{f}_2} + \omega^L_{H^+\tilde{W}^+\tilde{Z}}\alpha^d_{\tilde{f}_2\tilde{Z}_i}\mathcal{C}^u_{H^+ff'}\beta^{\tilde{W}_j}_{\tilde{f}_2}], \tag{A.756}$$

$$\mathcal{V}^{(2)}_{H^{\pm}\tilde{f}_2} = (\omega^R_{H^+\tilde{W}^+\tilde{Z}}\alpha^d_{\tilde{f}_2\tilde{Z}_i}\mathcal{C}^u_{H^+ff'}\alpha^{\tilde{W}_j}_{\tilde{f}_2} + \omega^L_{H^+\tilde{W}^+\tilde{Z}}\beta^d_{\tilde{f}_2\tilde{Z}_i}\mathcal{C}^d_{H^+ff'}\beta^{\tilde{W}_j}_{\tilde{f}_2}]|m_{\tilde{Z}_i}|m_{f'}, \tag{A.757}$$

$$\mathcal{V}^{(3)}_{H^{\pm}\tilde{f}_2} = -[\omega^L_{H^+\tilde{W}^+\tilde{Z}}L\alpha^d_{\tilde{f}_2\tilde{Z}_i}\mathcal{C}^d_{H^+ff'}\alpha^{\tilde{W}_j}_{\tilde{f}_2} + \omega^R_{H^+\tilde{W}^+\tilde{Z}}\beta^d_{\tilde{f}_2\tilde{Z}_i}\mathcal{C}^u_{H^+ff'}\beta^{\tilde{W}_j}_{\tilde{f}_2}]m_f|m_{\tilde{W}_j}|(-1)^{\theta_i}, \tag{A.758}$$

$$\mathcal{V}^{(4)}_{H^{\pm}\tilde{f}_2} = -[\omega^R_{H^+\tilde{W}^+\tilde{Z}}\alpha^d_{\tilde{f}_2\tilde{Z}_i}\mathcal{C}^d_{H^+ff'}\alpha^{\tilde{W}_j}_{\tilde{f}_2} + \omega^L_{H^+\tilde{W}^+\tilde{Z}}\beta^d_{\tilde{f}_2\tilde{Z}_i}\mathcal{C}^u_{H^+ff'}\beta^{\tilde{W}_j}_{\tilde{f}_2}]|m_{\tilde{Z}_i}|m_f, \tag{A.759}$$

$$\mathcal{V}^{(5)}_{H^{\pm}\tilde{f}_2} = [(-1)^{\theta_i}\omega^L_{H^+\tilde{W}^+\tilde{Z}}\alpha^d_{\tilde{f}_2\tilde{Z}_i}\mathcal{C}^u_{H^+ff'}\alpha^{\tilde{W}_j}_{\tilde{f}_2} + \omega^R_{H^+\tilde{W}^+\tilde{Z}}\beta^d_{\tilde{f}_2\tilde{Z}_i}\mathcal{C}^d_{H^+ff'}\beta^{\tilde{W}_j}_{\tilde{f}_2}]m_{f'}|m_{\tilde{W}_j}|, \tag{A.760}$$

$$\mathcal{V}^{(6)}_{H^{\pm}\tilde{f}_2} = -[\omega^L_{H^+\tilde{W}^+\tilde{Z}}\beta^d_{\tilde{f}_2\tilde{Z}_i}\mathcal{C}^d_{H^+ff'}\alpha^{\tilde{W}_j}_{\tilde{f}_2} + \omega^R_{H^+\tilde{W}^+\tilde{Z}}\alpha^d_{\tilde{f}_2\tilde{Z}_i}\mathcal{C}^u_{H^+ff'}\beta^{\tilde{W}_j}_{\tilde{f}_2}]|m_{\tilde{Z}_i}||m_{\tilde{W}_j}|(-1)^{\theta_i}(-1)^{\theta_j}, \tag{A.761}$$

$$\mathcal{V}^{(7)}_{H^{\pm}\tilde{f}_2} = [\omega^R_{H^+\tilde{W}^+\tilde{Z}}\beta^d_{\tilde{f}_2\tilde{Z}_i}\mathcal{C}^u_{H^+ff'}\alpha^{\tilde{W}_j}_{\tilde{f}_2} + \omega^L_{H^+\tilde{W}^+\tilde{Z}}\alpha^d_{\tilde{f}_2\tilde{Z}_i}\mathcal{C}^d_{H^+ff'}\beta^{\tilde{W}_j}_{\tilde{f}_2}]m_{f'}m_f, \tag{A.762}$$

$$\mathcal{V}^{(8)}_{H^{\pm}\tilde{f}_2} = 2[(-1)^{\theta_i}\omega^L_{H^+\tilde{W}^+\tilde{Z}}\beta^d_{\tilde{f}_2\tilde{Z}_i}\mathcal{C}^u_{H^+ff'}\alpha^{\tilde{W}_j}_{\tilde{f}_2} + \omega^R_{H^+\tilde{W}^+\tilde{Z}}\alpha^d_{\tilde{f}_2\tilde{Z}_i}\mathcal{C}^d_{H^+ff'}\beta^{\tilde{W}_j}_{\tilde{f}_2}]|m_{\tilde{Z}_i}|m_{f'}m_f|m_{\tilde{W}_j}|(-1)^{\theta_j}. \tag{A.763}$$

If it's a chargino decaying:

$$\mathcal{V}^{(1)}_{H^{\pm}\tilde{f}_2} = \frac{1}{2}[\omega^L_{H^+\tilde{W}^+\tilde{Z}}\beta^{\tilde{W}_j}_{\tilde{f}_2}\mathcal{C}^u_{H^+ff'}\alpha^d_{\tilde{f}_2\tilde{Z}_i} + (-1)^{\theta_j}\omega^R_{H^+\tilde{W}^+\tilde{Z}}\alpha^{\tilde{W}_j}_{\tilde{f}_2}\mathcal{C}^d_{H^+ff'}\beta^d_{\tilde{f}_2\tilde{Z}_i}], \tag{A.764}$$

$$\mathcal{V}^{(2)}_{H^{\pm}\tilde{f}_2} = -[\omega^L_{H^+\tilde{W}^+\tilde{Z}}\alpha^{\tilde{W}_j}_{\tilde{f}_2}\mathcal{C}^d_{H^+ff'}\alpha^d_{\tilde{f}_2\tilde{Z}_i} - (-1)^{\theta_j}\omega^R_{H^+\tilde{W}^+\tilde{Z}}\beta^{\tilde{W}_j}_{\tilde{f}_2}\mathcal{C}^u_{H^+ff'}\beta^d_{\tilde{f}_2\tilde{Z}_i}]|m_{\tilde{Z}_i}|m_f], \tag{A.765}$$

$$\mathcal{V}^{(3)}_{H^{\pm}\tilde{f}_2} = [(-1)^{\theta_j}\omega^R_{H^+\tilde{W}^+\tilde{Z}}\alpha^{\tilde{W}_j}_{\tilde{f}_2}\mathcal{C}^u_{H^+ff'}\alpha^d_{\tilde{f}_2\tilde{Z}_i} - \omega^L_{H^+\tilde{W}^+\tilde{Z}}\beta^{\tilde{W}_j}_{\tilde{f}_2}\mathcal{C}^d_{H^+ff'}\beta^d_{\tilde{f}_2\tilde{Z}_i}]m_{f'}|m_{\tilde{W}_j}|, \tag{A.766}$$

$$\mathcal{V}^{(4)}_{H^{\pm}\tilde{f}_2} = (\omega^L_{H^+\tilde{W}^+\tilde{Z}}\alpha^{\tilde{W}_j}_{\tilde{f}_2}\mathcal{C}^u_{H^+ff'}\alpha^d_{\tilde{f}_2\tilde{Z}_i} - (-1)^{\theta_j}\omega^R_{H^+\tilde{W}^+\tilde{Z}}\beta^{\tilde{W}_j}_{\tilde{f}_2}\mathcal{C}^d_{H^+ff'}\beta^d_{\tilde{f}_2\tilde{Z}_i})|m_{\tilde{Z}_i}|m_{f'}, \tag{A.767}$$

$$\mathcal{V}^{(5)}_{H^{\pm}\tilde{f}_2} = -[(-1)^{\theta_j}\omega^R_{H^+\tilde{W}^+\tilde{Z}}\alpha^{\tilde{W}_j}_{\tilde{f}_2}\mathcal{C}^d_{H^+ff'}\alpha^d_{\tilde{f}_2\tilde{Z}_i} + \omega^L_{H^+\tilde{W}^+\tilde{Z}}\beta^{\tilde{W}_j}_{\tilde{f}_2}\mathcal{C}^u_{H^+ff'}\beta^d_{\tilde{f}_2\tilde{Z}_i}]m_f|m_{\tilde{W}_j}|, \tag{A.768}$$

$$\mathcal{V}^{(6)}_{H^{\pm}\tilde{f}_2} = (\omega^R_{H^+\tilde{W}^+\tilde{Z}}\beta^{\tilde{W}_j}_{\tilde{f}_2}\mathcal{C}^u_{H^+ff'}\alpha^d_{\tilde{f}_2\tilde{Z}_i} + \omega^L_{H^+\tilde{W}^+\tilde{Z}}\alpha^{\tilde{W}_j}_{\tilde{f}_2}\mathcal{C}^d_{H^+ff'}\beta^d_{\tilde{f}_2\tilde{Z}_i})|m_{\tilde{W}_j}||m_{\tilde{Z}_i}|, \tag{A.769}$$

$$\mathcal{V}^{(7)}_{H^{\pm}\tilde{f}_2} = -(-1)^{\theta_j}[\omega^L_{H^+\tilde{W}^+\tilde{Z}}\beta^{\tilde{W}_j}_{\tilde{f}_2}\mathcal{C}^d_{H^+ff'}\alpha^d_{\tilde{f}_2\tilde{Z}_i} + \omega^R_{H^+\tilde{W}^+\tilde{Z}}\alpha^{\tilde{W}_j}_{\tilde{f}_2}\mathcal{C}^u_{H^+ff'}\beta^d_{\tilde{f}_2\tilde{Z}_i}]m_f m_{f'}, \tag{A.770}$$

$$\mathcal{V}^{(8)}_{H^{\pm}\tilde{f}_2} = 2[(-1)^{\theta_j}\omega^R_{H^+\tilde{W}^+\tilde{Z}}\beta^{\tilde{W}_j}_{\tilde{f}_2}\mathcal{C}^d_{H^+ff'}\alpha^d_{\tilde{f}_2\tilde{Z}_i} - \omega^L_{H^+\tilde{W}^+\tilde{Z}}\alpha^{\tilde{W}_j}_{\tilde{f}_2}\mathcal{C}^u_{H^+ff'}\beta^d_{\tilde{f}_2\tilde{Z}_i}]m_f m_{f'}|m_{\tilde{W}_j}||m_{\tilde{Z}_i}|. \tag{A.771}$$

The integrals and overall contribution are given exactly as for $H^{\pm}\tilde{f'}_2$ but $m_{\tilde{f'}_2} \to m_{\tilde{f}_2}$. Remember the integrals labelling depends on whether it's a neutralino decaying (to a chargino) or a chargino decaying (to a neutralino).

$\underline{\Gamma_{\tilde{f'}_1\tilde{f'}_2}}$

Here the coupling combinations for the interference of the two positively charged sfermions depend upon whether the decay is neutralino to chargino or chargino to neutralino. For neutralino to chargino:

$$\mathcal{V}^{(1)}_{\tilde{f'}_2\tilde{f'}_2} = (\beta^u_{\tilde{f}_1\tilde{Z}_i}\beta^u_{\tilde{f}_2\tilde{Z}_i} + \alpha^u_{\tilde{f}_1\tilde{Z}_i}\alpha^u_{\tilde{f}_2\tilde{Z}_i})(-1)^{\theta_i}, \tag{A.772}$$

$$\mathcal{V}^{(2)}_{\tilde{f'}_2\tilde{f'}_2} = (\alpha^u_{\tilde{f}_1\tilde{Z}_i}\beta^u_{\tilde{f}_2\tilde{Z}_i} + \beta^u_{\tilde{f}_1\tilde{Z}_i}\alpha^u_{\tilde{f}_2\tilde{Z}_i})(-1)^{\theta_i}, \tag{A.773}$$

$$\mathcal{V}^{(3)}_{\tilde{f}'_2\tilde{f}'_2} = (-\alpha^{\tilde{W}_j}_{\tilde{f}'_1}\alpha^{\tilde{W}_j}_{\tilde{f}'_2} + \beta^{\tilde{W}_j}_{\tilde{f}'_1}\beta^{\tilde{W}_j}_{\tilde{f}'_2})(-1)^{\theta_i}, \tag{A.774}$$

$$\mathcal{V}^{(4)}_{\tilde{f}'_2\tilde{f}'_2} = (\beta^{\tilde{W}_j}_{\tilde{f}'_1}\alpha^{\tilde{W}_j}_{\tilde{f}'_2} - \alpha^{\tilde{W}_j}_{\tilde{f}'_1}\beta^{\tilde{W}_j}_{\tilde{f}'_2})(-1)^{\theta_i}(-1)^{\theta_j}, \tag{A.775}$$

whilst for chargino to neutralino:

$$\mathcal{V}^{(1)}_{\tilde{f}'_2\tilde{f}'_2} = -\beta^{\tilde{W}_j}_{\tilde{f}'_1}\beta^{\tilde{W}_j}_{\tilde{f}'_2} + \alpha^{\tilde{W}_j}_{\tilde{f}'_1}\alpha^{\tilde{W}_j}_{\tilde{f}'_2}(-1)^{\theta_j}, \tag{A.776}$$

$$\mathcal{V}^{(2)}_{\tilde{f}'_2\tilde{f}'_2} = (-1)^{\theta_j}\alpha^{\tilde{W}_j}_{\tilde{f}'_1}\beta^{\tilde{W}_j}_{\tilde{f}'_2} - \alpha^{\tilde{W}_j}_{\tilde{f}'_2}\beta^{\tilde{W}_j}_{\tilde{f}'_2}, \tag{A.777}$$

$$\mathcal{V}^{(3)}_{\tilde{f}'_2\tilde{f}'_2} = (-\alpha^{u}_{\tilde{f}_1\tilde{Z}_i}\alpha^{u}_{\tilde{f}_2\tilde{Z}_i} + (-1)^{\theta_j}\beta^{u}_{\tilde{f}_1\tilde{Z}_i}\beta^{u}_{\tilde{f}_2\tilde{Z}_i}), \tag{A.778}$$

$$\mathcal{V}^{(4)}_{\tilde{f}'_2\tilde{f}'_2} = (-\alpha^{u}_{\tilde{f}_1\tilde{Z}_i}\beta^{u}_{\tilde{f}_2\tilde{Z}_i} + (-1)^{\theta_j}\alpha^{u}_{\tilde{f}_2\tilde{Z}_i}\beta^{u}_{\tilde{f}_1\tilde{Z}_i}). \tag{A.779}$$

The integrals are as follows with
$s = m^2_{\tilde{Z}_i} + m^2_{f'} - 2|m_{\tilde{Z}_i}|E$ and $\lambda = \sqrt{(s-(m_f+m_{\tilde{W}_j})^2)(s-(m_f-m_{\tilde{W}_j})^2}$:

$$I^1_{\tilde{f}'_1\tilde{f}'_2} = 2|m_{\tilde{Z}_i}|\int_{m_{f'}}^{E_{upper}} 2|m_{\tilde{Z}_i}|\sqrt{E^2-m^2_{f'}}\frac{\lambda}{s(s-m^2_{\tilde{f}'_1})(s-m_{\tilde{f}'_2})^2)}, \tag{A.780}$$

$$I^2_{\tilde{f}'_1\tilde{f}'_2} = 2|m_{\tilde{Z}_i}|\int_{m_{f'}}^{E_{upper}} 2|m_{\tilde{Z}_i}|\sqrt{E^2-m^2_{f'}}\frac{(s-m^2_f-m^2_{\tilde{W}_j})\lambda}{s(s-m^2_{\tilde{f}'_1})(s-m_{\tilde{f}'_2})^2)}, \tag{A.781}$$

$$I^3_{\tilde{f}'_1\tilde{f}'_2} = 2|m_{\tilde{Z}_i}|\int_{m_{f'}}^{E_{upper}} 2|m_{\tilde{Z}_i}|\sqrt{E^2-m^2_{f'}}\frac{2|m_{\tilde{Z}_i}|E\lambda}{s(s-m^2_{\tilde{f}'_1})(s-m_{\tilde{f}'_2})^2)}, \tag{A.782}$$

$$I^4_{\tilde{f}'_1\tilde{f}'_2} = 2|m_{\tilde{Z}_i}|\int_{m_{f'}}^{E_{upper}} 2|m_{\tilde{Z}_i}|\sqrt{E^2-m^2_{f'}}\frac{(s-m^2_f-m^2_{\tilde{W}_j})2|m_{\tilde{Z}_i}|E\lambda}{s(s-m^2_{\tilde{f}'_1})(s-m_{\tilde{f}'_2})^2)}. \tag{A.783}$$

Now if it's instead a chargino decaying, as described before, swap the chargino and neutralino masses throughout, but also here you must relabel the integrals $I^2_{\tilde{f}'_1\tilde{f}'_2} \leftrightarrow I^3_{\tilde{f}'_1\tilde{f}'_2}$. Also for a chargino decaying one must interchange m_f and $m_{f'}$. For a neutralino decaying:

$$\begin{aligned}\Gamma_{\tilde{f}'_1\tilde{f}'_2} =& -4\mathcal{V}^{(2)}_{\tilde{f}'_2\tilde{f}'_2}\mathcal{V}^{(4)}_{\tilde{f}'_2\tilde{f}'_2}|m_{\tilde{Z}_i}||m_{\tilde{W}_j}|m_{f'}m_f I^1_{\tilde{f}'_1\tilde{f}'_2} + 2\mathcal{V}^{(2)}_{\tilde{f}'_2\tilde{f}'_2}\mathcal{V}^{(3)}_{\tilde{f}'_2\tilde{f}'_2}|m_{\tilde{Z}_i}|m_{f'}I^2_{\tilde{f}'_1\tilde{f}'_2} \\ & - 2\mathcal{V}^{(1)}_{\tilde{f}'_2\tilde{f}'_2}\mathcal{V}^{(4)}_{\tilde{f}'_2\tilde{f}'_2}m_f|m_{\tilde{W}_j}|I^3_{\tilde{f}'_1\tilde{f}'_2} + \mathcal{V}^{(1)}_{\tilde{f}'_2\tilde{f}'_2}\mathcal{V}^{(3)}_{\tilde{f}'_2\tilde{f}'_2}I^4_{\tilde{f}'_1\tilde{f}'_2}.\end{aligned} \tag{A.784}$$

$\underline{\Gamma_{\tilde{f}_1\tilde{f}_2}}$

For this interference contribution the coupling combinations used are as follows:

$$\mathcal{V}^{(1)}_{\tilde{f}_1\tilde{f}_2} = -[(-1)^{\theta_c}\alpha^{d}_{\tilde{Z}_i\tilde{f}_1}\alpha^{d}_{\tilde{Z}_i\tilde{f}_2} + \beta^{d}_{\tilde{Z}_i\tilde{f}_1}\beta^{d}_{\tilde{Z}_i\tilde{f}_2}](-1)^{\theta_j}, \tag{A.785}$$

$$\mathcal{V}^{(2)}_{\tilde{f}_1\tilde{f}_2} = [(-1)^{\theta_i}\beta^{d}_{\tilde{Z}_i\tilde{f}_1}\alpha^{d}_{\tilde{Z}_i\tilde{f}_2} - \alpha^{d}_{\tilde{Z}_i\tilde{f}_1}\beta^{d}_{\tilde{Z}_i\tilde{f}_2}](-1)^{\theta_j}(-1)^{\theta_c}, \tag{A.786}$$

$$\mathcal{V}^{(3)}_{\tilde{f}_1\tilde{f}_2} = [\beta^{\tilde{W}}_{\tilde{f}_1}\beta^{\tilde{W}}_{\tilde{f}_2} - \alpha^{\tilde{W}}_{\tilde{f}_1}\alpha^{\tilde{W}}_{\tilde{f}_2}](-1)^{\theta_i}, \tag{A.787}$$

$$\mathcal{V}^{(4)}_{\tilde{f}_1\tilde{f}_2} = (\alpha^{\tilde{W}}_{\tilde{f}_1}\beta^{\tilde{W}}_{\tilde{f}_2} - \beta^{\tilde{W}}_{\tilde{f}_1}\alpha^{\tilde{W}}_{\tilde{f}_2})(-1)^{\theta_c}. \tag{A.788}$$

The integrals are as follows, now with:

$$s = m^2_{\tilde{Z}_i} + m^2_f - 2|m_{\tilde{Z}_i}|E, \tag{A.789}$$

$$\lambda = \sqrt{(s-(m_{f'}-m_{\tilde{W}_j})^2)(s-(m_{f'}+m_{\tilde{W}_j})^2)}, \tag{A.790}$$

$$I^1_{\tilde{f}_1\tilde{f}_2} = 2|m_{\tilde{Z}_i}| \int_{m_f}^{E_{upper2}} dE \frac{2|m_{\tilde{Z}_i}|}{s} \lambda \sqrt{E^2 - m_f^2} \frac{1}{(s - m^2_{\tilde{f}_1})(s - m^2_{\tilde{f}_2})}, \tag{A.791}$$

$$I^2_{\tilde{f}_1\tilde{f}_2} = 2|m_{\tilde{Z}_i}| \int_{m_f}^{E_{upper2}} dE \frac{2|m_{\tilde{Z}_i}|}{s} \lambda \sqrt{E^2 - m_f^2} \frac{s - m^2_{\tilde{W}_j} - m^2_{f'}}{(s - m^2_{\tilde{f}_1})(s - m^2_{\tilde{f}_2})}, \tag{A.792}$$

$$I^3_{\tilde{f}_1\tilde{f}_2} = 2|m_{\tilde{Z}_i}| \int_{m_f}^{E_{upper2}} dE \frac{2|m_{\tilde{Z}_i}|}{s} \lambda \sqrt{E^2 - m_f^2} \frac{2|m_{\tilde{Z}_i}|E}{(s - m^2_{\tilde{f}_1})(s - m^2_{\tilde{f}_2})}, \tag{A.793}$$

$$I^4_{\tilde{f}_1\tilde{f}_2} = 2|m_{\tilde{Z}_i}| \int_{m_f}^{E_{upper2}} dE \frac{2|m_{\tilde{Z}_i}|}{s} \lambda \sqrt{E^2 - m_f^2} \frac{2|m_{\tilde{Z}_i}|E(s - m^2_{\tilde{W}_j} - m^2_{f'})}{(s - m^2_{\tilde{f}_1})(s - m^2_{\tilde{f}_2})}, \tag{A.794}$$

The expression for the overall contribution as a product of these couplings and integrals is:

$$\begin{aligned}\Gamma_{\tilde{f}_1\tilde{f}_2} = -\Big[&(-1)^{\theta_i}(-1)^{\theta_c}\mathcal{V}^{(1)}_{\tilde{f}_1\tilde{f}_2}\mathcal{V}^{(3)}_{\tilde{f}_1\tilde{f}_2}I^4_{\tilde{f}_1\tilde{f}_2} + 2(-1)^{\theta_i}\mathcal{V}^{(1)}_{\tilde{f}_1\tilde{f}_2}\mathcal{V}^{(4)}_{\tilde{f}_1\tilde{f}_2}m_f|m_{\tilde{W}_j}|I^2_{\tilde{f}_1\tilde{f}_2} \\ &+ 2(-1)^{\theta_c}\mathcal{V}^{(2)}_{\tilde{f}_1\tilde{f}_2}\mathcal{V}^{(3)}_{\tilde{f}_1\tilde{f}_2}|m_{\tilde{Z}_i}|m_{f'}I^3_{\tilde{f}_1\tilde{f}_2} + 4\mathcal{V}^{(2)}_{\tilde{f}_1\tilde{f}_2}\mathcal{V}^{(4)}_{\tilde{f}_1\tilde{f}_2}|m_{\tilde{Z}_i}||m_{\tilde{W}_j}|m_f m_{f'}I^1_{\tilde{f}_1\tilde{f}_2})\Big].\end{aligned} \tag{A.795}$$

It should be noted the partial widths of the decays $\tilde{Z}_i \to \tilde{W}_j f' \bar{f}$ and the "reverse" decay $\tilde{W}_j \to \tilde{Z}_i f' \bar{f}$ may show strong dependence on the quark masses taken for kinematic masses and for the running masses (which is used to set Yukawa couplings), of course depending on the details of the exact spectrum considered. These mass choice effects, along with the fact that `sPHENO` allows (small) mixing in the first two generations of sfermions whereas it is neglected in `SoftSusy`, can cause larger differences between `SoftSusy` and `sPHENO` of around 25%. If the same mass choices are made and `sPHENO`'s small mixing angles inserted by hand into the `SoftSusy` code then these differences are reduced to around 10%.

A.4.3 Chargino 3-body Decays

$\underline{\tilde{W}_j \to \tilde{Z}_i f' \bar{f}}$

It is detailed above in the formulae for $\tilde{Z}_i \to \tilde{W}_j f' \bar{f}$ how to adapt the formula for the chargino decaying into the neutralino rather than the neutralino decaying into the chargino.

$\underline{\tilde{W}_1 \to \tilde{Z}_1 \pi^{\pm} \pi^0}$

For the lightest neutralino-lightest chargino quasi-mass degenerate case, the lightest chargino partial decay width into two pions and the lightest neutralino is [289]:

$$\begin{aligned}\Gamma(\tilde{W}_1^+ \to \tilde{Z}_1 \pi^+) = &\frac{G_F^2}{192\pi^3 m^2_{\tilde{W}_1}} \int_{4m_\pi^2}^{(M_{\tilde{Z}_1} - M_{\tilde{W}_1})^2} dq^2 \left|\tilde{F}(q^2)\right|^2 \left(1 - \frac{4m_\pi^2}{q^2}\right)^{3/2} \lambda\left(m_{\tilde{W}_1},\ m_{\tilde{Z}_1}, \sqrt{q^2}\right) \\ &\times \left\{ \left[(O^L_{11})^2 + (O^R_{11})^2\right] \left[q^2(m^2_{\tilde{W}_1} + m^2_{\tilde{Z}_1} - 2q^2) + (m^2_{\tilde{W}_1} - m^2_{\tilde{Z}_1})^2\right] - 12 O^L_{11} O^R_{11} q^2 m_{\tilde{Z}_1} m_{\tilde{W}_1} \right\},\end{aligned}$$

where $O^{L,R}_{11}$ are defined in Eq. A.74 and

$$\tilde{F}(q^2) = \frac{BW_\rho(q^2) + \beta BW_{\rho'}(q^2)}{1 + \beta}, \tag{A.796}$$

where $\beta = -0.145$ and BW_V refers to the Breit-Wigner pole of meson $V \in \{\rho,\ \rho'\}$:

$$BW_V(q^2) = \frac{m_V^2}{m_V^2 - q^2 - i\sqrt{q^2}\Gamma_V(q^2)}. \tag{A.797}$$

Here, $m_\rho = 0.773\,\text{GeV}$ and $m_{\rho'} = 1.370\,\text{GeV}$ are used as well as

$$\Gamma_V(q^2) = \frac{\Gamma_V m_V^2}{q^2}\left(\frac{q^2 - 4m_\pi^2}{m_V^2 - 4m_\pi^2}\right)^{3/2}, \tag{A.798}$$

where $\Gamma_\rho = 0.145\,\text{GeV}$ and $\Gamma_{\rho'} = 0.510\,\text{GeV}$.

A.5 Decays to Gravitinos

In certain SUSY-breaking scenarios, particularly gauge-mediated SUSY breaking (GMSB), the gravitino can be very light and therefore may be the Lightest Supersymmetric Particle (LSP). Moreover, the gravitino has longitudinal components from the Goldstino which couple much more strongly than gravitational strength, this therefore provides interactions relevant to collider phenomenology, resulting in gravitino-SUSY-SM couplings that affect collider signatures, when the gravitino is the LSP. Consequently Next-to-Lightest Supersymmetric Particle (NLSP) decays to gravitino LSPs may be of interest and are included within our decay calculator program `SoftSusy`. The following decay modes are relevant when the initial SUSY particle is the NLSP:

1. $\tilde{g} \to g\tilde{G}$
2. $\tilde{q}_i \to q\tilde{G}$
3. $\tilde{l} \to l\tilde{G}$
4. $\tilde{Z}_i \to \gamma\tilde{G}$
5. $\tilde{Z}_i \to Z\tilde{G}$
6. $\tilde{Z}_i \to \phi\tilde{G}$

Decays of Higgs bosons to the gravitino are not relevant as there are always other decays available to the Higgs (whether h or A) which dominate its branching ratio, for example even a Higgs boson were the NLSP then decays to $\gamma\gamma$ would be available and occur much more quickly than the Planck suppressed decays to gravitinos. The formulae used were re-derived but nonetheless are as provided in [65]:

$$\Gamma(\tilde{g} \to g\tilde{G}) = \frac{m_{\tilde{g}}^5}{48\pi m_{\tilde{G}}^2 M_P^{red\,2}}. \tag{A.799}$$

$$\Gamma(\tilde{q} \to q\tilde{G}) = \frac{(m_{\tilde{q}}^2 - m_q^2)^4}{48\pi m_{\tilde{q}}^3 m_{\tilde{G}}^2 M_P^{red\,2}}. \tag{A.800}$$

$$\Gamma(\tilde{Z}_i \to \gamma\tilde{G}) = \frac{|m_{\tilde{Z}_i}|^5}{48\pi m_{\tilde{G}}^2 M_P^{red\,2}}[N_{1i}\cos\theta_W + N_{2i}\sin\theta_W]^2. \tag{A.801}$$

$$\Gamma(\tilde{Z}_i \to Z\tilde{G}) = \frac{(m_{\tilde{Z}_i}^2 - m_Z^2)^4}{96\pi m_{\tilde{G}}^2 M_P^{red\,2}|m_{\tilde{Z}_i}|^3}\left[2(N_{1i}\sin\theta_W - N_{2i}\cos\theta_W)^2 + (N_{4i}\sin\beta - N_{3i}\cos\beta)^2\right]. \tag{A.802}$$

$$\Gamma(\tilde{Z}_i \to \phi\tilde{G}) = \frac{(m_{\tilde{Z}_i}^2 - m_\phi^2)^4}{96\pi m_{\tilde{G}}^2 M_P^{red\,2}|m_{\tilde{Z}_i}|^3}\mathcal{C}_{h/H/A}^2, \tag{A.803}$$

where

$$\mathcal{C}_{h/H/A} = \begin{cases} N_{4i}\cos\alpha - N_{3i}\sin\alpha, \text{ for h,} \\ N_{4i}\sin\alpha + N_{3i}\cos\alpha, \text{ for H,} \\ N_{4i}\cos\beta + N_{3i}\sin\beta, \text{ for A.} \end{cases} \tag{A.804}$$

Note that $M_P^{red} = \frac{M_P}{\sqrt{8\pi}} \approx 2.4 \times 10^{18}\,\text{GeV}$.

A.6 NMSSM Decays

Only 2-body decays have been included in the NMSSM, this does however include the important loop decays of the neutral Higgs bosons to $\gamma\gamma$, $Z\gamma$ and gg, as well as QCD corrections to the neutral Higgs decays to $q\bar{q}$ and gg. We do however include the decays $\phi \to WW^* \to Wf'\bar{f}$ and $\phi \to ZZ^* \to Zf\bar{f}$.[5] Note that throughout $S(A,B)$ is the now 3×3 CP even Higgs mixing matrix and $P(A,B)$ is the 2×3 CP odd Higgs mixing matrix (with Goldstone excluded). The additional NMSSM variables include λ (distinct from the $\tilde{\lambda}(A,B,C)$ used for kinematic part of decay widths given above), κ and $\mu_{eff} = \frac{\lambda\langle S\rangle}{\sqrt{2}}$. The conventions used for the NMSSM decay formulae were detailed earlier in section 3.3.2, with differences with respect to the `SoftSusy` NMSSM manual [118] noted. The conventions are those of `NMSSMTools` [126–128, 159], against which the formulae were checked for consistency and which provided a useful guide.

The NMSSM simply involves the addition of a gauge singlet chiral superfield to the MSSM, therefore the NMSSM has an additional neutralino, additional CP even neutral Higgs and additional CP odd neutral Higgs, therefore any decays not involving the extended neutralino or extended Higgs sectors are as in the MSSM.

A.6.1 CP Even Higgs Decays

First the decay to a fermion and antifermion, with no QCD corrections (QCD corrected formulae given later in A.7).

$$\Gamma(h_i \to f\bar{f}) = \frac{N_c G_F m_{h_i}}{\sqrt{2}4\pi} m_q^2 \Big(1 - 4\frac{m_q^2}{m_{h_i}^2}\Big)^{\frac{3}{2}} \mathcal{A}_{h_i ff}^{NMSSM}, \tag{A.805}$$

$$\mathcal{A}_{h_i ff}^{NMSSM} = \begin{cases} \frac{S(i,1)}{\sin\beta}, \text{ for 'u'-type fermions,} \\ \frac{S(i,2)}{\cos\beta}, \text{ for 'd'-type fermions.} \end{cases} \tag{A.806}$$

For squarks of the same handedness of the first two generations (so no mixing and negligible quark masses) the decay widths for the CP even Higgs i (i=1,2,3 are mass ordered CP even neutral Higgs bosons) are

$$\Gamma(h_i \to \tilde{q}_{L/R}\tilde{q}_{L/R}) = \frac{N_c}{16\pi m_{h_i}} \tilde{\lambda}^{\frac{1}{2}}(m_{h_i}, m_{\tilde{q}_{L/R}}, m_{\tilde{q}_{L/R}}) \mathcal{C}^2, \tag{A.807}$$

$$\mathcal{C} = \begin{cases} g\Big(m_W(\frac{1}{2} - \frac{\tan^2\theta_W}{6})[\sin\beta S(i,1) - \cos\beta S(i,2)] - \frac{m_q^2 S(i,1)}{m_W \sin\beta}\Big) \text{ , for up-type LH squarks,} \\ g\Big(m_W(-\frac{1}{2} - \frac{\tan^2\theta_W}{6})[\sin\beta S(i,1) - \cos\beta S(i,2)] - \frac{m_q^2 S(i,2)}{m_W \cos\beta}\Big) \text{ , for down-type LH squarks,} \\ g\Big(\frac{2}{3} m_W \tan^2\theta_W [\sin\beta S(i,1) - \cos\beta S(i,2)] - \frac{m_q^2 S(i,1)}{m_W \sin\beta}\Big) \text{ , for up-type RH squarks,} \\ g\Big(\frac{-1}{3} m_W \tan^2\theta_W [\sin\beta S(i,1) - \cos\beta S(i,2)] - \frac{m_q^2 S(i,2)}{m_W \cos\beta}\Big) \text{ , for down-type RH squarks.} \end{cases} \tag{A.808}$$

For sleptons the same formulae apply but without the factor of 3 in the pre-factor from N_c and with the coupling $\mathcal{C}$ now ("down type" here means the charged sleptons):

$$\mathcal{C} = \begin{cases} g\Big(m_W(\frac{1}{2} + \frac{\tan^2\theta_W}{2})[\sin\beta S(i,1) - \cos\beta S(i,2)]\Big) \text{ , for sneutrinos (i.e. equivalent of up-type LH),} \\ g\Big(m_W(\frac{1}{2} - \frac{\tan^2\theta_W}{6})[\sin\beta S(i,1) - \cos\beta S(i,2)] - \frac{m_q^2 S(i,2)}{m_W \cos\beta}\Big) \text{ , for down-type LH sleptons,} \\ g\Big(m_W(\tan^2\theta_W [\sin\beta S(i,1) - \cos\beta S(i,2)] - \frac{m_q^2 S(i,1)}{m_W \cos\beta}\Big) \text{ , for down-type RH sleptons.} \end{cases} \tag{A.809}$$

[5] The decays $\phi \to WW^* \to Wf'\bar{f}$ and $\phi \to ZZ^* \to Zf\bar{f}$, whilst strictly being 3-body, are classified as having NDA (Number of Daughters) of 2 according to SLHA conventions.

For squarks of opposite handedness:

$$\Gamma(h_i \to \tilde{q}_{L/R}\tilde{q}_{R/L}) = \frac{N_c}{16\pi m_{h_i}}\tilde{\lambda}^{\frac{1}{2}}(m_{h_i}, m_{\tilde{q}_L}, m_{\tilde{q}_R})\mathcal{D}^2, \tag{A.810}$$

where

$$\mathcal{D} = \begin{cases} \frac{gm_q}{2m_W \sin\beta}[A_q S(i,1) - \mu_{eff} S(i,2) - \lambda\frac{\sqrt{2}m_W\cos\beta}{gS(i,3)}] \text{ , for up-type squarks of different handedness,} \\ \frac{gm_q}{2m_W \cos\beta}[A_q S(i,2) - \mu_{eff} S(i,1) - \lambda\frac{\sqrt{2}m_W\sin\beta}{gS(i,3)}] \text{ , for down-type squarks of different handedness.} \end{cases} \tag{A.811}$$

For the decay to two sleptons with different handedness then we can use the same formulae as for two squarks of opposite handedness above but dividing by 3 to account for the fact sleptons aren't coloured (i.e. no factor N_c). Note that as only LH sneutrinos exist, only decays to charged sleptons of opposite handedness are possible, i.e. only "down-type sleptons" of different handedness. For third generation squarks and sleptons the formulae are more complicated ($j = 1, 2$ indicates $\tilde{t}_1$ and $\tilde{t}_2$):

$$\Gamma(h_i \to \tilde{t}_j\tilde{t}_j) = \frac{3}{16\pi m_{h_i}}\tilde{\lambda}^{\frac{1}{2}}(m_{h_i}, m_{\tilde{t}_j}, m_{\tilde{t}_j})\mathcal{C}^2_{t_j t_j}, \tag{A.812}$$

where

$$\begin{aligned}\mathcal{C}_{t_1t_1} =& \cos^2\theta_t\sqrt{2}\Big[h_u^2\langle h_1\rangle S(i,1) + (\frac{g'^2}{12} - \frac{g^2}{4})\{\langle h_1\rangle S(i,1) - \langle h_2\rangle S(i,2)\}\Big] + \sin^2\theta_t\sqrt{2}\Big[h_u^2\langle h_1\rangle S(i,1) \\ &- \frac{g'^2}{3}\{\langle h_1\rangle S(i,1) - \langle h_2\rangle S(i,2)\}\Big] + 2\cos\theta_t\sin\theta_t\frac{h_u}{\sqrt{2}}\Big(A_t S(i,1) - \mu_{eff}S(i,2) - \lambda\langle h_2\rangle S(i,3)\Big).\end{aligned} \tag{A.813}$$

This was for $j = 1$ i.e. for $\tilde{t}_1\tilde{t}_1$. For $j = 2$, make the replacements $\cos\theta_t \to -\sin\theta_t$ and $\sin\theta_t \to \cos\theta_t$.

For different stops:

$$\Gamma(h_i \to \tilde{t}_1\tilde{t}_2) = \frac{3}{16\pi m_{h_i}}\tilde{\lambda}^{\frac{1}{2}}(m_{h_i}, m_{\tilde{t}_j}, m_{\tilde{t}_j})\mathcal{C}^2_{t_1 t_2}, \tag{A.814}$$

where

$$\begin{aligned}\mathcal{C}_{t_1t_2} =& \cos\theta_t\sin\theta_t\Big[\sqrt{2}\Big(h_u^2\langle h_1\rangle S(i,1) - \frac{g'^2}{3}\{\langle h_1\rangle S(i,1) - \langle h_2\rangle S(i,2)\}\Big) \\ &- \sqrt{2}\Big(h_u^2\langle h_1\rangle S(i,1) + (\frac{g'^2}{12} - \frac{g^2}{4})\{\langle h_1\rangle S(i,1) - \langle h_2\rangle S(i,2)\}\Big)\Big] \\ &+ (\cos^2\theta_t - \sin^2\theta_t)\frac{h_u}{\sqrt{2}}\Big(A_t S(i,1) - \mu_{eff}S(i,2) - \lambda\langle h_2\rangle S(i,3)\Big).\end{aligned} \tag{A.815}$$

Note that $\langle h_1\rangle = \frac{\sqrt{2}m_W\sin\beta}{g}$ and $\langle h_2\rangle = \frac{\sqrt{2}m_W\cos\beta}{g}$, whilst $h_u = \frac{m_t^{run}}{\langle h_1\rangle}$.

For decays to sbottoms the decay formulae are the same (with the expected mass changes) except:

$$\begin{aligned}\mathcal{C}_{b_1b_1} =& \cos^2\theta_b\sqrt{2}\Big[h_d^2\langle h_2\rangle S(i,2) + (\frac{g'^2}{12} + \frac{g^2}{4})\{\langle h_1\rangle S(i,1) - \langle h_2\rangle S(i,2)\}\Big] \\ &+ \sin^2\theta_b\sqrt{2}\Big[h_d^2\langle h_2\rangle S(i,2) + \frac{g'^2}{6}\{\langle h_1\rangle S(i,1) - \langle h_2\rangle S(i,2)\}\Big] \\ &+ 2\cos\theta_b\sin\theta_b\frac{h_d}{\sqrt{2}}\Big(A_b S(i,2) - \mu_{eff}S(i,1) - \lambda\langle h_1\rangle S(i,3)\Big),\end{aligned} \tag{A.816}$$

$$\begin{aligned}\mathcal{C}_{b_1b_2} =& \cos\theta_b\sin\theta_b\Big[\sqrt{2}\Big(h_d^2\langle h_2\rangle S(i,2) + \frac{g'^2}{6}\{\langle h_1\rangle S(i,1) - \langle h_2\rangle S(i,2)\}\Big) \\ &- \sqrt{2}\Big(h_d^2\langle h_2\rangle S(i,2) + (\frac{g'^2}{12} + \frac{g^2}{4})\{\langle h_1\rangle S(i,1) - \langle h_2\rangle S(i,2)\}\Big)\Big] \\ &+ (\cos^2\theta_b - \sin^2\theta_b)\frac{h_d}{\sqrt{2}}\Big(A_b S(i,2) - \mu_{eff}S(i,1) - \lambda\langle h_1\rangle S(i,3)\Big).\end{aligned} \tag{A.817}$$

Note that $h_d = \frac{m_b^{run}}{\langle h_2 \rangle}$. Again to get the $\tilde{b}_2\tilde{b}_2$ coupling from the $\tilde{b}_1\tilde{b}_1$, make the changes $\cos\theta_b \to -\sin\theta_b$ and $\sin\theta_b \to \cos\theta_b$. For staus:

$$\Gamma(h_i \to \tilde{\tau}_j\tilde{\tau}_k) = \frac{1}{16\pi m_{h_i}}\tilde{\lambda}^{\frac{1}{2}}(m_{h_i}, m_{\tilde{\tau}_j}, m_{\tilde{\tau}_k})\mathcal{C}^2_{\tau_j\tau_k}, \tag{A.818}$$

where here we have

$$\begin{aligned}\mathcal{C}_{\tau_1\tau_1} =& \sin^2\theta_\tau\sqrt{2}\Big[h_\tau^2\langle h_2\rangle S(i,2) + (-\frac{g'^2}{4} + \frac{g^2}{4})\{\langle h_1\rangle S(i,1) - \langle h_2\rangle S(i,2)\}\Big] \\ &+ \cos^2\theta_\tau\sqrt{2}\Big[h_\tau^2\langle h_2\rangle S(i,2) + \frac{g'^2}{2}\{\langle h_1\rangle S(i,1) - \langle h_2\rangle S(i,2)\}\Big] \\ &+ 2\cos\theta_\tau\sin\theta_\tau\frac{h_\tau}{\sqrt{2}}\Big(A_\tau S(i,2) - \mu_{eff}S(i,1) - \lambda\langle h_1\rangle S(i,3)\Big),\end{aligned} \tag{A.819}$$

$$\begin{aligned}\mathcal{C}_{\tau_2\tau_2} =& \cos^2\theta_\tau\sqrt{2}\Big[h_\tau^2\langle h_2\rangle S(i,2) + (-\frac{g'^2}{4} + \frac{g^2}{4})\{\langle h_1\rangle S(i,1) - \langle h_2\rangle S(i,2)\}\Big] \\ &+ \sin^2\theta_\tau\sqrt{2}\Big[h_\tau^2\langle h_2\rangle S(i,2) + \frac{g'^2}{2}\{\langle h_1\rangle S(i,1) - \langle h_2\rangle S(i,2)\}\Big] \\ &- 2\cos\theta_\tau\sin\theta_\tau\frac{h_\tau}{\sqrt{2}}\Big(A_\tau S(i,2) - \mu_{eff}S(i,1) - \lambda\langle h_1\rangle S(i,3)\Big),\end{aligned} \tag{A.820}$$

and

$$\begin{aligned}\mathcal{C}_{\tau_1\tau_2} =& -\cos\theta_\tau\sin\theta_\tau\Big[\sqrt{2}\Big(h_\tau^2\langle h_2\rangle S(i,2) + \frac{g'^2}{2}\{\langle h_1\rangle S(i,1) - \langle h_2\rangle S(i,2)\}\Big) \\ &- \sqrt{2}\Big(h_\tau^2\langle h_2\rangle S(i,2) + (-\frac{g'^2}{4} + \frac{g^2}{4})\{\langle h_1\rangle S(i,1) - \langle h_2\rangle S(i,2)\}\Big)\Big] \\ &+ (\sin^2\theta_\tau - \cos^2\theta_\tau)\frac{h_\tau}{\sqrt{2}}\Big(A_\tau S(i,2) - \mu_{eff}S(i,1) - \lambda\langle h_1\rangle S(i,3)\Big).\end{aligned} \tag{A.821}$$

Now the decays to charginos, first of all decays to the same chargino:

$$\Gamma(h_i \to \tilde{W}_j\tilde{W}_j) = \frac{m_{h_i}}{8\pi}\tilde{\lambda}^{\frac{3}{2}}(m_{h_i}, m_{\tilde{W}_j}, m_{\tilde{W}_j})\mathcal{F}^2_{jj}, \tag{A.822}$$

where

$$\mathcal{F}_{jj} = \begin{cases} \frac{\lambda}{\sqrt{2}}S(i,3)\cos\theta_L\cos\theta_R + \frac{g}{\sqrt{2}}[S(i,1)\sin\theta_L\cos\theta_R + S(i,2)\cos\theta_L\sin\theta_R], \text{ for } j=1, \\ \frac{\lambda}{\sqrt{2}}S(i,3)\sin\theta_L\sin\theta_R - \frac{g}{\sqrt{2}}[S(i,1)\cos\theta_L\sin\theta_R + S(i,2)\sin\theta_L\cos\theta_R], \text{ for } j=2. \end{cases} \tag{A.823}$$

For decays to different charginos:

$$\Gamma(h_i \to \tilde{W}_1\tilde{W}_2) = \frac{m_{h_i}}{16\pi}\tilde{\lambda}^{\frac{1}{2}}(m_{h_i}, m_{\tilde{W}_1}, m_{\tilde{W}_2})\left[(c_1^2 + c_2^2)\frac{1}{m_{h_i}^2}(m_{h_i}^2 - m_{\tilde{W}_1}^2 - m_{\tilde{W}_2}^2) - 4c_1c_2\frac{m_{\tilde{W}_1}m_{\tilde{W}_2}}{m_{h_i}^2}\right], \tag{A.824}$$

where

$$c_1 = \frac{\lambda}{\sqrt{2}}S(i,3)\cos\theta_L\sin\theta_R + \frac{g}{\sqrt{2}}\left(S(i,1)\sin\theta_L\sin\theta_R - S(i,2)\cos\theta_L\cos\theta_R\right), \tag{A.825}$$

$$c_2 = \frac{\lambda}{\sqrt{2}}S(i,3)\sin\theta_L\cos\theta_R - \frac{g}{\sqrt{2}}\left(S(i,1)\cos\theta_L\cos\theta_R - S(i,2)\sin\theta_L\sin\theta_R\right). \tag{A.826}$$

Now the decays to neutralinos:

$$\Gamma(h_i \to \tilde{Z}_j \tilde{Z}_k) = \frac{\alpha_{jk} m_{h_i}}{16\pi}(1 - (\frac{m_{\tilde{Z}_j} + m_{\tilde{Z}_k}}{m_{h_i}})^2)\tilde{\lambda}^{\frac{1}{2}}(m_{h_i}, m_{\tilde{Z}_j}, m_{\tilde{Z}_k})\mathcal{G}^2_{ijk}, \tag{A.827}$$

where

$$\begin{aligned}\mathcal{G}_{ijk} =& \frac{\lambda}{\sqrt{2}}\Big[S(i,1)(N_{3j}N_{5k} + N_{5j}N_{3k}) + S(i,2)(N_{4j}N_{5k} + N_{5j}N_{4k}) + S(i,3)(N_{3j}N_{4k} + N_{4j}N_{3k})\Big] \\ & - \sqrt{2}\kappa S(i,3)N_{5j}N_{5k} + \frac{g'}{2}\Big[- S(i,1)(N_{1j}N_{4k} + N_{1k}N_{4j}) + S(i,2)(N_{1j}N_{3k} + N_{3j}N_{1k})\Big] \\ & + \frac{g}{2}\Big[S(i,1)(N_{2j}N_{4k} + N_{4j}N_{2k}) - S(i,2)(N_{2j}N_{3k} + N_{3j}N_{2k})\Big].\end{aligned} \tag{A.828}$$

Here N_{ab} is the neutralino mixing matrix which is now 5×5 as the singlino mixes with the four original neutralinos. The neutralinos here are in order of increasing mass. The conventions for the NMSSM were detailed previously in section 3.3.2. Note that the α_{jk} is 2 if $j \neq k$ and 1 if $j = k$ in order to account for indistinguishability of particles.

The neutral Higgs decays to CP odd neutral Higgs bosons are given by:

$$\Gamma(h_i \to A_j A_k) = \frac{1}{16\pi m_{h_i}}\tilde{\lambda}^{\frac{1}{2}}(m_{h_i}, m_{A_j}, m_{A_k})\mathcal{Q}^2_{jk}, \tag{A.829}$$

where

$$\begin{aligned}\mathcal{Q}_{jk} =& \frac{g^2 + g'^2}{4\sqrt{2}}\Big[\langle h_1\rangle\{\mathcal{C}(i,j,k,1,1,1) - \mathcal{C}(i,j,k,1,2,2)\} + \langle h_2\rangle\{\mathcal{C}(i,j,k,2,2,2) - \mathcal{C}(i,j,k,2,1,1)\}\Big] \\ & + \frac{\lambda A_\lambda}{\sqrt{2}}\{\mathcal{C}(i,j,k,1,2,3) + \mathcal{C}(i,j,k,2,1,3) + \mathcal{C}(i,j,k,3,1,2)\} - \frac{\kappa A_\kappa}{\sqrt{2}}\mathcal{C}(i,j,k,3,3,3) \\ & + \frac{\lambda^2}{\sqrt{2}}\Big[\langle h_1\rangle\{\mathcal{C}(i,j,k,1,2,2) + \mathcal{C}(i,j,k,1,3,3)\} + \langle h_2\rangle\{\mathcal{C}(i,j,k,2,1,1) + \mathcal{C}(i,j,k,2,3,3)\} \\ & + \frac{\mu_{eff}}{\lambda}\{\mathcal{C}(i,j,k,3,1,1) + \mathcal{C}(i,j,k,3,2,2)\}\Big] + \frac{\kappa^2\sqrt{2}\mu_{eff}}{\lambda}\mathcal{C}(i,j,k,3,3,3) \\ & + \frac{\lambda\kappa}{\sqrt{2}}\Big[\langle h_1\rangle\{\mathcal{C}(i,j,k,2,3,3) - 2\mathcal{C}(i,j,k,3,2,3)\} + \langle h_2\rangle\{\mathcal{C}(i,j,k,1,3,3) - 2\mathcal{C}(i,j,k,3,1,3)\} \\ & + 2\frac{\mu_{eff}}{\lambda}\{\mathcal{C}(i,j,k,3,1,2) - \mathcal{C}(i,j,k,1,2,3) - \mathcal{C}(i,j,k,2,1,3)\}\Big].\end{aligned} \tag{A.830}$$

The $\mathcal{C}(i,j,k,x,y,z)$ is the same coupling which appears later in (A.919).

$$\Gamma(h_i \to A_j Z) = \frac{(g^2 + g'^2)m^3_{h_i}}{64\pi m^2_Z}\tilde{\lambda}^{\frac{3}{2}}(m_{h_i}, m_{A_j}, m_Z)\mathcal{R}^2_{ij}, \tag{A.831}$$

where

$$\mathcal{R}_{ij} = (S(i,1)\cos\beta - S(i,2)\sin\beta)(P(j,1)\cos\beta - P(j,2)\sin\beta). \tag{A.832}$$

$$\Gamma(h_i \to H^+H^-) = \frac{1}{16\pi m_{h_i}}\tilde{\lambda}^{\frac{1}{2}}(m_{h_i}, m_{H^\pm}, m_{H^\pm})\mathcal{S}^2_i, \tag{A.833}$$

where

$$\begin{aligned}\mathcal{S}_i =& \frac{\lambda\mu_{eff}}{\sqrt{2}}\Big[2S(i,3)\cos^2\beta + 2S(i,3)\sin^2\beta\Big] - \frac{\lambda^2 m_W \sin\beta}{g}(2S(i,2)+2S(i,1))\cos\beta\sin\beta \\ &+ \mu_{eff}\kappa 2\sqrt{2}S(i,3)\cos\beta\sin\beta + \lambda A_\lambda\sqrt{2}S(i,3)\cos\beta\sin\beta \\ &+ \frac{g'^2}{4}\frac{m_W}{g}\Big[\sin\beta(2S(i,1)\cos^2\beta - 2S(i,1)\sin^2\beta) + \cos\beta(2S(i,2)\sin^2\beta - 2S(i,2)\cos^2\beta)\Big] \\ &+ \frac{g m_W}{4}\Big[\sin\beta(2S(i,1)\sin^2\beta - 2S(i,2)\cos^2\beta + 4S(i,2)\sin\beta\cos\beta) \\ &\qquad + \cos\beta(2S(i,2)\cos^2\beta + 2S(i,2)\sin^2\beta + 4S(i,1)\sin\beta\cos\beta)\Big].\end{aligned} \tag{A.834}$$

$$\Gamma(h_i \to W^\pm H^\pm) = \frac{G_F m_{h_i}^3}{8\pi}[S(i,1)\cos\beta - S(i,2)\sin\beta]^2\tilde{\lambda}^{\frac{3}{2}}(m_{h_i}, m_{W^\pm}, m_{H^\pm}). \tag{A.835}$$

In this equation a factor of 2 has been included as it could be either W^+H^- or W^-H^+.

$$\Gamma(h_i \to h_j h_k) = \frac{\alpha_{jk}}{32\pi m_{h_i}}\tilde{\lambda}^{\frac{1}{2}}(m_{h_i}, m_{h_j}, m_{h_k})[\mathcal{C}^{NMSSM}_{h_i h_j h_k}]^2, \tag{A.836}$$

where again $\alpha_{jk} = 1$ if $j = k$ and 2 otherwise.

Also remember that:

$$\mu_{eff} = \frac{\lambda\langle s\rangle}{\sqrt{2}}, \tag{A.837}$$

$$\langle h_1\rangle = \frac{\sqrt{2}m_W\sin\beta}{g}, \tag{A.838}$$

$$\langle h_2\rangle = \frac{\sqrt{2}m_W\cos\beta}{g}, \tag{A.839}$$

where λ is a parameter of the NMSSM which couples the singlino to Higgsinos.

Here $\mathcal{C}^{NMSSM}_{h_i h_j h_k}$ is given by:

$$\begin{aligned}\mathcal{C}^{NMSSM}_{h_i h_j h_k} =& \frac{g^2+g'^2}{4\sqrt{2}}\Big[\langle h_1\rangle[S_{ijk}(1,1,1) - S_{ijk}(1,2,2)] + \langle h_2\rangle[S_{ijk}(2,2,2) - S_{ijk}(2,1,1)]\Big] \\ &+ \frac{\kappa A_\kappa}{3\sqrt{2}}S_{ijk}(3,3,3) + \frac{\lambda^2}{\sqrt{2}}\Big[\langle h_1\rangle[S_{ijk}(1,2,2) + S_{ijk}(1,3,3)] + \langle h_2\rangle[S_{ijk}(2,1,1) + S_{ijk}(2,3,3)] \\ &+ \frac{\mu_{eff}}{\lambda}[S_{ijk}(3,1,1) + S_{ijk}(3,2,2)]\Big] + \kappa^2\sqrt{2}\frac{\mu_{eff}}{\lambda}S_{ijk}(3,3,3) - \frac{\lambda A_\lambda}{\sqrt{2}}S_{ijk}(1,2,3) \\ &- \frac{\lambda\kappa}{\sqrt{2}}[\langle h_1\rangle S_{ijk}(3,2,3) + \langle h_2\rangle S_{ijk}(3,1,3) + 2\frac{\mu_{eff}}{\lambda}S_{ijk}(1,2,3)],\end{aligned} \tag{A.840}$$

where $S_{ijk}(x,y,z)$ is just the symmetric combination of triples of S matrix elements with each of i,j,k with each of x,y,z, i.e.:

$$\begin{aligned}S_{ijk}(x,y,z) =& S(i,x)S(j,y)S(k,z) + S(i,x)S(k,y)S(j,z) + S(j,x)S(i,y)S(k,z) \\ &+ S(j,x)S(i,z)S(k,y) + S(k,x)S(i,y)S(j,z) + S(k,x)S(j,y)S(i,z).\end{aligned} \tag{A.841}$$

Decays to two vector bosons are complicated by the consideration of whether the Higgs boson mass is greater than twice the mass of the vector boson, just as they were complicated in the MSSM. Included in `SoftSusy` for the NMSSM are the cases both where the Higgs has mass $m_{h/H/H3} > 2m_V$, and so decays to two on-shell vector bosons, and also the case where the Higgs has mass $m_V < m_{h/H/H3} < 2m_V$ so that it may only undergo a decay to one on-shell vector boson and one off-shell vector boson, which then decays into a fermion-antifermion pair, i.e. $h/H/H3 \to WW^* \to Wf'\bar{f}$ and $h/H/H3 \to ZZ^* \to Zf\bar{f}$, exactly as were included for the MSSM.

As in the MSSM, first consider $m_V < m_{h/H/H3} < 2m_V$. The only difference compared with the MSSM formulae is in the couplings $c_{h/H/H3VV}$.

$$\Gamma(h/H/H3 \to ZZ^*) = \frac{G_F^2 m_{h/H/H3} m_W^4 c_{h/H/H3VV}^2}{64\pi^3 \cos^4\theta_W} F(\epsilon_Z)\left[7 - \frac{40}{3}\sin^2\theta_W + \frac{160}{9}\sin^4\theta_W\right], \quad \text{(A.842)}$$

$$\Gamma(h/H/H3 \to WW^*) = \frac{3G_F^2 m_W^4 m_{h/H/H3} c_{h/H/H3VV}^2}{16\pi^3} F(\epsilon_W), \quad \text{(A.843)}$$

where here

$$\epsilon_V = \frac{m_V}{m_{h/H/H3}}, \quad \text{(A.844)} \qquad c_{hVV} = S(1,1)\sin\beta + S(1,2)\cos\beta, \quad \text{(A.845)}$$

$$c_{HVV} = S(2,1)\sin\beta + S(2,2)\cos\beta, \quad \text{(A.846)} \qquad c_{H3VV} = S(3,1)\sin\beta + S(3,2)\cos\beta, \quad \text{(A.847)}$$

and as before

$$F(\epsilon_V) = \frac{3(1 - 8\epsilon_V^2 + 20\epsilon_V^4)}{\sqrt{4\epsilon_V^2 - 1}}\cos^{-1}\left[\frac{3\epsilon_V^2 - 1}{2\epsilon_V^3}\right] - (1 - \epsilon_V^2)\left(\frac{47}{2}\epsilon_V^2 - \frac{13}{2} + \frac{1}{\epsilon_V^2}\right) - 3(1 - 6\epsilon_V^2 + 4\epsilon_V^4)\log(\epsilon_V). \quad \text{(A.848)}$$

If however $m_{h/H/H3} > 2m_V$ then the decay to two on-shell vector bosons occurs instead and the formulae are then:

$$\Gamma(h/H/H3 \to WW) = \frac{G_F m_{h/H/H3}^3}{8\pi\sqrt{2}} \tilde{\lambda}^{\frac{1}{2}}(m_{h/H/H3}, m_W, m_W)(1 - r^2 + \frac{3}{4}r^4) c_{h/H/H3WW}^2, \quad \text{(A.849)}$$

$$\Gamma(h/H/H3 \to ZZ) = \frac{G_F m_{h/H/H3}^3}{16\pi\sqrt{2}} \tilde{\lambda}^{\frac{1}{2}}(m_{h/H/H3}, m_Z, m_Z)(1 - r^2 + \frac{3}{4}r^4) c_{h/H/H3ZZ}^2. \quad \text{(A.850)}$$

Remember $r = 2\frac{m_V}{m_{h/H/H3}}$.

Now onto the loop decays of the neutral Higgs bosons in the NMSSM:

$$\Gamma(h_i \to \gamma\gamma) = \frac{G_F}{\sqrt{2}} \frac{m_{h_i}^3 \alpha_{em}^2(m_{h_i})}{32\pi^2} |M_{\gamma\gamma}|^2, \quad \text{(A.851)}$$

$$\begin{aligned} |M_{\gamma\gamma}|^2 = &\Big[I_t^r + I_b^r + I_c^r + I_\tau^r + I_{\tilde{W}_1}^r + I_{\tilde{W}_2}^r + I_W^r + I_{H^\pm}^r + I_{\tilde{c}_L}^r + I_{\tilde{c}_R}^r + I_{\tilde{s}_L}^r + I_{\tilde{s}_R}^r + I_{\tilde{\mu}_L}^r + I_{\tilde{\mu}_R}^r + I_{\tilde{t}_1}^r + I_{\tilde{t}_2}^r \\ &+ I_{\tilde{b}_1}^r + I_{\tilde{b}_2}^r + I_{\tilde{\tau}_1}^r + I_{\tilde{\tau}_2}^r\Big]^2 + \Big[I_t^i + I_b^i + I_c^i + I_\tau^i + I_{\tilde{W}_1}^i + I_{\tilde{W}_2}^i + I_W^i + I_{H^\pm}^i + I_{\tilde{c}_L}^i + I_{\tilde{c}_R}^i + I_{\tilde{s}_L}^i \\ &+ I_{\tilde{s}_R}^i + I_{\tilde{\mu}_L}^i + I_{\tilde{\mu}_R}^i + I_{\tilde{t}_1}^i + I_{\tilde{t}_2}^i + I_{\tilde{b}_1}^i + I_{\tilde{b}_2}^i + I_{\tilde{\tau}_1}^i + I_{\tilde{\tau}_2}^i\Big]^2. \end{aligned} \quad \text{(A.852)}$$

The $I_a^{r/i}$ are given below and are the real (r) and imaginary (i) parts.

$$I_a = c_a k_a, \quad \text{(A.853)}$$

where the c_a is the coupling for particle a and the k_a is the kinetic part for particle a. The coupling is real whilst the kinetic part may be complex, it is from the kinetic part therefore that we get real and imaginary contributions. The couplings of the various loop particles are:

$$c_t = \frac{4}{3}\frac{S(i,1)}{\sin\beta}, \quad \text{(A.854)} \qquad c_c = \frac{4}{3}\frac{S(i,1)}{\sin\beta}, \quad \text{(A.855)}$$

$$c_b = \frac{1}{3}\frac{S(i,2)}{\cos\beta}, \quad \text{(A.856)} \qquad c_\tau = \frac{S(i,2)}{\cos\beta}, \quad \text{(A.857)}$$

$$c_W = S(i,1)\sin\beta + S(i,2)\cos\beta, \tag{A.858}$$

$$c_{\tilde{W}_1} = \frac{1}{\sqrt{\sqrt{2}G_F}m_{\tilde{W}_1}}\frac{\lambda}{\sqrt{2}}S(i,3)\cos\theta_L\cos\theta_R + \frac{g}{\sqrt{2}}\left[S(i,1)\sin\theta_L\cos\theta_R + S(i,2)\cos\theta_L\sin\theta_R\right], \tag{A.859}$$

$$c_{\tilde{W}_2} = \frac{1}{\sqrt{\sqrt{2}G_F}m_{\tilde{W}_2}}\frac{\lambda}{\sqrt{2}}S(i,3)\sin\theta_L\sin\theta_R - \frac{g}{\sqrt{2}}\left[S(i,1)\cos\theta_L\sin\theta_R + S(i,2)\sin\theta_L\cos\theta_R\right], \tag{A.860}$$

$$c_{\tilde{c}_L} = \frac{4}{3}\frac{2m_W}{gm^2_{\tilde{c}_L}}[\frac{g'^2}{12} + \frac{g^2}{4}]\frac{2m_W}{g}(\sin\beta S(i,1) - \cos\beta S(i,2)), \tag{A.861}$$

$$c_{\tilde{c}_R} = \frac{4}{3}\frac{2m_W}{gm^2_{\tilde{c}_R}}\frac{g'^2}{6}\frac{2m_W}{g}(\sin\beta S(i,1) - \cos\beta S(i,2)), \tag{A.862}$$

$$c_{\tilde{s}_L} = \frac{1}{3}\frac{2m_W}{gm^2_{\tilde{s}_L}}[\frac{g'^2}{12} + \frac{g^2}{4}]\frac{2m_W}{g}(\sin\beta S(i,1) - \cos\beta S(i,2)), \tag{A.863}$$

$$c_{\tilde{s}_R} = \frac{1}{3}\frac{2m_W}{gm^2_{\tilde{s}_R}}\frac{g'^2}{6}\frac{2m_W}{g}(\sin\beta S(i,1) - \cos\beta S(i,2)), \tag{A.864}$$

$$c_{\tilde{\mu}_L} = \frac{2m_W}{gm^2_{\tilde{\mu}_L}}[\frac{-g'^2}{4} + \frac{g^2}{4}]\frac{2m_W}{g}(\sin\beta S(i,1) - \cos\beta S(i,2)), \tag{A.865}$$

$$c_{\tilde{\mu}_R} = \frac{2m_W}{gm^2_{\tilde{\mu}_R}}\frac{g'^2}{2}\frac{2m_W}{g}(\sin\beta S(i,1) - \cos\beta S(i,2)), \tag{A.866}$$

$$\begin{aligned} c_{\tilde{t}_1} = \frac{1}{2\sqrt{\sqrt{2}G_F}m^2_{\tilde{t}_1}}\Big\{ & \cos^2\theta_t\sqrt{2}\frac{\sqrt{2}m_W}{g}\Big[f_t^2\sin\beta S(i,1) + (\frac{g'^2}{12} - \frac{g^2}{4})(\sin\beta S(i,1) - \cos\beta S(i,2))\Big] \\ & + \sin^2\theta_t\sqrt{2}\frac{\sqrt{2}m_W}{g}\Big[f_t^2\sin\beta S(i,1) - \frac{g'^2}{3}\{\sin\beta S(i,1) - \cos\beta S(i,2)\}\Big] \\ & + 2\sin\theta_t\cos\theta_t\frac{f_t}{\sqrt{2}}\Big[A_t S(i,1) - \mu_{eff}S(i,2) - \lambda\frac{\sqrt{2}m_W\cos\beta}{g}S(i,3)\Big]\Big\}, \end{aligned} \tag{A.867}$$

$$\begin{aligned} c_{\tilde{t}_2} = \frac{1}{2\sqrt{\sqrt{2}G_F}m^2_{\tilde{t}_2}}\Big\{ & \sin^2\theta_t\sqrt{2}\frac{\sqrt{2}m_W}{g}\Big[f_t^2\sin\beta S(i,1) + (\frac{g'^2}{12} - \frac{g^2}{4})\{\sin\beta S(i,1) - \cos\beta S(i,2)\}\Big] \\ & + \cos^2\theta_t\sqrt{2}\frac{\sqrt{2}m_W}{g}\Big[f_t^2\sin\beta S(i,1) - \frac{g'^2}{3}\{\sin\beta S(i,1) - \cos\beta S(i,2)\}\Big] \\ & - 2\sin\theta_t\cos\theta_t\frac{f_t}{\sqrt{2}}\Big[A_t S(i,1) - \mu_{eff}S(i,2) - \lambda\frac{\sqrt{2}m_W\cos\beta}{g}S(i,3)\Big]\Big\}, \end{aligned} \tag{A.868}$$

$$\begin{aligned} c_{\tilde{b}_1} = \frac{1}{2\sqrt{\sqrt{2}G_F}m^2_{\tilde{b}_1}}\Big\{ & \cos^2\theta_b\sqrt{2}\Big[f_b^2\sqrt{2}\frac{m_W\cos\beta}{g}S(i,2) + (\frac{g'^2}{12} + \frac{g^2}{4})\{\frac{\sqrt{2}m_W\sin\beta}{g}S(i,1) \\ & - \frac{\sqrt{2}m_W\cos\beta}{g}S(i,2)\}\Big] + \sin^2\theta_b\sqrt{2}\Big[f_b^2\frac{\sqrt{2}m_W\cos\beta}{g}S(i,2) + \frac{g'^2}{6}\{\frac{\sqrt{2}m_W\sin\beta}{g}S(i,1) \\ & - \frac{\sqrt{2}m_W\cos\beta}{g}S(i,2)\}\Big] + 2\sin\theta_b\cos\theta_b\frac{f_b}{\sqrt{2}}\Big[A_b S(i,2) - \mu_{eff}S(i,1) - \lambda\frac{\sqrt{2}m_W\sin\beta}{g}S(i,3)\Big]\Big\}, \end{aligned} \tag{A.869}$$

$$c_{\tilde{b}_2} = \frac{1}{2\sqrt{\sqrt{2}G_F}m^2_{\tilde{b}_2}}\Big\{ \sin^2\theta_b\sqrt{2}\Big[f_b^2\sqrt{2}\frac{m_W\cos\beta}{g}S(i,2) + (\frac{g'^2}{12}+\frac{g^2}{4})\{\frac{\sqrt{2}m_W\sin\beta}{g}S(i,1) - \frac{\sqrt{2}m_W\cos\beta}{g}S(i,2)\}\Big] + \cos^2\theta_b\sqrt{2}\Big[f_b^2\frac{\sqrt{2}m_W\cos\beta}{g}S(i,2) + \frac{g'^2}{6}\{\frac{\sqrt{2}m_W\sin\beta}{g}S(i,1) - \frac{\sqrt{2}m_W\cos\beta}{g}S(i,2)\}\Big] - 2\sin\theta_b\cos\theta_b\frac{f_b}{\sqrt{2}}\Big[A_bS(i,2) - \mu_{eff}S(i,1) - \lambda\frac{\sqrt{2}m_W\sin\beta}{g}S(i,3)\Big]\Big\}, \tag{A.870}$$

$$c_{\tilde{\tau}_1} = \frac{1}{2\sqrt{\sqrt{2}G_F}m^2_{\tilde{\tau}_1}}\Big\{ \cos^2\theta_\tau\sqrt{2}\Big[f_\tau^2\sqrt{2}\frac{m_W\cos\beta}{g}S(i,2) + (-\frac{g'^2}{4}+\frac{g^2}{4})\{\frac{\sqrt{2}m_W\sin\beta}{g}S(i,1) - \frac{\sqrt{2}m_W\cos\beta}{g}S(i,2)\}\Big] + \sin^2\theta_\tau\sqrt{2}\Big[f_\tau^2\frac{\sqrt{2}m_W\cos\beta}{g}S(i,2) + \frac{g'^2}{2}\{\frac{\sqrt{2}m_W\sin\beta}{g}S(i,1) - \frac{\sqrt{2}m_W\cos\beta}{g}S(i,2)\}\Big] + 2\sin\theta_\tau\cos\theta_\tau\frac{f_\tau}{\sqrt{2}}\Big[A_\tau S(i,2) - \mu_{eff}S(i,1) - \lambda\frac{\sqrt{2}m_W\sin\beta}{g}S(i,3)\Big]\Big\}, \tag{A.871}$$

$$c_{\tilde{\tau}_2} = \frac{1}{2\sqrt{\sqrt{2}G_F}m^2_{\tilde{\tau}_2}}\Big\{ \sin^2\theta_\tau\sqrt{2}\Big[f_\tau^2\sqrt{2}\frac{m_W\cos\beta}{g}S(i,2) + (-\frac{g'^2}{4}+\frac{g^2}{4})\{\frac{\sqrt{2}m_W\sin\beta}{g}S(i,1) - \frac{\sqrt{2}m_W\cos\beta}{g}S(i,2)\}\Big] + \cos^2\theta_\tau\sqrt{2}\Big[f_\tau^2\frac{\sqrt{2}m_W\cos\beta}{g}S(i,2) + \frac{g'^2}{2}\{\frac{\sqrt{2}m_W\sin\beta}{g}S(i,1) - \frac{\sqrt{2}m_W\cos\beta}{g}S(i,2)\}\Big] - 2\sin\theta_\tau\cos\theta_\tau\frac{f_\tau}{\sqrt{2}}\Big[A_\tau S(i,2) - \mu_{eff}S(i,1) - \lambda\frac{\sqrt{2}m_W\sin\beta}{g}S(i,3)\Big]\Big\}, \tag{A.872}$$

$$\begin{aligned} c_{H^\pm} =& \frac{\lambda\mu_{eff}}{\sqrt{2}}\Big[2S(i,3)\cos^2\beta + 2S(i,3)\sin^2\beta\Big] - \lambda^2\frac{m_W\sin\beta}{g}2S(i,2)\cos\beta\sin\beta \\ &- \frac{m_W\sin\beta}{g}2S(i,1)\cos\beta\sin\beta + \mu_{eff}\kappa 2\sqrt{2}S(i,3)\cos\beta\sin\beta + \frac{\lambda A_\lambda}{\sqrt{2}}2S(i,3)\cos\beta\sin\beta \\ &+ \frac{g'^2}{4}\frac{m_W}{g}\Big[\sin\beta\{2S(i,1)\cos^2\beta - 2S(i,1)\sin^2\beta\} + \cos\beta\{2S(i,2)\sin^2\beta - 2S(i,2)\cos^2\beta\}\Big] \\ &+ \frac{gm_W}{4}\Big[\sin\beta\{2S(i,1)\cos^2\beta + 2S(i,1)\sin^2\beta + 4S(i,2)\sin\beta\cos\beta\} \\ &+ \cos\beta\{2S(i,2)\cos^2\beta + 2S(i,2)\sin^2\beta + 4S(i,1)\sin\beta\cos\beta\}\Big], \end{aligned} \tag{A.873}$$

where we remember that

$$f_t = \frac{gm_t}{\sqrt{2}m_W\sin\beta}, \quad f_b = \frac{gm_b}{\sqrt{2}m_W\cos\beta}, \quad f_\tau = \frac{gm_\tau}{\sqrt{2}m_W\cos\beta}. \tag{A.874}$$

The kinetic parts meanwhile are as follows, they depend upon the $f(\tau)$ given in Eq. (A.2).

For fermions (spin $\frac{1}{2}$), i.e. the quarks and the charginos:

$$k_a = 2\tau_a[1 - \tau_a f(\tau_a)]. \tag{A.875}$$

For scalars (e.g. sfermions and $H^\pm$):

$$k_a = \tau_a(\tau_a f(\tau_a) - 1). \tag{A.876}$$

For spin 1 (i.e $W^\pm$ bosons):

$$k_a = -[2 + 3\tau_a + 3\tau_a(2-\tau_a)f(\tau_a)]. \tag{A.877}$$

That is all the information needed for $h_i \to \gamma\gamma$.

$$\Gamma(h_i \to Z\gamma) = \frac{G_F}{\sqrt{2}} \frac{m_{h_i}^3 \alpha_{em}^2(m_{h_i})}{64\pi^3} \Big(1 - \big(\frac{m_Z}{m_{h_i}}\big)^2\Big)^3 |M_{Z\gamma}|^2, \tag{A.878}$$

where

$$|M_{Z\gamma}|^2 = \Big(\mathcal{I}_t^r + \mathcal{I}_b^r + \mathcal{I}_c^r + \mathcal{I}_{\tilde{W}_1}^r + \mathcal{I}_{\tilde{W}_2}^r + \mathcal{I}_W^r + \mathcal{I}_{H^\pm}^r\Big)^2 + \Big(\mathcal{I}_t^i + \mathcal{I}_b^i + \mathcal{I}_c^i + \mathcal{I}_{\tilde{W}_1}^i + \mathcal{I}_{\tilde{W}_2}^i + \mathcal{I}_W^i + \mathcal{I}_{H^\pm}^i\Big)^2. \tag{A.879}$$

Again $\mathcal{I}_a^{r/i}$ are the real and imaginary parts of each contribution and $\mathcal{I}_a = c_a k_a$, where now the c_a and k_a are different to above as this is now for decays to $Z\gamma$. Now the couplings are:

$$c_t = -2(1 - \frac{8}{3}\sin^2\theta_W) \frac{1}{\sin\theta_W \cos\theta_W} \frac{S(i,1)}{\sin\beta}, \tag{A.880}$$

$$c_c = -2(1 - \frac{8}{3}\sin^2\theta_W) \frac{1}{\sin\theta_W \cos\theta_W} \frac{S(i,1)}{\sin\beta}, \tag{A.881}$$

$$c_b = (-1 + \frac{4}{3}\sin^2\theta_W) \frac{1}{\sin\theta_W \cos\theta_W} \frac{S(i,2)}{\cos\beta}, \tag{A.882}$$

$$c_W = -\frac{g}{g'}[S(i,1)\sin\beta + S(i,2)\cos\beta], \tag{A.883}$$

$$\begin{aligned} c_{\tilde{W}_1} =& \frac{4m_W}{m_{\tilde{W}_1} g \sin\theta_W \cos\theta_W} \Big[\frac{\lambda}{\sqrt{2}} S(i,3)\cos\theta_L \cos\theta_R + \frac{g}{\sqrt{2}}\{S(i,1)\sin\theta_L\cos\theta_R + S(i,2)\cos\theta_L\sin\theta_R\}\Big] \\ & \times [-\sin^2\theta_R - \frac{1}{2}\cos^2\theta_R + 2\sin^2\theta_W - \sin^2\theta_L - \frac{1}{2}\cos^2\theta_L], \end{aligned} \tag{A.884}$$

$$\begin{aligned} c_{\tilde{W}_2} =& \frac{4m_W}{m_{\tilde{W}_2} g \sin\theta_W \cos\theta_W} \Big[\frac{\lambda}{\sqrt{2}} S(i,3)\sin\theta_L \sin\theta_R - \frac{g}{\sqrt{2}}\{S(i,1)\cos\theta_L\sin\theta_R + S(i,2)\sin\theta_L\cos\theta_R\}\Big] \\ & \times [-\cos^2\theta_R - \frac{1}{2}\sin^2\theta_R + 2\sin^2\theta_W - \cos^2\theta_L - \frac{1}{2}\sin^2\theta_L], \end{aligned} \tag{A.885}$$

$$\begin{aligned} c_{H^\pm} =& (1 - 2\sin^2\theta_W) \frac{1}{2\sin\theta_W\cos\theta_W m_{H^\pm}^2} \frac{1}{\sqrt{\sqrt{2}G_F}} \Big\{ \frac{\lambda\mu_{eff}}{\sqrt{2}}[2S(i,3)\cos^2\beta + 2S(i,3)\sin^2\beta] \\ & - \frac{\lambda^2 m_W \sin\beta}{g} 2S(i,2)\cos\beta\sin\beta - \frac{\lambda^2 m_W \sin\beta}{g} 2S(i,1)\cos\beta\sin\beta + \mu_{eff}\kappa 2\sqrt{2}S(i,3)\cos\beta\sin\beta \\ & + \lambda A_\lambda \sqrt{2} S(i,3)\cos\beta\sin\beta + \frac{g'^2}{4}\frac{m_W}{g}[\sin\beta(2S(i,1)\cos^2\beta - 2S(i,1)\sin^2\beta] \\ & + \cos\beta[2S(i,2)\sin^2\beta - 2S(i,2)\cos^2\beta] + \frac{g m_W}{4}\Big(\sin\beta[2S(i,1)\cos^2\beta + 2S(i,1)\sin^2\beta \\ & + 4S(i,2)\sin\beta\cos\beta] + \cos\beta[2S(i,2)\cos^2\beta + 2S(i,2)\sin^2\beta + 4S(i,1)\sin\beta\cos\beta]\Big)\Big\}. \end{aligned} \tag{A.886}$$

Now the kinetic parts depend upon $f(\tau_a)$ in Eq. (A.2), $g(\tau_a)$ in Eq. (A.3) and $f(\tau_{aZ})$, $g(\tau_{aZ})$, where $\tau_{aZ} = 4(\frac{m_a}{m_Z})^2$ and $\tau_a = 4(\frac{m_a}{m_{h_i}})^2$.

For the spin $\frac{1}{2}$ particles (quarks or charginos):

$$k_a = \frac{\tau_a\tau_{aZ}}{2(\tau_a - \tau_{aZ})} + \frac{(\tau_a\tau_{aZ})^2}{2(\tau_a - \tau_{aZ})^2}[f(\tau_a) - f(\tau_{aZ})] + \frac{\tau_a^2\tau_{aZ}}{(\tau_a - \tau_{aZ})^2}[g(\tau_a) - g(\tau_{aZ})] + \frac{\tau_a\tau_{aZ}}{2(\tau_a - \tau_{aZ})}[f(\tau_a) - f(\tau_{aZ})]. \tag{A.887}$$

For scalars (charged Higgs bosons):

$$k_a = \frac{\tau_a\tau_{aZ}}{2(\tau_a - \tau_{aZ})} + \frac{(\tau_a\tau_{aZ})^2}{2(\tau_a - \tau_{aZ})^2}[f(\tau_a) - f(\tau_{aZ})] + \frac{\tau_a^2\tau_{aZ}}{(\tau_a - \tau_{aZ})^2}[g(\tau_a) - g(\tau_{aZ})]. \tag{A.888}$$

For the spin 1 bosons (W bosons):

$$k_a = -4(3-\tan^2\theta_W)\frac{\tau_a\tau_{aZ}}{2(\tau_a-\tau_{aZ})}[f(\tau_a)-f(\tau_{aZ})] + \{(1+\frac{2}{\tau_a})\tan^2\theta_W - (5+\frac{2}{\tau_a})\}\Big[\frac{\tau_a\tau_{aZ}}{2(\tau_a-\tau_{aZ})} + \frac{(\tau_a\tau_{aZ})^2}{2(\tau_a-\tau_{aZ})^2}[f(\tau_a)-f(\tau_{aZ})] + \frac{\tau_a^2\tau_{aZ}}{(\tau_a-\tau_{aZ})^2}[g(\tau_a)-g(\tau_{aZ})]\Big]. \tag{A.889}$$

That's all the information required for $h_i \to Z\gamma$.

Next consider gluon gluon:

$$\Gamma(h_i \to gg) = \frac{G_F m_{h_i}^3 \alpha_s^2(m_{h_i})}{64\sqrt{2}\pi^3}|M_{gg}|^2, \tag{A.890}$$

where

$$\begin{aligned}|M_{gg}|^2 =&[J_t^r + J_b^r + J_c^r + J_{\tilde{c}_L}^r + J_{\tilde{c}_R}^r + J_{\tilde{s}_L}^r + J_{\tilde{s}_R}^r + J_{\tilde{t}_1}^r + J_{\tilde{t}_2}^r + J_{\tilde{b}_1}^r + J_{\tilde{b}_2}^r]^2 \\ &+ [J_t^i + J_b^i + J_c^i + J_{\tilde{c}_L}^i + J_{\tilde{c}_R}^i + J_{\tilde{s}_L}^i + J_{\tilde{s}_R}^i + J_{\tilde{t}_1}^i + J_{\tilde{t}_2}^i + J_{\tilde{b}_1}^i + J_{\tilde{b}_2}^i]^2.\end{aligned} \tag{A.891}$$

As usual each of the J_a are given by $J_a = c_a k_a$, where the coupling parts c_a are given here whilst the kinetic parts are then exactly as in the $h_i \to \gamma\gamma$ case.

$$c_t = \frac{S(i,1)}{\sin\beta}, \tag{A.892}$$

$$c_c = \frac{S(i,1)}{\sin\beta}, \tag{A.893}$$

$$c_b = \frac{S(i,2)}{\cos\beta}, \tag{A.894}$$

$$c_{\tilde{c}_L} = \frac{2m_W}{g m^2_{\tilde{c}_L}}\Big(\frac{g'^2}{12}+\frac{g^2}{4}\Big)\frac{2m_W}{g}[\sin\beta S(i,1) - \cos\beta S(i,2)], \tag{A.895}$$

$$c_{\tilde{c}_R} = \frac{2m_W}{g m^2_{\tilde{c}_R}}\frac{g'^2}{6}\frac{2m_W}{g}[\sin\beta S(i,1) - \cos\beta S(i,2)], \tag{A.896}$$

$$c_{\tilde{s}_L} = \frac{2m_W}{g m^2_{\tilde{s}_L}}\Big(\frac{g'^2}{12}+\frac{g^2}{4}\Big)\frac{2m_W}{g}[\sin\beta S(i,1) - \cos\beta S(i,2)], \tag{A.897}$$

$$c_{\tilde{s}_R} = \frac{2m_W}{g m^2_{\tilde{s}_R}}\frac{g'^2}{6}\frac{2m_W}{g}[\sin\beta S(i,1) - \cos\beta S(i,2)], \tag{A.898}$$

$$\begin{aligned}c_{\tilde{t}_1} =&\frac{m_W}{g m^2_{\tilde{t}_1}}\Big[\cos^2\theta_t\sqrt{2}\Big(f_t^2\sqrt{2}\frac{m_W\sin\beta}{g}S(i,1) + (\frac{g'^2}{12}-\frac{g^2}{4})\{\sqrt{2}\frac{m_W}{g}(S(i,1)\sin\beta - \cos\beta S(i,2))\}\Big) \\ &+ \sin^2\theta_t\sqrt{2}\Big(f_t^2\sqrt{2}\frac{m_W\sin\beta}{g}S(i,1) - \frac{g'^2}{3}\{\sqrt{2}\frac{m_W}{g}(\sin\beta S(i,1) - \cos\beta S(i,2))\}\Big) \\ &+ 2\sin\theta_t\cos\theta_t\frac{f_t}{\sqrt{2}}\Big(A_t S(i,1) - \mu_{eff}S(i,2) - \lambda\sqrt{2}\frac{m_W\cos\beta}{g}S(i,3)\Big)\Big],\end{aligned} \tag{A.899}$$

$$\begin{aligned}c_{\tilde{t}_2} =&\frac{m_W}{g m^2_{\tilde{t}_2}}\Big[\sin^2\theta_t\sqrt{2}\Big(f_t^2\sqrt{2}\frac{m_W\sin\beta}{g}S(i,1) + (\frac{g'^2}{12}-\frac{g^2}{4})\{\sqrt{2}\frac{m_W}{g}(S(i,1)\sin\beta - \cos\beta S(i,2))\}\Big) \\ &+ \cos^2\theta_t\sqrt{2}\Big(f_t^2\sqrt{2}\frac{m_W\sin\beta}{g}S(i,1) - \frac{g'^2}{3}\{\sqrt{2}\frac{m_W}{g}(\sin\beta S(i,1) - \cos\beta S(i,2))\}\Big) \\ &- 2\sin\theta_t\cos\theta_t\frac{f_t}{\sqrt{2}}\Big(A_t S(i,1) - \mu_{eff}S(i,2) - \lambda\sqrt{2}\frac{m_W\cos\beta}{g}S(i,3)\Big)\Big],\end{aligned} \tag{A.900}$$

$$c_{\tilde{b}_1} = \frac{m_W}{g m^2_{\tilde{b}_1}} \Big[\cos^2\theta_b \sqrt{2} \Big(f_b^2 \sqrt{2} \frac{m_W \cos\beta}{g} S(i,2) + (\frac{g'^2}{12} + \frac{g^2}{4}) \{ \sqrt{2} \frac{m_W}{g} (S(i,1)\sin\beta - \cos\beta S(i,2)) \} \Big)$$
$$+ \sin^2\theta_b \sqrt{2} \Big(f_b^2 \sqrt{2} \frac{m_W \cos\beta}{g} S(i,2) + \frac{g'^2}{6} \{ \sqrt{2} \frac{m_W}{g} (\sin\beta S(i,1) - \cos\beta S(i,2)) \} \Big)$$
$$+ 2\sin\theta_b \cos\theta_b \frac{f_b}{\sqrt{2}} \Big(A_b S(i,2) - \mu_{eff} S(i,1) - \lambda \sqrt{2} \frac{m_W \sin\beta}{g} S(i,3) \Big) \Big], \tag{A.901}$$

$$c_{\tilde{b}_2} = \frac{m_W}{g m^2_{\tilde{b}_2}} \Big[\sin^2\theta_B \sqrt{2} \Big(f_b^2 \sqrt{2} \frac{m_W \cos\beta}{g} S(i,2) + (\frac{g'^2}{12} + \frac{g^2}{4}) \{ \sqrt{2} \frac{m_W}{g} (S(i,1)\sin\beta - \cos\beta S(i,2)) \} \Big)$$
$$+ \cos^2\theta_b \sqrt{2} \Big(f_b^2 \sqrt{2} \frac{m_W \cos\beta}{g} S(i,2) + \frac{g'^2}{6} \{ \sqrt{2} \frac{m_W}{g} (\sin\beta S(i,1) - \cos\beta S(i,2)) \} \Big)$$
$$- 2\sin\theta_b \cos\theta_b \frac{f_b}{\sqrt{2}} \Big(A_b S(i,2) - \mu_{eff} S(i,1) - \lambda \sqrt{2} \frac{m_W \sin\beta}{g} S(i,3) \Big) \Big]. \tag{A.902}$$

A.6.2 CP Odd Higgs Decays

First of all decays to a quark and an antiquark:

$$\Gamma(A_i \to q\bar{q}) = \frac{3 G_F}{4\pi\sqrt{2}} m_q^2 m_{A_i} \sqrt{1 - \frac{4m_q^2}{m^2_{A_i}}} \mathcal{A}, \tag{A.903}$$

where

$$\mathcal{A} = \begin{cases} [\frac{S(i,1)}{\sin\beta}]^2, \text{ for up-type quarks (u,c,t)}, \\ [\frac{S(i,2)}{\cos\beta}]^2, \text{ for down-type quarks (d,s,b)}. \end{cases} \tag{A.904}$$

Use the same formulae for decays to leptons but divide by 3 as the 3 in the pre-factor is N_c. Now decays to sfermions, because of CP conservation, decays can only go to sfermions of different handedness.

$$\Gamma(A_i \to \tilde{q}_L \tilde{q}_R^*) = \frac{1}{16\pi m_{A_i}} \tilde{\lambda}^{\frac{1}{2}}(m_{A_i}, m_{\tilde{q}_L}, m_{\tilde{q}_R}) \mathcal{C}^2_{A_i \tilde{q}\tilde{q}}, \tag{A.905}$$

$$\mathcal{C}_{A_i \tilde{q}\tilde{q}} = \begin{cases} \frac{f_q}{\sqrt{2}} [A_{\tilde{q}} P(i,1) + \mu_{eff} P(i,2) + \lambda\sqrt{2} \frac{m_W \cos\beta}{g} P(i,3)], \text{ for } u\text{-type squarks}, \\ \frac{f_q}{\sqrt{2}} [A_{\tilde{q}} P(i,2) + \mu_{eff} P(i,1) + \lambda\sqrt{2} \frac{m_W \sin\beta}{g} P(i,3)], \text{ for } d\text{-type squarks}. \end{cases} \tag{A.906}$$

Remember that the expression for f_q differs for up type and down type quarks, for example see (A.11).

Note that (A.905) holds even for third generation squarks; as we see in the MSSM, in the NMSSM the decays of CP odd Higgs bosons to squarks are independent of the sfermion mixing angles. The formulae for the decays to squarks also hold for decays to sleptons, but again one must divide by 3.

Decays to neutralinos:

$$\Gamma(A_i \to \tilde{Z}_j \tilde{Z}_k) = \frac{m_{A_i}}{16\pi} \Big[1 - (\frac{m_{\tilde{Z}_j} - m_{\tilde{Z}_k}}{m_{A_i}})^2 \Big] \tilde{\lambda}^{\frac{1}{2}}(m_{A_i}, m_{\tilde{Z}_j}, m_{\tilde{Z}_k}) \alpha_{ij} \mathcal{C}^2_{A_i \tilde{Z}_j \tilde{Z}_k}, \tag{A.907}$$

where, as for the CP even decays to neutralinos, the α_{jk} factor accounts for indistinguishability and so is 1 if $j = k$ (i.e. decay to two of the same neutralinos) and 2 if $j \neq k$ (i.e. decays to two different neutralino mass eigenstates). The coupling is given by:

$$\mathcal{C}_{A_i\tilde{Z}_j\tilde{Z}_k} = \frac{\lambda}{\sqrt{2}}\Big[P(i,1)(N_{3j}N_{5k}+N_{5j}N_{3k})+P(i,2)(N_{4j}N_{5k}+N_{5j}N_{4k})+P(i,3)(N_{3j}N_{4k}+N_{4j}N_{3k})\Big] - \sqrt{2}\kappa P(i,3)N_{5j}N_{5k} - \tan\theta_W\frac{g}{2}\Big[-P(i,1)(N_{1j}N_{4k}+N_{4j}N_{1k})+P(i,2)(N_{1j}N_{3k} + N_{3j}N_{1k})\Big] - \frac{g}{2}\Big[P(i,1)(N_{2j}N_{4k}+N_{4j}N_{2k})-P(i,2)(N_{2j}N_{3k}+N_{3j}N_{2k})\Big]. \tag{A.908}$$

Decays to charginos, first consider decays to the two of the same chargino:

$$\Gamma(A_i \to \tilde{W}_j\tilde{W}_j) = \frac{m_{A_i}}{8\pi}\tilde{\lambda}^{\frac{1}{2}}(m_{A_i}, m_{\tilde{W}_j}, m_{\tilde{W}_j})S^2, \tag{A.909}$$

here

$$S = \begin{cases} \frac{\lambda}{\sqrt{2}}P(i,3)\cos\theta_L\cos\theta_R - \frac{g}{\sqrt{2}}[P(i,1)\sin\theta_L\cos\theta_R + P(i,2)\cos\theta_L\sin\theta_R], \text{ for } j=1, \\ \frac{\lambda}{\sqrt{2}}P(i,3)\sin\theta_L\sin\theta_R + \frac{g}{\sqrt{2}}[P(i,1)\cos\theta_L\sin\theta_R + P(i,2)\sin\theta_L\cos\theta_R], \text{ for } j=2. \end{cases} \tag{A.910}$$

Meanwhile for decays to different charginos:

$$\Gamma(A_i \to \tilde{W}_1\tilde{W}_2) = \frac{m_{A_i}}{8\pi}\tilde{\lambda}^{\frac{1}{2}}(m_{A_i}, m_{\tilde{W}_1}, m_{\tilde{W}_2})\Big[(c_1^2+c_2^2)\frac{1}{m_{A_i}^2}(m_{A_i}^2 - m_{\tilde{W}_1}^2 - m_{\tilde{W}_2}^2) + 4c_1c_2\frac{m_{\tilde{W}_1}m_{\tilde{W}_2}}{m_{A_i}^2}\Big], \tag{A.911}$$

now

$$c_1 = \frac{\lambda}{\sqrt{2}}P(i,3)\cos\theta_L\sin\theta_R - \frac{g}{\sqrt{2}}[P(i,1)\sin\theta_L\sin\theta_R - P(i,2)\cos\theta_L\cos\theta_R], \tag{A.912}$$

$$c_2 = \frac{\lambda}{\sqrt{2}}P(i,3)\sin\theta_L\cos\theta_R + \frac{g}{\sqrt{2}}[P(i,1)\cos\theta_L\cos\theta_R - P(i,2)\sin\theta_L\sin\theta_R]. \tag{A.913}$$

Decays to CP even neutral Higgs bosons and a Z boson:

$$\Gamma(A_i \to h_jZ) = \frac{G_F m_{A_i}^3}{8\pi\sqrt{2}}\tilde{\lambda}^{\frac{3}{2}}(m_{A_i}, m_{h_j}, m_Z)\mathcal{C}^2_{A_ih_jZ}, \tag{A.914}$$

where

$$\mathcal{C}_{A_ih_jZ} = \begin{cases} [S(1,1)\cos\beta - S(1,2)\sin\beta]\cos\theta_A, \text{ for } i=j=1, \\ [S(1,1)\cos\beta - S(1,2)\sin\beta]\sin\theta_A, \text{ for } i=2,\ j=1, \\ [S(2,1)\cos\beta - S(2,2)\sin\beta]\cos\theta_A, \text{ for } i=1,\ j=2, \\ [S(2,1)\cos\beta - S(2,2)\sin\beta]\sin\theta_A, \text{ for } i=j=2, \\ [S(3,1)\cos\beta - S(3,2)\sin\beta]\cos\theta_A, \text{ for } i=1,\ j=3, \\ [S(3,1)\cos\beta - S(3,2)\sin\beta]\sin\theta_A, \text{ for } i=2,\ j=3. \end{cases} \tag{A.915}$$

The decay of a CP odd neutral Higgs to a charged Higgs and a W boson in the NMSSM is given by:

$$\Gamma(A \to H^\pm W^\pm) = \frac{G_F m_A^3}{8\pi\sqrt{2}}\tilde{\lambda}^{\frac{3}{2}}(m_A, m_{H^\pm}, m_W)\cos^2\theta_A, \tag{A.916}$$

for A_2 undergoing the same decay transform $\cos\theta_A \to \sin\theta_A$ and $m_A \to m_{A_2}$.

$$\Gamma(A_2 \to Ah_i) = \frac{1}{16\pi m_{h_i}}\tilde{\lambda}^{\frac{1}{2}}(m_{A_2}, m_A, m_{h_i})[\mathcal{C}^{NMSSM}_{AA2h_i}]^2, \tag{A.917}$$

where the coupling $\mathcal{C}^{NMSSM}_{AA2h_i}$ is:

$$\begin{aligned}\mathcal{C}^{NMSSM}_{AA2h_i} =& \frac{g^2+g'^2}{4\sqrt{2}}\Big[\langle h_1\rangle[C(i,1,2,1,1,1)-C(i,1,2,1,2,2)]+\langle h_2\rangle[C(i,1,2,2,2,2)-C(i,1,2,2,1,1)]\Big]\\ &+\frac{\lambda A_\lambda}{\sqrt{2}}[C(i,1,2,1,2,3)+C(i,1,2,2,1,3)+C(i,1,2,3,1,2)]-\frac{\kappa A_\kappa}{\sqrt{2}}C(i,1,2,3,3,3)\\ &+\frac{\lambda^2}{\sqrt{2}}\Big[\langle h_1\rangle[C(i,1,2,1,2,2)+C(i,1,2,1,3,3)]+\langle h_2\rangle[C(i,1,2,2,1,1)+C(i,1,2,2,3,3)]\\ &+\mu_{eff}\lambda[C(i,1,2,3,1,1)+C(i,1,2,3,2,2)]\Big]+\frac{\kappa^2\sqrt{2}\mu_{eff}}{\lambda}C(i,1,2,3,3,3)\\ &+\frac{\lambda\kappa}{\sqrt{2}}\Big[\langle h_1\rangle[C(i,1,2,2,3,3)-2C(i,1,2,3,2,3)]+\langle h_2\rangle[C(i,1,2,1,3,3)-2C(i,1,2,3,1,3)]\\ &+2\frac{\mu_{eff}}{\lambda}[C(i,1,2,3,1,2)-C(i,1,2,1,2,3)-C(i,1,2,2,1,3)]\Big],\end{aligned} \tag{A.918}$$

where here $C(i,1,2,x,y,z)$ is notation for

$$C(i,1,2,x,y,z) = S(i,x)[P(1,y)P(2,z)+P(1,z)P(2,y)]. \tag{A.919}$$

Now the loop decays of the CP odd Higgs bosons. First consider decays to $\gamma\gamma$:

$$\Gamma(A_i\to\gamma\gamma) = \frac{G_F m^3_{A_i}\alpha^2_{em}(m_{A_i})}{32\pi^3\sqrt{2}}|M_{A_i\gamma\gamma}|^2, \tag{A.920}$$

where

$$|M_{A_i\gamma\gamma}|^2 = (\mathcal{J}^r_t+\mathcal{J}^r_b+\mathcal{J}^r_c+\mathcal{J}^r_\tau+\mathcal{J}^r_{\tilde{W}_1}+\mathcal{J}^r_{\tilde{W}_2})^2+(\mathcal{J}^i_t+\mathcal{J}^i_b+\mathcal{J}^i_c+\mathcal{J}^i_\tau+\mathcal{J}^i_{\tilde{W}_1}+\mathcal{J}^i_{\tilde{W}_2})^2. \tag{A.921}$$

The $\mathcal{J}^{r/i}_a$ here are the real and imaginary parts respectively of $c_a k_a$ where the c_a and k_a for this decay mode are given below:

$$c_t = \frac{4}{3}\frac{P(i,1)}{\sin\beta}, \qquad c_b = \frac{1}{3}\frac{P(i,2)}{\cos\beta}, \qquad c_c = \frac{4}{3}\frac{P(i,1)}{\sin\beta}, \qquad c_\tau = \frac{P(i,2)}{\cos\beta}, \tag{A.922}$$

$$c_{\tilde{W}_1} = \frac{2m_W}{gm_{\tilde{W}_1}}[\frac{\lambda}{\sqrt{2}}P(i,3)\cos\theta_L\cos\theta_R-\frac{g}{\sqrt{2}}(P(i,1)\sin\theta_L\cos\theta_R+P(i,2)\cos\theta_L\sin\theta_R)], \tag{A.923}$$

$$c_{\tilde{W}_2} = \frac{2m_W}{gm_{\tilde{W}_2}}[\frac{\lambda}{\sqrt{2}}P(i,3)\sin\theta_L\sin\theta_R+\frac{g}{\sqrt{2}}(P(i,1)\cos\theta_L\sin\theta_R+P(i,2)\sin\theta_L\cos\theta_R)]. \tag{A.924}$$

Meanwhile the kinetic parts are, for the quarks or the charginos (as both are spin $\frac{1}{2}$):

$$k_a = \tau_a f(\tau_a). \tag{A.925}$$

The next loop decay is to $Z\gamma$:

$$\Gamma(A_i\to Z\gamma) = \frac{G_F}{\sqrt{2}}\frac{m^3_{A_i}\alpha^2_{em}(m_{A_i})}{64\pi^3}\Big(1-(\frac{m_Z}{m_{A_i}})^2\Big)|M_{A_iZ\gamma}|^2, \tag{A.926}$$

where

$$|M_{A_iZ\gamma}|^2 = (\mathcal{K}^r_t+\mathcal{K}^r_b+\mathcal{K}^r_c+\mathcal{K}^r_{\tilde{W}_1}+\mathcal{K}^r_{\tilde{W}_2})^2+(\mathcal{K}^i_t+\mathcal{K}^i_b+\mathcal{K}^i_c+\mathcal{K}^i_{\tilde{W}_1}+\mathcal{K}^i_{\tilde{W}_2})^2. \tag{A.927}$$

As usual each $\mathcal{K}_a^{r/i}$ is the real/imaginary part of $c_a k_a$ where the c_a and k_a for this mode are given below:

$$c_t = -2(1 - \frac{8}{3}\sin^2\theta_W)\frac{1}{\sin\theta_W\cos\theta_W}\frac{P(i,1)}{\sin\beta}, \quad c_c = -2(1 - \frac{8}{3}\sin^2\theta_W)\frac{1}{\sin\theta_W\cos\theta_W}\frac{P(i,1)}{\sin\beta}, \tag{A.928}$$

$$c_b = (-1 + \frac{4}{3}\sin^2\theta_W)\frac{1}{\sin\theta_W\cos\theta_W}\frac{P(i,2)}{\cos\beta}, \tag{A.929}$$

$$\begin{aligned} c_{\tilde{W}_1} = 4\frac{m_W}{m_{\tilde{W}_1} g \sin\theta_W\cos\theta_W}\Big[&-\sin^2\theta_R - \frac{1}{2}\cos^2\theta_R - \sin^2\theta_L - \frac{1}{2}\cos^2\theta_L + 2\sin^2\theta_W\Big] \\ &\times \Big(\frac{\lambda}{\sqrt{2}}P(i,3)\cos\theta_L\cos\theta_R - \frac{g}{\sqrt{2}}[P(i,1)\sin\theta_L\cos\theta_R + P(i,2)\cos\theta_L\sin\theta_R]\Big), \end{aligned} \tag{A.930}$$

$$\begin{aligned} c_{\tilde{W}_2} = 4\frac{m_W}{m_{\tilde{W}_2} g \sin\theta_W\cos\theta_W}\Big[&-\cos^2\theta_R - \frac{1}{2}\sin^2\theta_R - \cos^2\theta_L - \frac{1}{2}\sin^2\theta_L + 2\sin^2\theta_W\Big] \\ &\times \Big(\frac{\lambda}{\sqrt{2}}P(i,3)\sin\theta_L\sin\theta_R + \frac{g}{\sqrt{2}}[P(i,1)\cos\theta_L\sin\theta_R + P(i,2)\sin\theta_L\cos\theta_R]\Big), \end{aligned} \tag{A.931}$$

The kinetic parts are all of the following form, where remember $\tau_{aZ} = 4(\frac{m_a}{m_Z})^2$ and $\tau_a = 4(\frac{m_a}{m_\phi})^2$:

$$k_a = \frac{\tau_a\tau_{aZ}}{2(\tau_a - \tau_{aZ})}[f(\tau_a) - f(\tau_{aZ})]. \tag{A.932}$$

Finally, for the loop decay to gg:

$$\Gamma(A_i \to gg) = \frac{G_F}{\sqrt{2}}\frac{m_{A_i}^3\alpha_s^2(m_{A_i})}{16\pi^3}|M_{A_i gg}|^2, \tag{A.933}$$

where

$$|M_{A_i gg}|^2 = (\mathcal{R}_t^r + \mathcal{R}_b^r + \mathcal{R}_c^r)^2 + (\mathcal{R}_t^i + \mathcal{R}_b^i + \mathcal{R}_c^i)^2. \tag{A.934}$$

Again the $\mathcal{R}_a^{r/i}$ are the real and imaginary parts of $c_a k_a$, where for this mode they are:

$$c_t = \frac{P(i,1)}{\sin\beta}, \quad c_b = \frac{P(i,2)}{\cos\beta}, \quad c_c = \frac{P(i,1)}{\sin\beta}. \tag{A.935}$$

The kinetic parts are just:

$$k_a = \tau_a f(\tau_a). \tag{A.936}$$

A.6.3 Decays into Higgs Bosons

$$\Gamma(\tilde{b}_2 \to \tilde{b}_1 h_i) = \frac{1}{16\pi m_{\tilde{b}_2}}\tilde{\lambda}^{\frac{1}{2}}(m_{\tilde{b}_2}, m_{\tilde{b}_1}, m_{h_i})\Big[\cos\theta_b\sin\theta_b(c_R - c_L) + (\cos^2\theta_b - \sin^2\theta_b)c_{LR}\Big]^2, \tag{A.937}$$

where

$$c_L = -\sqrt{2}\left[f_b^2\langle h_2\rangle S(i,2) + (\frac{g'^2}{12} + \frac{g^2}{4})[\langle h_1\rangle S(i,1) - \langle h_2\rangle S(i,2)]\right], \tag{A.938}$$

$$c_R = -\sqrt{2}\left[f_b^2\langle h_2\rangle S(i,2) + (\frac{g'^2}{6})[\langle h_1\rangle S(i,1) - \langle h_2\rangle S(i,2)]\right], \tag{A.939}$$

$$c_{LR} = -\frac{f_b}{\sqrt{2}}\left[A_b S(i,2) - \mu_{eff} S(i,1) - \lambda\langle h_1\rangle S(i,3)\right]. \tag{A.940}$$

$$\Gamma(\tilde{t}_2 \to \tilde{t}_1 h_i) = \frac{1}{16\pi m_{\tilde{t}_2}} \tilde{\lambda}^{\frac{1}{2}}(m_{\tilde{t}_2}, m_{\tilde{t}_1}, m_{h_i}) \Big[\cos\theta_t \sin\theta_t (c_R - c_L) + (\cos^2\theta_t - \sin^2\theta_t) c_{LR} \Big]^2, \quad \text{(A.941)}$$

where

$$c_L = -\sqrt{2} \left[f_t^2 \langle h_1 \rangle S(i,1) + (\frac{g'^2}{12} - \frac{g^2}{4})[\langle h_1 \rangle S(i,1) - \langle h_2 \rangle S(i,2)] \right], \quad \text{(A.942)}$$

$$c_R = -\sqrt{2} \left[f_t^2 \langle h_1 \rangle S(i,1) - (\frac{g'^2}{3})[\langle h_1 \rangle S(i,1) - \langle h_2 \rangle S(i,2)] \right], \quad \text{(A.943)}$$

$$c_{LR} = -\frac{f_t}{\sqrt{2}} \left[A_t S(i,1) - \mu_{eff} S(i,2) - \lambda \langle h_2 \rangle S(i,3) \right]. \quad \text{(A.944)}$$

$$\Gamma(\tilde{\tau}_2 \to \tilde{\tau}_1 h_i) = \frac{1}{16\pi m_{\tilde{\tau}_2}} \tilde{\lambda}^{\frac{1}{2}}(m_{\tilde{\tau}_2}, m_{\tilde{\tau}_1}, m_{h_i}) \Big[\cos\theta_\tau \sin\theta_\tau (c_R - c_L) + (\cos^2\theta_\tau - \sin^2\theta_\tau) c_{LR} \Big]^2, \quad \text{(A.945)}$$

where

$$c_L = -\sqrt{2} \left[f_\tau^2 \langle h_2 \rangle S(i,2) + (\frac{-g'^2}{4} + \frac{g^2}{4})[\langle h_1 \rangle S(i,1) - \langle h_2 \rangle S(i,2)] \right], \quad \text{(A.946)}$$

$$c_R = -\sqrt{2} \left[f_\tau^2 \langle h_2 \rangle S(i,2) + (\frac{g'^2}{2})[\langle h_1 \rangle S(i,1) - \langle h_2 \rangle S(i,2)] \right], \quad \text{(A.947)}$$

$$c_{LR} = -\frac{f_\tau}{\sqrt{2}} \left[A_\tau S(i,2) - \mu_{eff} S(i,1) - \lambda \langle h_1 \rangle S(i,3) \right]. \quad \text{(A.948)}$$

$$\Gamma(\tilde{b}_2 \to \tilde{b}_1 A_i) = \frac{1}{16\pi m_{\tilde{b}_2}} \tilde{\lambda}^{\frac{1}{2}}(m_{\tilde{b}_2}, m_{\tilde{b}_1}, m_{\tilde{A}_i}) [\cos^2\theta_b - \sin^2\theta_b]^2 A_{LR}^2, \quad \text{(A.949)}$$

where

$$A_{LR} = \frac{f_b}{\sqrt{2}} \left[A_b P(i,2) + \mu_{eff} P(i,1) + \lambda \langle h_1 \rangle P(i,3) \right]. \quad \text{(A.950)}$$

For $\tilde{\tau}_2 \to \tilde{\tau}_1 A_i$ the formulae are the same except the changes $\theta_b \to \theta_\tau$, $m_b \to m_\tau$ and now A_{LR} is given by:

$$A_{LR} = \frac{f_\tau}{\sqrt{2}} \left[A_\tau P(i,2) + \mu_{eff} P(i,1) + \lambda \langle h_1 \rangle P(i,3) \right]. \quad \text{(A.951)}$$

For $\tilde{t}_2 \to \tilde{t}_1 A_i$ the formulae are the same except the changes $\theta_b \to \theta_t$, $m_b \to m_t$ and now A_{LR} is given by:

$$A_{LR} = \frac{f_t}{\sqrt{2}} \left[A_t P(i,1) + \mu_{eff} P(i,2) + \lambda \langle h_2 \rangle P(i,3) \right]. \quad \text{(A.952)}$$

The chargino decays to lighter charginos and a CP even neutral Higgs:

$$\Gamma(\tilde{W}_2 \to \tilde{W}_1 h_i) = \frac{1}{32\pi |m_{\tilde{W}_2}|} \tilde{\lambda}^{1/2}(m_{\tilde{W}_2}, m_{\tilde{W}_1}, m_{h_i}) \Big[(c_1^2 + c_2^2)(m_{\tilde{W}_1}^2 + m_{\tilde{W}_2}^2 - m_{h_i}^2) + 4 c_1 c_2 m_{\tilde{W}_1} m_{\tilde{W}_2} \Big]^2, \quad \text{(A.953)}$$

here the c_1 and c_2 are:

$$c_1 = \frac{\lambda}{\sqrt{2}} S(i,3) \cos\theta_L \sin\theta_R + \frac{g}{\sqrt{2}} [S(i,1) \sin\theta_L \sin\theta_R - S(i,2) \cos\theta_L \cos\theta_R], \quad \text{(A.954)}$$

$$c_2 = \frac{\lambda}{\sqrt{2}} S(i,3) \sin\theta_L \cos\theta_R - \frac{g}{\sqrt{2}} [S(i,1) \cos\theta_L \cos\theta_R - S(i,2) \sin\theta_L \sin\theta_R]. \quad \text{(A.955)}$$

The chargino decays to lighter charginos and a CP odd neutral Higgs:

$$\Gamma(\tilde{W}_2 \to \tilde{W}_1 A_i) = \frac{1}{32\pi |m_{\tilde{W}_2}|} \tilde{\lambda}^{1/2}(m_{\tilde{W}_2}, m_{\tilde{W}_1}, m_{A_i}) \Big[(C_1^2 + C_2^2)(m_{\tilde{W}_1}^2 + m_{\tilde{W}_2}^2 - m_{h_i}^2) + 4 C_1 C_2 m_{\tilde{W}_1} m_{\tilde{W}_2} \Big]^2, \quad \text{(A.956)}$$

here the C_1 and C_2 are:

$$C_1 = \frac{\lambda}{\sqrt{2}} P(i,3)\cos\theta_L \sin\theta_R - \frac{g}{\sqrt{2}}[P(i,1)\sin\theta_L \sin\theta_R - P(i,2)\cos\theta_L \cos\theta_R], \tag{A.957}$$

$$C_2 = \frac{\lambda}{\sqrt{2}} P(i,3)\sin\theta_L \cos\theta_R + \frac{g}{\sqrt{2}}[P(i,1)\cos\theta_L \cos\theta_R - P(i,2)\sin\theta_L \sin\theta_R]. \tag{A.958}$$

The formulae for $\Gamma(H^\pm \to W h_i)$ are just as above for $\Gamma(h_i \to W H^\pm)$ in (A.835) but with $m_{h_i} \leftrightarrow m_{H^\pm}$. Similarly the formulae for $\Gamma(H^\pm \to W A_i)$ are just as above for $\Gamma(A_i \to W H^\pm)$ in (A.916) but with the replacement $m_{A_i} \leftrightarrow m_{H^\pm}$.

A.6.4 Neutralino Decays

$$\Gamma(\tilde{Z}_i \to \tilde{q}_{L/R}\bar{q}) = \frac{N_c g^2}{32\pi |m_{\tilde{Z}_i}|} \tilde{\lambda}^{\frac{1}{2}}(m_{\tilde{Z}_i}, m_{\tilde{q}_{L/R}}, m_q) \mathcal{C}_{\mathcal{L}/\mathcal{R}}{}^2 (m^2_{\tilde{Z}_i} - m^2_{\tilde{q}_{L/R}} + m^2_q), \tag{A.959}$$

where

$$C_L = \begin{cases} -\sqrt{2}[\frac{2}{3}c(1)\sin\theta_W + (\frac{1}{2} - \frac{2}{3}\sin^2\theta_W)\frac{c(2)}{\cos\theta_W}], \text{ for } \tilde{u}_L, \\ \sqrt{2}[\frac{1}{3}c(1)\sin\theta_W + (\frac{1}{2} - \frac{1}{3}\sin^2\theta_W)\frac{c(2)}{\cos\theta_W}], \text{ for } \tilde{d}_L, \\ \sqrt{2}[-c(1)\sin\theta_W + (\frac{1}{2} - \sin^2\theta_W)\frac{c(2)}{\cos\theta_W}], \text{ for } \tilde{l}_L, \\ \frac{-c(2)}{\sqrt{2}}\cos\theta_W, \text{ for } \tilde{\nu}_L, \end{cases} \tag{A.960}$$

$$C_R = \begin{cases} -\sqrt{2}\frac{2}{3}\sin\theta_W \Big[c(2)\tan\theta_W - c(1)\Big], \text{ for } \tilde{u}_R, \\ \sqrt{2}\frac{1}{3}\sin\theta_W \Big[c(2)\tan\theta_W - c(1)\Big], \text{ for } \tilde{d}_R, \\ \sqrt{2}\sin\theta_W \Big[c(2)\tan\theta_W - c(1)\Big], \text{ for } \tilde{l}_R, \\ 0, \text{ for } \tilde{\nu}_R. \end{cases} \tag{A.961}$$

Here $N_c = 3$ for quarks and 1 for leptons and $c(1)$ and $c(2)$ are given by:

$$c(1) = N_{1i}\cos\theta_W + N_{2i}\sin\theta_W, \qquad c(2) = -N_{1i}\sin\theta_W + N_{2i}\cos\theta_W. \tag{A.962}$$

For the third generation, the generalisation is as expected but with extra Yukawa interactions:

$$\Gamma(\tilde{Z}_i \to \tilde{t}_{1/2}\bar{t}) = \frac{3g^2}{32\pi |m_{\tilde{Z}_i}|} \tilde{\lambda}^{\frac{1}{2}}(m_{\tilde{Z}_i}, m_{\tilde{t}_{1/2}}, m_t) \left[(c_1^2 + c_2^2)(m^2_{\tilde{Z}_i} - m^2_{\tilde{t}_{1/2}} + m_t^2) + 4 m_t m_{\tilde{Z}_i} c_1 c_2\right], \tag{A.963}$$

where

$$c_1 = \begin{cases} \sqrt{2}\cos\theta_t[-\frac{2}{3}c(1)\sin\theta_W + (-\frac{1}{2} + \frac{2}{3}\sin^2\theta_W)\frac{c(2)}{\cos\theta_W}] - \sin\theta_t \frac{f_t}{g} N_{4i}, \text{ for } \tilde{t}_1, \\ -\sqrt{2}\sin\theta_t[-\frac{2}{3}c(1)\sin\theta_W + (-\frac{1}{2} + \frac{2}{3}\sin^2\theta_W)\frac{c(2)}{\cos\theta_W}] - \cos\theta_t \frac{f_t}{g} N_{4i}, \text{ for } \tilde{t}_2, \end{cases} \tag{A.964}$$

$$c_2 = \begin{cases} -\sqrt{2}\sin\theta_t \frac{2}{3}\sin\theta_W[c(2)\tan\theta_W - c(1)] - \cos\theta_t \frac{f_t}{g} N_{4i}, \text{ for } \tilde{t}_1, \\ -\sqrt{2}\cos\theta_t \frac{2}{3}\sin\theta_W[c(2)\tan\theta_W - c(1)] + \sin\theta_t \frac{f_t}{g} N_{4i}, \text{ for } \tilde{t}_2, \end{cases} \tag{A.965}$$

$$\Gamma(\tilde{Z}_i \to \tilde{b}_{1/2}\bar{b}) = \frac{3g^2}{32\pi |m_{\tilde{Z}_i}|} \tilde{\lambda}^{\frac{1}{2}}(m_{\tilde{Z}_i}, m_{\tilde{b}_{1/2}}, m_b) \left[(c_1^2 + c_2^2)(m^2_{\tilde{Z}_i} - m^2_{\tilde{b}_{1/2}} + m_b^2) + 4 m_b m_{\tilde{Z}_i} c_1 c_2\right], \tag{A.966}$$

where

$$c_1 = \begin{cases} \sqrt{2}\cos\theta_b[\frac{1}{3}c(1)\sin\theta_W + (\frac{1}{2} - \frac{1}{3}\sin^2\theta_W)\frac{c(2)}{\cos\theta_W}] - \sin\theta_b\frac{f_b}{g}N_{3i}, \text{ for } \tilde{b}_1, \\ -\sqrt{2}\sin\theta_b[\frac{1}{3}c(1)\sin\theta_W + (\frac{1}{2} - \frac{1}{3}\sin^2\theta_W)\frac{c(2)}{\cos\theta_W}] - \cos\theta_b\frac{f_b}{g}N_{3i}, \text{ for } \tilde{b}_2, \end{cases} \tag{A.967}$$

$$c_2 = \begin{cases} \sqrt{2}\sin\theta_b\frac{1}{3}\sin\theta_W[c(2)\tan\theta_W - c(1)] - \cos\theta_b\frac{f_b}{g}N_{3i}, \text{ for } \tilde{b}_1, \\ \sqrt{2}\cos\theta_b\frac{1}{3}\sin\theta_W[c(2)\tan\theta_W - c(1)] + \sin\theta_b\frac{f_b}{g}N_{3i}, \text{ for } \tilde{b}_2. \end{cases} \tag{A.968}$$

$$\Gamma(\tilde{Z}_i \to \tilde{\tau}_{1/2}\bar{\tau}) = \frac{g^2}{32\pi|m_{\tilde{Z}_i}|}\tilde{\lambda}^{\frac{1}{2}}(m_{\tilde{Z}_i}, m_{\tilde{\tau}_{1/2}}, m_\tau)\left[(c_1^2 + c_2^2)(m_{\tilde{Z}_i}^2 - m_{\tilde{\tau}_{1/2}}^2 + m_\tau^2) + 4m_\tau m_{\tilde{Z}_i}c_1c_2\right], \tag{A.969}$$

where

$$c_1 = \begin{cases} \sqrt{2}\cos\theta_\tau[c(1)\sin\theta_W + (\frac{1}{2} - \sin^2\theta_W)\frac{c(2)}{\cos\theta_W}] - \sin\theta_\tau\frac{f_\tau}{g}N_{3i}, \text{ for } \tilde{\tau}_1, \\ -\sqrt{2}\sin\theta_\tau[c(1)\sin\theta_W + (\frac{1}{2} - \sin^2\theta_W)\frac{c(2)}{\cos\theta_W}] - \cos\theta_\tau\frac{f_\tau}{g}N_{3i}, \text{ for } \tilde{\tau}_2, \end{cases} \tag{A.970}$$

$$c_2 = \begin{cases} \sqrt{2}\sin\theta_\tau\sin\theta_W[c(2)\tan\theta_W - c(1)] - \cos\theta_\tau\frac{f_\tau}{g}N_{3i}, \text{ for } \tilde{\tau}_1, \\ \sqrt{2}\cos\theta_\tau\sin\theta_W[c(2)\tan\theta_W - c(1)] + \sin\theta_\tau\frac{f_\tau}{g}N_{3i}, \text{ for } \tilde{\tau}_2. \end{cases} \tag{A.971}$$

Neutralino decays to a chargino and W boson:

$$\Gamma(\tilde{Z}_i \to W\tilde{W}_1) = \frac{g^2}{32\pi|m_{\tilde{Z}_i}|}\tilde{\lambda}^{1/2}(m_{\tilde{Z}_i}, m_{\tilde{W}_1}, m_W)\Big[-12m_{\tilde{Z}_i}m_{\tilde{W}_j}c_Lc_R + (c_L^2 + c_R^2)\{(m_{\tilde{W}_1}^2 + m_{\tilde{Z}_i}^2 - m_W^2) + (m_{\tilde{Z}_i}^2 + m_W^2 - m_{\tilde{W}_j}^2)(m_{\tilde{Z}_i}^2 - m_W^2 - m_{\tilde{W}_j}^2)\frac{1}{m_W^2}\}\Big], \tag{A.972}$$

where

$$c_L = \frac{-1}{\sqrt{2}}N_{4i}\cos\theta_R + N_{2i}\sin\theta_R, \tag{A.973}$$

$$c_R = \frac{1}{\sqrt{2}}N_{3i}\cos\theta_L + N_{2i}\sin\theta_L. \tag{A.974}$$

For $\tilde{W}_2$ just take $m_{\tilde{W}_1} \to m_{\tilde{W}_2}$, $\cos\theta_R \to \sin\theta_R$, $\cos\theta_L \to \sin\theta_L$, $\sin\theta_R \to -\cos\theta_R$ and $\sin\theta_L \to -\cos\theta_L$.

Neutralino decays to a chargino and charged Higgs boson:

$$\Gamma(\tilde{Z}_i \to H^\pm\tilde{W}_1) = \frac{1}{32\pi|m_{\tilde{Z}_i}|}\tilde{\lambda}^{1/2}(m_{\tilde{Z}_i}, m_{\tilde{W}_1}, m_{H^\pm})\Big[(\mathcal{C}_L^2 + \mathcal{C}_R^2)\{(m_{\tilde{W}_1}^2 + m_{\tilde{Z}_i}^2 - m_{H^\pm}^2) + 4\mathcal{C}_L\mathcal{C}_Rm_{\tilde{Z}_i}m_{\tilde{W}_1}\}\Big], \tag{A.975}$$

here

$$\mathcal{C}_L = \lambda\cos\beta N_{5i}\cos\theta_L - \frac{\sin\beta}{\sqrt{2}}[g'N_{1i} + gN_{2i}]\cos\theta_L + g\sin\beta N_{3i}\sin\theta_L, \tag{A.976}$$

$$\mathcal{C}_R = \lambda\sin\beta N_{5i}\cos\theta_R + \frac{\cos\beta}{\sqrt{2}}[g'N_{1i} + gN_{2i}]\cos\theta_R + g\cos\beta N_{4i}\sin\theta_R. \tag{A.977}$$

Again for $\tilde{W}_2$, $m_{\tilde{W}_1} \to m_{\tilde{W}_2}$, $\cos\theta_R \to \sin\theta_R$, $\cos\theta_L \to \sin\theta_L$, $\sin\theta_R \to -\cos\theta_R$ and $\sin\theta_L \to -\cos\theta_L$.

Neutralino decays to a lighter neutralino and Z boson:

$$\Gamma(\tilde{Z}_i \to Z\tilde{Z}_j) = \frac{g^2}{32\pi|m_{\tilde{Z}_i}|}\tilde{\lambda}^{\frac{1}{2}}(m_{\tilde{Z}_i}, m_{\tilde{Z}_j}, m_Z)\Big[-12m_{\tilde{Z}_i}m_{\tilde{Z}_j}c_{LZ}c_{RZ} + (c_{LZ}^2 + c_{RZ}^2)\{(m_{\tilde{Z}_i}^2 + m_{\tilde{Z}_j}^2 - m_Z^2) + (m_{\tilde{Z}_i}^2 - m_{\tilde{Z}_j}^2 + m_Z^2)(m_{\tilde{Z}_i}^2 - m_{\tilde{Z}_j}^2 - m_Z^2)\frac{1}{m_Z^2}\}\Big], \tag{A.978}$$

here we have:

$$c_{LZ} = -c_{RZ} = \frac{1}{2\cos\theta_W}[N_{3i}N_{3j} - N_{4i}N_{4j}]. \tag{A.979}$$

Neutralino decays to a lighter neutralino and CP even neutral Higgs boson:

$$\Gamma(\tilde{Z}_i \to h_k \tilde{Z}_j) = \frac{1}{4\pi |m_{\tilde{Z}_i}|} \tilde{\lambda}^{\frac{1}{2}}(m_{\tilde{Z}_i}, m_{h_k}, m_{\tilde{Z}_j}) \mathcal{C}^2_{\tilde{Z}_i \tilde{Z}_j h_k} \left[m^2_{\tilde{Z}_i} + m^2_{\tilde{Z}_j} - m^2_{h_k} + 2 m_{\tilde{Z}_i} m_{\tilde{Z}_j} \right], \tag{A.980}$$

where

$$\begin{aligned} \mathcal{C}_{\tilde{Z}_i \tilde{Z}_j h_k} =& \frac{\lambda}{2\sqrt{2}} \Big[S(k,1)(N_{3i}N_{5j} + N_{3j}N_{5i}) + S(k,2)(N_{4i}N_{5j} + N_{4j}N_{5i}) + S(k,3)(N_{3i}N_{4j} + N_{4i}N_{3j}) \Big] \\ & - \sqrt{2}\kappa S(k,3) N_{5i} N_{5j} + \frac{g'}{2} \Big[- S(k,1)(N_{1i}N_{4j} + N_{1j}N_{4i}) + S(k,2)(N_{1i}N_{3j} + N_{1j}N_{3i}) \Big] \\ & + \frac{g}{2} \Big[S(k,1)(N_{2i}N_{4j} + N_{2j}N_{4i}) - S(k,2)(N_{2i}N_{3j} + N_{2j}N_{3i}) \Big]. \end{aligned} \tag{A.981}$$

Neutralino decays to a lighter neutralino and CP odd neutral Higgs boson:

$$\Gamma(\tilde{Z}_i \to A_k \tilde{Z}_j) = \frac{1}{4\pi |m_{\tilde{Z}_i}|} \tilde{\lambda}^{\frac{1}{2}}(m_{\tilde{Z}_i}, m_{A_k}, m_{\tilde{Z}_j}) [\mathcal{G}^2_{\tilde{Z}\tilde{Z}A_k}] [m^2_{\tilde{Z}_i} + m^2_{\tilde{Z}_j} - m^2_{A_k} - 2 m_{\tilde{Z}_i} m_{\tilde{Z}_j}], \tag{A.982}$$

where

$$\begin{aligned} \mathcal{G}_{\tilde{Z}_i \tilde{Z}_j A_k} =& \frac{-\lambda}{2\sqrt{2}} \Big[P(k,1)(N_{3i}N_{5j} + N_{3j}N_{5i}) + P(k,2)(N_{4i}N_{5j} + N_{4j}N_{5i}) + P(k,3)(N_{3i}N_{4j} + N_{4i}N_{3j}) \Big] \\ & - \sqrt{2}\kappa P(k,3) N_{5i} N_{5j} - \frac{g'}{2} \Big[- P(k,1)(N_{1i}N_{4j} + N_{1j}N_{4i}) + P(k,2)(N_{1i}N_{3j} + N_{1j}N_{3i}) \Big] \\ & - \frac{g}{2} \Big[P(k,1)(N_{2i}N_{4j} + N_{2j}N_{4i}) - P(k,2)(N_{2i}N_{3j} + N_{2j}N_{3i}) \Big]. \end{aligned} \tag{A.983}$$

Note that the $\mathcal{C}$ and $\mathcal{G}$ couplings here are similar to those given for the reverse decays of Higgs bosons to neutralinos earlier, with i, j, k permuted accordingly.

A.6.5 Decays into Neutralinos

For the first two generations of quarks and squarks:

$$\Gamma(\tilde{q}_{L/R} \to q \tilde{Z}_i) = \frac{g^2}{16\pi m_{\tilde{q}_{L/R}}} B^2_{\tilde{q}_{L/R}} \tilde{\lambda}^{\frac{1}{2}}(m_{\tilde{q}_{L/R}}, m_{\tilde{Z}_i}, m_q) [m^2_{\tilde{q}_{L/R}} - m^2_{\tilde{Z}_i} - m^2_q], \tag{A.984}$$

where:

$$B_{\tilde{q}_{L/R}} = \begin{cases} -\sqrt{2}[\frac{2}{3} c(1) \sin\theta_W + (\frac{1}{2} - \frac{2}{3}\sin^2\theta_W) \frac{c(2)}{\cos\theta_W}], \text{ for } \tilde{u}_L \text{ type}, \\ -\sqrt{2}\frac{2}{3} \sin\theta_W [c(2)\tan\theta_W - c(1)], \text{ for } \tilde{u}_R \text{ type}, \\ \sqrt{2}[c(1)\frac{1}{3}\sin\theta_W + (\frac{1}{2} - \frac{1}{3}\sin^2\theta_W)\frac{c(2)}{\cos\theta_W}], \text{ for } \tilde{d}_L \text{ type}, \\ \sqrt{2}\frac{1}{3}\sin\theta_W [c(2)\tan\theta_W - c(1)], \text{ for } \tilde{d}_R \text{ type}. \end{cases} \tag{A.985}$$

The decay formulae for decays of the first two generations of sleptons to leptons and neutralinos are the same as for the squarks here but with the coupling change $B_{\tilde{q}_{L/R}} \to B_{\tilde{l}_{L/R}}$ and squark masses exchanged for slepton masses and quark masses for lepton masses:

$$B_{\tilde{l}_{L/R}} = \begin{cases} -\frac{c(2)}{\sqrt{2}\cos\theta_W}, \text{ for } \tilde{\nu}_L \text{ type}, \\ 0, \text{ for } \tilde{\nu}_R \text{ type (as no RH sneutrinos)}, \\ \sqrt{2}[c(1)\sin\theta_W + (\frac{1}{2} - \sin^2\theta_W)\frac{c(2)}{\cos\theta_W}], \text{ for } \tilde{l}_L \text{ type}, \\ \sqrt{2}\sin\theta_W [c(2)\tan\theta_W - c(1)], \text{ for } \tilde{l}_R \text{ type}. \end{cases} \tag{A.986}$$

For the third generation:

$$\Gamma(\tilde{t}_{1/2} \to t\tilde{Z}_i) = \frac{g^2}{16\pi m_{\tilde{t}_{1/2}}} \Big[(d_1^2 + d_2^2)(m^2_{\tilde{t}_{1/2}} - m_t^2 - m^2_{\tilde{Z}_i}) - 4d_1 d_2 m_t m_{\tilde{Z}_i}\Big] \tilde{\lambda}^{\frac{1}{2}}(m_{\tilde{t}_{1/2}}, m_{\tilde{Z}_i}, m_t), \quad \text{(A.987)}$$

where

$$d_1 = \begin{cases} \cos\theta_t\sqrt{2}[-\frac{2}{3}c(1)\sin\theta_W + (-\frac{1}{2} + \frac{2}{3}\sin^2\theta_W)\frac{c(2)}{\cos\theta_W}] - \sin\theta_t \frac{f_t}{g} N_{4i}, \text{ for } \tilde{t}_1, \\ -\sin\theta_t\sqrt{2}[-\frac{2}{3}c(1)\sin\theta_W + (-\frac{1}{2} + \frac{2}{3}\sin^2\theta_W)\frac{c(2)}{\cos\theta_W}] - \cos\theta_t \frac{f_t}{g} N_{4i}, \text{ for } \tilde{t}_2, \end{cases} \quad \text{(A.988)}$$

$$d_2 = \begin{cases} -\frac{2}{3}\sin\theta_t\sqrt{2}\sin\theta_W[c(2)\tan\theta_W - c(1)] - \cos\theta_t \frac{f_t}{g} N_{4i}, \text{ for } \tilde{t}_1, \\ -\frac{2}{3}\cos\theta_t\sqrt{2}\sin\theta_W[c(2)\tan\theta_W - c(1)] + \sin\theta_t \frac{f_t}{g} N_{4i}, \text{ for } \tilde{t}_2. \end{cases} \quad \text{(A.989)}$$

$$\Gamma(\tilde{b}_{1/2} \to b\tilde{Z}_i) = \frac{g^2}{16\pi m_{\tilde{b}_{1/2}}} \Big[(f_1^2 + f_2^2)(m^2_{\tilde{b}_{1/2}} - m_b^2 - m^2_{\tilde{Z}_i}) - 4f_1 f_2 m_b m_{\tilde{Z}_i}\Big] \tilde{\lambda}^{\frac{1}{2}}(m_{\tilde{b}_{1/2}}, m_{\tilde{Z}_i}, m_b), \quad \text{(A.990)}$$

where

$$f_1 = \begin{cases} \cos\theta_b\sqrt{2}[\frac{1}{3}c(1)\sin\theta_W + (\frac{1}{2} - \frac{1}{3}\sin^2\theta_W)\frac{c(2)}{\cos\theta_W}] - \sin\theta_b \frac{f_b}{g} N_{3i}, \text{ for } \tilde{b}_1, \\ -\sin\theta_b\sqrt{2}[\frac{1}{3}c(1)\sin\theta_W + (\frac{1}{2} - \frac{1}{3}\sin^2\theta_W)\frac{c(2)}{\cos\theta_W}] - \cos\theta_b \frac{f_b}{g} N_{3i}, \text{ for } \tilde{b}_2, \end{cases} \quad \text{(A.991)}$$

$$f_2 = \begin{cases} \frac{1}{3}\sin\theta_b\sqrt{2}\sin\theta_W[c(2)\tan\theta_W - c(1)] - \cos\theta_b \frac{f_b}{g} N_{3i}, \text{ for } \tilde{b}_1, \\ \frac{1}{3}\cos\theta_b\sqrt{2}\sin\theta_W[c(2)\tan\theta_W - c(1)] + \sin\theta_b \frac{f_b}{g} N_{3i}, \text{ for } \tilde{b}_2. \end{cases} \quad \text{(A.992)}$$

$$\Gamma(\tilde{\tau}_{1/2} \to \tau\tilde{Z}_i) = \frac{g^2}{16\pi m_{\tilde{\tau}_{1/2}}} \Big[(g_1^2 + g_2^2)(m^2_{\tilde{\tau}_{1/2}} - m_\tau^2 - m^2_{\tilde{Z}_i}) - 4g_1 g_2 m_\tau m_{\tilde{Z}_i}\Big] \tilde{\lambda}^{\frac{1}{2}}(m_{\tilde{\tau}_{1/2}}, m_{\tilde{Z}_i}, m_\tau), \quad \text{(A.993)}$$

where

$$g_1 = \begin{cases} \cos\theta_\tau\sqrt{2}[c(1)\sin\theta_W + (\frac{1}{2} - \sin^2\theta_W)\frac{c(2)}{\cos\theta_W}] - \sin\theta_\tau \frac{f_\tau}{g} N_{3i}, \text{ for } \tilde{\tau}_1, \\ -\sin\theta_\tau\sqrt{2}[c(1)\sin\theta_W + (\frac{1}{2} - \sin^2\theta_W)\frac{c(2)}{\cos\theta_W}] - \cos\theta_\tau \frac{f_\tau}{g} N_{3i}, \text{ for } \tilde{\tau}_2, \end{cases} \quad \text{(A.994)}$$

$$g_2 = \begin{cases} \sin\theta_\tau\sqrt{2}\sin\theta_W[c(2)\tan\theta_W - c(1)] - \cos\theta_\tau \frac{f_\tau}{g} N_{3i}, \text{ for } \tilde{\tau}_1, \\ \cos\theta_\tau\sqrt{2}\sin\theta_W[c(2)\tan\theta_W - c(1)] + \sin\theta_\tau \frac{f_\tau}{g} N_{3i}, \text{ for } \tilde{\tau}_2. \end{cases} \quad \text{(A.995)}$$

Remember the $c(1)$ and $c(2)$ were given previously in (A.962).

Sneutrino decays into neutralinos are given by:

$$\Gamma(\tilde{\nu}_{\tau_{1/2}} \to \nu_\tau \tilde{Z}_i) = \frac{g^2}{16\pi m_{\nu_{\tau^{\sim}_{1/2}}}} \tilde{\lambda}^{\frac{1}{2}}(m_{\nu_{\tau^{\sim}_{1/2}}}, 0, m_{\tilde{Z}_i})(m^2_{\nu_{\tau^{\sim}_{1/2}}} - m^2_{\tilde{Z}_i})\Big(\frac{c(2)}{\sqrt{2}\cos\theta_W}\Big)^2. \quad \text{(A.996)}$$

For chargino decays into neutralinos and charged Higgs bosons the partial width is given by:

$$\begin{aligned}\Gamma(\tilde{W}_1 \to H^\pm \tilde{Z}_j) =& \frac{g^2}{32\pi|m_{\tilde{W}_1}|} \tilde{\lambda}^{\frac{1}{2}}(m_{\tilde{W}_1}, m_{\tilde{Z}_j}, m_{H^\pm})\Big[(c1^2_{\tilde{W}_1 H^\pm \tilde{Z}_j} + c2^2_{\tilde{W}_1 H^\pm \tilde{Z}_j})(m^2_{\tilde{Z}_j} + m^2_{\tilde{W}_1} - m^2_{H^\pm}) \\ &+ 4c1^2_{\tilde{W}_1 H^\pm \tilde{Z}_j} c2^2_{\tilde{W}_1 H^\pm \tilde{Z}_j} m_{\tilde{Z}_j} m_{\tilde{W}_1}\Big],\end{aligned} \quad \text{(A.997)}$$

where:

$$c1_{\tilde{W}_1 H^\pm \tilde{Z}_j} = \frac{1}{g}[\lambda \sin\beta N_{5j} \cos\theta_R + \frac{\cos\beta}{\sqrt{2}}(g' N_{1j} + g N_{2j}) \cos\theta_R + g \cos\beta N_{4j} \sin\theta_R], \tag{A.998}$$

$$c2_{\tilde{W}_1 H^\pm \tilde{Z}_j} = \frac{1}{g}[\lambda \cos\beta N_{5j} \cos\theta_L - \frac{\sin\beta}{\sqrt{2}}(g' N_{1j} + g N_{2j}) \cos\theta_L + g \sin\beta N_{3j} \sin\theta_L]. \tag{A.999}$$

For $\tilde{W}_2$ the formulae are the same, just make the replacements $m_{\tilde{W}_1} \to m_{\tilde{W}_2}$, $\cos\theta_{L/R} \to \sin\theta_{L/R}$ and $\sin\theta_{L/R} \to -\cos\theta_{L/R}$.

$$\Gamma(\tilde{W}_1 \to W \tilde{Z}_j) = \frac{g^2}{32\pi |m_{\tilde{W}_1}|} \tilde{\lambda}^{\frac{1}{2}}(m_{\tilde{W}_1}, m_{\tilde{Z}_j}, m_W) \Bigg[-12 m_{\tilde{W}_1} m_{\tilde{Z}_j} cL_{\tilde{W}_1 W \tilde{Z}_j} cR_{\tilde{W}_1 W \tilde{Z}_j}$$
$$+ (cL^2_{\tilde{W}_1 W \tilde{Z}_j} + cR^2_{\tilde{W}_1 W \tilde{Z}_j}) \Big\{ (m^2_{\tilde{W}_1} + m^2_{\tilde{Z}_j} - m^2_W) + (m^2_{\tilde{W}_1} + m^2_W - m^2_{\tilde{Z}_j})(m^2_{\tilde{W}_1} - m^2_{\tilde{Z}_j} - m^2_W) \frac{1}{m^2_W} \Big\} \Bigg], \tag{A.1000}$$

where:

$$cL_{\tilde{W}_1 W \tilde{Z}_j} = -\frac{1}{\sqrt{2}} N_{4j} \cos\theta_R + N_{2j} \sin\theta_R, \tag{A.1001}$$

$$cR_{\tilde{W}_1 W \tilde{Z}_j} = \frac{1}{\sqrt{2}} N_{3j} \cos\theta_L + N_{2j} \sin\theta_L. \tag{A.1002}$$

Again for $\tilde{W}_2$ the formulae are the same, just make the replacements $m_{\tilde{W}_1} \to m_{\tilde{W}_2}$, $\cos\theta_{L/R} \to \sin\theta_{L/R}$ and $\sin\theta_{L/R} \to -\cos\theta_{L/R}$.

A.7 QCD Corrections to Decays

Note, for the decays of neutral Higgs bosons to quarks or gluons, that the possibility of including QCD corrections is included in the program, by default the QCD corrections are on. The formulae are those provided in `HDECAY-3.4` in `SUSYHIT` [131,132] and `NMSSMTools-4.2.1` in `NMHDECAY` [126,159]. With QCD corrections incorporated our formulae become as follows:

$$\Gamma(h \to qq)_{\text{QCDcorr}} = \Gamma(h -> qq)_{\text{tree}} \left(1 + \frac{4\alpha_s(m_h)}{3\pi} [\frac{A(\tilde{\beta})}{\tilde{\beta}} + \frac{3 + 34\tilde{\beta}^2 - 13\tilde{\beta}^4}{16\tilde{\beta}^3} \log\frac{1+\tilde{\beta}}{1-\tilde{\beta}} + \frac{3}{8\tilde{\beta}^2}(7\tilde{\beta}^2 - 1)]\right). \tag{A.1003}$$

This formula applies for all the CP even neutral Higgs bosons, whether in the MSSM or NMSSM, the difference between the MSSM and NMSSM comes in the tree-level formula. Note that α_s is evaluated at the mass of the decaying Higgs boson. Also note that then $\tilde{\beta} = \sqrt{1 - 4m_q^2/m_h^2}$ and $A(\tilde{\beta})$ is given by:

$$\begin{aligned} A(\tilde{\beta}) =& (1+\tilde{\beta}^2)\Big[4Li_2(\frac{1-\tilde{\beta}}{1+\tilde{\beta}}) + 2Li_2(\frac{\tilde{\beta}-1}{\tilde{\beta}+1}) - 3\log(\frac{1+\tilde{\beta}}{1-\tilde{\beta}})\log\frac{2}{1+\tilde{\beta}} - 2\log(\frac{1+\tilde{\beta}}{1-\tilde{\beta}})\log\tilde{\beta}\Big] \\ & - 3\tilde{\beta}\log\frac{4}{1-\tilde{\beta}^2} - 4\tilde{\beta}\log\tilde{\beta}. \end{aligned} \tag{A.1004}$$

This is exactly as given in equations (16) and (25) of [182]. Li_2 is the di-logarithm function (Spence's function).

For the CP odd Higgs bosons we have:

$$\Gamma(A \to qq)_{\text{QCDcorr}} = \Gamma(A -> qq)_{\text{tree}} \left(1 + \frac{4\alpha_s(m_A)}{3\pi} [\frac{A(\tilde{\beta})}{\tilde{\beta}} + \frac{19 + 2\tilde{\beta}^2 + 3\tilde{\beta}^4}{16\tilde{\beta}} \log\frac{1+\tilde{\beta}}{1-\tilde{\beta}} + \frac{3}{8}(7 - \tilde{\beta}^2)]\right). \tag{A.1005}$$

$\tilde{\beta}$ and $A(\tilde{\beta})$ are as given above but with the change $m_h \to m_A$ as appropriate. This formula is as given in equations (25) and (26) of [182]. It should be noted that when QCD corrections are applied one should use the pole quark masses (as we do within `SoftSusy` here), rather than the running masses, as otherwise the formulae double count $O(\alpha_s)$ effects [174, 184].

The QCD corrections for $h \to gg$ are more complicated as they involve both standard QCD corrections due to gluons being radiated, gluons in the loop, tops, bottoms and other quarks, and additional SUSY-QCD corrections due to gluinos, stops, sbottoms and other squarks. This complicates matters as whilst the usual "fermionic" QCD (FQCD) corrections apply to all particles in the loop, the SUSY-QCD (SQCD) corrections only apply to the scalar squark contributions, therefore rather than multiply the whole width by a correction factor (as was the case for $h \to qq$) we must now correct the SM and SUSY loop contributions separately. The usual MSSM equation for $h \to gg$ with no corrections is:

$$\Gamma(\phi \to gg)_{\text{1-loop}} = \frac{\alpha_s^2(m_\phi)}{128\pi^3}\frac{G_F}{\sqrt{2}} m_\phi^3 \frac{9}{8} |\Sigma I^\phi_{\text{loop}}|^2. \tag{A.1006}$$

Here the α_s is run to the mass of the decaying Higgs boson. The I_{loop} can be split into I_{quark} and I_{squark} loop contributions. So $I^\phi_{\text{looptot}} = I^\phi_{\text{qtot}} + I^\phi_{\text{sqtot}}$, where $I^\phi_{\text{qtot}} = I^\phi_t + I^\phi_b + I^\phi_c$ and $I^\phi_{\text{sqtot}} = I^\phi_{\tilde{t}_1} + I^\phi_{\tilde{t}_2} + I^\phi_{\tilde{b}_1} + I^\phi_{\tilde{b}_2} + I^\phi_{\tilde{c}_L} + I^\phi_{\tilde{c}_R} + I^\phi_{\tilde{s}_L} + I^\phi_{\tilde{s}_R} + I^\phi_{\tilde{u}_L} + I^\phi_{\tilde{u}_R} + I^\phi_{\tilde{d}_L} + I^\phi_{\tilde{d}_R}$.

To account for the usual QCD corrections, i.e. "FQCD" corrections, as these affect all the loop contributions, the whole partial width is multiplied by δ_{FQCD}:

$$\delta_{FQCD}^{CPevenHiggs} = 1 + \frac{\alpha_s(m_\phi)}{\pi}\left(\frac{95}{4} - \frac{7}{6}N_f\right), \tag{A.1007}$$

$$\delta_{FQCD}^{CPoddHiggs} = 1 + \frac{\alpha_s(m_\phi)}{\pi}\left(\frac{97}{4} - \frac{7}{6}N_f\right). \tag{A.1008}$$

N_f is the number of active fermion flavours. The SUSY QCD corrections, i.e. "SQCD" corrections, apply only to the squark loop contributions. Therefore to incorporate these in the final partial width you must multiply both the squark loop squared contributions and the interference terms of the squark loops with the quark loops by the correction factor. Therefore the $|I_{loop}|^2$ (which comes from the matrix element squared) above with both FQCD and SQCD corrections included becomes:

$$|I^\phi_{looptot}|^2 = \delta^\phi_{FQCD}|I^\phi_{looptot}|^2 + Re[(I^\phi_{looptot})^* I^\phi_{sqtot}]\delta_{SQCD}. \tag{A.1009}$$

To be clear the $(I^\phi_{looptot})^*$ here means the complex conjugate of $I^\phi_{looptot}$, given this is an interference term. The δ_{SQCD} correction factor is the same for CP even and CP odd neutral Higgs bosons and is given by (A.1010) below, note that α_s is run to the mass of the decaying Higgs boson:

$$\delta_{SQCD} = \frac{17\alpha_s(m_\phi)}{6\pi}. \tag{A.1010}$$

Consequently in the MSSM the overall formula for the QCD and SUSY-QCD corrected $h \to gg$ decay (at 2-loop) is:

$$\Gamma(\phi \to gg)_{1-loop+QCDcorr} = \frac{\alpha_s^2(m_\phi)}{128\pi^3}\frac{G_F}{\sqrt{2}} m_\phi^3 \frac{9}{8}\left[\delta^\phi_{FQCD}|I^\phi_{looptot}|^2 + Re[(I^\phi_{looptot})^* I^\phi_{sqtot}]\delta_{SQCD}\right]. \tag{A.1011}$$

ϕ is a CP even neutral Higgs here as CP odd Higgs bosons do not have squark loop contributions because of CP invariance of the decays. For the CP odd Higgs A in the MSSM we therefore only have the quark loops and FQCD corrections:

$$\Gamma(A \to gg)_{1-loop+QCDcorr} = \frac{\alpha_s^2(m_A)}{128\pi^3}\frac{G_F}{\sqrt{2}} m_A^3 \frac{9}{8}\left[\delta^A_{FQCD}|I^A_{qtot}|^2\right]. \tag{A.1012}$$

The FQCD corrections for CP even and CP odd neutral Higgs bosons in the MSSM are as given in Ref. [183] in equations (7) and (15) but with the log terms dropped as the scale of alphas is run to the masses of the decaying Higgs. As the corrections are purely coloured and the NMSSM only alters the Higgs and neutralino sectors, the form of the QCD corrections is exactly the same in the NMSSM. The alterations to the Higgs sector in the NMSSM however result in the couplings of the neutral Higgs bosons to other particles, and therefore the leading order (i.e. 1-loop) formula for the loop contributions to $h \to gg$, being altered. The formula in the uncorrected NMSSM (i.e. at 1-loop) is (as detailed previously) as follows, with the α_s evaluated at the scale of the decaying Higgs boson:

$$\Gamma(h_i \to gg)_{1-loop} = \frac{G_F m_{h_i}^3 \alpha_s^2(m_{h_i})}{64\sqrt{2}\pi^3} |M_{gg}|^2, \tag{A.1013}$$

where

$$\begin{aligned} |M_{gg}^{\phi}|^2 =& [J_t^r + J_b^r + J_c^r + J_{\tilde{u}_L}^r + J_{\tilde{u}_R}^r + J_{\tilde{d}_L}^r + J_{\tilde{d}_R}^r + J_{\tilde{c}_L}^r + J_{\tilde{c}_R}^r + J_{\tilde{s}_L}^r + J_{\tilde{s}_R}^r + J_{\tilde{t}_1}^r + J_{\tilde{t}_2}^r + J_{\tilde{b}_1}^r + J_{\tilde{b}_2}^r]^2 \\ &+ [J_t^i + J_b^i + J_c^i + J_{\tilde{u}_L}^i + J_{\tilde{u}_R}^i + J_{\tilde{d}_L}^i + J_{\tilde{d}_R}^i + J_{\tilde{c}_L}^i + J_{\tilde{c}_R}^i + J_{\tilde{s}_L}^i + J_{\tilde{s}_R}^i + J_{\tilde{t}_1}^i + J_{\tilde{t}_2}^i + J_{\tilde{b}_1}^i + J_{\tilde{b}_2}^i]^2, \end{aligned} \tag{A.1014}$$

where the J_X contributions are different to those in the MSSM as the couplings are different. Here the ^{r} and ^{i} were used as shorthand for real and imaginary parts. The $|M_{gg}|^2$ is therefore just the mod square of the sum of the complex loop contributions.

In order to incorporate the FQCD and SQCD corrections we again group the loop contributions into quark and squark so that $J_{qtot}^{\phi} = J_t^{\phi} + J_b^{\phi} + J_c^{\phi}$, $J_{sqtot}^{\phi} = J_{\tilde{u}_L}^{\phi} + J_{\tilde{u}_R}^{\phi} + J_{\tilde{d}_L}^{\phi} + J_{\tilde{d}_R}^{\phi} + J_{\tilde{c}_L}^{\phi} + J_{\tilde{c}_R}^{\phi} + J_{\tilde{s}_L}^{\phi} + J_{\tilde{s}_R}^{\phi} + J_{\tilde{t}_1}^{\phi} + J_{\tilde{t}_2}^{\phi} + J_{\tilde{b}_1}^{\phi} + J_{\tilde{b}_2}^{\phi}$ and $J_{looptot}^{\phi} = J_{qtot}^{\phi} + J_{sqtot}^{\phi}$. Then $|M_{gg}|^2$ becomes:

$$|M_{gg}^{\phi}|^2 = \left[\delta_{FQCD}^{\phi} |J_{looptot}^{\phi}|^2 + Re[(J_{looptot}^{\phi})^* J_{sqtot}^{\phi}]\delta_{SQCD}\right], \tag{A.1015}$$

because the FQCD and SQCD corrections apply to the loop contributions exactly as in the MSSM, however the loop contributions themselves have changed between the MSSM and NMSSM. So overall in the NMSSM, the QCD corrected partial width for neutral Higgs decays to gluons is as follows, again the α_s is evaluated at the scale of the mass of the decaying Higgs boson:

$$\Gamma(h_i \to gg)_{1-loop+QCDcorr} = \frac{G_F m_{h_i}^3 \alpha_s^2(m_{h_i})}{64\sqrt{2}\pi^3} \left[\delta_{FQCD}^{\phi} |J_{looptot}^{\phi}|^2 + Re[(J_{looptot}^{\phi})^* J_{sqtot}^{\phi}]\delta_{SQCD}\right]. \tag{A.1016}$$

Again ϕ here is a CP even neutral Higgs boson as CP odd Higgs bosons do not have squark loop contributions because of CP invariance of the decays, as in the MSSM. Therefore CP odd Higgs bosons have only quark loop contributions and so only receive FQCD corrections, without corrections the formula was:

$$\Gamma(A_i \to gg)_{1-loop} = \frac{g^2 \alpha_s^2(m_{A_i}) m_{A_i}^3}{128\pi^3 m_W^2} |M_{A_i gg}|^2, \tag{A.1017}$$

remembering that the $\alpha_s(m_{A_i})$ means α_s evaluated at the mass of the decaying CP odd Higgs boson A_i. Here $|M_{A_i gg}|^2$ is:

$$|M_{A_i gg}|^2 = (\mathcal{R}_t^r + \mathcal{R}_b^r + \mathcal{R}_c^r)^2 + (\mathcal{R}_t^i + \mathcal{R}_b^i + \mathcal{R}_c^i)^2. \tag{A.1018}$$

The corrections are incorporated by multiplying by δ_{FQCD}^A, so with the QCD corrections the CP odd Higgs decays in the NMSSM are given by:

$$\Gamma(A_i \to gg)_{1-loop+QCDcorr} = \frac{g^2 \alpha_s^2(m_{A_i}) m_{A_i}^3}{128\pi^3 m_W^2} |M_{A_i gg}|^2 \delta_{FQCD}^A. \tag{A.1019}$$

Throughout, the formulae used are those given in `HDECAY-3.4` [132] (and hence `SUSYHIT` [131]) and `NMSSMTools-4.2.1` [126–128, 159].

Appendix B

reSolve Theory further information

B.1 Resummation Coefficients

In this section we provide expressions and references for the resummation coefficients introduced in Chapter 6.2.3 in order to be as comprehensive as possible. We begin with the process-independent coefficients, the first coefficients to be given are the $g^{(n)}$ representing the leading logarithm, next-to-leading logarithm and next-to-next-to-leading logarithm all-order resummations for $n = 1, 2, 3$ respectively in the Sudakov factor, as outlined in equation 6.20:

$$\bar{g}^{(1)} = \frac{A^{(1)}}{\beta_0}\frac{\lambda + \log(1-\lambda)}{\lambda}\,, \tag{B.1}$$

$$\bar{g}^{(2)} = \frac{B^{(1)}}{\beta_0}\log(1-\lambda) - \frac{A^{(2)}}{\beta_0^2}\left(\frac{\lambda}{1-\lambda} + \log(1-\lambda)\right) + \frac{A^{(1)}\beta_1}{\beta_0^3}\left(\frac{1}{2}\log^2(1-\lambda) + \frac{\log(1-\lambda)}{1-\lambda} + \frac{\lambda}{1-\lambda}\right)\,, \tag{B.2}$$

$$\begin{aligned}\bar{g}^{(3)} = &-\frac{A^{(3)}}{2\beta_0^2}\frac{\lambda^2}{1-\lambda} - \frac{B^{(2)}}{\beta_0}\frac{\lambda}{1-\lambda} + \frac{A^{(2)}\beta_1}{\beta_0^3}\left(\frac{\lambda(3\lambda-2)}{2(1-\lambda)^2} - \frac{(1-2\lambda)\log(1-\lambda)}{(1-\lambda)^2}\right)\\ &+ \frac{B^{(1)}\beta_1}{\beta_0^2}\left(\frac{\lambda}{1-\lambda} + \frac{\log(1-\lambda)}{1-\lambda}\right)\\ &+ A^{(1)}\left[\frac{\beta_1^2}{2\beta_0^4}\frac{1-2\lambda}{(1-\lambda)^2}\log^2(1-\lambda) + \log(1-\lambda)\left(\frac{\beta_0\beta_2 - \beta_1^2}{\beta_0^4} + \frac{\beta_1^2}{\beta_0^4(1-\lambda)}\right)\right];\end{aligned} \tag{B.3}$$

where the $\log(Q^2b^2)$ terms are contained in the variable λ:

$$\lambda = \frac{1}{\pi}\beta_0\alpha_s(Q^2)\log(Q^2b^2/b_0^2)\,. \tag{B.4}$$

These are the terms currently implemented in the `reSolve`, which can thus perform resummations up to NNLL.

These $\bar{g}^{(n)}$ functions are just an alternative representation of the $A^{(n)}$ and $B_c^{(n)}$ functions, hence their dependence upon them, and are related to these by expanding the exponential in equation 6.16. The soft $A^{(n)}$ and flavour-conserving collinear $B_c^{(n)}$ perturbative coefficients themselves are given in terms of the standard QCD constants, which we give here before listing the $A^{(n)}$ and $B_c^{(n)}$ coefficients:

$$\begin{aligned}
&T_R:\ \mathrm{tr}(t^a t^b) = T_R\,\delta_{ab} && \to \text{fundamental colour matrices normalisation,}\\
&C_A \equiv C_g = N_c && \to \mathrm{SU}(N_c)\text{ adjoint representation Casimir,}\\
&C_F \equiv C_q \equiv C_{\bar{q}} = T_R\frac{N_c^2-1}{N_c} && \to \mathrm{SU}(N_c)\text{ fundamental representation Casimir,}\\
&N_f && \to \text{Number of active (effectively massless) flavours,}\\
&\zeta_n && \to \text{Value of Riemann Zeta function on point } n.
\end{aligned} \tag{B.5}$$

We also attempt to be as general as possible here and banish any confusion which can arise from reading

the literature, where many of the perturbative coefficients listed have different normalisation choices between papers in their expansions. We therefore define an arbitrary constant k to account for this, with common choices in the literature $k = 1,\ 2,\ 4$. A generic perturbative function $Z(\alpha_s)$ is then:

$$Z(\alpha_s) = \sum_n \left(\frac{\alpha_s}{k\pi}\right)^n Z^{(n)} \,. \tag{B.6}$$

We must also report the β function (defined as in equation 6.18 and present in equation 6.19) coefficients (taken from reference [222] equation (28) and reference [236] equation (B5)):

$$\beta_0 = \frac{k}{12}(11C_A - 4T_R N_f), \tag{B.7}$$

$$\beta_1 = \frac{k^2}{24}(17C_A^2 - 10C_A T_R N_f - 6C_F T_R N_f), \tag{B.8}$$

$$\beta_2 = \frac{k^3}{64}\left(\frac{2857}{54}C_A^3 - \frac{1415}{27}C_A^2 T_R N_f - \frac{205}{9}C_A C_F T_R N_f \ + 2C_F^2 T_R N_f + \frac{158}{27}C_A T_R^2 N_f^2 + \frac{44}{9}C_F T_R^2 N_f^2\right). \tag{B.9}$$

Finally we can list the perturbative $A^{(n)}$ and $B_c^{(n)}$ coefficients up to NNLO, all coefficients are defined in the hard scheme, explained in Chapter 6.2.3, unless otherwise specified. The $A_c^{(n)}$ coefficients are resummation scheme independent, being independent of the transformations in equation 6.30. The $A_c^{(n)}$ coefficients are taken from reference [222] equation (47) for $A_c^{(1,2)}$ and reference [236] equations (51), (74) and (B3) for $A_c^{(3)}$. The $B_c^{(n)}$ are from reference [222] eq. (49) for $B^{(1)}$ and reference [251] eq. (34)-(36) for $B_c^{(2)}$:

$$A_c^{(1)} = k\, C_c, \tag{B.10}$$

$$A_c^{(2)} = \frac{k^2}{2}C_c\left[\left(\frac{67}{18} - \frac{\pi^2}{6}\right)C_A - \frac{10}{9}T_R N_f\right], \tag{B.11}$$

$$\begin{aligned} A_g^{(3)} =& C_A\frac{k^3}{16}\left[C_A^2\left(\frac{245}{6} - \frac{134}{27}\pi^2 + \frac{11}{45}\pi^4 + \frac{22}{3}\zeta_3\right)\right. \\ &\left. + C_A T_R N_f\left(-\frac{418}{27} + \frac{40}{27}\pi^2 - \frac{56}{3}\zeta_3\right) + C_F T_R N_f\left(-\frac{55}{3} + 16\zeta_3\right) + \frac{16}{27}T_R^2 N_f^2\right], \end{aligned} \tag{B.12}$$

$$A_q^{(3)} = A_{\bar{q}}^{(3)} = \frac{C_F}{C_A}A_g^{(3)} + 2\beta_0\frac{k^2}{16}C_F\left[C_A\left(\frac{808}{27} - 28\zeta_3\right) - \frac{224}{27}T_R N_f\right], \tag{B.13}$$

$$B_g^{(1)} = -\frac{k}{6}(11C_A - 4T_R N_f), \tag{B.14}$$

$$B_q^{(1)} = B_{\bar{q}}^{(1)} = -k\,\frac{3}{2}\,C_F, \tag{B.15}$$

$$B_c^{(2)} = k\left(\frac{\gamma_c^{(1)}}{16} + \pi\beta_0 C_c\zeta_2\right). \tag{B.16}$$

The $\gamma_c^{(1)}$ coefficients are the $\delta(1-z)$ parts of the first order Altarell-Parisi splitting kernels:

$$\begin{aligned} \gamma_q^{(1)} = \gamma_{\bar{q}}^{(1)} &= k\left[C_F^2(-3 + 24\zeta_2 - 48\zeta_3) + C_A C_F\left(-\frac{17}{3} - \frac{88}{3}\zeta_2 + 24\zeta_3\right) + C_F T_R N_f\left(\frac{2}{3} + \frac{16}{3}\zeta_2\right)\right], \\ \gamma_g^{(1)} &= k\left[C_A^2\left(-\frac{64}{3} - 24\zeta_3\right) + \frac{16}{3}C_A T_R N_f + 4C_F T_R N_f\right]. \end{aligned} \tag{B.17}$$

Meanwhile we must also give the collinear expressions, which are dependent on the leading order process which initiates the hard scatter. All $C_{ab}^{(n)}$ coefficients are given here in z-space; in `reSolve`

however the corresponding Mellin space expressions are actually used. We begin with the first order coefficients, taken from reference [251], equations (29)-(33):

$$C_{qq}^{(1)}(z) = \frac{k}{2} C_F (1-z), \tag{B.18}$$

$$C_{gq}^{(1)}(z) = \frac{k}{2} C_F z, \tag{B.19}$$

$$C_{qg}^{(1)}(z) = \frac{k}{2} z(1-z), \tag{B.20}$$

$$C_{gg}^{(1)}(z) = C_{q\bar{q}}^{(1)}(z) = C_{qq'}^{(1)}(z) = C_{q\bar{q}'}^{(1)}(z) = 0. \tag{B.21}$$

Finally, for NNLL resummation, we also require the 2$^{\text{nd}}$ order collinear coefficients, $C_{ab}^{(2)}$; these expressions are very long and so we report them in terms of more fundamental objects whose definitions can be found in the listed references, the formulae are extracted from [251], equations (37)-(40) and nearby text:

$$C_{qq}^{(2)}(z) = \frac{k^2}{2}\left\{\mathcal{H}_{q\bar{q}\leftarrow q\bar{q}}^{DY(2)}(z)|_{\text{no } \delta(1-z)} - \frac{C_F^2}{4}\left[(2\pi^2-18)(1-z) - (1+z)\log z\right]\right\}, \tag{B.22}$$

$$C_{q\bar{q}}^{(2)}(z) = k^2\,\mathcal{H}_{q\bar{q}\leftarrow qq}^{DY(2)}(z), \tag{B.23}$$

$$C_{qq'}^{(2)}(z) = k^2\,\mathcal{H}_{q\bar{q}\leftarrow q\bar{q}'}^{DY(2)}(z), \tag{B.24}$$

$$C_{qg}^{(2)}(z) = k^2\left\{\mathcal{H}_{q\bar{q}\leftarrow qg}^{DY(2)}(z) - \frac{C_F}{4}\left[z\log z + \frac{1}{2}(1-z^2) + (\pi^2-8)z(1-z)\right]\right\}, \tag{B.25}$$

$$C_{q\bar{q}'}^{(2)}(z) = C_{qq'}^{(2)}(z), \text{ by eqs. (24), (26) and (35) of [290];} \tag{B.26}$$

$$C_{gq}^{(2)}(z) = k^2\left\{\mathcal{H}_{gg\leftarrow gq}^{H(2)}(z) + C_F^2\frac{3z}{4} - \frac{C_A C_F}{z}\left[(1+z)\log z + 2(1-z) - \frac{5+\pi^2}{4}z^2\right]\right\}, \tag{B.27}$$

$$C_{gg}^{(2)}(z) = \frac{k^2}{2}\left\{\mathcal{H}_{gg\leftarrow gg}^{H(2)}(z)|_{\text{no } \delta(1-z)} + C_A^2\left[\frac{1+z}{z}\log z + 2\frac{1-z}{z}\right]\right\}. \tag{B.28}$$

The $\mathcal{H}_{q\bar{q}\leftarrow q\bar{q}}^{DY(2)}(z)$, $\mathcal{H}_{q\bar{q}\leftarrow qq}^{DY(2)}(z)|_{\text{no } \delta(1-z)}$, $\mathcal{H}_{q\bar{q}\leftarrow q\bar{q}'}^{DY(2)}(z)|_{\text{no } \delta(1-z)}$ and $\mathcal{H}_{q\bar{q}\leftarrow qg}^{DY(2)}(z)$ are defined in equations (23), (24), (25) and (32) of [290]; whilst $\mathcal{H}_{gg\leftarrow gq}^{H(2)}(z)$ and $\mathcal{H}_{gg\leftarrow gg}^{H(2)}(z)$ are defined in equations (23) and (24) of [291].

Whilst these equations are very complex, we owe some reduction in complexity to flavour and $\mathcal{C}$ symmetry. All flavour indices in equation 6.11 could in principle assume 13 different values (from $\bar{t}$ to t plus g). However, since quark mass effects are not included in this formalism, given we work in a fixed flavour scheme, the coefficients are related by flavour symmetry. This reduces the number of possible c indices in coefficients $A_c^{(n)}$ and B_c^n to $c = q, \bar{q}$ or g. For the collinear coefficients C_{ab} there is a further need to distinguish diagonal and non-diagonal flavour contributions - there are combinations $C_{qq'}$, $C_{\bar{q}\bar{q}'}$, $C_{q\bar{q}'}$ and $C_{\bar{q}q'}$. Furthermore, due to $\mathcal{C}$ symmetry, all coefficients are invariant under barring of all indices so that $A_q = A_{\bar{q}}$, $B_q^F = B_{\bar{q}}^F$ to all orders. As a result there are just seven independent combinations for the C_{ab} coefficients: C_{gg}^F, C_{qq}^F, C_{qg}^F, C_{gq}^F, $C_{q\bar{q}}^F$, $C_{qq'}^F$ and $C_{q\bar{q}'}^F$.

Lastly, we must list the hard factors, which are process-dependent, absorbing the remaining process dependence of the resummation formalism. Here we list the diphoton, Drell-Yan and Higgs hard factor coefficients in the hard scheme, with only the diphoton and Drell-Yan processes so far included in the `reSolve` program. In actuality, as described in Chapter 6.2.3, in `reSolve` we use the DY-Higgs scheme and so our Drell-Yan (and Higgs once this process is added) hard factors are taken to be 0, nonetheless one can use the resummation transformation of equation 6.30 to switch between resummation schemes. The formulae listed here are given in the paper [251]: equations (82-83) are for Drell-Yan, equations (88-91)

are for diphoton, and equations (85, 87) are for Higgs production[1].

$$H_q^{DY(1)} = k\, C_F \left(\frac{\pi^2}{2} - 4\right), \tag{B.29}$$

$$\begin{aligned} H_q^{DY(2)} =& k^2 \left[C_F C_A \left(\frac{59}{18}\zeta_3 - \frac{1535}{192} + \frac{215}{216}\pi^2 - \frac{\pi^4}{240}\right) + \frac{1}{4} C_F^2 \left(-15\zeta_3 + \frac{511}{16} - \frac{67}{12}\pi^2 + \frac{17}{45}\pi^4\right) \right. \\ &\left. + \frac{1}{864} C_F T_R N_f (192\zeta_3 + 1143 - 152\pi^2) \right], \end{aligned} \tag{B.30}$$

$$\begin{aligned} H_q^{\gamma\gamma(1)} =& k\, \frac{C_F}{2} \left[\pi^2 - 7 + \frac{1}{(1-v)^2 + v^2} \Big[((1-v)^2 + 1) \log^2(1-v) \right. \\ &\left. + v(v+2)\log(1-v) + (v^2+1)\log^2 v + (1-v)(3-v)\log v \Big] \right], \end{aligned} \tag{B.31}$$

$$\begin{aligned} H_q^{\gamma\gamma(2)} =& \frac{k^2}{4\mathcal{A}_{\rm LO}} \left[\mathcal{F}^{0\times 2}_{inite,q\bar{q}\gamma\gamma;s} + \mathcal{F}^{1\times 1}_{inite,q\bar{q}\gamma\gamma;s} \right] + 3\zeta_2 C_F H_q^{\gamma\gamma(1)} - \frac{45}{4} C_F^2 \\ &+ C_F C_A \left(\frac{607}{324} + \frac{1181}{144}\zeta_2 - \frac{187}{144}\zeta_3 - \frac{105}{32}\zeta_4\right) + C_F T_R N_f \left(-\frac{41}{162} - \frac{97}{72}\zeta_2 + \frac{17}{72}\zeta_3\right), \end{aligned} \tag{B.32}$$

$$H_g^{H(1)} = k \left[C_A \frac{\pi^2}{2} + \frac{5C_A - 3C_F}{2} \right], \tag{B.33}$$

$$\begin{aligned} H_g^{H(2)} =& k^2 \left[C_A^2 \left(\frac{3187}{288} + \frac{7}{8} L_Q + \frac{157}{72}\pi^2 + \frac{13}{144}\pi^4 - \frac{55}{18}\zeta_3\right) + C_A C_F \left(-\frac{145}{24} - \frac{11}{8} L_Q - \frac{3}{4}\pi^2\right) \right. \\ &\left. + \frac{9}{4} C_F^2 - \frac{5}{96} C_A - \frac{1}{12} C_F - C_A T_R N_f \left(\frac{287}{144} + \frac{5}{36}\pi^2 + \frac{4}{9}\zeta_3\right) + C_F T_R N_f \left(-\frac{41}{24} + \frac{1}{2} L_Q + \zeta_3\right) \right]. \end{aligned} \tag{B.34}$$

(B.35)

For the Higgs case $L_Q = \log(m_H^2/m_t^2)$, whilst for the diphoton process $v = -u/s$ (partonic Mandelstam variables), and $\mathcal{A}_{\rm LO}$ is proportional to the LO matrix element $u/t + t/u$ (and to `KinFac` in our code):

$$\mathcal{A}_{\rm LO} = -8N_c \left(\frac{u}{t} + \frac{t}{u}\right) = 8N_c \frac{1 - 2v + 2v^2}{v(1-v)}\,. \tag{B.36}$$

The $\mathcal{F}^{0\times 2}_{inite,q\bar{q}\gamma\gamma;s}$, $\mathcal{F}^{1\times 1}_{inite,q\bar{q}\gamma\gamma;s}$ are defined elsewhere in the literature in [293], equations. (4.6) and (5.3), see also Appendices A and B in the same reference, they are IR-subtracted loop amplitudes with 0×2 being interferences of LO and 2-loop and 1×1 being the 1-loop squared. A subtlety which appears in the $\gamma\gamma$ process is that as the photon couples proportional to charge so the $\mathcal{F}^{0\times 2}_{inite,q\bar{q}\gamma\gamma;s}$ factor, and thus $H_q^{\gamma\gamma(2)}$, is actually dependent on the electric charge (squared) of the involved quark. There are therefore two different $H_q^{\gamma\gamma(2)}$ coefficients, $H_u^{\gamma\gamma(2)}$ and $H_d^{\gamma\gamma(2)}$. In the $\gamma\gamma$ case, the gg channel contributes with the LO term for this initiation given by the $gg \to \gamma\gamma$ box (see Figure 6.4 in Chapter 6.4.1), so that $H_{gg}^{\gamma\gamma} \neq 0$. However, the $gg \to \gamma\gamma$ partonic process is suppressed by α_s^2 with respect to the $q\bar{q}$-initiated one (which is $\mathcal{O}(\alpha_s^0)$, a purely electromagnetic process at LO), so a non-trivial $H_{gg}^{\gamma\gamma}$ is only needed beyond N^{2}LL, and so is not included in `reSolve`.

[1] The Higgs hard factors were obtained in the large m_t limit. For Higgs at NLO, also the contribution for finite top mass is known: see for instance [292], equations. (21)-(30).

B.2 Mellin Space

In our `reSolve` formalism, we rely on transforming from momentum fraction space for each parton to Mellin space $(z_1, z_2) \to (N_1, N_2)$ in order to simplify the resummation and the evaluation of the spectra. The reason for this is that in our master formula for transverse momentum resummation, we naturally develop a "multiplicative convolution" (by which we mean a product analogue of the standard convolutions used in Fourier theory) as the partons emerge from the hadrons with momentum fractions $\frac{x_1}{z_1}$ and $\frac{x_2}{z_2}$ before emitting collinear radiation which reduces their momentum fractions by a further factor to z_1 and z_2. We consequently develop integrals of the schematic form:

$$\int_{x_1}^{1} \frac{dz_1}{z_1} C(z_1, \dots) f(\frac{x_1}{z_1}, \dots). \tag{B.37}$$

Mellin transforms simplify such expressions as they are invariant under scale transformations, reflecting the fact that mathematically scaling all the momentum fractions in such multiplicative convolutions leaves the problem unchanged. The Mellin transform $\mathcal{M}$ of a function $g(x)$ into Mellin space s is defined in equation B.38. The "Haar measure" $\frac{dx}{x}$ ensures the Mellin transform is invariant under dilatations, i.e. it is scale invariant. Compare this with Fourier transformations where the measure is invariant under translations and so simplifies standard (i.e. additive) convolutions.

$$\{\mathcal{M}(f)\}(s) := \phi(s) = \int_0^\infty x^{s-1} g(x) dx = \int_0^\infty x^s g(x) \frac{dx}{x}. \tag{B.38}$$

Meanwhile, inverse Mellin transforms $\mathcal{M}^{-1}$ must be done along a contour in the complex plane:

$$\{\mathcal{M}^{-1}(\phi)\}(x) := g(x) = \frac{1}{2\pi i} \int_{c-i\infty}^{c+i\infty} x^{-s} \phi(s) ds, \tag{B.39}$$

here the standard is to integrate over a vertical line in the complex plane as indicated, however in `reSolve` we integrate over a contour at 45 degrees in the complex plane so as to aid convergence.

To see that such transforms will simplify our "multiplicative convolutions" in our master formula, let us consider a general form $\int_0^\infty K(x/y) g(y) \frac{dy}{y}$. Then its Mellin transform is given by:

$$\mathcal{M}\Big(\int_0^\infty K(x/y) g(y) \frac{dy}{y} \Big) = \int_0^\infty x^{s-1} \Big(\int_0^\infty K(x/y) g(y) \frac{dy}{y} \Big) dx = \int_0^\infty g(y) \Big(\int_0^\infty x^{s-1} K(x/y) dx \Big) \frac{dy}{y}. \tag{B.40}$$

In the last step we interchanged the order of integration. We now change variables, let $u = x/y$ so that $\frac{du}{u} = \frac{dx}{x}$:

$$\begin{aligned} \mathcal{M}(\int_0^\infty K(x/y) g(y) \frac{dy}{y}) &= \int_0^\infty g(y) \Big(\int_0^\infty y^s u^s K(u) \frac{du}{u} \Big) \frac{dy}{y} = \int_0^\infty g(y) \Big(\int_0^\infty y^{s-1} u^{s-1} K(u) du \Big) dy \\ &= \int_0^\infty g(y) y^{s-1} dy \int_0^\infty u^{s-1} K(u) du = \{\mathcal{M}(g)\}(s) \times \{\mathcal{M}(K)\}(s). \end{aligned} \tag{B.41}$$

So our multiplicative convolution becomes a simple product in Mellin space, so for our applications we can implement the multiplicative convolution in the Master formula equation 6.11 as a simple product in Mellin space, making the formalism much more straightforward to reproduce computationally.

B.3 reSolve Monte Carlo Integration

Here we wish to provide an overview of the Monte Carlo integration technique applied in the k_vegas built-in, self-written integrator which is an implementation of Lepage's VEGAS algorithm [265]. In order to estimate an integral based on randomly sampling numbers from a flat distribution we can calculate the integrand for each input variable x, sum the integrands and divide by the total number of samples:

$$I = \int f(x)dx \approx \frac{1}{N}\sum_{i=1}^{N} f_i. \tag{B.42}$$

The square error estimate in this case for this approximate integration is as follows, with the additional $\frac{1}{N-1}$ prefactor obtaining the variance in the mean rather than in the overall distribution:

$$\sigma^2 = \frac{1}{N-1}\Big[\frac{1}{N}\sum_{i=1}^{N} f_i^2 - \Big(\frac{1}{N}\sum_{i=1}^{N} f_i\Big)^2\Big]. \tag{B.43}$$

In this case however, the points were sampled from a flat distribution, clearly this is not the optimal sampling strategy to reduce the variance of the estimate made. Indeed if we sample from a probability distribution with normalised probability density function $p(x)$ we essentially perform a change of variables $dP(x) = p(x)dx$:

$$I = \int f(x)dx = \int \frac{f(x)}{p(x)}p(x)dx = \int \frac{f(x)}{p(x)}dP(x). \tag{B.44}$$

The estimate for I and its error squared are then

$$I \approx \frac{1}{N}\sum_{i=1}^{N}\frac{f_i}{p_i} = \frac{1}{N}\sum_{i=1}^{N} f_i w_i, \tag{B.45}$$

$$\sigma^2 = \frac{1}{N-1}\Big[\frac{1}{N}\sum_{i=1}^{N}(f_i w_i)^2 - \Big(\frac{1}{N}\sum_{i=1}^{N} f_i w_i\Big)^2\Big], \tag{B.46}$$

where the w_i are the weights and are the inverse of the probabilities of choosing the value of x at that specific point.

The challenge for Monte Carlo integration methods is to choose the probability distribution $p(x)$ such that the variance is minimised, one method of doing this is importance sampling, i.e. sampling the distribution where it is largest. In particular, if you were to sample from the actual function $f(x)$ (which would require knowing its functional form across the entire x range rather than just evaluating it at specific points numerically) you would expect to minimise variance as you would be summing the contributions of the integrand with probabilities set by the integrand, replicating analytic integration. Therefore importance sampling aims to do just this, sampling the integrand function where it is largest

$$p(x) = \frac{|f(x)|}{\int f(x)dx}, \tag{B.47}$$

so the sampling probability is proportional to the function value. As the weights of individual points are the inverse of the probabilities of obtaining that point, the weights are correspondingly smaller for larger values of the integrand as these have larger probabilities of being selected. Of course, to normalise this probability density function $p(x) \propto |f(x)|$ as in equation B.47, you need to know the value of I itself - but this is what we are aiming for! The Lepage VEGAS algorithm, and various other importance sampling methods, are therefore an attempt to minimise the variance by circumventing this circularity in the argument.

VEGAS works by dividing the problem of obtaining a Monte Carlo integral estimate into iterations, the estimate of the integral for the previous iterations can then be used to normalise the probability distribution and ensure in the following iteration the integrand is sampled where it is largest.

1. In the first iteration a uniform probability density function is used and the integral and variance estimates are simply given by equations B.42 and B.43 respectively.
2. Given there is now an estimate for the function at various values of x we can produce a grid in x which is weighted such that it reflects the value of the function in different regions of x, this can then be used to define the probability density function $p(x)$ as in equation B.47.
3. In the second iteration the x values sampled are given by the Monte Carlo grid so that the probability density function approximates the integrand function. The integral and variance estimates for the second iteration are then given by equations B.45 and B.46 respectively. The Monte Carlo grid is then updated using the new values of the function sampled in this second iteration. It is updated by weighted average using the variance estimates of the first and second iterations to weight their contributions to the grid.
4. This iterative procedure is repeated until the specified number of iterations have been performed, each time the integral estimate should get more accurate, as indicated by a reduced variance estimate.
5. Iteration on iteration a total estimate of the integral, $\tilde{I}$, and the error, $\sigma_{\tilde{I}}$, are made using all previous iterations. This is done by weighted averaging with the variance for each iteration estimate used as the weighting, the error in this overall estimate is then:

$$\sigma_{\tilde{I}} = \Big[\sum_j \frac{1}{\sigma_j^2}\Big]^{-\frac{1}{2}}, \tag{B.48}$$

   where j is the iteration number and σ_j is the variance of an individual iteration estimate. The overall estimate of the integral up to that point is the weighted average of the individual iteration integral estimates (I_j) and is given by:

$$\tilde{I} = \sigma_{\tilde{I}}^2 \sum_j \frac{I_j}{\sigma_j^2}. \tag{B.49}$$

6. A χ^2 estimate can be made iteration on iteration for the goodness of the iteration estimate for the integral using this overall estimate:

$$\chi^2 = \sum_j \frac{(I_j - \tilde{I})^2}{\sigma_j^2}, \tag{B.50}$$

   sometimes this may additionally be weighted by I_j^2/σ_j^2. For the total estimate to be trusted, the χ^2 value should not exceed the number of iterations minus 1, this is the "χ^2 per degree of freedom" printed by `reSolve` and should decrease iteration on iteration, again after the first few iterations are performed.
7. Iteration on iteration the grid is improved, once the optimal grid is obtained the error estimate is proportional to the standard $1/\sqrt{n}$ with n the number of integrand evaluations in the iteration. For this reason the number of evaluations per iteration is increased in `reSolve` so as to reduce the Monte Carlo error.

This described the procedure for obtaining the overall cross-section and its error, integrated over all phase space variables. In reality, `reSolve` is targeted at differential cross-sections, where the summing of

contributions is done over all but one (or perhaps more) phase space variables. In this case the procedure is similar, except first the events (samples) are divided into bins in the relevant differential variable, as specified by the histogrammer through the input file. In each of these bins the cross-section estimate and error estimate is made as in the step-by-step guide above. This essentially integrates over the other phase space variables to obtain a cross-section estimate in each bin in the differential variable, thereby obtaining the differential distribution.

This description has been one of importance sampling, an alternative technique to improve the Monte Carlo error estimate is stratified sampling, we will not go into details on this other than to mention its basic strategy is to sub-divide the integration region into smaller volumes and perform a Monte Carlo integration in each smaller region. The size of the regions are varied, as well as their relative locations, iteratively in order to ensure the contribution to the total variance is equal from each sub-region. This minimises the overall variance as expressions of the form of equation B.48 are dominated by the smallest $\frac{1}{\sigma_j^2}$, i.e. by the largest variance. In fact, VEGAS and hence `reSolve` use both stratified sampling and importance sampling, as the grid described requires a stratification of the values of the phase space variables sampled. Essentially the individual estimates are histogrammed in all variables in order to define the grid from which to sample the random values. However, in order to avoid the number of bins in the grid growing rapidly as K^d with the number of dimensions, where K is the number of bins per dimension d, which is a problem with stratified sampling, the probability density function is assumed to be separable in each variable: $g(x_1, x_2, x_3, \dots) = g_1(x_1)g_2(x_2)g_3(x_3)\dots$, this reduces the number of bins required to define the grid to Kd. This imposes a constraint on VEGAS however, meaning it is most efficient when the peaks of the integrand function are localised in the separate phase space variables. Much more information on the precise strategy applied are given in Lepage's original VEGAS paper [265].

Bibliography

[1] B. C. Allanach, T. Cridge, The Calculation of Sparticle and Higgs Decays in the Minimal and Next-to-Minimal Supersymmetric Standard Models: SOFTSUSY4.0, Comput. Phys. Commun. 220 (2017) 417–502. arXiv:1703.09717, doi:10.1016/j.cpc.2017.07.021.

[2] F. Coradeschi, T. Cridge, reSolve - A Transverse Momentum Resummation ToolarXiv:1711.02083.

[3] W. Porod, SPheno, a program for calculating supersymmetric spectra, SUSY particle decays and SUSY particle production at e+ e- colliders, Comput. Phys. Commun. 153 (2003) 275–315. arXiv:hep-ph/0301101, doi:10.1016/S0010-4655(03)00222-4.

[4] W. Porod, F. Staub, SPheno 3.1: Extensions including flavour, CP-phases and models beyond the MSSM, Comput. Phys. Commun. 183 (2012) 2458–2469. arXiv:1104.1573, doi:10.1016/j.cpc.2012.05.021.

[5] L. Cieri, F. Coradeschi, D. de Florian, Diphoton production at hadron colliders: transverse-momentum resummation at next-to-next-to-leading logarithmic accuracy, JHEP 06 (2015) 185. arXiv:1505.03162, doi:10.1007/JHEP06(2015)185.

[6] L. Cieri, F. Coradeschi, D. de Florian, N. Fidanza, Transverse-momentum resummation for the signal-background interference in the H channel at the LHC, Phys. Rev. D96 (5) (2017) 054003. arXiv:1706.07331, doi:10.1103/PhysRevD.96.054003.

[7] G. Bozzi, S. Catani, G. Ferrera, D. de Florian, M. Grazzini, Production of Drell-Yan lepton pairs in hadron collisions: Transverse-momentum resummation at next-to-next-to-leading logarithmic accuracy, Phys. Lett. B696 (2011) 207–213. arXiv:1007.2351, doi:10.1016/j.physletb.2010.12.024.

[8] S. Catani, D. de Florian, G. Ferrera, M. Grazzini, Vector boson production at hadron colliders: transverse-momentum resummation and leptonic decay, JHEP 12 (2015) 047. arXiv:1507.06937, doi:10.1007/JHEP12(2015)047.

[9] J. Ellis, TikZ-Feynman: Feynman diagrams with TikZ, Comput. Phys. Commun. 210 (2017) 103–123. arXiv:1601.05437, doi:10.1016/j.cpc.2016.08.019.

[10] F. Abe, et al., Observation of top quark production in $\bar{p}p$ collisions, Phys. Rev. Lett. 74 (1995) 2626–2631. arXiv:hep-ex/9503002, doi:10.1103/PhysRevLett.74.2626.

[11] S. Abachi, et al., Observation of the top quark, Phys. Rev. Lett. 74 (1995) 2632–2637. arXiv:hep-ex/9503003, doi:10.1103/PhysRevLett.74.2632.

[12] G. Aad, et al., Observation of a new particle in the search for the Standard Model Higgs boson with the ATLAS detector at the LHC, Phys. Lett. B716 (2012) 1–29. arXiv:1207.7214, doi:10.1016/j.physletb.2012.08.020.

[13] S. Chatrchyan, et al., Observation of a new boson at a mass of 125 GeV with the CMS experiment at the LHC, Phys. Lett. B716 (2012) 30–61. arXiv:1207.7235, doi:10.1016/j.physletb.2012.08.021.

[14] M. E. Peskin, D. V. Schroeder, An introduction to quantum field theory, Westview, Boulder, CO, 1995, includes exercises. URL https://cds.cern.ch/record/257493.

[15] M. Srednicki, Quantum Field Theory, Cambridge Univ. Press, Cambridge, 2007.
URL `https://cds.cern.ch/record/1019751`

[16] M. Thomson, Modern particle physics, Cambridge University Press, New York, 2013.
URL `http://www-spires.fnal.gov/spires/find/books/www?cl=QC793.2.T46::2013`

[17] R. K. Ellis, W. J. Stirling, B. R. Webber, QCD and collider physics, Camb. Monogr. Part. Phys. Nucl. Phys. Cosmol. 8 (1996) 1–435.

[18] J. Collins, Foundations of perturbative QCD, Camb. Monogr. Part. Phys. Nucl. Phys. Cosmol. 32 (2011) 1–624.

[19] M. L. Mangano, Introduction to QCD, in: Particles and fields. Proceedings, 10th Jorge Andre Swieca Summer School, Sao Paulo, Brazil, February 6-12, 1999, 1998, pp. 53–97, [,53(1998)].

[20] M. K. Gaillard, P. D. Grannis, F. J. Sciulli, The standard model of particle physics, Rev. Mod. Phys. 71 (1999) S96–S111. doi:10.1103/RevModPhys.71.S96. URL https://link.aps.org/doi/10.1103/RevModPhys.71.S96.

[21] M. M. Nojiri, Beyond the Standard Model, in: Proceedings, 1st Asia-Europe-Pacific School of High-Energy Physics (AEPSHEP): Fukuoka, Japan, October 14-27, 2012, 2014, pp. 137–149. arXiv:1406.1410, doi:10.5170/CERN-2014-001.137. URL https://inspirehep.net/record/1299320/files/arXiv:1406.1410.pdf.

[22] B. C. Allanach, Beyond the Standard Model Lectures for the 2016 European School of High-Energy Physics, in: Proceedings, 2016 European School of High-Energy Physics (ESHEP2016): Skeikampen, Norway, June 15-28 2016, 2017, 2017, pp. 123–152. arXiv:1609.02015, doi:10.23730/CYRSP-2017-005.123.
URL https://inspirehep.net/record/1485569/files/arXiv:1609.02015.pdf

[23] G. Bertone, D. Hooper, J. Silk, Particle dark matter: Evidence, candidates and constraints, Phys. Rept. 405 (2005) 279–390. arXiv:hep-ph/0404175, doi:10.1016/j.physrep.2004.08.031.

[24] M. Lisanti, Lectures on Dark Matter Physics, in: Proceedings, Theoretical Advanced Study Institute in Elementary Particle Physics: New Frontiers in Fields and Strings (TASI 2015): Boulder, CO, USA, June 1-26, 2015, 2017, pp. 399–446. arXiv:1603.03797, doi:10.1142/9789813149441_0007.
URL https://inspirehep.net/record/1427360/files/arXiv:1603.03797.pdf

[25] J. L. Feng, Dark Matter Candidates from Particle Physics and Methods of Detection, Ann. Rev. Astron. Astrophys. 48 (2010) 495–545. arXiv:1003.0904, doi:10.1146/annurev-astro-082708-101659.

[26] A. D. Sakharov, Violation of CP Invariance, C Asymmetry, and Baryon Asymmetry of the Universe, Soviet Journal of Experimental and Theoretical Physics Letters 5 (1967) 24.

[27] Y. Ashie, et al., A Measurement of atmospheric neutrino oscillation parameters by SUPER-KAMIOKANDE I, Phys. Rev. D71 (2005) 112005. arXiv:hep-ex/0501064, doi:10.1103/PhysRevD.71.112005.

[28] M. H. Ahn, et al., Measurement of Neutrino Oscillation by the K2K Experiment, Phys. Rev. D74 (2006) 072003. arXiv:hep-ex/0606032, doi:10.1103/PhysRevD.74.072003.

[29] Q. R. Ahmad, et al., Direct evidence for neutrino flavor transformation from neutral current interactions in the Sudbury Neutrino Observatory, Phys. Rev. Lett. 89 (2002) 011301. arXiv:nucl-ex/0204008, doi:10.1103/PhysRevLett.89.011301.

[30] M. Apollonio, et al., Search for neutrino oscillations on a long baseline at the CHOOZ nuclear power station, Eur. Phys. J. C27 (2003) 331–374. arXiv:hep-ex/0301017, doi:10.1140/epjc/s2002-01127-9.

[31] S. Abe, et al., Precision Measurement of Neutrino Oscillation Parameters with KamLAND, Phys. Rev. Lett. 100 (2008) 221803. arXiv:0801.4589, doi:10.1103/PhysRevLett.100.221803.

[32] D. V. Naumov, New Results from the Daya Bay Reactor Neutrino Experiment, PoS NEUTEL2017 (2018) 008.

[33] C. Patrignani, et al., Review of Particle Physics, Chin. Phys. C40 (10) (2016) 100001. doi:10.1088/1674-1137/40/10/100001.

[34] P. Langacker, The standard model and beyond, Series in High Energy Physics, Cosmology and Gravitation, Taylor and Francis, Boca Raton, FL, 2010. URL https://cds.cern.ch/record/1226768.

[35] S. F. King, Neutrino mass models, Rept. Prog. Phys. 67 (2004) 107–158. arXiv:hep-ph/0310204, doi:10.1088/0034-4885/67/2/R01.

[36] M. Gell-Mann, P. Ramond, R. Slansky, in Sanibel Talk, CALT-68-709, Feb 1979 and in Supergravity (North Holland, Amsterdam 1979).

[37] T. Yanagida, in Proc. of the Workshop on Unified Theory and Baryon Number of the Universe, KEK, Japan, 1979.

[38] S. Glashow, Cargese Lectures (1979).

[39] R. N. Mohapatra, G. Senjanović, Neutrino mass and spontaneous parity nonconservation, Phys. Rev. Lett. 44 (1980) 912–915. doi:10.1103/PhysRevLett.44.912. URL https://link.aps.org/doi/10.1103/PhysRevLett.44.912.

[40] J. Schechter, J. W. F. Valle, Neutrino decay and spontaneous violation of lepton number, Phys. Rev. D 25 (1982) 774–783. doi:10.1103/PhysRevD.25.774. URL https://link.aps.org/doi/10.1103/PhysRevD.25.774.

[41] R. N. Mohapatra, Understanding neutrino masses and mixings in the seesaw framework, in: Neutrino telescopes. Proceedings, 10th International Workshop, Venice, Italy, March

11-14, 2003. Vol. 1+2, 2003, pp. 279–299, [,279(2003)]. arXiv:hep-ph/0306016. URL http://www.slac.stanford.edu/spires/find/video/www?irn=18899.

[42] R. D. Peccei, H. R. Quinn, CP conservation in the presence of pseudoparticles, Phys. Rev. Lett. 38 (1977) 1440–1443. doi:10.1103/PhysRevLett.38.1440. URL https://link.aps.org/doi/10.1103/PhysRevLett.38.1440.

[43] A. M. Sirunyan, et al., Search for physics beyond the standard model in events with high-momentum Higgs bosons and missing transverse momentum in proton-proton collisions at 13 TeV, Submitted to: Phys. Rev. Lett.arXiv:1712.08501.

[44] Search for selectrons and smuons at $\sqrt{s} = 13$ TeV, Tech. Rep. CMS-PAS-SUS-17-009, CERN, Geneva (2017. URL https://cds.cern.ch/record/2297116).

[45] M. Aaboud, et al., Search for dark matter and other new phenomena in events with an energetic jet and large missing transverse momentum using the ATLAS detector, JHEP 01 (2018) 126. arXiv:1711.03301, doi:10.1007/JHEP01(2018)126.

[46] M. Aaboud, et al., Search for top squarks decaying to tau sleptons in pp collisions at $\sqrt{s} = 13$ TeV with the ATLAS detector arXiv:1803.10178.

[47] S. P. Martin, A Supersymmetry primer (1997) 1–98[Adv. Ser. Direct. High Energy Phys.18,1(1998)]. arXiv:hep-ph/9709356, doi:10.1142/9789812839657_0001, 10.1142/9789814307505_0001.

[48] A. Salam, J. A. Strathdee, Supergauge Transformations, Nucl. Phys. B76 (1974) 477–482. doi:10.1016/0550-3213(74)90537-9.

[49] A. Salam, J. Strathdee, Superfields and fermi-bose symmetry, Phys. Rev. D 11 (1975) 1521–1535. doi:10.1103/PhysRevD.11.1521. URL https://link.aps.org/doi/10.1103/PhysRevD.11.1521.

[50] F. A. Berezin, INTRODUCTION TO SUPERANALYSIS, 1987.

[51] P. C. West, Introduction to supersymmetry and supergravity, 1990.

[52] K. A. Intriligator, N. Seiberg, Lectures on Supersymmetry Breaking, Class. Quant. Grav. 24 (2007) S741–S772, [Les Houches87,125(2008)]. arXiv:hep-ph/0702069, doi:10.1088/0264-9381/24/21/S02, 10.1016/S0924-8099(08)80020-0.

[53] M. Dine, J. D. Mason, Supersymmetry and Its Dynamical Breaking, Rept. Prog. Phys. 74 (2011) 056201. arXiv:1012.2836, doi:10.1088/0034-4885/74/5/056201.

[54] A. H. Chamseddine, R. Arnowitt, P. Nath, Locally supersymmetric grand unification, Phys. Rev. Lett. 49 (1982) 970–974. doi:10.1103/PhysRevLett.49.970. URL https://link.aps.org/doi/10.1103/PhysRevLett.49.970.

[55] R. Barbieri, S. Ferrara, C. Savoy, Gauge models with spontaneously broken local supersymmetry, Physics Letters B 119 (4) (1982) 343 – 347. doi:https://doi.org/10.1016/0370-2693(82)90685-2.
URL http://www.sciencedirect.com/science/article/pii/0370269382906852

[56] N. Ohta, Grand unified theories based on local supersymmetry, Progress of Theoretical Physics 70 (2) (1983) 542–549. arXiv:/oup/backfile/content_public/journal/ptp/70/2/10.1143/ptp.70.542/2/70-2-542.pdf, doi:10.1143/PTP.70.542.
URL http://dx.doi.org/10.1143/PTP.70.542

[57] L. Hall, J. Lykken, S. Weinberg, Supergravity as the messenger of supersymmetry breaking, Phys. Rev. D 27 (1983) 2359–2378. doi:10.1103/PhysRevD.27.2359. URL https://link.aps.org/doi/10.1103/PhysRevD.27.2359.

[58] M. Dine, A. E. Nelson, Dynamical supersymmetry breaking at low energies, Phys. Rev. D 48 (1993) 1277–1287. doi:10.1103/PhysRevD.48.1277. URL https://link.aps.org/doi/10.1103/PhysRevD.48.1277.

[59] M. Dine, A. E. Nelson, Y. Nir, Y. Shirman, New tools for low-energy dynamical supersymmetry breaking, Phys. Rev. D53 (1996) 2658–2669. arXiv:hep-ph/9507378, doi:10.1103/PhysRevD.53.2658.

[60] L. Randall, R. Sundrum, Out of this world supersymmetry breaking, Nuclear Physics B 557 (1) (1999) 79 – 118. doi:https://doi.org/10.1016/S0550-3213(99)00359-4.
URL http://www.sciencedirect.com/science/article/pii/S0550321399003594

[61] G. F. Giudice, M. A. Luty, H. Murayama, R. Rattazzi, Gaugino mass without singlets, JHEP 12 (1998) 027. arXiv:hep-ph/9810442, doi:10.1088/1126-6708/1998/12/027.

[62] S. Dimopoulos, H. Georgi, Softly broken supersymmetry and su(5), Nuclear Physics B 193 (1) (1981) 150 – 162. doi:https://doi.org/10.1016/0550-3213(81)90522-8.
URL http://www.sciencedirect.com/science/article/pii/0550321381905228

[63] S. Deser, B. Zumino, Broken supersymmetry and supergravity, Phys. Rev. Lett. 38 (1977) 1433–1436. doi:10.1103/PhysRevLett.38.1433. URL https://link.aps.org/doi/10.1103/PhysRevLett.38.1433.

[64] R. Casalbuoni, S. De Curtis, D. Dominici, F. Feruglio, R. Gatto, A Gravitino - Goldstino High-Energy Equivalence Theorem, Phys. Lett. B215 (1988) 313–316. doi:10.1016/0370-2693(88)91439-6.

[65] H. Baer, X. Tata, Weak scale supersymmetry: From superfields to scattering events, Cambridge University Press, 2006. URL http://www.cambridge.org/9780521290319.

[66] B. C. Allanach, SOFTSUSY: a program for calculating supersymmetric spectra, Comput. Phys. Commun. 143 (2002) 305–331. arXiv:hep-ph/0104145, doi:10.1016/S0010-4655(01)00460-X.

[67] K. Abe, et al., Search for proton decay via $p \to e^+\pi^0$ and $p \to \mu^+\pi^0$ in 0.31megatonyears exposure of the Super-Kamiokande water Cherenkov detector, Phys. Rev. D95 (1) (2017) 012004. arXiv:1610.03597, doi:10.1103/PhysRevD.95.012004.

[68] B. C. Allanach, M. A. Bernhardt, Including R-parity violation in the numerical computation of the spectrum of the minimal supersymmetric standard model: SOFTSUSY, Comput. Phys. Commun. 181 (2010) 232–245. arXiv:0903.1805, doi:10.1016/j.cpc.2009.09.015.

[69] B. C. Allanach, C. H. Kom, M. Hanussek, Computation of Neutrino Masses in R-parity Violating Supersymmetry: SOFTSUSY3.2, Comput. Phys. Commun. 183 (2012) 785–793. arXiv:1109.3735, doi:10.1016/j.cpc.2011.11.024.

[70] L. J. Hall, M. Suzuki, Explicit r-parity breaking in supersymmetric models, Nuclear Physics B 231 (3) (1984) 419 – 444. doi:https://doi.org/10.1016/0550-3213(84)90513-3.
URL http://www.sciencedirect.com/science/article/pii/0550321384905133

[71] S. P. Martin, Implications of supersymmetric models with natural R-parity conservation, Phys. Rev. D54 (1996) 2340–2348. arXiv:hep-ph/9602349, doi:10.1103/PhysRevD.54.2340.

[72] D. I. Kazakov, Beyond the standard model: In search of supersymmetry, in: 2000 European School of high-energy physics, Caramulo, Portugal, 20 Aug-2 Sep 2000: Proceedings, 2000, pp. 125–199. arXiv:hep-ph/0012288.

[73] M. Beck, F. Bensch, J. Bockholt, G. Heusser, H. Klapdor-Kleingrothaus, B. Maier, F. Petry, A. Piepke, H. Strecker, M. Vllinger, K. Zuber, A. Balysh, S. Belyaev, A. Demehin, A. Gurov, I. Kondratenko, V. Lebedev, A. Mller, Searching for dark matter with the enriched ge detectors of the heidelberg-moscow experiment, Physics Letters B 336 (2) (1994) 141 – 146. doi:https://doi.org/10.1016/0370-2693(94)01000-5.
URL http://www.sciencedirect.com/science/article/pii/0370269394010005

[74] G. Jungman, M. Kamionkowski, K. Griest, Supersymmetric dark matter, Physics Reports 267 (5) (1996) 195 – 373. doi:https://doi.org/10.1016/0370-1573(95)00058-5.
URL http://www.sciencedirect.com/science/article/pii/0370157395000585

[75] P. Gondolo, J. Edsjo, P. Ullio, L. Bergstrom, M. Schelke, E. A. Baltz, DarkSUSY: Computing supersymmetric dark matter properties numerically, JCAP 0407 (2004) 008. arXiv:astro-ph/0406204, doi:10.1088/1475-7516/2004/07/008.

[76] T. Bringmann, J. Edsj, P. Gondolo, P. Ullio, L. Bergstrm, DarkSUSY 6 : An Advanced Tool to Compute Dark Matter Properties NumericallyarXiv:1802.03399.

[77] J. Edsj, T. Bringmann, P. Gondolo, P. Ullio, L. Bergstrm, M. Schelke, E. Baltz, G. Duda, Darksusy (2018).
URL http://www.darksusy.org

[78] G. Belanger, F. Boudjema, A. Pukhov, A. Semenov, MicrOMEGAs: A Program for calculating the relic density in the MSSM, Comput. Phys. Commun. 149 (2002) 103–120. arXiv:hep-ph/0112278, doi:10.1016/S0010-4655(02)00596-9.

[79] G. Belanger, F. Boudjema, A. Pukhov, A. Semenov, MicrOMEGAs 2.0: A Program to calculate the relic density of dark matter in a generic model, Comput. Phys. Commun. 176 (2007) 367–382. arXiv:hep-ph/0607059, doi:10.1016/j.cpc.2006.11.008.

[80] G. Aad, et al., Combined Measurement of the Higgs Boson Mass in pp Collisions at $\sqrt{s} = 7$ and 8 TeV with the ATLAS and CMS Experiments, Phys. Rev. Lett. 114 (2015) 191803. arXiv:1503.07589, doi:10.1103/PhysRevLett.114.191803.

[81] P. Draper, H. Rzehak, A Review of Higgs Mass Calculations in Supersymmetric Models, Phys. Rept. 619 (2016) 1–24. arXiv:1601.01890, doi:10.1016/j.physrep.2016.01.001.

[82] M. Carena, H. E. Haber, Higgs boson theory and phenomenology, Prog. Part. Nucl. Phys. 50 (2003) 63–152. arXiv:hep-ph/0208209, doi:10.1016/S0146-6410(02)00177-1.

[83] B. C. Allanach, A. Voigt, Uncertainties in the Lightest CP Even Higgs Boson Mass Prediction in the Minimal Supersymmetric Standard Model: Fixed Order Versus Effective Field Theory Prediction, Eur. Phys. J. C78 (7) (2018) 573. arXiv:1804.09410, doi:10.1140/epjc/s10052-018-6046-z.

[84] A. Djouadi, The Anatomy of electro-weak symmetry breaking. II. The Higgs bosons in the minimal supersymmetric model, Phys. Rept. 459 (2008) 1–241. arXiv:hep-ph/0503173, doi:10.1016/j.physrep.2007.10.005.

[85] L. E. Ibanez, G. G. Ross, Discrete gauge symmetries and the origin of baryon and lepton number conservation in supersymmetric versions of the standard model, Nuclear Physics B 368 (1) (1992) 3 – 37. doi:https://doi.org/10.1016/0550-3213(92)90195-H. URL http://www.sciencedirect.com/science/article/pii/055032139290195H.

[86] T. Banks, Y. Grossman, E. Nardi, Y. Nir, Supersymmetry without R-parity and without lepton number, Phys. Rev. D52 (1995) 5319–5325. arXiv:hep-ph/9505248, doi:10.1103/PhysRevD.52.5319.

[87] B. C. Allanach, A. Dedes, H. K. Dreiner, R parity violating minimal supergravity model, Phys. Rev. D69 (2004) 115002, [Erratum: Phys. Rev.D72,079902(2005)]. arXiv:hep-ph/0309196, doi:10.1103/PhysRevD.69.115002, 10.1103/PhysRevD.72.079902.

[88] D. A. Demir, G. L. Kane, T. T. Wang, The Minimal U(1)' extension of the MSSM, Phys. Rev. D72 (2005) 015012. arXiv:hep-ph/0503290, doi:10.1103/PhysRevD.72.015012.

[89] G. Blanger, J. Da Silva, U. Laa, A. Pukhov, Probing U(1) extensions of the MSSM at the LHC Run I and in dark matter searches, JHEP 09 (2015) 151. arXiv:1505.06243, doi:10.1007/JHEP09(2015)151.

[90] T. D. Lee, SPONTANEOUS T VIOLATION, in: T.D. LEE: SELECTED PAPERS. VOL. 2: FIELD THEORY AND SYMMETRY PRINCIPLES, 1973, pp. 531–554.

[91] G. C. Branco, P. M. Ferreira, L. Lavoura, M. N. Rebelo, M. Sher, J. P. Silva, Theory and phenomenology of two-Higgs-doublet models, Phys. Rept. 516 (2012) 1–102. arXiv:1106.0034, doi:10.1016/j.physrep.2012.02.002.

[92] U. Ellwanger, C. Hugonie, A. M. Teixeira, The Next-to-Minimal Supersymmetric Standard Model, Phys. Rept. 496 (2010) 1–77. arXiv:0910.1785, doi:10.1016/j.physrep.2010.07.001.

[93] M. Maniatis, The Next-to-Minimal Supersymmetric extension of the Standard Model reviewed, Int. J. Mod. Phys. A25 (2010) 3505–3602. arXiv:0906.0777, doi:10.1142/S0217751X10049827.

[94] S. Dawson, SUSY and such, NATO Sci. Ser. B 365 (1997) 33–80. arXiv:hep-ph/9612229, doi:10.1007/978-1-4615-5963-4_2.

[95] H. Baer, et al., Low-energy supersymmetry phenomenology,arXiv:hep-ph/9503479, doi:10.2172/72994.

[96] P. Binétruy, Supersymmetry: Theory, Experiment, and Cosmology, Oxford graduate texts, Oxford University Press, 2006. URL https://books.google.co.uk/books?id=Sja2kQEACAAJ.

[97] H. Baer, V. Barger, P. Huang, D. Mickelson, M. Padeffke-Kirkland, X. Tata, Natural susy with a bino- or wino-like lsp, Phys. Rev. D 91 (2015) 075005. doi:10.1103/PhysRevD.91.075005.
URL `https://link.aps.org/doi/10.1103/PhysRevD.91.075005`

[98] G. Aad, et al., Measurements of the Higgs boson production and decay rates and coupling strengths using pp collision data at $\sqrt{s} = 7$ and 8 TeV in the ATLAS experiment, Eur. Phys. J. C76 (1) (2016) 6. arXiv:1507.04548, doi:10.1140/epjc/s10052-015-3769-y.

[99] M. Aaboud, et al., Searches for the $Z\gamma$ decay mode of the Higgs boson and for new high-mass resonances in pp collisions at $\sqrt{s}$ = 13 TeV with the ATLAS detector, JHEP 10 (2017) 112. arXiv:1708.00212, doi:10.1007/JHEP10(2017)112.

[100] H. E. Haber, M. J. Herrero, H. E. Logan, S. Penaranda, S. Rigolin, D. Temes, Decoupling properties of MSSM particles in Higgs and top decays, in: Proceedings, 5th International Symposium on Radiative Corrections - RADCOR 2000, 2001. arXiv:hep-ph/0102169. URL http://www.slac.stanford.edu/econf/C000911/.

[101] M. Aaboud, et al., Search for additional heavy neutral Higgs and gauge bosons in the ditau final state produced in 36 fb[1] of pp collisions at $\sqrt{s}$ = 13 TeV with the ATLAS detector, JHEP 01 (2018) 055. arXiv:1709.07242, doi:10.1007/JHEP01(2018)055.

[102] J. F. Gunion, S. Dawson, H. E. Haber, G. L. Kane, The Higgs hunter's guide, Vol. 80, Brookhaven Nat. Lab., Upton, NY, 1989, in the second printing (1990) by Perseus Books in the collection Frontiers in physics, no 80, a number of errors and omissions are corrected and the references at the end of each chapter are updated. A paperback reprint of the 1990 edition has been published in 2000. URL https://cds.cern.ch/record/425736.

[103] M. Aaboud, et al., Search for new phenomena using the invariant mass distribution of same-flavour opposite-sign dilepton pairs in events with missing transverse momentum in $\sqrt{s}$ = 13 TeV pp collisions with the ATLAS detectorarXiv:1805.11381.

[104] M. Aaboud, et al., Search for a scalar partner of the top quark in the jets plus missing transverse momentum final state at $\sqrt{s}$=13 TeV with the ATLAS detector, JHEP 12 (2017) 085. arXiv:1709.04183, doi:10.1007/JHEP12(2017)085.

[105] M. Aaboud, et al., Search for supersymmetry in events with b-tagged jets and missing transverse momentum in pp collisions at $\sqrt{s}$ = 13 TeV with the ATLAS detector, JHEP 11 (2017) 195. arXiv:1708.09266, doi:10.1007/JHEP11(2017)195.

[106] M. Aaboud, et al., Search for squarks and gluinos in final states with jets and missing transverse momentum using 36fb^{-1} of $\sqrt{s}$ = 13TeV pp collision data with the ATLAS detector, Phys. Rev. D97 (11) (2018) 112001. arXiv:1712.02332, doi:10.1103/PhysRevD.97.112001.

[107] M. Aaboud, et al., Search for electroweak production of supersymmetric particles in final states with two or three leptons at $\sqrt{s}$ = 13 TeV with the ATLAS detectorarXiv:1803.02762.

[108] ATLAS Collaboration, Summary plots from the atlas higgs physics group - bsm higgs exclusion in the hmssm.
URL `https://atlas.web.cern.ch/Atlas/GROUPS/PHYSICS/CombinedSummaryPlots/HIGGS/, 2018-30-06`

[109] ATLAS Collaboration, Summary plots from the atlas supersymmetry physics group - mass reach of atlas searches for supersymmetry. url https://atlas.web.cern.ch/atlas/groups/physics/combinedsummaryplots/susy/, 2018-30-06.

[110] G. Aad, et al., Summary of the searches for squarks and gluinos using $\sqrt{s}$ = 8 TeV pp collisions with the ATLAS experiment at the LHC, JHEP 10 (2015) 054. arXiv:1507.05525, doi:10.1007/JHEP10(2015)054.

[111] G. Aad, et al., Search for the electroweak production of supersymmetric particles in $\sqrt{s}$=8 TeV pp collisions with the ATLAS detector, Phys. Rev. D93 (5) (2016) 052002. arXiv:1509.07152, doi:10.1103/PhysRevD.93.052002.

[112] A. Barr, J. Liu, First interpretation of 13 TeV supersymmetry searches in the pMSSMarXiv:1605.09502.

[113] G. F. Giudice, A. Romanino, Split supersymmetry, Nucl. Phys. B699 (2004) 65–89, [Erratum: Nucl. Phys.B706,487(2005)]. arXiv:hep-ph/0406088, doi:10.1016/j.nuclphysb.2004.11.048, 10.1016/j.nuclphysb.2004.08.001.

[114] T. Han, Collider phenomenology: Basic knowledge and techniques, in: Physics in D ¿= 4. Proceedings, Theoretical Advanced Study Institute in elementary particle physics, TASI 2004, Boulder, USA, June 6-July 2, 2004, 2005, pp. 407–454. arXiv:hep-ph/0508097, doi:10.1142/9789812773579_0008.

[115] M. Spira, Higgs boson production and decay at the Tevatron, in: Physics at Run II: Workshop on Supersymmetry / Higgs: Summary Meeting Batavia, Illinois, November 19-21, 1998, 1998. arXiv:hep-ph/9810289.

[116] B. C. Allanach, SUSY Predictions and SUSY Tools at the LHC, Eur. Phys. J. C59 (2009) 427–443. arXiv:0805.2088, doi:10.1140/epjc/s10052-008-0695-2.

[117] B. C. Allanach, A. Bednyakov, R. Ruiz de Austri, Higher order corrections and unification in the minimal supersymmetric standard model: SOFTSUSY3.5, Comput. Phys. Commun. 189 (2015) 192–206. arXiv:1407.6130, doi:10.1016/j.cpc.2014.12.006.

[118] B. C. Allanach, P. Athron, L. C. Tunstall, A. Voigt, A. G. Williams, Next-to-Minimal SOFTSUSY, Comput. Phys. Commun. 185 (2014) 2322–2339. arXiv:1311.7659, doi:10.1016/j.cpc.2014.04.015.

[119] B. C. Allanach, S. P. Martin, D. G. Robertson, R. Ruiz de Austri, The Inclusion of Two-Loop SUSYQCD Corrections to Gluino and Squark Pole Masses in the Minimal and Next-to-Minimal Supersymmetric Standard Model: SOFTSUSY3.7, Comput. Phys. Commun. 219 (2017) 339–345. arXiv:1601.06657, doi:10.1016/j.cpc.2017.05.006.

[120] P. Athron, J.-h. Park, D. Stckinger, A. Voigt, FlexibleSUSYA spectrum generator generator for supersymmetric models, Comput. Phys. Commun. 190 (2015) 139–172. arXiv:1406.2319, doi:10.1016/j.cpc.2014.12.020.

[121] P. Athron, M. Bach, D. Harries, T. Kwasnitza, J.-h. Park, D. Stckinger, A. Voigt, J. Ziebell, FlexibleSUSY 2.0: Extensions to investigate the phenomenology of SUSY and non-SUSY models, Comput. Phys. Commun. 230 (2018) 145–217. arXiv:1710.03760, doi:10.1016/j.cpc.2018.04.016.

[122] F. E. Paige, S. D. Protopopescu, H. Baer, X. Tata, ISAJET 7.69: A Monte Carlo event generator for pp, anti-p p, and e+e- reactionsarXiv:hep-ph/0312045.

[123] D. Chowdhury, R. Garani, S. K. Vempati, SUSEFLAV: Program for supersymmetric mass spectra with seesaw mechanism and rare lepton flavor violating decays, Comput. Phys. Commun. 184 (2013) 899–918. arXiv:1109.3551, doi:10.1016/j.cpc.2012.10.031.

[124] A. Djouadi, J.-L. Kneur, G. Moultaka, SuSpect: A Fortran code for the supersymmetric and Higgs particle spectrum in the MSSM, Comput. Phys. Commun. 176 (2007) 426–455. arXiv:hep-ph/0211331, doi:10.1016/j.cpc.2006.11.009.

[125] S. Heinemeyer, W. Hollik, G. Weiglein, FeynHiggs: A Program for the calculation of the masses of the neutral CP even Higgs bosons in the MSSM, Comput. Phys. Commun. 124 (2000) 76–89. arXiv:hep-ph/9812320, doi:10.1016/S0010-4655(99)00364-1.

[126] U. Ellwanger, J. F. Gunion, C. Hugonie, NMHDECAY: A Fortran code for the Higgs masses, couplings and decay widths in the NMSSM, JHEP 02 (2005) 066. arXiv:hep-ph/0406215, doi:10.1088/1126-6708/2005/02/066.

[127] U. Ellwanger, C. Hugonie, NMSPEC: A Fortran code for the sparticle and Higgs masses in the NMSSM with GUT scale boundary conditions, Comput. Phys. Commun. 177 (2007) 399–407. arXiv:hep-ph/0612134, doi:10.1016/j.cpc.2007.05.001.

[128] D. Das, U. Ellwanger, A. M. Teixeira, NMSDECAY: A Fortran Code for Supersymmetric Particle Decays in the Next-to-Minimal Supersymmetric Standard Model, Comput. Phys. Commun. 183 (2012) 774–779. arXiv:1106.5633, doi:10.1016/j.cpc.2011.11.021.

[129] F. Staub, SARAH 4 : A tool for (not only SUSY) model builders, Comput. Phys. Commun. 185 (2014) 1773–1790. arXiv:1309.7223, doi:10.1016/j.cpc.2014.02.018.

[130] J. Baglio, R. Grber, M. Mhlleitner, D. T. Nhung, H. Rzehak, M. Spira, J. Streicher, K. Walz, NMSSMCALC: A Program Package for the Calculation of Loop-Corrected Higgs Boson Masses and Decay Widths in the (Complex) NMSSM, Comput. Phys. Commun. 185 (12) (2014) 3372–3391. arXiv:1312.4788, doi:10.1016/j.cpc.2014.08.005.

[131] A. Djouadi, M. M. Muhlleitner, M. Spira, Decays of supersymmetric particles: The Program SUSY-HIT (SUspect-SdecaY-Hdecay-InTerface), Acta Phys. Polon. B38 (2007) 635–644. arXiv:hep-ph/0609292.

[132] A. Djouadi, J. Kalinowski, M. Spira, HDECAY: A Program for Higgs boson decays in the standard model and its supersymmetric extension, Comput. Phys. Commun. 108 (1998) 56–74. arXiv:hep-ph/9704448, doi:10.1016/S0010-4655(97)00123-9.

[133] A. Djouadi, J. Kalinowski, M. Muehlleitner, M. Spira, HDECAY: Twenty$_{++}$ Years AfterarXiv:1801.09506.

[134] M. Muhlleitner, A. Djouadi, Y. Mambrini, SDECAY: A Fortran code for the decays of the supersymmetric particles in the MSSM, Comput. Phys. Commun. 168 (2005) 46–70. arXiv:hep-ph/0311167, doi:10.1016/j.cpc.2005.01.012.

[135] M. D. Goodsell, S. Liebler, F. Staub, Generic calculation of two-body partial decay widths at the full one-loop level, Eur. Phys. J. C77 (11) (2017) 758. arXiv:1703.09237, doi:10.1140/epjc/s10052-017-5259-x.

[136] T. Sjstrand, S. Ask, J. R. Christiansen, R. Corke, N. Desai, P. Ilten, S. Mrenna, S. Prestel, C. O. Rasmussen, P. Z. Skands, An Introduction to PYTHIA 8.2, Comput. Phys. Commun. 191 (2015) 159–177. arXiv:1410.3012, doi:10.1016/j.cpc.2015.01.024.

[137] M. Bahr, et al., Herwig++ Physics and Manual, Eur. Phys. J. C58 (2008) 639–707. arXiv:0803.0883, doi:10.1140/epjc/s10052-008-0798-9.

[138] J. Bellm, et al., Herwig 7.0/Herwig++ 3.0 release note, Eur. Phys. J. C76 (4) (2016) 196. arXiv:1512.01178, doi:10.1140/epjc/s10052-016-4018-8.

[139] T. Gleisberg, S. Hoeche, F. Krauss, A. Schalicke, S. Schumann, J.-C. Winter, SHERPA 1. alpha: A Proof of concept version, JHEP 02 (2004) 056. arXiv:hep-ph/0311263, doi:10.1088/1126-6708/2004/02/056.

[140] T. Gleisberg, S. Hoeche, F. Krauss, M. Schonherr, S. Schumann, F. Siegert, J. Winter, Event generation with SHERPA 1.1, JHEP 02 (2009) 007. arXiv:0811.4622, doi:10.1088/1126-6708/2009/02/007.

[141] J. Alwall, R. Frederix, S. Frixione, V. Hirschi, F. Maltoni, O. Mattelaer, H. S. Shao, T. Stelzer, P. Torrielli, M. Zaro, The automated computation of tree-level and next-to-leading order differential cross sections, and their matching to parton shower simulations, JHEP 07 (2014) 079. arXiv:1405.0301, doi:10.1007/JHEP07(2014)079.

[142] W. Beenakker, R. Hopker, M. Spira, PROSPINO: A Program for the production of supersymmetric particles in next-to-leading order QCDarXiv:hep-ph/9611232. URL http://www.ph.ed.ac.uk/ tplehn/prospino/.

[143] J. de Favereau, C. Delaere, P. Demin, A. Giammanco, V. Lematre, A. Mertens, M. Selvaggi, DELPHES 3, A modular framework for fast simulation of a generic collider experiment, JHEP 02 (2014) 057. arXiv:1307.6346, doi:10.1007/JHEP02(2014)057.

[144] J. P. Miller, E. de Rafael, B. L. Roberts, Muon (g-2): Experiment and theory, Rept. Prog. Phys. 70 (2007) 795. arXiv:hep-ph/0703049, doi:10.1088/0034-4885/70/5/R03.

[145] P. Kant, R. V. Harlander, L. Mihaila, M. Steinhauser, Light MSSM Higgs boson mass to three-loop accuracy, JHEP 08 (2010) 104. arXiv:1005.5709, doi:10.1007/JHEP08(2010)104.

[146] R. V. Harlander, J. Klappert, A. Voigt, Higgs mass prediction in the MSSM at three-loop level in a pure $\overline{\text{DR}}$ context, Eur. Phys. J. C77 (12) (2017) 814. arXiv:1708.05720, doi:10.1140/epjc/s10052-017-5368-6.

[147] R. Ruiz de Austri, R. Trotta, F. Feroz, Superbayes (2018).
URL `http://www.ft.uam.es/personal/rruiz/superbayes/index.php?page=main.html`

[148] R. Trotta, F. Feroz, M. P. Hobson, L. Roszkowski, R. Ruiz de Austri, The Impact of priors and observables on parameter inferences in the Constrained MSSM, JHEP 12 (2008) 024. arXiv:0809.3792, doi:10.1088/1126-6708/2008/12/024.

[149] R. Lafaye, T. Plehn, M. Rauch, D. Zerwas, Measuring Supersymmetry, Eur. Phys. J. C54 (2008) 617–644. arXiv:0709.3985, doi:10.1140/epjc/s10052-008-0548-z.

[150] P. Bechtle, K. Desch, P. Wienemann, Fittino, a program for determining MSSM parameters from collider observables using an iterative method, Comput. Phys. Commun. 174 (2006) 47–70. arXiv:hep-ph/0412012, doi:10.1016/j.cpc.2005.09.002.

[151] B. C. Allanach, S. Kraml, W. Porod, Theoretical uncertainties in sparticle mass predictions from computational tools, JHEP 03 (2003) 016. arXiv:hep-ph/0302102, doi:10.1088/1126-6708/2003/03/016.

[152] B. C. Allanach, A. Djouadi, J. L. Kneur, W. Porod, P. Slavich, Precise determination of the neutral Higgs boson masses in the MSSM, JHEP 09 (2004) 044. arXiv:hep-ph/0406166, doi:10.1088/1126-6708/2004/09/044.

[153] F. Staub, P. Athron, U. Ellwanger, R. Grber, M. Mhlleitner, P. Slavich, A. Voigt, Higgs mass predictions of public NMSSM spectrum generators, Comput. Phys. Commun. 202 (2016) 113–130. arXiv:1507.05093, doi:10.1016/j.cpc.2016.01.005.

[154] D. de Florian, et al., Handbook of LHC Higgs Cross Sections: 4. Deciphering the Nature of the Higgs Sector arXiv:1610.07922.

[155] B. Allanach, S. Kraml, W. Porod, Comparison of SUSY mass spectrum calculations, in: Supersymmetry and unification of fundamental interactions. Proceedings, 10th International Conference, SUSY'02, Hamburg, Germany, June 17-23, 2002, 2002, pp. 904–910. arXiv:hep-ph/0207314.
URL http://www-library.desy.de/preparch/desy/proc/proc02-02/Proceedings/pa.1b/kraml_pr.pdf

[156] P. Z. Skands, et al., SUSY Les Houches accord: Interfacing SUSY spectrum calculators, decay packages, and event generators, JHEP 07 (2004) 036. arXiv:hep-ph/0311123, doi:10.1088/1126-6708/2004/07/036.

[157] B. C. Allanach, et al., SUSY Les Houches Accord 2, Comput. Phys. Commun. 180 (2009) 8–25. arXiv:0801.0045, doi:10.1016/j.cpc.2008.08.004.

[158] F. Staub, W. Porod, Improved predictions for intermediate and heavy Supersymmetry in the MSSM and beyond, Eur. Phys. J. C77 (5) (2017) 338. arXiv:1703.03267, doi:10.1140/epjc/s10052-017-4893-7.

[159] U. Ellwanger, C. Hugonie, NMHDECAY 2.0: An Updated program for sparticle masses, Higgs masses, couplings and decay widths in the NMSSM, Comput. Phys. Commun. 175 (2006) 290–303. arXiv:hep-ph/0508022, doi:10.1016/j.cpc.2006.04.004.

[160] F. Domingo, U. Ellwanger, Updated Constraints from B Physics on the MSSM and the NMSSM, JHEP 12 (2007) 090. arXiv:0710.3714, doi:10.1088/1126-6708/2007/12/090.

[161] U. Ellwanger, C. C. Jean-Louis, A. M. Teixeira, Phenomenology of the General NMSSM with Gauge Mediated Supersymmetry Breaking, JHEP 05 (2008) 044. arXiv:0803.2962, doi:10.1088/1126-6708/2008/05/044.

[162] F. Domingo, A New Tool for the study of the CP-violating NMSSM, JHEP 06 (2015) 052. arXiv:1503.07087, doi:10.1007/JHEP06(2015)052.

[163] T. Hahn, S. Heinemeyer, W. Hollik, H. Rzehak, G. Weiglein, FeynHiggs 2.7, Nucl. Phys. Proc. Suppl. 205-206 (2010) 152–157. arXiv:1007.0956, doi:10.1016/j.nuclphysbps.2010.08.035.

[164] S. Heinemeyer, W. Hollik, G. Weiglein, The Masses of the neutral CP - even Higgs bosons in the MSSM: Accurate analysis at the two loop level, Eur. Phys. J. C9 (1999) 343–366. arXiv:hep-ph/9812472, doi:10.1007/s100529900006.

[165] G. Degrassi, S. Heinemeyer, W. Hollik, P. Slavich, G. Weiglein, Towards high precision predictions for the MSSM Higgs sector, Eur. Phys. J. C28 (2003) 133–143. arXiv:hep-ph/0212020, doi:10.1140/epjc/s2003-01152-2.

[166] M. Frank, T. Hahn, S. Heinemeyer, W. Hollik, H. Rzehak, G. Weiglein, The Higgs Boson Masses and Mixings of the Complex MSSM in the Feynman-Diagrammatic Approach, JHEP 02 (2007) 047. arXiv:hep-ph/0611326, doi:10.1088/1126-6708/2007/02/047.

[167] T. Hahn, S. Heinemeyer, W. Hollik, H. Rzehak, G. Weiglein, High-Precision Predictions for the Light CP -Even Higgs Boson Mass of the Minimal Supersymmetric Standard Model, Phys. Rev. Lett. 112 (14) (2014) 141801. arXiv:1312.4937, doi:10.1103/PhysRevLett.112.141801.

[168] K. Ender, T. Graf, M. Muhlleitner, H. Rzehak, Analysis of the NMSSM Higgs Boson Masses at One-Loop Level, Phys. Rev. D85 (2012) 075024. arXiv:1111.4952, doi:10.1103/PhysRevD.85.075024.

[169] T. Graf, R. Grober, M. Muhlleitner, H. Rzehak, K. Walz, Higgs Boson Masses in the Complex NMSSM at One-Loop Level, JHEP 10 (2012) 122. arXiv:1206.6806, doi:10.1007/JHEP10(2012)122.

[170] M. Mhlleitner, D. T. Nhung, H. Rzehak, K. Walz, Two-loop contributions of the order $\mathcal{O}(\alpha_t\alpha_s)$ to the masses of the Higgs bosons in the CP-violating NMSSM, JHEP 05 (2015) 128. arXiv:1412.0918, doi:10.1007/JHEP05(2015)128.

[171] S. F. King, M. Muhlleitner, R. Nevzorov, K. Walz, Exploring the CP-violating NMSSM: EDM Constraints and Phenomenology, Nucl. Phys. B901 (2015) 526–555. arXiv:1508.03255, doi:10.1016/j.nuclphysb.2015.11.003.

[172] B. C. Allanach, D. P. George, B. Nachman, Investigating Multiple Solutions in the Constrained Minimal Supersymmetric Standard Model, JHEP 02 (2014) 031. arXiv:1311.3960, doi:10.1007/JHEP02(2014)031.

[173] I. Jack, D. R. Timothy Jones, S. P. Martin, M. T. Vaughn, Y. Yamada, Decoupling of the -scalar mass in softly broken supersymmetry, Phys. Rev. D. 50 (1994) 5481–5483. arXiv:hep-ph/9407291.

[174] M. Drees, K.-i. Hikasa, NOTE ON QCD CORRECTIONS TO HADRONIC HIGGS DECAY, Phys. Lett. B240 (1990) 455, [Erratum: Phys. Lett.B262,497(1991)]. doi:10.1016/0370-2693(90)91130-4.

[175] W. H. Press, S. A. Teukolsky, W. T. Vettering, B. P. Flannery, Numerical Recipes in Fortran 77: The Art of Scientific Computing, Vol. 1, Cambridge University Press, 1992.

[176] G. Passarino, M. Veltman, One-loop corrections for e+e annihilation into + in the Weinberg model, Nuc. Phys. B. 160 (1979) 151–207. doi:10.1016/0550-3213(79)90234-7.

[177] A. Djouadi, Y. Mambrini, M. Muhlleitner, Chargino and neutralino decays revisited, Eur. Phys. J. C20 (2001) 563–584. arXiv:hep-ph/0104115, doi:10.1007/s100520100679.

[178] H. Baer, C.-h. Chen, M. Drees, F. Paige, X. Tata, Supersymmetry reach of Tevatron upgrades: The Large tan Beta case, Phys. Rev. D58 (1998) 075008. arXiv:hep-ph/9802441, doi:10.1103/PhysRevD.58.075008.

[179] J. Hernandez-Sanchez, M. A. Perez, G. Tavares-Velasco, J. J. Toscano, Decay H+ —¿ W+ gamma in a nonlinear R(xi)-gauge, Phys. Rev. D69 (2004) 095008. arXiv:hep-ph/0402284, doi:10.1103/PhysRevD.69.095008.

[180] A. Djouadi, Y. Mambrini, Three body decays of SUSY particles, Phys. Lett. B493 (2000) 120–126. arXiv:hep-ph/0007174, doi:10.1016/S0370-2693(00)01102-3.

[181] A. Djouadi, M. Drees, U. Ellwanger, R. Godbole, C. Hugonie, S. King, S. Lehti, S. Moretti, A. Nikitenko, I. Rottlnder, M. Schumacher, A. Teixeira, Benchmark scenarios for the nmssm, Journal of High Energy Physics 2008 (07) 002. URL http://stacks.iop.org/1126–6708/2008/i=07/a=002.

[182] M. Spira, Higgs Boson Production and Decay at Hadron Colliders, Prog. Part. Nucl. Phys. 95 (2017) 98–159. arXiv:1612.07651, doi:10.1016/j.ppnp.2017.04.001.

[183] A. Djouadi, M. Spira, P. M. Zerwas, QCD corrections to hadronic Higgs decays, Z. Phys. C70 (1996) 427–434. arXiv:hep-ph/9511344, doi:10.1007/s002880050120.

[184] A. L. Kataev, V. T. Kim, The Effects of the QCD corrections to Gamma (H0 —¿ b anti-b), in: 3rd International Workshop on Software Engineering, Artificial Intelligence and Expert systems for High-energy and Nuclear Physics (AIHENP 93) Oberammergau, Germany, October 4-8, 1993, 1993.

[185] S. S. AbdusSalam, et al., Benchmark Models, Planes, Lines and Points for Future SUSY Searches at the LHC, Eur. Phys. J. C71 (2011) 1835. arXiv:1109.3859, doi:10.1140/epjc/s10052-011-1835-7.

[186] A. Buckley, PySLHA: a Pythonic interface to SUSY Les Houches Accord data, Eur. Phys. J. C75 (10) (2015) 467. arXiv:1305.4194, doi:10.1140/epjc/s10052-015-3638-8.

[187] A. Djouadi, P. Gambino, Qcd corrections to higgs boson self-energies and fermionic decay widths, Phys. Rev. D 51 (1995) 218–228. doi:10.1103/PhysRevD.51.218. URL https://link.aps.org/doi/10.1103/PhysRevD.51.218.

[188] A. Denner, S. Heinemeyer, I. Puljak, D. Rebuzzi, M. Spira, Standard Model Higgs-Boson Branching Ratios with Uncertainties, Eur. Phys. J. C71 (2011) 1753. arXiv:1107.5909, doi:10.1140/epjc/s10052-011-1753-8.

[189] A. Djouadi, Y. Mambrini, Three body decays of top and bottom squarks, Phys. Rev. D63 (2001) 115005. arXiv:hep-ph/0011364, doi:10.1103/PhysRevD.63.115005.

[190] H. Baer, T. Krupovnickas, Radiative neutralino decay in supersymmetric models, JHEP 09 (2002) 038. arXiv:hep-ph/0208277, doi:10.1088/1126-6708/2002/09/038.

[191] S. Kraml, H. Eberl, A. Bartl, W. Majerotto, W. Porod, SUSY QCD corrections to scalar quark decays into charginos and neutralinos, Phys. Lett. B386 (1996) 175–182. arXiv:hep-ph/9605412, doi:10.1016/0370-2693(96)00944-6.

[192] A. Djouadi, W. Hollik, C. Junger, QCD corrections to scalar quark decays, Phys. Rev. D55 (1997) 6975–6985. arXiv:hep-ph/9609419, doi:10.1103/PhysRevD.55.6975.

[193] A. Bartl, H. Eberl, K. Hidaka, S. Kraml, W. Majerotto, W. Porod, Y. Yamada, Susy-qcd corrections to top and bottom squark decays into higgs bosons, Phys. Rev. D 59 (1999) 115007. doi:10.1103/PhysRevD.59.115007.
URL `https://link.aps.org/doi/10.1103/PhysRevD.59.115007`

[194] A. Bartl, H. Eberl, K. Hidaka, S. Kraml, W. Majerotto, W. Porod, Y. Yamada, SUSY QCD corrections to stop and sbottom decays into W+- and Z0 bosons, Phys. Lett. B419 (1998) 243–252. arXiv:hep-ph/9710286, doi:10.1016/S0370-2693(97)01475-5.

[195] W. Beenakker, R. Hopker, P. M. Zerwas, SUSY QCD decays of squarks and gluinos, Phys. Lett. B378 (1996) 159–166. arXiv:hep-ph/9602378, doi:10.1016/0370-2693(96)00379-6.

[196] W. Beenakker, R. Hopker, T. Plehn, P. M. Zerwas, Stop decays in SUSY QCD, Z. Phys. C75 (1997) 349–356. arXiv:hep-ph/9610313, doi:10.1007/s002880050478.

[197] S. Weinberg, The quantum theory of fields. Vol. 2: Modern applications, Cambridge University Press, 2013.

[198] S. Weinberg, Infrared photons and gravitons, Phys. Rev. 140 (1965) B516–B524. doi:10.1103/PhysRev.140.B516.
URL https://link.aps.org/doi/10.1103/PhysRev.140.B516

[199] F. Bloch, A. Nordsieck, Note on the radiation field of the electron, Phys. Rev. 52 (1937) 54–59. doi:10.1103/PhysRev.52.54. URL https://link.aps.org/doi/10.1103/PhysRev.52.54.

[200] T. Kinoshita, Mass singularities of feynman amplitudes, Journal of Mathematical Physics 3 (4) (1962) 650–677. arXiv:https://doi.org/10.1063/1.1724268, doi:10.1063/1.1724268. URL https://doi.org/10.1063/1.1724268.

[201] T. D. Lee, M. Nauenberg, Degenerate systems and mass singularities, Phys. Rev. 133 (1964) B1549–B1562. doi:10.1103/PhysRev.133.B1549. URL https://link.aps.org/doi/10.1103/PhysRev.133.B1549.

[202] R. Field, Applications of perturbative QCD, Frontiers in physics, Addison-Wesley, The Advanced Book Program, 1989. URL https://books.google.co.uk/books?id=_rbvAAAAMAAJ.

[203] G. Dissertori, I. Knowles, M. Schmelling, Quantum Chromodynamics: High Energy Experiments and Theory, International Series of Monographs on Physics, Clarendon Press, 2003.
URL https://books.google.co.uk/books?id=9PtKDgAAQBAJ

[204] G. F. Sterman, Partons, factorization and resummation, in: QCD and beyond. Proceedings, Theoretical Advanced Study Institute in Elementary Particle Physics, TASI-95, Boulder, USA, June 4-30, 1995, 1995, pp. 327–408. arXiv:hep-ph/9606312.

[205] P. Skands, Introduction to QCD, in: Proceedings, 2nd Asia-Europe-Pacific School of High-Energy Physics (AEPSHEP 2014): Puri, India, November 0417, 2014, 2013, pp. 341–420, [,63(2107)]. arXiv:1207.2389, doi:10.1142/9789814525220_0008, 10.23730/CYRSP-2017-002.63.
URL https://inspirehep.net/record/1121892/files/arXiv:1207.2389.pdf

[206] D. Amati, R. Petronzio, G. Veneziano, Relating Hard QCD Processes Through Universality of Mass Singularities. 2., Nucl. Phys. B146 (1978) 29–49. doi:10.1016/0550-3213(78)90430-3.

[207] S. B. Libby, G. Sterman, Jet and lepton-pair production in high-energy lepton-hadron and hadron-hadron scattering, Phys. Rev. D 18 (1978) 3252–3268. doi:10.1103/PhysRevD.18.3252. URL https://link.aps.org/doi/10.1103/PhysRevD.18.3252.

[208] R. Ellis, H. Georgi, M. Machacek, H. Politzer, G. G. Ross, Perturbation theory and the parton model in qcd, Nuclear Physics B 152 (2) (1979) 285 – 329. doi:https://doi.org/10.1016/0550-3213(79)90105-6.
URL http://www.sciencedirect.com/science/article/pii/0550321379901056

[209] J. C. Collins, D. E. Soper, The theorems of perturbative qcd, Annual Review of Nuclear and Particle Science 37 (1) (1987) 383–409. doi:10.1146/annurev.ns.37.120187.002123. URL https://doi.org/10.1146/annurev.ns.37.120187.002123.

[210] T. Plehn, LHC Phenomenology for Physics Hunters, in: Proceedings of Theoretical Advanced Study Institute in Elementary Particle Physics on The dawn of the LHC era (TASI 2008): Boulder, USA, June 2-27, 2008, 2010, pp. 125–180. arXiv:0810.2281, doi:10.1142/9789812838360_0003.
URL https://inspirehep.net/record/799244/files/arXiv:0810.2281.pdf

[211] G. Altarelli, G. Parisi, Asymptotic Freedom in Parton Language, Nucl. Phys. B126 (1977) 298–318. doi:10.1016/0550-3213(77)90384-4.

[212] L. N. Lipatov, The parton model and perturbation theory, Sov. J. Nucl. Phys. 20 (1975) 94–102, [Yad. Fiz.20,181(1974)].

[213] V. N. Gribov, L. N. Lipatov, Deep inelastic e p scattering in perturbation theory, Sov. J. Nucl. Phys. 15 (1972) 438–450, [Yad. Fiz.15,781(1972)].

[214] Y. L. Dokshitzer, Calculation of the Structure Functions for Deep Inelastic Scattering and e+ e- Annihilation by Perturbation Theory in Quantum Chromodynamics., Sov. Phys. JETP 46 (1977) 641–653, [Zh. Eksp. Teor. Fiz.73,1216(1977)].

[215] L. A. Harland-Lang, A. D. Martin, P. Motylinski, R. S. Thorne, Parton distributions in the LHC era: MMHT 2014 PDFs, Eur. Phys. J. C75 (5) (2015) 204. arXiv:1412.3989, doi:10.1140/epjc/s10052-015-3397-6.

[216] R. D. Ball, et al., Parton distributions with LHC data, Nucl. Phys. B867 (2013) 244–289. arXiv:1207.1303, doi:10.1016/j.nuclphysb.2012.10.003.

[217] S. Dulat, T.-J. Hou, J. Gao, M. Guzzi, J. Huston, P. Nadolsky, J. Pumplin, C. Schmidt, D. Stump, C. P. Yuan, New parton distribution functions from a global analysis of quantum chromodynamics, Phys. Rev. D93 (3) (2016) 033006. arXiv:1506.07443, doi:10.1103/PhysRevD.93.033006.

[218] S. J. Brodsky, M. Mojaza, X.-G. Wu, Systematic Scale-Setting to All Orders: The Principle of Maximum Conformality and Commensurate Scale Relations, Phys. Rev. D89 (2014) 014027. arXiv:1304.4631, doi:10.1103/PhysRevD.89.014027.

[219] V. V. Sudakov, Vertex parts at very high-energies in quantum electrodynamics, Sov. Phys. JETP 3 (1956) 65–71, [Zh. Eksp. Teor. Fiz.30,87(1956)].

[220] R. Sghedoni, Transverse momentum distribution in B decays, Ph.D. thesis, Parma U. (2004). arXiv:hep-ph/0405291.

[221] U. Aglietti, R. Sghedoni, L. Trentadue, Full O(alpha(s)) evaluation for b —¿ s gamma transverse momentum distribution, Phys. Lett. B585 (2004) 131–143. arXiv:hep-ph/0310360, doi:10.1016/j.physletb.2004.02.010.

[222] G. Bozzi, S. Catani, D. de Florian, M. Grazzini, Transverse-momentum resummation and the spectrum of the Higgs boson at the LHC, Nucl. Phys. B737 (2006) 73–120. arXiv:hep-ph/0508068, doi:10.1016/j.nuclphysb.2005.12.022.

[223] J. Collins, D. E. Soper, G. Sterman, Transverse momentum distribution in drell-yan pair and w and z boson production, Nuclear Physics B 250 (1) (1985) 199 – 224. doi:https://doi.org/10.1016/0550-3213(85)90479-1.
URL http://www.sciencedirect.com/science/article/pii/0550321385904791

[224] E. laenen, Resummation for observables at tev colliders, Pramana 63 (6) (2004) 1225. doi:10.1007/BF02704892.
URL https://doi.org/10.1007/BF02704892

[225] T. Becher, R. Frederix, M. Neubert, L. Rothen, Automated NNLL + NLO resummation for jet-veto cross sections, Eur. Phys. J. C75 (4) (2015) 154. arXiv:1412.8408, doi:10.1140/epjc/s10052-015-3368-y.

[226] S. Marzani, L. Schunk, G. Soyez, A study of jet mass distributions with grooming, JHEP 07 (2017) 132. arXiv:1704.02210, doi:10.1007/JHEP07(2017)132.

[227] S. Frixione, B. R. Webber, Matching NLO QCD computations and parton shower simulations, JHEP 06 (2002) 029. arXiv:hep-ph/0204244, doi:10.1088/1126-6708/2002/06/029.

[228] P. Nason, A New method for combining NLO QCD with shower Monte Carlo algorithms, JHEP 11 (2004) 040. arXiv:hep-ph/0409146, doi:10.1088/1126-6708/2004/11/040.

[229] S. Frixione, P. Nason, C. Oleari, Matching NLO QCD computations with Parton Shower simulations: the POWHEG method, JHEP 11 (2007) 070. arXiv:0709.2092, doi:10.1088/1126-6708/2007/11/070.

[230] S. Catani, F. Krauss, R. Kuhn, B. R. Webber, QCD matrix elements + parton showers, JHEP 11 (2001) 063. arXiv:hep-ph/0109231, doi:10.1088/1126-6708/2001/11/063.

[231] S. Hoeche, F. Krauss, N. Lavesson, L. Lonnblad, M. Mangano, A. Schalicke, S. Schumann, Matching parton showers and matrix elements, in: HERA and the LHC: A Workshop on the implications of HERA for LHC physics: Proceedings Part A, 2005, pp. 288–289. arXiv:hep-ph/0602031, doi:10.5170/CERN-2005-014.288.
URL http://inspirehep.net/record/709818/files/arXiv:hep-ph_0602031.pdf

[232] J. Alwall, et al., Comparative study of various algorithms for the merging of parton showers and matrix elements in hadronic collisions, Eur. Phys. J. C53 (2008) 473–500. arXiv:0706.2569, doi:10.1140/epjc/s10052-007-0490-5.

[233] K. Hamilton, P. Nason, E. Re, G. Zanderighi, NNLOPS simulation of Higgs boson production, JHEP 10 (2013) 222. arXiv:1309.0017, doi:10.1007/JHEP10(2013)222.

[234] S. Alioli, C. W. Bauer, C. Berggren, F. J. Tackmann, J. R. Walsh, Drell-Yan production at NNLL+NNLO matched to parton showers, Phys. Rev. D92 (9) (2015) 094020. arXiv:1508.01475, doi:10.1103/PhysRevD.92.094020.

[235] T. Becher, A. Broggio, A. Ferroglia, Introduction to Soft-Collinear Effective Theory, Lect. Notes Phys. 896 (2015) pp.1–206. arXiv:1410.1892, doi:10.1007/978-3-319-14848-9.

[236] T. Becher, M. Neubert, Drell-Yan Production at Small q_T, Transverse Parton Distributions and the Collinear Anomaly, Eur. Phys. J. C71 (2011) 1665. arXiv:1007.4005, doi:10.1140/epjc/s10052-011-1665-7.

[237] T. Becher, M. Neubert, D. Wilhelm, Electroweak Gauge-Boson Production at Small q_T: Infrared Safety from the Collinear Anomaly, JHEP 02 (2012) 124. arXiv:1109.6027, doi:10.1007/JHEP02(2012)124.

[238] Y. Dokshitzer, D. Dyakonov, S. Troyan, Hard processes in quantum chromodynamics, Physics Reports 58 (5) (1980) 269 – 395. doi:https://doi.org/10.1016/0370-1573(80)90043-5.
URL http://www.sciencedirect.com/science/article/pii/0370157380900435

[239] G. Parisi, R. Petronzio, Small transverse momentum distributions in hard processes, Nuclear Physics B 154 (3) (1979) 427 – 440. doi:https://doi.org/10.1016/0550-3213(79)90040-3.
URL http://www.sciencedirect.com/science/article/pii/0550321379900403

[240] G. Curci, M. Greco, Y. Srivastava, Qcd jets from coherent states, Nuclear Physics B 159 (3) (1979) 451 – 468. doi:https://doi.org/10.1016/0550-3213(79)90345-6.
URL http://www.sciencedirect.com/science/article/pii/0550321379903456

[241] S. D. Ellis, W. J. Stirling, Quark form factors and leading double logarithms in quantum chromodynamics, Phys. Rev. D 23 (1981) 214–226. doi:10.1103/PhysRevD.23.214. URL https://link.aps.org/doi/10.1103/PhysRevD.23.214.

[242] J. C. Collins, D. E. Soper, Back-to-back jets in qcd, Nuclear Physics B 193 (2) (1981) 381 – 443. doi:https://doi.org/10.1016/0550-3213(81)90339-4.
URL http://www.sciencedirect.com/science/article/pii/0550321381903394

[243] J. C. Collins, D. E. Soper, Back-to-back jets: Fourier transform from b to kt, Nuclear Physics B 197 (3) (1982) 446 – 476. doi:https://doi.org/10.1016/0550-3213(82)90453-9.
URL http://www.sciencedirect.com/science/article/pii/0550321382904539

[244] J. Kodaira, L. Trentadue, Summing soft emission in qcd, Physics Letters B 112 (1) (1982) 66 – 70. doi:https://doi.org/10.1016/0370-2693(82)90907-8.
URL http://www.sciencedirect.com/science/article/pii/0370269382909078

[245] G. Altarelli, R. Ellis, M. Greco, G. Martinelli, Vector boson production at colliders: A theoretical reappraisal, Nuclear Physics B 246 (1) (1984) 12 – 44. doi:https://doi.org/10.1016/0550-3213(84)90112-3.
URL http://www.sciencedirect.com/science/article/pii/0550321384901123

[246] C. T. H. Davies, B. R. Webber, W. J. Stirling, Drell-Yan Cross-Sections at Small Transverse Momentum, Nucl. Phys. B256 (1985) 413, [1,I.95(1984)]. doi:10.1016/0550-3213(85)90402-X.

[247] S. Catani, E. D'Emilio, L. Trentadue, The gluon form factor to higher orders: Gluon-gluon annihilation at small qt, Physics Letters B 211 (3) (1988) 335 – 342. doi:https://doi.org/10.1016/0370-2693(88)90912-4.
URL http://www.sciencedirect.com/science/article/pii/0370269388909124

[248] D. de Florian, M. Grazzini, Next-to-next-to-leading logarithmic corrections at small transverse momentum in hadronic collisions, Phys. Rev. Lett. 85 (2000) 4678–4681. arXiv:hep-ph/0008152, doi:10.1103/PhysRevLett.85.4678.

[249] S. Catani, M. Grazzini, QCD transverse-momentum resummation in gluon fusion processes, Nucl. Phys. B845 (2011) 297–323. arXiv:1011.3918, doi:10.1016/j.nuclphysb.2010.12.007.

[250] S. Catani, D. de Florian, M. Grazzini, Universality of non-leading logarithmic contributions in transverse-momentum distributions, Nuclear Physics B 596 (1) (2001) 299 – 312. doi:https://doi.org/10.1016/S0550-3213(00)00617-9.
URL http://www.sciencedirect.com/science/article/pii/S0550321300006179

[251] S. Catani, L. Cieri, D. de Florian, G. Ferrera, M. Grazzini, Universality of transverse-momentum resummation and hard factors at the NNLO, Nucl. Phys. B881 (2014) 414–443. arXiv:1311.1654, doi:10.1016/j.nuclphysb.2014.02.011.

[252] C. Balazs, C. P. Yuan, Soft gluon effects on lepton pairs at hadron colliders, Phys. Rev. D56 (1997) 5558–5583. arXiv:hep-ph/9704258, doi:10.1103/PhysRevD.56.5558.

[253] C. Balazs, E. L. Berger, P. M. Nadolsky, C. P. Yuan, All-orders resummation for diphoton production at hadron colliders, Phys. Lett. B637 (2006) 235–240. arXiv:hep-ph/0603037, doi:10.1016/j.physletb.2006.04.017.

[254] D. de Florian, G. Ferrera, M. Grazzini, D. Tommasini, Higgs boson production at the LHC: transverse momentum resummation effects in the H-¿2gamma, H-¿WW-¿lnu lnu and H-¿ZZ-¿4l decay modes, JHEP 06 (2012) 132. arXiv:1203.6321, doi:10.1007/JHEP06(2012)132.

[255] M. Grazzini, H. Sargsyan, Heavy-quark mass effects in Higgs boson production at the LHC, JHEP 09 (2013) 129. arXiv:1306.4581, doi:10.1007/JHEP09(2013)129.

[256] S. Catani, M. Grazzini, A. Torre, Transverse-momentum resummation for heavy-quark hadroproduction, Nucl. Phys. B890 (2014) 518–538. arXiv:1408.4564, doi:10.1016/j.nuclphysb.2014.11.019.

[257] S. Catani, M. Grazzini, Qcd transverse-momentum resummation in gluon fusion processes, Nuclear Physics B 845 (3) (2011) 297 – 323. doi:https://doi.org/10.1016/j.nuclphysb.2010.12.007.
URL http://www.sciencedirect.com/science/article/pii/S0550321310006528

[258] T. Ooura, M. Mori, The double exponential formula for oscillatory functions over the half infinite interval, Journal of Computational and Applied Mathematics 38 (1) (1991) 353 – 360. doi:https://doi.org/10.1016/0377-0427(91)90181-I.
URL http://www.sciencedirect.com/science/article/pii/037704279190181I

[259] J. C. Collins, D. E. Soper, Back-To-Back Jets: Fourier Transform from B to K-Transverse, Nucl. Phys. B197 (1982) 446–476. doi:10.1016/0550-3213(82)90453-9.

[260] A. Kulesza, W. J. Stirling, Nonperturbative effects and the resummed Higgs transverse momentum distribution at the LHC, JHEP 12 (2003) 056. arXiv:hep-ph/0307208, doi:10.1088/1126-6708/2003/12/056.

[261] G. Bozzi, S. Catani, D. de Florian, M. Grazzini, Higgs boson production at the lhc: Transverse-momentum resummation and rapidity dependence, Nuclear Physics B 791 (1) (2008) 1 – 19. doi:https://doi.org/10.1016/j.nuclphysb.2007.09.034.
URL http://www.sciencedirect.com/science/article/pii/S0550321307007298

[262] F. James, M. Roos, Minuit - a system for function minimization and analysis of the parameter errors and correlations, Computer Physics Communications 10 (6) (1975) 343 – 367. doi:https://doi.org/10.1016/0010-4655(75)90039-9.
URL http://www.sciencedirect.com/science/article/pii/0010465575900399

[263] J. C. Collins, D. E. Soper, Angular distribution of dileptons in high-energy hadron collisions, Phys. Rev. D 16 (1977) 2219–2225. doi:10.1103/PhysRevD.16.2219. URL https://link.aps.org/doi/10.1103/PhysRevD.16.2219.

[264] T. Hahn, CUBA: A Library for multidimensional numerical integration, Comput. Phys. Commun. 168 (2005) 78–95. arXiv:hep-ph/0404043, doi:10.1016/j.cpc.2005.01.010.

[265] G. P. Lepage, A new algorithm for adaptive multidimensional integration, Journal of Computational Physics 27 (1978) 192–203. doi:10.1016/0021-9991(78)90004-9.

[266] S. Catani, L. Cieri, D. de Florian, G. Ferrera, M. Grazzini, Diphoton production at hadron colliders: a fully-differential QCD calculation at NNLO, Phys. Rev. Lett. 108 (2012) 072001, [Erratum: Phys. Rev. Lett.117,no.8,089901(2016)]. arXiv:1110.2375, doi:10.1103/PhysRevLett.108.072001, 10.1103/PhysRevLett.117.089901.

[267] T. Binoth, J. P. Guillet, E. Pilon, M. Werlen, A Full next-to-leading order study of direct photon pair production in hadronic collisions, Eur. Phys. J. C16 (2000) 311–330. arXiv:hep-ph/9911340, doi:10.1007/s100520050024.

[268] Z. Bern, L. J. Dixon, C. Schmidt, Isolating a light Higgs boson from the diphoton background at the CERN LHC, Phys. Rev. D66 (2002) 074018. arXiv:hep-ph/0206194, doi:10.1103/PhysRevD.66.074018.

[269] J. M. Campbell, R. K. Ellis, Y. Li, C. Williams, Predictions for diphoton production at the LHC through NNLO in QCD, JHEP 07 (2016) 148. arXiv:1603.02663, doi:10.1007/JHEP07(2016)148.

[270] P. M. Nadolsky, C. Balazs, E. L. Berger, C. P. Yuan, Gluon-gluon contributions to the production of continuum diphoton pairs at hadron colliders, Phys. Rev. D76 (2007) 013008. arXiv:hep-ph/0702003, doi:10.1103/PhysRevD.76.013008.

[271] M. Chiesa, N. Greiner, M. Schnherr, F. Tramontano, Electroweak corrections to diphoton plus jets, JHEP 10 (2017) 181. arXiv:1706.09022, doi:10.1007/JHEP10(2017)181.

[272] S. D. Drell, T.-M. Yan, Massive lepton-pair production in hadron-hadron collisions at high energies, Phys. Rev. Lett. 25 (1970) 316–320. doi:10.1103/PhysRevLett.25.316. URL https://link.aps.org/doi/10.1103/PhysRevLett.25.316.

[273] C. Davies, W. Stirling, Non-leading corrections to the drell-yan cross section at small transverse momentum, Nuclear Physics B 244 (2) (1984) 337 – 348. doi:https://doi.org/10.1016/0550-3213(84)90316-X.
URL `http://www.sciencedirect.com/science/article/pii/055032138490316X`

[274] M. Schmaltz, D. Tucker-Smith, Little Higgs review, Ann. Rev. Nucl. Part. Sci. 55 (2005) 229–270. arXiv:hep-ph/0502182, doi:10.1146/annurev.nucl.55.090704.151502.

[275] Y. Li, F. Petriello, Combining QCD and electroweak corrections to dilepton production in FEWZ, Phys. Rev. D86 (2012) 094034. arXiv:1208.5967, doi:10.1103/PhysRevD.86.094034.

[276] F. Landry, R. Brock, P. M. Nadolsky, C. P. Yuan, Tevatron Run-1 Z boson data and Collins-Soper-Sterman resummation formalism, Phys. Rev. D67 (2003) 073016. arXiv:hep-ph/0212159, doi:10.1103/PhysRevD.67.073016.

[277] Q.-H. Cao, C. P. Yuan, Combined effect of QCD resummation and QED radiative correction to W boson observables at the Tevatron, Phys. Rev. Lett. 93 (2004) 042001. arXiv:hep-ph/0401026, doi:10.1103/PhysRevLett.93.042001.

[278] S. Catani, L. Cieri, G. Ferrera, D. de Florian, M. Grazzini, Vector boson production at hadron colliders: a fully exclusive QCD calculation at NNLO, Phys. Rev. Lett. 103 (2009) 082001. arXiv:0903.2120, doi:10.1103/PhysRevLett.103.082001.

[279] A. D. Martin, W. J. Stirling, R. S. Thorne, G. Watt, Parton distributions for the LHC, Eur. Phys. J. C63 (2009) 189–285. arXiv:0901.0002, doi:10.1140/epjc/s10052-009-1072-5.

[280] A. Airapetian, et al., ATLAS: Detector and physics performance technical design report. Volume 2.

[281] The CMS electromagnetic calorimeter project: Technical Design Report, no. CERN/LHCC 97-33 in Technical Design Report CMS, CERN, Geneva, 1997.
URL `https://cds.cern.ch/record/349375`

[282] T. Binoth, J. P. Guillet, E. Pilon, M. Werlen, Beyond leading order effects in photon pair production at the Tevatron, Phys. Rev. D63 (2001) 114016. arXiv:hep-ph/0012191, doi:10.1103/PhysRevD.63.114016.

[283] M. Aaboud, et al., Measurements of integrated and differential cross sections for isolated photon pair production in pp collisions at $\sqrt{s} = 8$ TeV with the ATLAS detector, Phys. Rev. D95 (11) (2017) 112005. arXiv:1704.03839, doi:10.1103/PhysRevD.95.112005.

[284] J. M. Campbell, R. K. Ellis, An Update on vector boson pair production at hadron colliders, Phys. Rev. D60 (1999) 113006. arXiv:hep-ph/9905386, doi:10.1103/PhysRevD.60.113006.

[285] J. M. Campbell, R. K. Ellis, C. Williams, Vector boson pair production at the LHC, JHEP 07 (2011) 018. arXiv:1105.0020, doi:10.1007/JHEP07(2011)018.

[286] J. M. Campbell, R. K. Ellis, W. T. Giele, A Multi-Threaded Version of MCFM, Eur. Phys. J. C75 (6) (2015) 246. arXiv:1503.06182, doi:10.1140/epjc/s10052-015-3461-2.

[287] R. Boughezal, J. M. Campbell, R. K. Ellis, C. Focke, W. Giele, X. Liu, F. Petriello, C. Williams, Color singlet production at NNLO in MCFM, Eur. Phys. J. C77 (1) (2017) 7. arXiv:1605.08011, doi:10.1140/epjc/s10052-016-4558-y.

[288] M. R. Whalley, D. Bourilkov, R. C. Group, The Les Houches accord PDFs (LHAPDF) and LHAGLUE, in: HERA and the LHC: A Workshop on the implications of HERA for LHC physics. Proceedings, Part B, 2005, pp. 575–581. arXiv:hep-ph/0508110.

[289] C. H. Chen, M. Drees, J. F. Gunion, A Nonstandard string / SUSY scenario and its phenomenological implications, Phys. Rev. D55 (1997) 330–347, [Erratum: Phys. Rev.D60,039901(1999)]. arXiv:hep-ph/9607421, doi:10.1103/PhysRevD.60.039901, 10.1103/PhysRevD.55.330.

[290] S. Catani, L. Cieri, D. de Florian, G. Ferrera, M. Grazzini, Vector boson production at hadron colliders: hard-collinear coefficients at the NNLO, Eur. Phys. J. C72 (2012) 2195. arXiv:1209.0158, doi:10.1140/epjc/s10052-012-2195-7.

[291] S. Catani, M. Grazzini, Higgs Boson Production at Hadron Colliders: Hard-Collinear Coefficients at the NNLO, Eur. Phys. J. C72 (2012) 2013, [Erratum: Eur. Phys. J.C72,2132(2012)]. arXiv:1106.4652, doi:10.1140/epjc/s10052-012-2013-2, 10.1140/epjc/s10052-012-2132-9.

[292] U. Aglietti, R. Bonciani, G. Degrassi, A. Vicini, Analytic Results for Virtual QCD Corrections to Higgs Production and Decay, JHEP 01 (2007) 021. arXiv:hep-ph/0611266, doi:10.1088/1126-6708/2007/01/021.

[293] C. Anastasiou, E. W. N. Glover, M. E. Tejeda-Yeomans, Two loop QED and QCD corrections to massless fermion boson scattering, Nucl. Phys. B629 (2002) 255–289. arXiv:hep-ph/0201274, doi:10.1016/S0550-3213(02)00140-2.